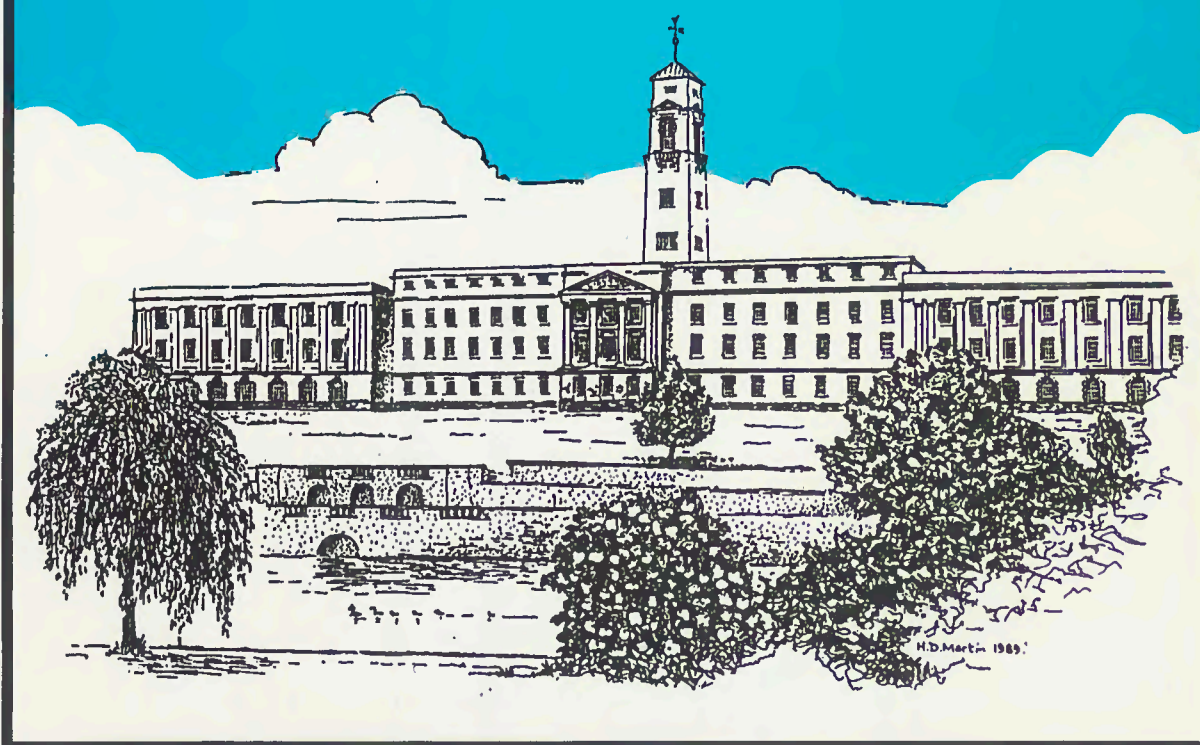


**FOURTH INTERNATIONAL  
CONFERENCE  
ON ELECTRIC FUSES  
AND THEIR APPLICATIONS**



**23rd-25th SEPTEMBER 1991  
UNIVERSITY OF NOTTINGHAM, UK**





**PROCEEDINGS OF THE  
FOURTH INTERNATIONAL CONFERENCE  
ON ELECTRIC FUSES  
AND THEIR APPLICATIONS**

**University of Nottingham  
United Kingdom**

**23rd-25th September 1991**

**These Proceedings are sponsored by S.O.C. Corporation, Japan**

© UNIVERSITY OF NOTTINGHAM

ISBN 0 9514828 1 5

Proceedings of the Fourth International Conference  
on Electric Fuses and their Applications  
(paperback)

Published by

Department of Electrical and Electronic Engineering  
University of Nottingham  
University Park  
Nottingham NG7 2RD  
United Kingdom

The University of Nottingham and the Fourth International Conference on Electric Fuses and their Applications Technical and Organising Committees are not responsible for the opinions expressed in the papers published in these Proceedings. The contents of the papers express entirely the views of the authors.

Printed in Great Britain by Quorn Selective Repro Ltd, Queens Road, Loughborough,  
Leicestershire, LE11 1HH

## FOREWORD

Today, when several billions of fuses are manufactured each year, it is not generally known that they were used to protect submarine telegraph cables as long ago as 1864. Few were produced at that time and it was not until after the establishment of electricity-supply systems, some 100 years ago, that their use started to increase greatly.

Most people today are familiar with fuses and know how to replace them after they have operated. They are generally regarded as very simple devices which contain metal wires or strips that melt when currents above certain levels flow through them. It would therefore surprise the majority of people, and certainly those who first developed fuses, to know that their behaviour is still not fully understood and that much research is being conducted on them around the world as the end of the 20th century approaches.

The extent of the research and development effort in recent years is evident from the fact that successful international conferences on fuses were held at Liverpool Polytechnic in the UK in 1976 and at the Technical Universities of Norway in Trondheim and Eindhoven in the Netherlands in 1984 and 1987 respectively. A total of exactly 100 papers were presented at these conferences.

The University of Nottingham is pleased to host the Fourth International Conference at which over 50 papers are to be presented, the authors being from 16 countries. The delegates who are to be present are from many countries around the world and this provides further evidence of the international interest in electric fuses. A very warm welcome is extended to all of them and it is hoped that they will find the Conference activities to be both interesting and enjoyable.

Dr Howe and I wish to thank the members of the Conference Organising and Technical Committees for their assistance. Thanks are also due to both Hawker Fusegear Ltd for the support they have provided and SOC Corporation for their generous sponsorship.

Arthur Wright  
Chairman  
Technical Committee

## LOCAL ORGANISING COMMITTEE

Dr A F Howe (Chairman)

Mr A Brindle (Treasurer)

Mrs C Everard (Publicity)

Miss S Hollingsworth (Secretary)

Mr P G Newbery

Mr N P M Nurse

Mr P Rosen

Professor A Wright

## INTERNATIONAL TECHNICAL COMMITTEE

Professor A Wright (Chairman)  
University of Nottingham, UK

Professor G Cantarella  
Politecnico di Torino, Italy\*

Mr W H Curtis  
Bussman-Cooper Industries, USA\*

Dr J E Daalder  
ABB, Norway\*

Mr R Deshayes  
Ferraz, France\*

Professor A Hirose  
SOC Corporation, Japan\*

Dr A F Howe  
University of Nottingham, UK

Mr D J Krueger  
Littelfuse Inc, USA\*

Dr J G Leach  
Hi-Tech Fuses Incorporated, USA\*

Professor M Lindmayer  
Technische Universitat Braunschweig,  
Germany\*

Professor T Lipski  
Technical University of Gdansk,  
Poland\*

Mr P G Newbery  
Hawker Fusegear Ltd, UK

Mr N P M Nurse  
Hawker Fusegear Ltd, UK

Mr P Rosen  
Hawker Fusegear Ltd, UK

Professor A D Stokes  
University of Sydney, Australia\*

Dr C Turner  
ERA Technology, UK

Mr H W Turner  
ERA Technology, UK

Dr L Vermij  
Littelfuse Tracor BV, The Netherlands\*

Mr J S Wall  
Gould Inc, USA\*

Professor Wang Ji-Mei  
University of Xi'an Jiaotong,  
P R China\*

Dr R Wilkins  
Consultant, UK

\* Corresponding Member

INTERNATIONAL TECHNICAL COMMITTEE  
ESTABLISHED 1981

- |                                    |  |
|------------------------------------|--|
| Mr. R. J. ...<br>Hawke ... Ltd. UK | Prof. ... A. Wright (Chairman)<br>University of Nottingham, UK |
| Mr. P. ...<br>... Ltd. UK          | Prof. ... G. ...<br>... Ltd. UK                                |
| Mr. ...<br>... Ltd. UK             | Mr. W. ...<br>... USA  |
| Prof. ... B. ...<br>... Austria    | Dr. J. ...<br>...  |
| Dr. ...<br>EPA Technology, UK      | Mr. ...<br>...   |
| Mr. W. ...<br>EPA Technology, UK   | Prof. ...<br>...   |
| Dr. ...<br>... UK                  | Dr. ...<br>University of ... UK                                |
| Mr. J. ...<br>Gold Inc. USA        | Mr. ...<br>USA   |
| Dr. ...<br>... USA                 | Dr. ...<br>USA   |
| Dr. ...<br>Canada, UK              | Prof. ...<br>...   |
| ...                                | Prof. ...<br>...   |

## CONTENTS

<b>Opening Address</b>		Page
FEENAN J	Low Voltage Fuses	1
<b>Session 1: Fuse Design I</b>		
BRECHTKEN D, KONIG D & MULLER B	Thermal processes in SF <sub>6</sub> -filled fuses below the minimum melting current	7
WILKINS R	Steady-state current-sharing in fuses with asymmetrical arrangements of parallel elements	13
COSTA S F, RANGEL L P & BASTOS R G	Overload tests for fuses in rolling-mills	17
REX H G	A simple method to calculate the maximum voltage that arises when a fuse link breaks a DC short circuit current	23
CAO L J & STOKES A D	Spectrum analysis of an ablation-stabilised arc in ice	27
<b>Session 2: Fuse Design II</b>		
WANG JI-MEI	Research on horse-shoe type axial magnetic field vacuum fuse	33
SHEN MEIHAN	An experimental investigation of interrupting performance of HV expulsion fuses	37
WILKINS R, WILKINSON A & CLINE C	Endurance of semiconductor fuses under cyclic loading	43
AKHMEROV N, AZIZOV E & JAGNOV V	The electrically exploding wires application in the power circuit breakers	49
WOLNY A	Fuse-element in SF <sub>6</sub> atmosphere	53
<b>Session 3: Fuse Design III</b>		
NAMITOKOV K K, ILYINA N A, ZHEMEROV G G & SHKLOVSKY I G	Semiconductor fuses with aluminium current-carrying parts: the problems and prospects	59
GOMEZ J C, TOURN D & McEWAN P M	Investigation of the pre-arcing behaviour of dissimilar uniform double-elemented filled fuses, using FE CAD techniques	65

		Page
NUTSCH G & ROTHER W	Investigation for the use of copper as an element material in HV-HBC fuses	68
NAMITOKOV K K, ILYINA N A, ZHEMEROV G G & SHKLOVSKY I G	Principal manufacture technologies for semiconductor fuses	74
ELIADE R & BUDASCU E	Contributions concerning new extinction media in ultra-fast fuses up to 2000 V a.c.	81
<b>Session 4: Miniature Fuses</b> <i>Chair</i>		
HARRISON R D, HOWE A F & HARRISON, I	Ageing of film fuses on substrates	85
TAKAHASHI H & HIROSE K	A semiconductor fuse-link on a ceramic substrate	92
VAN RIETSCHOTEN P, JASPAR J & VERMIJ L	Some design and application aspects of very small fuses	96
JASPAR J, VAN RIETSCHOTEN P & VERMIJ L	A theoretical approximation of the time-current characteristic of miniature fuses	100
HIROSE A & MATSUZAKI H	Breaking tests of low breaking capacity miniature fuse-links	103
LINDMAYER M & LUTHER M	Fusing and short circuit interruption behaviour of metal film fuses	107
<b>Session 5A: Motor Control Fuses</b>		
FLOOD A J	Protection of motor controllers using North American time delay fuses	115
ARATO D & CANTARELLA G	Contactors protected by fuses: risk of contact welding	119
ARATO D & DUGHERA C	Starters protected by fuses: thermal stress on overload relays during short circuit currents	125
BRET M	Coordination of fuses-starters: new standards, new needs	131
DESHAYES R	"aM" fuse and its coordination with starters	137
SCHAFFER S	Dual-element time-delay class J fuses for protection of motor circuits utilizing IEC controllers	143
OSSOWICKI J & CWIDAK K	The distribution of constrictions in corrugated fuse-elements	146
<b>Session 5B: Fundamental Processes I</b>		
BOTTAUSCIO O, CROTTI G & FARINA G	Non-adiabatic process in fuse elements with heavy current faults	151
SASU M & OARGA CH	Mathematical modelling of the heat transfer phenomena in variable section fusible elements	156

	Page
CHEIM L A V & HOWE A F	Calculating fuse pre-arcing times by transmission-line modelling (TLM) 162
NAMITOKOV K K, ILYINA N A, ZHEMEROV G G & SHKLOVSKY I G	Identification and optimization as main application areas for mathematical methods in fuse design 168
XIE YUNXIANG	The computer analysis of breaking current process in sand filler fuses 173
GARRIDO C & CIDRAS J	Analysis of pre-arcing time-current characteristic of fuselinks 178

### Session 6A: Fuse Testing

HALLERBERG D A	Underwriters Laboratories Inc Standards for Safety for fuses 185
PORTEUS D	Developments in small dimension fuse technology and the impact on a third party independent certification organization 190
WAFER R V & OSYPIW D	The effects of supply frequency on the performance of AC fuses 195
BOTTAUSCIO O, CROTTI G & FARINA G	Influence of short-circuit power factor on the cut-off current of low voltage fuses 201
SLOOT J G J & MENG XIAN ZHONG	Choices for the presentation of fuse melting curves 206

### Session 6B: Fundamental Processes II

WILKINS R, SUURONEN D & O'SHIELDS L	Developments in the modelling of fuse breaking tests 211
JAKUBIUK K, LIPSKI T & PISANKO A	An integrated physical model of the h.b.c. fuse arcing process 216
BARROW D R & HOWE A F	The use of optical spectroscopy in the analysis of electric fuse arcing 221
JAKUBIUK K	Electrothermal fuse-element disintegrating mechanism by short-circuit currents 226
BARROW D R & HOWE A F	A comparison of the computer modelling of electric fuse arcing and their real-life performance 231
FRENCKEL Z	The calculation of the parameters of the plasma of the arc in a fuse 235

### Session 7: Applications and Trends

TURNER H W, TURNER C & WILLIAMS D J A	Performance criteria for compact industrial fuselinks 241
--	---

	Page
TURNER C, TURNER H W & WILLIAMS D J A	Requirements for Universal Modular Fuses (UMFs) 246
ARAI S	Application of the expert system for the selection of capacitor fuses 252
WILLIAMS D J A & TURNER H W	Protection of ESI equipment where private generators are connected to the distribution system 258
NEWBERY P G	Future trends in low voltage fuse systems 264

## INDEX OF AUTHORS

	Page No.		Page No.
Akhmerov, N	49	McEwan, P M	65
Arai, S	252	Matsuzaki, H	103
Arato, D	119, 125	Meng, XianZhong	206
Azizov, E	49	Muller, B	7
Barrow, D R	221, 231	Namitokov, K K	59, 74, 168
Bastos, R G	17	Newbery, P G	264
Bottauscio, O	151, 201	Nutsch, G	68
Brechtken, D	7	O'Shields, L	211
Bret, M	131	Oarga, C H	156
Budascu, E	81	Ossowicki, J	146
Cantarella, G	119	Osypiw, D	195
Cao, L J	27	Pisanko, A	216
Cheim, L A V	162	Porteus, D	190
Cidras, J	178	Rangel, L P	17
Cline, C	43	Rex, H G	23
Costa, S F	17	Rother, W	68
Crotti, G	151, 201	Sasu, M	156
Cwidak, K	146	Schaffer, S	143
Deshayes, R	137	Shen Meihan	37
Dughera, C	125	Shklovsky, I G	59, 74, 168
Eliade, R	81	Sloot, J G J	206
Farina, G	151, 201	Stokes, A D	27
Feenan, J	1	Suuronen, D	211
Flood, A J	115	Takahashi, H	92
Frenckel, Z	235	Tourn, D	65
Garrido, C	178	Turner, C	241, 246
Gomez, J C	65	Turner, H W	241, 246, 258
Hallerberg, D A	185	Van Rietschoten, P	96, 100
Harrison, I	85	Vermij L	96, 100
Harrison, R D	85	Wafer, R V	195
Hirose, A	103	Wang Ji-mei	33
Hirose, K	92	Wilkins, R	13, 43, 211
Howe, A F	85, 162, 221, 231	Wilkinson, A	43
Ilyina, N A	59, 74, 168	Williams, D J A	241, 246, 258
Jagnov, V	49	Wolny, A	53
Jakubiuk, K	216, 226	Xie, Yunxiang	173
Jaspar, J	96, 100	Zhemerov, G G	59, 74, 168
Konig, D	7		
Lindmayer, M	107		
Lipski, T	216		
Luther, M	107		

INDEX OF AUTHORS

Page No.	Page No.	Page No.
107	107	107
108	108	108
109	109	109
110	110	110
111	111	111
112	112	112
113	113	113
114	114	114
115	115	115
116	116	116
117	117	117
118	118	118
119	119	119
120	120	120
121	121	121
122	122	122
123	123	123
124	124	124
125	125	125
126	126	126
127	127	127
128	128	128
129	129	129
130	130	130
131	131	131
132	132	132
133	133	133
134	134	134
135	135	135
136	136	136
137	137	137
138	138	138
139	139	139
140	140	140
141	141	141
142	142	142
143	143	143
144	144	144
145	145	145
146	146	146
147	147	147
148	148	148
149	149	149
150	150	150
151	151	151
152	152	152
153	153	153
154	154	154
155	155	155
156	156	156
157	157	157
158	158	158
159	159	159
160	160	160
161	161	161
162	162	162
163	163	163
164	164	164
165	165	165
166	166	166
167	167	167
168	168	168
169	169	169
170	170	170
171	171	171
172	172	172
173	173	173
174	174	174
175	175	175
176	176	176
177	177	177
178	178	178
179	179	179
180	180	180
181	181	181
182	182	182
183	183	183
184	184	184
185	185	185
186	186	186
187	187	187
188	188	188
189	189	189
190	190	190
191	191	191
192	192	192
193	193	193
194	194	194
195	195	195
196	196	196
197	197	197
198	198	198
199	199	199
200	200	200

## **Opening Address**

Opening Address

## LOW VOLTAGE FUSES 1919-1991

J Feenan  
Consultant  
GEC ALSTHOM Installation Equipment Ltd  
Liverpool UK

I am honoured to be asked to present the opening paper to this, the Fourth International Conference on Electric Fuses and Their Applications. These conferences are now established as an important event in the technical progress of fuses. The wide range of papers from an international assembly of authors reflects the extensive research which is continuing on what is probably the oldest electrical protective device - the fuse.

In contrast to the detailed academic content of the majority of papers to be presented during this conference, I intend to concern myself with an historical review, together with a somewhat practical assessment of present and future trends. I have concentrated on low voltage fuses because this has been my main interest, although, as the conference papers show, tremendous strides in the design of high-voltage fuses have, and are taking place, and there are now exciting developments in miniature fuses.

The first recorded discussion on fuses was in the early 1880's and in the first edition of the IEE Wiring Regulations in 1882, there is a reference to the fuse.

Regulation II 9 states

"Every part of the circuit should be so determined that the gauge of wire to be used is properly proportioned to the currents it will have to carry, and changes of circuit from a larger to a smaller conductor should be sufficiently protected with suitable safety fuses so that no portion of the conductor should ever be allowed to attain a temperature exceeding 150°F.

NB. These fuses are the very essence of safety. They should always be enclosed in incombustible cases. Even if wires become perceptibly warmed by the ordinary current, it is a proof that they are too small for the work they have to do and that they ought to be replaced by larger wires".

I am sure all delegates to this conference will heartily endorse the sentiments expressed in the note but it is also an interesting fact that even in the first IEE Wiring regulations a major consideration was the thermal protection of circuit conductors, which, as will be discussed later, has always been, and still is a very important design parameter for the low voltage fuse.

The time scale of 1919 to 1991 given in the title of this paper covers a period from the first edition of the British Standard BS88 'Low-voltage fuses' to the present day.

Table 1 is a summary of the development of this standard from 1919 to the present time and it produces some interesting information on such subjects as :

Breaking capacity  
Temperature rise  
Minimum fusing current

What this summary does not reflect is the challenges which continuously arose during this period as electrical distribution grew and new applications emerged, testing the ingenuity of fuse designers, who as we know were proved equal to the task. Some examples of novel applications were fuses for warships, aircraft and rotating rectifiers. The shock, vibration and 'g' forces required to satisfy these applications are perhaps the most onerous to which any protective device is submitted and which few, if any, could equal.

The ability to interrupt modest over-currents on highly inductive dc circuits, (e.g., traction applications and aluminium pot-lines) required detailed investigation into the design parameters of fuses suitable for these duties. Here again, satisfactory designs emerged and are in widespread use. The protection of large capacitor banks, particularly series-parallel arrangements, posed particular protection problems in which the ability of the fuse to exhibit effective cut-off even on high discharge currents with a rate of rise of  $10^9$ A/sec enabled satisfactory protection to be obtained.

### Breaking Capacity

The summary of BS88 requirements (Table 1) shows that the cartridge fuse (or HBC fuse), first included in the 1937 edition, was only tested at  $I_1$  (maximum prospective current).

These requirements, both for ac and dc, have grown steadily more searching and more severe as knowledge of the various onerous combinations of voltage, current, and power factor (or time constant) emerged, until, with the present edition which reflects IEC 269, a very comprehensive and very reliable test series is specified which is adequate for the most onerous application requirements.

### Let through current and $I^2t$

Breaking capacity alone, however, is not sufficient in modern installations: limitation of peak current and let through  $I^2t$  is essential for the protection of other components of the electrical circuit, particularly as they become more compact and efficient. The two outstanding examples of associated equipment which require precise protection are semi-conductor devices and the modern compact motor starter.

TABLE 1 Summary of requirements for fuses to BS88, showing how the standard has evolved between 1919 and 1991

Date	Title	Scope	Breaking Capacity	Temperature Rise	Minimum Fusing Current	Dimensions	Other Requirements
1919	Electric Cut-Outs for Low Pressure Type 'O'	Semi-Enclosed Fuses up to 100A	DC Test with no voltage or prospective current specified	None Specified	$2I_n$	Overall Dimensions	None Specified
1931	Electric Cut-Outs Type 'O'	As 1919 Edition	Various prospective currents up to 6500A DC at 260V	Fuse Contact - 60°C Terminal - 28°C	$1.9I_n$	None Specified	None Specified
1937	Electric Fuses up to 80A and 250V to Earth	Semi-Enclosed and Cartridge Fuses up to 800A and 400V	Test at 440V AC 33 kA or 250V AC 16kA, 500A 0.3PF also refers to DC testing at 250V. Recovery voltage 95% of test voltage. Tested in metal enclosure connected to earth via fine wire fuse.	Fuse Contact - 60°C Terminal - 35°C	1.4In for overload and SC protection. Higher values for SC protection only.	None Specified	Shrouding of Contacts Specified
1939	As 1937 Edition	As 1937 Edition	As 1937 but PF graded to duty and time constants specified for DC.	As 1937 Edition	As 1937 Edition	None Specified	As 1937 Edition
1947	Electric fuses for Low and Medium Voltage	Semi-Enclosed and Cartridge Fuses up to 1200A at 600V AC and 460V DC	As 1939 but with introduction of Test Duty 2 and point on-wave closure	Fuse Contacts - 55°C Fixed Terminals - 46°C	Fusing Factor Class P = $1.25 I_n$ Class Q = $1.75 I_n$ Class R = $1.75 I_n$	None Specified	Arc Voltage limit introduced. Discrimination defined.
1952	Electric Fuses for Circuits of Voltage Ratings up to 660V	As 1947 Edition	As 1947 Edition	Fuse Contacts - 55°C Fixed Terminals: Up to 60A - 40°C Above 60A - 46°C	As 1947 Edition	Dimensions Of cartridge fuses included. Reference allocated to dimensions.	Test for determining time current characteristics introduced.
1967	Part 1 : Cartridge Fuses of Voltage Ratings up to 660 V Part 2 : Covers Fuse Holders	Cartridge Fuses up to 1200A 660V AC and 500V DC	As 1947 but prospective current increased to 80kA	Tested in Test Rig Additional Temperature Rise - 30°C	Class P = $1.25 I_n$ Class Q <sub>1</sub> = $1.5 I_n$ Class Q <sub>2</sub> = $1.75 I_n$ Class R = $2.5 I_n$	As 1952 Edition	1st described
1975	Cartridge Fuses for Voltages up to and including 1000V AC 1500V DC. Part 1 : General Requirements Part 2 : Supplementary Requirements for Fuses of Standard Dimensions for Industrial Purposes	Cartridge Fuses up to 1250A 1000V AC and 1500V DC	Tests aligned with IEC 269 I <sub>1</sub> , I <sub>2</sub> , I <sub>3</sub> & I <sub>4</sub> for AC & DC Arcing Angle specified	As 1967 Edition	Class P and Q <sub>1</sub> Also I <sub>1</sub> = $1.6 I_n$ I <sub>2</sub> = $1.2 I_n$	As 1952 Edition	Aligned with IEC269 - 1968
1988	As 1975 Edition	As 1975 Edition	As 1975 Edition	As 1967 Edition	Fusing factors removed I <sub>1</sub> = $1.6 I_n$ I <sub>2</sub> = $1.25 I_n$	As 1952 Edition	Aligned with IEC 269-1986

Perhaps the most significant development during the period under review was the emergence of semi-conductor fuses for the protection of semi-conductor devices with their ever increasing capability and application. The parallel evolution of suitable fuses for the protection of these devices is one of the great success stories and the fuse industry can claim to be a major contributor to the continuing development of the application of solid state devices.

Papers included in this conference reflect the continuing development work on this subject.

The other example, the protection of the modern compact motor starter, is of more recent origin. With the advent of these designs of starters, the question of their proper protection in electrical installations has arisen, mainly due to the need to comply with the requirements of the IEC Wiring Regulations and rapidly increasing demands for safety in electrical installations in many countries (exemplified in UK by the introduction of the "Electricity at Work Regulations - 1989" which is a mandatory document).

The fuse is undoubtedly the best means of providing the most economical and efficient means of protection to motor starters. This fact is widely recognised and the efforts of the Low-Voltage Fuse Committee IEC SC32B/WG8 to determine internationally agreed parameters for let-through current and  $I^2t$  for fuses for such applications is to be commended. When this work is complete it will add to the IEC fuse standard limiting values of  $I^2t$  and  $I_p$  for L.V. fuses. This will improve the standard significantly and greatly assist the world-wide application of fuses to motor circuits, emphasising their superiority over other forms of protection.

#### Time current characteristics

Another significant achievement of IEC SC32B is the agreement reached on standardised time current characteristics for gG fuses in IEC269. This, coupled with the finalised agreements of  $I^2t$  and  $I_p$ , will result in complete electrical interchangeability of fuses complying with IEC 269. The benefits of this achievement to the Fuse Industry are very significant, and it is up to the industry to exploit this achievement. For example, the 16th Edition of the IEE Wiring Regulations (which aligns with the IEC Wiring Regulations) includes one set of characteristics for fuses to BS88 (IEC 269-2-2) and five sets of characteristics for MCB's. The five sets of characteristics result from a combination of the types 1, 2 and 3 characteristics of MCB's to BS 3871:1965 and types B and C characteristics of IEC 898 which are now included in a revision to BS3871.

A table of values of  $Z_s$  (earth loop impedance) for disconnecting times of 0.1, 0.2, 0.4 and 5 seconds is given for each type of MCB compared with one Table of  $Z_s$  values for fuses to BS88:Part 2 and Part 6 (Part 6 fuses are the compact types submitted to IEC 32B for inclusion in IEC269).

Therefore the simplicity of fuse application and interchangeability compares very favourably with the very complicated problem of interchanging MCB's. In fact, it is true to say that despite the great effort which the MCB Industry has made towards dimensional standardisation, the proliferation of time current characteristics, coupled with the other design variations, such as position of arc chutes etc, makes a nonsense of dimensional interchangeability of these devices. This must be to the advantage of the fuse.

#### Overload Protection

Perhaps the most controversial problem for the modern fuse concerns the overload protection of cables, one which was mentioned in the first edition of IEE Wiring Regulations. This problem is more theoretical than practical because there is no record to suggest that the modern low-voltage fuse properly applied does not provide adequate overload protection to cables. This is particularly true of installations complying with the IEC Wiring Regulations which specify that circuits should be so designed that they are not subjected to repeated overloads of long duration.

A study of the changes to minimum fusing current in the various editions of BS88 shows violent fluctuations, particularly in the earlier editions, until after considerable debate the values of  $I_f = 1.6 I_n$  and  $I_{nf} = 1.25 I_n$  were agreed and included in IEC 269 and reflected in BS88:1988. Even with the agreed value of  $I_f$  there is a need for an additional requirement to the fuse standard, called the conventional cable overload test, to prove that the fuse will protect a PVC insulated cable on a current of  $1.45 I_z$  ( $I_z$  is the installation rating of cable) because this is a requirement of IEC364 'Wiring Regulations'. This agreement is now under further review in IECSC32B because the new MCB specification includes tripping currents of  $1.45 I_n$  and this has produced a demand from certain countries that the fuse standard should be changed so that  $I_f = 1.45 I_n$ .

This situation is further complicated by the fact that in IEC364 the rules of overload protection of cables still make reference to the characteristics of gI and gII fuses. It has already been agreed that these requirements must be reviewed in the light of the agreement now reached on gG fuses which replace the gI and gII types. The international cable overload protection problem is further compounded by the fact that the North American Code requires that overload protective devices shall have a fusing or tripping current of  $1.35 I_n$ .

Against this background there is a simplistic view by some national users that the fuse should have an  $I_f$  of  $1.45 I_n$  and various complicated test arrangements are being investigated in an attempt to achieve this objective and solve a 'non-problem'.

A review of the trends in cable insulation and overload protection requirements over the period covered in Table 1 produces some interesting information. Initially vulcanised rubber was used for low voltage cable insulation and the minimum fusing requirement was  $\approx 2 I_n$ . This was based upon the use of semi-enclosed fuses and is still valid today for the protection of PVC insulated cables by semi-enclosed fuses. Obviously the thermal capabilities of the cables were not fully utilised by this requirement.

With the introduction of the cartridge fuse and the achievement of lower minimum fusing currents without thermal penalties at rated current, the value was reduced to  $1.4 I_n$  but later increased to  $1.75 I_n$ , as higher temperature rises were permitted on terminals. It is not clear why such a large variation was permitted but what is certain is that with the introduction of PVC insulated cables the value acceptable for close protection of these cables was agreed as  $I_f = 1.5 I_n$ . Subsequent discussion in IEC32B resulted in agreement on the value of  $1.6 I_n$ . This was a compromise based on existing fuse characteristics in the various national systems. The IEC364 requirement of  $I_f = 1.45 I_z$  permits fuses with an  $I_f = 1.6 I_n$  to comply with the overload protection rules of IEC364 without the necessity of derating the cable. It utilises the fact that the  $I_z$  of a cable, is with few exceptions, larger than the  $I_n$  of the protective device. Therefore in practice the fuse with  $I_f$  of  $1.6 I_n$  is used on an equal basis to the MCB for the overload protection of PVC insulated cables.

If we review the North American requirement of  $I_f = 1.35 I_n$  it should be noted that there is an exception which permits the use of the next highest rating of fuse if the cable and fuse-rating do not coincide, thus effectively providing a much higher ratio between the  $I_f$  of the fuse and the installation current rating of the cable. I presented a paper on this subject to the 1984 International Fuse Conference in Trondheim. This fact is being taken into account in the IEC32B discussions aimed at including some types of North American fuses into IEC269.

A further change is now taking place in the insulation used for low voltage cables. There is an increasing trend towards the use of cables with thermo setting insulation (XLPE) in preference to PVC in general wiring practice. Certainly in UK there is an increasing use of this type of cable which can run at  $90^\circ\text{C}$  compared with  $70^\circ\text{C}$  for PVC. Because of its greater fire resistance and reduced toxicity compared with PVC, this cable is being supplied without economic penalties because cable manufacturers, like other product manufacturers, have to consider the safety aspects of installations and their legal liabilities under modern safety regulations. There is no doubt that the use of thermo-setting insulation considerably reduces fire and toxicity risks, and cables so insulated are in increasing demand in a number of countries.

The problem of its increasing use to LV equipment manufacturers will in future not lie with the question of overload protection, but with the possible derating of cable or equipment required to avoid overheating in normal service. This is because all LV equipment is rated on the basis of the use of  $70^\circ\text{C}$  PVC insulated cables and terminal temperature-rises at rated current are limited to  $70^\circ\text{C}$ . The popular use of cables with  $90^\circ\text{C}$  thermo-setting insulation will bring with it the need to consider either the derating of equipment or the decision that the extra thermal capability of the cable can only be used for higher ambient situations. There is already a warning in the IEC Wiring Regulations concerning the use of higher temperature cables with low voltage equipment.

This aspect should figure largely in the future discussions of IEC TC64 when reviewing the rules for overload protection of cables. These may well reveal that an  $I_f = 1.6 I_n$  is a satisfactory value for the future, and there is certainly no case for making a further intermediate change to an  $I_f = 1.45 I_n$  to satisfy the simplistic view mentioned earlier. I cannot stress too strongly the importance of an effective presence from the Fuse Industry in this most influential IEC TC64 Committee because their decisions will affect future practice. I hope that the various national delegates at this conference will bear this in mind.

#### Alternative Protective Devices

In addition to the technical challenges facing the fuse arising from new applications and new materials, there is the challenge of alternative devices for the more popular applications, mainly the MCB and MCCB. There is no doubt that the MCB is the most popular device in new domestic installations because it is more user friendly than the fuse, and the modern current limiting MCB can quite easily cope with the fairly simple requirements of most domestic installations. In a number of countries, certainly in UK, it has apparent advantage over the semi-enclosed fuse which it is replacing. The increasing demand for residual current protection against electric shock is also more readily met with an MCB/ RCD package than with a fuse/RCD package.

There is now an increasing use of MCB's in industrial applications but in this area there are many pitfalls for the MCB. Inadequate breaking capacity and the inability to provide proper protection to motor circuits are examples. The first problem can and is dealt with by proper co-ordination with the back-up fuse. This is another application problem which should be thoroughly investigated. The second can only be solved by accepting damage to the starter on certain faults and the use of a cable of the same current rating as the MCB, which is a considerable economic disadvantage.

If the Fuse Industry is to fight back against these threats from alternative devices it must speak out more forcefully about the benefits of fuses.

The one thing that the MCB Industry has done very effectively is to advertise its products: this cannot be said of the Fuse Industry. As electrical installation practice becomes more precise and safety rules are more rigorously enforced, the advantages of fuses should weigh more heavily with the installers and users. For example :

1. Full electrical and physical interchangeability with fuses of any make complying with IEC269 and a given set of dimensions.
2. Simplified planning of discrimination and co-ordination with final decision on fuse dimensions made at a later date.
3. Unequalled limitation of damage at seat of fault. Now a very important consideration from the viewpoint of operator safety.
4. Discrimination with a ratio as low as 1.6:1 between major and minor fuse ratings.

With regard to 1 and 2, as stated earlier the MCB cannot be readily interchanged electrically because of the variety of characteristics available and the various forms of arc dispersion used in the standardised dimensional package and the user is effectively tied to one make of MCB.

With regard to 3, this is of great importance even within the breaking capacity of MCB's but absolutely essential in situations of high fault level.

With regard to 4, no mechanical tripping device can match this performance and it can produce many economies in circuit lay-out.

In the domestic application, fuse isolators dimensionally interchangeable with MCB's are emerging and becoming popular for those circuits where the MCB cannot provide the same reliability as the fuse. In the industrial sector the emergence of compact ranges of fuses for the 240/415V applications has offset one of the criticisms of low voltage industrial fuses, i.e., the relatively large dimensions compared with MCB's. Fuse combination units utilising these compact fuses, having dimensions comparable with MCCB's, are already on the market and increasing in popularity (see Figs 1 & 2). This trend is happening with all dimensional systems of fuses.

#### The Future

There is no doubt that, despite the improvements in the technology of low-voltage fuses, the threat from the MCB and MCCB in popular applications is serious. The work in IEC32B to standardise the characteristics of fuses has made fuse application much easier. This point must be made forcefully to the Installer and User.

Thought must continue to be given to ways of making the fuse more 'user friendly': for example, by ensuring safe and simple interchange of fuse-links by providing adequate shrouding of live parts. It is no longer acceptable to provide less shrouding on fuses for use by authorised persons than that provided on fuses for use by unskilled persons.

Modern safety legislation is producing an increasing demand for a high degree of safety to Operators in all situations.

One area of application which requires further exploration is the combination of an automatic overload tripping device with the fuse to combine the benefits of both the fuse and circuit-breaker. This is not a new idea with MCCB's but the problems of protecting modern motor circuits with MCCB's gives a new impetus to this arrangement and it could also apply to Fuse/MCB combinations. The economic benefits of compact fuses and fusegear is the subject of some papers at this conference and perhaps this theme can be developed further.

I have concentrated on low-voltage fuses with particular emphasis on practical aspects of applications, past, present and future. A similar picture could be presented on high-voltage fuses, where technical improvements are emerging at an impressive pace. The same can be said about the miniature fuse developments. All of these subjects will be discussed at length during this conference, from which we will gain further information and incentive to improve the technical excellence of the fuse and also improve appeal to the user.

Considerable steps along these twin routes have already been observed since the first conference and the subject matter of this conference indicates that progress will continue. It is however essential to recognise the competition faced in the international electrical industry from other protective devices and we must ensure that the achievements which have and will be made are well publicised so that fuses and fusegear will continue to enjoy the popularity they have had in the past. I look forward, as you all do, to the presentations and discussions which will take place during this conference. I am sure they will be both informative and challenging and hopefully will further promote the benefits of the fuse which, as long ago as 1882, was described as being "The Very Essence of Safety".

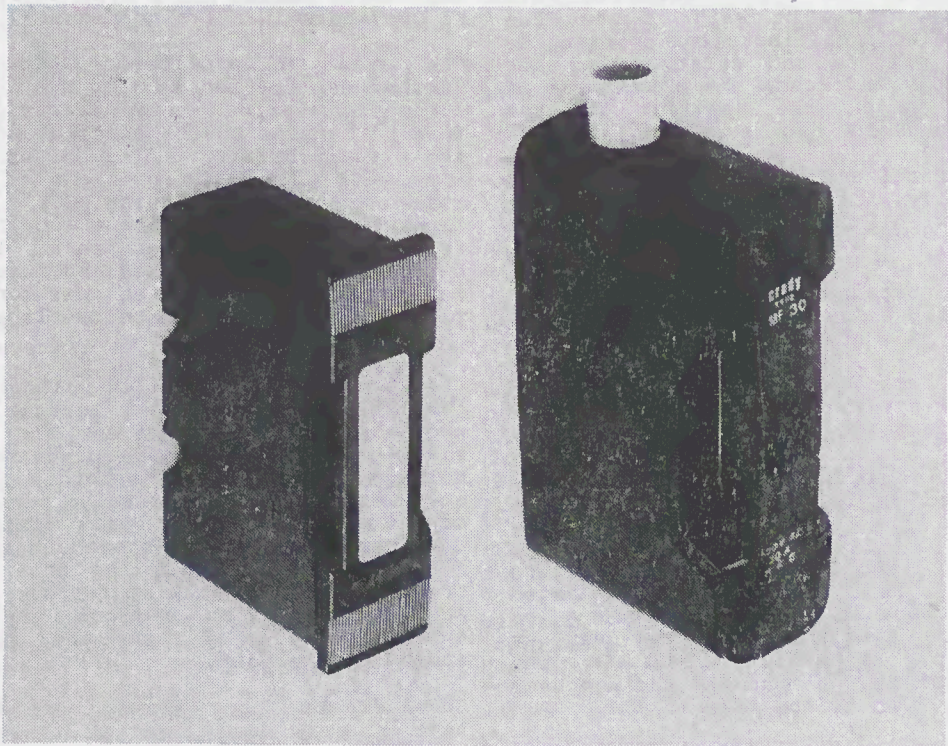


Fig.1 Comparison of 32A compact fuse (BS88:Pt 6) with 32A conventional fuse (BS88:Pt 2)

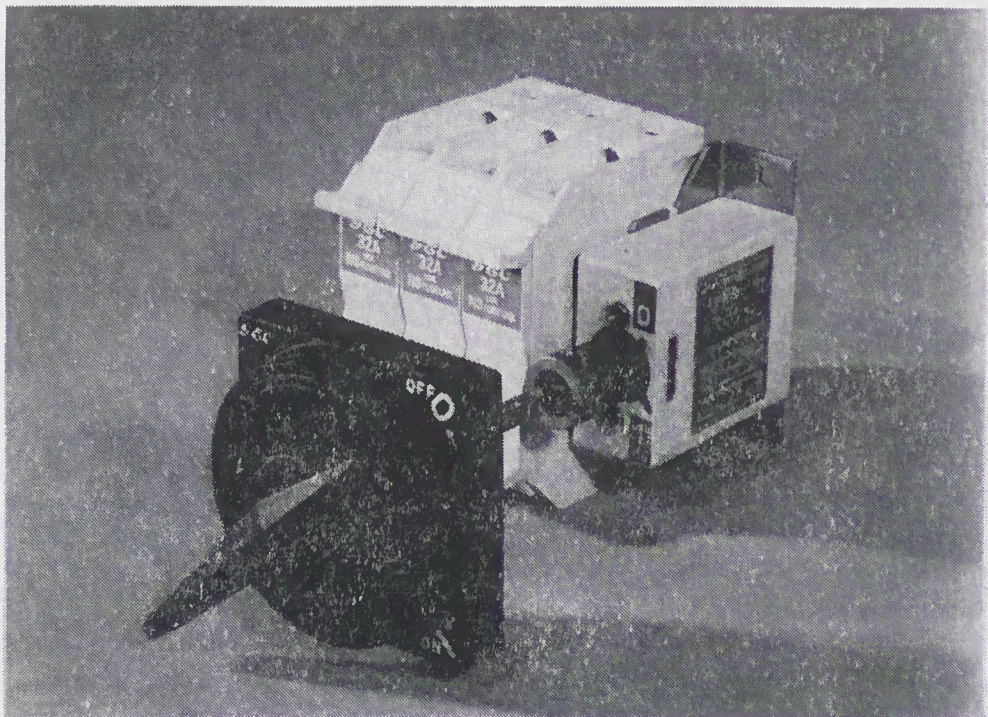


Fig.2 Compact 32A fuse combination unit with fuse-links to BS88:Pt 6

**Session 1**  
**FUSE DESIGN I**



# THERMAL PROCESSES IN SF<sub>6</sub> - FILLED FUSES BELOW THE MINIMUM MELTING CURRENT

D. Brechtken, D. König  
Technical University Darmstadt  
High Voltage Laboratory  
Germany

B. Müller  
Fa. Jean Müller GmbH  
Eltille  
Germany

## Summary

In conventional sand-filled fuses, heat transfer is predominantly determined by conduction. However, in case of gas-filled fuses, the influence of convection and radiation must be taken into account.

The investigations described aim at calculating the temperature distribution in the fuse and thus determine the minimum melting current using an approximation procedure. The calculated results are compared with measurements on test samples. The comparison shows that the calculation model applied is a suitable one.

## 1. Introduction

Conventional high voltage fuses in general have a zone of an uncertain arc quenching capability and by this show an uncertain switching performance in the low overcurrent region. A fuse filled with SF<sub>6</sub> overcomes this disadvantage by a quick lengthening of the arc happens and thus a fast recovery of the dielectric strength after current zero can be achieved [1]. In that case extinguishing of the arc can be reached and all currents above the minimum melting current can be switched off reliably.

One of the major remaining problems is the exact determination of the minimum melting current, which leads to disintegration of the fuse wire. Therefore, a study might be useful, which aims at its determination by calculating of the relevant temperature field. In order to check the accuracy of these computations, the calculated temperatures are to be compared with measured ones.

## 2. Minimum Melting Current I<sub>mm</sub>

During high short-circuit currents heat transfer phenomena are assumed to be negligible. The expected melting time of the fuse wire can be calculated for this adiabatic case from [2]:

$$\int_0^{t_m} J^2 dt = const. \quad (1)$$

where,  $t_m$  - melting time  
 $J$  - current density  
 $t$  - time

For each fuse exists a current level, at which melting would theoretically commence after an infinite long time. This current, which is important for theoretical considerations, is called the minimum melting current I<sub>mm</sub>. For currents above the minimum melting current I<sub>mm</sub>, equ.(1) can be modified to

$$(I - I_{mm})^2 * t = a \quad (2)$$

where,  $a$  characterizes the stored heat energy Q<sub>wire</sub> in the fuse wire. If heat flow from the fuse wire in axial and radial direction becomes more important, which is the case for decreasing currents, one more term must be added for the stored energy in the surroundings Q<sub>sur</sub>.

Q<sub>sur</sub> may be assumed according to the empirical equation

$$Q_{sur} = b * t^{1/3} \quad (3)$$

in which  $b$  is a constant.

Thus, equ. (2) may be expanded by the term given by equ.(3) to

$$(I - I_{mm})^2 * t = a + b * t^{1/3} \quad (4)$$

In principle, the unknown parameters  $a$ ,  $b$  and I<sub>mm</sub> can be evaluated from the time-current characteristic by at least three independent experiments [2]. However, the evaluation of the minimum melting current I<sub>mm</sub> as defined above is associated with a fairly high uncertainty.

## 3. Test Arrangement

Fig. 1 shows the subject of investigations in horizontal position as used for measurements and calculations. The fuse wire (1) is placed concentric in the insulating tube (4), which is closed by metal end caps (3) and filled with SF<sub>6</sub>.

Due to the movement of the gas, upper parts of the model are at other temperatures than lower parts at the same distance of the wire. This was confirmed by measurements.

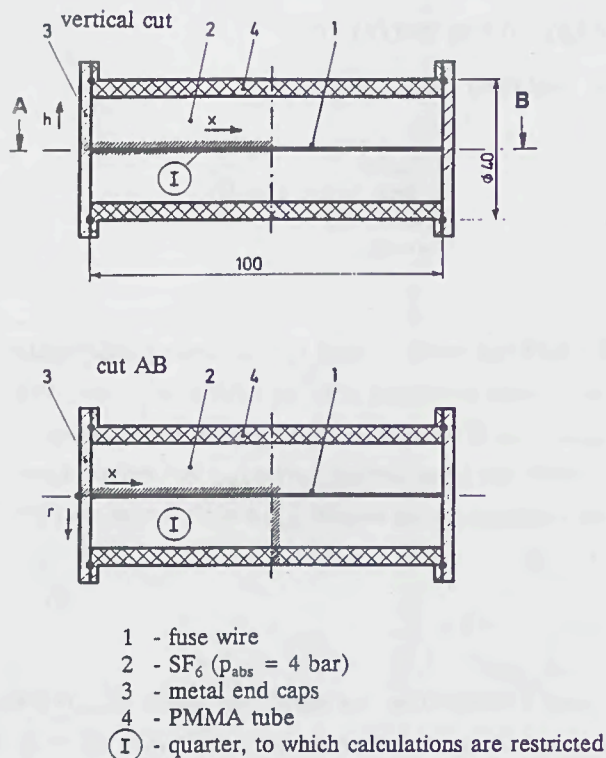


Fig. 1: Test Arrangement

Because these differences of temperature between upper and lower parts are smaller than 60 °C, it is useful to restrict measurements and calculations to the plain section with the height  $h=0$ , marked by "I" in Fig. 1. The influence of the thermo couples on the gas flow is neglected. Thus axial and radial symmetry is assumed and further considerations are restricted to the quarter marked by "I".

The test circuit and the measuring equipment is shown in Fig. 2. The specimen can be stressed by currents up to 60 A. The fuse wire and its surroundings is heated up by the current. The actual temperatures in the surroundings are measured with Ni-NiCr thermo couples, which are usable up to 1000 °C. Table 1 gives their axial and radial horizontal positions.

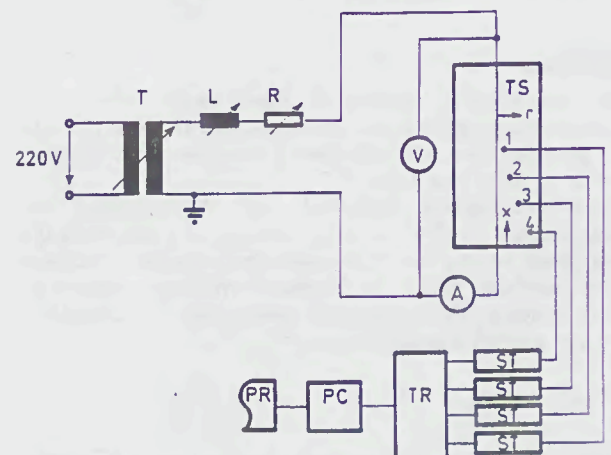
Table 1: Positions of the thermo couples in the test specimen

number of thermo couples	axial position	radial position
	x	r
1	42 mm	2 mm
2	22 mm	3 mm
3	41 mm	6 mm
4	22 mm	14 mm

The signals of the thermo couples are converted in a special

signal transformer (ST) (Typ AD594, Manufacturer: Analog Devices) to a voltage proportional to the temperature. This voltage is led to a transient recorder (TR). The personal computer (PC) stores the measuring results for further usage.

It seems to be unfavourable to measure the temperature of



- T - transformer
- L - variable inductance
- R - variable resistance
- TS - test specimen
- TR - transient recorder
- PC - personal computer
- PR - printer
- 1,2,3,4 - number of the thermo couples (tc)
- x,r - position of the thermo couples (tc)
- ST - signal transformer

Fig. 2: Test circuit and Measuring Arrangement

the fuse wire with the help of a thermo couple, since it could cause an undesirable cooling of the relevant wire section. Therefore a different way to evaluate the wire temperature was used. Since with increasing temperature of the fuse wire the resistance and consequently the voltage drop at the fuse increases, too, this voltage drop is a measure for the wire temperature, provided that the current is kept constant. The measuring accuracy of the voltage drop is less than  $\pm 5$  mV.

#### 4. Calculation Model

Heat is transferred by three basic modes: conduction, convection and radiation. The physical mechanisms and laws of heat transfer are different for each of these three modes. The influence of each mode on heat transfer depends on the physical properties of the materials, the geometry and the temperature gradients.

Heat transfer can be described with the help of a system of differential equations. But, for most of the heat transfer

problems, which are of practical importance, an analytical solution does not exist [3,4]. Therefore it is necessary to find other possibilities for solution. One of these could be the theory of geometric similarity [5], from which the relevant thermal processes can be deduced as depending on "dimensionless numbers". If these numbers are known, a known solution may be transferred to similar problems.

The desired "dimensionless numbers" are defined as follows:

$$\text{Grashof number} \quad Gr = \beta * \frac{g * l^3}{\nu^2} * \Delta \vartheta \quad (5)$$

$$\text{Prandtl number} \quad Pr = \frac{\eta * c_p}{\lambda} \quad (6)$$

$$\text{Nusselt number} \quad Nu = \alpha * \frac{l}{\lambda} \quad (7)$$

where is

- $\beta$  = coefficient of thermal expansion
- $g$  = acceleration due to gravity
- $l$  = significant length
- $\nu$  = kinematic viscosity
- $\vartheta$  = temperature
- $\eta$  = dynamic viscosity
- $c_p$  = specific heat at constant pressure
- $\lambda$  = thermal conductivity
- $\alpha$  = heat transfer coefficient

The **Grashof number** can be interpreted as the ratio of fluid flow inertia forces to viscous forces [6].

The **Prandtl number** compares the kinematic viscosity for pulse transport by friction with the energy transport by conduction [4].

The **Nusselt number** can be interpreted physically as the ratio of the temperature gradient in the fluid in contact with the surface to a reference temperature gradient [6].

However, in the following  $Nu$  was not used, since  $\alpha$  is unknown for this relevant problem.

With the help of these numbers, the different mechanisms of leading away the heat generated in the fuse wire can be investigated.

The area of the quarter section of the fuse model is subdivided in segments with an area of 1 mm<sup>2</sup>. The generated power per increment of the fuse wire  $dP$  is

$$dP = I^2 * \rho(\vartheta) * \frac{dx}{A} \quad (8)$$

where

- $I$  - current
- $\rho$  - specific resistance
- $\vartheta$  - temperature
- $dx$  - incremental length of the wire
- $A$  - area of cross section of the wire

For all currents below the minimum melting current  $I_{mm}$ , this power has to be carried off to the surroundings. Thus the considerations can be restricted to the steady state [7].

In the gas, heat is transferred in radial direction by conduction, convection and radiation. Due to the cylindrical form of the fuse, the heat transported by conduction in radial direction  $Q_{lr}$  can be written as:

$$Q_{lr} = \frac{2\pi * \lambda_{SF_6} * l}{\ln \frac{r_a}{r_i}} * \Delta \vartheta \quad (9)$$

- $\lambda_{SF_6}$  - thermal conductivity of SF<sub>6</sub>
- $l$  - length of the fuse wire
- $r_a$  - outside radius of the incremental layer
- $r_i$  - inner radius of the incremental layer
- $\Delta \vartheta$  - temperature difference between  $r_a$  and  $r_i$

The influence of convection  $Q_c$  depends on the type of flow. In the vicinity of the wire, a boundary layer exists with a laminar flow. Inside this boundary layer, no heat transfer by convection, but only by conduction, exists. Outside this section, the influence of convection can be taken into account by an "effective" thermal conductivity  $\lambda_{eff}$ . Since  $\lambda_{eff}$  is a function of the product of the Grashof and the Prandtl number, it can be written [3]:

$$10^0 < Gr * Pr < 10^3$$

$$\frac{\lambda_{eff}}{\lambda} = 1 \quad (10)$$

$$10^3 < Gr * Pr < 10^6$$

$$\frac{\lambda_{eff}}{\lambda} = 0,105 * (Gr * Pr)^{0,3} \quad (11)$$

$$10^6 < Gr * Pr < 10^{10}$$

$$\frac{\lambda_{eff}}{\lambda} = 0,4 * (Gr * Pr)^{0,2} \quad (12)$$

Equ. (12) signifies that the total heat transfer is considered as resulting only from conduction. The decrease of  $\lambda_{eff}$  for large values of the argument ( $Gr \cdot Pr$ ) in equ. (12) can be explained with reciprocal disturbances between streams of rising and falling gas.

Using the idea that an "effective" thermal conductivity  $\lambda_{eff}$  exists, which takes into account convection effects, thermal resistances can be established to figure the influence of convection. Thus, the relevant heat  $Q_c$  can be calculated by replacing  $\lambda_{SF6}$  in equ. (9) by the term  $(\lambda_{eff} - \lambda_{SF6})$ . Additional to conduction and convection, heat is transported by radiation  $Q_{rad}$  as given by [3]:

$$Q_{rad} = \epsilon_{Ag}(\vartheta) * A * C * \left\{ \left( \frac{\vartheta_{Ag}}{100} \right)^4 - \left( \frac{\vartheta_W}{100} \right)^4 \right\} \quad (13)$$

$\epsilon_{Ag}$  - emission coefficient of silver  
 $A$  - surface area of the fuse wire  
 $C$  - radiation number  
 $\vartheta_{Ag}$  - temperature of the fuse wire  
 $\vartheta_W$  - temperature of the wall

In solid materials, such as fuse wire and fuse wall, heat is transferred only by conduction. Heat is transferred from the outer surface of the fuse to the surroundings by conduction, convection and radiation.

Heat is transferred in axial direction only by conduction  $Q_{ia}$ .

$$Q_{ia} = \lambda_m * \frac{\pi * (r_a^2 - r_i^2)}{\Delta l} * \Delta \vartheta \quad (14)$$

$\lambda_m$  - thermal conductivity of the medium  
 $\Delta l$  - incremental length  
 $r_a$  - outside radius of the incremental layer  
 $r_i$  - inner radius of the incremental layer  
 $\Delta \vartheta$  - difference of temperature along  $\Delta l$

Based on the described considerations, a thermal equivalent circuit was developed. Thermal resistances are calculated taking into account the different relevant heat transfer mechanisms. This network has thermal current sources in each increment which correspond to the heat generated. Calculation of the temperature is reduced to a calculation of the network's potentials.

From these potentials, the temperatures in the fuse are known. Knowing the melting temperature of the fuse wire, the minimum melting current is calculatable. The knowledge of the temperatures and the resistances enable to analyse the contribution of the different mechanisms of heat transfer.

## 5. Results

As shown by Fig. 3 the temperatures at different test points, as given in Table 1, do not further increase after a time of 90 minutes which signifies that the "steady state" is reached. In that state the measured values can be compared

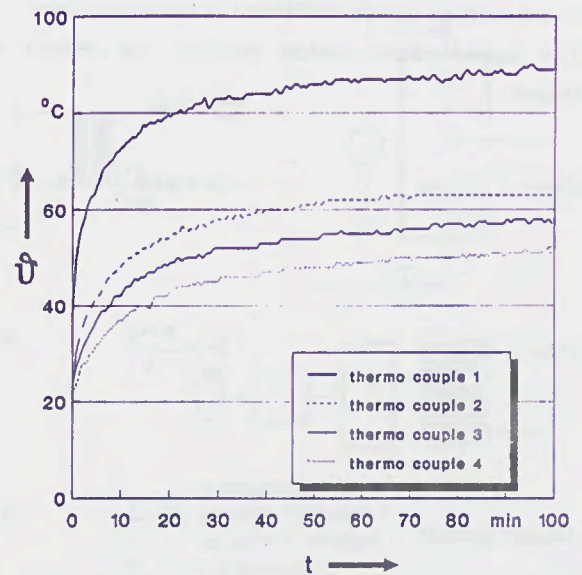
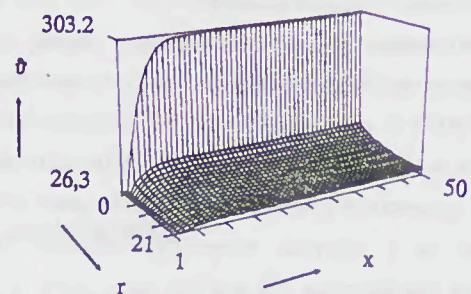


Fig. 3: Measured temperatures as a function of time at the positions of the thermo couples number 1-4  
 Parameters:  $I = 14.5 \text{ A}$   
 fuse wire diameter  $0.4 \text{ mm}$

with those, which we calculated. Fig. 4 shows a calculated temperature distribution over the quarter of the specimen as marked in Fig. 1. Noticeable are the very strong temperature gradients in radial direction and in axial direction close to the caps. At 10 mm from the caps the temperature of the



$x$  - control variable for the axial position  
 $r$  - control variable for the radial position  
 $\vartheta$  - temperature

Fig. 4: Calculated temperature distribution in a quarter of the cross section of the test body.

Parameters:  $I = 11.04 \text{ A}$   
 fuse wire diameter  $0.35 \text{ mm}$

fuse wire has reached 95 % of the maximum value (303 °C). The temperature in the SF<sub>6</sub>-atmosphere is in the middle relatively low (about 50 °C).

For the same conditions the temperatures were measured with the equipment according to Fig. 2. Fig. 5 shows the comparison between the calculated and the measured values in the four positions of the thermo couples. The deviations are smaller than 20%. This might be due to the applied simplifications.

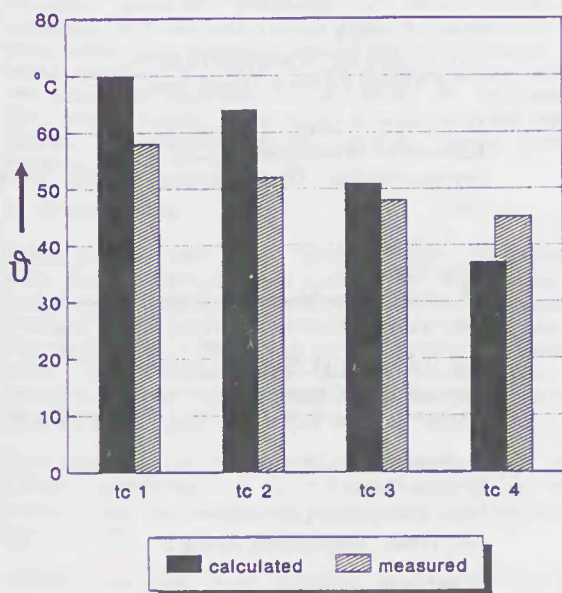


Fig. 5: Comparison between measured and calculated temperatures at the positions of the thermo couples (tc).

Parameters:  $I = 11.04 \text{ A}$   
fuse wire diameter 0.35 mm

Fig. 6 shows a comparison of the measured voltage across the fuse and the calculated voltage drop calculated with the described model. These voltages differ essentially.

By dividing the voltage difference by the relevant current, a constant contact resistance was obtained, which was 54 mΩ in the case of Fig. 6. This resistance is given by the clip positions of the wire. Considering these contact voltage drops, the deviations between calculated and measured voltage are smaller than 60 mV, which is a fairly good agreement.

Furthermore, Fig. 6 shows the calculated maximum fuse wire temperature. At 960 °C [8], the melting temperature is reached. The corresponding current value is 15.8 A, while the minimum melting current  $I_{mm}$  as determined in chapter 2 is 15.0 A. Measured and calculated values of the minimum melting current  $I_{mm}$  are in a good agreement.

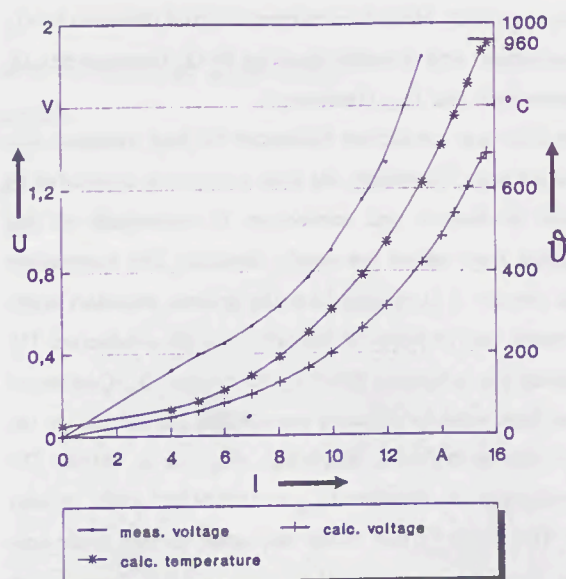


Fig. 6: Comparison between calculated maximum fuse wire temperature, calculated and measured voltage drop across the fuse wire as a function of current for a fuse wire diameter of 0.32 mm.

The different mechanisms of transporting the heat from one wire element to the neighbouring is investigated. The wire diameter here is 0.32 mm and the current 15.6 A. Fig. 7

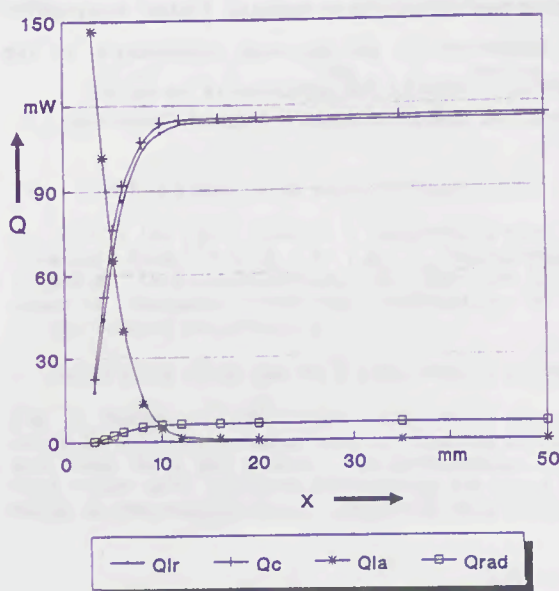


Fig. 7: Transported heat portions per wire increment by different mechanisms such as radial conduction  $Q_{lr}$ , convection  $Q_c$ , axial conduction  $Q_{la}$  and radiation  $Q_{rad}$ .  
Parameters:  $I = 15.6 \text{ A}$   
fuse wire diameter 0.32 A

gives the result. Heat is transferred in axial direction by  $Q_{ia}$  (conduction) and in radial direction by  $Q_{ir}$  (conduction),  $Q_c$  (convection) and  $Q_{rad}$  (radiation).

The axial heat conduction influences the heat transport only near the caps. Thereafter, the heat transport is dominated by radial conduction and convection. Coincidentally in this example their values are nearly identical. The surprisingly high portion of  $Q_{ir}$  results from the laminar boundary layer, in which heat transfer is possible only by conduction [3]. Outside this boundary layer,  $Q_c$  dominates  $Q_{ir}$ . Combining these conditions by applying two parallel resistances for the first segment in the  $SF_6$ -gas, a high value for  $Q_{ir}$  results. The contribution of radiation  $Q_{rad}$  to the heat transfer is only 5%. This might be due to the very small surface of the fuse wire. Thus, the important mechanisms in radial direction are conduction and convection.

#### 6. Conclusions

Approximate calculations of the heat transferred from the fuse wire to the surroundings with help of a model as described in chapter 4 enable to calculate the temperature distribution in a fuse filled with  $SF_6$ .

Based on the calculated wire temperatures, the minimum melting current can be determined. Furthermore the heat transfer mechanisms can be analysed. Further investigation are under way to get improved informations on the permissible limits for the application of the model.

#### 7. References

- [1] J. Trott  
Untersuchungen zur Lichtbogenlöschung in Hochspannungs-Hybridsicherungen  
Dissertation TH Darmstadt 1988
- [2] H.H. Johann  
Eine Formel für die Strom-Zeit-Kennlinie von Schmelzsicherungen und ihre Anwendung zur Ermittlung von Kennwerten.  
Elektrotechnische Zeitschrift 58. Jahrgang, Heft 25, 24.6.1937, S. 684-686.
- [3] M.A. Michejew  
Grundlagen der Wärmeübertragung  
VEB Verlag Technik, Berlin 1964.
- [4] G. P. Merker (Hrsg.: U. Grigull)  
Konvektive Wärmeübertragung  
Springer-Verlag Berlin/Heidelberg/New York 1987.
- [5] A. J. Chapman  
Heat Transfer  
2<sup>nd</sup> edition, The Macmillan Company,  
New York 1967.
- [6] J. P. Todd and H. B. Ellis  
Applied Heat Transfer  
Harper & Row, Publishers, Inc., New York 1982.
- [7] A. Wright & P. Newbery  
Electric Fuses  
Peter Peregrinus Ltd., 1982  
IEE Power Engineering Series 2
- [8] Rüdtenberg  
Elektrische Schaltvorgänge  
5. überarbeitete Auflage Heidelberg / New York  
Springer Verlag 1974

STEADY-STATE CURRENT-SHARING IN FUSES WITH ASYMMETRICAL ARRANGEMENTS  
OF PARALLEL ELEMENTS

R. Wilkins  
Consultant  
Heswall, UK

Summary

The paper is concerned with calculation of the steady-state temperature distribution in fuses with multiple parallel elements, in cases where the elements have unequal radial thermal impedances. In such cases some elements run hotter than others, and their share of the total current diminishes, due to the positive temperature coefficient of resistance. The paper gives methods of calculating the radial thermal resistances and the current share between elements.

1. Introduction

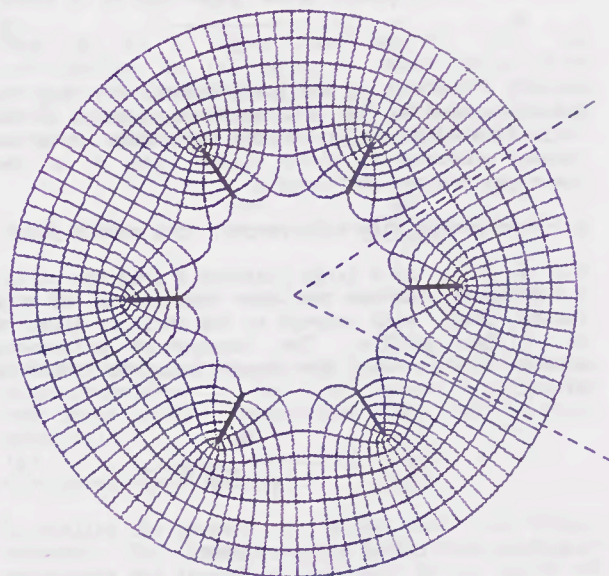
Calculation of the steady-state temperature distribution for fuses is useful for prediction of temperature rises and voltage drops under specified loading conditions, and determination of the minimum fusing current. For fuses with parallel elements, such calculations are usually based upon the assumption that the elements share the total current equally.

Most fuse designs have cylindrical symmetry, which allows reduction to a 2-dimensional (r,z) form, rather than the very complicated truly 3-dimensional form. [1,2].

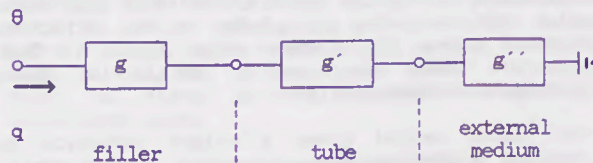
Current-carrying fuse elements lose heat firstly by axial conduction to the ends, and secondly by "radial" conduction through the filler and fuse body to the ambient. A further common assumption is to consider these two loss paths separately. This is equivalent to neglecting axial flow of heat in the filler.

This paper is principally concerned with calculation of the radial loss. Fig. 1 (a) shows the heat-flux lines and isothermals produced by six equal infinitely long strip sources of heat (computed by methods to be described later). At a relatively short distance from the strips, the isothermals become circular, and we can choose one of these to coincide with the inner diameter of the fuse tube, which permits calculation of the thermal resistance between the elements and the inside of the tube. Since the problem has cylindrical symmetry, heat flow from each element is restricted to an angle  $2\pi/n$  and so the equivalent thermal resistance model shown in Fig.1(b) can be used, for a typical element. [1,2].

However, for many practical fuse designs the thermal impedance differs from element to element, e.g. when they are arranged in rows, or when one layer of elements is enclosed within another. Elements in the middle of a group get hotter than the average. Heat generation in them is increased due to the temperature coefficient, but this is offset by a decrease in current in the hotter elements, due to their higher resistance. In this paper a method for calculating the radial thermal impedances for a general, asymmetric, arrangement of strips is given, together with an iterative procedure for determining the share of current between elements. Application to practical designs for fuses of finite length with notched elements is also discussed.



(a) isothermals and heat-flux lines



(b) equivalent thermal resistance model, per sector

Fig. 1 Heated strips with axial symmetry ( $n=6$ )

In Fig. 1 (b) the element temperature-rise is obtained from  $\theta = q.(g + g' + g'')$ . Calculation of  $g'$  and  $g''$  is straightforward [1]. The rest of this paper is concerned with the calculation of the filler thermal resistance  $g$ .

2. Temperature field due to a strip source of heat.

Fig. 2 shows an infinitely thin strip source of width  $2a$  emitting a total heat  $q$ , located at  $(0,0)$  and lying along the x-axis. The isothermals for this case are ellipses surrounding the strip [3], which is represented as an infinitely thin ellipse.

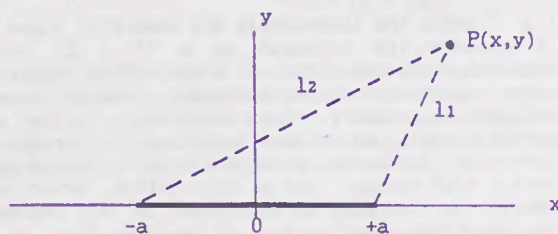


Fig. 2 Strip source of heat located at the origin.

The isothermals and the heat-flux lines correspond to constant values of the potential function  $\theta$  and the flux function  $\phi$  respectively in the inverse cosine transformation [3]

$$\theta + j\phi = \cos^{-1}(x + jy) \quad (1)$$

From (1) the potential at P with respect to the strip is easily obtained. The form used by Sato [4] is convenient, i.e.

$$\theta = -\frac{q}{2\pi k} \ln \frac{S + \sqrt{S^2 - a^2}}{a} \quad (2)$$

where  $S = (l_1 + l_2)/2$  and the distances  $l_1$  and  $l_2$  are as defined by Fig. 2.  $S$  may be thought of as the "effective distance" of P from the strip.  $k$  is the thermal conductivity of the filler, and  $q$  is the power emitted per unit length.

### 2.1 Temperature rise with respect to a remote point

For a point at a large distance  $R$  from the strip,  $S \approx R$  and  $S \gg a$ , so that the temperature of the remote point with respect to the strip is given by  $\theta_R = (1/2\pi k) \ln(2R/a)$ . The temperature difference between P(x,y) and the remote point is therefore given by

$$\theta_P = \frac{q}{2\pi k} \ln \frac{2R}{S + \sqrt{S^2 - a^2}} \quad (3)$$

### 2.2 Superposition of strip sources

For a number of sources an approximation to the total temperature rise at any point P can be obtained by adding the contributions from each strip using (3),  $S$  being calculated as the "effective distance" from P to each strip in turn. This procedure has been used to obtain the field distribution shown in Fig. 1.

The above method gives a slight variation in computed temperature across the width of each strip. For a given strip the temperature rise due to its own heat generation is constant across its width, but the field due to the other strips gives rise to a variation. If the strips were perfect thermal conductors there would be no such variation. To obtain the field in this case a true Green's function would need to be used [5], with a very great increase in the complexity of the calculations.

For fuse elements, which are good but not perfect thermal conductors, and which are thin, there will be a slight variation of temperature across the strip, such as can be seen in Fig. 1, so the solution obtained by superposition method used here may well be as accurate as a true Green's function solution.

### 3. Radial thermal resistance matrix

Fig. 3 shows the isothermals and heat-flux lines for 15 heated strips arranged as a (5 x 3) array, computed using the method of superposition described above. Although the arrangement does not possess cylindrical symmetry, the isothermals again soon become circular as we move away from the strips. The outermost isothermal shown deviates by less than 2% from a true circle, and so very little error will result in choosing an isothermal in this region to represent the inner surface of the fuse tube. In the case shown the heat emitted is the same for all strips. Note that the element in the centre is hotter than the others.

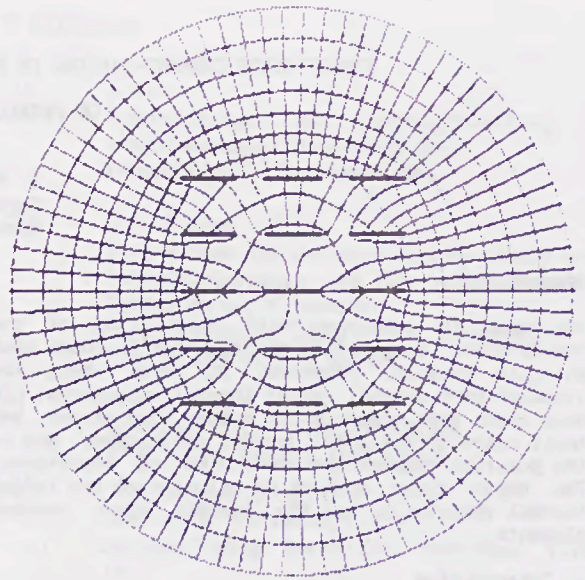


Fig. 3 Strips without cylindrical symmetry

Let us assume that the inner radius of the fuse tube is  $R$ . By superposition of potential contributions given by (3) we can obtain the temperature rise at any point with respect to  $R$ , but our main interest is in the temperature of the strips. These are given by :

$$\begin{aligned} \theta_1 &= g_{11}q_1 + g_{12}q_2 + \dots + g_{1n}q_n \\ &\cdot \\ &\cdot \\ \theta_i &= g_{i1}q_1 + \dots + g_{ij}q_j \dots + g_{in}q_n \\ &\cdot \\ &\cdot \\ \theta_n &= g_{n1}q_1 + g_{n2}q_2 + \dots + g_{nn}q_n \end{aligned}$$

or in matrix form,

$$[\theta] = [g][q] \quad (4)$$

where  $[\theta]$  is a vector of the strip temperature rises,  $[g]$  is an  $(n \times n)$  thermal resistance matrix, and  $[q]$  a vector of powers emitted from the strips.

The element  $g_{ij}$  of the thermal resistance matrix may be interpreted as the temperature rise produced at strip  $i$  due to unit power emitted from strip  $j$  with all other powers set to zero. Using (3) this is given by :

$$g_{ij} = \frac{1}{2\pi k} \ln \frac{2R}{S_{ij} + \sqrt{S_{ij}^2 - a^2}} \quad (5)$$

The diagonal elements of  $[g]$  are all equal to  $(1/2\pi k) \ln(2R/a)$ , but there is some ambiguity about the off-diagonal elements, depending upon the point on strip  $j$  for which  $S_{ij}$  is calculated - as already stated, use of the strip function gives rise to a variation in temperature across strip  $j$ . This can be resolved by calculating  $S_{ij}$  at selected points on strip  $j$ . This is repeated for  $S_{ji}$  and the geometric mean of all the distances is taken to be  $S_{ij} (= S_{ji})$ .

$[g]$  is then a symmetric matrix, and is easily assembled given a list of the coordinates of each strip and its inclination to the x-axis.

#### 4. Solution for strip temperatures

##### 4.1 Equal current sharing and zero temperature coefficient

Although this is not a realistic situation, it provides the starting point for analysis. If the strips have an electrical resistance  $r_0$  per unit length and share the total current  $I$  equally the power generation is the same for all elements, i.e.,

$$q_i = (I/n)^2 r_0 = Q = \text{constant, for all } i$$

From (4) the temperature rise of strip  $i$  is then

$$\theta_i = g_{i1}Q + g_{i2}Q + \dots + g_{in}Q$$

$$\text{or } \theta_i = g_i^* Q \quad (6)$$

$$\text{where } g_i^* = \sum_{j=1}^n g_{ij}$$

$g_i^*$  is the sum of row  $i$  of  $[g]$  and is the effective thermal resistance of strip  $i$ , a value which takes account of the self heating and the mutual heating. The situation can be represented by the thermal resistance model shown in Fig. 4.

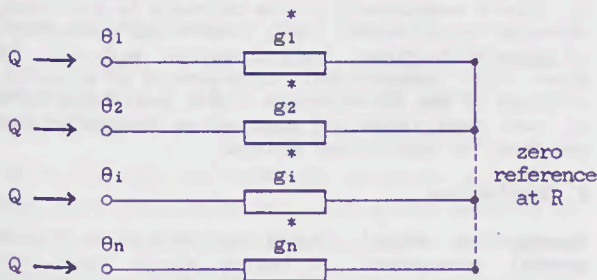


Fig. 4 Thermal resistance model for  $q = \text{constant}$

The average temperature-rise of the  $n$  strips is

$$\theta_{av} = \frac{1}{n} \sum_{i=1}^n \theta_i = \frac{1}{n} \sum_{i=1}^n g_i^* Q$$

$$\text{i.e. } \theta_{av} = g_{av} Q \quad (7)$$

where  $g_{av}$  is the average thermal resistance per strip, and is the average of the rowsums of  $[g]$ . The average strip temperature-rise can then be found from the very simple model shown in Fig. 5.



Fig. 5 Thermal resistance model for determining  $\theta_{av}$

The individual strip temperature-rises can be evaluated if  $\theta_{av}$  is known, by using (6) and (7), to give

$$\theta_i = \frac{g_i^*}{g_{av}} \theta_{av} \quad (8)$$

##### 4.2 Effect of temperature coefficient alone

If we assume for the moment that equal sharing of the current is maintained, but the strip temperature coefficient ( $\alpha$ ) is positive, the heat generation in the hotter strips will be enhanced, and the "spread" of temperatures between the strips will be increased. For strip  $i$ ,

$$q_i = (I/n)^2 r_0 (1 + \alpha\theta_i) = q_0 (1 + \alpha\theta_i)$$

where  $q_0$  is the "cold" strip power,  $(I/n)^2 r_0$ .

Thus  $[q]$  is a linear function of  $[\theta]$ , and substitution in (4) gives a relationship which requires the inversion of  $[g]$  to determine  $[\theta]$ . A good initial approximation to  $[\theta]$  can be obtained however, using the "average" model of Fig. 6.



Fig. 6 Approximate model for average temperature

Solving the thermal network of Fig. 6 the average temperature rise is  $\theta_{av} = q_0 / \{(1/g_{av}) - \alpha q_0\}$ . The individual strip temperatures can then be found using (8).

##### 4.3 Current-shift effect

In reality the current per strip does not remain constant. The hotter strips will have a higher resistance and therefore there will be a shift of current away from these strips to the cooler strips. This current-shift has an effect opposite to that described above due to the temperature-coefficient alone, in that it reduces the heat generation in the hotter strips, and reduces the spread in strip temperatures. The current-shift effect is about twice as strong as the effect of temperature coefficient alone.

The current in strip  $i$  is given by  $r_t I / r_i$ , where  $r_t$  is the resistance per unit length of all the strips in parallel. This then gives

$$I_i = \frac{1}{(1 + \alpha\theta_i) \sum_{j=1}^n \frac{1}{(1 + \alpha\theta_j)}} \cdot I \quad (9)$$

and the heat generation in each strip is then obtained as

$$q_i = n^2 q_0 \frac{1}{(1 + \alpha\theta_i) \left[ \sum_{j=1}^n \frac{1}{(1 + \alpha\theta_j)} \right]^2} \quad (10)$$

Substitution for the  $q_i$  in (4) gives a non-linear set of equations for the temperatures which cannot be solved directly for  $[\theta]$ , but an iterative solution is possible. Substituting for  $q_i$  in the  $i$ 'th equation of (4), we obtain

$$\theta_i = C \left[ \frac{g_{i1}}{1 + \alpha\theta_1} + \dots + \frac{g_{in}}{1 + \alpha\theta_n} \right] \quad (11)$$

$$\text{where } C = n^2 q_0 / \left[ \sum_{j=1}^n \frac{1}{(1 + \alpha \theta_j)} \right]^2$$

Equation (11) is suitable for iterative calculation of the strip temperature-rises. At the start of each iterative sweep the multiplier  $C$  is evaluated using the temperatures from the previous iteration, while the term in square brackets is evaluated using the Gauss-Seidel procedure, i.e. using the latest available estimates of  $\theta_i$ . The process converges rapidly.

Typical results are given in the table below, which is for an array of 15 strips positioned as shown in Fig. 3, carrying a total current of 300A. The strips were assumed to be 4mm x 0.1mm silver in a tube with  $R = 20\text{mm}$  and  $k = 4 \times 10^{-4} \text{ Wmm}^{-1}\text{degC}^{-1}$ .

21.34	20.01	21.34
90.83	111.68	90.83
19.98	18.64	19.98
112.27	136.38	112.27
19.59	18.25	19.59
118.94	144.18	118.94
19.98	18.64	19.98
112.27	136.38	112.27
21.34	20.01	21.34
90.83	111.68	90.83

In the table the figure above the line is the strip current in A, while the lower figure is the temperature rise in degC. Equal current sharing would give 20A per strip, but the current in the centre strip is significantly lower than this. Despite its lower current the centre strip is much hotter than those at the corners.

#### 5. Application to practical designs

The methods described above are for infinitely long strips, for which the heat loss is solely radial. Practical fuse elements are of finite length, and the axial heat loss along the elements to the ends is considerable. Furthermore practical fuse elements usually have reduced sections along their length, so that the element width also varies in the axial direction.

Nevertheless the ideas in section 4 can be used to obtain an approximate solution for real fuses with asymmetrical arrangements of elements, by the following procedure:

- From the coordinates of the elements evaluate  $[g]$  and hence  $g_{av}$  using the full widths of the elements in the calculation.
- Replace the actual asymmetric arrangement of elements by an *equivalent circular arrangement* which the same number of elements, like the one shown in Fig. 1. The *only* parameter to be determined for the equivalent circular arrangement is the radius of the circle around which the elements are to be situated ( $R_p$ ). The basis for determining  $R_p$  must be that the average thermal resistance is the same as for the real fuse.  $R_p$  can be found by a very simple iterative process.

- Solve for the complete temperature distribution in the equivalent circular arrangement, by any convenient method, e.g. the finite difference or finite element method. Then by integration axially along the element in the equivalent circular arrangement, determine the average element temperature-rise,  $\theta_{av}$ .

- Calculate the value of  $q_0$  corresponding to this value of  $\theta_{av}$ . From Fig. 6 this is found to be

$$q_0 \text{ (av)} = \frac{\theta_{av}}{g_{av} (1 + \alpha \theta_{av})} \quad (12)$$

- Use the iterative procedure (11) to generate the "spread" of average temperature-rises for the real element system.

- Assuming that the "shape" of the axial temperature distribution is the same for all elements, determine the maximum element temperature, the element resistances and the volt drop, and the current in each element.

The justification for using the full element width for evaluating  $[g]$  and  $R_p$  is that the bulk of the heat loss to the filler is lost from the full strip, since the notch zones only constitute a small fraction of the total element surface area.

It has not been possible to verify these predictions by direct measurement of the currents in individual elements within a real fuse. However the predictions of temperature-rises, volt-drops and m.f.c.'s for fuses with asymmetrical arrangements of elements, obtained by the above method, have been found to be of the same order of accuracy as the predictions obtained for symmetrical designs.

#### 6. Conclusions

Steady-state radial losses by conduction from an general arrangement of heated strips have been calculated using the inverse cosine transformation to represent each strip and superposition to obtain the total temperature-rise and heat flux. From this a formulation for the radial thermal resistance matrix has been developed, which relates the strip temperature rises to the emitted powers.

An iterative procedure may be used to determine the strip currents, and this can be used in modified form for real fuses with asymmetrical arrangements of elements. By replacing the real system of elements by an equivalent circular arrangement, the need for solving a truly 3-dimensional problem is avoided.

#### 7. References

- Wilkins R. Simulation of fuselink temperature-rise tests. ICEFA, Trondheim 1984, 24-33.
- Sloot J.G.J. Analog simulation of the heat flow in a high voltage fuse. ICEFA, Eindhoven 1987, 7-11.
- Ramo S., Whinnery J.R. and Van Duzer T. Fields and waves in communication electronics. (Wiley 1984).
- Sato S., Menju T., Aoyagi K. and Honda M. Electric field calculation in 2-dimensional multiple dielectric by the use of elliptic cylinder charge. Int. Symp. on High-Voltage Engineering, Milan 1978.
- Chorlton F. Boundary value problems in physics and engineering. (Van Nostrand 1969).

## OVERLOAD TESTS FOR FUSES IN ROLLING-MILLS

S. F. Costa  
CEPEL-Electrical Energy Research Center  
Rio de Janeiro, BRAZIL

and

L.P. Rangel, R. G. Bastos  
Companhia Siderúrgica de Tubarão  
Vitória, BRAZIL

### Summary

Recently the authors were involved in the solution of problems related to frequent premature operation of fuses for the protection of rolling-mills used in the lamination of steel ingots which are subjected to frequent overload currents.

Based on this experience and existing literature, some applications and typical circuits are presented including a description of the inherent thermal and dynamical effects. Standardized tests and their comparison with actual situations are described. Finally, in order to facilitate the user some suggestions are given to improve the current technical standards.

### 1. Introduction

Being an equilibrium point between users and manufacturers, international standards represent the state of the art of products and have a very large number of readers all over the world.

Due to the very big number of specific situations that they shall cover it is not always possible to describe in a sufficiently clear way to the medium reader, the fundamentals/objectives of some of the specifications, which are clear to the experts during the preparation of the standards.

It is a natural fact that the higher the development of one country in one knowledge area the bigger is its concern regarding to the participation in the elaboration of the standard.

Even when not participating many other countries will use these documents in the whole or as the main reference for the national ones, sometimes without a good understanding of the extent.

In a certain way this is the main reason for this paper in which it is tried to resume in an easy way to the user some aspects related to overload cycles inherent to the application of fuses in the protection of circuits involving semi-conductors, in particular for the protection of variable speed dc motors used in the rolling of steel ingots.

For these fuses it is very important to the user to supply the manufacturer with the correct informations about the actual use.

Only with these informations it is possible to the manufacturer to indicate the adequate fuse avoiding

consequences as fast deterioration of the fuse-element, premature operation and bad performance when the fuse operates in severe failures.

For the good understanding of the text it is valuable to resume some definitions as used in IEC Publication 269-4:

- a) Pulsed current - an unidirectional current the instantaneous value of which varies cyclically and includes intervals of small values of current as in Figure 1.
- b) Rated-current - a value assigned by the manufacturer and verified by temperature rise and repetitive duty tests.
- c) Tests for the verification of rated current - composed of a temperature rise test at rated current of the fuse and one test consisting of the application during 100 h of a cycle with an on-period of the conventional time with 1.05 rated current and an off-period of 10% the on-period.
- d) Overload tests - a test in which the fuse is subjected to 100 load cycles, each having a total duration equal to 0.2 the conventional time. The currents and durations are based on the conventional overload curve to be verified. The "on" periods have a current value and duration corresponding to the coordinates of the curve, the "off" forming the rest of interval.

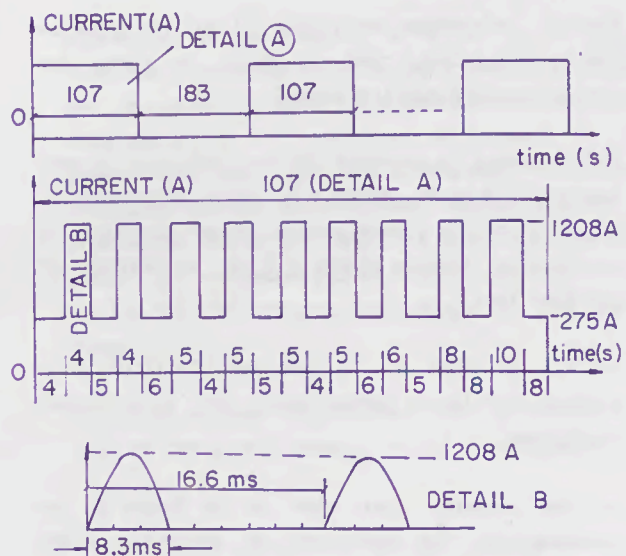


FIGURE 1- ACTUAL CYCLE IN A FUSE FOR ROLLING-MILLS.

## 2. Typical Application of Fuses in Rolling-Mills

One typical application is shown in Figure 2. Currents/cycles as in Figure 1 may be applied to the fuses about  $10^5$  times per year. In Section 4 a comparison is made between the actual cycle and the conventional overload cycle for overload tests.

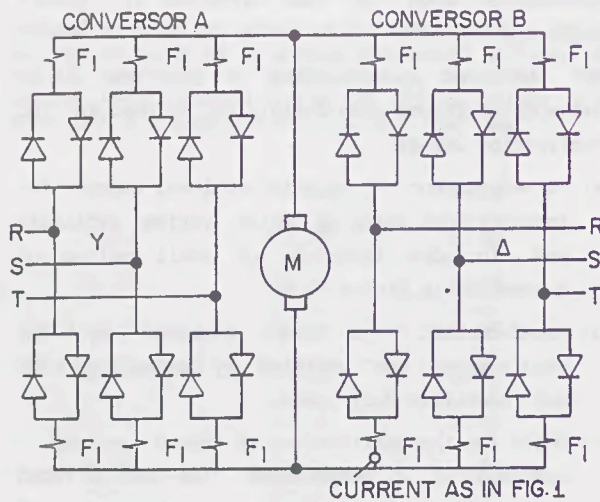


FIGURE 2-TYPICAL APPLICATION OF FUSES IN ROLLING-MILLS.

## 3. Thermal and Dynamical Effects of Overloads

Both effects conduct to ageing during these fuses life as the overload currents are the usual ones and considerably greater than the rated current  $I_N$  (3 up to 6  $I_N$ ).

### 3.1 Thermal Effects

Several references among them [1] and [2] describe the thermal effects that may occur in fuses for semi-conductors applications.

They present approaches on the influence of many factors as type of materials, sand compactation, rigidity of the fuse-elements, values and duration of overload, looking always for the estimation of the fuse life.

In all of them it is not possible to define a general calculation method valid for all general conditions.

To the readers that want to go deeper in the fundamentals of the behaviour of materials under cyclic loading at low and high temperatures

references [3] to [5] are plenty of useful informations. In these references the processes of fatigue, creep and crack propagation inherent to the materials are described under several points of view. Basically the common objective is also how to predict the service life of materials and/or components considering temperatures, cycles and frequency of application, mean stress applied, environment, finishing of materials, tests, elastic stresses distribution around a notch and others. It can be seen that general formulas are not also available for simultaneous conditions. One resume of the more relevant points from these references as they were interpreted by the authors is in the lines below.

Every time one material (or a part of one equipment) is subjected to compression or tension stresses strains are produced. These strains may be elastic with the material, from the macroscopic point of view, returning to its original dimensions after the end of stress or plastic when one limit is exceeded. In this case the material after the end of the stress does not recover its previous dimensions. The effect can be seen by an hysteresis curve as in Figure 3.

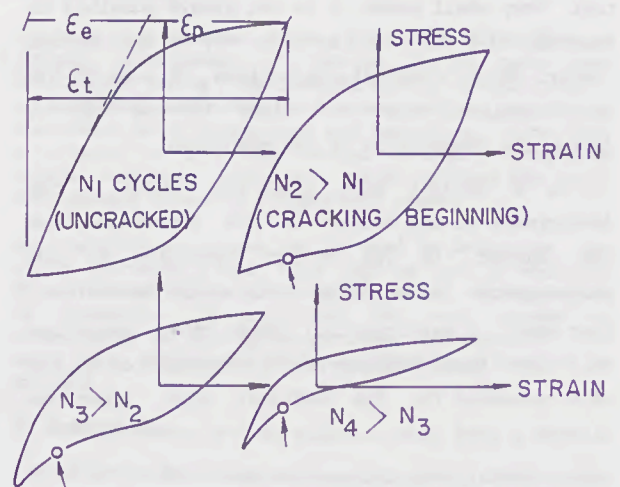


FIGURE 3-TYPICAL HYSTRESIS LOOP DURING CYCLING TEST SHOWING CRACK INDICATIONS.

From the microscopic point of view if one material is perfectly plain and a percentage of the elastic limit is not exceeded, stress cycles could be applied indefinitely without reduction of the life.

As this does not occur materials may exhibit fatigue characteristics due to the propagation of a

surface microcrack from some initial defect or flaw. If the cyclic stress level is sufficiently high the microcrack will spread across the surface and penetrate into the body by continuing to-and-from slip processes until it has reached such a size that it is able to grow as a macrocrack, that is, its growth will depend on the amount it opens and closes under the normal cyclic stress across its faces.

A fuse subjected to an up and down current may be seen as a beam fixed in the two ends (Figure 4). When the current and consequently temperature increases the length of the element tends to increase. As the ends are fixed the internal stresses increase leading eventually to the rupture of the element (if it is very rigid). When the current is lowered the temperature and the length decreases. The repetition of the processes is exactly what is shown in Figure 3 and the consequence is the propagation of microcracks along the time.

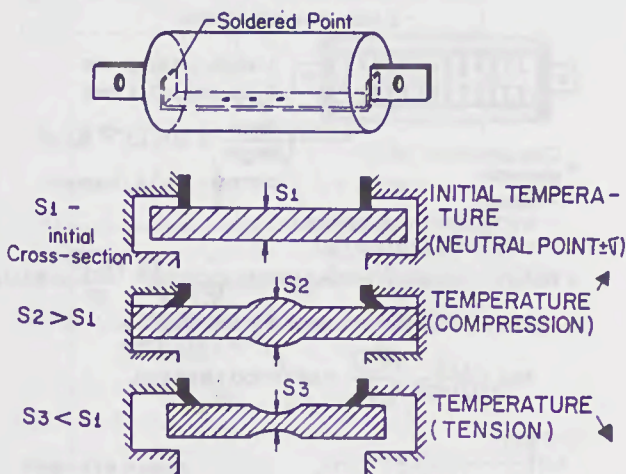


FIGURE 4 - FUSE - MECHANICAL SYSTEM X VARIATION IN TEMPERATURE

This could also be seen as if in each cycle one small plastic strain is retained and is "added" to the previous one up to the point of rupture.

In reference [1] a good description is made on how to minimize the stresses increasing the life by reducing the rigidity of the fuse element. It is also stated that fuse elements without bends shall not be used.

In the literature whichever is the application of

the material the estimation of the life is based in stress-strain and thermal tests and leads to a formula of the type:

$$N^\alpha \cdot \epsilon_p = C \quad (1)$$

where  $N$  is the number of load cycles up to failure (as in Figure 3),  $\epsilon_p$  is the plastic strain,  $C$  is a constant dependent on the temperature taking for a fixed one the form of:

$$C = \frac{1}{2} \epsilon_f = \frac{1}{2} \ln \left( \frac{1}{1 - \beta} \right) \quad (2)$$

$\epsilon_f$  being the fracture ductility and  $\beta$  the percentual reduction in cross-sectional area when the rupture occurs after a fatigue test at a specific temperature as in Figure 3.

The higher is the test temperature the lower is  $C$ . It shall be mentioned that the plastic strain ( $\epsilon_p$ ) is the difference between the total strain (elastic + plastic) and the elastic one ( $\epsilon_e$ ). In the case of fuses the total strain is:

$$\epsilon_t = \beta \cdot \Delta\theta \quad (3)$$

- the temperature coefficient and  $\Delta\theta$  the temperature difference.

For this reason it is not very good to assume for calculations that the plastic strain is nearly equal to the total strain specially when the ratio overload/rated current is not high. In these cases the plastic strain may reach insignificant values.

Concerning to the constant  $\alpha$ , we go to the point that the literature mentions two types of processes as in Figure 5. When low endurance are involved, lets say  $N < 10^4$ , the fatigue process is the predominant one. For long endurance ( $> 10^7$ ) creep processes are the relevant ones. Values of  $\alpha$  to be considered are in the range 0.3 up to 0.5 (the most used) for low-temperatures fatigue and from 0.6 up to 1.0 for high-temperature-fatigue in the creep range.

For these reasons expressions for prediction of life as the useful example showed in Reference [2]:

$$N = \frac{1}{(\beta \cdot \Delta\theta \cdot m)^2} \cdot \left( \frac{C}{K} \right)^2 \cdot \left( \frac{1}{S^2} \right)^2 \quad (4)$$

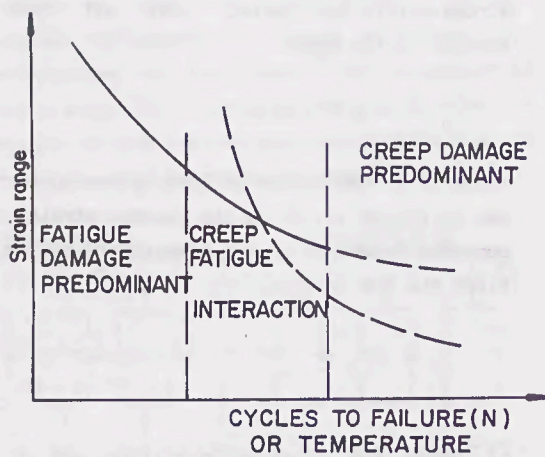


FIGURE 5 - PREDOMINANT PROCESSES TO FAILURE

where  $\Delta\theta_m$  is the temperature rise of the melting point,  $K$  - factor to consider the rigidity of the fuse-element and  $S$  - ratio between overload-current and current from the melting-time characteristic for the same pulse duration, shall be used with special attention for the conditions that they are developed from assumptions as  $\alpha = 0.5$  and  $\Delta\theta = \Delta\theta_m \cdot S^2$  for any value of  $S$  and consequently temperature.

The effects of local concentration of stresses due to the existence of notches and of the mean value of the applied stresses (function of the higher and lower temperatures during the cycle and not only of the difference) may be seen by expressions like:

$$\sigma_{nm} = \frac{\sigma_0}{Kt} \left(1 - \frac{\sigma_m}{\sigma}\right) \quad (5)$$

where:

$\sigma_{nm}$  - the nominal notched fatigue strength, at a given endurance  $N$

$\sigma_0$  - the plain (without notches) fatigue strength at zero mean load (as in Figure 3) at the same endurance

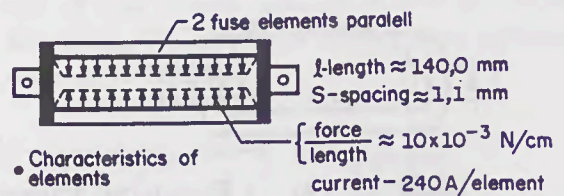
$\sigma_m$  - the applied nominal tensile mean stress

$\sigma$  - the tensile strength of the material

$K_t$  - geometric elastic stress concentration factor =  $\sigma_{notch}/\sigma$  applied

### 3.2 Dynamical Effects

In the used references there were no specific details about these effects but it is a known phenomena that the circulation of currents in neighbour conductors generate electro-dynamical forces/stresses as in Figure 6, the way as these forces will stress the "fuse-element beam" dependent on the ratio between the natural frequency of the beam and the frequency of the overload current. As the natural frequency changes with the span length and there are several micro-span formed by conductor-sand grain it is reasonable to assume that even when the dynamical forces are not high they actuate in parallel fuse-elements forming a high frequency vibrator and trying to reduce the distance between them. Along the time the tendency is that more and more it will be difficult for the fuse-element to recover to its original dimensions and consequently giving a contribution for the growth of cracks.



- Characteristics of elements
  - silver
  - 6x0,3mm (cross-section)
  - weight - 0,2 kg/cm (gt)
- Natural frequency (without sand) =  $f_{01} = \frac{112}{l^2} \frac{\sqrt{E \cdot J}}{gt} \approx 43 \text{ Hz}$
- Natural frequency (with sand  $\phi 1 \text{ mm}$ ) =  $f_{02} = \frac{112}{2(l/140)^2} \frac{\sqrt{E \cdot J}}{gt} \approx 140^2 \cdot f_{01} = 845 \text{ kHz}$

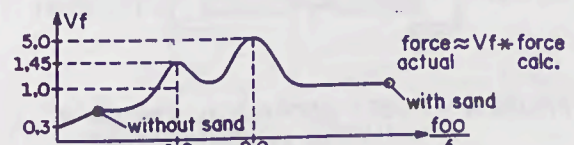


Figure 6 - Electro-dynamical stresses

Maybe this aspect explains one statement in Reference [1] about the increase in the thermal stability of some tested fuses when the sand compactation decreases, in despite of the poorer heat exchange through the sand.

### 4. Standardized Tests and Comparisons with Actual Situations

In IEC Standard 269-4 it is specified one test related to overloads as explained in Section 1 of this paper.

This text is used only to verify if overloads within the limits of the conventional overload curve supplied by the manufacturer can be applied to the fuse  $10^2$  times without problems.

If the actual duty cycle of a fuse is known then, it is possible by transforming the actual duty in an equivalent conventional one to know by comparison with the conventional overload curve if the fuse is adequate to the  $10^2$  cycles.

The conversion is done by integrating  $I^2t$  (actual) along  $0.2^*$  conventional time, and using the maximum value of actual current ( $I_{max}$ ). The "on" period duration is equal to  $I^2t$  (actual) /  $I_{max}^2$ .

As an example we will take one fuse rated  $I_N = 500$  A with pre-arcing and conventional overload curves as in Figure 7 and an actual duty cycle in service as in Figure 1.

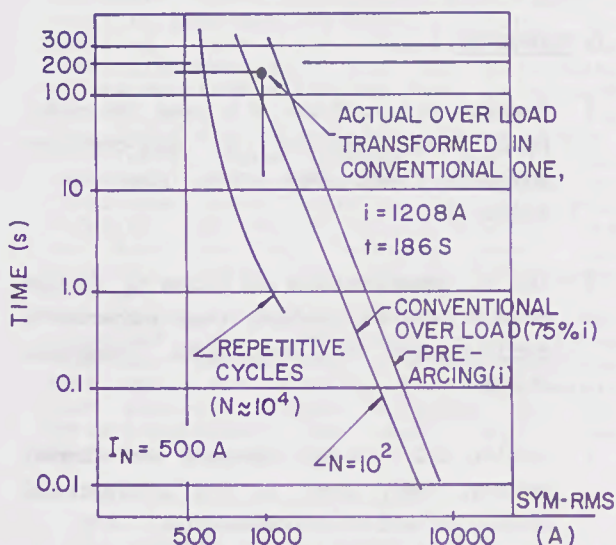


FIGURE 7 - EXAMPLE OF OVER LOAD CURVES ( $N=10^2$  -  $N=10^4$ )

To convert the actual cycle in a conventional one it is necessary to integrate  $I^2t$  (actual) along  $0.2 * 4 h = 48$  min. This integral is around  $27,60 * 10^6 A^2.s$ .

As the maximum actual current is 1208 A the "on" time for the conversion to conventional cycle would be  $t_{on} = 27 * 10^6 / 1208^2 = 180$  s and the "off" period would be  $48 * 60 - 180 = 2700$  s.

If we go to Figure 7 it can be seen that 1208 A can be applied on fuse during approximately 20 s 100 times.

As the obtained point is to the right side of the conventional overload curve the fuse would probably melt before 100 cycles. An adequate fuse to resist more than 100 cycles should have a higher rated current in this case.

The main problem in this actual example of a fuse protecting one very big slab mill is that the actual cycle may in certain occasions occur around  $10^4$  times per month or  $10^5$  per year and for this 500 A fuse the "informed  $N = 10^4$  overload curve" is as in Figure 7, although the experience in use indicates higher values of N.

##### 5. Proposals for Improvements in Standards

Taking into account all the observations in the previous paragraphs it can be stated that the great number of informations which the user shall supply the manufacturer to obtain the appropriated fuse are normally, in the first moments, out of the understanding of the medium user.

Improvements in the standards are necessary in order to facilitate the user and to avoid waste of money and time until the understanding of the reasons for frequent failures leads to the satisfactory solution.

Some suggestions for inclusion in IEC 269-4 are:

- a) to include a note concerning to the 100 cycles overload test mentioning that the test itself provides only a relative comparison between fuses of different manufacture, but gives, in the present state of the art, no real indication of the ability of the fuses to withstand a very large number of pulses during their service life. By that it is meant that the conventional overload curve is only applicable to an occasional pulse situation, where in the lifetime of the fuse-link it will only be subjected to a small number of such overloads
- b) to include one statement mentioning that when required the manufacturer may provide additionally to the conventional overload curve ( $10^2$  pulses), overload curves for  $10^4$  and  $10^6$  pulses (without the inclusion of a test for verification)
- c) to reevaluate the conventional overload test

method as the values of  $t$  (on) and  $t$  (off) are very different from the actual cycle (compare Figure 1 with transformed curve in Section 4). The much higher values of  $t$  (off) in the conventional cycle may generate a mean value of the applied stresses (see Equation 5) much lower than the actual one.

Maybe this is one part of the explanation for a fact that is occurring with one test that is still running giving unexpected results.

One fuse of the type in Figure 7 is being subjected to a continuous cycle as in Figure 8 in the last months. After 17000 cycles the resistance of the fuse and the temperature rise of the end caps which are under measurement from the beginning did not show variations greater than 11%. The test will run until the fuse melts.

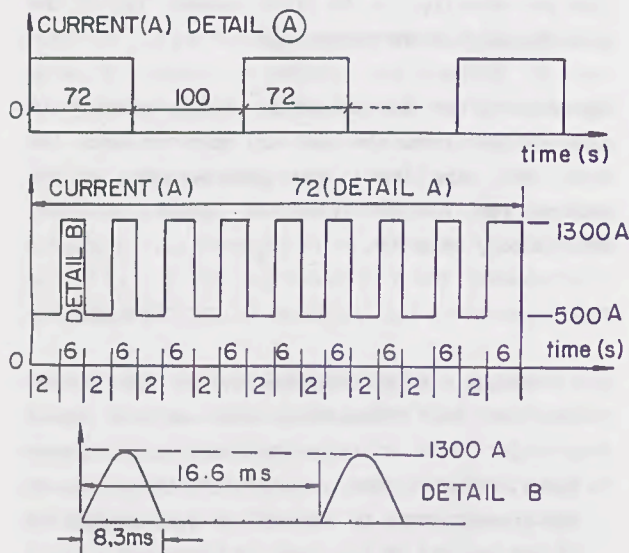


FIGURE 8 - CYCLE FOR TEST RUNNING FOR FUSE IN FIG.7.

## 6. CONCLUSIONS

When we started to develop this work, based on previous experiences with frequent fuses failures the purposes were in addition to clarify some aspects to fuses users, to better understand the reasons for the failures and also to propose some calculation method for evaluation of fuse life under overload conditions. After consultation to the referred literature and some studies a good experience was reached.

It was not possible to obtain the calculation

method and we think that now with a better understanding of the parameters involved this is very difficult and a task for manufacturers which shall involve at the same time electrical engineers and experts actuating in materials<sup>3,4,5</sup>.

We think that the objective of reporting in easy words the aspects related to overload in fuses was reached up to the point of our limited knowledge on the subject.

The main conclusion was that if this subject is still not very clear for us after the end of the work, it is much more difficult for the medium user to know and to evaluate the informations to be supplied to the manufacturer to specify or to replace a fuse for the applications in the scope of this paper. By this reason we are sure that the proposals for improvements in standards are valid and have space for consideration from the experts in this subject.

## 7. REFERENCES

- 1 Namitokov K.K., Ilyina N.A. and Shklovsky, Pulse Withstandability of semi-conductor protection fuses, 1989, Proc. ICSAP-Lodz - Poland, 205-211.
- 2 Arai S., Deteriorations and Cycles to failure of H.V. Current-limiting fuses subjected to cyclic loading, 1984, Proc. ICEFA, Trondheim, 252-261.
- 3 Littler, D.J., Thermal stresses and Thermal fatigue, 1969, Proc. of the International Conference held at Gloucestershire, 1-576.
- 4 Carden A.E., Mc Evily A.J., Wells C.H., Fatigue at elevated temperatures, 1972, ASTM special technical publication 520, 1-801.
- 5 Frost N.E., Marsh K.J., Pook L.P., Metal fatigue, 1974, Clarendon Press, Oxford, 1-500.
- 6 Costa S.F., Electromechanical stresses in electrical energy rigid bus-bar systems, 1979, M.Sc Thesis, COPPE/UFRJ, Rio de Janeiro, Brazil.

*v simple  
no allowance for burn back  
we can always fix after the event*

A SIMPLE METHOD TO CALCULATE THE MAXIMUM VOLTAGE THAT ARISES  
WHEN A FUSE LINK BREAKS A DC SHORT CIRCUIT CURRENT.

Hans-Günter Rex , Berlinerstraße 5 , D-6902 Sandhausen

The breaking of a short circuit current needs a rising resistance of the breaking gap in the melting element of a fuse link. The voltage across the breaking gap increases simultaneously to a maximum value. In some cases this maximum value reaches ten times the value of the driving voltage. In the time interval before the maximum voltage experiments have demonstrated that the electric arc has a positive characteristic. The rise of the voltage has been found to depend always in the same way on the arcing time. On the following pages a simple method developed from experiments is described to calculate the maximum voltage with good accuracy for melting elements with one or more rows of restrictions and for dc short circuit currents of more than 20 times the rated current.

Das Unterbrechen eines Kurzschlußstromes erfordert einen zunehmenden Widerstand in der Schaltstrecke des Schmelzleiters. Die Spannung über der Schaltstrecke des Schmelzleiters wächst mit dem Widerstand zu bis zu einem maximalen Wert. In einigen Fällen kann der maximale Wert das Zehn-fache der Betriebsspannung erreichen. Experimente haben gezeigt, daß in dem Zeitraum vor der maximalen Spannung der Lichtbogen eine positive Charakteristik aufweist. Es hat sich auch gezeigt, daß das Ansteigen der Spannung immer auf dieselbe Weise von der Lichtbogenzeit abhängt. Auf den folgenden Seiten wird ein einfaches aus Versuchen abgeleitetes Programm beschrieben mit ausreichender Genauigkeit für Schmelzleiter mit einer oder mehreren Engstellenreihen und für Kurzschlußströme von mehr als dem 20-fachen Nennstrom.

Equ.(6) is the base assumption for the model of the arcing process. All experiments were done at a time constant of 15ms. The melting element differs in the shape of the restrictions, in the number of the row of the restrictions and in the material.

The model informs about the voltage along the fuse link during the arcing period. We only develop a model which gives necessary information about the current breaking process. The information is sufficient accurate and available in a few minutes without much effort.

In this paper I refer to melting elements with one or more rows of restrictions. The technical data of a manufactured fuse allow to develop a safe-fuse model and compare the calculated results with the experiment. You get necessary data with a minimum of experiments.

In the Lodz paper 1989 I did some assumptions to the arcing process in an ac circuit (L8). I had the opportunity to get detailed information about experiments in ac circuits (L9). When I compared the calculated results with the experimental values I found the error to be less than +- 10 percent. The short circuit current in an ac circuit is limited to the breaking time of about 15 ms. This is nearly the time of the first half wave of a 50 cycle ac current. In a dc circuit the region of the short circuit current is widened up to about 50ms breaking time. The arcing time sometimes exceeds 10ms. This needs a more precise model for the arcing process. Therefore I modified some assumptions of the Lodz paper 1989.

The dc-circuit model calculates ac circuits too.

The model is for a safe-operating fuse link only and not when limiting values are reached.

2. mathematical model of the arcing process

When we discuss electrical processes we refer to diagram no. 1. This means a circuit build up with dc voltage source  $U_0$  with the internal resistance  $R_i$ , resistor  $R_0$  and inductance  $L$  to control the short circuit current without fuse link, the resistor  $R_s$  of the fuse link solid melting element, a rising arc resistance  $R_a$ , a constant dc voltage  $U_e$  for each arcing gap in the element and switch  $s$  for breaking the melting current and for starting the arcing process.

Switch  $s$  in the closed position means the melting process is going on.

When switch  $s$  opens arcing begins. The current does not change very abruptly.

When a restriction is cut its Joulian resistance is replaced by an arc resistance  $R_a$  and a minimum arcing voltage  $U_e$ , the ignition voltage of the arc.

A changing current  $i(t)$  creates in the inductance  $L$  a counter voltage  $U_l(t)$  which delays the changing of the current.

1. The purpose of the model and the range of application

In the last 15 years succesful attempts have been accomplished to get information about the current breaking process inside a fuse link (L3, L4, L5, L6). Today pc-programs are available to calculate the melting and the arcing process (L2, L7).

This paper deals with the arcing process inside a fuse link. The model of the arcing process is a mixture of theory and experiment.

This model informs about the reaction of a h.r.c. fuse link with the melting element embedded in quartz sand of optimum grain size 4mm and its reactions to dc short circuit currents and breaking times up to 50 milliseconds.

If you know the numerical values of the arcing process evaluated for one characteristic experiment you can calculate the values for other experiments.

This effect can be expressed by

$$U_1(t) = -L \cdot (di/dt) \quad (1)$$

The values of voltage and current in the circuit can be calculated by means of the differential equation

$$U_0 = i(t) \cdot (R_0 + R_i + R_s) + i(t) \cdot n \cdot R_a + n \cdot U_e + U_1(t) \quad (2)$$

The values  $R_s$ ,  $R_0$ ,  $R_i$ ,  $L$  and  $U_0$  are known from the fuse link and the circuit. The values  $R_a$  and  $U_e$  belong to each cut restriction of the melting element. That means they do not belong to the solid restrictions during the melting period.

Inside the fuse link body shall be a melting element which contains  $n$  rows of equally shaped restrictions with the cross section  $Q_e$ . Each restriction and the part next to it forms a single breaking device. This does not limit the applicability of the model.

In the prearcing period the fuse link in the circuit behaves like a resistor  $R_s$ . The value  $R_s$  and the whole melting process can be calculated by known methods.

In the prearcing period there is no arcing voltage  $U_e$  and no arc resistance  $R_a$ . When the melting element disrupts the resistance of each row of restrictions turns into a rising arc resistance value  $R_a$  and a voltage value  $U_e$ . We simplify and state the resistance  $R_s$  of the solid melting element material remains at nearly the same value  $R_s$ .

The process of creating the arc resistance  $R_a$  needs a minimum of time and energy. Therefore I propose the variable resistance  $R_a$  for the arcing process to be a function  $f(E)$  of the arcing energy  $E$  already done in a single arc. Other authors do assume other functions.

The breaking moment is set to zero and the arcing time begins at  $t=0$ . Thus after disruption of  $n$  rows of restrictions of the melting element the current  $i$  that flows through the melting element creates an arcing voltage value  $U_a$  measured along the fuse link.

$$U_a = n \cdot U_e + i(t) \cdot (R_s + n \cdot R_a \cdot f(E)) \quad (3)$$

Therefore equ.(2) changes into

$$U_0 = i(t) \cdot (R_0 + R_i + R_s + n \cdot R_a \cdot f(E)) + n \cdot U_e + L \cdot di/dt \quad (4)$$

We look in equ.(4) for the derivation  $di$  of the current in the time interval  $dt$

$$di/dt = (1/L) \cdot (U_0 - n \cdot U_e - i(t) \cdot (R_0 + R_i + R_s + n \cdot R_a \cdot f(E))) \quad (5)$$

Nearly all numerical values belong to the prearcing process. The value  $U_e$  belongs to the arcing process and does not depend on any cross section of the melting element. The numerical value of  $U_e$  has little influence on the result.

The product  $R_a \cdot f(E)$  must create a sufficient steep rise of the arcing voltage  $U_a$  and begin at a minimum value for  $t=0$ . The method try and error delivered for the function

$$R_a \cdot f(E) = A_0/q \cdot i \cdot t \cdot dt \quad (6)$$

The arcing factor  $A_0$  is of the dimension  $mOhm \cdot mm^2 / (W \cdot s)$ .

The numerical value of  $A_0$  depends on the fuse link body and on the melting element. The value  $q$  is the cross section of the restrictions of the melting element in a defined fuse link body.

For the arcing process no significant difference between Ag- and Cu-material has been measured. The model therefore does not know any difference between the arcing of copper or silver material.

The current value  $i(0)$  in the moment  $t=0$  at the beginning of the arcing process is the known melting current is. The voltage value  $i(t) \cdot R_s$  is very small.

In the first time interval  $dt$  the energy  $dE(0)$  is

$$dE(0) = (R_a \cdot i_s \cdot i_s \cdot dt) / n \quad (7)$$

In each following time interval the arcing energy increases with the value  $dE(t)$

$$dE(t) = (R_a \cdot i(t) \cdot i(t) \cdot dt) \cdot n \quad (8)$$

Equ.(8) delivers the value of the variable arcing voltage at the end of the first time interval.

We calculate the value  $di/dt$  in the moment  $t=0$  according to equ.(5) and determine the alteration  $di$  of the current within the time interval  $dt$ . In the moment (1) current has changed to

$$i(1) = i(0) + dt \cdot (di(0)/dt) \quad (9)$$

$$i(t) = i(t-1) + dt \cdot (di(t-1)/dt) \quad (10)$$

The formulas (3), (5) and (8) are simple equations to calculate the breaking process of a melting element inside a fuse link body for a wide variety of test conditions. The time interval  $dt = 25\mu s$  delivers a good resolution in a program for accurate calculation and plotting. The program calculates simultaneously the arc voltage curve given by equ.(3).

We always get the result within one minute and have always sufficient accuracy. But we must not forget it must be a safe-operating fuse link.

The accuracy of the calculation is comparable with the accuracy of the experiment.

### 3. The melting element

A fuse can be designed with single strip or multiple strip melting element. When the melting process ends, the last row of restrictions in each strip is cut in the same moment. The arcing process starts when the melting current cuts the first row of restriction.

In order to get sufficient voltage withstand capability the disintegrated restrictions need a minimum gap and a minimum build-up energy. The necessary arc cross section carries the arc current, builds up an area with rising arc resistance  $R_a$  and develops the ability to withstand the rising voltage.

In real melting elements the cross section in each row of equally shaped restrictions is not equal. A difference in the cross section of +1% means an increase of the melting time of about 100  $\mu s$ . This means that the beginning of the arcing is

delayed about 100us, too. When we take into account this uncertainty of the beginning of the arcing process in each row of restrictions then the measured rise of the arcing voltage along the melting element is delayed and can show several steps.

There are melting elements with very much lead in the middle of one restriction. The heating up and the melting of such a restriction sometimes can be delayed so much that the restriction breaks only when current goes to zero. The arcing process then is controlled by one row less than intended. That means that less rows join the arcing process than the operator running the experiment expects.

It is easy to calculate a single or double strip melting element in a fuse link body. When there are three or more strips then often the arcing process does not need all strips. The arcing current reduces the necessary cross section and the arcing curve changes.

The value of the arcing resistance  $R_a$  increases.

You can calculate the arcing voltage when you reduce the value of the cross section for one strip less and when you reduce additionally the value of the inner cross section of the fuse link body proportional to the cross section of the melting element. The arcing process needs at least two strips of a multiple strip melting element.

Equ.(3) delivers the curve for the arcing voltage and equ.(10) the curve of the arcing current of a melting element.

The arcing process is controlled by the arcing factor  $A_e$ . Now the value  $A_e$  does not depend on the cross section of the restrictions.

#### 4. The spacings of the dividing gaps

Stepwise calculation delivers both the voltage and the current.

Charge carriers leave the current path, carry away energy and go into the sand around the electric arc. Therefore I use a kind of non-adiabatic model.

When we have equally shaped rows of restrictions with equal spacings then all material between these restrictions is heated up by the arc current and especially by the arc heat and will change from liquid to gaseous within a few usec. This result in a remarkable decrease of the number  $n$  of the rows of restrictions and therefore in the values  $n \cdot U_e$  and  $n \cdot R_a$ . The current and the arcing voltage change.

It is significant for a well designed fuse element that this occurs only when the arcing voltage has passed its maximum value.

Melting elements with unequal spacings can be calculated or estimated separately for each spacing.

It is not difficult to calculate the arcing energy and adds it up until the necessary vaporizing energy of the gap connecting material is reached.

When we calculate the arcing process with a model that takes into account the breaking of the gap connecting material, then the displayed arcing voltage of the calculation shows the breaking of arcing voltage often at exact the same moment as the experiment.

#### 5. The arcing voltage

In the first 25 usec a cutting voltage  $U_e$  is created along each gap and must be added to the voltage drop  $R_s \cdot i(t)$  along the fuse element.

The arc resistance  $R_a$  increases and controls the arcing process. Gradually the current changes.

The rising arc resistance  $R_a$  and the falling current result in a maximum voltage within a few milliseconds after the beginning of the arcing process. Then the voltage decreases to supply voltage even when no disturbing process is going parallel.

When the current has fallen to zero the measured voltage becomes the emf-value of the voltage source.

We assume that  $n$  dividing gaps exist all over the arcing time. The gaps are separated by the gap connecting material (gcm). Then equ.(2) describes the arcing voltage curve.

When arcing begins the surrounding sand is an excellent insulating material and withstands high voltage values. When arcing goes on heat energy, electrons and positive ions leave the electric arc, disappear into the surrounding sand and heat it up. When the inner surface of the arc channel has reached a minimum temperature value then the inner surface of the arc channel begins to carry a resistive current parallel to the falling arc current. In this moment measurements show that the arcing voltage breaks to the supply voltage. The insulating capability of the sand decreases.

The arc resistance  $R_a$  increases.

#### 6. Inside the volume of the fuse link body

The inner volume of the fuse link body influences the arcing process due to the pressure of the arcing material. The inner cross section of the fuse link body controls the arcing resistivity value  $A_e$  and changes the voltage value  $U_e$ .

The rising arc resistance can be realized by the increase of the gas pressure in the arc and by the decrease of the temperature in the arc.

When sand is not packed with normal density the compressibility of the sand increases and the arc quenching effect is lowered. Then the voltage rises less fast and arcing is delayed.

When the gap connecting material of the melting element vaporizes then gaseous material is added to increase the pressure in the arc channel. This results in a better arc quenching but it lowers the arc voltage because it decreases the number of rows of restrictions.

When the arc is burning inside the quartz sand in a fuse link body then the surrounding sand is heated up and slowly begins to carry a fault current. When arcing does not decrease fast enough the fault current reaches a value equal to the arcing current. Then the arcing voltage falls to zero. The fault current is maintained.

7. How to use the program in practice

It is necessary to have the evaluated measurements of at least one experiment with the specified fuse link. Set the arcing factor  $A_e$  to 1 and calculate according to the above mentioned formulas. When the result is not as desired then change the arcing factor  $A_e$  and repeat the calculation until you get good approximation. Then calculate the fuse link with this same arcing factor  $A_e$  at modified test conditions.

Enter the complete mechanical information of the fuse link and the short circuit test conditions. Define the initial conditions for the beginning of the arcing process. Then the calculation is continued to the end of the breaking process.

It also helps to know the critical conditions of a given melting element. It helps to know the behaviour of a "not yet built" fuse link under various short circuit test conditions.

In practice it is important to get information fast and sufficient accurate. Extreme accuracy is not needed. The program asks a minimum of questions and gives the needed information.

When the calculation is done it delivers numerical values about the arcing process, the arc current, arcing integral and arcing voltage.

At the beginning we did the limitation of equally shaped restrictions. We can neglect this limitation when we do extra calculation for each type of restriction as described above.

With modern small personal computers the calculation of the arcing process of a simple melting element needs about five minutes dialog time between computer and operator and less than one minute run-time.

The before mentioned method is part of a comfortable computer program STROMex. The program does not only the calculation of the arcing process of a simple fuse link but additional the melting process and heating up processes. It displays the curve on the monitor or external plotter and allows curve discussion.

Handling of the program is most simple. The answer is brought very fast. You can test various short circuit conditions without danger to material and with nearly no extra costs.

8. Literature

1. VDE-test-reports and technical data of h.r.c. fuse links
2. Rex: STROMex, das Rechnen mit Strömen. A program for model calculation developed for the MS-DOS-PC
3. Daalder, Schreurs: arcing phenomena in high voltage fuses, EUT-report, 1983

Liverpool papers 1976

4. Dolegowski : calculation of the course of the current and voltage of a current limiting fuse

Trondheim papers 1984

5. Paukert: electr. conductivity for arc extinguishing media for low voltage fuses
6. Leistad, Kongsjorden, Kulsetas: simulation of short circuit testing of high voltage fuses
7. Wilkins, Wade, Floyd: A suite of interactive programs for fuese design and development

Lodz papers 1989

8. Rex: The process of the breaking of an ac current in lv-hrc-fuse links calculated by means of a model in a personal computer
9. Ossowicki, Pisanko: influence of the distance of the contractions in the strip fuse element on breaking short circuit

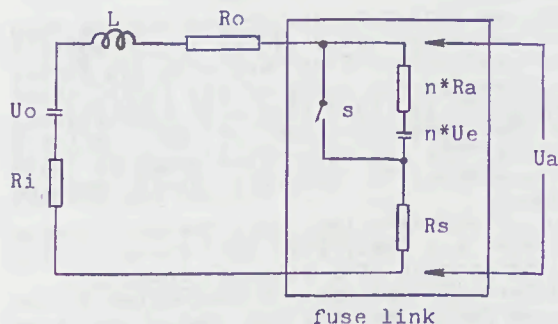


diagram no.1: circuit diagram

$U_{max}/U_o$

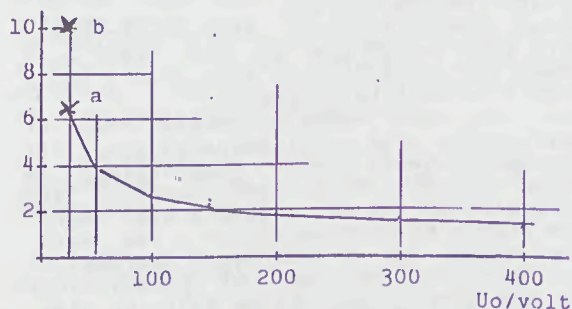


diagram no.2:

max. arcing voltage vs. supply voltage  $U_o$

melting element: double strip  
 material : Ag  
 cross section :  $.1 \text{ mm}^2$   
 number of rows : 3  
 fuse link body  
 inner cross section:  $380 \text{ mm}^2$   
 test current : 1200 A  
 measured values: a , b

The calculation of the arcing process delivers both values.

$U_{max}$ , calculated as double strip: a  
 $U_{max}$ , " " single strip: b

# Spectrum Analysis of An Ablation-Stabilised Arc in Ice

L. J. Cao and A. D. Stokes  
School of Electrical Engineering  
The University of Sydney  
NSW 2006, Australia

## Abstract

The spectrum of an ablation-stabilised arc has been recorded using ice as the test material. The intensity of neutral oxygen lines was found to reach the blackbody radiation limit and subsequently the temperature of the vapour layer was determined by the Planck function. The arc diameter, pressure at stagnation point, arc column temperature and vapour temperature were measured by spectroscopic methods. The results are in agreement with a two-zone, isothermal arc model [7].

## 1 Introduction

The ablation-stabilised arc is very common in expulsion fuses and puffer circuit breakers. The arc is of high current-density being confined in a narrow channel and radiation is the dominant energy-transfer process. Strong radiation causes wall material ablation and a vapour layer exists between the arc column and wall. High pressure is built up and the arc column consists mainly of wall materials [6,7,9].

Under the powerful ablation conditions associated with expulsion fuses, it is normally impossible to view the interior space of the high-current arc. By selecting ice as the confining material, no solid products were produced during arc ablation and it has been possible to record the spectrum of such an arc without the obscuring effect of solid particles.

Among the previous experimental measurements of the arc characteristics [10,11,12], there has been no attempt at spectroscopic temperature measurement. In this paper, the spectrum of the ablation-stabilised arc was taken by side-on spectroscopy and was recorded on a photographic plate. The arc temperature, pressure and diameter were measured by using these results. The test material was a block of ice. The length of the bore was 110 mm and the diameter 10 mm. The theoretical characteristics of such an arc have been calculated in advance [6,11].

## 2 Preliminaries

### 2.1 Optical setup

A ray-tracing method [4] was used to calculate the optical setup, in which Gaussian optics is described by matrices. Two doublets were used in this system so that the location of the images and object-to-image ratio could be easily determined. By considering the diameter of the lens and the maximum aperture angle of the spectrograph, a simple program was written to calculate the position of each lens. Figure 1 is the actual optical setup during the experiment.

A shutter was placed at position S to control the exposure. Exposure time was around 2 ms and it was used in all

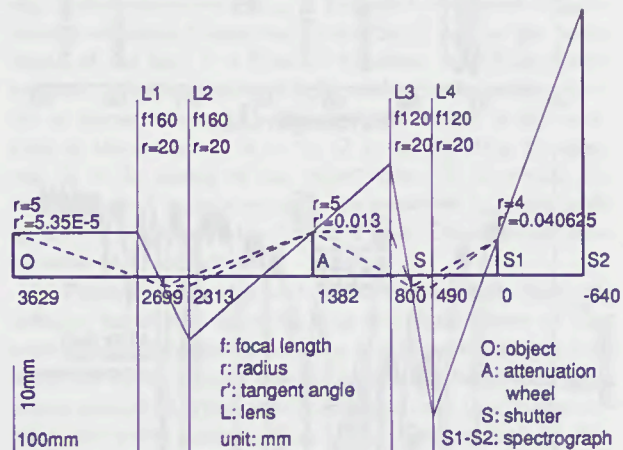


Figure 1: Optical layout of spectrum measurement.

spectral measurements. A Helium-Neon laser beam was used to align the optical elements on the optic axis. A Steinheil universal spectrograph, model GH, and type I-N Kodak photographic plates were used to photograph the arc spectrum. To construct the H-D curve of the plate, an intensity reference spectrum was taken from a standard tungsten filament lamp with an attenuation wheel between the lamp and the spectrograph.

### 2.2 Influence of the fuse wire

It is well known that metal vapour contamination markedly increases the net radiation emission [13,14], because excitation energy levels of metal atoms are much lower than that of nitrogen and oxygen. The arc column of the ablation-stabilised arc was assumed to be composed of wall-ablation materials.

To investigate the influence of the metal wire on the arc column, two copper wires of different diameters (0.07 mm and 0.35 mm) were used. Spectra were taken from the onset time (0 ms) of the main current to the 9th ms of the first half cycle, in 1 ms steps. The exposure times were around 2 ms. A photomultiplier was mounted inside the spectrograph and its voltage signal was sent to an oscilloscope so that precise exposure time could be recorded.

For a given wire,  $\int [i \sin(\omega t)]^2 dt$  is a constant. Experimental results showed that it took 0.32 ms to evaporate a 0.07-mm wire at 2.4 kA. Copper lines were observed in the spectra for observation times up to 3-5 ms from onset of the main current. No copper lines were observed for 4-6 ms observation times. Figure 2 shows the spectra of a 2.4-kA arc taken between 2.0-3.9 ms and 4.9-6.8 ms. Strong copper lines can be clearly distinguished for the early exposure (top), while there are no copper lines in the later exposure (bottom).

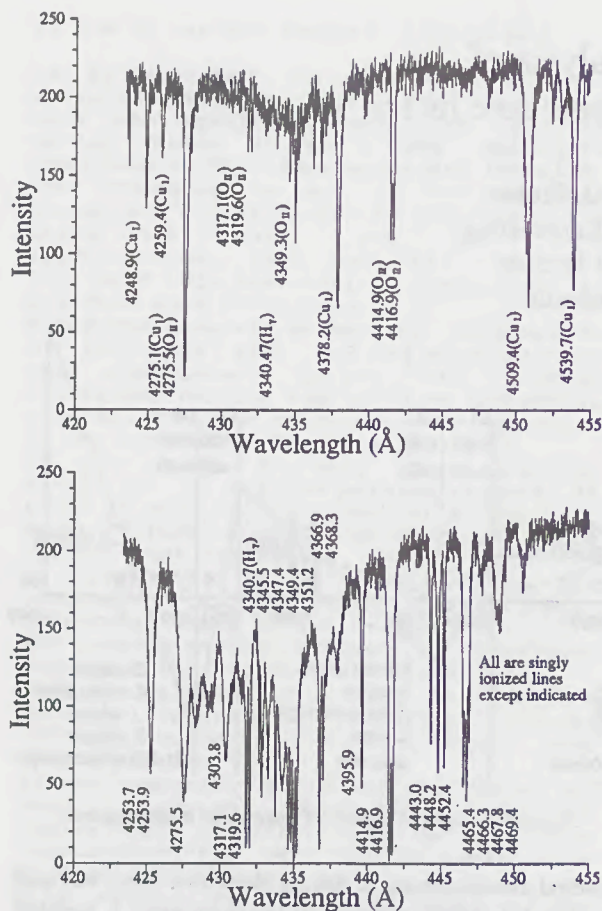


Figure 2: Spectra at 2.0 ms (top) and 4.9 ms (bottom), 0.07-mm wire, 2.4 kA.

By contrast, it took 1.78 ms to evaporate a 0.35-mm wire for a current of 2.4 kA, and copper lines were detected on the plate throughout the first half cycle. Since 0.07-mm fuse wire was used for all experiments, it was not necessary to consider the effect of metal vapour on arc behaviour.

### 2.3 Spectral line reconstruction

The photographic plate containing the image of the spectral lines was scanned by a microdensitometer. A spectral line reconstruction code [5] was modified to meet the present requirements. The program calculated the H-D curve from scanned data and converted the emulsion density to exposure according to the H-D curve. Then FFT filtering was performed to eliminate noise due to plate granularity, line rotating and bending techniques were used to eliminate the astigmatic effect and Abel inversion was performed to recover the emissivity of the arc cross-section. The maximum exposure was kept below the upper limit of the linear region of the H-D curve.

Figure 3 shows a typical spectral line recovery process on the Or line at 466.1 nm. From top to bottom, there are three-dimensional and contour plots of the emulsion density of the photographic plate, radiance after correction and recovered spectral emissivity, respectively. For the three-dimensional plots, the X axis is in the wavelength direction and the Y axis is in the radial (arc diameter) direction. The axis notation for contour plots is the opposite.

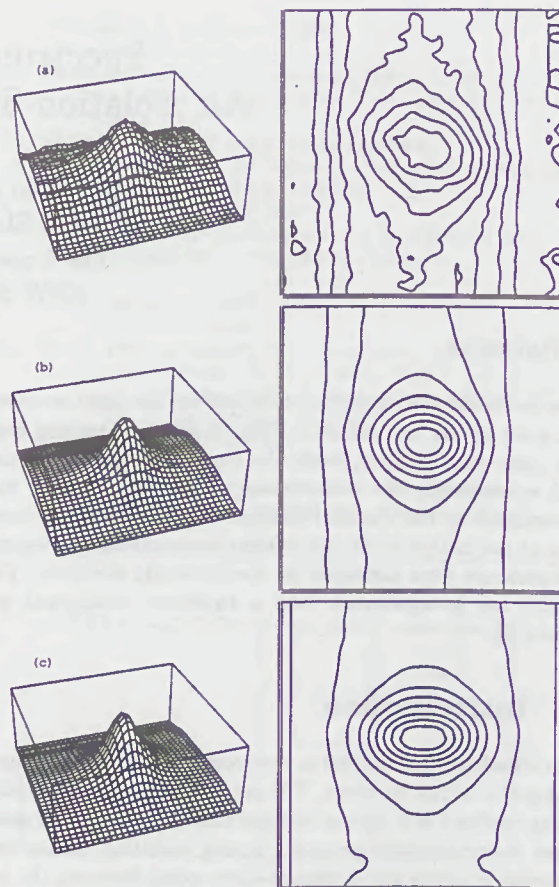


Figure 3: Typical process of spectrum line reconstruction on the singly ionised oxygen line 466.1 nm. See text.

### 3 Electron density and pressure measurement

If inelastic collisions can be ignored, line broadening by charged particles is mainly attributed to the linear Stark effect in the case of hydrogen. The half-width of the line depends on the electron and ion densities and may be used to measure  $N_e$  [15].

The effect of Doppler broadening is much smaller than that of Stark broadening in such a high-pressure arc. The half-width contributed by Doppler broadening is

$$\delta\nu_D = 7.16 \times 10^{-7} \nu_0 (T/M)^{1/2},$$

where  $M$  is the mass number. At 20 000 K the half-widths of  $H_\alpha$  and  $H_\beta$  are 0.66 Å and 0.49 Å, respectively, while they are over 100 Å in this experiment. The effect of Doppler broadening was thus ignored.

For quasi-static (ionic) broadening, the line width is proportional to  $N_e^{2/3}$  [1]. The hydrogen lines are well described by the quasi-static model in which the smearing effect from electron impacts changes the line profile but has little effect on the actual half-value width.  $N_e$  can be obtained from the relation

$$N_e = C(N_e, \lambda)(\Delta\lambda)^{3/2},$$

where  $C$  depends only weakly on  $N_e$  and  $T$  and it can be found from tables [1,3]. Figure 4 shows the measured half-width and electron number density calculated by equation (3). Fig-

ure 5 shows the calculated pressure [11] and evaluated pressure from measured electron number density. Since, in the LTE condition, the material functions are uniquely determined by temperature and pressure, the pressure was evaluated from the calculated material function table by assuming a theoretical temperature.

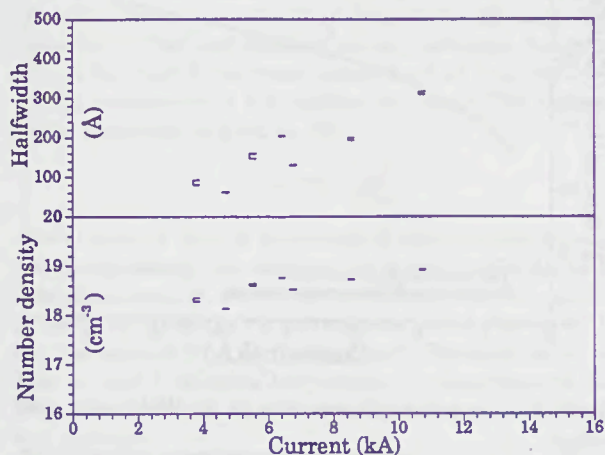


Figure 4: Measured half-width and electron number density.

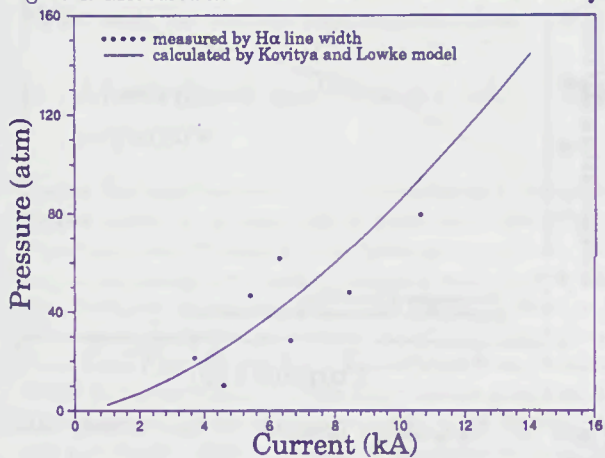


Figure 5: Calculated and measured pressures.

The half-width of the  $H_{\alpha}$  line was widely broadened since the pressure inside the tube was very high. The half-widths of the  $H_{\beta}$  and  $H_{\gamma}$  lines were so wide that these lines interfered with each other and therefore could not be used for measurement.

## 4 Temperature measurement

The transitions of internal energy levels of atoms and ions can be classified into three groups, that is, bound-bound, bound-free and free-free transitions. Bound-bound transitions occur at a particular spectral wavelength and produces a line spectrum of the atomic species. The other two kinds of transition produce a radiation continuum.

Spectroscopic analysis includes measurement of the spectral radiance and identification of the atomic and molecular processes giving rise to the observed spectra. The temperature determination may depend on measurements at a single spectral frequency or on some relationship among measurements at several frequencies.

### 4.1 Absolute line intensity

Gas temperature can be determined by measuring radiance integrated over the frequency bandwidth of a single line. When self-absorption is negligible, the integrated radiance ( $I_{nm}$  in  $\text{W m}^{-3} \text{ster}^{-1}$ ) of an atomic emission line is [16,17]

$$I_{nm} = \frac{hc}{4\pi} \rho_0 \frac{g_n A_{nm}}{Q \lambda_{nm}} e^{-E_n/kT},$$

where the subscripts  $n$  and  $m$  refer to the upper and lower energy states respectively,  $A_{nm}$  is Einstein's coefficient of spontaneous emission (transition probability),  $\lambda_{nm}$  is the wavelength of the line,  $h$  is Planck's constant,  $k$  is Boltzmann's constant,  $c$  is the velocity of light, and  $\rho_0$  is the number density of atoms or ions,  $g_n$  is the statistical weight of the upper state of the transition  $n \rightarrow m$ ,  $Q$  is the partition function, and  $E_n$  is the energy of the upper state. To determine the temperature of a gas specimen, one measures  $I_{nm}$ , and looks up the temperature on the  $I_{nm}$  vs.  $T$  plot. One does not solve equation (4.1) explicitly.

Figure 6 shows a typical measurement result. Since the radiance varies with approximately the fourth power of temperature, the decrease of radiance is much greater than that of temperature. Beyond the arc boundary, the measured radiance reduces to a very small value and even to a "negative" value, due to the granular noise of the photograph plate. The edge of the temperature profile then was simply taken as the abrupt of intensity. It can also be seen that the temperature profile is not flat but is higher in the centre.

Figure 7 plots both the measured temperature by the absolute line intensity method and the calculated temperature [11]. Since the temperature profile over radius was not a constant, the experimental points were plotted as a range rather than a point. The upper boundary is the temperature at the arc centre and the lower boundary is the temperature taken at one third of the radius from the arc centre since the variation of radiance and temperature at the edge of the arc column are quite large and can lead to a certain degree of uncertainty there.

### 4.2 Boltzmann plot and line intensity ratio

Temperature can also be determined from the relative intensities of spectral lines of the same atomic species. When the lines belong to the same ionisation level, the partition functions and number densities of particles in the ground state are the same.

Equation (4.1) can conveniently be re-written [8] to perform the Boltzmann plot,

$$\log \frac{I_{nm} \lambda_{nm}}{g_n A_{nm}} = \text{const} - \frac{E_n}{kT}.$$

A plot of  $\log I\lambda/gA$  against  $E$  for several spectral lines of the same ionisation level should be a straight line of slope  $1/kT$ . Deviations from the Boltzmann distribution should show up as deviations from the straight line, due to optical depth (absorption). Figure 8 shows such a plot of a 2.4-kA arc.

To compare the intensities of two lines by using equation (4.1), we obtain the equation for the line intensity ratio method [8],

$$\frac{I_1}{I_2} = \frac{A_1 g_1 \lambda_2}{A_2 g_2 \lambda_1} e^{-\frac{E_1 - E_2}{kT}},$$

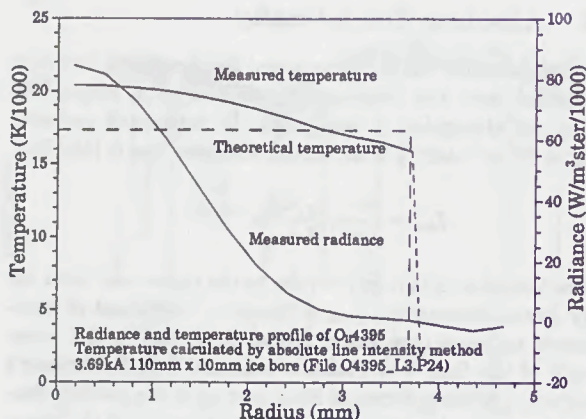


Figure 6: Radiance and temperature profile over arc radius.

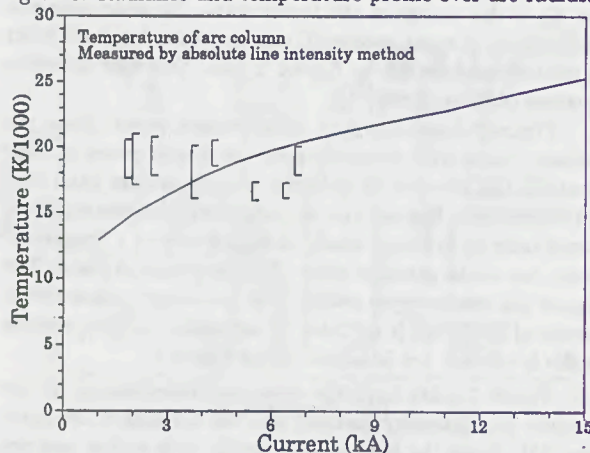


Figure 7: Temperature measured by absolute line intensity method.

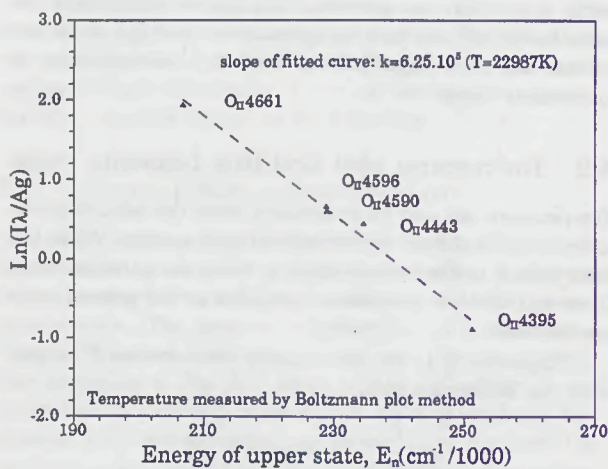


Figure 8: Boltzmann plot.

where the indices 1 and 2 refer to the first and the second line respectively. To be able to evaluate the temperature accurately, the energy difference of the upper terms of the two lines,  $E_1 - E_2$ , must be large ( $\geq 2\text{eV}$ ).

The line intensity ratio method and Boltzmann plot method offer the possibility to evaluate the temperature without knowledge of the number densities and partition functions of the atomic species, which will hopefully bring down the calculation errors. These two methods are basically the

same. Figures 9 and 10 are the results of the measurements. The measured temperatures are higher than those calculated, which indicates significant self-absorption.

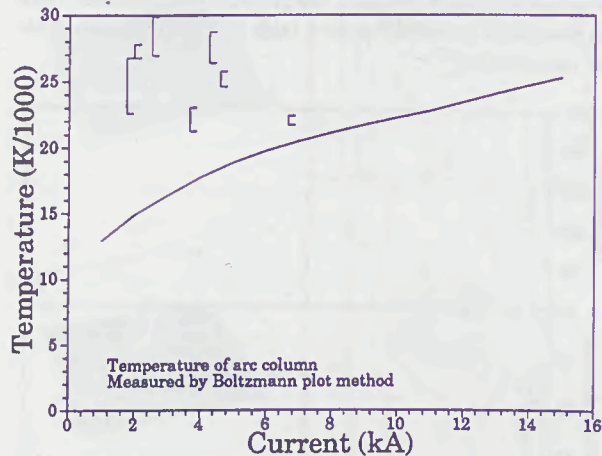


Figure 9: Temperature measurement by Boltzmann plot method.

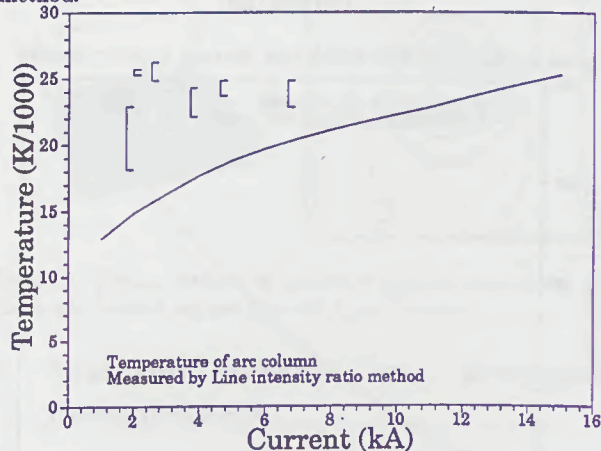


Figure 10: Temperature measured by line intensity ratio method.

### 4.3 Relative line intensity

As in equation (4.1), the radiance of a single line increases with increase of plasma temperature and number density of the atomic species. At a constant pressure, increase of plasma temperature is accompanied by decrease of number density. As temperature goes higher, the influence of the decrease of number density on the radiance will eventually surpass the influence of the increase of temperature. The radiance will then start to fall off. If a line radiance profile has an off-axis peak, its temperature can be determined by considering the relative intensity of the atomic line, the Fowler-Milne method [2].

One then normalises the maximum of the  $I$  vs.  $T$  plot with the maximum of the  $I$  vs.  $r$  plot. The temperature profile can be determined by matching the maxima of both radiance plots. In the current experiment, neutral oxygen and hydrogen lines were found to have off-centre peaks. It was further found that the measured radiance was 50-100 times lower than expected. With such heavy absorption, the Abel inversion and line intensity methods were no longer applicable. These lines were dealt with differently, as described in

section 5.

#### 4.4 Absolute continuum intensity

Continuum radiation arises from the interaction of initially free electrons with the positive ions or atoms that are present. The interactions may be either free-free transitions (Bremsstrahlung) or free-bound transitions (recombination radiation). The total intensity at any particular frequency  $I(\nu)$  is the sum of the contributions from all such processes having components at the specified frequency. The radiance of the continuum is given as [15]

$$I(\nu) = C(\nu) \frac{N_e N_i}{T^{1/2}},$$

where constant  $C(\nu)$  is a function of wavelength but not of population density nor temperature in the wavelength range considered here.  $N_e$  and  $N_i$  are the electron and ion densities respectively. From the known temperature distribution of the arc, the value of  $C(\nu)$  can be calculated. The same value can then be used to calculate temperature at other pressures and population densities since it is independent of temperature and pressure.

During the analysis, it was found that  $C(\nu)$  was not a constant. It decreases with the increase of current. Again this indicated that self-absorption has taken place.

### 5 Absorption and vapour layer temperature

The arc has been described by a two-dimensional, isothermal channel model [7]. At large optical depth, each photon must be absorbed and re-emitted many times on its way out. The surface brightness must reach a saturation value equal to that of a blackbody at some points. Thus the major fraction of the energy is dissipated by radiation, which is absorbed in the cooler outer regions of the arc. This self-absorption produces a shelf in the temperature profile as a function of radius. As a consequence, a zone of vapour usually exists between the wall and the arc plasma. Not all of the radiation from the centre of the arc is of a wavelength short enough to ionise the ablated material from the wall. The vapour is transparent to some of the radiation.

As in section 4.3, the intensities of neutral lines was much lower than those of theoretical predictions. A typical radiance profile (OI715.6nm) is shown in Figure 11. It can be clearly observed that line profile is flat over a large distance from the axis, which can be explained by Figure 12. At the particular wavelength, the blackbody radiation limit is reached and radiation from the arc core is absorbed almost completely. The line profile recorded on the plate is the intensity profile of the vapour layer. It reaches the saturation value of blackbody radiation. The flat profile is evidence of extremely heavy absorption of the arc radiation.

As the pressure inside the bore becomes large, the radiation intensity approaches the blackbody radiation limit. The line shape will saturate by redistributing its energy within a larger bandwidth. The half-width of singly ionised oxygen lines in this experiment is around  $3 \text{ \AA}$  while that of neutral lines is around  $12 \text{ \AA}$ . Widely spread line-width is further evidence that the blackbody radiation limit has been attained.

On the other hand, larger amounts of particles are concentrated at the related energy levels (centre frequency).

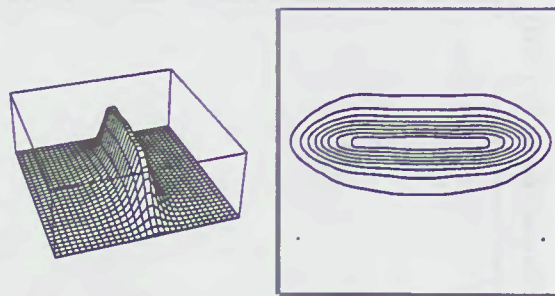


Figure 11: Typical radiance profile of the neutral oxygen line 715.6 nm, continuum extracted).

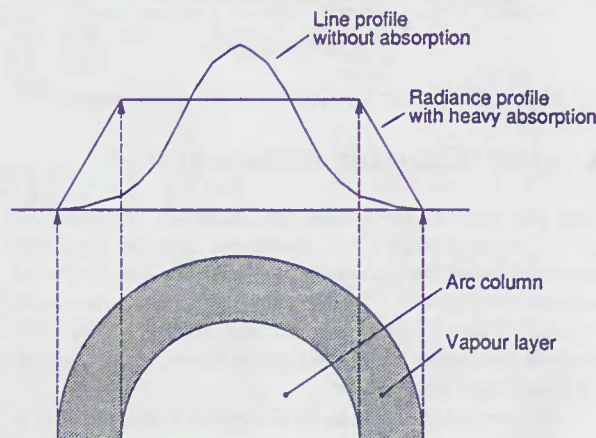


Figure 12: Radiation profile with and without heavy absorption.

This, in turn, will lead to heavy absorption at the line centre. It was observed that both the  $H_\alpha$  and  $H_\beta$  lines recorded had a dip at the line centre. This is contrary to the predicted Stark profile for  $H_\alpha$  because there are no shifted central Stark components in  $H_\alpha$  as there are in  $H_\beta$ . This provides more evidence that heavy absorption is present in the neutral atomic lines. The dip is caused by absorption from particles of very high population density at the centre frequency.

Equation (4.1) was also integrated to evaluate theoretically the extent of line radiation. It was found that the integrated intensity of neutral line radiance approached the blackbody radiation limit under the high pressures in this experiment (same order of magnitude), while that of a singly ionised oxygen lines was far less than the limit (two orders of magnitude lower).

It was thus assumed that the radiation of neutral lines attained the blackbody radiation limit. The distribution of blackbody radiation is governed by the Planck function [15],

$$I_0(\nu, T) = \frac{2h\nu^3}{c^2} \frac{1}{e^{h\nu/kT} - 1}.$$

Thus the vapour layer temperature can be determined from the radiance profile of a neutral line. Figure 13 shows the vapour temperature calculated by this method. We can see that the vapour temperature is almost independent of current. It should be related to a temperature high enough to evaporate all possible solid materials.

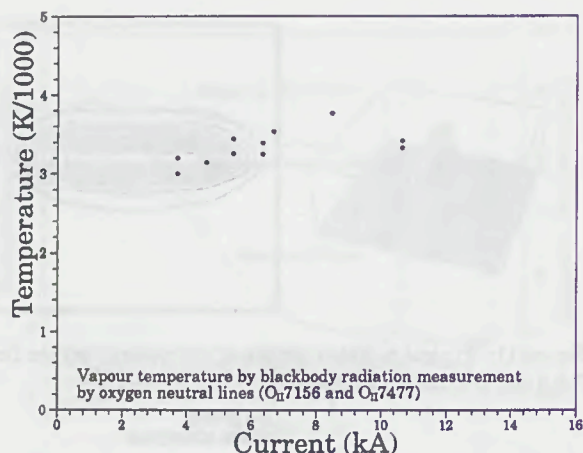


Figure 13: Vapour layer temperature measurement.

## 6 Arc diameter measurement

Since the spectral line profile was faithfully reconstructed, the arc diameter could also be measured. Two methods were used to measure the diameter of the arc. The first method is illustrated in Figure 6. The arc temperature profile calculated by absolute line intensity method falls abruptly. The point at which this occurs is regarded as the boundary between the arc column and vapour layer.

The second method can be illustrated with references to Figure 11. The flat top of the radiance profile indicates the arc column. The position of the edge is taken as the midpoint between the "shoulder" and "toe". Figure 14 shows the results of diameter measurement by these two methods. The measurement fits well with the theoretical prediction.

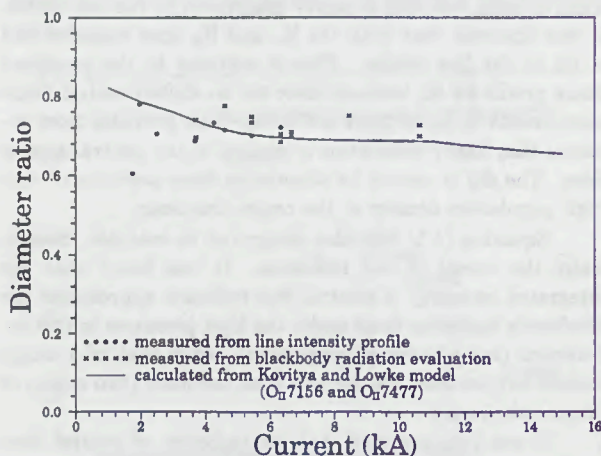


Figure 14: Diameter measurement.

## 7 Discussion

Because of the presence of self-absorption, temperature calculation through intensity measurements in Section 4 is not very accurate. As the current density and pressure increase, spectral transmissivity decreases. Thus, temperature measured by absolute line intensity of singly ionised oxygen lines is lower at higher current (Figure 7). Absorption leads to a higher population of atoms at lower excitation energy levels.

As a result, the measured intensities at lower energy level are lower than they should be, because radiation at these levels is more likely to be absorbed. Because of this reason, the points on the left side of Figure 8 are lower than they should be. Subsequently, the slope is too low and temperatures on Figure 9 and 10 are too high.

The Stark broadening mechanism is independent of the state of LTE. The pressure evaluation in section 3 is fairly accurate, by using measured electron number density and theoretical temperature. This in turn indicates that the temperature predicted is correct.

Comparing Figures 3(b) with Figure 11, we can see that the radiance of the neutral oxygen line is spread through the outer layer while the radiance of the singly ionised oxygen line is concentrate at the centre. This is because there are two zones in the channel, a high temperature arc column and a low temperature vapour layer. It also explains why lines of different energy level are present on the same photographic plate.

## Acknowledgment

The authors wish to thank Prof. T. Lipski and Dr. A. J. D. Farmer for helpful advice.

## References

- [1] J Cooper. *Reports on progress in physics*, Vol.29(Part 1):35-130, 1966.
- [2] R H Fowler and E A Milne. *Monthly Notices Roy. Astron. Soc. (London)*, Vol.83, 1923.
- [3] H R Griem. *Plasma spectroscopy*, McGraw-Hill Book Company, 1964.
- [4] K Halbach. *Am. J. Phys.*, Vol.32:90-108, 1964.
- [5] C A Schmidt-Harms. Internal Report, School of Elec. Eng., Univ of Sydney, 1985.
- [6] P Kovitya. *IEEE Tran. on Plasma Science*, Vol.15:294-301, 1987.
- [7] P Kovitya and J J Lowke. *J. Phys. D: Appl. Phys.*, Vol.17:1197-1212, 1984.
- [8] W Lochte-Holtgreven. *Plasma diagnostics*, North-Holland Publishing Company, 1968.
- [9] L Niemeyer. *IEEE Tran on PAS*, Vol.97:950-958, 1978.
- [10] C B Ruchti and L Niemeyer. *IEEE Trans on Plasma Science*, Vol.14:423-434, August 1986.
- [11] A D Stokes and L J Cao *J. Phys. D: Appl. Phys.*, Vol.22:1697-1701, 1989
- [12] A D Stokes, H Sibilski and P Kovitya. *J. Phys. D: Appl. Phys.*, Vol.22:1702-1707, 1989
- [13] D C Strachan. *Proc. IEE*, Vol.123(11), 1976.
- [14] D C Strachan. *J. Phys. D: Appl. Phys.*, Vol.10:361-370, 1977.
- [15] A P Thorne, *Spectrophysics*, Chapman and Hall & Science Paperbacks, 1972.
- [16] R H Tourin, *Spectroscopic gas temperature measurement*, Elsevier Publishing Company, 1966.
- [17] W L Wiese, M W Smith and B M Glennon, *Atomic transition probabilities*, Vol.1, NBS 4, 1966; Vol.2, NBS 22, 1969.

## **Session 2**

# **FUSE DESIGN II**

Section 2

ELISE VESPER

what is the point  
now C-L

RESEARCH ON HORSE SHOE CORE TYPE AXIAL  
MAGNETIC FIELD VACUUM FUSE

Wang Jimei  
Xi'an Jiaotong University  
The People's Republic of China

INTRODUCTION

In recent years the interrupters of the vacuum circuit breakers are applied various configurations of the axial magnetic field which are to really effective to improve the interrupting performance. Here we apply this method into our newly developed vacuum fuse which was not only successfully preventing local overheating of an electrode when it interrupted large current, but also simplified the coil type of the original axial magnetic field configuration which is adopted horse shoe core type axial magnetic field.

This vacuum fuse shows an excellent interrupting capacity in a wide current range from a overload fault current to a larger short-circuit fault current. Thus, it can be reliably used as a general purpose fuse especially as a motor protection fuse.

CONFIGURATION, OPERATING PRINCIPLE AND ADVANTAGES

The configuration of vacuum fuse is similar to ordinary fuses. It consists of element, dielectric for extinguishing arc, envelop and conducting rod. The main difference is dielectric which is vacuum. It is usually provided with an axial magnetic field device for improving the interrupting capacity.

Figure 1 shows a general type vacuum fuse of early products with rated voltage 15kV, rated current 300A and interrupting capacity 12kA [1].

Figure 2 shows an axial magnetic field coil type vacuum fuse, an experimental product made in 1985 by Japan; the rated voltage, rated current and interrupting capacity being 12kV, 630A and 21kA respectively [2].

Figure 3(b) shows a horse shoe core type of axial magnetic field vacuum fuse, a research sample made by our university's factory in 1988; the rated voltage, rated current and interrupting capacity being 10kV, 250A and 31.5kA respectively [3].

In this type of the vacuum fuse, the axial magnetic field is produced by two plates of horse shoe iron core located on the back of electrodes. The principal configuration is showing in Figure 4. When the short-circuit current passes through to the vacuum fuse,

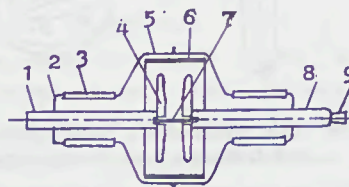


Fig. 1 A General Type of Vacuum Fuse  
1-conducting rod, 2-end cap, 3-porcelain tube, 4-arc electrode, 5-metal envelop, 6-shield, 7-fuse element, 8-conducting rod, 9-seal

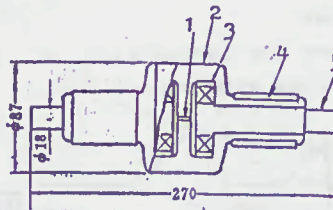


Fig. 2 An Axial Magnetic Field Coil Type Vacuum Fuse  
1-fuse element, 2-shield, 3-arc electrode, 4-porcelain tube, 5-conducting rod

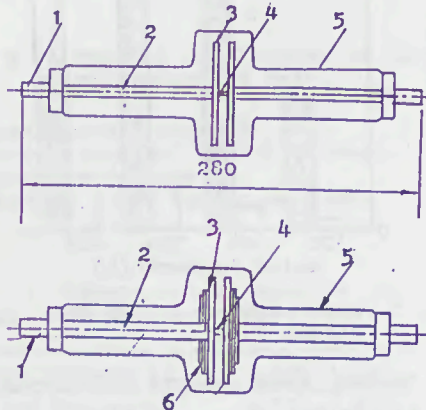


Fig. 3 A Horse Shoe Core Type of Axial Magnetic Field Vacuum Fuse  
1-conducting rod, 2-glass tube, 2-electrode, 4-fuse element, 5-glass tube, 6-horse shoe iron core

the fuse element operates and produces arc between the two electrodes. Meanwhile, the surfaces of electrodes will build an axial magnetic field which is produced by two plates of horse shoe iron core. Due to two opposite axial magnetic field on the surfaces of the electrodes, most of eddy current will be cancelled out each other. Hence, the surfaces of the electrodes leave out cutting slot.

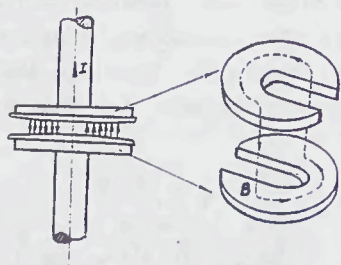


Fig. 4 The Principal Configuration of horse shoe iron core

The advantages of the vacuum fuse are:

(1) The fuse element is very short, only few millimeters and its power loss is lower than that of any other types of fuse. The power loss is nearly only 10% of same rated current of other types.

Figure 5 shows the comparison of the power loss of HRC fuse with vacuum fuse.

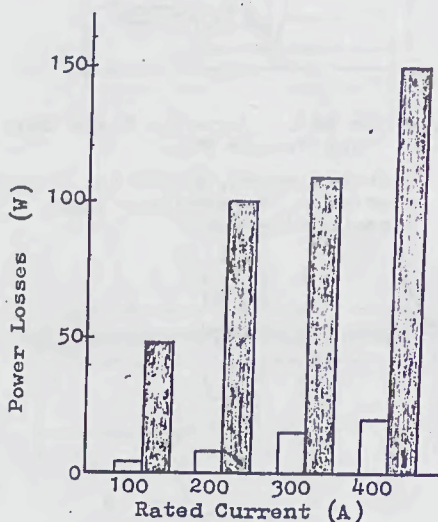


Fig. 5 Power Losses of HRC Fuse and Vacuum Fuse

(2) The vacuum fuse always interrupts fault current at current zero, so there is no over voltage occurred.

(3) The heat-capacity of connecting terminal of vacuum fuse is large and its conducting heat is better. So that, under rated current condition, its temperature rise is small in

comparison with the same rated current of other types. It is only 30-50%.

(4) Many times of over current tests of vacuum fuse, there is no deterioration phenomena and no resistance deviation of fuse element. Hence, it is fit for applications of the frequent operation such as for motor protection. Figure 6 shows the number of tests against over current ratio S of the vacuum fuse and HRC fuse.

$$\text{(Over current ratio } S = \frac{\text{over current during 10 sec.}}{\text{10 sec. fusing current}})$$

(5) During operation, no explosion, no gas spraying out and no noise will occur.

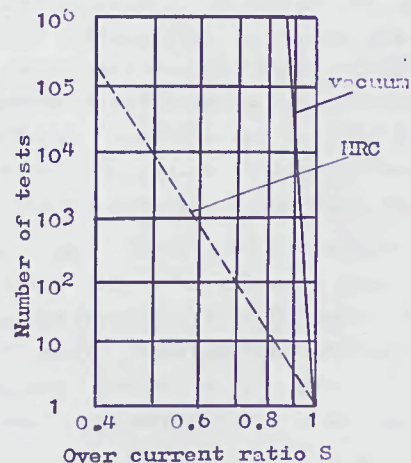


Fig. 6 The Number of Tests Against Over Current Ratio S of The Vacuum Fuse and HRC Fuse.

#### THE CHARACTERISTICS OF VACUUM FUSE

The operation process of the vacuum fuse during over load current or short circuit current is similar to that of the general fuse involving melting, vaporizing, restriking and arcing. Finally, the vacuum fuse quenches this arc at current zero. The conducting rod of vacuum fuse is made by a good conductive material (Cu) having large heat-capacity. Therefore it has lower temperature rise at normal working condition and higher overload ability. When the vacuum fuse suddenly happens short-circuit current fault, the fuse element temperature rise will be attained very rapidly to the melting point until the arc produced. This is nearly an adiabatic process. But at low overload current, the melting time will be increased more and more. Therefore the prearcing characteristic of the vacuum fuse becomes a steep curve. Figure 7

shows a steep time-current characteristic of the vacuum fuse.

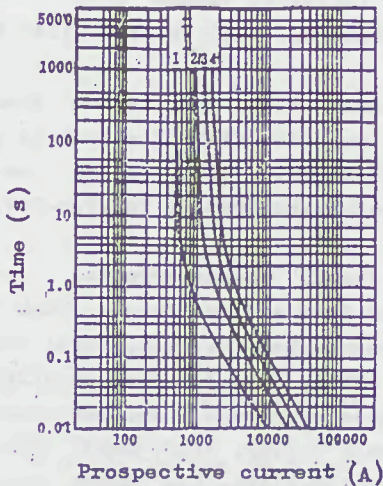


Fig. 7 Time-current characteristics of vacuum fuse

T. Tanaka et al [2] gave the optimizing data of flux density against interrupting current for axial magnetic field type vacuum fuse as shown in Figure 8. In Figure 8 it shows that when the electrode diameter of the vacuum fuse equals 50mm, the optimization of the flux density is  $(8-13.6) \times 10^{-3} \text{ Wb. m}^{-2} \text{ kA}^{-1}$ ; when the electrode diameter of the vacuum fuse equals 60mm, the optimization of the flux density is  $(8.2-14) \times 10^{-3} \text{ Wb. m}^{-2} \text{ kA}^{-1}$ .

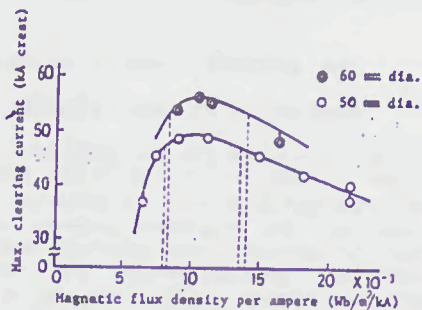


Fig. 8 The Clearable current limit as a function of magnetic flux density per ampere

If the flux density is lower than the optimization value, the max. interrupting current will be decreased rapidly with the decrease of the flux density. If the flux density is higher than the optimization value, the max. interrupting current will be decreased slowly with the increase of the flux density. The reason is that when the axial magnetic field is too weak, the arc between the two electrodes will become a

constriction state easily. On the contrary, when the axial magnetic field is too strong, the arc between the two electrodes will maintain a diffusion state, but the charge particles move along the axial magnetic field longer path than the optimization flux density. So that the voltage drop between the electrodes will be increased slightly, but the interrupting current will be decreased.

#### TESTS AND RESULTS

Two typical samples are shown in Figure 3. One is designed for a lower interrupting capacity without horse shoe iron core structure, that is no axial magnetic field producing in the surfaces of the electrodes. The other is designed for a higher interrupting capacity with horse shoe iron core structure which can produce axial magnetic field under the test. Figure 9 shows the short circuit test result of the latter one with prospective current being 32kA. The temperature rise measured at the ends of the connecting terminals on these two typical samples were  $5.8^{\circ}\text{C}$  and  $14.3^{\circ}\text{C}$  respectively. Table 1 shows an experimental temperature rise test [5].

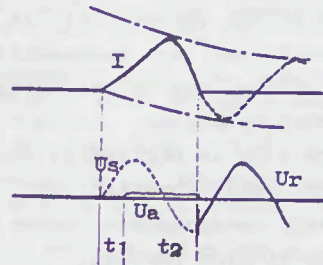


Fig. 9 A Typical Oscillogram of Short Circuit Current Test

I-Short circuit current,  
Us-Source voltage, Ua-Arc voltage,  
Ur-Recovery voltage,  
t1-Melting time, t2-Arcing time,

Table 1 Experimental Results of Temperature Rise Test

Rated Current(A)	100	250
Tested Current(A)	101	253
Temperature rise( $^{\circ}\text{C}$ ) (Connecting Terminal)	5.8	14.3
Area of connected wire( $\text{mm}^2$ )	100	225

#### APPLICATIONS

Horse shoe iron core type vacuum fuse has many advantages in comparison with a current limiting fuse. The applications of this newly developed vacuum fuse are as follows:

- (1) Overload and short circuit protection of a high voltage motor of large capacity.
- (2) Protection of main transformer, distribution transformer and protection on overhead or underground distribution lines.
- (3) Protection of capacitor banks.
- (4) Other special devices for required low over voltage.

Furthermore, this type vacuum fuse with a higher rated voltage is easily developed without any serious increase in dimensions such as for 35kV system.

#### CONCLUSION

The axial magnetic field makes the arc column stable and keeps it in diffusion state, so that it has an excellent interrupting capacity.

The small over current can be interrupted without any trouble.

No over voltage is occurred during operation, because the current is interrupted always at its current zero.

Power loss of the vacuum fuse is about 1/10 in comparison to a current limiting fuse with same rating, due to the fusible element being short length.

Temperature rise is negligibly small.

Fuse element deterioration and deformation are scarcely recognizable after repetitive application of over current.

It is affirmed that the vacuum fuse having such advanced characteristics can be adopted in various fields, so that it will be developed widely in the future.

#### REFERENCES

- [1] J. M. Lafferty, Vacuum arcs theory and application, 1980 by John Wiley & Sons, Inc.
- [2] T. Tanaka et al, The vacuum fuse with axial magnetic field for general purpose applications, IEEE Trans. on Power Apparatus, and System, Vol.Pas-104, No.9, Sept. 1985.
- [3] Wang Jimei, Characteristics of the vacuum fuse and its future, High Voltage Apparatus, Vol.26, No.2, April 1990.
- [4] Wang Jimei, et al, Construction and analysis of vacuum fuse, Electrotechnical Journal, Vol.69, No.9, Sept. 1988.
- [5] Zhao Quing-liang, The horse shoe iron core type vacuum fuse, Ms. D. Thesis Xi'an Jiaotong University, China. 1989.
- [6] H. Schellekers et al, Axial magnetic field type vacuum circuit breaker based on exterior coil and horse shoe, XIIth International Symposium on Discharges and Electrical Insulation in Vacuum, 1986.

AN EXPERIMENTAL INVESTIGATION OF INTERRUPTING  
PERFORMANCE OF HV EXPULSION FUSES

Shen Meihan

Xi'an High Voltage Apparatus

Research Institute

P.R.China

**Abstract:** In this paper some factors affecting the arc-extinguishing behaviors of HV expulsion fuse are dealt with and the construction, and behaviors of the newly-developed 11.5-40.5 KV expulsion fuse and its use and prospect in China are introduced. Moreover, suggestions regarding the relevant regulations for interrupting tests of the IEC 282-2 "Expulsion and Similar Fuses" are made.

### 1 General Introduction

The 11.5-40.5 KV HV expulsion fuse has found extensive application in the 10-35 KV power systems in China. Being simple in construction, reasonable in price and convenient in use and maintenance and relatively satisfactory in protection behavior, the fuse, which is well accepted by numerous users, is one of the most widely-used electric HV apparatuses in the power systems in China. It is mainly connected in series on the HV side of the 10-35 KV distributing transformer in urban and rural areas, or installed on the main and branch lines of the distributing networks to protect the transformer and lines from accidents. In the 10-35 KV power systems in China, the number of this kind of fuses is as great as about several millions and its annual output some hundreds thousand each year.

### 1.1 Investigation of Factors Affecting Arc-Extinguishing Behaviors of the Fuses

Detailed specifications are made in the IEC 282-2 standard and C37.41-1981 of the American ANSI/IEEE standard concerning the interrupting behaviors of the fuse. The standards demand that the fuse should be able to make and break the interrupting current ratings and any short-circuiting and over-load currents below them, i.e. to make and break 5 series of current values such as  $1 + 5\%$ ,  $0.7-0.8$ ,  $1.0-2.0$ ,  $3$ ,  $400-500$  A, and the 2.7-3.3 times fuse link rating. As these demands are quite severe, and the arc-extinguishing behaviors are affected by a great number of factors, among which are chiefly the material, construction and size of the fuse tube, it is the key problem to design the reasonable fuse construction, to select the arc-extinguishing material with satisfactory properties and to make out the rational fuse size to resolve the contradiction of making and breaking large and small currents. The paper, considering a numerous tests and investigations conducted over the past few years concerning the new type 11.5-40.5 KV fuses and the experience in the manufacturing testing and operation of fuses gained in China for more than 30 years, deals with a few important factors affecting the arc-extinguishing behaviors of the fuse as follows:

### 1. The Influence of the Material and Size of the Fuse Tube

The fuse tube is the most important part of the expulsion fuse and it consists generally of the inner gas-generating arc-extinguishing tube and the outer protecting tube. When the fuse-element is blown out and the arc is produced, the material of the inner arc-extinguishing tube under the action of the arc, generates a large amount of deionizing gas, thus causing the pressure in the tube to rise rapidly and the high pressure gas injects from the open end of the fuse tube blowing the arc perpendicularly so that the arc is elongated quickly and cooled intensively and caused to be extinguished.

After carrying out investigations and tests of the short-circuiting interrupting current by using gas-generating materials such as plexiglass, PVC, fibere, amino resin cellulose, etc. we have found that with PVC, which has a satisfactory arc-extinguishing behavior, a high impact strength, and a moderate consumption, with gas generated under the action of the arc, a great number of carbonized particles are produced on its surface. Other materials such as plexiglass, amino resin cellulose etc., in spite of their good properties in many fields, the mechanical strengths, mainly the impact strength, are not good enough. After the gas is generated and the arc is extinguished, there are cracks at the bottom end of the inner tube. After the second

successive interrupting, the bottom end of the inner arc-extinguishing tube is cracked for 8 to 10 cm, the part broken in pieces flying out of the tube fuse together with the gas so that it cannot be used again. At present, it is considered that only the fiber material is relatively suited for making of the inner arc-extinguishing tube. Therefore, this material is selected for making the arc-extinguishing tube with the epoxy resin cloth wound around it to act as its outer protecting tube so as to increase the strength against mechanical impact. The outer surface of the tube is coated with moisture-proof insulation lacquer. However, the greatest disadvantage of the fiber material is that it is likely to be deformed when absorbing moisture. To combat this drawback, we have designed a fuse tube construction with its top end closed under normal operating conditions to keep rain from getting into the tube directly. It has been proved that the construction in which the top end is closed and step-by-step gas discharge is adopted is successful thus avoiding completely the disadvantages of the fiber.

When the arc-extinguishing material has been selected, another key issue is how to determine the size of the fiber inner arc-extinguishing tube in the fuse tube in order to satisfy the demands of the large and small interrupting short-circuit and overload currents. As in the fuse tube, the arc is extinguished by generating

the gas from the inner arc-extinguishing tube, it is clear that, if a larger internal diameter is chosen, the pressure will be moderate when making and breaking the rated interrupting current. However, when making and breaking a small over-load current, the gas will not be generated enough to extinguish the arc because the internal diameter of the arc-extinguishing tube is too large resulting in an insufficient amount of the gas generated. When a smaller internal diameter is chosen, a sufficient amount of gas will be generated when making and breaking small currents, but there can be cases when an explosion occurs because, when making and breaking the rated interrupting current, the amount of the gas generated is too large and the pressure in the tube is too high so that the fuse tube fails to withstand such a high pressure. As up to now there has been no formula for determining accurately the size of the arc-extinguishing tube, it is mandatory to determine the suitable size of the arc-extinguishing tube through the interrupting tests of research nature. As far as the fuses for different voltage ratings and rated interrupting currents, the size of the arc-extinguishing tubes is different from other. Through a lot of tests and research, we have determined the sizes of the arc-extinguishing tube of the fuses for various specifications for the rated voltage of 11.5-40.5 KV, rated current of 100 and 200 A and rated interrupting currents of 6.3, 8, 10, 12.5 KA. Valuable experimental data have been obtained from hundreds of interrupting tests for various current ratings and relatively deeper understanding has been gained concerning varied factors affecting the interrupting properties. It has been found from the tests that only depending on the suitable selection of the tube material and size, is it still not possible to meet the demands for the fuse tube with the same size to make and break both large and small short-circuit currents. To overcome this difficulty, it is necessary to take steps with regard to the construction of the fuse tube. Furthermore, supplementary technical measures for arc-extinguishing should be taken. This is the second and third problems we are going to discuss in the following.

## 2. Influence of the Fuse Tube Construction

The fuse tube we have designed is one of the step-by-step gas discharge construction (see Fig. 1), where the button-type fuselink is employed (see Fig. 2). The fuselink is inserted from one end and the button is pressed by the pressure-releasing piece at the top. When tightening the pressure-releasing cap, the fuselink button will be pressed against the moving contact to ensure a good and stable contact of the fuselink button and the low temperature rise. During the designing, attention has been paid to making suitable selection of the material, size and thickness of the pressure-releasing piece and the choice of the parts such as pressure-releasing caps etc. to make them suit the following requirements:

1) When the interrupting current is 30% less than the rated interrupting current value, the pressure-releasing piece will not be actuated and the tube discharges gas downwards in the one-way manner so as to keep comparatively high pressure within the fuse tube beneficial for extinguishing small short-circuit and over-load currents.

2) When the interrupting current is 30% larger than the rated interrupting current value, the fuse button will shear and break the pressure-releasing piece owing to the action of the pressure in the tube which is relatively great. The button and the pressure-releasing piece will be forced out by the gas current. At this time, the fuse tube discharges gas to both ends so as to enable the high-pressure gas generated under the large short-circuit current to

force out of the fuse tube rapidly, thus reducing the mechanical stress applied to the fuse tube when making and breaking the large currents. When using the step-by-step gas discharge construction, the fuse is enabled to increase its rated interrupting current value and to cut off small currents, thereby expanding the range of the interrupting currents and effectively removing the contradiction of the large and small interrupting currents for the arc-extinguishing apparatuses with self gas generation.

The material, diameter and thickness of the pressure-releasing piece should be determined through the designing and interrupting tests. As far as the fuses for various voltage ratings, rated currents and interrupting currents are concerned, the size is different from each other.

In addition, with the step-by-step gas discharge fuses, the fuse tube and top moving contact should be adhered to each other by using epoxy resin and fastened by riveting. This is a technical key point, as in the interrupting instant, the pressure in the tube acts on the top moving contact through the fuselink button, pressure-releasing piece and cap. The force produced causes the top contact to separate from the fuse tube. If the adhesion is not tight enough, the top moving contact is likely to get away from the top end of the fuse tube and bring about interrupting failure. It is shown in experiments that where the adhesive force between the top moving contact and the fuse tube is concerned, tension tests should be made on the mechanical tester. If a two-tons tension strength can be withstood, there will be no removal phenomenon as mentioned above.

## 3 The Influence of the Size, Position and Installation Manner of the Auxiliary Arc-Extinguishing Tube of the Fuselink.

The construction of the tube fuse with step-by-step gas discharge is conducive to improving the interrupting characteristics. But further steps should be taken to meet the requirements specified in the 4th and 5th interrupting series of the IEC 282-2 standard. We have taken the measure to install an auxiliary small arc-extinguishing tube on the fuse-element. When interrupting a current less than 500A, the small arc-extinguishing tube is mainly used to generate gas for extinguishing the arc and the extinguishing tube in the fuse tube does not produce gas for consumption. When making and breaking the currents larger than 500 A, the small auxiliary arc-extinguishing tube will be burst, and the gas generated in the arc-extinguishing tube will be used for extinguishing the arc. In this case, the small auxiliary arc-extinguishing tube will be broken into pieces and removed out of the fuse tube together with the gas without affecting the rated interrupting currents.

Grouped contrast experiments have been performed in connection with such factors as the material, diameter, wall thickness, and length of the small auxiliary arc-extinguishing tube, the change of the behaviors over the long period of heating of the fuse-element, the manner and location of the installation on the fuse tube, etc. The analyses can be given as follows:

1) Material: As far as the material of the small auxiliary arc-extinguishing tube is concerned, it is required that it produce sufficient amount of gas under the action of the interrupting current less than 500 A so as to be helpful to the extinguishing of small currents. Under the action of large short-circuit currents, it should be broken quickly into pieces without blocking the gas-discharging passage.

During the normal operation, under the action of high temperature, it should not be aged and deteriorated. In addition it should be low in cost and easy in machining.

In the contrast experiments by using materials such as plexiglass, fiber, raw cotton paper soaked with specially prepared arc-extinguishing solution, etc., we have found that the last material is better than the first two materials. Therefore it is employed for the purpose.

2) Size: As the internal diameter of the small auxiliary arc-extinguishing tube is limited by the external diameter of the copper hoop of the fuselink, it should be 1 mm larger. In this way, the copper loop can move freely in the tube. When extinguishing the current that is 2.7-3.3 times fuse link rating, the small arc-extinguishing tube will stay basically unaffected and when the fuse-element is blown out, the fuse tube will drop properly. If the internal diameter is too small, it will be seized between the two copper hoops of the fuselink so that, after the blowing-out of the fuselink, the fuse tube cannot drop because the small auxiliary arc-extinguishing tube is seized between the two copper hoops. The external diameter of the small auxiliary arc-extinguishing tube should be 2 mm smaller than the internal diameter of the arc-extinguishing tube. In this way, when making and breaking the rated interrupting current, there will be smooth gas discharge. Otherwise, because of the blockage of the gas discharge, there will be fuse tube explosion, or because of the weak perpendicular blowing of the arc, the arc will get out to continue burning as it is blocked in the tube thus leading to the flash along the outer surface of the fuse tube and failing in extinguishing the arc. It is confirmed through experiments that it is desirable to adopt the wall thickness of 1 mm for the small auxiliary arc-extinguishing tube.



Fig. 1. The step-by-step gas discharge construction of fuse tube.

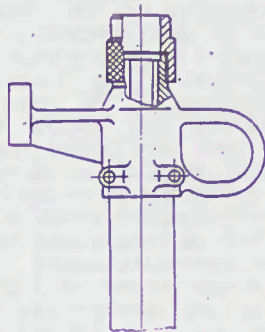


Fig. 2. The bottom-type fuselink.

The installation position of the small auxiliary arc-extinguishing tube has an important impact on the arc-extinguishing behaviors. The top end of the small auxiliary arc-extinguishing tube should be fitted closely with the fuselink button so that, when extinguishing the small current, the gas generated will not leak and discharge along the lower end of the small tube to blow the arc in a perpendicular way. In Fig 3 are shown the oscillograms of the 40.5 KV fuse when interrupting the current of 500 A. On the top diagram, as there is a seam between the top end and the fuselink button, when extinguishing the 500-A current, the interrupting fails because the gas generated leaks along the seam. With other conditions unchanged, the mere replacement of the small extinguishing arc-extinguishing tube which is closely fitted to the fuselink button, the interrupting of 500 A current is cleared smoothly (see lower diagram). The length of the small auxiliary arc-extinguishing tube increases with the rise of the rated voltage of the fuse. It has also been found during the interrupting experiments that, on account of the rise of the rated voltage of the fuse, the successful step for extinguishing the small 11.5 KV current fails to function on the 40.5 KV fuse. Clearly, various measures for extinguishing small currents should be taken to fuses with different voltage ratings.

In the experiments it has also been found that that torsion force for the lower fuse to send forth the plate spring also has an impact on the interrupting of the small current. Under its action, the fuselink, after blowing out, will be pushed down rapidly, the speed being particularly sensitive to the interrupting of small currents. The torsion force of the spring has an influence on the time-current characteristics of fuselinks. A suitable torsion force of the spring which is determined through experiments is not only helpful to the interrupting of small currents, but has no influence on the time-current characteristics of fuselinks as well.

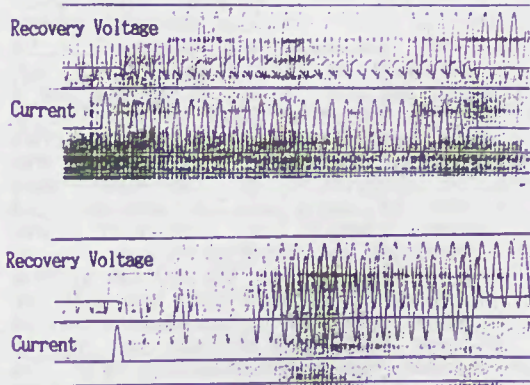


Fig. 3. The oscillograms of the 40.5 KV fuse when interrupting the current of 500 A.

#### 4. The Influence of the Position of the Fuse-element In the Fuse Tube

The position of the fuse-element in the fuse has an importance influence on the interrupting behaviors. As far the fuse with single end discharge of gas used abroad is concerned, the fuse-element is close to the buttonhead. Hence, after the fuse-element is blown out, the arc is produced and the gas generated in the arc-extinguishing tube under the action of the arc blows down and in a perpendicularly manner along the tube, which

is conducive to the extinguishing of the arc. The fuse tube designed by us is of the type of step-by step discharge of gas. As a result, the fuse-element is not located close to the buttonhead. If the fuse-element is still close to the buttonhead, the gas generated after the blowing-out will quickly break the pressure-releasing piece and get out of the fuse tube, which is not helpful to the perpendicular blowing and cooling of the arc and often makes the arc get out of the fuse tube and continue the burning. Such a phenomenon has been confirmed through a lot of interrupting experiments. If the fuse-element is situated in the middle position, the arrangement is not good for extinguishing small currents. It has been verified that good results can be obtained when the fuse-element is located at the top end away from the button to some extent. Such a treatment is helpful to the interrupting of both large and small currents. However, the location for 11.5-40.5 KV fuses with various voltage ratings should be different from each other and no identical distance can be used.

### 5. The Influence of the Other Factors

When large short-circuit currents are interrupted in the fuse tube, the incandescent gas injected out of the top and lower ends of the fuse tube, the length of the visible light observed by the unaided eye is about 0.3-0.4 m, the top opening being shorter than the lower one and the diameter of the injected gas being 0.2-0.3 m. The injected gas looks like a flame. When the high-speed camera is used to take pictures, the injected gas at high speed from the middle is as long as 1-2 m. In the gas, there are a lot of evaporated metal particles which are produced through the gasification of the melting fuse-element and the tail lead of the fuselink under the action of high temperature of the arc. The length varies with the period of the AC current. It is also dependent on the voltage and interrupting current. This incandescent gas which includes metal vapor will be reflected when meeting an obstacle. As a result, at the top and lower ends, there should be no obstacles within the above mentioned scope. Otherwise, when the gas current injects on to the obstacle, there will be counter injection from it with the result that the outer surface of the fuse tube is coated with a thin metal layer full of a lot of copper vapor, leading to a flash on the outer surface of the fuse tube and re-burning. Therefore, when designing the construction of the fuse, steps must be taken to avoid such a problem. The above factors should be considered when testing, installing and operating the fuse. It has been found through the data analysis of a large number of interrupting experiments that with the 11.5 KV fuse, there cannot be any obstacle in the space 2m away from the top and lower end openings and the distance from the lower end opening of the fuse tube to the ground and other parts such as the support and the case cover of the transformer should be more than 2 m, the distance between two phases should be greater than 0.6 m. With the 40.5 KV fuse, the corresponding distance should be above 3 m and the distance between two phases should also be more than 1 m accordingly.

### III The Development of the new type 11.5-40.5 KV Expulsion Fuse

Based on the experiments and investigation of the factors affecting the behaviors of the fuse, we have developed the 11.5-40.5 KV fuses the main technical data of which are shown in Table. 1. The type test of the fuses is done in accordance with the IEC 282-2 standard. Among the new fuses, the RW11-12/100-8 type fuse was tested both in China and the "KEMA" Test Station in Holland resulting in interrupting

successfully the 8 KA rated interrupting current (symmetrical) and the 17 A minimum interrupting current. The RW11-12/100-8 type fuse has found wide application in China. The 15 and 27 KV fuses were developed chiefly for meeting the demands of export.

In order to implement the electrification of the rural areas in China, a model plan of the rural substation has been determined as shown in Fig. 4. According to the plan, 40.5 KV fuses will be used in great numbers on the HV side of the 35 KV substations for protecting the transformer from short-circuiting and over-loading. The fuse to be used every year will amount to about 10,000.

Table 1 Technical Parameters of 11.5--40.5 Fuses

Voltage Rating (kV)	Current Rating (A)	Interrupting Ratings (rms amps sym)
12	100	8000
12	200	12500
15	100	10000
27	100	8000
40.5	100	6300
40.5	200	8000

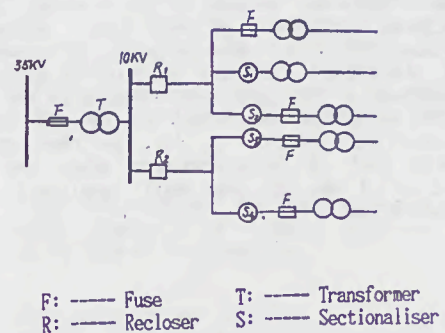


Fig 4. A model plan of the rural substation.

### IV A Few Suggestions

Through a great number of interrupting tests, numerous valuable data have been provided for developing new products and at the same time significant information has been accumulated for the revision of the testing standard of "Expulsion and Similar Fuses". It has been confirmed through hundreds of interrupting tests that in accordance with the related regulations for the interrupting tests specified in the IEC 282-2 standard, a fuse must pass 5 series of interrupting tests among which, as far as the first series for testing the rated interrupting current is concerned, the three interrupting tests for installing the fuselink for the minimum rated current are more severe than the three interrupting tests for installing the fuselink for the maximum rated current and accordingly the consumption of the inner arc-extinguishing tube in the fuse tube is larger. This is because under the condition of the same rated interrupting current I, the fuselink for the minimum rated current is blown out earlier than that for the maximum rated current, thus generating the arc. As the tail lead of the fuselink for the small rated current is small in diameter, light in mass and low in heat capacity, under the action of the arc, the section of the tail lead burned out is long; there is a long distance of the arc between the two tail leads; there is a large area of contact between the arc-

extinguishing tube and arc; there is a large amount of gas generated and high pressure in the fuse tube. Especially, when a new tube does interrupting for the first time, and the making angle after voltage zero is  $-5$  to  $+15$  (at this time the non-periodical component is maximum) the strength of the fuse tube undergoes the most severe examination. It has been confirmed through the statistical data of hundreds of interrupting tests that during the three interrupting tests for installing the fuselink for the minimum rated current, the consumption of the inner arc-extinguishing tube in the fuse tube is 50% larger than that for the three interrupting tests for installing the fuse for the maximum rated current. The RW 11-12/100-8 type fuses were used at the same time; it shows that after the three interrupting tests for installing the 100 A fuselink; the internal diameter of the arc-extinguishing tube increased from 13mm to 14.5mm and that after the three interrupting tests for installing the 5A fuselink, the internal diameter of the arc-extinguishing tube increased from 13mm to 15.3mm. The above conclusion is the same for the arc-extinguishing tubes made of different materials and those made with the same material but produced by different manufacturers. Thus we hold that for the first series of interrupting tests, it is only necessary to make the three interrupting tests for the minimum rated fuselink or to conduct two tests for the minimum rated fuselink and one test for the maximum rated fuselink.

In the four interrupting tests for the second series for 0.7 to 0.8 I (there are two tests for the fuselink for the maximum and minimum currents respectively), the consumption of the fuse tube is still larger than that for the three interrupting tests for installing

the fuselink for the minimum rated current so that the test of the electric life of the fuse tube is more severe than the first series. We made several rounds of interrupting tests of fuses. In the first series, the three tests for installing the maximum and minimum rated currents fuselinks respectively all cleared, but in the four tests for the second series of 0.7 - 0.8 I, the first three succeeded in interrupting, whereas the fourth test failed because the diameter of the fuse tube was increased so that the amount of gas generated was not enough. It has also been found in the tests that in the second series of tests, if two tests for installing the fuselink for the maximum rated current was done first and then the two tests for installing the fuselink for the minimum rated current, it was easy to pass the tests. On the contrary, if the two tests for installing the fuselink for the minimum rated current were done first and then the two tests for the maximum fuselink were done, the tests might not be passed. This is due to the fact that when doing the two tests for installing the maximum fuselink, the consumption of the internal diameter of the arc-extinguishing tube is small; when the minimum fuselink is installed, the internal diameter of the arc extinguishing tube has been increased so that the amount of gas generated and the consumption are less than when doing the test for installing the small fuselink in the new tube but larger than when conducting the test for installing large fuselink; thus the test can be passed successfully. Therefore it is to be suggested that the order for the tests of the second series should be specified clearly as follows: two tests for installing the minimum fuselink and then two tests for installing the maximum fuselink.

Table 2

Parameters	Class	Test series				
		Series 1	Series 2	Series 3	Series 4	Series 5
Power-frequency recovery voltage	1 and 2	Rated voltage $+5\%$ $-0\%$				
Natural frequency of transient recovery voltage (See Note 3)	1	Column (B) of Table IVB			Under consideration	Not applicable
	2	Column (A) of Table IVB				
Amplitude factor (See Note 3)	1	From 1.4 to 1.5			From 0.3 to 0.5	From 0.6 to 0.8
	2	From 1.3 to 1.4				
R.M.S. symmetrical value of prospective current	1 and 2	$I \pm 5\%$ $0\%$	From 0.7 I to 0.8 I	From 0.2 I to 0.3 I	From 400 A to 500 A (1) (2)	From 2.7 $I_n$ to 3.3 $I_n$ with a minimum of 15 A (1)
Power-factor	1	Lower than 0.10			From 0.3 to 0.5	From 0.6 to 0.8
	2	Lower than 0.15			From 0.3 to 0.5	From 0.6 to 0.8
Making angle related to voltage zero (degrees)	1 and 2	1st test: $-5$ to $+15$ 2nd test: 85 to 105 3rd test: 130 to 150	1st test: $-5$ to $+15$ 2nd test: 85 to 105	For all tests, from 85 to 105	Random timing	
Current rating of fuse-links	1 and 2	Min.    Max.	Min.    Max.	Min.    Max.	Min.	Min.
Number of tests	1 and 2	1    1	1    1	1    1	2	2
Number of fuse-links to be tested for each fuse-carrier	1 and 2	4		2		4

Notes 1. -- If the test involves an operating time appreciably higher than 2 s, the test shall be made with a higher current to obtain an operating time of approximately 2 s.

2. -- If the values are lower than those of series 5, test series 5 need not be made.

3. -- It is expected that service natural frequencies and amplitude factors will usually not exceed the specified values.

In order to reduce the number of tests without lowering the demands for the comprehensive examination of the interrupting behaviors of the fuse, it is to be suggested that the current value, testing order and the number of tests for the interrupting tests for the first and second series should be revised again by the working group for the IEC fuse standard.

It has been found through tests that the fuses which had succeeded in passing the interrupting tests of the first and second series were all able to succeed in passing the tests for the third series for 0.2 - 0.3 I. Since the interrupting testing current value in the third series, is not the critical interrupting current value for the expulsion fuse, it is suggested that in order to reduce the number of interrupting tests the regulations for the tests in the third series should be removed or at least that with the fuse products which have passed all the type tests and finalized the design, the tests for the third series be not needed when the same product is reproduced in a second manufacturer by using the same drawings, technologies and materials.

The purpose of the interrupting tests for the fourth and fifth series is to examine the ability of the fuse to interrupt small accident currents and overload currents. This requirement is indispensable. It is mandatory to conduct the tests for the fourth and fifth series when testing the newly-developed fuses. It has been confirmed from our tests that as the interrupting test for these two series aim mainly at testing the arc-extinguishing behaviors of the auxiliary arc-extinguishing tube, and the inner arc-extinguishing tube in the fuse tube does not act at this time, all the fuses which have succeeded in passing all the interrupting type tests and finalized in the design are able to succeed in passing the interrupting tests for the fourth and fifth series when they are produced by a second manufacturer through the use of the same drawings, technologies and materials. We have done six contrast tests like this fully indicating that when the material, construction, size and installation manner for the small auxiliary arc-extinguishing tube of the fuselink are the same, the products are able to pass the interrupting tests for the fourth and fifth series successfully without any exception. Therefore we should like to suggest that when a second manufacturer makes repeated product, the tests for the fourth and fifth series should not be done.

From hundreds of interrupting tests and investigations and through the analysis of the data of the grouped contrast tests it is concluded that under the condition of ensuring the full and reasonable testing of the interrupting behaviors of the expulsion fuses, it is required to reduce as much as possible the number of unnecessary tests. We should like to make the following suggestions (Table 2) for providing some references for the working group for drafting the IEC fuse standard and revising the IEC 282-2 "expulsion and similar fuses" standard.

## ENDURANCE OF SEMICONDUCTOR FUSES UNDER CYCLIC LOADING

R. Wilkins  
Consultant  
Heswall, UK

and

A. Wilkinson, C. Cline  
Gould Shawmut  
Newburyport, USA

### Summary

Current practice in selecting fuses for pulsed and cyclic loading duty is reviewed, and improved methods of selection are proposed, based upon the use of new thermal modelling methods and computer predictions of the temperature distribution within the fuse. Combination of the thermal predictions with a simple metal-fatigue model allows the prediction of life curves for arbitrary duty cycles. Each fuse can be characterised by a single factor which represents its ability to withstand cycling.

### List of principal symbols

$C_b$  natural convection loss constant  
 $C_i$  thermal capacity of subvolume  $i$ ,  $J/deg C$   
 $D$  effective diameter for convection loss,  $m$   
 $h$  surface power loss coefficient  $W/m^2/deg C$   
 $K$  fuse fatigue constant  
 $m, x$  exponents in fatigue equation  
 $N$  number of cycles to fatigue failure  
 $n$  time step index  
 $P_{oi}$  "cold" value of  $P_i$   
 $P_i$  Joulean heating power in subvolume  $i$ ,  $W$   
 $R_c$  thermal resistance (transient heat storage)  
 $R_{ik}$  intervolum thermal resistance,  $deg C/W$   
 $[G]$  thermal admittance matrix  
 $[q]$  vector of power terms  
 $[\theta]$  vector of subvolume temperature rises  
 $\alpha$  temperature coefficient of resistivity,  $deg C^{-1}$   
 $\beta$  lateral strain deflection factor  
 $\gamma$  coefficient of linear expansion  $deg C^{-1}$   
 $\Delta t$  integration time step  
 $\Delta \theta$  p/p temperature fluctuation at hotspot,  $deg C$   
 $\Delta \epsilon$  maximum p/p strain fluctuation at hotspot  
 $\epsilon_b$  surface emissivity  
 $\epsilon$  total strain  
 $\sigma$  Stefan-Boltzmann constant  
 $\theta_{av}$  average element temperature at hotspot,  $deg C$   
 $\theta_i$  temperature rise of subvolume  $i$ ,  $deg C$

### 1. Introduction

Fuses are usually rated for continuous current duty, but fuses for the protection of power semiconductors usually carry a current which is not continuous, and selection of the correct fuse for a given application can only be made after the effects of pulsed and cyclic overloads [1] have been considered. Fuse standards usually require some tests to ensure that fuses have, in general, adequate ability to withstand pulsed and cyclic overloads, but very often the actual service duty is different from that which was used in the standard tests. In these cases recourse is usually made to "rules-of-thumb" in order to select the correct fuselink.

Computer simulation of cyclic loading behaviour requires large-scale modelling because of the need to follow both short-duration and long-duration transients. An approach to this is described which uses finite-difference methods formulated in terms of the RC-network analogue and solved using sparse matrix methods with ordered elimination. Reliable methods of dealing with the non-linear boundary conditions are also given.

The construction of a typical fuse for the protection of semiconductors is illustrated in Fig.1. There are one or more silver or copper notched elements, with no M-effect, within a sand-filled cartridge. Problems of long-term ageing due to the use of M-effect [2] require a separate approach, and are not considered here.

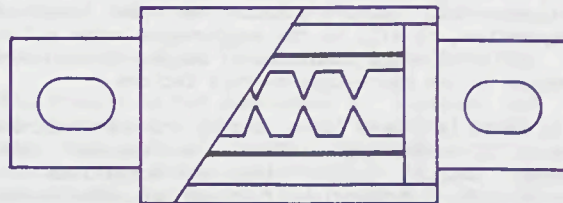


Fig. 1 Typical semiconductor-protection fuse

### 2. Rules-of-thumb for fuse selection

The first type of overload to be considered is the non-repetitive pulsed overload, or "occasional" overload [1]. This occurs only a few times during the service life of the fuse. Manufacturers usually recommend the selection of a fuse such that the current during the pulse does not exceed say 75% of the current which would cause operation of the fuse in a time equal to the duration of the pulse, according to the fuse's time-current characteristic. In fact, the fundamental requirement should be that the maximum temperature of the fuse element should not exceed a certain level, and this is not guaranteed by use of a fixed percentage-current value. Some of the difficulties which can arise by using a fixed percentage-current have been pointed out by Newbery [3], and often in practice the percentage allowed is varied in the light of experience for different fuse designs and overload conditions.

The second type of duty to be considered is the repetitive or cyclic load. Fuse selection in these cases is usually made on the basis that

- (a) the r.m.s. value of the current over the whole cycle is below the rated fuse current, and
- (b) if a sliding time-window of width  $T$  is moved across the fuse current waveshape, the r.m.s. current over the time  $T$  must not exceed a certain percentage of the current to produce melting in a time  $T$ , according to the time-current characteristic, and this must be true for all values of  $T$ .

In this case the percentage current allowed is significantly lower than for occasional overloads, typically 50% or less according to the fuse design and the nature of the load cycle. The relationship between the percentage current and the physical phenomena which may cause fuse deterioration in this case is much less clear. It is necessary to ensure

that the peak temperature reached by the fuse-element during cycling does not exceed a certain level - a condition similar to that required for a single pulse. However, a more important requirement is to guard against mechanical fatigue. Semiconductor-protection fuses necessarily have very narrow notch zones, and repeated heating and cooling can give rise to fatigue failures if the temperature excursions during cycling are too high [4]. This is a thermo-mechanical process which is only indirectly related to the time-current characteristic.

It is possible to produce cyclic load withstand characteristics giving the number of cycles to failure as a function of current for fuses under given loading conditions and use these to predict the expected life [1], but it is difficult to modify these characteristics for different duty cycles. Furthermore extensive testing is required to evaluate each new fuse design if this approach is used.

Just as the continuous current rating is affected by environmental factors such as the ambient temperature, so will be the performance under pulsed or cyclic loading conditions, making it even more complex to use percentage-current factors.

Thus there is a need for a simpler and more accurate method of assessing a fuse's performance under pulsed and/or cyclic loading conditions. A prerequisite for this is a fast and accurate method of calculating the steady-state and transient temperature distributions within the fuse. A method for doing this is described in the next section.

### 3. Computer modelling of fuse thermal behaviour

The simplest model of fuse thermal behaviour is that it can be represented by a fixed thermal impedance and a single thermal time-constant. Whilst this may be useful for investigating general trends [5],[6] it is not sufficiently accurate for our purpose. When a real fuse is heated, there are very fast thermal responses, in the sub-millisecond region, associated with the notch zones. These are followed by phenomena in the 0.1-1s region, associated with transient losses from element to filler; in the 1-10s region, associated with heat loss along the elements to the ends; followed by the much slower responses, over half an hour or longer, of the bulk of the fuse filler, the body, and the connecting cables. A single time-constant is not sufficient to model all these phenomena.

For accurate calculations it is necessary to use numerical solution methods based upon finite-differences or finite-elements [7],[8],[9], but the application of these methods is not straightforward. The set of equations which results from the application of these methods is non-linear, because of the nature of the convective and radiative heat-loss from the fuse body, endcaps and cables to the surrounding medium. If iterative methods are used to solve these equations convergence is frequently impossible [10], and recent work has shown that for transient studies, iterative methods can fail even if the equations are forcibly linearised. For some studies, simplifying assumptions can be made (e.g. neglect of heat loss to the filler for short-times), but in the case of cyclic loading there are very few simplifications that can be made. Heat transfer through the whole fuse to the surroundings needs to be calculated to determine the background temperature distribution, upon which fluctuations are superimposed due to the cycling. To model these fluctuations accurately, the transient losses to the filler near to the element need to be calculated [11], requiring a large number of nodes in this region of space,

together with a model of the notch zones with sufficient resolution to follow the rapid temperature transients in these zones. The net result of these requirements is that a model with around 10,000 nodes is needed, and since iterative solution methods cannot be used, it is essential to exploit the sparsity [12] of the system of equations.

#### 3.1 General method

The method described here is fundamentally a finite-difference method but there are considerable practical advantages in formulating this in terms of an equivalent RC network analogue [13]. The fuse and its connecting cables are divided into subvolumes, and a typical subvolume is shown in Fig.2. The power balance equation for subvolume  $i$  is

$$C_i \frac{d\theta_i}{dt} = P_i + \sum_k \frac{\theta_i - \theta_k}{R_{ik}} \quad (1)$$

By this process the partial differential equation governing the flow of heat has been reduced to a set of (non-linear) ordinary differential equations [14]. Since the inherent time-constants within the system vary so widely, the set of equations is "stiff" [14]. Open-type integration schemes such as the Runge-Kutta methods are not suitable, as the integration time step is restricted by the shortest time constant in the system. In the case of fuses this requires time-steps of the order of tens of microseconds, giving impossibly long computing times. For stiff systems implicit methods are best, since the methods are stable regardless of the time-step chosen. Trapezoidal-rule integration [15] is one popular method, and this can easily be shown to be exactly equivalent to the Crank-Nicholson method, applied to the original PDE. The Crank-Nicholson method has previously been applied with success in fuse studies [8], but experience with the method applied to cyclic loading studies has given some problems. A flexible and robust solution method requires the integration time step to be altered dynamically during solution, but with the Crank-Nicholson method this can generate oscillations in the numerical solutions which decay only very slowly. These oscillations are well-documented [14]. Experience shows that the fully-implicit method is better for general-purpose use. Although the truncation errors are higher than the Crank-Nicholson method they can be easily controlled. The implicit method is unconditionally stable for all values of the time-step, and no oscillations occur, even for very large changes of time-step.

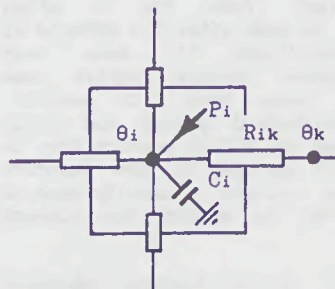


Fig. 2 Typical subvolume

For insulating materials the power generated within each subvolume is zero. For conductors the Joulean heating term  $P_i$  can be represented as  $P_{0i}(1 + \alpha\theta_i)$  where  $P_{0i}$  is the power generation if the subvolume were at ambient temperature (the "cold" power). Applying now the implicit approximation to the time derivative in (1) we obtain

$$C_i \frac{\theta_i^{n+1} - \theta_i^n}{\Delta t} = P_{oi}^{n+1} (1 + \alpha \theta_i^{n+1}) + \sum_k \frac{\theta_i^{n+1} - \theta_k^{n+1}}{R_{ik}} \quad (2)$$

Rearranging now so that all unknown temperature rises are on the left-hand side,

$$-\sum_k \frac{\theta_k^{n+1}}{R_{ik}} + \left[ \sum_k \frac{1}{R_{ik}} + \frac{1}{R_{ci}} - \alpha P_{oi}^{n+1} \right] \theta_i^{n+1} = P_{oi}^{n+1} + \frac{\theta_i^n}{R_{ci}} \quad (3)$$

where  $R_{ci} = \Delta t / C_i$ . If this equation is written for each subvolume we obtain the matrix equation

$$[G][\theta] = [q] \quad (4)$$

which has to be solved at each time step to give the new subvolume temperature rises  $[\theta]$ .  $[G]$  is the thermal admittance matrix, which can easily be assembled from a list of thermal resistances and capacitances. Each off-diagonal element  $G_{ij}$  is minus the thermal admittance connecting node  $i$  to node  $j$ . Each diagonal element  $G_{ii}$  is the sum of all admittances terminating on node  $i$ , plus a thermal capacitance term  $1/R_{ci}$  minus a term  $\alpha P_{oi}$  which allows for the temperature coefficient of resistivity. It has been assumed that the generated power at time  $(n+1)\Delta t$  is a known quantity. This means that in cases where the circuit current is time-varying, the new current needs to be calculated before (4) is solved for the new temperature rises.

Software has been developed to automatically generate the subvolumes, thermal resistances and capacitances for a design such as that shown in Fig.1, in such a way that the subvolumes are concentrated in the regions where the temperature gradients are highest, e.g. around the notch zones and in the filler near to the element. This procedure reduces the truncation errors in the replacement of partial space derivatives by a network of thermal resistances. The power generation in the subvolumes is found by a separate field solution for the electrical current-density distribution, using methods based upon those which have been described previously [8], but extended for other element profiles.

### 3.2 Boundary conditions

For subvolumes on the interface with the surrounding ambient air, a thermal resistance needs to be included in the heat loss path from the subvolume to the ambient (reference) node, to allow for the loss of heat by natural convection and radiation. The surface heat transfer coefficient [13] is given by

$$h = C_b(\theta/D)^{0.25} + \epsilon_b \sigma \left[ (\theta + T_a)^2 + T_a^2 \right] (\theta + 2T_a) \quad (5)$$

where  $T_a$  is the ambient temperature in K. A first estimate of the convection coefficient  $C$  can be obtained from standard data for the loss from horizontal or vertical cylinders of diameter  $D$ , but fine tuning of the model requires adjustment of  $C$  for each particular fuse design.

If the surface area presented to the ambient by the boundary subvolume is  $A$  the required thermal resistance in the heat loss path is  $1/(hA)$ . This is a non-linear function of temperature, and so  $[G]$  is a (weakly) non-linear function of  $[\theta]$ .

### 3.3 Steady-state temperature distribution

If the thermal capacitance terms in (3) are omitted (or an infinitely large time step is chosen) the steady-state temperature distribution is obtained, by a single solution of (4). In this case the non-linear boundary conditions must be correctly modelled, since in the steady-state the whole of the heat generated within fuse and cables is balanced by the total heat losses from their surfaces, so accurate assessment of these losses is crucial. In order to assemble  $[G]$  some estimate of the temperature vector  $[\theta]$  is needed since the external thermal resistances are functions of  $[\theta]$ . The following iterative refinement procedure has been found suitable for solution of this problem.

1. Assume an initial set of temperature rises  $[\theta]$
2. Assemble  $[G]$ . Solve for the temperatures  $[\theta]^{new}$
3. Calculate the vector  $[\Delta\theta] = [\theta]^{new} - [\theta]^{old}$
4. Adjust temperatures using  $[\theta]^{adj} = [\theta]^{old} + u [\Delta\theta]$
5. Go to step 2 and repeat until converged

This process is not guaranteed to converge but it has been found to do so in all practical cases if a very high set of initial temperatures is used together with under-relaxation ( $u < 1$ ). In this way convergence can be obtained in about 20 iterations, provided that the applied current is below the thermal runaway current.

### 3.4 Computation of minimum fusing current

It is frequently important to know the steady-state current which will just cause melting of the fuse (i.e. operation in an infinite time). This can be done by successive calls to the steady temperature calculation routine, with increasing current, until the melting point is straddled, final convergence towards the m.f.c. being achieved using the secant method [16].

### 3.5 Transient temperature response

When using the method described in section 3.1 to compute the transient temperature response, the main problem is that of coping with those thermal resistors which are non-linear functions of  $\theta$ . One possible method may be termed the "time-lag" method [15], in which the temperatures at the previous time-step are used to calculate the resistors and hence in the assembly of  $[G]$ . This method is effectively an explicit method, and is only stable if small time steps are used. Experience has shown that it is not suitable for a general purpose program in which freedom to vary the time step without instability is required, to avoid impossibly long computing times.

A much better solution is to linearise the problem by replacing the non-linear resistors by fixed resistors, the values of which are calculated at some appropriate quiescent point. In the modelling of fuse behaviour there are two important situations in which this need arises, which can be dealt with as follows.

- (a) for the calculation of the time-current characteristic, and the response to a single pulse, a preliminary computation of the minimum fusing current is made and the resistors are then fixed at the values obtained at the end of this procedure. This means that when these values are used, the computed long-time end of the time-current characteristic will tend to the correct m.f.c. For shorter times the thermal

resistances external to the fuse and cables play little part in determining the melting time, and so their actual values are not significant.

- (b) for cyclic loading studies, the steady-state temperature rises are calculated using the r.m.s. value of the complete wave to obtain a quiescent temperature distribution, from which a set of external thermal resistors is derived. These are then fixed for the subsequent calculation of the superimposed fluctuations due to cycling.

### 3.6 Sparsity of [G] and solution methods

[G] is a network admittance matrix, and is symmetric, and sparse, the vast majority of entries being zero. Solution of (4) for the temperatures for models with sizes of the order of 10000 nodes cannot be achieved without exploiting the properties of [G] using sparse matrix technology [12], and ordered elimination to minimise the number of non-zero elements generated during solution. Provided that the negative term in the diagonal elements of [G] does not dominate, [G] is also a positive-definite matrix, and can be factorised into sparse upper triangular form, solution for the temperatures then being obtained by forward- and back-substitution. This factorisation process only needs to be repeated during solution if a change in time-step occurs. For transient studies with high currents it is possible that too large a time step could result in [G] not being positive definite, so if factorisation fails for this reason the time-step is progressively reduced until computation can continue.

### 3.7 Typical results

Fig.3 shows the computed maximum element temperature rise as a function of time for constant-current pulses of four different amplitudes applied to a fuse with a rating of approximately 120A. The temperature-time transients are plotted over a range of more than 6 decades of time, and several time zones can be identified. Also shown is a growth curve such as would be obtained from a model with a single time-constant, which has a constant initial rate-of-rise, with a slope of unity when logarithmic axes are used (curve A).

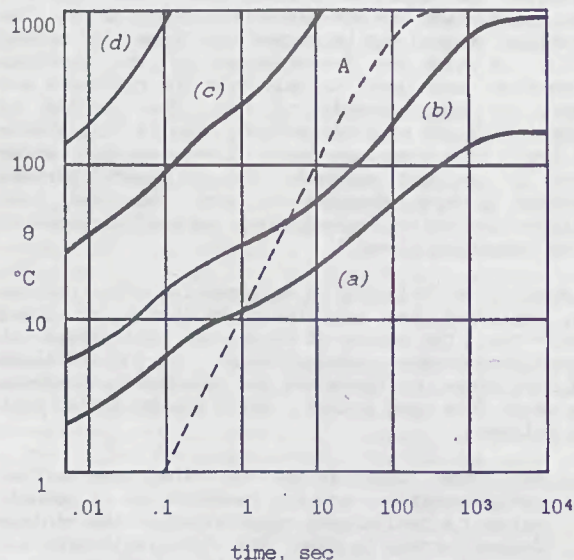


Fig. 3 Element hotspot temperature-rise  
(a) at  $I_n$  (b)  $1.55I_n$  (c)  $3.5I_n$  (d)  $6.8I_n$

For times much less than 0.001 sec (not shown on Fig.3) the computed temperature-rise transients have an initial slope identical to that of curve A. This corresponds to the time zone when truly adiabatic heating of the notch zones is occurring. However, in the 0.01-0.1s time zone the computed rates-of-rise are much lower than curve A, mainly due to the effect of transient heat losses from the element notch zones to the cooler full element sections. In the 0.1-1s time zone the rates-of rise are further reduced because of the very high transient heat loss from element to the adjacent filler, the radial temperature gradients being very steep in this zone. After about 10s the radial gradients fall, the temperature-wave having penetrated by this time to the outside of the fuse body. The rate-of-rise of maximum element temperature then begins to increase noticeably, and the body temperature also begins to rise rapidly. For currents lower than the minimum fusing current, the temperature then continues to rise beyond about 1000s, but at an ever-decreasing rate, until eventual thermal equilibrium is achieved. For high currents which cause melting times less than about 0.1s the effect of the positive temperature-coefficient of resistivity can be clearly seen, as the rate-of-rise of temperature increases monotonically. Fig.3 shows that representation of fuse heating under constant current cannot be achieved by a single time-constant model even over a very limited time-zone, confirming the need for finite-difference or finite-element modelling.



Fig.4 Cyclic loading transient (cold start)

Fig.4 shows the computed maximum element temperature for a repetitive cyclic loading condition of 150A for 1 minute followed by a 2 minute OFF period. Starting from cold, i.e. with all subvolume temperatures initially at ambient, the temperature-rise "ratchets" upwards, with the peak-to-peak excursion in temperature gradually increasing due to the effect of the temperature-coefficient. Automatic adjustment of the time-step during the solution was used to achieve a preset numerical accuracy. Eventually a quasi-stable equilibrium is reached, with constant-amplitude excursions superimposed on a quiescent temperature distribution. The time taken for the stabilisation to be reached will be of the order of thousands of seconds, and if the period of the cycle is short, say 1s ON followed by 1s OFF, the computer time required before stabilisation is excessive. The main purpose of the simulations is to compute the peak-to-peak temperature excursions after stabilisation has been reached, and the computer time needed can be reduced dramatically by using a "hot-start" condition, in which the temperature distribution in the fuse and cables is

set initially to the values obtained from a steady-state solution for a steady current having the same r.m.s. value as the cyclic wave to be applied. Fig.5 shows the case of Fig.4 but with a hot-start condition. Stabilisation occurs within a few cycles, making the estimation of cyclic duty feasible even for very short duty cycles.

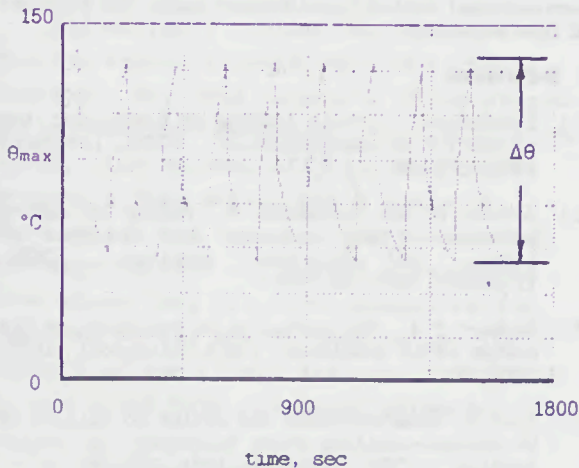


Fig.5 Cyclic loading transient (hot start)

#### 4. Occasional overloads

Using the computational procedure described in the previous section, assessment of the effect of a single pulsed overload is straightforward. Temperature transients like those in Fig.3 are computed and terminated after the duration of the pulse. The maximum temperature reached by the fuse-element is then known, and this must be limited to some predetermined value, based upon the chemical and metallurgical nature of the material used for the element.

Rules-of-thumb based upon the use of a fixed percentage of the melting current imply that the heating curves for different currents are parallel, but Fig.3 shows that this is not so. Studies have shown that for a given fuse, with a pulse amplitude which is a fixed percentage of the melting current for the pulse duration, the maximum temperature rises produced vary by about 10% about an average value, due to the differing magnitudes of the heat losses in the various time zones previously discussed. This suggests that the rule-of-thumb for occasional overloads is quite good for a specific fuse, but there are large variations in the allowable percentage limit for different fuses, depending upon the size of the fuse and its design, so the computational model is much more convenient to use in practice.

#### 5. Assessment of life under cyclic loading

Computation of thermal responses such as those shown in Fig.4 and Fig.5 will show immediately whether the fuse element is likely to melt under the influence of a cyclic loading condition, and will also give the number of cycles which can be tolerated before melting occurs. This is however not very often likely to be a serious practical problem.

More important is the thermal fatigue effect. When the fuse heats up the elements expand considerably more than the fuse body, firstly because the average element temperature is much higher, and secondly because the element material usually has a very much larger expansion coefficient. A thermal stress is set up, which causes the element to deflect laterally, resulting in a thermal strain which

depends upon the temperature-rise [4]. Under the action of cycling the strain fluctuates, following the peak-to-peak temperature fluctuation, and thus has a time-variation which follows the shape of Fig.4.

Non-ferrous metals such as those used for fuse elements have no fatigue limit. If the peak-to-peak strain during cycling is  $\Delta\epsilon$  the number of cycles to failure can be estimated using the relationship [17]

$$\Delta\epsilon = CN^{-m} \quad (6)$$

The exponent  $m$  in (6) varies in the approximate range 0.2-0.5, depending upon the metal and whether the elastic component, plastic component, or the total strain is used. In the case of cycling in fuses we cannot separate the components, so  $\epsilon$  must be interpreted as the total strain (the sum of elastic and plastic deformations).

If we assume that strain is proportional to temperature-rise, the peak-to-peak strain will be given by

$$\Delta\epsilon = \beta\gamma\Delta\theta \quad (7)$$

Here  $\gamma$  is the expansion coefficient and  $\beta$  is a coefficient which relates the actual strain which occurs when the element deflects laterally to the thermal strain  $\gamma\Delta\theta$ .  $\beta$  is thus a measure of the way the mechanical design of the fuse affects its ability to withstand cycling.

Combining (6) and (7), the number of cycles to failure can be related to  $\Delta\theta$ . However the relationship (6) is for strain cycling at a constant temperature. The fatigue strength of silver and copper falls as the average temperature is increased [4]. Over a limited temperature range this can be allowed for by assuming that  $C$  falls with temperature according to a power-law [4], i.e.  $C = \mu\theta_{av}^{-x}$ . This then gives

$$\beta\gamma\Delta\theta = \mu\theta_{av}^{-x} N^{-m} \quad (8)$$

Solving for the number of cycles to failure

$$N = K \left[ \Delta\theta.\theta_{av}^x \right]^{-1/m} \quad (9)$$

Where  $K = [\mu/(\beta\gamma)]^{1/m}$  and is a constant for a given fuse design. The higher the value of  $K$  the better the fuse's ability to withstand cycling.

The relationship (9) has been tested using the results of cyclic loading endurance tests on a number of semiconductor fuses with silver elements, of various designs. For each test the number of cycles to failure  $N$  is known, and the temperature terms  $\Delta\theta$  and  $\theta_{av}$  were found for the given loading condition using the computer model. To achieve higher accuracy in the calculations, the following method was used. First the time-current characteristic for each fuse was obtained using the computer model. The cyclic performance was then computed using ON-state currents which were the same percentage of the computed time-current characteristic as was used in the tests, relative to the actual characteristic. This ensured good accuracy in the temperature values.

Application of multiple regression analysis to the results showed that :

(a) there was, as expected, a strong dependence of  $N$

upon  $\Delta\theta$ . The best-fit value for  $1/m$  was 3.85, giving  $m=0.26$ , which is within the expected range for the fatigue law of equation (6).

- (b) there was a much weaker dependence of  $N$  upon  $\theta_{av}$ . The best-fit value for  $x/m$  was 0.658, giving  $x=0.171$ , which is a measure of the fall in fatigue strength with temperature.
- (c) the values of  $K$  showed a consistent pattern which gave a direct measure of the ability of a given design to withstand cyclic loading.

Fig.6 shows how the life curves for two different fuses conform to equation (9). The test results were obtained using a variety of different duty cycles, but use of the computer model to convert these test conditions to values of  $\Delta\theta$  and  $\theta_{av}$  bring all the results together into a band. There is a scatter in life of about one power of ten, which is typical of fatigue failures, but the general trend is in agreement with the fatigue model of equation (9).

This then gives a quick method of assessing expected life of a fuse under given cyclic loading conditions, or, conversely, of selecting a fuselink for an application to ensure that an acceptable life is achieved.

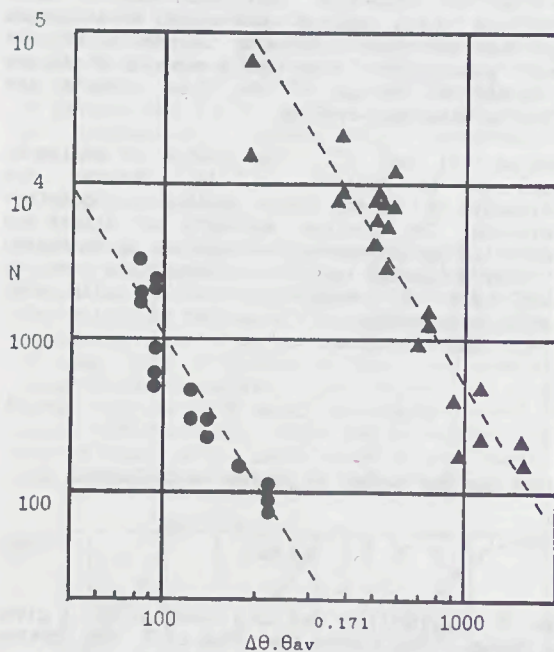


Fig. 6 Typical endurance characteristics

## 6. Conclusions

Simulation of the thermal behaviour of fuses for the protection of semiconductors under pulsed and/or cyclic loading conditions requires a comprehensive finite-difference model with a number of nodes of the order of 10,000 if accurate results are to be obtained from the simulation. The development and testing of such a simulation method has been undertaken, based upon the use of the RC-network analogue, and using sparse matrix methods with ordered elimination to obtain rapid solutions.

From drawings of a fuse design and knowledge of the materials used in its construction and their properties, predictions of the element temperature distributions can be obtained, and used to assess the fuse's suitability for a given application. A simple fatigue model has been developed which enables selection of a fuse to withstand a given

number of cycles.

For straightforward cases, applications engineers will no doubt continue to use the rules-of-thumb for fuse selection when these are known by experience to give good results, but in those special cases which arise so frequently in protection problems involving power semiconductors, the availability of the new computational method considerably eases the problems of fuse selection.

## 7. References

- [1] Stevenson G. Cyclic loading of fuses for the protection of semiconductors. ICEFA, Liverpool 1976, 276-283.
- [2] Hofmann M and Lindmayer M. Fusing and ageing behaviour of fuse elements with M-effect at medium- and long-time overload. ICEFA, Trondheim 1984, 280-296.
- [3] Newbery P.G. The influence of standards on the design of LV fuselinks. ICEFA, Liverpool 1976, 317-326.
- [4] Arai S. Deteriorations and cycles to failure of HV current-limiting fuses subjected to cyclic loading. ICEFA, Trondheim 1984, 252-261.
- [5] Naot Y. How far is an insulated conductor protected by a fuse?, *ibid*, 87-94.
- [6] Brown R. Surge performance of miniature fuses. ICEFA, Eindhoven 1987, 127-131.
- [7] Leach J.G., Newbery P.G., and Wright A. Analysis of high-rupturing-capacity fuselink prearcing phenomena by a finite-difference method. *Proc IEE*, 120(9), 1973, 987-993.
- [8] Wilkins R. and McEwan P.M. AC short-circuit performance of notched fuse elements. *ibid*, 122(3), 1975, 289-292.
- [9] Meng X-Z. and Wang J-M. The simulation of prearcing characteristics of fuse elements in the Finite-Element Method. ICEFA, Eindhoven 1987, 24-29.
- [10] McEwan P.M. Numerical prediction of the pre-arcing performance of h.r.c. fuses. Ph.D. Thesis, Liverpool Polytechnic, 1975.
- [11] McEwan P.M. and Wilkins R. A decoupled method for predicting the time-current characteristics of HRC fuses. ICEFA, Liverpool 1976, 33-41.
- [12] Pissanetzky S. Sparse matrix technology (Academic Press, 1984).
- [13] Sloop J.G.J. Analog simulation of the heat flow in a high voltage fuse. ICEFA, Eindhoven 1987, 7-11.
- [14] Smith G.D. Numerical solution of partial differential equations: finite difference methods. (Oxford University Press, 1985)
- [15] Dommell H.W. and Scott Meyer W. Computation of electromagnetic transients. *Proceedings IEEE*, 62(7), 1974, 983-993.
- [16] Conte S.D. and De Boor C. Elementary numerical analysis. (McGraw-Hill, 1981)
- [17] Frost N.E., Marsh K.J. and Pook L.P. Metal fatigue. (Clarendon Press, 1974)

THE ELECTRICALLY EXPLODING WIRES APPLICATION  
IN THE POWER CIRCUIT BREAKERS.

N. Akhmerov, E. Aziziv, V. Jagnov.

Kurchatov Institute of Atomic Energy, Moscow, USSR.

Abstract.

Pulsed power systems based upon the inductive energy storage require circuit breakers. For this purpose a three-staged-switch has been developed comprising a relatively slow mechanically-driven current breaker, a fuse switch and a resistor. This switch has been designed, assembled and experimented on. Recent experiments have shown that the three-staged-switch operates safely and is able to provide current pulses of all the required shapes in the loads with the broad parameter range.

2. Introduction.

In the large energetic pulsed devices for the switch-off the current or its commutation many-step commutation schemes are preferable. Usually the mechanical contact breakers are used in the scheme for the first step. The combination of thyristors with fuse or an other element with nonlinear property are used for the second and next stages. Similar schemes are discussed for example in [1,2].

In the operation regime the total current is flowing through the contacts of a mechanical key but the next keys have not a current. The commutation process proceeds in some steps: the first- mechanical break of contacts by a fast destruction. As a result, the total current is commutated for some time in the next key ( an example, a shunting wire - "SW"). Then the electrical of the wire happens and the current must be switched-off or commutated to the next electrical chain.

The agreement of two processes for the stable operation in that scheme is necessary: the arc blows out in the first key and the electrical exploding occurs in the wire in the next steps.

The voltage growth rate and the voltage value should be correlated with the media condition in the contact for the recovery of electrical strength.

The key of the second step as a rule is fuse. When the operation current increases one have to make the parallel connection of a similar fuse design.

In our report the operation of the many-step switch-off in the power supply based upon the inductive energy storages discussed.

3. About the commutation process model.

As an example of the three-staged circuit breakers, which is shown in figure 1 the process of commutation is considered.

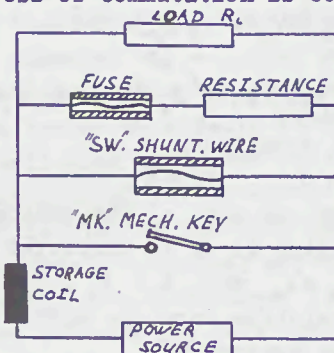


Fig.1. Basic diagram of an inductive energy storage system.

Here, the fuse and the resistor connected seriesly were used as the third key. It is necessary to form the front of the current impulse in the loading (in scheme  $R_L$ ). It is assumed, that initial resistance  $R_{L_0}$  is essentially more than the resistance of the second shunting wire at the moment of explosion, which makes it possible to disregard the loading current in the analysis.

For the contact key the model of the linear increase of the voltage is

$$U_p = Evt = at \quad (1)$$

It's assumed, that "a" doesn't depend on the current value, the scheme inductance and fuse parameters.

The growth of the fuse resistance is defined by a specific energy  $q = Q/m$ , where  $Q = \int_0^t i_s^2 R_s dt$  - total deposite energy in the fuse,  $m$  - wire mass.

the specific deposite energy  $q_t$  and

resistance  $R_t$  are related to the melting point (for the copper wire  $q_t = 0.468$  kJ/g,  $R_t/R_0 = 5.96$ ), for the total melting of wire -  $q_m$  and  $R_m$  and for boiling point  $q_b$  and  $R_b$ .

For the heating stage in the solid state ( $q \leq q_t$ ,  $R_s \leq R_t$ )

$$R_s/R_0 = 1 + (\alpha/C_p) \cdot q = 1 + q/q_1 \quad (2)$$

Where  $-\alpha$  - temperature coefficient of resistance,

$C_p$  - specific heat capacity of metal

$q_1$  - specific energy deposit, when specific resistance doubles.

For the other two stages this coefficient can be written in the form of

$$R_s/R_0 = f(q/q_1) = f(Q/Q_1) \quad (3)$$

where  $Q_1 = q_1 \cdot m$ .

The current commutation from MK to SW is described as

$$L(di_s/dt) + i_s R_s = at \quad (4)$$

$$(1/R_0)(dR_s/dt) = (i_s^2 R_s / Q_1) \pm R_s/R_0 \quad (5)$$

with initial conditions

$$i_s = 0; \quad R_s = R_0 \quad (6)$$

To define the time of the ending time this equation is to be completed by the condition  $i_s = i_0$  when  $t = \tau_4$ .

In the relative form the system equation shall be written as

$$\beta y' yx = x, \quad z' = y^2 x^2 \quad (7)$$

with an initial conditions

$$x = 0, \quad y = 0, \quad z = 1 \quad (8)$$

$$x = x_*, \quad y = \gamma \quad (9)$$

where

$$x = t/\tau_4; \quad y = i_s/i_0; \quad z = R_s/R_0 \quad (10)$$

$$\tau_4 = (R_0 Q_1 / a)^{1/3}; \quad i_0 = (a Q_1 / R_0^2)^{1/2} \quad (11)$$

$$\beta = L \left( \frac{a^2}{R_0^2 Q_1} \right)^{1/3} = \frac{L \rho}{l^{2/3}} \left( \frac{a^2}{\rho_0^2 q_1 \delta} \right)^{1/3} \quad (12)$$

$$\gamma = i_0 \left( \frac{R_0^2}{a Q_1} \right)^{1/3} = \frac{i_0 l^{1/3}}{S} \left( \frac{\rho_0^2}{a q_1 \delta} \right)^{1/3} \quad (13)$$

here,  $l$  - length of SW;  $S$  - section square

$\rho_0$  - specific resistance

$\delta$  - metal density.

Two independent relative parameters and  $\gamma$  can be considered as dimensionless inductance and relative current, accordingly.

The solution of (7) and (8) is the function family  $y(x, \beta)$  and  $z(x, \beta)$ . The curves  $y(x, \beta)$ ,  $z(x, \beta)$  are dependences of the dimensionless current in the SW and resistance SW on the relative

time (fig.2)

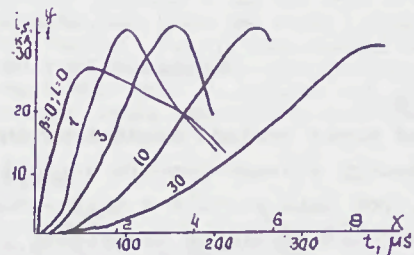


Fig. 2a. Variation of relative current as a function of relative time

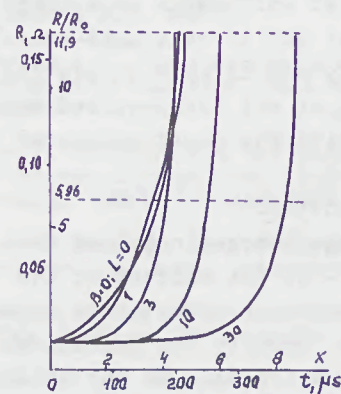


Fig. 2b. Curves showing the SW resistance as a function of time.

Here,  $i_0$  and  $\tau_4$  are calculated for the support points ( $a = 10^7$  V/s,  $l = 80$  cm,  $S = 1$  mm<sup>2</sup>,  $Q = 676$  J,  $R_0 = 1.38 \cdot 10^{-2}$   $\Omega$ ).

The condition of successful commutation is given by the inequality  $y < y_{max}(\beta)$ , when  $y > y_{max}(\beta)$  the current changes its direction (here we denote term "counter-current" as "CC") and equation (10) isn't true in this case. Thus,  $y_{max}$  is a critical value, which defines a boundary of commutative field  $y_{max}(\beta) = \gamma_{cz}(\beta)$ .

Figure 3 shows the field boundary of the successful commutation in the  $(\beta, \gamma)$  plane as well as the direct lines where the relative parameters are constant.

The proposed current commutation model provides possibility to predict, that at some regimes, in which a correlation takes place the first key arc current starts to increase again. The current direction changes from a very small value of specific energy deposition. For example, the CC arises at the first stage of the heating SW when  $R_s/R_0 = \sqrt{3}$  and  $T^0 = 160^\circ$  C. Therefore, for  $\epsilon_0 > 1.35$  kJ/g the commutation will be impossible.

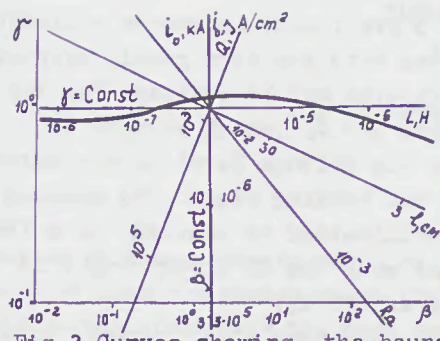


Fig. 3 Curves showing the boundary of the successful commutation.

The critical current density for is defined as

$$J_c = 0.83(aq, \delta / \rho_0^2 l)^{1/3} \quad (14)$$

For the copper wire

$$J_c = 5.5 \cdot 10^4 (a/l)^{1/3}, [A/cm^2] \quad (15)$$

where  $a$  is the rate in V/cm,  $l$  - in cm.

#### 4. Experiments.

The experimental investigation of the commutative processes was carried out in two stages: 1) the investigation of the wire electrical explosion and the current commutation by fuse to loading; 2) the study of the three-step scheme commutation.

At the first stage of wire explosion electrical characteristics were investigated as a dependence of the tube channel diameter upon the wire diameter  $\gamma = d_{ch}/d_w$  ratio. It was shown that the wire explosion in the fuse is similar to the air case when  $\gamma \geq 10$ . The current and voltage characteristics very rapidly change when  $\gamma \leq 7$  and the explosion time is decreasing. The high speed shocking have been performed for better understanding of wire explosion processes in the tube channel. The wire (0.7 mm diameter, 0.38 mm<sup>2</sup> section area, 100 mm long and  $R_w \approx 1.5 \cdot 10^{-5} \Omega$ ) exploded in the glass tube,  $\gamma = 2.83$ . The standard scheme of the capacitor impulse power supply was used with the storage voltage and the energy  $U = 1500$  V and  $W = 6.2$  kJ, respectively. It melts down to  $U = 1300$  V after the wire explosion. So the explosion energy were  $W_w = 2.2$  kJ and  $W_s = 6.4$  kJ/E, respectively.

A typical explosion result in the glass tube is shown in fig. 4



Fig. 4 The frames of the wire explosion.

This picture was taken with the high-speed SFR-camera. The time interval between the frames is 4.05 μs. The melting stage as a light wave is spreading with average speed 2 km/s and intimating to the middle of the wire. The wire is exploded after intimidation of the light wave. The commutation of the current  $I = 10 + 100$  kA to the loading was investigated. By means of several fuses ( $d_w = 0.7$  mm) with the tube channel diameter  $d_{ch} = 3.5$  mm and 220 mm long the commutation was performed the specific energy  $W_s = 12 + 15$  kJ/wire.

We will pick out three problems :

- 1) the mechanical force action on the fuse tube;
- 2) the flow of the wire explosion products from the channel apertures and the possible face breakdown;
- 3) the channel breakdown and the arc development in the channel.

The solution of the first problem lies in the strengthening of chamber design. For the second case we developed special chambers on the dielectric tube ends (see fig. 5).

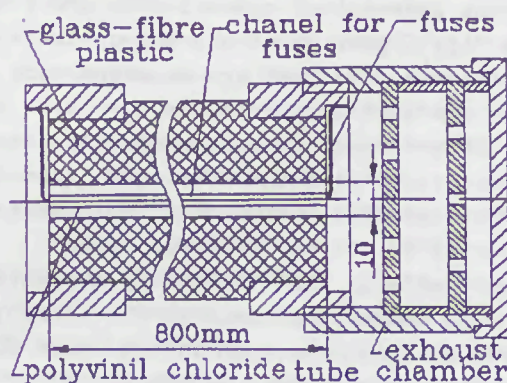


Fig. 5. Cross-sectional view of the shunting wire element.

The most complicated problem is the third one. The choice of the channel length and the parameter  $\gamma = d_{ch}/d_w$  can help solved this problem, though.

The previous experiments permitted to

begin the investigation using the total scheme (fig.1) with the mechanical contact interrupter [3] and the fuse.

On the first step we used the explosive high-speed breaker. It was the dural tube (76 mm diameter, 200 mm long) with 10 mm wall thickness. The tube was filled with paraffin. A cylindrical explosive of 10 mm diameter was on the tube axis. In order to catch the splinters the tube breaker was placed into the closed dielectric chamber.

As a result of the explosion the metal cylinder is destructed, the arc is burned. When the splinter velocity  $v = 10^4$  cm/s the voltage rise rate reached up to  $a = \epsilon v = 10^7$  V/s. It should be noted that this parameter is weakly dependent on the current initial value from 10 to 100 kA. The arc voltage drop is increasing when  $\tau = \text{const}$  during  $\tau = 0.5 \cdot 10^{-3}$  s to  $U_p = 3$  kV. When  $\tau = 1 \cdot 10^{-3}$  s the contact voltage drop was fast decreased to  $U_p = 10^2$  V. The dynamical voltage-ampere characteristics (VAC) for the current commutation shows that the current is almost constant in a large time interval.

On the second stage one or several wires (200 + 300 mm long,  $R = 10^{-2}$ ) are connected in parallel to the mechanical switch. On figure 5 the design of SW is shown. This design allows us to solve all problems of the commutation when the current changes from 10 kA and the voltage from 10 kV to 30 kV. An advantage of that design is the presence of special chambers (on the fig. 5 pos. 5) at the end of the dielectric tube that are catching wire electric explosion products.

SW and resistor connected with each other are used in the loading to form the current profile. The initial resistance of assembly  $R = 0.1 + 10$ . It was shown experimentally that the energy characteristics is weakly dependent on the length, cross section area, quantity of wire when the wire is warmed up to the melt; temperature and the current density  $j = 10 + 35$  kA/mm<sup>2</sup>. A deviation from monotonous character of function  $R/R_0 = f(Q)$  takes place on explosion when  $Q > 1.5$  kJ/g.

More rapid growth of the relative resistance is observed when the SW length

(for  $i_0, R_0, S$  are fixed) increases exploding wire regime with the very gently sloping characteristics may be realized for the wire length  $l < l_c$ , which permits to stabilize the voltage level on the current input to the loading stage. The voltage level stabilization is reached in a few hundred  $\mu$ s when the SW energy input is as large as 200 kJ.

In the mentioned above current interval and switch design the electrical breaking strength of the explosion products was no more  $E = 1$  kV/cm. The input energy limit was 2 + 3 kJ on the length unit.

#### Summary.

Thus, we have created the elements of many-staged commutation scheme. They are: the explosion breaker [3] and many-shut commutator, which is discussed in detail in [4] and switch on the wire electrical explosive bases. All switches have been tested in experimental installations. Using this devices the current commutation was produced from the inductive energy storage with the storage energy of several dozens MJ to the different loading.

This equipment may also be used on the energy plants.

#### References

- 1 Salge J., Braunsberger U., Schwaz U., Circuit breaking by exploding wires in magnetic energy storage systems, proc. 6<sup>th</sup> symp. on eng. Problems of Fusion Research, 1975, Asti-Torino, Itali, 477-480.
- 2 Larionov B., Stolov A., Akhmerov N., Физика и техника мощных импульсных систем, 1987, Энергосатомиздат, 105-127.
- 3 Azizov E., Akhmerov N., Jagnov V., Письма в ЖТФ, 1976, т.2, №7, 316-321.
- 4 Akhmerov N., Gerasimov V., Godojuk V., Egorov Ju., Gavoronkov M., Smoljak A., Приборы и техника эксперимента, 1983, Москва, №4, 132-136.

very useful expil data  
SF<sub>6</sub> and Air  
nat. cond.

## FUSE-ELEMENT IN SF<sub>6</sub> ATMOSPHERE

A. Wolny

Technical University of Gdańsk  
Gdańsk, Poland.

### 1. Abstract.

Behavior of fuse-elements made of copper, silver or aluminum heated up to the melting point in SF<sub>6</sub> atmosphere has been described. Heat transfer from fuse-element was investigated as well as corrosive influence of SF<sub>6</sub> on the metals. For comparison the tests were repeated for air and argon. At the temperature of several hundreds degrees of Celsius was observed less difference between heat transfer in SF<sub>6</sub> and air. Pressure had little influence in these conditions.

It was proved that aluminum is resistant at high temperature in contrast to copper and silver which corroded rapidly over 300°C.

### 2. Introduction.

Application of SF<sub>6</sub> to circuit-breakers, load-switches and encapsulated switch-gear does not involve higher temperature than 200°C, if very short arcing times are not taken into account. So, the all experience on SF<sub>6</sub> low chemical activity towards most metals and insulating materials, as well as on its thermal properties concerns rather the moderate temperature.

Recently more and more interest in SF<sub>6</sub> fuses has been observed, both as independent devices [1,2] and as parts of hybrid ones [3]. Investigation of the behavior of fuse-elements in SF<sub>6</sub> atmosphere up to melting point became imperative.

To provide good extinguishing conditions the amount of metal vapour in quenching chamber should be limited, therefore good conductors only, such as silver, copper and aluminum can be considered for fuse-elements. Melting temperatures of the two first metals approach 1000°C. Therefore one can expect certain grade of dissociation of SF<sub>6</sub> particles, which may change heat transfer conditions and provoke corrosion [4].

Aluminum melts easier, but its melting point at 659°C seems still to be high

enough to expect any changes of SF<sub>6</sub>.

### 3. Experimental.

Test chamber was made of quartz glass cylinder 40 mm in diameter, 132 mm long. Its walls were 4 mm thick. Electrodes cross-section of 50 mm<sup>2</sup> permitted application of currents up to 50 A without excessive heating.

Tested fuse-elements were made of copper, silver or aluminum wires, 0.8, 0.85, and 1.6 mm in diameter correspondingly. Their total length was 70 mm, but only a straight segment about 35 mm long was investigated. To diminish axial flow of heat the both ends of fuse-element were curled. Two turns 4 mm in diameter, separated 2.5 mm were applied. Each sample was equipped with two welded probes 0.3 mm in diameter, 32 mm apart for voltage drop measuring and on this way determination of temperature.

The fuse-elements surface was degreased before their installation.

The test chamber was positioned horizontally. After having hermetised it air was evacuated and argon let in. Tested fuse-element was heated up to the red glow to uniform its structure and stabilize resistivity. After such conditioning over several minutes the gas was pumped out and then the chamber was filled up with SF<sub>6</sub> under desired pressure. The sample was fed with stabilized current not exceeding 50 A DC, until the voltage drop got stable magnitude. This took several minutes. The last (stable) reading was used for calculation of temperature. First three terms of series representing the resistivity-temperature function were applied. The temperature was calculated from the formulae:

$$\Delta T = K_1 \cdot [(K_2 \cdot R/R_0 - 1) + \sqrt{(K_2 \cdot R/R_0 - 1)^2 + (R/R_0 - 1)}] \cdot K_3$$

$$\text{where: } K_1 = A_1/2A_2, \quad K_2 = A_7/A_1, \quad K_3 = 4A_2/A_1^2(1)$$

$A_1, A_2, A_7$  are material constants taken from [5]. They denote:  $A_1, A_2$  are the first and second thermal resistivity constants and  $A_7$  is the dilatation constant. If any changes of the sample surface were not observed a different current or pressure was established and the test was repeated. Results of the experiment were extrapolated to examine their convergence to independently measured FMC. The deviation of temperature was less than 5 percent.

$SF_6$  heat transfer investigations were carried out at pressures 50, 100, 180, 260, 340 and 420 kPa and temperature up to approximately 800 °C. Bulk of results was obtained for the copper wire.

Applying the same test method comparison was made with air and argon.

After having built approximated  $i-T$  profiles serving for determination of the temperature due to the set current the corrosive activity of  $SF_6$  was investigated under the pressure of 100 kPa. The test current was maintained over 3 hours. Next the sample was thoroughly examined. Tenfold optical magnification was applied.

#### 4. Results.

##### 4.1. Heat transfer.

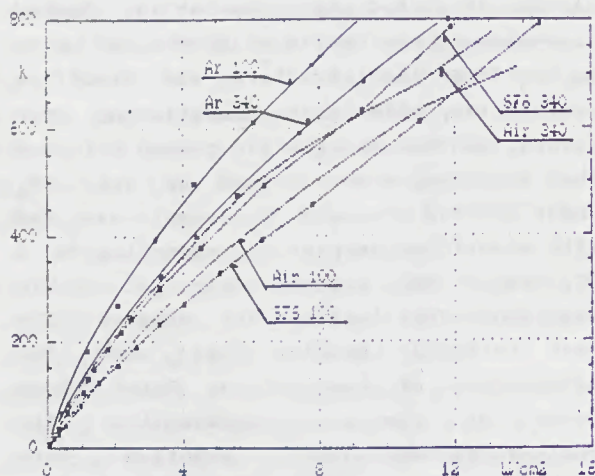


Fig. 1. Temperature rise of cooper fuse-element in  $SF_6$ , air and argon (100, 340 kPa)

The temperature rise versus heat power flux profiles for  $SF_6$ , air and argon under the pressure of 100 kPa and 340 kPa are given in Fig.1 One can see that the advantageous

cooling features of  $SF_6$  known for moderate temperature are not true over 600°C for copper wire, although pressure has still propitious influence. Up to this temperature under any pressure the difference between  $SF_6$  and air is never greater than several percent only and seems to be slightly less than that measured for larger objects [6].

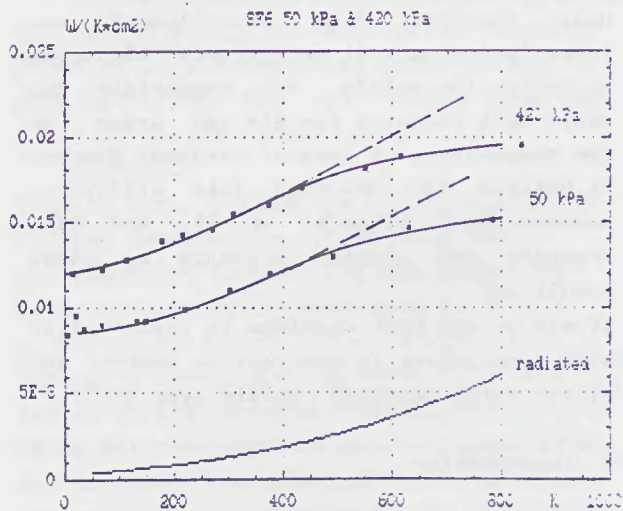


Fig. 2. Heat transfer coefficient  $K_{ht}$  for  $SF_6$  (50 kPa and 420 kPa).

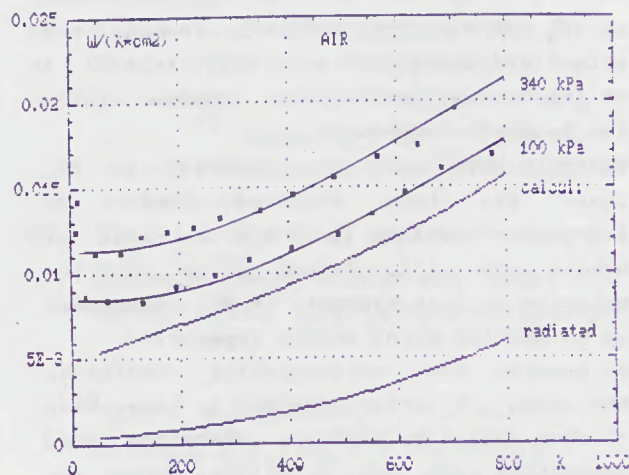


Fig. 3. Heat transfer coefficient  $K_{ht}$  for air, measured and calculated (100 kPa).

Pressure rise enhances heat transfer but in a very moderate way. The increase from 50 kPa to 420 kPa at 200°C gives 42% in profit only. At higher temperature it is even less, due to influence of radiation, which is independent from gas pressure.

The SF<sub>6</sub> generalized heat transfer coefficient K<sub>ht</sub> in function of temperature rise for full range of tested pressures is presented in Fig. 2.

$$K_{ht} = P / [S \cdot (T - T_0)] \quad (2)$$

P = ΔU · I - dissipated heat power,

S - sample surface,

T, T<sub>0</sub> - sample and ambient temperature.

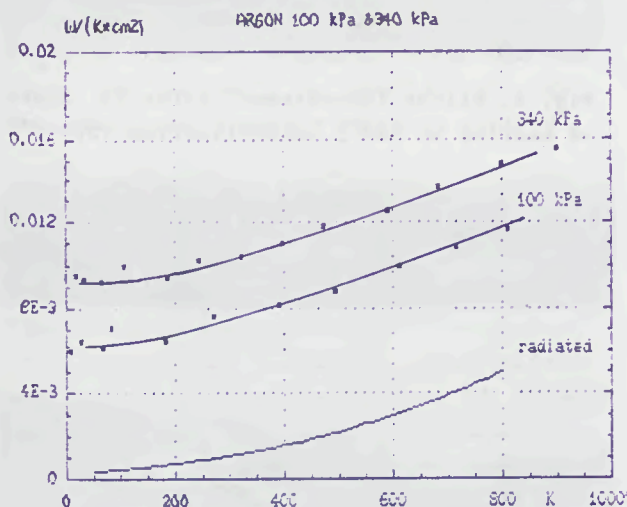


Fig. 4. Heat transfer coefficient for argon (100 kPa and 340 kPa).

Data for the lowest (50 kPa) and the highest (420 kPa) pressures, determining the belt filled with intermediate values for other conditions are given only. Similar results for air and argon, but for more narrow range (100-340 kPa) are shown in Fig. 3 and Fig. 4. On both of them radiation heat transfer coefficient K<sub>r</sub> is also plotted providing emissivity ε=0.6 for SF<sub>6</sub> and air or ε=0.5 for argon. It is supposed that copper oxides layer enhancing emissivity is more transparent in argon.

$$K_r = \epsilon \cdot \sigma \cdot (T^4 - T_0^4) / (T - T_0) \quad (3)$$

At higher temperature close to 600°C the K<sub>ht</sub> coefficient in SF<sub>6</sub> begins to rise slower and slower, differently than in other gases. The trend similar to argon or air should follow the dashed line charted in the Fig. 2.

The K<sub>ht</sub> coefficient calculated for free convection in air in natural conditions based on the data given by Szargut [7] is

also shown in Fig. 3. The table data were approximated. The results of measurements indicate that the cooling conditions in the experiment were better than those supposed in calculation, maybe partly because of not fully compensated axial heat flow.

Comparison of K<sub>ht</sub> coefficients for SF<sub>6</sub> and air at 100 kPa and 340 kPa is presented in the Fig. 5. The difference is several percent. The curves are very similar up to about 500°C. Above this threshold the cooling properties of SF<sub>6</sub> decline in tests with copper fuse-element

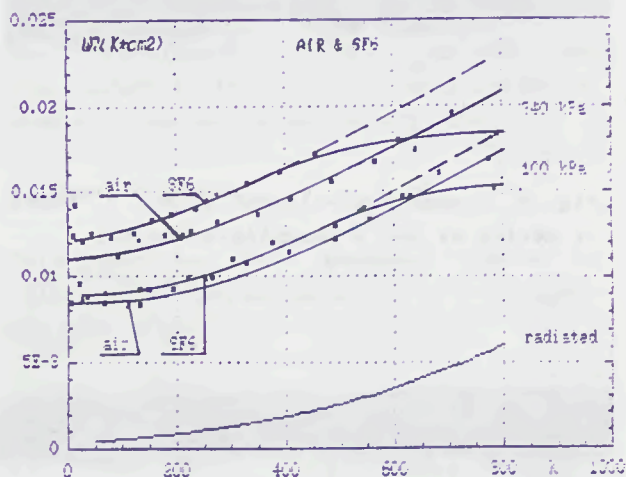


Fig. 5. Heat transfer coefficient K<sub>ht</sub> for SF<sub>6</sub> and air (100 kPa and 340 kPa).

Used method of measurement is less accurate for very low (small voltage drop and possible inhomogeneity) and very high temperature rises (possible oxidation). Therefore larger deviation of results has been observed in these conditions.

#### 4.2. Corrosive properties of SF<sub>6</sub>.

Up to about 250 - 300°C nothing special was observed, but over 300°C, gas initially colorless turned very slightly yellowish. Glass walls lost their transparency and became a little milky. After having opened the test chamber the sharp, irritating smell was felt. No chemical analysis was done because of the small volume of the chamber.

The first alterations of copper fuse-element were observed at 300°C. Over 400°C it got dark patches, and next a dark brown surface layer built of tiny

bubble-like formations (Fig. 6). The diameter of wire increased in 50%. Further temperature rise consolidated that layer. It was fragile and split easily while bending the wire (Fig. 7).

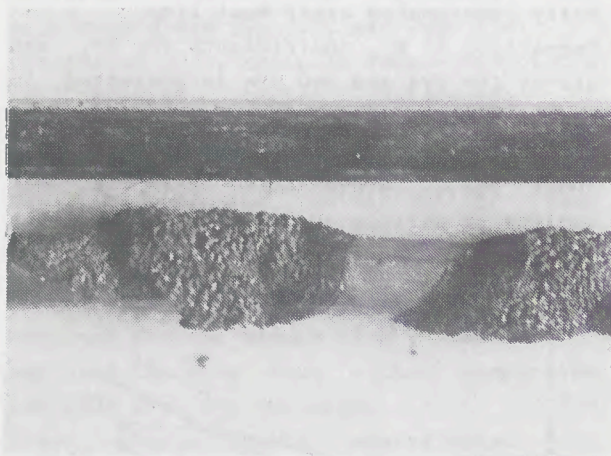


Fig. 6. Copper fuse-element after 3 hours of heating at 660°C (magnification 15).

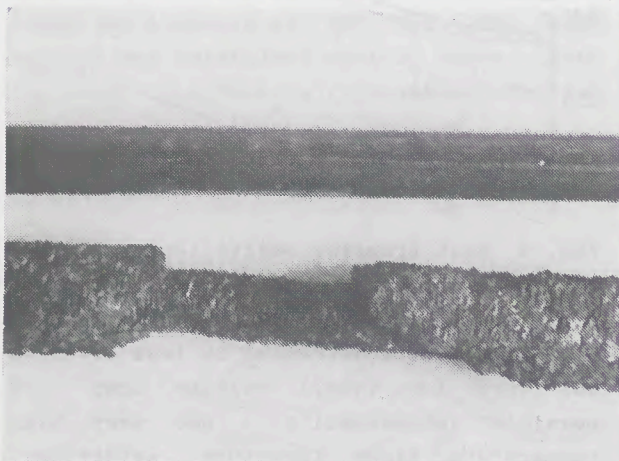


Fig. 7. Copper fuse-element after 3 hours of heating at 830°C (magnification 15).

The silver fuse-element began changing at a little higher temperature. At about 400°C white powder was observed on the surface, that became more cohesive during the heating. The corrosion product layer was thinner than that on the copper wire, but still the diameter increased in 35%. It split also facile (Fig. 8).

The aluminum wire did not change at all even close to melting point (Fig. 9).

Any inhomogeneity of surface could produce differences of features of created corrosion product layers (Fig. 5).

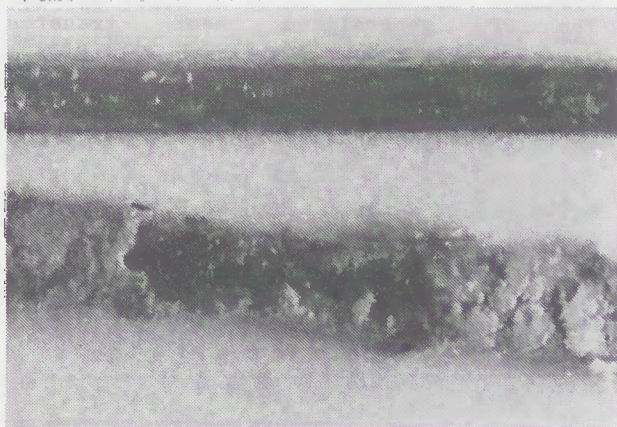


Fig. 8. Silver fuse-element after 3 hours of heating at 780°C (magnification 15).

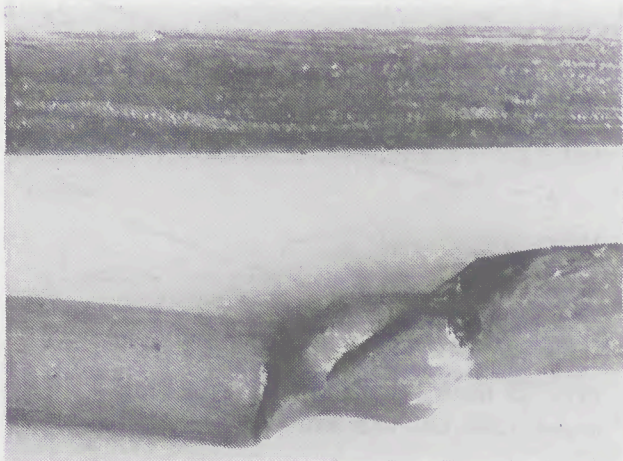


Fig. 9. Aluminum fuse-element after 3 hours of heating at 625°C (magnification 15).

## 5. Discussion.

### 5.1. Heat transfer.

The chamber and fuse-element diameters ratio is so big that the heat conduction can be fully omitted.

At low temperature radiation may be also neglected but over 300-400°C this is not the case. At 600°C it can constitute almost 30% of the heat flux (Figs. 2-5). Luckily it is easy to calculate if emissivity of fuse-element is known.

The real problem creates convection. Its heat transfer coefficient  $K_k$  is defined by Nusselt number correlation

$$Nu = K_k \cdot d / \lambda = C \cdot (Gr \cdot Pr)^m \quad (4)$$

where the Grashof number  $Gr$  is defined as

the Prandtl number  $Pr = c_p \cdot \rho \cdot \nu / \lambda$ . (6)

The thermal capacity  $c_p$ , thermal conductivity  $\lambda$ , kinematic viscosity  $\nu$ , and the gas density  $\rho$  are functions of temperature and pressure. The constants  $C$ , and  $m$  depend upon the value of  $Gr Pr$  product and should be determined experimentally. For  $SF_6$  it lacks such data for the fuse operation conditions. Therefore it seems convenient to compare  $SF_6$  fuse thermal features with the air ones. Up to  $600^\circ C$  a coefficient ( $K_p$ ) dependent upon pressure could be applied

$$K_{ht}(SF) = K_{ht}(air) \cdot K_p \quad (6)$$

Its value may be constant for a given pressure and the pressure influence can be linearised as show results. Errors should not exceed few percent. Investigations carried out at lower temperature by Majzel [6] indicated also that pressure rise caused almost linear increase of the heat transfer coefficient.

Over  $600^\circ C$  the sharp drop of rate of rise of the  $K_{ht}$  coefficient value may be probably provoked by coating of the sample with corrosion product layer. Therefore no interpretation of this feature and methods of evaluation can be given until additional experiments with materials chemically more resistant are completed.

Rate of rise of  $K_{ht}$  value slightly increases with the temperature rise for argon and air in the full range of tested temperatures. So, the oxidation of copper wire in air would have less influence than the corrosive activity of  $SF_6$ .

## 5.2. Chemical activity.

In accordance to the observations made, there is no doubt that the dissociation of  $SF_6$  particles occurs over  $300^\circ C$ , what can provoke corrosion. It was stated that the most endangered is copper and the most resistant is aluminum, unlikely to Howard's report [8] concerning lower temperature. Silver can be positioned in between.

In practice it could be said that exclusively aluminum is suitable for fuse-elements. Copper and silver could be

used for short-circuit or time-lag with low melting point M-effect protection only.

## 6. Conclusions.

In large range of temperature the  $SF_6$  thermal features are very similar to those of air, although  $SF_6$  is several percent better one.

Therefore, the heating calculations could be performed in the same way as for air, using the same parameters but applying additionally a correction factor greater than 1.

The fuse-element in  $SF_6$  applied for overcurrent protection preferably should be made of aluminum or coated with it.

## 7. Acknowledgement

This paper has been prepared thanks to valuable help in measurements of Mr Targonski M.Sc.E.E.

## 8. References.

- [1] Akers D.J.,  $SF_6$  designs improve distribution switching and fusing, 1989 Power Technol. Intern., 267-268.
- [2] Reason J., Revolution in switchgear, 1989, Electr. World (USA), 203, 57-62.
- [3] Kacprzak B, Lipski T, Wolny A., Dwucieczowy, piaskowo-prozniowy bezpiecznik wielkiej mocy o nieograniczonej zdolności wylaczenia malych pradow, 1987, Zeszyty Naukowe Politechniki Poznanskiej, Elektryka, 34, 51-58.
- [4] Artur A., Preparation proprietes physiques, chimiques et applications generales de l'hexafluorure de soufre, Bull. SFE, 34, 514-523.
- [5] Rex H.G., Calculation of models for adiabatic processes, 1984, Int. Conf. on Electrical Fuses and Their Appl., 35-51.
- [6] Majzel E.S., Issledovanie teplovykh svoistv gazovoj izolacii primeniajemoj v elektrotechnicheskikh ustrojstwach, 1962, Elektrizestvo, 4, 54-57.
- [7] Szorgut J., Termodynamika, 1976, PWN, Warszawa, Poland.
- [8] Howard P.R., Insulating properties of compressed electronegative gases, 1957, Proc. IEE, 104, 123-137.

Faint, illegible text at the top of the left page.

Faint, illegible text in the middle of the left page.

Faint, illegible text in the lower middle of the left page.

Faint, illegible text in the lower part of the left page.

Faint, illegible text at the bottom of the left page.

Faint, illegible text at the top of the right page.

Faint, illegible text in the middle of the right page.

Faint, illegible text in the lower middle of the right page.

Faint, illegible text at the bottom of the right page.

**Session 3**

**FUSE DESIGN III**

Baselton J

BASELTON J

Why all not  
they used?

SEMICONDUCTOR FUSES WITH ALUMINIUM CURRENT-CARRYING PARTS: PROBLEMS  
AND PROSPECTS

K.K. Mamitokov, K.A. Ilyina, G.G. Zhemerov, and I.G. Shklovsky

The Kharkov Institute of Engineers of Municipal Economy

Importance of the problem. At present, fuse elements of quick-breaking protection fuses are made of silver ( $Ag$ ), which material is characterized by a variety of valuable properties. The world production of silver (without USSR) in 1983 approached 9869 metric tons, with a 5000 ton deficit<sup>1</sup>. Yearly irreparable losses of  $Ag$  exceed 4000 tons, with electrical industries responsible for the major part of this figure<sup>2</sup>. This is the situation where instability of market prices, with a tendency towards a considerable growth, is only too natural. Thus, the price of silver doubled five times over the period of 1983-1985, occasionally falling down<sup>3</sup>. While in 1960 the price of 1 gram of  $Ag$  was 2.8 cents, it rose to 26-36 cents in 1980's, even reaching 1.5 \$<sup>1</sup>. By the year 2000, the production of silver in developed countries is expected to reach 6000 tons, with the demand three times as high. Hence, a radical solution to the problem would be replacement of silver by another material.

Requirements to high-speed fuses. The technically severe operation conditions of semiconductor devices with high-speed fuses and the emergencies that may arise give rise to contradictory requirements that the fuses should meet. On the one hand, the fuses must provide long-term reliability under the repeated action of arbitrarily varying loads and/or overloads, without demanding reductions in the rated current values through the circuit. On the other hand, if a fault condition develops, the fuse must disconnect the faulty subcircuit, while retaining its own mechanical integrity and preventing inadmissible consequences for the major system. This is achieved through extinguishing the arc at the lowest possible level of its energy and optimizing the values of the Joule integral for the fuses, semiconductor devices and other protection equipment. E.g., in the case of internal short circuiting the condition must

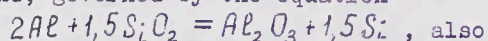
be met

$$W_1 \leq [n(1-K) + K]^2 W_2,$$

where  $W_1$  is the let-through  $\int i^2 dt$  integral of the fuse,  $W_2$  the prearcing integral,  $n$  the number of parallel circuit branches, and  $K$  the nonuniformity coefficient of current sharing. This condition is particularly hard to satisfy for the values often encountered in practice, i.e.  $n = 2$ ,  $K = 0.3$  and  $U_{arc} \leq U_{main}$ . In the case of adiabatic heating, i.e. with high values of the short-circuit current (about  $(250 \text{ to } 400) \times I_{rated}$ ), the integrals assume values between 1.31 and 4.36, which may fail to satisfy the above condition at the level of 2.89. Difficulties can also arise in matching the parameters of automatic circuit breakers or semiconductor devices with performance characteristics of the fuse (such as the peak current, arc energy,  $\int i^2 dt$  integrals, etc.). Optimization of the fuse parameters is not an easy task even with the use of silver elements.

Characteristics of aluminium. Compared with silver, aluminium is characterized by lower (nearly by a factor of two) values of the thermal and electric conductivity, much lower Meyer constant ( $37 \text{ A}^2 \text{ sec/mm}^4$  against  $72 \times 10^3 \text{ A}^2 \text{ sec/mm}^4$ ), lower mechanical strength ( $8 \text{ kgf/mm}^2$  compared with  $15 \text{ kgf/mm}^2$ ), and lower melting point. At low temperatures, the mechanical strength of both  $Ag$  and  $Al$  increases (almost by a factor of two at  $-200 \text{ }^\circ\text{C}$ ), while at higher temperatures it decreases monotonously to become  $1 \text{ kgf/mm}^2$  (at  $900 \text{ }^\circ\text{C}$  for  $Ag$  and  $600 \text{ }^\circ\text{C}$  for  $Al$ ). The oxide film present on  $Al$  has a noticeable strengthening effect at high temperatures. E.g., specimens of aluminium foil (thickness of  $0.1 \text{ mm}$ ,  $99.997 \%$  pure) annealed at  $600 \text{ }^\circ\text{C}$  showed a strength of  $2.45 \times 10^6 \text{ Pa}$  and a  $12 \%$  plasticity. With the oxide film removed through chemical solution the same foil showed a  $1.35 \times 10^6 \text{ Pa}$  strength and a  $39 \%$  plasticity. If the oxide film is removed mechanically, aluminium interacts

vigorously with water and aqueous solutions of acids or alkalis. The properties of aluminium specimens are markedly influenced by their chemical purity. E.g., the tests performed at 350 °C for two kinds of 99.99 % pure aluminium specimens have revealed ageing and failure effects after 308 and 376 hours, while for specimens of lower purity (99.95 %) after 121 and 206 hours<sup>1</sup>. Silver specimens subjected to mechanical straining at high temperatures also showed a noticeable ageing effect. E.g., after 3 hours at 250 °C the mechanical strength was 7.85 kgf/mm<sup>2</sup> with a relative elongation of 70 %, which values reduced to 6.45 kgf/mm<sup>2</sup> with a 50 % elongation after 58 hours. At 400 °C, the 3.95 kgf/mm<sup>2</sup> strength shown after 6 hours dropped down to 2.35 kgf/mm<sup>2</sup> after 178 hrs. The transition to a melted condition is accompanied by a nearly three-fold increase in the electric resistivity of both Al and Ag (from 8.65x10<sup>-6</sup> to 25.1x10<sup>-6</sup> Ohm·cm in the case of Ag). Aluminium is characterized by an extremely high energy of compound formation with oxygen, sulphur and carbon (specifically, 1672 kJ/mol, whereas the figures for silver and copper are 30.5 kJ/mol and 167 kJ/mol, respectively). The aluminium-oxygen interaction results in the Al<sub>2</sub>O<sub>3</sub> oxide, or alumina which is a stable chemical compound. The corresponding exothermal reaction may occur in accordance with the two equations given below<sup>4</sup>. As follows from the calculation, the oxidation reaction,  $2Al + 1.5O_2 = Al_2O_3$ , should liberate 33.4 kJ of thermal energy resulting from a complete combustion of 1 g Ag. However, this reaction requires 0.672 litre of oxygen per 1 g, while the closed cartridge of a semiconductor fuse, e.g. ПП-60, contains about 0.005 l of oxygen, or 0.7 % of the necessary amount. This quantity is definitely insufficient for supporting the reaction and liberating the heat. In open air, there is enough oxygen to maintain the oxidation reaction but analysis of the literature data on electrically exploded aluminium wires shows no effects of the exothermal reaction. The alloying reaction of aluminium with quartz sand, governed by the equation



should be associated, in accordance with the Hess rule, with the release of 33.4 kJ per 1 g of reacting Al independently of intermediate stages. However, the exothermal oxidation reaction is accompanied by an endothermal reaction, namely reduction of silicon from silica, SiO<sub>2</sub>. It consumes 27.6 kJ of thermal energy per 1 g of the reacting aluminium. Hence, 1 g of completely burned aluminium theoretically is able to release 5.8 kJ of extra thermal energy, which is about 25 % of the arc energy. This extra energy has not been revealed in our special experiments which will be described in more detail below. According to paper<sup>5</sup>, the interaction of an aluminium element with a chemically active medium containing hydrogen peroxide in a relatively high concentration had but a "modest" effect on the fuse performance. Nor have we found in our investigations a noticeable chemical impact of the colloidal silica suspension, N<sub>2</sub>O · n · SiO<sub>2</sub> · H<sub>2</sub>O (plus heating), on the performance of aluminium elements. Thus, despite the high reactivity of Al it is stable against many chemical reagents, owing to the oxide film on its surface. Therefore, the rate of corrosion of aluminium decreases with time in a majority of media. On a freshly worked surface the oxide film becomes 10<sup>-9</sup> m thick after about 10<sup>-5</sup> sec. As a result of 20 years of corrosion tests in air, it has been found that the major part of corrosive destruction of Al, with a 40 % loss of strength, occurs over the first year<sup>6</sup>. Voytovich and Golovko<sup>7</sup> investigated high temperature oxidation of aluminium in air under isothermal conditions, using thermometry and mass measurements, with continuous 8-hour monitoring of the specimen mass. At temperatures close to the melting point the increase in the oxide mass per unit area of the material surface was very low, specifically (0.1 to 0.3) mg/cm<sup>2</sup>, which is evidence for its high resistance to corrosion. Whereas the loss in the mass of silver specimens resulting from corrosion in air is (0.01-0.3) mg/cm<sup>2</sup>hr, depending on the resistance group of Ag<sup>1</sup>.

Experimental results. Long-term thermal performance. Laboratory experiments and

trial operation have shown that aluminium fuse elements of geometry identical with silver elements and thickness greater by a factor of 1.8 or 1.9 allow producing a quick-breaking fuse with practically the same thermal parameters as those of the prototype with silver elements, provided the aluminium terminals are 2.0 to 2.5 times thicker than copper terminals, in order to compensate for the lower electric conductivity of  $Al$ . E.g., the fuses for  $U_{rate} = 660$  V and  $I_{rate} = 400$  A with silver elements  $\Delta = 0.1$  mm and aluminium elements  $\Delta = 0.18$  mm, and terminals of either copper ( $\Delta = 4$  mm) or  $Al$  ( $\Delta = 10$  mm) have shown practically the same values of  $R = (210 - 215) \times 10^{-6} \Omega m$ , temperature rise of the terminals (82 to 87 °C) and power loss (52 to 57 W). Disc-shaped fuses with two-side water cooling (water consumption 3.5 to 4.5 litre/min at  $T = 30$  °C), aluminium elements  $\Delta = 0.3$  mm, 10 mm thick aluminium terminals and aluminium current-carrying parts ( $U_{rate} = 380$  V and  $I_{rate} = 1600$  A) have shown the same values of basic parameters as fuses with  $Ag$  elements, i.e.  $R = (45-55) \times 10^{-6} \Omega m$ , power loss (160-170) W and temperature rise below 85 °C under natural cooling. The pressure force against the converter wires was 60 kN. Thus, in the nominal operation duty the temperature of constricted parts does not exceed 300 °C and the oxide film grows by a few angströms which leads to a (0.1-0.2) % increase in the resistance. This results in a high stability of losses both in the elements and terminals and integrity of the contact. Using a hard filler improved the thermal characteristics in both cases by nearly 10 %. With the use of water cooling, the thermal parameter of temperature rise at the terminals becomes meaningless. The parameter of principal importance remains the voltage drop. In a reasonably designed fuse, this latter should be 1.4 to 1.5 times as great as the initial value, i.e. the product of the fuse resistance by the current.

Calculations of the current density and temperature fields in  $Al$  and  $Ag$  elements show practically coincident patterns for the above listed thicknesses of aluminium parts.

Duties with cyclic and arbitrarily repeated loads and overloads. The tests were performed for various duties with repeated loads described in more detail in paper<sup>11</sup>. Fuses with planar elements made of aluminium (rated current 400 A at 660 V) loaded by the nominal current with 18 min on and off periods failed after 89 to 127 cycles. Fuses with planar elements made of silver withstood over 200 loading cycles. To attain a similar withstandability with  $Al$  fuses, the rated current had to be reduced by 12 to 15 %. In the case of ageing by a rated current (8 hours under a sinusoidal current and a 16 hour pause) fuses with elements failed after 31 or 33 cycles. With other patterns of current loading the level of withstandability shown by fuses with planar  $Ag$  elements again could be attained by  $Al$  fuses if the rated current were reduced by 12 to 18 %. Comparative tests of fuses with bended  $Al$  and  $Ag$  elements have shown that equal levels of cycling withstandability can be attained by fuses with aluminium elements if their rated currents are reduced by 10 %, or even 5 % if a hard filler is employed. Similar regularities have been established for transient overload duties, like for instance interruption by a circuit breaker of an emergency regime in a converter. The total number of such uncontrolled overloads (up to  $(6-10) I_{rate}$ ) lasting for  $\leq 0.2$  sec can reach  $20-25$  over the fuse lifetime. In our experiments that involved interruption of a d.c. circuit with a superquick circuit breaker the current through fuses reached the level of  $10 I_{rate}$  in 3 msec and then dropped down to zero in another 3 msec. The fuse withstood 15 such pulses (one in every 10 or 20 minutes) without changing its resistance.

As is known<sup>8</sup>, the fracture mechanics has not yet developed, because of the complexity of the physics involved, an adequate theory of metal fatigue that could predict specimen durability, i.e. the dynamics of crack growth as a function of the number of load cycles. The development of a theory of fatigue failure in constricted portions of fuses subjected to cyclic loads is even more complex as the phenomenon involves a

variety of interdependent electrical, thermal and mechanical effects. The formulation and analysis of nonlinear coupled field-theoretic problems that could lead to a living theory, face conceptual difficulties. A theory like that should provide a qualitative and quantitative description of both stages of fatigue failure in constrictions, i.e. i) changes in the metal structure leading to crack formation, and ii) growth of the crack, ending in a fracture of the constricted part. It should be noted that development of a theory relating the fuse longevity to its design parameters, number of loading cycles and load characteristics (such as intensity and waveform of the current, duration of the on-current and currentless periods, etc.) is complicated by the pronounced effect of manufacture technology, sequence of various stages, etc. that are virtually unaccountable for. On the other hand, the present amount of practical expertise is sufficient for designing durable quick-breaking fuses, including those with aluminium current-carrying parts, that combine optimized geometries of the bended fuse element, employment of a hard filler and a reasonable choice of the rated current density through constricted portions. In our experiments, laboratory prototypes with  $Al$  elements withstood 100000 loading cycles (each cycle consisted of 15 sec of a  $2 I_{rate}$  current flow and a 45 sec currentless pause) applied for 8 to 9 hours daily during one year. At the end of these tests, the fuse resistance remained practically unchanged.

Fault current interruption. The higher cathode voltage drop, characteristic of arcing between aluminium electrodes (16.2 to 18.6 V) as compared with silver electrodes (12.1 to 13.6 V), facilitates arc extinguishing in protection fuses with aluminium elements. Moreover, the oxide film favours inertial storage and further explosive dissipation of energy, thus ensuring excellent switching capabilities of  $Al$  elements. The rate of voltage growth during fusion of the constricted portions can be as high as  $10^6$  V/sec. Special features revealed in the experiments are as follows.

A.c. interruption. Fuses with  $Al$  elements

have demonstrated the capability to reliably interrupt currents ranging from  $3 I_{rate}$  to  $(300+400) I_{rate}$ . No effect of the exothermal reaction that could be expected from theoretical considerations has been revealed either in oscillograms or in the condition of sand fulgurites. Moreover, the highest values of let-through currents and Joule integrals were practically the same for  $Al$ -based fuses and their  $Ag$  prototypes. This conclusion is in agreement with the results of Japanese writers (Ueda et al.) who have found that in a fuse with  $Ag$  elements arcing occurs in the atmosphere of an evaporated filler. The claimed independence of arcing of the element  $Ag$  material thus is true for  $Al$  too.

The arc energy shows no pronounced maximum as a function of the circuit current. In a wide range of available currents ( $(10-100) I_{rate}$ ) the arc energy for  $\Psi = 0^\circ$  did not deviate from its maximum value by more than 10 %. Of great importance is the knowledge of conditions when the let-through current is maximal. The maximum current is observed under interruption conditions with  $\Psi = 53-57^\circ$ , which is also close to the arc energy maximum.

An objective characteristic of the fuse performance at the arc extinguishing stage is provided by the ratio of the total  $\int i^2 dt$  integral to its prearcing value. This ratio can be used to obtain fairly accurate quality estimates of different fuses, including those for different current and voltage ratings. By connecting two or more fuses in parallel their reliability can be greatly increased, and all protective qualities generally improved, especially at high current values. During transient prearcing operation,  $Al$ -based fuses show special points and zones of performance characteristics similar to those described in paper<sup>9</sup> for  $Ag$ .

Silver and aluminium actually show close values of another theoretically important parameter, namely the adiabatic pressure produced during adiabatic heating and melting of constrictions under the condition that the volume of the gaseous phase should be the same as of the constriction material (the values are  $160 \times 10^8$  and

$155 \times 10^8$  Pa for Ag and Al, respectively). This pressure is calculated from the familiar Mendeleev-Klapeyron equation. In fact, a pressure as high as this, conditioned by the fact that the gas volume under normal conditions would be tens of thousands times greater than that of the melted metal, never exists in protection fuses. Indeed, the filler sand is a non-Newtonian liquid, hence the pressure wave arriving at the cartridge walls is weakened and never exceeds  $10^6$  Pa, irrespective of the fuse element material. Meanwhile, electrical explosion of an Al wire in water which is a classic Newtonian liquid is accompanied by a pressure pulse up to  $10^9$  Pa with a temperature about  $4 \times 10^4$  K<sup>5</sup>. The corresponding electric field strength reaches 15 kV/cm, which value is one order of magnitude higher than in the case of sand.

D.c. interruption. Tests have shown that fuses with Al elements can interrupt quite easily currents as high as  $(200 \sim 400) I_{rate}$ , even with rather great values of  $\tau$  like  $\tau = 35$  msec. Similar as in the a.c. case, effects of an exothermal reaction are not detected. Moreover, the peak voltage can be increased by another 8 or 12 %. The problems that exist relate to the interruption of low currents  $(6 \sim 10) I_{rate}$  with  $\tau = 35$  msec or more. The difficulties are characteristic of all quick-breaking fuses, independently of the fuse element material. They are associated with the reactive energy stored in the circuit inductance, which component may reach 75 % of the total arc energy<sup>10</sup>. The physics of interrupting low currents has been investigated for fuse elements of various lengths, with the highest admissible voltage at which the circuit can be reliably interrupted fixed for each length. Besides, the authors have discovered a special feature in the process of interrupting low currents with great  $\tau$  by Al-based protection fuses. It consists of the restriking effect, when the current through the fuse starts to increase some 40 or 100 msec after it has dropped down to zero. The energy dissipated in the fuse before occurrence of the effect happens to

be 20 to 40 % lower than in the a.c. case, which manifested itself through a shorter length of the sand fulgurite. Reliable interruption could be achieved by reducing the length of Al fuse elements by 12 to 20 % or reducing the circuit voltage (or time constant) by the same fraction. The interruption of low and medium currents in circuits with high time constants,  $\tau = 35$  to 70 msec, was accompanied by nonuniform burn-out of the fuse elements. While some of the elements were burnt nearly completely, others retained about one half of their metal and still others were damaged near constricted portions only. On some occasions, just a single element burnt completely brought about piercing of the end cap independently of the element material.

#### REFERENCES

- [1] V.V. Malyshev and D.V. Rumyantsev. Silver, 1987, "Metallurgiya" Publ. Co., Moscow (in Russian).
- [2] G. Tornbitz. Optimierung des Edelmetall. Einsatzes bei Schaltern und Schaltgeräten, 1981, Electr. Anz., vol. 34, No. 14, 25-29.
- [3] J.G. Leach. New application flexibility for medium voltage current-limiting fuses, 1985, IEEE Transactions on Industr. Applications, vol. , No 4, 1075-1080.
- [4] T. Lipski. Bezpieczniki nizkonapie- rowe, 1969, Warszawa, 299 p.
- [5] R.E. Runovsky. Fuse opening switches for pulse power applications: Open switches, 1987, 209-232.
- [6] Corrosion (A Reference Book). Russian Translation of the English Edition, 1981, "Metallurgiya" Publ. Co., Moscow.
- [7] R.F. Voytovich and E.I. Golovko. High temperature oxidation of metals and alloys, 1980, "Naukova Dumka" Publ. Co., Kiev, (in Russian).
- [8] David Broek. Elementary Engineering: Fracture Mechanics, 1980, Noordhoff Int'l Publishing Co., Leyden (Russian Translation: "Vysshaya Shkola", Moscow, 368 p.).

- [9] K.K. Namitokov, N.A. Ilyina, and I.G. Shklovsky. A finite element analysis of the thermal behaviour of notched fuse elements in semiconductor fuses, 1989, Sixth Int'l Conference on Switching Arc Phenomena, 12-15 September, Lodz, Poland, 212-217.
- [10] K.K. Namitokov, N.A. Ilyina, and I.G. Shklovsky. Protection of semiconductor devices. 1988, Energoatomizdat, Moscow.
- [11] K.K. Namitokov, N.A. Ilyina, and I.G. Shklovsky. Pulse withstandability of semiconductor protection fuses, 1989, Six Int'l Conference on Switching Arc Phenomenon, 12-15 September, Conference Materials, 205-211, Lodz, Poland.

# INVESTIGATION OF THE PRE-ARCING BEHAVIOUR OF DISSIMILAR UNIFORM DOUBLE-ELEMENTED FILLED FUSES, USING FE CAD TECHNIQUES

J C Gomez, D Tourn  
University of Rio Cuarto  
ARGENTINA

and

P M McEwan  
Sheffield City Polytechnic  
Sheffield, UK

## Summary

Dissimilar uniform strip elements in filled fuses have been studied using Finite Element CAD techniques to investigate 'M effect' time-current type fuse melting behaviour. The results of simulations indicate significant time delay operation is feasible for Ag-Ag and Ag-Sn element material and that FE CAD techniques may be used with confidence to analyse this class of problem.

## Introduction

The use of low-melting point alloys to produce 'M effect' in fuses is known to introduce conditions where the fuse can operate outside its declared time-current characteristic. The use of parallel elements of different material and dimensions, to produce the similar time-delays in the overload region of time-current characteristics without the shortcomings of 'M effect' was considered to be feasible but very difficult to investigate experimentally. The FE CAD simulation technique (1), which could be verified by experiment, was considered to be the most suitable method for investigating the time-lag performance of dissimilar elements.

Finite element CAD simulation studies were consequently used to investigate the time-delay low-overload pre-arcing performance of fuses containing two dissimilar uniform strip elements of different materials, surface area and relative positions in filler.

## Fuse Models

Two fuse models were developed to simulate the transient heating of two parallel current-carrying uniform strip elements, in filled fuses. The period of interest was over the region 1s to 10s, consistent with the 'M effect' overload time-delay region of fuse time-current characteristics. Over this time range, the model has to take account of heat conduction to end terminations, convection from all fuse surfaces and the temperature dependency of the electrical and thermal properties of all the fuse components (2).

A simple model was developed, which eliminated the external heat transfer effects. The model was useful, and is recommended, for quick assessment of the accuracy of representation and for estimating the assumptions of the

model, since it requires fewer nodes and much shorter computer run times.

A more detailed model fig 1 had to be limited to 1000 nodes. The model includes variations in thermal conductivity, specific heat and electrical conductivity with temperature change, of all the fuse components. The fuse modelled was a DIN standard NH00 fuse (maximum external body dimensions 30 x 30 cm in section and 46 cm long). The filler was granulated silica quartz and the body was made of ceramic material. The end plates were brass and knife blade contacts, made of copper, were assumed to be connected to standard lengths of cable held at 20°C, 50 cm from the cable/fuse terminations.

At the end of each time step of the computation, the redistribution of the current between the two elements is determined by computing the electrical resistances of the elements, until one of the elements reaches its melting temperature. When one of the elements reaches its melting temperature, the whole current is transferred to the other element.

The detailed model required 990 nodes, which enabled solutions to be obtained using a Personal Computer fitted with a mathematics co-processor.

## Results

Simulation studies were undertaken with the detailed model for pairs of similarly dimensioned strip elements made from silver, copper, aluminium, tin and zinc combinations. The Cu-Ag, Cu-Al and Ag-Al combinations shared current almost equally and consequently produced virtually no time delay effect compared with the Ag-Sn combination. Similarly, element combinations of similar low melting point metals produced no noticeable 'M effect' type characteristics.

Simulation studies were undertaken on pairs of Ag-Ag element of same cross section, but different widths and thicknesses and therefore different surface areas. The results of the respective simulation studies given in Table 1 and fig 2, indicate 'M effect' type melting time-current behaviour.

Ag-Sn element combinations indicated the most promise so studies were concentrated on this pair of element

materials. Simulation studies were undertaken on Ag-Sn strip of different widths and thickness but with the same combined cross sections. These results are also given in table 1 and figures 3 and 4 for two samples carrying a current of 300A.

Table 1 - Operating Melting Time for Sample Parallel Elements

Sample	Element Material 1	Element Material 2	Operating Time (s) (I = 300A)
	Dimension	Dimension	
A	Ag W = 3.18 T = 0.1	Ag W = 3.18 T = 0.1	8
B	Ag W = 3.18 T = 0.1	Ag W = 0.56 T = 0.56	4
C	Ag W = 3.18 T = 0.1	Sn W = 0.56 T = 0.56	1.25
D	Sn W = 3.18 T = 0.1	Ag W = 0.56 T = 0.56	0.7

W = width (mm)  
T = thickness (mm)  
csa = 0.318 mm<sup>2</sup>

The four fuse samples, Table 1, were simulated for current-carrying conditions approaching their estimated rated currents. The simulation temperature profiles of a section through the fuse at the hottest point, is shown in fig 5 for the fuse samples A, B and C.

In order to check the accuracy of these latter simulations the respective fuse combinations were made up and volt drop and temperature measurement tests performed. Correlation better than  $\pm 5\%$  was obtained between the experimental and simulated results.

#### Conclusions

The studies indicate that 'M effect' time-delay type operation can be obtained without using low melting point alloys by varying the element geometry of parallel fuse elements

comprising similar or dissimilar material. The FE CAD studies were undertaken on uniform strip elements in order to examine basic principles and to assess the accuracy of the simulations in predicting the performance of practical filled fuses in the 1s to 10s time-current characteristic region. The results of all the simulations compared sufficiently well with experimentally derived results to establish a high degree of confidence in the FE CAD technique.

It is considered that the 'M effect' type characteristic may be further improved by varying the relative disposition of elements and for practical dissimilar strip elements with reduced sections. These latter investigations are to be followed up in the next stage of the studies, although practical problems are anticipated in fixing low melting element material to fuse end plates.

#### References

- 1 Gomez J.C. and McEwan P.M., Determination of the Time/Current Characteristic of Fuses Using Finite Element Methodology, 6th IntSAP Conf, Lodz, 1989.
- 2 McEwan P.M., Numerical Prediction of the Pre-arcing Performance of HRC Fuses, PhD Thesis, Liverpool Polytechnic, 1975.

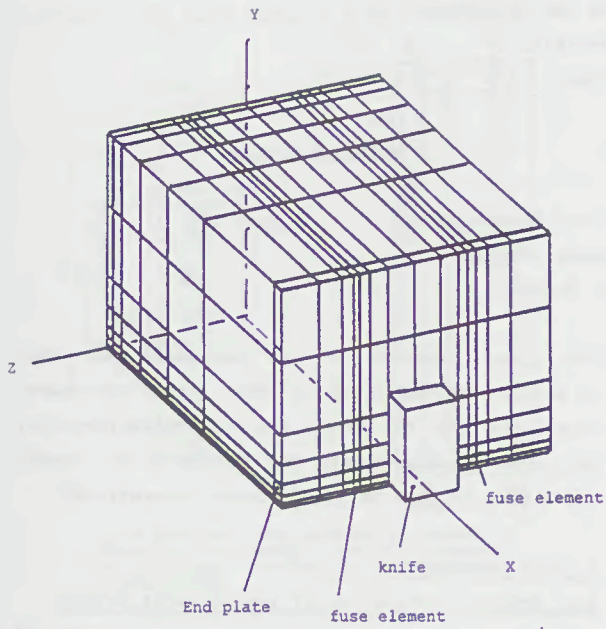


Figure 1 Finite Element Fuse Model

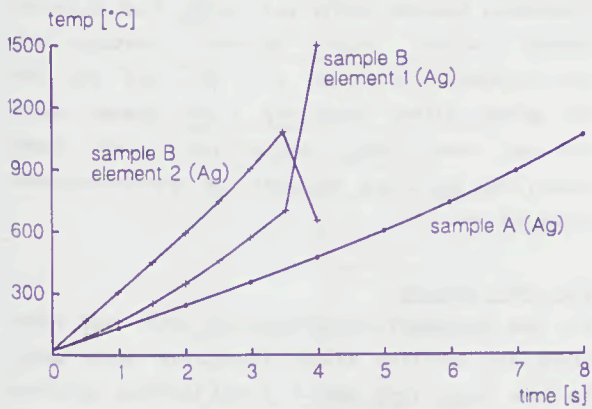


Figure 2 Critical Time-current Temperature Rise of Sample A and Sample B Silver Strip Elements ( $I = 300A$ )

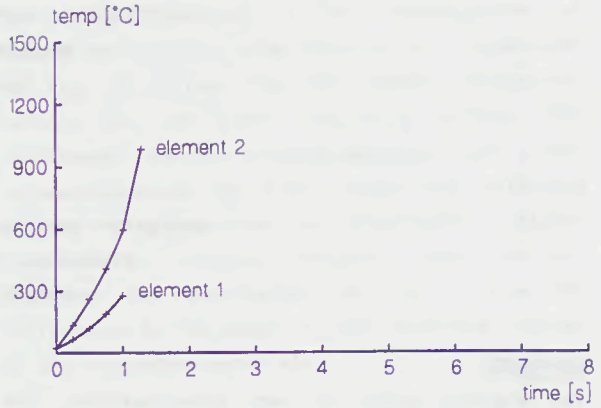


Figure 3 Critical time-current Temperature Rise of Sample C Sn-Ag Strip Elements ( $I = 300A$ )

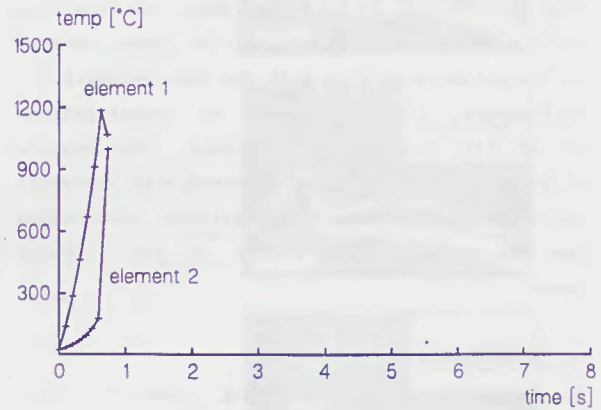


Figure 4 Critical Time-current Temperature Rise of Sample D Ag-Sn Strip Elements ( $I = 300A$ )

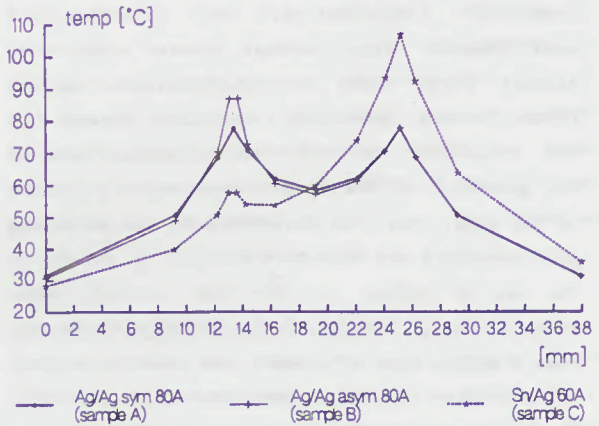


Figure 5 Section View of Fuse Steady-State Temperature Profile of Sample Parallel Elements Types A, B and C

INVESTIGATION FOR THE USE OF COPPER  
AS AN ELEMENT MATERIAL IN  
HV-HBC-FUSES

Gabriele Nutsch

and

Wolfgang Rother

Fachgebiet Schaltgeräte und Plasmatechnik  
Technische Hochschule Ilmenau  
0-6300 Ilmenau, Germany

ABSTRACTS

The starting point of our investigations has been the question whether one can substitute the silver by copper in high voltage fuses without changing the geometry of the fusible elements.

Some results will be presented about the prearcing and the arcing phase of copper wire fuses related to the silver wire fuse with the same geometry.

Furthermore, it is reported on investigations of the life time of copper fuses. The results of the experiments will be compared with numerical computations. By the investigations conclusions were derived for using copper in high voltage fuses.

1. INTRODUCTION

In low-voltage high breaking capacity fuses copper is often used as fuse element. In case of high-voltage high breaking capacity fuses, however, silver serves as the material for the fuse element.

For producing cheaper hv-hbc-fuses, the problem of replacing silver by copper had to be taken into our consideration. The investigations made regarded high voltage fuses with fuse element wires which were manufactured in the former German Democratic Republic. Caused by the conditions of the manufacturing process the geometry of the fuse element should always be the same, while the parameters of the switching process should not deteriorate.

The use of copper as the fuse element seems to be difficult because of the possible oxidation. Fuse elements made of copper can oxidate already at low rated operation temperatures (/1/, /2/). The oxidation decreases the conductive cross-section, and the current density increases. Thus, the temperature of the fuse element also increase, the oxidation being further accelerated. This might lead to the early break-up of the fuse link and could possibly destroy it.

For these reasons it was necessary not only to perform current breaking test duties of copper fuse-links and to check the t-I-characteristic, but also to investigate the behaviour of copper fuse-links in case of rated current operation.

2. TEST PARAMETERS

2.1. Physical properties of fuse-element metals

If silver is replaced by copper, the changed properties of the material have to be considered.

For our calculations we used the values according to /3/.

In some cases, copper fuse elements with silver coatings are used for low-voltage fuse-links. Therefore, besides silver and copper fuse elements copper wires with silver coatings, were investigated, too. Wires with 10, 30, 150 and 260 gramms silver layer per 1,000 gramms basic material were used, respectively. For these cases, the following designations are introduced: Cu/Ag 10 etc.

2.2. Test samples

For the necessary investigations both test fuse-links and modified hv-hbc fuse-links were used. In fuse links type HWSF-B 3,6kV/10A the Ag-wires was replaced by Cu-wire or Cu-wire with Ag-coating of the same dimensions. The current breaking tests demanded according to IEC 282-1 were performed in the test plant "Institut Prüffeld für elektrische Hochleistungstechnik"(IPH) in Berlin.

The investigations of test fuse-links which were made in the test field of the Ilmenau Institute of Technology served as basic investigations of the behaviour of the various metals for fuse elements. Model 1 (Fig. 1a) is used for short-circuit current breaking tests, while model 2 (Fig. 1b) is used for investigating the fusing by overload, where the fuse element is so long that the axial heat conduction to the fuse end caps can be neglected

similar to the conditions in a hv fuse-link.

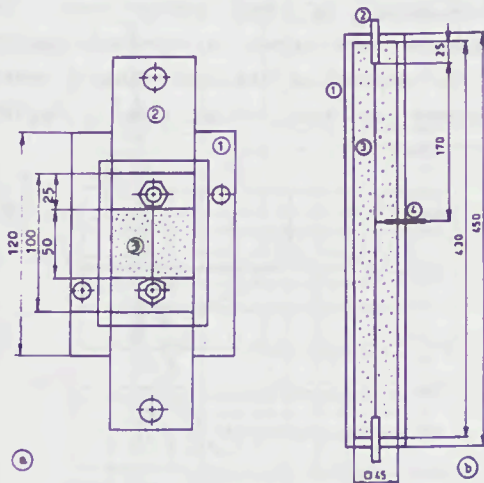


Fig. 1: Test fuse-links: (a)-Model 1, (b)-Model 2  
1-body, made from organic textolite, 2-terminal and fuse element connection, 3-fuse element, 4-thermoelement

### 3. INVESTIGATION OF THE SHORT-CIRCUIT CURRENT BREAKING

#### 3.1. Investigation of test fuse-links

Both wires with uniform cross-section and wires with restrictions were investigated.

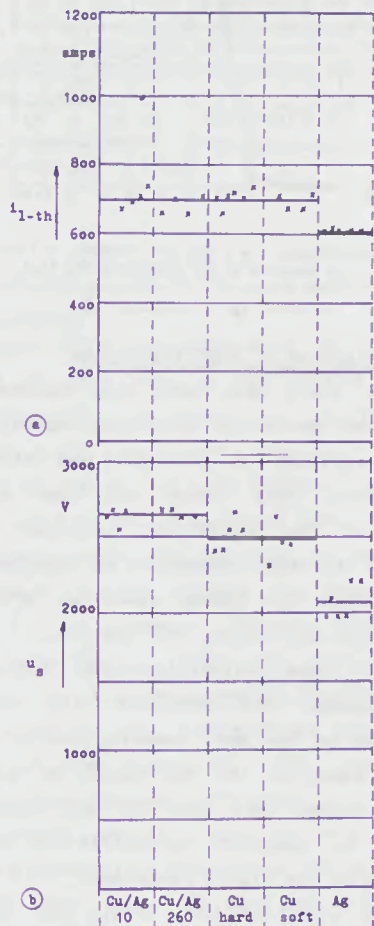


Fig. 2: Let-through current ( a ) and switching voltage ( b ) of uniform fuse-element wires with model 1

The results gathered in the investigation of a wire with uniform cross section are illustrated in Fig. 2: Silver has the lowest let-through current and the lowest switching voltage. The let-through current of the various copper wires is approximately the same, while the switching voltage of Cu/Ag-wires is considerably higher than that of uncoated Cu-wires, which was not expected. The oscillograms in Fig. 3 show the differences in the peaks of the switching voltage of the respective materials.

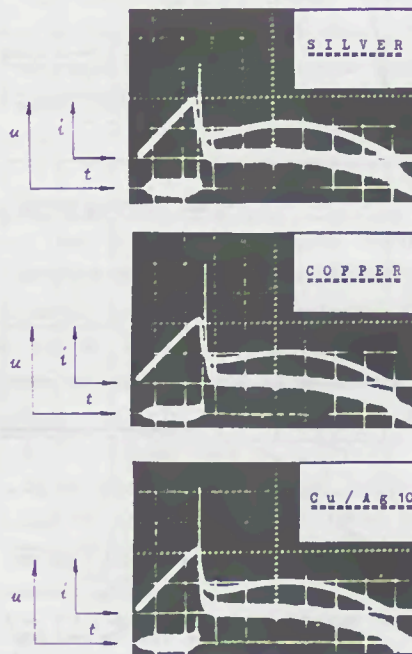


Fig. 3: Oscillograms with model 1  
i: 316 amps/div., u: 500 volts/div., t: 1msec./div.

The generally very high switching voltage is generated by the uncontrolled disintegration of uniform wires due to self-magnetic forces and surface tension. As a result, a large number of single arcs is formed which cause the high switching voltage. Out of a variety of calculations possible for this kind of voltage, the formula by Johann /4/ matches best with our results.

#### 3.2. Modified hv-hbc fuse-links

Modified 3,6kV/10A fuse-links with copper fuse elements and Cu/Ag 10 fuse elements, respectively, were tested for the test duties 1 and 2 and compared to silver wire fuse-links. All fuse-links with copper fuse elements (about 100) stood the tests, safely interrupting the current. The Figures 4 and 5 illustrate the results. These results confirm our measurements of the

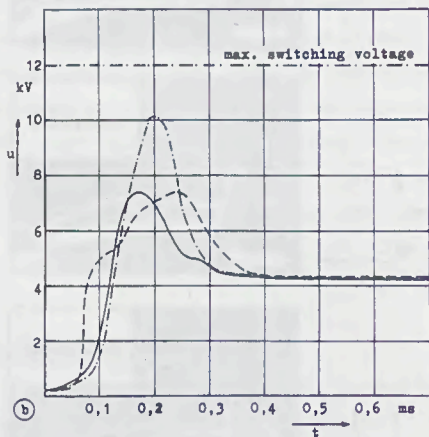
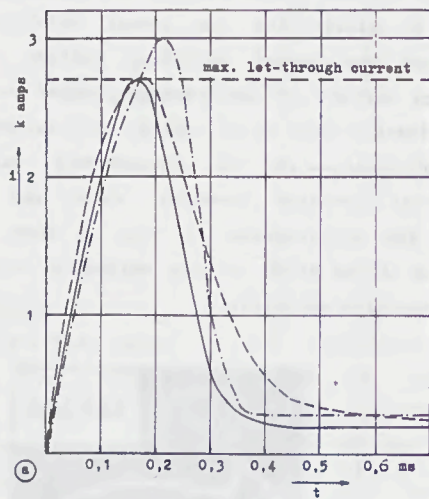


Fig.4: Current ( a ) and arc voltage ( b ) as a function of the time from the test duty 1  
 — Ag ——— Cu — · — Cu/Ag 10  
 ( cut - out )

test fuse-links: Cu/Ag-wires have worse breaking characteristics than copper wires and silver wires. Copper wires can be compared to silver wires with regard to their current-breaking capability, in fact they are even better in some cases because of their lower switching voltage with equal arcing time.

#### 4. MEASUREMENTS OF THE $t$ - $I$ -CHARACTERISTIC

The fusing time of the fuse-wire in case of overload depends not only on the material properties of the fuse element such as resistivity, heat capacity, fusion heat, and cross section, but also on the properties of the quartz sand surrounding the fuse element. The smaller the current and the longer the fusing time, the

greater the influence of the heat transfer to the surroundings by the quartz sand. The investigations were aimed at proving whether or not the material of the fuse element exerts an influence on the fusing time - current characteristic.

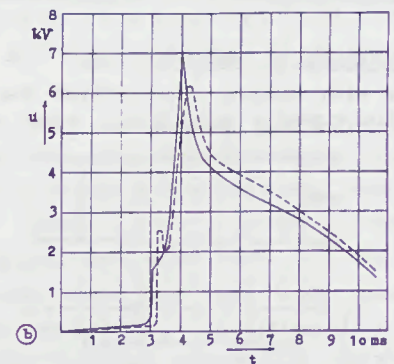
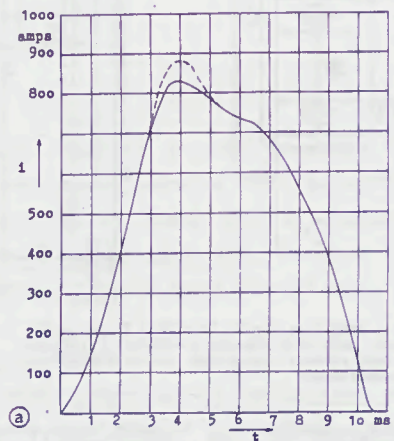


Fig.5: Current ( a ) and arc voltage ( b ) as a function of the time from the test duty 2  
 — Ag ——— Cu

#### 4.1. Investigation of test fuse-links

In model 2 there are used long uniform wires made of the materials mentioned above. Within our investigations we did not use wires with solder spots. This leaves out the different behaviour of the solder on the fuse elements and enables the sheer comparison of materials.

Figure 6 shows the fusing times as a function of the effective value of the a.c. breaking current for some materials. The fusing time is approximately the same for all materials. This is due to the heat transfer characteristics of quartz sand, on the one hand. On the other hand, the higher heat capacity and fusion heat of copper as compared to silver is obviously compensated by the higher resistance.

The dashed line is the result of numerical calculation by Wintergerst /5/ for the copper elements.

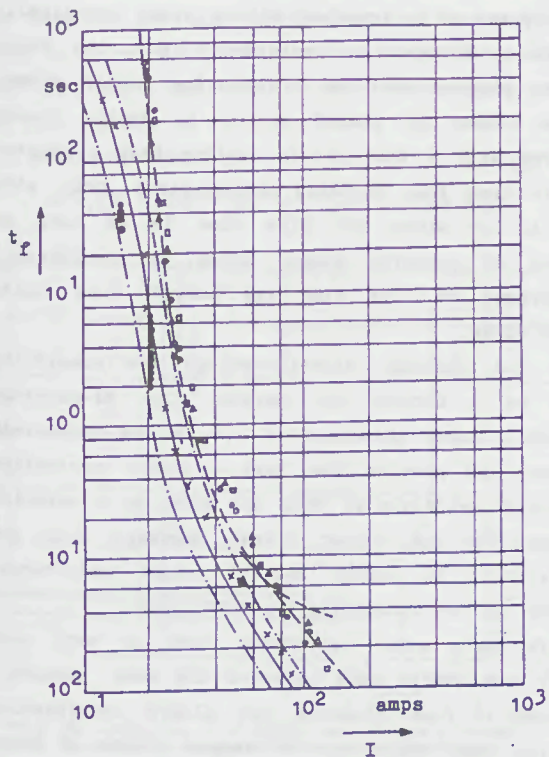


Fig.6: Fusing time versus current  
 - model 2 with uniform cross-section wires  
 O Cu, □ Ag, △ Cu/Ag 260, test results  
 ----- calculation by Wintergerst /5/  
 - HV-HBC-fuses 3,6kV/10A, related of the current per one element  
 x Cu, ■ Ag, ● Cu - test duty 3  
 ——— time-current-curve with —·— the permitted tolerance range

#### 4.2. Modified fuse-links: $t$ - $I$ -characteristic and test duty 3

The results of the measurements of the fusing time and of test duty 3 for HwsF-B 3,6kV/10A copper fuse-links as well as single results of HwsF-B 3,6kV/10A silver fuse-links are also indicated in Fig. 6. For this purpose, the characteristic curve of the latter ones with the permitted tolerance range was included in the diagram. The current flowing through the fuse-link was related to the current flowing through each single conductor in order to facilitate the comparison to the measurements performed with model 2. Due to the restrictions of the fuse elements of the fuse-links, the fusing times are below those measured with model 2.

The conditions are the same as with model 2: the fusing times of Cu-fuse-links are only slightly different from those of Ag-fuse-links, all of them being within the permitted tolerance range.

The HwsF-B 3,6kV/10 A fuse-link has a minimum

breaking current of 40 A (see test duty 3). This current was also used for testing the Cu-fuse-links. With the fusing times resulting from these tests being within the tolerance range according to the IEC 282-1 standard. The fuse-links safely switched off the current. Some fuse-links were additionally tested with  $I = 30$  A under the conditions of test duty 3. The current was safely switched off. The fusing times are within the tolerance range, as can be seen in the figure 6, too.

These results and the results of the investigations of test fuse-links were confirmed. Silver and copper used as fuse elements do not have different breaking characteristics. The copper-fuse-links meet the conditions of the test duties extra ordinarily well.

#### 5. OXIDATION ON OF FUSE ELEMENTS

The thermal load of the fuse element that occurs in the operation may cause irreversible changes of the material by diffusion processes and the formation of an alloy between the solder and the conductor material as well as by the oxidation of the conductor material. The process of material changing in the solder spot is generally called "ageing". It is often the subject of investigation e.g. by Klepp /6/ and Hoffmann /7/. This process, however, was not investigated within the framework of our research programm.

#### 5.1. Determination of the temperature of the fusible element

As described in another paper /8/, the temperature of the fuse element determines decisively the oxidation rate. In the range of rated current, the temperature was calculated according to Vermij /3/ by measuring the heat transfer coefficient  $G$ , and theoretically by using the finite element method. For both procedures, the material values and, as in case of the latter, also the properties of the quartz sand had to be taken from literature. Since the values indicated by the various authors differ very much, we used the results gathered from the measurement of the temperature of the fuse element as a basis for our investigations.

The measurements were made with Ni-Ci-Ni thermocouples, mainly for model 2, and with potential probes of thin Cu-wires, the latter method being applied for the modified HV-hbc-fuses. Here, the voltage drop at the respective current measured

over a definite part of the fuse element by two probe wires was used for determining the resistance of this part. Its temperature was determined on the basis of the well-known temperature dependence  $R = R_0 (1 + \beta \vartheta)$ . Preferably,  $R_0$  is not determined by the help of the material values taken from literature as in /9/, but are measured with the same arrangement. If the distance between the probe wires is small, the course of temperature along the fuse element can be determined. On the other hand, the respective measurements revealed that, due to the trapezoidal course of temperature, it is sufficient to determine a mean temperature of the fuse element on the basis of the measurement of the resistance of the fuse-link.

### 5.2. Life tests of various materials for fusible elements

For these investigations, the uniform wires of model 2 were fixed in open air and periodically loaded with a current 1.4 times higher than the rated current of the fuse element. The duration of current flow was 1 hour, the currentless break being 1 hour, too. Caused by the "breathing", a high thermal load of the fuse element follows from the repeated heating-up to a temperature of 400 to 600 °C and the following cooling to room temperature, so that the effects of oxidation can be determined already after a relatively short time. The resistance is measured at the end of the currentless break. The results of the increase of resistance with the number of cycles are illustrated in Fig. 7.

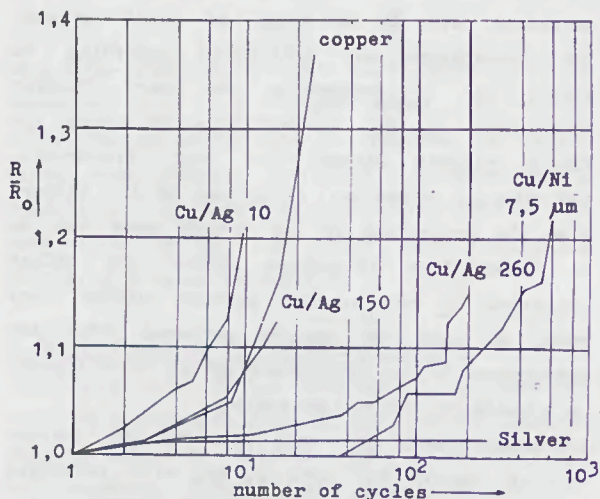


Fig. 7: Relative increase of resistance of fuse element materials

As it was to be expected, silver wires practically show no increase of resistance. Thus, the tests were stopped after 240 cycles. For copper wires, the number of passed cycles is small. Copper wires with a thin silver coating have a shorter life time than uncoated copper wires. Only with Cu/Ag 150 wires the life time is as long as that of uncoated copper wires. A considerable increase of life time was proved with Cu/Ag 260 wires.

In the plating, nickel-coatings are considered to be a barrier for oxygen. The Ni-coatings with a layer thickness of 7,5 μm are relatively dense and provide the best possible protection against oxidation if they are used as a covering layer for the copper wires. However, they are difficult to deform and to solder and, thus, they can not be applied for fuse-links.

Life tests under continuous load in both open air and quartz sand revealed the same tendency: Cu/Ag 10 fuse elements are always considerably worse than those made of copper. Figure 8 shows a metallographic for illustrating oxidation even below thicker Ag-coatings.



Fig.8: Metallographic of Cu/Ag 260 wire

### 5.3. Calculation of the life time of modified HV-hbc-fuse-links

As mentioned above, the authors of /8/ introduced a simple model for calculating the life time of fuse-links in case of continuous load. The calculations are based on the equation by Vermij /3/ for determining the temperature of the fuse element, into which the decrease of radius by oxidation was included.

$$\vartheta_{\max} = \frac{\vartheta_0}{(1 - \frac{x}{r_0})^4 - \beta \vartheta_0} \quad (1)$$

$$\text{with } \vartheta_0 = \frac{q_0 \cdot l^2}{G \cdot A_0^2} = \text{constant}$$

$$x = (k \cdot t)^{1/2} = r_0 - r_t = \text{decrease of radius}$$

The rate of reaction coefficient  $k$  for copper wires in quartz sand was determined experimentally (see /8/) as a function of the temperature of the fuse element as

$$k = A \exp(-B/T) \quad (2)$$

$$= 9,17 \cdot 10^{-11} \text{ cm}^2 \text{ s}^{-1} \exp(-4048 \text{ K}/T)$$

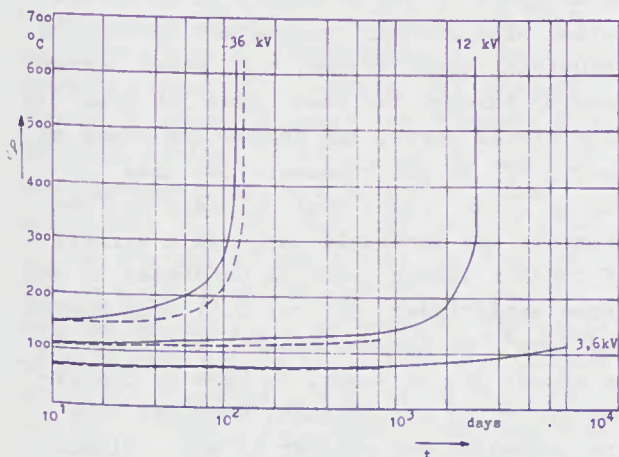


Fig.9: The temperature  $T$  of fuse elements versus life time  $t$  for different fuses with rated current  $I = 10$  amperes  
 ----- experiment, ——— calculation

For more than two years long-time tests have been made with 10 A copper fuse-links of different rated voltage values for checking the calculation model. Figure 9 illustrates the results gathered with this calculation model and compares them to the measured values gathered before December 31st, 1990. Here, the temperature of the fuse element was determined as mean temperature from the voltage drop of the fuse-link at rated current. The measurement results confirm the trends following from the calculation.

## 6. CONCLUSIONS

- The life time to be reached with a fuse-link is determined by the initial rated operational temperature.
- With a given fuse element, the initial rated operational temperature depends on the design of the fuse link. The rated power dissipation per fuse length being a decisive influencing factor.
- Out of the number of fuse-links investigated by us, only the 3,6kV/10A fuse-link provides a sufficient life time of 20 years.
- The dimensions of the fuse element being maintained, fuse-links with Cu-fuse elements, too, will meet the demands with regard to the  $t$ - $I$ -characteristic and the test duties according to IEC 282-1.

- The tolerances of the tests provide some freedom in varying the geometry of the fuse element, which can be used for lowering the rated operational temperature.

This offers the chance to guarantee a low enough oxidation rate for all types of fuse-links investigated.

The investigations necessary for this purpose are not yet completed.

## REFERENCE

- /1/ Schatz, J.  
Eignung von Kupfer-Silber-Manteldrähten zu Schmelzeinsätzen in elektrischen Sicherungen ETZ 65(1944) 43/44, pp. 341 ff.
- /2/ Bors, S.  
Beitrag zur Frage der Alterung von Schmelzsicherungen  
E. u. M. 7a(1961) 6, pp. 131
- /3/ Vermij, L.  
Behaviour of short-fuse elements associated with thermal effects  
Holectechnik 5(1975) pp. 76
- /4/ Johann, H.  
Ausschaltlichtbögen in elektrischen Sicherungen mit körnigem Löschmittel  
Teil 2: Elektrische Eigenschaften und ihre Parameter  
Siemens-Forschungs- und Entwicklungsberichte 9(1980), pp. 205
- /5/ Wintergerst, E.  
Über die Schmelzzeit von Schmelzsicherungen  
Z. für angewandte Physik II, 1950, 4, S. 167 - 173
- /6/ Klepp, G.  
Über das Abschmelzverhalten von Sicherungsschmelzleitern im Überlastbereich  
Diss. TU Braunschweig, 1982
- /7/ Hofmann, M.  
Experimentelle und rechnerische Untersuchung von Ansprechennlinien und Alterungsvorgängen bei Sicherungsschmelzleitern  
Diss. TU Braunschweig, 1986
- /8/ Nutsch, G.; Rother, W.  
Untersuchungen zur Oxidation von Kupferschmelzleitern  
Int. Wiss. Koll. TH Ilmenau, 1986
- /9/ Agarwal, M.S.; A.D. Stokes; P. Kovitya  
Prearcing behaviour of open fuse wires  
J. Phys. D: Appl. Phys. 20(1987)1237

*Quartz-  
sand-filler*

## PRINCIPAL MANUFACTURE TECHNOLOGIES FOR SEMICONDUCTOR FUSES

K.K. Namitokov, M.A. Ilyina, G.G. Zhemerov, and I.G. Shklovsky

The Kharkov Institute of Engineers of Municipal Economy

Problem formulation. The basic technical and cost parameters of semiconductor fuses are largely determined by the technology employed to produce the hard filler. The traditional methods<sup>1</sup>, in particular those involving thermal hardening of a binder-impregnated filler present certain difficulties as they require complex equipment and happen to be power consuming (over 10 kW.hr per unit). Besides, the technological procedures last for a long time (10 to 15 hr) and often result in fracturing of the fuse terminal coating in the furnace. The present writers have suggested a new technology<sup>2</sup> in which the filler is baked through heating of the current-carrying fuse pieces with electric current. In this approach, many of the technical problems are removed. Currently the method is subjected to practical tests and theoretic analysis in view of the its potential advantages.

Experimental set-up. The set-up involves an insulated base capable of accomodating as many as 10 ПП 60M fuses (rated current and voltage values are 630 A and 660 V); buses of variable length and cross-section area (40 to 300 mm and 30 to 400 mm<sup>2</sup>, respectively) used to seriesly connect the fuses, and an adjustable power supply to produce currents up to 30 kA at 4 V. The ПП 60M fuse is shown in Fig. 1. It consists of an ultraporcelain cartridge 1 containing bended fuse elements 2 made of copper that are welded to copper terminals 3. Cover caps 4 are at the top and bottom; the filler is charged through the opening 5 in the top end cap 4, which is shut by the lid 6. The drain opening in the bottom end cap 4 is screened with the gauze 7 adjacent to which is the outlet tube 8 to release products of the baking process. The fuse is fixed to the buses with terminals 3. It is filled with quartz sand and impregnated with a 30 % colloidal silica suspension in water.

Phenomenology of the hardening process; experimental results for standard parameters

For practical purposes, of interest would be analysis of the processes in an installation with standard parameters typical of industrial applications, e.g. rated current density through the fuse about 550 A/mm<sup>2</sup> in constricted parts, and conducting buses of length 175 mm and cross-section area 180 mm<sup>2</sup>. The Joule heat released in fuse elements and terminals supports a variety of complex thermodynamical processes in the dense sand/binder mixture. Following Barrow and Howe<sup>3</sup>, we assume chemical reactions to be absent or, at least, to have no important effect on the process, provided they are characterized neither by heat release or absorption, nor influence on the mass transfer in the liquid or vapour-gas phase. The preheating stage represents an increase to the boiling point in the temperature of the liquid component directly adjacent to the current-carrying parts. At this stage, no products are released through the drain opening, gauze screen or the outlet pipe. Objective external manifestations of this stage are a noticeably greater voltage drop across the fuse and a weakly increased temperature of the cartridge and terminals. The end to this stage is marked by the first liquid drop released from the drain opening. This occurs some 5 or 11 minutes after the onset of the process. The temperature of the first drop is close to the ambient temperature (i.e. 30 to 40 °C). At the following stage the liquid component is partially evaporized and the vapour expands to force part of the liquid through the pipe. During this stage which last for 13 to 19 minutes, the products are released mainly in the liquid phase, with the temperature and flow rate progressively increasing (Fig. 2). The hot liquid forced out by the vapour carries away various contaminants, thus performing "steam cleaning" of the filler. As a result, the fuse insulation resistance increases (to tens megohms after the breakdown current has been switched off). Of the 52 to 61 grams of

colloidal silica suspension introduced into the sand, it is hardly 15 grams that are released out of the fuse as a liquid. A stage close to the final is that of nucleate boiling. Under the action of overheated vapour (about 200 °C), individual bubbles appear first, at the end of the pipe, and later become a continuous flow of white steam of characteristic odour and growing temperature. Most of the product (up to 30 grams in mass) are released from the fuse during the stage, in the form of the gas-vapour mixture described. The stage does not last for more than 15 minutes. By the end of the stage, the outflow of the white steam becomes less intense and the vapour turns colourless. The stage of invisible vapour release is the longest among all (lasting for 40 to 50 min) and can be detected, e.g. with a sweating mirror. It is characterized by a rather quick increase in the temperature of all parts of the fuse and an increased voltage drop. An important practical criterion for the completion of the hardening process is cessation of the colourless vapour flow from the structure. The absolute criterion is provided by evaluation of the fuse mass. If the mass at the end of the hardening process is 0 to 2 g greater than before introduction of the colloidal silica, then the result may be considered excellent. With a 2 to 5 g mass increase the result is good, while with 5 to 11 g it is merely satisfactory. The complete cessation of the steam outflow and the nearly zero value of the mass increase speak in favour of the hypothesis suggesting a predominant role of heat and mass transfer effects without noticeable chemical transformations. With regard to performance characteristics, the quality of baking is estimated from the magnitudes of the Joule integral and the arc energy. The technology described does not have a destructive effect on the temperature sensitive parts of the fuse like constrictions or welding points, nor does it affect the fuse resistance. If the 10 fuses placeable on the base are baked simultaneously, then process stages in each piece are shifted in time with respect to other specimens (within a few minutes), so

that they should not interface.

Effects of different factors. The character of the hardening process is largely determined by two basic parameters which are the current density in the fuse elements and the bus geometry (i.e. cross-section area and length). With a proper allowance for the electric conductivity magnitude, the kind of the material the current carrying parts are made of is of no importance. By increasing the current density by 4 to 11 % against the rated value, the baking process can be greatly intensified (the total duration reduces by nearly 20 %), while all the stages mentioned remain. Further increase in the density of current through the fuse elements is not advisable for reliability reasons, while lower densities are impractical. The cross-section area and length of the conducting buses fully determine the course of the hardening process near the cartridge ends and have an important effect on the areas adjacent to the fuse elements. The effect of variations in the bus length within 40 to 300 mm is equivalent to changes of the cross-section area. For the sake of designer's convenience, we have selected buses of 170 mm in length for the experiments described, while the cross-section area could be varied from 30 to 400 mm<sup>2</sup>. With 30 mm<sup>2</sup>, the process of filler hardening was characterized by extreme intensity. The outgoing products appeared in the gas-vapour phase alone, although the outflow started with a noticeable delay (about 2 min). Note that the process developed within 30 minutes, which was 2 or 3 times quicker than for rated parameter values, and with excellent quality at that. (The excess mass was practically zero.) However, the copper buses showed heavy blackening and proved unfit for further use, while the fuse element constrictions and welding points remained in a good condition. In the case of the largest cross-section area, 400 mm<sup>2</sup>, the general pattern, as described for the rated parameter values, remained but the process lasted as long as 5 hours. The quantitative characteristics were sizably lower and the filler in the cartridge end portions did not solidify at all. Thus, buses of small cross-section area in fact play the part of a

heater, whereas larger buses act as a radiator.

Prior heating of the buses, e.g. owing to the preceding technological process, is of no special importance because of the quick cooling of the set-up (e.g., the temperature of buses drops from 110 to 35 °C over 4 minutes). Yet in some cases, the time necessary for the liquid component to appear in the outlet pipe reduced by 2 or 3 minutes. It seems noteworthy that the time interval between introduction of a binder in the filler and the beginning of the hot hardening process virtually has no effect either on the process or the condition of the (copper) fuse element, at least for times within 100 hours. On the other hand, decreasing the current value in the course of the process, even for a relatively short time, has a negative effect on the quality of baking. This is even more true for a fully halted baking process with a completely cooled set-up. The quality can be restored only by repeating the baking procedure all over again, even many months after the initial process. As a special aspect of investigations, the quartz sand-colloidal silica mixture in the cartridge in some experiments was blown through with air, prior to the baking procedure, the air being compressed to  $(0.35+0.45) \times 10^5$  Pa. Of the 52 to 61 g of the silica suspension introduced, about 22 to 31 g leave the cartridge through the drain opening during the initial 1 or 2 minutes of the blow-through. Further blowing, even during lengthy periods of time (10 to 18 minutes), of an air either at ambient temperature or at 120 to 150 °C, does not remove more of the suspension from the fuse cartridge. At other stages of the filler hardening process, the products are released practically in the gas-vapour phase alone, i.e. air blowing has suppressed the stage of liquid product release, thus reducing duration of the process by 30 or 40 %, with the high quality of the hard filler retained. By prolonging the procedure, a zero mass increment is guaranteed, however characteristics of the filler are not changed.

Temperature field measurements in the filler and the fuse element performed in the

course of the process have allowed determining the effective thermal conductivity  $\lambda_e$ .<sup>4</sup> If combined with the solution of the direct heat conduction problem, e.g. by the iterative technique<sup>6</sup>, this knowledge enables evaluating the effective heat capacity  $C_e$  of the filler. To that end, the calculated temperature field  $T_{calc}$  resulting from successive refinements of the input data was compared with the measured values  $T_{meas}$ . The value of  $C_e$  was chosen from the condition

$$|T_{calc}(x,y,z,t) - T_{meas}(x,y,z,t)| < \delta_0$$

where  $\delta_0$  is the limiting value of the mismatch which determines the solution accuracy. In the course of filler hardening,  $\lambda_e$  and  $C_e$  changed with time between 1.3 and 3.2 W/m deg, and 1.5 and 4.2 J/g deg, respectively, following rather complex laws. The values of  $\lambda_e$  and  $C_e$  obtained were employed to improve the mathematical model described below.

#### An attempt of theoretical description.

##### Problem formulation and basic equations.

We will analyze the physical processes in a fuse volume representing a cylindrical sector filled with a sand-liquid mixture. All the boundary surfaces, except the drain opening aperture, are assumed to be impenetrable, according to the symmetry conditions. The filler is heated by the fuse element whose thermal condition in the current carrying state is described by

$$\frac{\partial^2 T}{\partial R^2} + \frac{1}{R} \frac{\partial T}{\partial R} + \frac{1}{R} \frac{\partial^2 T}{\partial z^2} + \omega(R, \theta, z) = \frac{C_1 \lambda_1 \partial T}{\lambda_1 \partial z} \quad (1)$$

where  $T_1$ ,  $C_1$ ,  $\lambda_1$  and  $\lambda_1$  are the temperature, heat capacity, mass density and thermal conductivity of the fuse material, respectively. This equation is valid only for the fuse element of thickness  $\delta$  in the domain specified by the equations  $R_1 + \delta > R > R_1$ ;  $\theta_0 > \theta > 0$  and  $H > z > 0$ , where  $R_1$  is the radial location of the elements;  $\theta$  is the angle at the vertex of the sector considered, and  $H$  the sector height. The equation for the filler adjacent to the fuse elements from its both sides is

$$\frac{\partial^2 T_2}{\partial R^2} + \frac{1}{R} \frac{\partial T_2}{\partial R} + \frac{1}{R^2} \frac{\partial^2 T_2}{\partial \theta^2} + \frac{\partial^2 T_2}{\partial z^2} = \frac{c_2 \gamma_2}{\lambda_2} \frac{\partial T_2}{\partial \tau} \quad (2)$$

$R_1 > R > 0; \theta_0 > \theta > 0$  and  $\lambda_2 \frac{\partial T_2}{\partial z} \Big|_{H > z > 0}$

where  $T_2$ ,  $c_2$ ,  $\gamma_2$  and  $\lambda_2$  are, respectively, the temperature, heat capacity, mass density and thermal conductivity of the filler. The boundary conditions are

$$\frac{\partial T_i}{\partial z} \Big|_{z=0} = K_i (T_i - T_{amb}), \quad \lambda_1 \frac{\partial T_1}{\partial R} = \lambda_2 \frac{\partial T_2}{\partial R} \Big|_{R=R_1} \quad (3)$$

$\theta > \theta > 0$   
 $H > z > 0$

$$\frac{\partial T_j}{\partial R} \Big|_{R=R_2} = K_j (T_j - T_{amb});$$

$\theta_0 > \theta > 0$   
 $H > z > 0$

$$\frac{\partial T_i}{\partial \theta} \Big|_{R > R > 0} = 0; \quad \lambda_1 \frac{\partial T_1}{\partial R} = \lambda_2 \frac{\partial T_2}{\partial R} \Big|_{R=R_1+\sigma}$$

$H > z > 0$   
 $\theta > \theta > 0$   
 $H > z > 0$

As a result of heating, the temperature of some filler areas can reach the boiling point for the liquid component, hence the heating is accompanied by phase transitions. In such areas, the temperature field is described by the differential equation

$$\frac{\partial^2 T_i}{\partial R^2} + \frac{1}{R} \frac{\partial T_i}{\partial R} + \frac{1}{R^2} \frac{\partial^2 T_i}{\partial \theta^2} + \frac{\partial^2 T_i}{\partial z^2} - \frac{z \gamma'}{\lambda_2 \delta \tau} = \frac{c_2 \gamma_2}{\lambda_2} \frac{\partial T_i}{\partial \tau} \quad (4)$$

where  $z$  is the specific heat of vaporization and  $\gamma'$  the mass density of the liquid component. Boiling of the liquid is accompanied by an increase in pressure, hence the liquid is forced through the drain opening. The law followed by the varying pressure can be found from the material balance and energy balance equations and the equation of state. The material balance equation takes the form

$$M' - M'' = \frac{\partial}{\partial \tau} (\nu' \gamma' + \nu'' \gamma''), \quad (5)$$

where  $M'$  is the liquid mass arriving to an elemental volume,  $M''$  the mass of the vapour released,  $\nu'$  and  $\nu''$  are the liquid volume and that of the vapour, respectively, and  $\gamma'$  and  $\gamma''$  the liquid and vapour mass densities. The energy balance equation is

$$M' i' - M'' i'' + Q = \frac{d}{d\tau} (\nu' \gamma' i' + \nu'' \gamma'' i'' + G c_s T_s) \quad (6)$$

where  $i'$  is the liquid enthalpy,  $i''$  that of the vapour;  $M' i'$  is the amount of heat arriving to the elemental volume with the liquid and  $M'' i''$  the amount of heat leaving

the volume with the vapour;  $Q$  is the amount of heat transferred to the elemental volume either from neighbouring elemental volumes of the medium or from the fuse element;  $G$  the sand mass in the elemental volume;  $G c_s$  the specific heat capacity of the sand and  $T_s$  the sand temperature. The saturated vapour density and that of the boiling liquid both vary with pressure, therefore the equation of state is broken up in a series of equations like

$$\gamma' = \gamma'(P); \quad \gamma'' = \gamma''(P); \quad i' = i'(P), \quad \text{etc.} \quad (7)$$

As follows from geometrical considerations, the total volume of the vapour and the liquid component should be equal to  $\nu$  both under static and dynamic conditions; i.e.  $\nu = \nu' + \nu''$ , where  $\nu$  is the constant value of the elemental volume. This implies that time derivatives of  $\nu'$  and  $\nu''$  should be equal (apart from the sign). At this stage we can linearize the equation set (4-6), assuming for simplicity's sake that  $M' = M'' = 0$ . The latter condition implies that no liquid arrives to a boiling elemental volume from adjacent volumes, nor does it release vapour outwards. With allowance for the above mentioned equality of the time derivatives, we have

$$(\nu_0' \frac{d\gamma'}{dP} + \nu_0'' \frac{d\gamma''}{dP}) \frac{d\Delta P}{d\tau} + (\gamma' - \gamma'') \frac{d\nu'}{d\tau} = 0 \quad (8)$$

In fact, this is an incremental form of equation (5), with  $\nu_0'$  and  $\nu_0''$  denoting initial volumes. The energy balance equation becomes

$$dQ = (\nu_0' \frac{d\gamma'}{dP} i' + \nu_0'' \frac{d\gamma''}{dP} i'') \frac{d\Delta P}{d\tau} + (\gamma' i' - \gamma'' i'') \frac{d\nu'}{d\tau} + G c_s \frac{dT_s}{d\tau} \quad (9)$$

which form takes into account that  $M' = M'' = 0$ . Equation (9) implies that the heat arriving to the volume is spent to change the heat content of the sand, water and water vapour. To analyze equations (8) and (9), we substitute  $t'$  instead of  $T_s$ . These are equal values as the temperature of sand follows that of the liquid, and  $dT_s/d\tau = dt'/d\tau$ . Combining equation (7) with the solution of (8) and (9), we arrive at

$$\frac{d\Delta P}{d\tau} = \frac{\Delta Q}{\Phi} \rightarrow d\Delta P = \frac{\Delta Q}{\Phi} d\tau; \Phi = \Phi_1 + \Phi_2 + \Phi_3 \quad (10)$$

$$\text{with } \Phi_1 = \nu_0 \left( \frac{\gamma''_z}{\gamma' - \gamma''} \frac{d\gamma'}{dP} + \gamma' \frac{di'}{dP} \right)$$

$$\Phi_2 = \nu_0'' \left( \frac{\gamma''_z}{\gamma' - \gamma''} \frac{d\gamma''}{dP} + \gamma'' \frac{di''}{dP} \right)$$

$$\text{and } \Phi_3 = G C_s \frac{dt}{dP}$$

The relations derived permit determining the pressure whose increase shifts the boiling front, as well as the rate of liquid and vapour flow through the drain opening.

The temperature field and volume variations of the filler where liquid filtering occurs under the action of high-pressure vapour can be analysed with several simplifying assumptions. First, we shall assume that the porous medium obeys Darcy's law. Second, the viscous and the inertial term in the equation of motion will be neglected in view of the low values of Darcy's and Reynolds numbers. With these assumptions, the equation of mass, momentum and energy conservation in a non-stationary three-dimensional flow through an isotropic porous medium takes the form

$$\frac{\partial P}{\partial \tau} + \frac{\partial (RW_R)}{\partial R} + \frac{1}{R} \frac{\partial W_\theta}{\partial \theta} + \frac{\partial W_z}{\partial z} = 0 \quad (11)$$

Actual boundary conditions are

$$\frac{1}{R} \frac{\partial (RP)}{\partial R} + \frac{\mu}{K} W_R = 0; \frac{1}{R} \frac{\partial P}{\partial \theta} + \frac{\mu}{K} W_\theta = 0 \quad (12)$$

$$\text{and } \frac{\partial P}{\partial z} + \rho g + \frac{\mu}{K} W_z = 0.$$

These equations govern liquid flow through the porous medium, representing in fact the equation of filtration, with  $W_i$  denoting the velocity of motion in the  $i$ -th direction;  $\mu$  the liquid viscosity;  $K$  - the penetrability of the porous medium, and  $g$  the gravity forces acceleration. The thermal flux diffusion equation is

$$W_R = \frac{1}{R} \frac{\partial R(RT_i)}{\partial R} + W_\theta \frac{1}{R} \frac{\partial T_i}{\partial \theta} + W_z \frac{\partial T_i}{\partial z} =$$

$$= \frac{\partial^2 T_i}{\partial R^2} + \frac{1}{R} \frac{\partial T_i}{\partial R} + \frac{1}{R^2} \frac{\partial^2 T_i}{\partial \theta^2} + \frac{\partial^2 T_i}{\partial z^2} - \frac{c_2 \gamma_2}{\lambda} \frac{\partial T_i}{\partial \tau} = 0 \quad (13)$$

with the boundary conditions of equation (3). Equation (13) describes the thermal state of such elemental volumes that have not yet reached the boiling point, however accepts the liquid carrying heat away and

forced through the volume. The three terms in the left-hand side describe the heat carried out by water along the directions  $R$ ,  $\theta$  and  $z$ , respectively. Equations (2), (4), (12) and (13) with the boundary conditions (3) and (12) were solved in the mathematical simulation technique with the aid of an  $R$ -network processor. The calculation error was within 7 to 13 %.

Test results for the fuses manufactured in the technology described. The fuses  $\Pi\Pi 60M$  were developed for diode converters of electric railway locomotives. Therefore, the conditions of primary importance that dictated the choice of a hard filler were prevention of filler leakage during operation and strict maintenance of a fixed packing density through the fuse lifetime. Besides, the method has proven to be highly efficient for cyclic loading duties (the 60M fuses have withstood 200 thousand current pulses in 2 years). Technical details are described in<sup>5</sup>. Here we will rather dwell on the effect of technological parameters on the performance in the fault current interruption regime. The fuses were subjected to tests of two kinds. Specimens with a normal degree of filler compaction (5 types) were tested for easy circuit breaking conditions, i.e. a voltage of 730 V and effective current of 11 kA. The filler types were:

a) standard granular filler without a binding agent; b) granular filler with 52 g of a binder introduced during 1 min under a pressure of 0.35 atm; c) binder-impregnated filler blown through during 1 min at 0.35 atm. After the blown-down the specimens contained 25 g of the binder; d) binder-impregnated filler subjected to a 1 min blow-down at 0.35 m and drying. The specimens contained 3.8 or 10 g of the binder; e) binder-impregnated filler that was not blown-through but subjected to drying. The specimens contained 3.8 or 10 g of the binder.

All of these fuses have shown practically identical performance characteristics, specifically  $I_0 = 14-15$  kA,  $t_0 = 9-10$  ms and  $W_{\text{break}} = (600 \text{ to } 700) \times 10^3$  A<sup>2</sup> sec. Type b) specimens released 25 g of the binder suspension, forced through the gauze under the arc

pressure at the switch-off.

Heavy duty tests (730 V, 150 kA effective,  $\cos \psi = 0.1$  and  $\psi_{\text{sw on}} = 52$  to  $62^\circ$ ) were performed for specimens of two groups. The first group (normal degree of filler compaction) comprised fuses of three types, namely a) with a standard granular filler; b) with a binder-impregnated filler subjected to drying. The residual binder content is up to 5 g; and c) with a binder-impregnated and dried filler of a 15 to 19 g residual binder content. The peak current magnitudes fed through this group of fuses and total Joule integrals were 32 to 35; 27 to 28 and 38 to 41 kA, and  $1.5 \times 10^6$ ;  $0.85 \times 10^6$  and  $2.9 \times 10^6$  A<sup>2</sup>.sec for the three types, respectively. The second group (loosely packed filler) involved fuses of two types, namely a) with a standard granular filler and b) with a binder-impregnated and dried filler of residual binder content below 3 g. The peak currents and let-through Joule integrals were, respectively, 42.2 and 28.5 kA, and  $(2.4$  to  $3.2) \times 10^6$  and  $(1.6$  to  $1.7) \times 10^6$  A<sup>2</sup>.sec. Type a) specimens showed end cap spiking and arc bursts.

Conclusions. The undoubtful advantages resulting from the new technology are

- i) the high mechanical strength of the filler, plus longevity and structural and dielectric uniformity owing to "internal" heating and "steam cleaning";
- ii) improved protection characteristics of the fuse (i.e. peak currents, arc energy and let-through  $\int i^2 dt$  integral reduced by a factor of 1.5 or 2) with retained integrity of the terminal coating and good appearance;
- iii) the high productivity and low costs of the technological process. A single manufacturing set-up for 10 fuses can provide up to 40 thousand fuses per year if operated in two shifts. The power consumed to bake 10 fuses is below 4 or 6 kW/hr. The laboratory breadboard installation (operated by a team including the present writers) has yielded over 3 thousand fuses.

#### REFERENCES

- [1] US Patents No 3838375 (1975) and No 4003129 (1977).

- [2] USSR Author's Certificates No 1184026 (1985) and No 1474755 (1988)
- [3] D.R. Barrow and A.F. Howe. Chemical interaction during fuse arcing. 12-15 Sept., 1989, In: Sixth Int'l Conf. on Switching Arc Phenomena, Lodz, Poland, pp. 246-249.
- [4] K.K. Namitokov, N.A. Ilyina, and I.G. Shklovsky. A finite-element analysis of the thermal behaviour of notched fuse elements in semiconductor protection fuses, 12-15 Sept., 1989, In: Sixth Int'l Conf. on Switching Arc Phenomena, Lodz, Poland, pp. 212-217.
- [5] K.K. Namitokov, N.A. Ilyina, and I.G. Shklovsky. Pulse withstandability of semiconductor protection fuses. 12-15 Sept., 1989, In: Sixth Int'l Conf. on Switching Arc Phenomena, Lodz, Poland, pp. 205-211.
- [6] A.N. Tikhonov and V.J. Arsenin. Methods of solution of ill-posed problems, 1979, Nauka Publ. Co., Moscow (in Russian), p. 304.

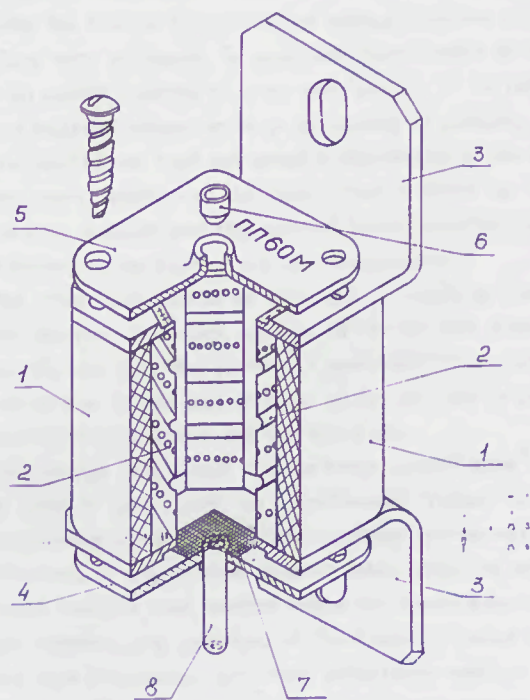


Fig. 1.

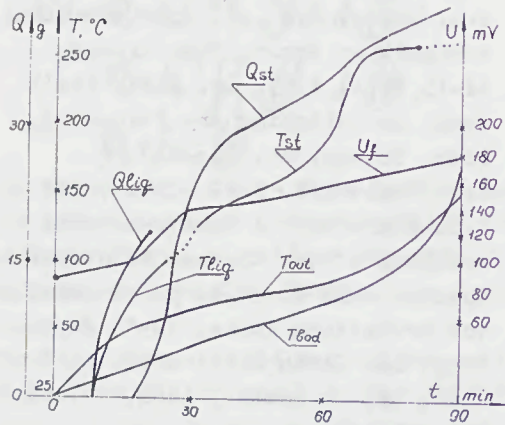


Fig. 2

Solid - filler  
No details given

CONTRIBUTIONS CONCERNING NEW EXTINCTION MEDIA IN ULTRA-FAST  
FUSES UP TO 2000 V a.c.

R.Eliade and E.Budascu  
Research Institute for Electrical Engineering-ICPE  
Bucharest, Romania

The authors' intention as it results from this paper is to present some of the researches made in our Institute in order to find out new extinction media for high-speed fuses. The new obtained extinction media have allowed significant improvements in these fuses performance: increase of electrical performances, decrease of the constructive overall dimensions comparing to the constructive version which uses the quartz sand as filler silver replacement by copper in fuse element manufacturing.

1. Introduction

The research of a new arc filler for high-speed fuses, another one different from the quartz sand, became more than necessary only two years ago when, by our government order the silver tape delivery was completely stopped. From that moment all our efforts were directed to find out a new filler which could allow the use of copper in fuse element manufacturing.

This new filler, which is a compact-rigid material, not only that it practically prevents copper oxidation whose negative effects are very well known, but, by its special properties concerning arc quenching and heat transfer, has allowed the decrease of the constructive overall dimensions and the increase of the nominal current within the given dimensions. Up till now, our researches have resulted in the certification in prototype phase, according to IEC 269-4-1986<sup>1</sup> of the following copper fuses:

- high-speed fuses of 660 V a.c, sizes 1, 2 and 3, fixing distance 80 mm, 100-630 A
- high-speed fuses of 660 V a.c, size OO, fixing distance 80 mm, 16-200 A
- high-speed fuses of 1000 V a.c, size 3, fixing distance 110 mm, 500 A and 630 A
- high-speed fuses of 1250 V a.c, size 3, 400 A, 800 A, 1150 A
- high-speed fuses of 1500 V a.c, sizes 2 and 3, fixing distance 140 mm, 350 A and 400 A
- high-speed fuses of 2000 V a.c, size 3, fixing distance 170 mm, 350 A

All these sizes are in conformity with DIN 43653 standard<sup>2</sup>. The last two types of fuses presented above have been made of silver fuse-elements and a compact-rigid filler. That is because of the ceramic body which, in our country hasn't reached the performance level obtained by the industrially de-

veloped countries.

Of course, this compact-rigid filler may be also applied to high-speed fuses with silver fuse-elements. Their performances will be clearly superior to those with copper fuse but their cost will be higher.

2. The compact-rigid filler

The compact-rigid filler generally consists of a refractory material with high resistivity and high dielectric rigidity and of an organic or anorganic binder. As refractory materials it is better to use oxides or nitrides of metals such as: silicon, magnesium, aluminium, beryllium, calcium or strontium and their mixtures.  $SiO_2$  having the highest electric resistivity among all the known insulators and being easily available as quartz sand, is generally much used for this purpose. Such materials are well settled within the fuse, the settling degree being maintained between exact limits. If these limits are exceeded the damping effect is no longer obtained. The refractory material is reinforced under the form of a rigid body by mixing it, before or after filling with an organic or anorganic binder which is added in an enough quantity to cover each particle of the refractory material without sensibly diminishing its porosity.

The used binder must not entail a degradation of the electric characteristics of the filler which is added to, when the fuse operates and the compact mass (material+binder) is subject to the electric arc high temperature.

The filler main role is to interrupt as rapidly as possible the electric arc which appears within the fuse when the shortcircuit cuts the current. A secondary but important role is that of the heat transfer within the fuse to the insulating body and from this one to the air.

The voltage on a single notches range, as Mr. Turner<sup>3</sup> says, is limited and can't be significantly raised without introducing current limits which condition fuse operation.

However, if the notches range number could be reduced (more volts on each notches range) this would mean a corresponding reduction of the dissipated power and of the fuse dimensions. All these advantages resulted from the new filler we have obtained as a better alternative to the quartz sand. During the latest years, we have developed a number of compact-rigid filler among which we have chosen the filler consisting of quartz sand and a reinforcing binder. This compact-rigid filler can be obtained

by applying a special compaction and reinforcing technology. As a result of the experiments made on electric fuses, it was found that this filler had higher properties comparing to quartz sand, concerning particularly three directions. The first direction consists of finding out a compact material which could prevent oxygen permeation to fuse elements and consequently their oxidation. The filler compaction was characterized by porosity determinations and water absorption. The filler porosity is 17%. The second direction was that of eliminating as much possible, the air thus improving the heat transfer. The third direction consists of laminating and cooling the electric arc, extinguishing it as rapidly as possible, with a strong decreasing evolution of the arc current. Therefore the fuses with compact rigid filler have a cut limited current and  $I^2t$  smaller than the fuses with quartz sand as filler.

As we have shown above, the base compact-rigid filler component is the quartz sand which in our country is mainly obtained at the Miorcani quarry. The quartz sand quality must provide a strong pressure and cooling of the electric arc. Thus, as Mr. Barbu<sup>4</sup> considers, a good quartz sand must include in its composition over 99%  $\text{SiO}_2$ ; under 0.03%  $\text{Fe}_2\text{O}_3$ ; under 0.5%  $\text{Al}_2\text{O}_3$ ; under 0.2%  $\text{CaO}$ ; under 0.04%  $\text{TiO}_2$ . The quartz sand action is connected with the metal vapour quantity produced by the material which constitutes the fuse-element. For instance, the silver or copper fuse-elements produce a smaller quantity of metal vapours in the electric arc, fact that favours its extinguishing. In their papers, Mr. Lipski<sup>5</sup> and Mr. Bratinov<sup>6</sup> mention that from the point of view of gases which are developed during the electric arc, the quartz sand produces the minimum pressure among all friable media. The quartz sand grains can store an energy of approximatively 2 kJ.

A very important problem is that of filler settling. The fuse ceramic body volume must be filled in proportion of 60...80% from the total volume, taking into consideration the dimensions, the particle distribution and their settling degree, the rest representing the vacancies among which the metal vapours can diffuse in order to cool and extinguish the arc.

The experimental results indicate the fact that, by the filling density increase, a series of fuse operation characteristics regarding fault current interruption are improved: arc time decrease, arc  $I^2t$ , arc energy and fulgurite length decrease.

However, as it also results from Mr. Namitokov's paper<sup>7</sup>, there are two parameters which deteriorate concurrently with the filling density increase: the arc voltage and the pressure of the ceramic body wall. While the arc voltage continuously raises together with the filling density, the pressure raises together with the filling density up to 1,73  $\text{g/cm}^3$  value, and then strongly decreases together with the filling density increase. Consequently, the compaction densi-

ty was chosen at minimum 1.74  $\text{g/cm}^3$  when all the fuse characteristics are considerably improved.

As we all know, with high speed fuses, the maximum admissible arc voltage in operation is 2,5 x utilization voltage for utilization voltages between (0.7...1.1) x the nominal voltage. There must also be attentively analysed the quartz sand components and their effects. For instance the components which can develop gases within the electric arc, such as  $\text{CaCO}_3$ , must be eliminated.  $\text{CaCO}_3$  elimination is made by quartz sand heating at approx. 950°C, obtaining in this way the following chemical reaction:



The water content is eliminated from the quartz sand by heating it at approx. 100°C before filling. The metal oxide content ( $\text{Al}_2\text{O}_3$  and  $\text{Fe}_2\text{O}_3$ ) has negative effects.

As not all the quartz sand deposits are rich in  $\text{SiO}_2$ , in many cases the respective sand must be enriched. One of the methods consists of its wash in HCl.

### 3. Fuse elements

The compact-rigid filler made possible, for the first time in our country, the use of copper instead of silver in the manufacturing of fuse elements meant to high-speed fuses. Our laboratory has, besides the research concerns in the field of low voltage fuses, also an operation plant for high-speed fuses meant as spare parts in different driving models in the cement industry, the aluminium industry, oil-field exploitation, transport, a.s.o. Therefore, for a couple of years we have manufactured high-speed copper fuses and their operation behaviour is very good.

Material choice for fuse element construction depends on the metal physical-mechanical parameters and of the fuse type. The main parameters that must be taken into account are presented comparatively for several metals, in Table 1.

Table 1

Material/ Parameters	Al	Ag	Cu
Resistivity $10^{-6} [\Omega \cdot \text{cm}]$	2.55	1.51	1.63
Density [ $\text{g/cm}^3$ ]	2.7	10.5	8.9
Specific heat [ $\text{W.s/g}^\circ\text{C}$ ]	0.86	0.23	0.38
Thermal conductivity [ $\text{W/cm}^\circ\text{C}$ ]	2.26	4.18	3.9
Melting temperature [ $^\circ\text{C}$ ]	659	961	1083
Vaporization temperature [ $^\circ\text{C}$ ]	2400	1950	2350
Mayr constant $10^8 [(\text{A/cm}^2)^2 \cdot \text{s}]$	2.94	6.64	9.55

It can be observed that silver has the best electrical properties and it's necessary to be used to high speed-fuses

with excellent performances: small operation  $I^2t$ , reduced dissipated powers, high lifetimes, a.s.o.

It is also known the fact that silver oxidizes during fuse operation, but the thickness of  $Ag_2O$  layer is ranged at  $10^{-9}$  m and the oxide formed in this way prevents the further oxidation of silver, silver oxide being a good conductor of electricity.

Copper is the most used in fuse element manufacturing for low voltage fuses mainly those of general use: rapidly fuses (gG type) and slow fuses (aM type), where notches have larger sections than high-speed fuses.

The use of copper in fuse elements manufacturing for high-speed fuses is avoided due to copper pronounced oxidation. We know from the literature<sup>8</sup> that copper oxide layer thickness which is not a good electricity conductor, increases in time, following the relation:

$$g = 30 (1 + \sqrt{t} \cdot e^{0.013 \cdot \Theta}) \quad [\text{\AA}]$$

where: t-is the operation time, in hours;  $\Theta$  is the operation temperature in K.

In order to verify electro-thermal stress effects on copper high-speed fuses with a compact-rigid filler we have made endurance tests according to IEC 269-4/1986 international standards<sup>1</sup>:

-100 cycles, each compound from an active time and a break time, equal between them and with 0.1 of the conventional time, the fuse current being its nominal current

-100 cycles with a total time for each of them of 0.2 of the conventional time, the active part of the cycle being of the 6 seconds, when the replacing element is traversed by the over load current equal with  $1.6 \cdot I_n$  for  $I_n \leq 100$  A, or with  $2I_n$ , for  $I_n > 100$  A

Besides these classical tests we have also made a whole series of special tests presented in the next chapter.

#### 4. Experimental results

The high-speed fuses with compact-rigid filler material presented in chapter 1 were subject to the whole test programme according to IEC 269-4/1986<sup>1</sup>, only in alternative current and certificated. The main electrical parameters obtained as a result of these tests, only for a few types of fuses are presented in Table 2.

As for the high-speed copper or silver fuses of 500 A, 660 V a.c and 1000 V a.c besides the tests imposed by standards, there were made a few special tests:

-the fuse of 500 A, 660 V a.c was continuously subject to a 400 A current. It already has 3321 operation hours and didn't blow. This current represents the equivalent current prescribed by the standards. As a matter of fact the firms LK-NES<sup>9</sup> and Ferraz<sup>10</sup> warrant the electric endurance of the high-speed fuses at  $0.8 I_n$

-the fuses of 500 A, 1000 V a.c both with copper and silver fuse-elements were subject to their nominal current in 24

Table 2

Electrical parameters Fuse type	Power loss [W]	$I^2t$ total at $U_n$ [A <sup>2</sup> s]x10 <sup>3</sup>	Arc voltage at $U_n$ [V]
UR-350A-660V-Cu size 1	55	109	1050
UR-500A-660V-Cu size 2	83	245	1027
UR-630A-660V-Cu size 3	103	390	1050
UR-200A-660V-Cu size OO	49	3	1229
UR-500A-1000V-Cu size 3	122	3	1850
UR-500A-1000V-Ag size 3	112	322	1860
UR-400A-1250V-Cu size 3	110	235	1960
UR-800A-1250V-Cu size 2x3	217	680	1950
UR-1150A-1250V-Cu size 2x3	308	1700	1960
UR-350A-1500V-Cu size 2	126	165	2800
UR-400A-1500V-Ag size 3	130	145	2400
UR-350A-2000V-Ag size 3	149	196	3540

minutes active cycles and 24 minutes break. The results are presented in Table 3.

Table 3

Crt. No.	Internal resistance [m $\Omega$ ]	Fuse material	Number of achieved cycles
1.	0.22	Ag	220
2.	0.26	Cu	227
3.	0.26	Cu	144
4.	0.26	Cu	484

-19 high-speed copper fuses of 500 A, 1000 V a.c which were stored during 1 year, were then tested at 1000 V.a.c. and currents between 4000 A and 38400 A. The fuses behaved very well considering the standards

-the 500 A, 1000 V a.c copper and silver fuses were subject within IPH-Berlin, to a test of the breaking capacity-160 kA, 1100 V a.c.

They worked very well. It resulted that the copper fuse parameters are close to silver fuse parameters. This is also due to the fact that the fuse system for the copper fuses is improved

-the copper fuses of 500 A, 1000 V a.c with a surrounding metal screen, were subject to 1100 V a.c, the current  $I_2 = 8000$  A. It wasn't observed any ionization and breaking of the space between fuse and screen

-silver and copper fuses of 500 A, 1000 V a.c wadding covered were also subject to 1100 V a.c, the current  $I_2$ . It

wasn't observed any exterior plasma ejection

As a result of these additional tests, we have drawn the conclusion that high speed copper fuses present guarantees in operation.

#### 5. Conclusions

-the fuse filler based on quartz sand, is reinforced under the form of a compact-rigid body, by means of a special technology

-the binder quantity provides the compaction and the reinforcing but, at the same time, keeps a certain porosity of the filler necessary to extinguish the electric arc

-the compact-rigid filler doesn't change neither during fuse operation under a nominal regime nor during the electric arc discharge as it results from the special tests which high speed fuses were subject to

-the compact-rigid filler prevents oxygen permeation to fuses and therefore their oxidation, improves the heat transfer from the fuses to the ceramic body and provides the strong lamination and cooling of the electric arc

-there have been manufactured and certificated high-speed copper fuses having a compact-rigid filler

-as a result of the special tests made, mainly regarding the electrical endurance, we have found that high-speed copper fuses behaved in accordance with the standards and present guarantees in exploitation

-taking into account the analysis of the electrical parameters of high-speed copper fuses and the compact-rigid filler we can find out that their values are close to the similar parameter values of high-speed silver fuses.

#### Bibliography

- [1] x x x Low voltage fuses. Supplementary requirements for fuse-links for the protection of semiconductor devices. IEC 269-4/1986.
- [2] x x x Hochleistungs Sicherungseinsätze Grosse 1 bis 3 und OO mit Anschvaublaschen für Halbleiter-Stromrichtere. DIN 43653/1982.
- [3] Turner H.W. The role of fuse filler in circuit protection. Conference of electric fuses and their applications, Liverpool 1976, p.80-89.
- [4] Barbu I. Sigurante electrice de joasa tensiune. Bucu - resti, Editura Tehnica, 1982, p.56.
- [5] Lipski T. Bezpieczniki niskonapieciowe Wydawnictwa Naukowo Techniczne, Warszawa, 1968.
- [6] Bratinov P. Electriciski predpaziteli za nisko naprajenje. Drjavno Izdatelstvo "TEHNIKA", Sofia, 1976.
- [7] Namitokov K. Influenta densitatii umpluturii de quart asupra proceselor cu arc in sigurantele fuzibile. Electrotehnica nr.8, Moscova, 1983.
- [8] Stainberg C. Teoria si proiectarea aparatelor electrice, vol.I, Editura Didactica si Pedagogica, Bucuresti, 1964.

[9] Norholm O. High speed fuses for the protection high power semiconductors. Third Conference on Power Electronics, Zagreb, 23-26 May 1978.

[10] x x x Cartouches portfusibles a très haut pouvoir de coupure pour la protection des semi-conducteurs de puissance. Prospect Ferraz-UR 1250 V/1981.

## **Session 4**

# **MINIATURE FUSES**

11

PLATE 10

MINIATURE PAPERS

## AGEING OF FILM FUSES ON SUBSTRATES

R D Harrison  
Hawker Fusegear Limited  
Burton-on-the-Wolds, Leics, UK

and

A F Howe, I Harrison  
University of Nottingham  
Nottingham, UK

### Abstract

The fabrication and long term behaviour of a simple film element fuse are described. The fuse comprised an alumina substrate with a combination of single layer screen printing and vapour deposited silver film to form the element. The fusing region was made solely from a single layer of vapour deposited silver. The long term behaviour of the fuse was tested under alternating current conditions. Although migrational effects are not normally associated with these conditions, such an effect did appear to occur. It was speculated that this migration was thermally induced by heat generation within the element. The paper further describes the effects of elevated temperature on various thicknesses of silver films, in relation to resistance changes and surface morphology.

### 1. Introduction

The continual development of fast-acting semi-conductor devices has made the protection of these products by fuses increasingly difficult. Consequently manufacturers have striven to produce fuses with very fast operating times and hence low let-through  $I^2t$ . Dr. Turner in her keynote speech to the Third International Conference on Electrical Fuses and Their Applications [1], pointed out that substrate fuses are capable of very high speed operation. To produce such fuses manufacturers are turning to technologies developed by the semi-conductor industry, which has experience of manufacturing good quality conductive metallic films in intimate contact with supporting, electrically insulating, ceramic substrates. The aims of this paper are to provide some insight into the viability of substrate fuses with respect to their long term stability.

De Cogan et al [2], showed that when a thin film fuse element is in intimate contact with a thermally conductive substrate, heat is dissipated from the hot element through the substrate allowing the elements to carry, in steady state, higher current densities than are possible with conventional fuse element designs surrounded by granular

quartz. However, under fault conditions, the small cross-sectional area of the film element, ensures rapid operation. Both the thermal and mechanical properties of the substrate are of paramount importance in affecting the overall fuse characteristics [3], [4]. De Cogan et al have shown that materials whose graphs of thermal time constant vs temperature, have positive slopes (e.g. alumina), are far more suitable for rapid fuse operation than those with negative slopes (e.g. silica). Since, in the former case, the heat generated during steady state conditions is readily dissipated from the restriction. Whereas under fault conditions the rate of heat dissipation is used to heat and vaporise the element. As the steady state fuse current is very dependent on the heat dissipation, the time vs current curves of this type of fuse are difficult to compile because their performance is greatly affected by the cooling provided for each element [5].

### 2. Initial Test Observations

Test samples were made by evaporating silver through a patterned foil mask, onto commercial grade alumina substrates. The silver element layout is shown in figure 1. These fuses were subjected to long term a.c. tests, and preliminary results indicated that these fuses were failing prematurely. On examination of the elements with a scanning electron microscope, surface features were found which suggested that migrational effects may have caused the unexpected operation of the fuses.

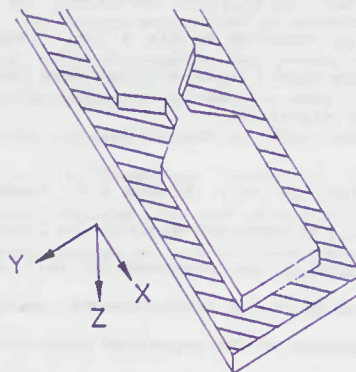


FIGURE 1.

SUBSTRATE FUSE ELEMENT  
RESTRICTION IN X-Y PLANE.

To enhance any possible migrational effects a special type of substrate fuse was constructed. Instead of forming the constriction in the width of the silver film as was done in the previously described substrate fuse, the constriction was formed in the thickness plane (or "Z" direction), of the film. This is illustrated in figure 2.

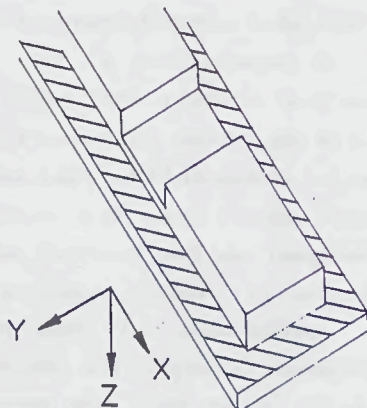


FIGURE 2.  
SUBSTRATE FUSE ELEMENT  
RESTRICTION IN Z PLANE.

### 3. Tests on Substrate Fuses by Other Workers

When single layer, silver element, substrate fuses were operated in d.c. circuits it was observed by Inameti [4] that there was a depletion of conductor material in the region of the restriction which was connected to the negative terminal of the supply. This reduction of conductor material was accompanied by an accumulation of material on the other side of the restriction. Inameti believed that this phenomenon was due to electromigration. To suppress the effect, he added thin super layers of chromium to his films. Whereas other authors [6] have used a layer of glass over the conductor to prevent any migration.

This problem not only affects d.c. fuses but also manifests itself in the micro-electronics industry, where integrated circuits are reported to fail due to the formation of voids in the interconnects, which have been caused by migration of the deposited conductor [7]. For this reason there has been a large amount of research into this effect.

Electromigration is found to be a major problem in thin film conductors because of the associated high current densities which can normally be in the region of  $10^4$  A/mm<sup>2</sup>. The phenomenon does not arise from any material transport caused by chemical potential gradients [8], but is caused by an interaction between the atoms of a conductor and a d.c. current flowing through the conductor. Electromigration, like other transport phenomena, in thin films often occurs via grain boundary diffusion. It is generally considered that the driving force behind the transport phenomenon is a combination of two effects. Firstly, there is an electrostatic interaction between the applied electric field and the ionic core of the atoms which have been stripped of their valence electrons, and an electrostatic frictional force between these ions and the flowing charge or current of electrons passing through the material.

Some workers [9] have noted a temperature dependence of electromigration by measuring an activation energy for the process,  $\Delta H$ . Their results indicated that for thin silver films at a temperature between 225°C and 280°C,  $\Delta H$  was approximately 0.95eV, which they suggested was typically due to ion movement in the grain boundaries. Whereas, at lower temperatures 160°C to 225°C, the reported value of  $\Delta H$  was 0.3eV which they assigned to surface dominated transport.

### 4. Fuse Fabrication

To produce a large aspect ratio at the restriction with the "Z" fuse (in figure 2.), conductive screen printed material was laid onto commercial grade alumina substrate (dimensions of 52mm x 14mm x 0.63mm) to a thickness of between 12 and 14  $\mu$ m, in two or more rectangular patterns each separated by 2mm. After ultra-sonic cleaning in acetone, the samples were mounted in a vacuum chamber which was evacuated to a pressure of about  $1 \times 10^{-3}$  N/m<sup>2</sup> ( $1 \times 10^{-5}$  mbar). Silver was then evaporated onto the exposed surfaces using an electrically heated tungsten boat to produce a fusing region which had a uniform thickness across the restriction. The thickness of the silver layer, which was controllable to an accuracy of 5nm, was between 0.25 $\mu$ m and 2.0 $\mu$ m for the current series of experiments.

The resulting film of silver is poly-crystalline in nature and each grain containing silver atoms arranged

in a face centred cubic arrangement [10]. The size of the grains can to some extent be changed by altering the deposition conditions. The rate of deposition used was in the order of 2.0nm/s. The adhesion of the silver to the alumina substrate was found to be adequate and therefore, it was unnecessary to deposit an intermediate layer of chromium as employed by Inameti [4].

##### 5. Long Term Ageing Effects

To assess the long term ageing effects of substrate fuses under a.c. conditions, it was necessary to examine an element immediately before the onset of arcing, since arcing would destroy any features of ageing in the fusing region of the silver element. To ensure that an element would be as close as possible to the point of operation without actually operating, two identical elements (within normal fabrication tolerances) were connected in series, so that when one fuse operated the other one was left in its aged but intact state. This approach ensured that there was no interference to a healthy restriction from the arcing and has proved to be more reliable than the examination of undamaged restrictions in multi-restriction elements which had operated.

A separate screen printed area was put on the reverse side of the substrate along the complete length. This area was then soldered to a solid copper base. To provide good electrical connections, copper connecting tags were soldered to the screen printed areas at each end of the element, see figure 3.

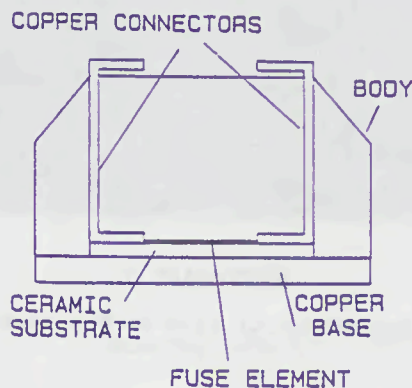
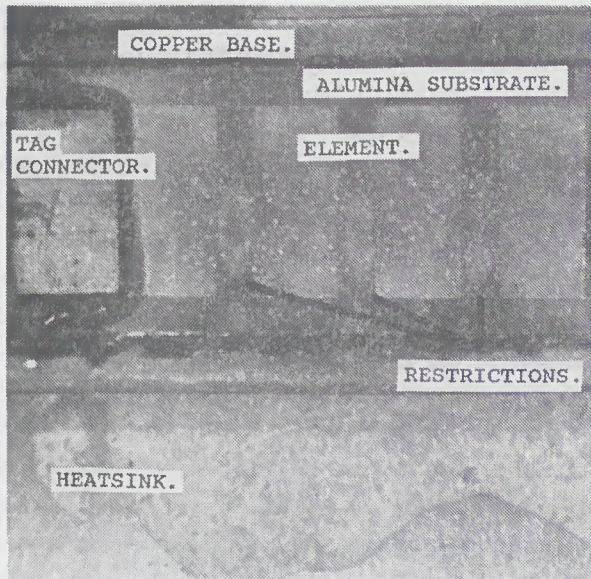


FIGURE 3.  
FUSE CONFIGURATION.

Two nominally identical fuses from a batch, each with fusing area dimension, 2mm long, 12mm wide and 1.0  $\mu\text{m}$  thick, were immersed in granular quartz, and then clamped to a fan cooled aluminium heatsink.

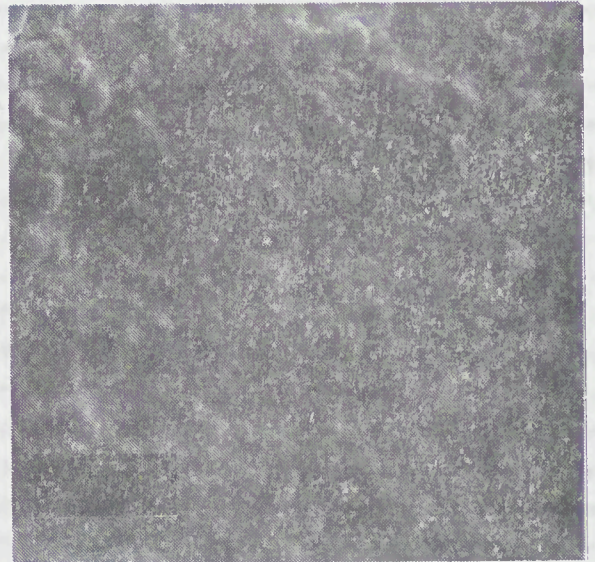
Over a period of about 1500 hours, the current through the fuses was gradually increased ( $\sim 1\text{A/day}$ ) from about 40A, until operation occurred in one of the elements. An average current density just prior to operation was in the order of  $8 \times 10^3 \text{A/mm}^2$  which corresponded to a current of approximately 95A. At this current level the heatsink temperature was around 50°C.

The fuses were removed from the heatsink and examined. Initial visual studies showed that the elements had tarnished slightly and the silver had taken on a pale yellow shade in places. Due to the non-uniformity of temperature along the element the extent of tarnishing varied. A distinct oval pattern was observed in the area of the restriction. In the region where the temperature is the highest one would expect the greatest amount of oxidation. It is therefore believed that the oval pattern showed the hottest regions. These patterns can be seen in photograph A. Further examination of the elements particularly in the fusing region, was undertaken with a scanning electron microscope. The results of which appear in photographs B to F. Although the fuses were subjected to alternating current the photographs show what appears to be migration of the material in the vapour deposited restriction. It can be seen in these photographs that there is random crystal growth, with some of the crystals appearing to be shaped like long whiskers (see photograph F). These crystals are occasionally seen in electromigrated films [11]. This is interesting since the fuses were operated in a.c. conditions and one would not expect electromigration effects. As electromigration is associated with d.c. conditions, this phenomenon can probably be discounted here, and the migration of the film seen in the photograph was possibly induced thermally. The temperature at the restriction in substrate fuses is higher than in conventional designs [3], and this elevated temperature may aggravate migration in the fusing region, as described above.



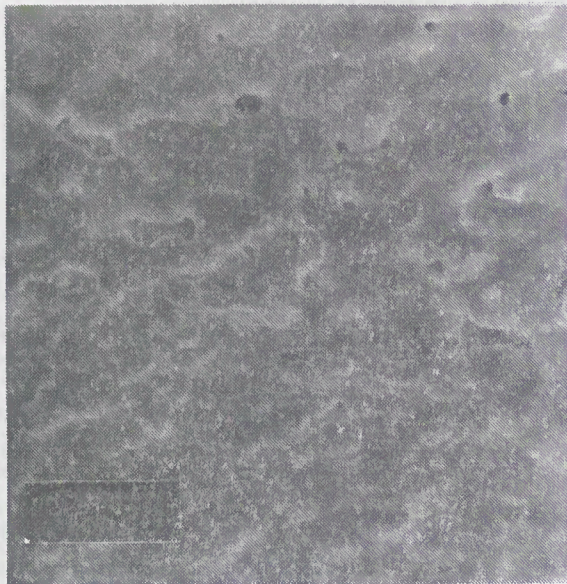
PHOTOGRAPH A.

This shows degradation of the film as oval patterns on the restrictions.



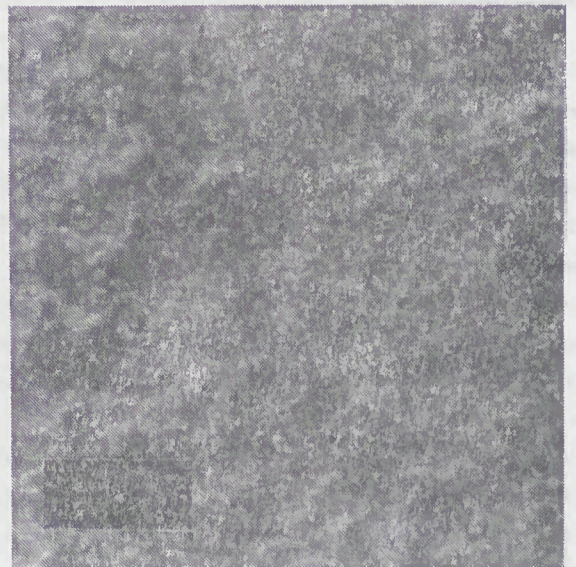
PHOTOGRAPH B.

Appearance of 1.0µm of silver film on alumina substrate, immediately after deposition.



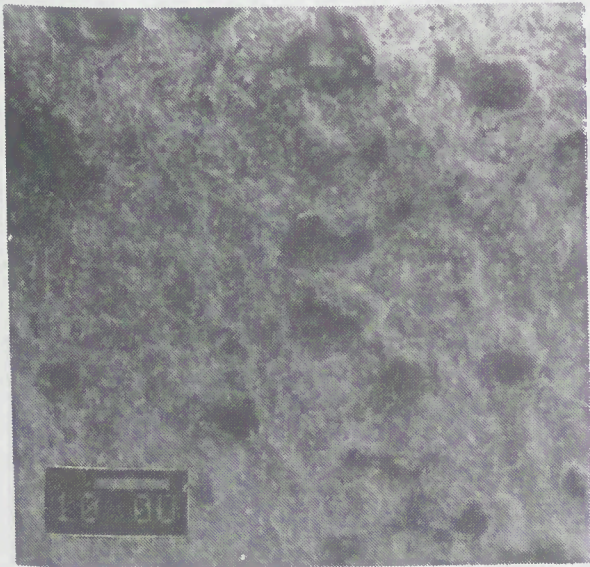
PHOTOGRAPH C

Edge of restriction showing screen printed area (top) and vapour deposited film (below)



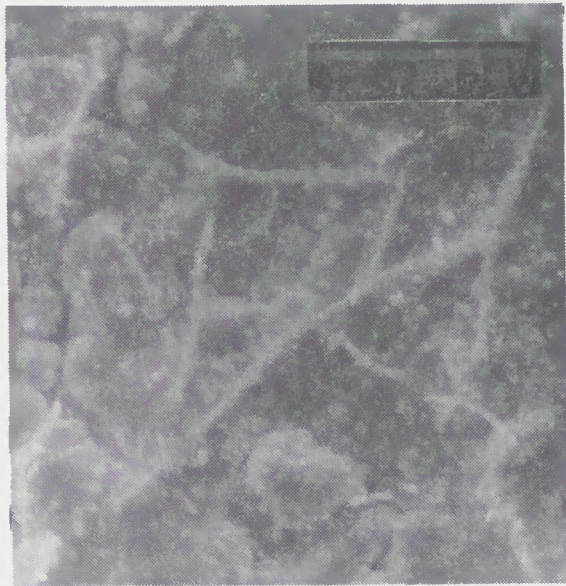
PHOTOGRAPH D.

Appearance of film at the edge of oval pattern.



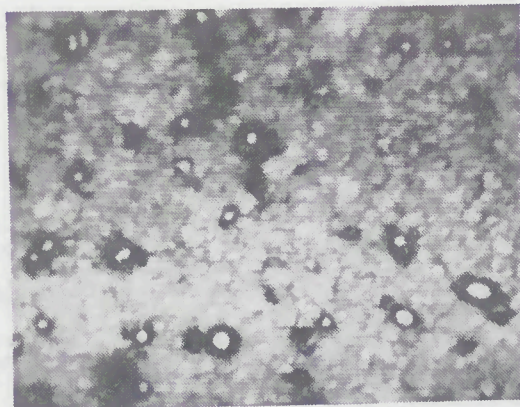
PHOTOGRAPH E.

Silver film at the centre of oval pattern showing migration features.



PHOTOGRAPH F.

Detail picture of migration showing whisker growth.



PHOTOGRAPH G.

Typical migration of heated films

6. Thickness Dependence of Migration

To find the changes in fuse resistance a four terminal system (sometimes called a four point probe) was used. A small direct current (which had a negligible heating effect) was supplied to the element via two terminals and the voltage across the restriction was measured via the other connections. Long term changes in the resistance were monitored using a digital multimeter which had been interfaced to a microprocessor.

Each film was heated by passing current through the electrically conductive screen printed strip on the reverse side of the substrate.

Figure 4 shows the results for tests done on elements with various thickness in the fusing region. All measurements were performed in a draught free environment

and the substrate temperature was about 350°C. It took on average 3 minutes for the temperature of the heater to reach steady state and this accounts for the depression in the curves in the graph at points labelled A. This fall in resistance may be attributed to annealing of the film with the relief of stress which had built up during condensation of the film from silver vapour. This may have been avoided if the silver had been evaporated onto heated substrates. At point B on the graph there is a second drop in resistance followed by a much steeper rise (labelled C) at which point it is thought that migrational features begin to appear. Examination of the films after they have passed point C (figure 4) show spherical growth on the silver surface. This can be seen clearly in photograph G as dark circles, and is thought to show crystallisation of the film.

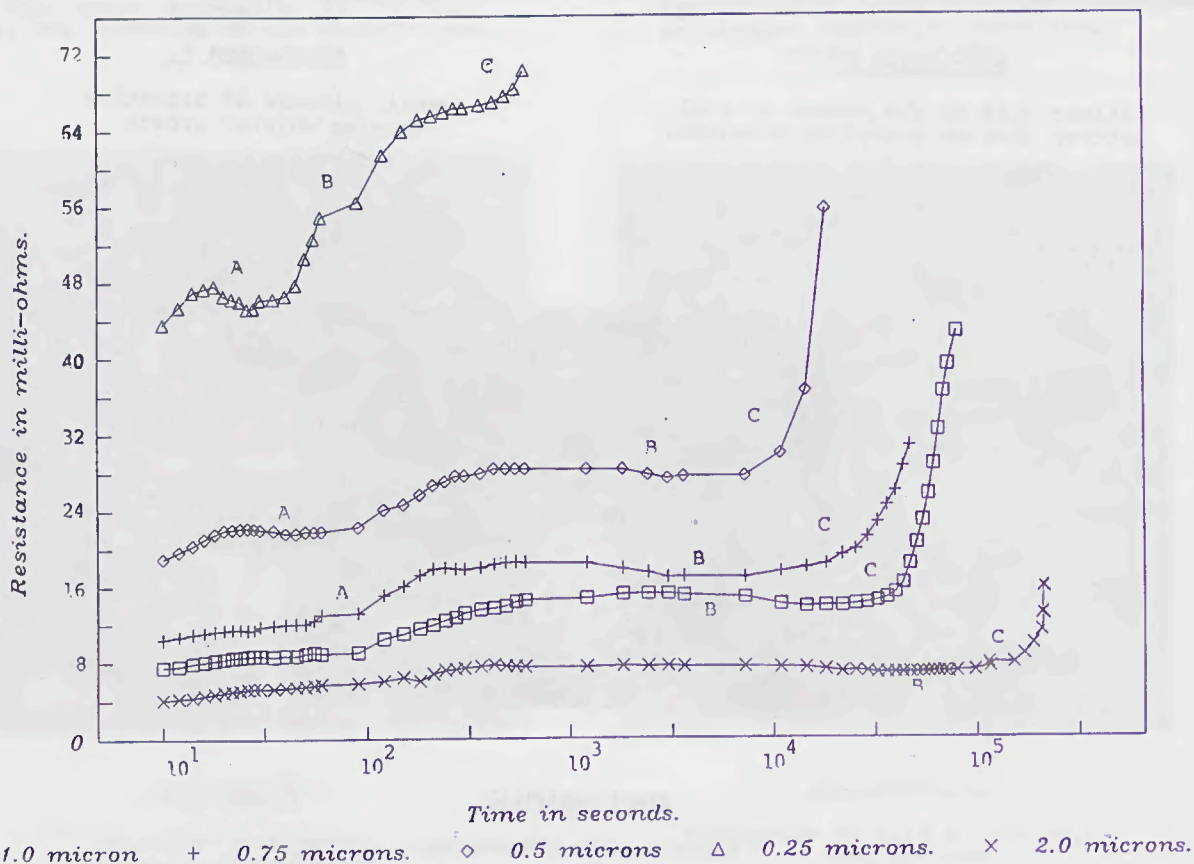


FIGURE 4.  
RESISTANCE CHANGES OF FILMS  
UPON HEATING

## 7. Discussion

The effects described above show that if a substrate fuse, with a single layer element design is used in a.c. applications, then migration of the element material, particularly in the fusing region, could pose a long term problem. The onset of migration at an elevated temperature was shown to be related to the thickness of the film with the thicker films remaining stable for longer periods. It may be possible to inhibit the migrational effects by the use of vacuum deposited super-layers over the elements, alternatively the silver film element can be made sufficiently thick to make any migrational effects insignificant. Research in this field is therefore continuing.

## 8. Acknowledgements

The authors wish to express their appreciation to Hawker Fusegear Limited for sponsoring the work and to the University of Nottingham for the facilities provided.

## 9. References

1. Proceedings of the Third International Conference on Electrical Fuses and Their applications. Eindhoven 1987.
2. D de Cogan, A F Howe, P W Webb. "Temperature Measurements of Thin Films on Substrates." IEE Proceedings Vol. 132 Pt 1 No 3 June 1985.
3. D de Cogan, M Henini. "TLM Modelling of the Thermal Behaviour of Conducting Films on Insulating Substrates." J. Phys D: Appl Phys. 20. (1987).
4. E. Inameti. Ph.D. Thesis University of Nottingham 1988.
5. J. G. J. Sloot. Sixth International Symposium on Switching Arc Phenomena, Lodz, Poland. September 1989.
6. F. M. D' Heurle and R. Rosenberg. Physics of Thin Films, Vol 7 (1973), 257.
7. Edited by M. J. Howes and D. V. Morgan. "Reliability and Degradation Semiconductor Devices and Circuits. John Wiley & Sons, 1981.
8. J. M. Poate, K. W. Tu and J. W. Mayer. "Thin Films - Interdiffusion and Reactions." John Wiley, New York (1978)
9. R. C. Hummel and H. J. Geier. "Activation Energy for Electrotransport in Thin Silver & Gold Films." Thin Solid Films 25, 335 (1975).
10. Modern Physical Metallurgy. R. E. Smallmann. Butterworth.
11. C. Maissel & R. Glaug. "Hand book of Thin Film Technology." Mc Graw Hill, New York, 1970.

# A SEMICONDUCTOR FUSE-LINK ON A CERAMIC SUBSTRATE

Hiroyuki Takahashi  
 Shibaura Institute of Technology

Dr. Kengo Hirose  
 Yoden Engineering Co. Ltd

## 1. Foreword

A fuse-link having element(s) of thin copper film, deposited on a ceramic tab and provided with high-precision small holes with electrolytical process, has been introduced as a new type of semiconductor fuse-links with very small operating I<sup>2</sup>t.

Ratings, construction and distinguished features of this fuse-link, as well as the test circuitry built especially for the development of this type of fuse-links are explained below.

## 2. Construction of the new fuse-links

Thin film of high purity copper is deposited on one side or both sides of a ceramic tab of thickness 1 mm.

The film thickness depends on the current rating, and the tab length on the voltage rating of the fuse-link. The highest current rating of a single tab is 60 A, with films deposited on both sides of the tab. For fuse-links of higher current ratings, two or more tabs in parallel are used.

The copper film on the tab is provided with high precision small holes by electrolytic process as illustrated in Fig.1. These holes give rise to a series of small parallel arcs between the neighbouring holes along the whole length of the tab when large overcurrent flows through it.

The surface of the tab is covered with thin film of silicon resin to protect the copper element from oxidation.

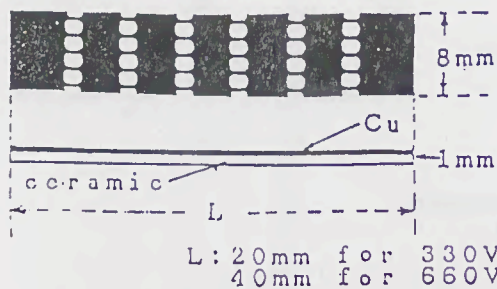


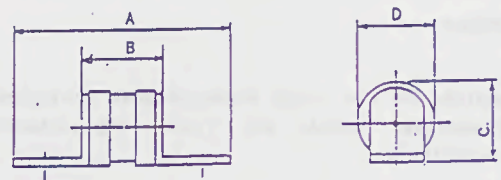
Fig. 1 Structure of fuse element

The barrel containing the tab is filled tightly with sand in just the same way as ordinary semiconductor fuse-links.

List of the fuse-links developed thus far is given in Table 1.

Table 1 List of fuses  
 AC 330V Fuses

TYPE	RATED VOLTAGE	RATED CURRENT	RATED BREAKING CURRENT	SIZE(mm)			
				A	B	C	D
UR31	AC: 330V	20 · 30 · 40 · 50 · 60A	100KA	55	26	19	18
UR32		60 · 80 · 100 · 120A		58	28	22	21
UR33		90 · 120 · 150 · 180A		60	30	27	27
UR35		150 · 200 · 250 · 300A		85	32	39	35



AC 660V Fuses

TYPE	RATED VOLTAGE	RATED CURRENT	RATED BREAKING CURRENT	SIZE(mm)			
				A	B	C	D
UR61	AC: 660V	20 · 30 · 40 · 50 · 60A	100KA	76	47	19	18
UR62		60 · 80 · 100 · 120A		90	48	22	21
UR63		90 · 120 · 150 · 180A		90	50	27	27
UR66		150 · 200 · 250 · 300A		106	52	39	36

AC 660V Fuses (combination type)

TYPE	RATED VOLTAGE	RATED CURRENT	RATED BREAKING CURRENT	SIZE(mm)			
				A	B	C	D
UR66-D	AC: 660V	390 · 495 · 580A	100KA	105	52	39	36
UR66DD		750 · 940 · 1128A		105	52	39	36

※ D: Double type  
 DD: Tow double type



### 3. Technical merits of the new fuse-links

Thanks to the high thermal conductivity due to high density of the substrate, heat generated in the narrow paths between the holes can easily be carried away into the substrate. This makes it possible to hold temperature rise of the narrow paths at a moderate level for normal current, although the electric resistance at the narrow paths is rather high.

The small cross-section of the narrow paths greatly reduces pre-arcing  $I^2t$  of this fuse-link for large overcurrents.

On the other hand, the high precision of the perforations equalizes voltage and current, hence power, of the multiple parallel and series arcs, preventing concentration of arc-energy on limited number of arcs. In addition to this, strong cooling of arcs by the ceramic substrate remarkably reduces arc time and arcing  $I^2t$  of the new fuse-links.

The combined very low value of total operating  $I^2t$  of the new fuse-links for large overcurrent is tabulated in Table 2.

Table 2 Test result of new fuse

TYPE	RATED VOLTAGE (V)	RATED CURRENT (A)	POWER DISSIPATION (W)	OPERATING $I^2t$ ( $A^2t$ )
UR61	660	20	6.5	100
		60	15.5	1,300
UR62	660	60	18.5	750
		120	21.6	7,500
UR63	660	90	21.3	2,400
		180	32.0	18,000
UR66	660	150	30.4	9,200
		300	50.0	58,000
UR66-D	660	390	77.0	92,000
		580	98.0	300,000
UR66DD	660	750	123.0	413,000
		1128	172.0	1,220,000

Fig.2 shows pre-arcing time-current characteristic of 660V/30A fuse-link, which depicts that adiabatic fusion of its element takes place only for very large currents for which pre-arcing time exceeds 0.3 ms.

The quick absorption of the heat generated in the narrow paths of the fuse-element by the substrate and the fast sticking of the paths onto the substrate prevent deformation of the narrow paths

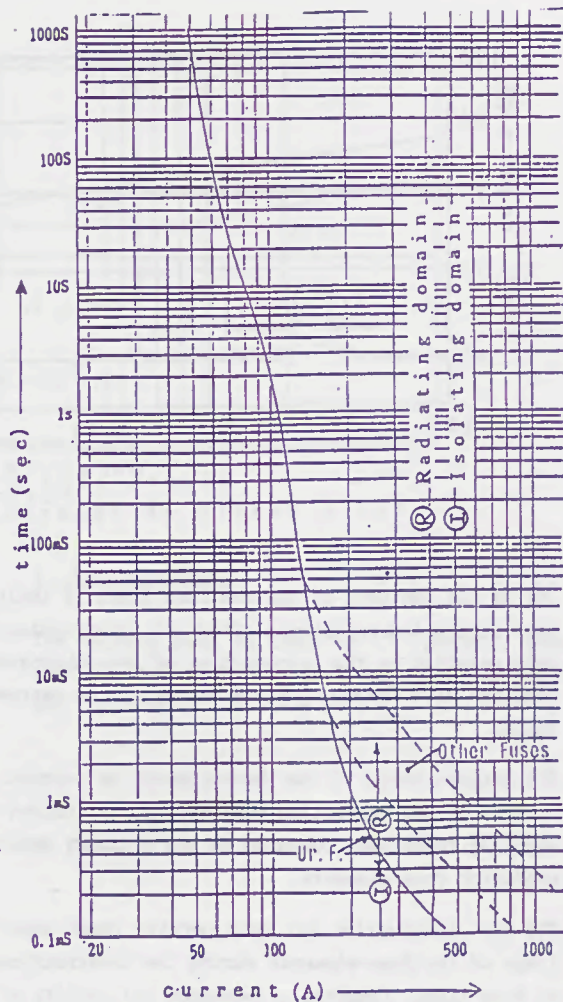


Fig. 2 Pre-arcing time-current characteristic of UR61-30A fuse.

caused by the temperature fluctuation by repetitive overloads.

Fig.3 shows the number of repetitive current cycles (on-period 1 sec/off-period 300 sec) that can be imposed on a 60 A fuse-link until its fusion as the function of the test current given in % of its 1-sec fusing current. It indicates that at a current of 70% 1-sec fusing current the fuse-link withstands 50,000 cycles of repetitive overload, which must be quite a remarkable value for a semiconductor fuse-link.

In general, low operating  $I^2t$  of a semiconductor fuse-link is incompatible with the longevity. However, in the case of the new fuse-links, they are compatible with each other.

The perforation through the element makes it rather easy to control arc voltage of the fuse-link. Hence, arc-voltage is no great a problem for our fuse-links.

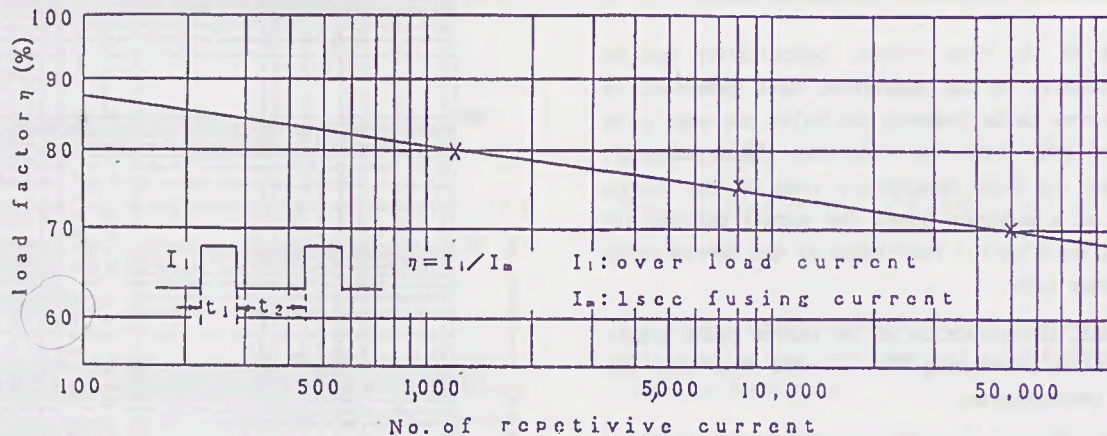


Fig. 3 Result of repetitive life test using UR62-80A

One of the features of the new fuse-links is their high insulation resistance after the interruption; made possible by the introduction of the substrate combined with the appropriate design of the narrow paths.

The largest merit of the fuse-element on ceramic, in view of the production engineering, is its outstanding robustness compared to the ordinary semiconductor fuse-elements.

The new construction not only permits rough handlings of the fuse-elements during the construction of fuse-links, remarkably increases reliability of the product.

#### 4. Breaking test facilities

To facilitate the development of new fuse-links, a special test circuit as indicated in Fig. 4 was introduced, where the capacitor charged up to about 5,000 V was discharged through the upper part of the coil to the fuse-link producing near-sinusoidal current of 50 kA at 100 Hz.

The initial rate of rise of the test current was set at  $44.4 \times 10^6$  A/s which corresponds to test current of 100 kA at 50 Hz as indicated in Fig. 5.

The highest arc voltage did not exceed 1.3 times the peak recovery voltage.

After the interruption of the current by the fuse-link, the discharge current flows through the entire coil and its frequency turns to 50 Hz producing recovery voltage of 50 Hz. Test results by this resonance circuit, which was very useful in developing our new fuse-links, were compared with those by a short-circuit test machine. The result showed good coincidence.

#### 5. Conclusion

A new type of semiconductor fuse-links with fuse-elements deposited on ceramic substrate has been introduced.

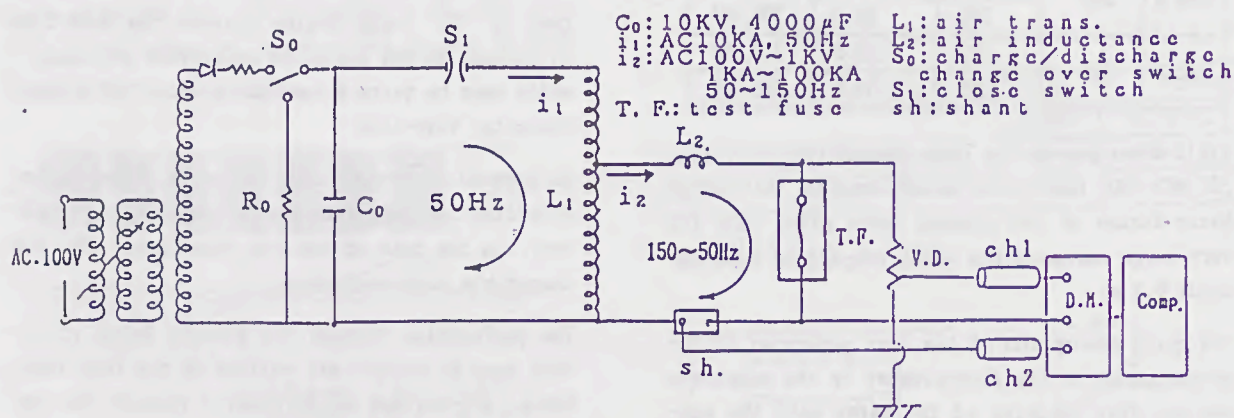


Fig. 4 Interrupting test circuit of AC 660V, 100KA fuses

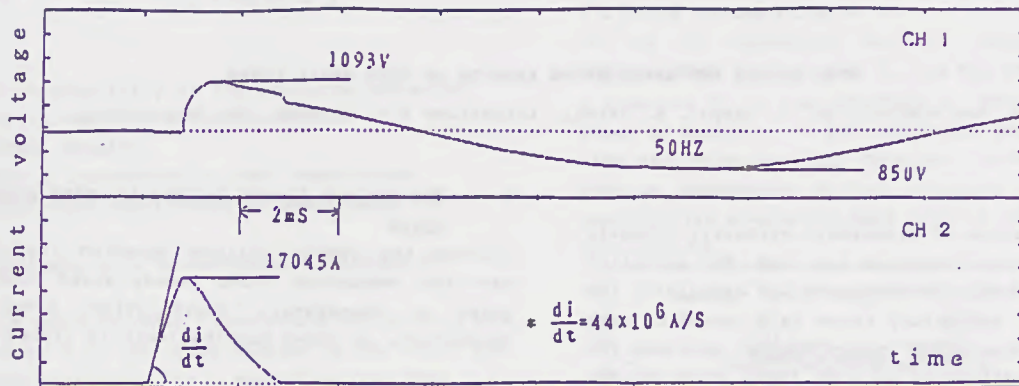


Fig. 5 UR66D-600A fusing test result by AC660V, 100KA circuit

Very low operating  $I^2t$  without sacrificing longevity is the most outstanding feature of this type of fuse-links.

Also the inherent sturdiness of the fuse-element has made handlings during the fuse production easy, resulting in higher reliability of new fuse-links.

#### 6. Acknowledgement

The authors wish to thank Mr. T. Umezaki, President of Yoden Engineering Co Ltd, for his support and encouragement of this work.

SOME DESIGN AND APPLICATION ASPECTS OF VERY SMALL FUSES

P. van Rietschoten, J. Jaspar, L. Vermij, Littelfuse B.V. Utrecht, The Netherlands.

**Abstract**

For the protection of electronic circuitry normally fuses with small dimensions are used. For so-called on-board protection on PC-boards and especially for surface mount technology there is a trend to very small sized fuses. This offers special problems for design and application of such fuses which do not occur in that extend with "normal" miniature fuses. On hand of some theoretical calculations and experimental results the influences as mentioned will be shown and principle solutions for these problems are indicated.

**1. Introduction**

In modern electronic equipment it is common practice to use components with smaller and smaller dimensions and with a high package density. This is especially true for the so-called surface mount technology. Also for fuses used for the protection of such circuitry there is a requirement for smaller dimensions. In figure 1 typical dimensions for a fuse as used for surface mount applications.

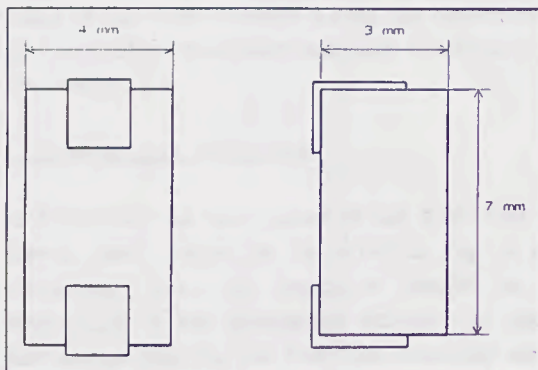


Figure 1: typical dimensioning of a fuse for surface mount technology.

These relatively small dimensions offer special problems for design and application which do not occur in that extend with 'normal' miniature fuses. It is obvious that the length of the fuse element in fuses of such dimensions is very small. Sometimes an 'active' fuse element length of less than 2 mm is formed in such fuses. Apart from the technological aspect of manufacturing such fuses in large quantities, there is the question of breaking capacity. But the very short length of the fuse element in such fuses may also create problems in getting a reproducible time-current characteristic. In the following sections these problems will be treated in more detail.

**2. The minimum fusing current for very short fuse wires**

Solving the energy balance equation for current carrying conductors under steady state conditions gives a temperature distribution along such conductors, as shown qualitatively in figure 2 [1].

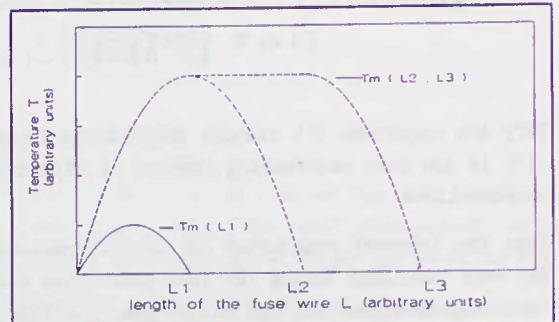


Figure 2: temperature distributions along short and long wires carrying the same current I.

In deriving such temperature distributions it is assumed that the wire is connected to two end blocks 1 and 2 which are kept at environmental temperature  $T_0$  (see figure 3). If the wire is long that means  $L \geq L_2$  (see figure 2) the highest temperature  $T_m$  is not influenced by the end effects. For short wires, that means wires with  $L < L_1$ , the highest value  $T_m$  may be influenced considerably by the length of the fuse wire. For these situations the heat transfer to the ends play the major role, radial heat transfer can be neglected. This means, however, that for short wires the value of the minimum fusing current  $I$ , depends on the length of the fuse wire. In case of short fuse wires, where only the heat transfer to the ends of the fuse wire is to be taken into account, the minimum fusing current can be calculated from the energy balance equation for steady state conditions:

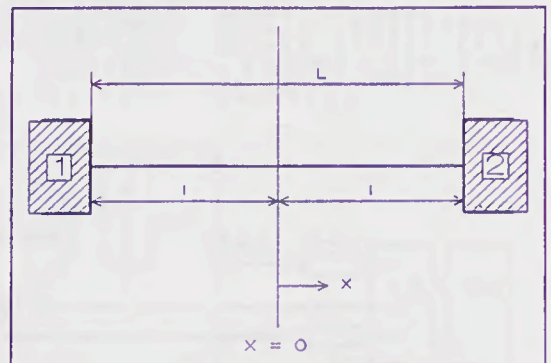


Figure 3: a wire connected to two end-blocks 1 and 2.

$$(1) \quad \lambda \frac{d^2 T}{dx^2} + J^2 \cdot \rho_0 \cdot (1 + \beta \cdot T) = 0$$

where:

- $\lambda$  : heat conductivity of the conductor material
- $T$  : temperature of the conductor at  $x$
- $J$  : current density
- $\rho_0$  : specific resistance at room temperature
- $\beta$  : temperature coefficient of resistance

The coordinate  $x$  is demonstrated in figure 3

At  $x=0$  is valid  $dT/dx=0$ . Introducing  $T=T_0$  at  $x=l$  and  $I=AJ$ , where  $A$  is the cross section of the wire, the following expression for  $I_s$  can be derived from (1), taking into account that the value of  $I_s$  is determined by the melting temperature  $T_m$ .

$$(2) \quad I_s^2 = A^2 \left[ \frac{\lambda}{l^2 \beta \rho_0} \left( \arccos \frac{1}{1 + \beta(T_m - T_0)} \right)^2 \right]$$

Assuming cylindrical wires for which is valid  $A = (\pi d^2)/4$  ( $d$  is wire diameter) then the graphs shown in figure 4 can be calculated from equation 2. These graphs show the relationship between  $I_s$  and  $d$  for different wire lengths

$L = 2l$  of the fuse wire and with the assumption that  $T_0=0$ .

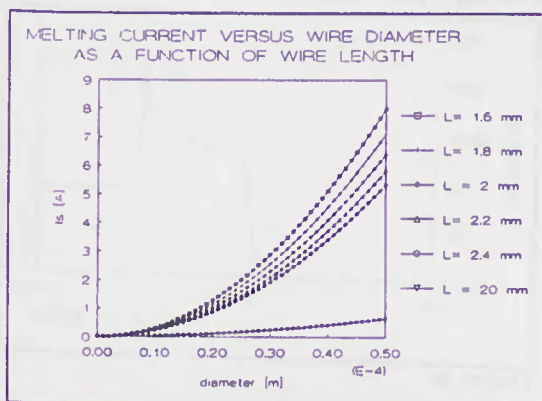


Figure 4: the minimum fusing current  $I_s$  as a function of the wire diameter of Cu-wires. The length  $L$  of the wire is parameter.

(For comparison also the value of a long fuse wire is plotted in this figure) The last assumption is more or less valid if the end blocks 1 and 2 in figure 3 have a relatively high heat capacity and a very good heat transfer to its surroundings. In many cases in practice such an assumption is not justified; the end blocks are heated up by the energy supplied by the fuse wire, that means that under steady state conditions the end blocks have a temperature  $T_0 = T_m$ , the value of which depends on the mounting conditions on e.g. a p.c.board. Such conditions are e.g. determined by differences in pad-sizes and amounts of solder as will be found with different soldering methods (see figure 5). Also differences

in cross sections of tracks on the p.c.board have an influence on the value of  $T_0$ .

To get an impression how the value of  $I_s$  is influenced by the value of  $T_0$ , one can calculate  $I_s$  as a function of  $T_0$  from equation 2. Some results are shown in figure 6 for some different length of fuse-wire and calculated for Cu-wires. Such curves just give an impression of the influence of  $T_0$ , for a quantitative evaluation more factors are to be taken into account.

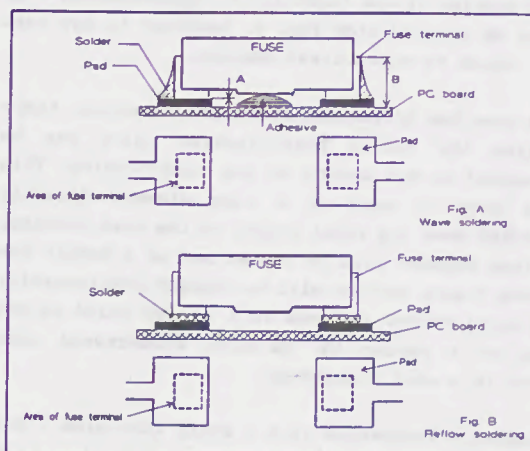


Figure 5: mounting by wave soldering (A) and reflow soldering (B).

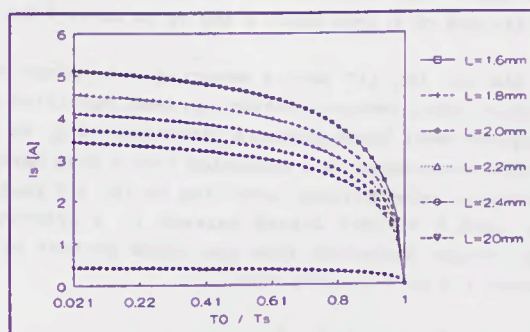


Figure 6: Minimum fusing current  $I_s$  in relation to the temperature  $T_0$  of the end-blocks, calculated for a Cu-wire of 40  $\mu$ m diameter.

In figure 6 the area close to the point  $T_0/T_s=1$  has only a theoretical meaning, the value of  $T_0$  can never be equal to  $T_m$  by heating the wire connections by the fusewire only.

What do we learn from the above?

Let us take an example.

From figure 4 it can be seen that the  $I_s$  value of a copper-wire with  $d=40 \mu$ m and  $l=2$  mm is 4 A, assuming that  $T_0=0$ . A change of the length of the wire from 1.8 to 2.2 mm, that means  $2 \text{ mm} \pm 0.2 \text{ mm}$ , changes its  $I_s$  value from approximately 4.6 A to 3.6 A. It is difficult if not impossible to get an accuracy in wire length of  $\pm 0.2$  mm or less by using soldering

technologies for the connection of the fuse-wire. It is common practice to solder the fuse wire in miniature fuses. From the above example it is obvious that connecting methods for very small fuses have to be changed to get a rather well defined value of the minimum fusing current  $I_1$ .

Another aspect is how to make such a small fuse for low current ratings? As an example, a 100 mA fuse with a copper fuse wire of 2 mm length requires a cross section of the fuse-wire of approximately  $7 \mu\text{m}$  as may be derived from fig. 4. Needless to say that this leads to unpractical designs.

Apart from the influences as mentioned before, there is also the radial heat-transfer which can be influenced by the design of the fuse-housing. This means that in case of a fuse element directly connected over its total length to the fuse housing, the fuse element will be cooled and as a result the minimum fusing current will be changed considerably. As a total effect a change in  $I_1$  can be found in the order of a factor 10, we have encountered this factor in a real fuses design.

We tested a fuses design with a short fuse wire (less than 2 mm) for which was quoted that the rated current was 500 mA. We created a situation in which this fuse didn't blow at 11 Amp! Mounted on a p.c.board with different conditions of soldering, pad-sizes and track cross sections, we found variations of  $I_1$  from about 1 Amp up to about 5 Amp.

In the new IEC 127 part 4 covering a.o. fuses for surface mount designs nothing has been specified or required about these possible variations of  $I_1$ . So in future there might be a situation that a fuse having a certain rated current according to IEC 127 part 4 may have a minimum fusing current in a practical application differing from the rated current by a factor 1.5 to 5 or even more.

### 3. Possible solutions

From the above it is clear that the longer the wire, the less vulnerable the fuse will be for mounting conditions and inaccuracies of fuse assembly methods.

If the wire is long ( $L > L_1$  in figure 2) then the radial heat transfer plays also a role which, in a properly designed fuse, has a compensating effect on influences from the outside.

Not only the length of a fuse-wire, but also the physical parameters of the fuse-wire material, determine if a fuse-wire has to be considered as long or not.

In fig. 7 a fuse design is shown which allows for a relatively long but well controlled length of the fuse wire. Such a design makes it also possible to get some degree of balancing between the heat transfer to the ends of the wire and the heat transfer via the fuse body. If moreover the proper fuse-wire material is selected then, under all practical circumstances as found on a p.c.-board, a change of  $I_1$ -value of less than 5% can be achieved. This requires of course also a rather high accuracy regarding the assembly of the fuse, which means that an assembly technology has to be developed which allows for this required high accuracy.

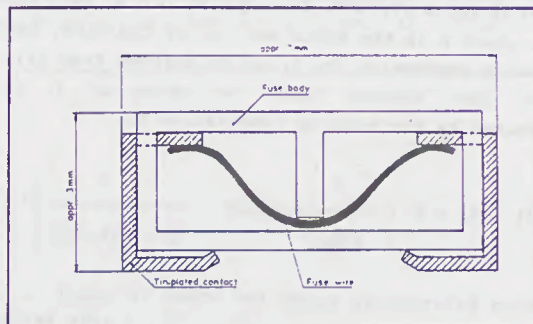


Figure 7

This "two-chamber" design not only makes it possible to design a fuse with a rather well defined  $I_t$ -curve, it realises also a better control of the arc voltage and a relatively high breaking capacity, without the use of any filler material in the cavities.

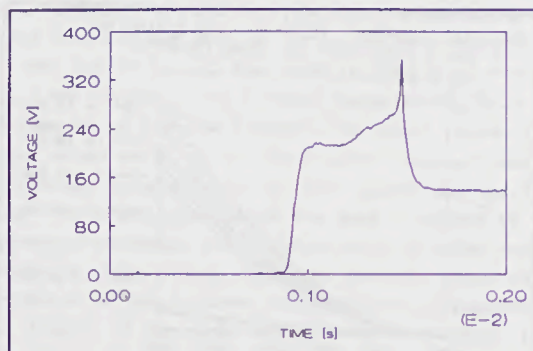


Figure 8a

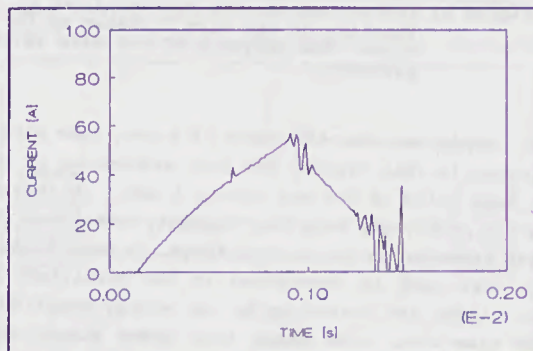


Figure 8b

Fig. 8 shows, as an example, the oscillogram taken at the interruption of a 150A effective current at 125V AC. From this oscillogram it can be seen that the max. value of the arc-voltage does not exceed 350 volts. As a remark for the basic design as shown in fig. 7 a European patent application nr. 89202921.6 has been filed.

Literature:

- [1]: Fischer, J., Die stationäre Temperatur stromdurchflossener, mässig langer Drahte. Arch.f.Elektrot. XL.band H3 (1951) 11, 171.

Abstract

It is known from experiments that a linear relationship exists on log-log scale between the minimum fusing current and the diameter of round metal wires, as used in miniature fuses. This can be explained by using a rather simple energy-balance. Extending the energy-balance with Nusselt-numbers, it is possible to predict the slope of the relationship from calculations only. Since for such wires the  $I^2t$ -value is known quantity, the limits of the time-current characteristic can be calculated.

1. Introduction

Normally, time-current ( $I_t$ )-characteristics for miniature fuses are presented on a log-log scale as shown in Fig. 1. Such an  $I_t$ -characteristic can be approximated by two asymptotic straight lines, one vertical line representing the minimum fusing current  $I$ , and one line under a well-known slope representing the  $I^2t$ -value [1]. These lines are also shown in Fig. 1. (lines 1 and 2 respectively).

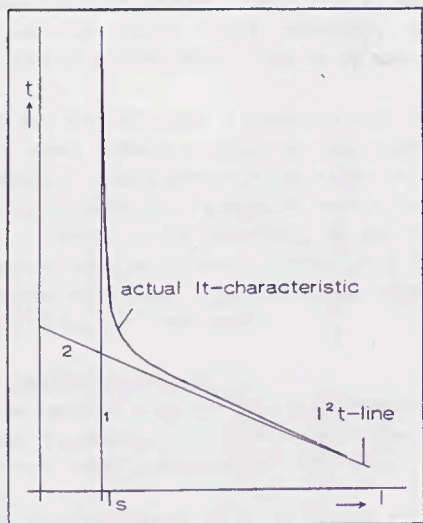


Figure 1: Approximation of the time-current characteristic.

In most cases line 2 can be calculated with rather good accuracy for a given fuse design, using Meyer's formula [2]. If the value of  $I$ , can also be calculated, then this means that the limits of the  $I_t$ -characteristic of a given fuse can be found from calculation only. For a first design of a miniature fuse such an information is mostly sufficient, as far as the  $I_t$ -characteristic is concerned.

In the following section it is shown how the value of  $I$ , can be determined for fuse designs as usual for 5 x 20 mm and 6.3 x 32 mm fuses.

2. Determining  $I$

In most cases the fuse-wire in a miniature cartridge fuse can be considered as a long wire, that means that the temperature of the wire at its hottest point (the middle of the wire) is not influenced by the heat transfer to the ends of the wire. Along the wire the well-known temperature distribution as shown qualitatively in fig. 2. occurs. In this figure it is also shown at what length  $L$ , of the fuse wire a transition takes place from a "long wire" to a "short wire", as long as a wire with constant cross-section over its length is considered.

The minimum fusing current  $I$ , is determined by the melting temperature  $T = T_m$  in the middle of the wire under steady state conditions. In this case a simple energy equation per unit volume is valid, viz:

$$J_s^2 \cdot \rho_0 \cdot (1 + \beta \cdot (T_s - T_0)) = G \cdot (T_s - T_0) \quad (2)$$

where

$J_s$  = the current density.

$\rho_0$  = the specific resistance at  $T_0$ .

$\beta$  = the temperature coefficient of the specific resistance

$G$  = the heat transfer in radial direction per unit volume and per degree C.

$T_0$  = ambient temperature.

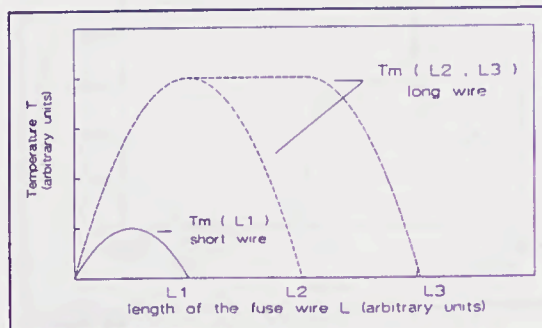


Figure 2: Temp. distribution along a wire carrying the same current  $I$ , depending on the length  $L$  of the wire.

Introducing  $I_s = \frac{1}{2} \pi d^2 J_s$ , where  $d$  is the diameter of the fuse-wire, considered to be cylindrical for the sake of simplicity, we then get:

$$I_s^2 = \frac{\pi^2}{16} d^4 \cdot \frac{G \cdot (T_s - T_0)}{\rho_0 (1 + \beta \cdot (T_s - T_0))} \quad (3)$$

or:

$$I_s^2 = G \cdot K_1 \cdot d^4 \quad (3a)$$

where  $K_1$  is a constant, only dependant on physical parameters of the fuse-wire material. Note that also for the case of a short conductor, it can be shown [3] that  $I_c^2 = K_2 \cdot d^4$  with  $K_2$  a constant different from the product  $G \cdot K_1$ .

It is a well known fact that if we plot the value of  $I_c$  of miniature-fuses as a function of the wire-diameter on a log-log scale, a straight line results as illustrated in Fig. 3. This relationship between  $I_c$  and  $d$  has already been described by Preece as early as 1884 [4] for straight long wires in air, and is sometimes referred to as Preece's law.

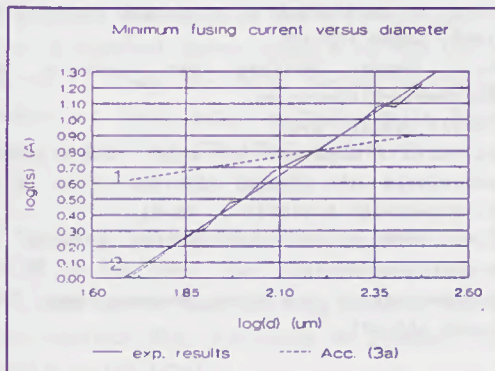


Figure 3: Relationship minimum fusing current  $I_c$  and wire diameter  $d$ .

If we plot in the same figure the relationship between  $I_c$  and  $d$  as predicted by eq. (3a) (line 1 in fig.3), then it is clear that the slope of this line differs from the slope as predicted by Preece's law (line 2 in fig. 3). Furthermore Fig. 3 shows a remarkable fit of Preece's law to the experimental results obtained from fuses with Sn-plated Cu-wires.

Obviously the factor  $G$  can not be a constant, but does depend on  $d$ . If, however,  $\log I_c$  is linearly related with  $\log d$ , as proven by experiment, then  $\log G$  should also have a linear relationship with  $\log d$ . This means that some power  $\alpha$  of  $d$  must exist, for which is valid:

$$G \cdot d^\alpha = \text{constant} \quad (3b)$$

From a comparison with experimental data and the relationship given by eq. (3a), it can be derived that  $\alpha = 1$  is valid. That means that the product  $G \cdot d$  is a constant as a function of  $d$ .

If we introduce  $G_4 = G \cdot d$  in eq. (3a), then it follows:

$$I_c^2 = K_1 \cdot G_4 \cdot d^3 \quad (4)$$

in which  $G_4$  is a constant. Equation (4) is exactly the relationship as described by Preece.

Numerous experiments revealed that  $G_4$  is indeed a constant for one specific metal. Different metals and alloys show different values of  $G_4$ . The only

metal we found in our experiments which does not follow eq. (4), at least for smaller diameters, is Nickel. The deviations from eq. (4) shown by Nickel are believed to be the result of a second order phase-change, which occurs at 357°C.

Furthermore it was found that the value of  $G_4$  depends on the surroundings of the wire (sand filler, air a.s.o), but is not so much influenced by the dimensions or the design of the fuse, as long as the fuse-wire can be considered to be "long".

Knowing values for  $G_4$  for different metals and alloys and for different fuse-wire surroundings,  $I_c$  can be calculated from eq. (4).

### 3. Some remarks with respect to Preece's law

A somewhat larger model is needed in order to obtain a relationship between the various values of  $G_4$  for different metals. With such a model it can be made plausible that  $G_4 = G \cdot d$  is indeed a constant.

In the above equation (2),  $G$  is the heat-transfer in radial direction, per unit of volume and per degree Celsius.

For round wires in air, the radial heat-transfer is given by:

$$Q = h_c \cdot (T_1 - T_0) \cdot \pi \cdot d \cdot l \quad (5)$$

with

$$h_c = \frac{Nu_4 \cdot K}{d}$$

and:

$$\begin{aligned} Q &= \text{radial heat transfer} & [W] \\ d &= \text{diameter of wire} & [m] \\ l &= \text{length of wire} & [m] \\ Nu_4 &= \text{Nusselt number related to } d \\ K &= \text{thermal conductivity of air} & [W/(m^\circ C)] \\ T_0 &= \text{ambient temperature} & [^\circ C] \end{aligned}$$

We then find:

$$(\frac{1}{4}\pi d^2) \cdot l \cdot G \cdot (T_1 - T_0) = \frac{Nu_4 \cdot K}{d} \cdot (T_1 - T_0) \cdot \pi \cdot d \cdot l$$

or:

$$G = \frac{4 \cdot Nu_4 \cdot K}{d^2} \quad (6)$$

Since for non-moving air, the Nusselt-number  $Nu_4$  is usually given as:

$$Nu_4 = A \cdot (Gr_4 \cdot Pr)^B \quad (7)$$

where:

$$\begin{aligned} A, B &= \text{constants} \\ Gr_4 &= \text{Grashof number related to } d \\ Pr &= \text{Prandtl number} \end{aligned}$$

Because the Grashof-number is proportional with

$(T_i - T_0)$  and with  $d^3$ , eq. (6) can be rewritten into:

$$G_i d^{(2-3B)} = \text{constant} \cdot (T_i - T_0)^B$$

Since in literature for B values are found to be around 0.25 to 0.33, we get in case of  $B = 0.33$  the same relationship as observed by Preece:

$$(2-3 \cdot 0.33) = 1 \rightarrow G_i d = \text{constant} \cdot (T_i - T_0)^{0.33} \quad (8)$$

Note that the constant in eq. (8) incorporates the physical properties of air, and is as a result temperature dependant.

Equation (8) makes it plausible that for different fuse-wire materials with different values of  $T_i$ , different values of  $G_i$  are found.

Furthermore it follows from the above, that the following relationship between the constants  $G_{i1}$  and  $G_{i2}$  of two different metals in the same straight wire fuse-design must exist:

$$\frac{G_{i1}}{G_{i2}} = \frac{K(T_{i1} - T_0) \cdot (\text{Pr}(T_{i1} - T_0) \cdot (T_{i1} - T_0))^B}{K(T_{i2} - T_0) \cdot (\text{Pr}(T_{i2} - T_0) \cdot (T_{i2} - T_0))^B} \quad (9)$$

Experimental results obtained so far, show that eq. (9) can be used as a rough estimate.

#### 4. Conclusion

For round long wires of various metals in air, a rather good fit can be obtained for the relationship between the minimum fusing current and the diameter, using Preece's law.

Since also the  $I^2t$ -value is a well-known quantity, the limits of the time-current characteristic as shown in Fig. 1. can be calculated quite well.

#### Literature:

- [1] L. Vermij, A. Mattheij: Time current characteristics of miniature fuses. Proc. of the ICEFA 3<sup>rd</sup> International Conference, 1987, pages 122-126.
- [2] G.J. Meyer: Beitrag zur Kenntnis der Abschmelz-Sicherungen. Thesis Berlin, 1906.
- [3] L. Vermij: Behaviour of short fuse-elements associated with thermal effects. Holectechniek 5 (1975) 3, 76-81.
- [4] W.H. Preece: On the heating effects of electric currents. Proceedings of the Royal Society, Apr. 1884 pages 464-471.

## BREAKING TESTS OF LOW BREAKING CAPACITY MINIATURE FUSE-LINKS

A. Hirose  
S.O.C. Corporation  
Yokohama, Japan

and

H. Matsuzaki  
S.O.C. Corporation  
Yokohama, Japan

### 1. Lbc and hbc miniature fuse-links

Standard rated breaking capacity for low-breaking capacity miniature fuse-links (lbc MFs), specified in Standard Sheets 2, 3 and 4 of IEC 127-2 and also in Standard Sheets 3 and 4 of IEC 127-3, is 35A or 10 times the rated current whichever is greater at their rated voltage; while Standard Sheets 1 and 2 of IEC 127-3 specify 50 A for the rated current of their lbc MFs.

In any case, the standard breaking capacity of the lbc MF is far lower than the corresponding value of 1,500A for the high-breaking capacity miniature fuse-links (hbc MFs) according to Standard Sheets 1 and 5 of IEC 127-2.

This large difference in breaking capability is attributable to the sand-filling of the hbc MFs. The sand, filled tightly in the fuse-envelope of the hbc MF, causes limitation of the overcurrent in the circuit, often reducing the actual breaking current of the fuse-link far below the prospective overcurrent.

The extent of the current-limitation depends on the ratio of the prospective overcurrent to the rated current of the fuse-link; for the larger ratio the limitation is stronger. Because of this, breaking performance of a hbc MF depends substantially on its rated current.

In the case of lbc MFs, however, no strong current limitation takes place, and the breaking current is essentially equal to the prospective overcurrent which is determined only by the circuit constants. Hence, the breaking performance of a lbc fuse-link depends on the prospective overcurrent but not so much on its rated current as in the case of hbc fuse-links.

### 2. Arc-energy of lbc MFs

In return for the freedom from the troublesome sand-filling, the glass envelope of the lbc MF is exposed to the intense heat of the arc. On the other hand, its moderate test current doesn't generate that violent and explosive vapourization of the fuse-element which sometimes destroys the en-

velopes of hbc fuse-links mechanically. Because of these two facts, almost all failures in the breaking tests of lbc MFs are of thermal, rather than mechanical, nature.

Just for this reason, arc-energy measurement during breaking tests of lbc MFs becomes very important for the estimation of their breaking capacity limit.

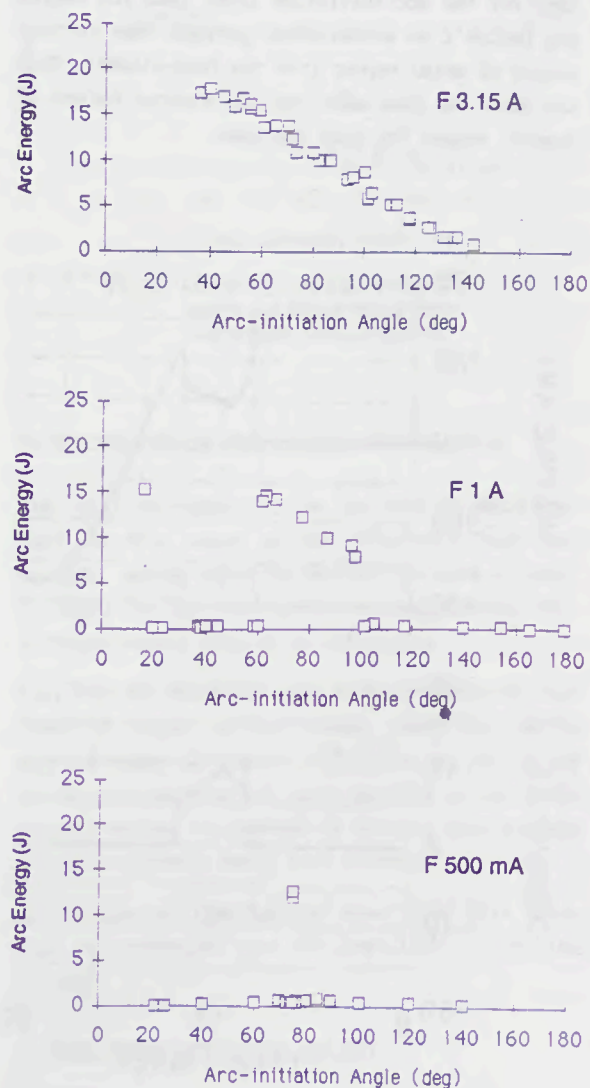


Fig. 1 Test results of 5 x 20 mm fuse-links to IEC 127-2, at 250 V - 35 A (Quick-acting, manufacture A)

### 3. Arc-energy versus arc-initiation angle

Fig. 1 shows three diagrams for arc-energy in terms of arc-initiation angle on the source voltage wave for 5 x 20 mm quick-acting fuse-links. Current ratings are 3.15, 1 and 0.5A from top, for test current 250V- 35A. All these test pieces were products of a single manufacturer, A.

The top diagram shows the arc-energy decreasing almost linearly with the increase in the arc-initiation angle, which implies that in every test arc lasted until the first voltage zero. This diagram is in general agreement with the arc-energy/arc-initiation diagram by H.W. Turner et al.<sup>1</sup>

The middle diagram for 1A fuse-links indicates that for the arc-initiation later than 100 degree arc couldn't be established, perhaps, due to poor supply of metal vapour from the fuse-element. This was also the case when the arc started before 60 degree, except for only one case.

For further smaller rated current of 500mA, arc was established only in three of the total 20 tests, at the arc-initiation angle about 75 degree. In all other cases, arc succeeded in starting but failed in establishment. Fig. 2 indicates the two cases, where arc was established (a) and was extinguished (b).

Interesting is the fact that when the arc is established arc-energy of the three kinds of fuse-links is nearly the same for a definite arc-initiation angle. This observation leads us to the conclusion that the fuse-element of a lbc fuse-link is only an arc-starter and that arc-current and energy during the operation of the fuse-link are determined by circuit constants.

Fig. 3 gives, corresponding to Fig. 1, diagrams for lbc time-lag fuse-links of differing ratings of the same size as before but produced by another manufacturer, B. It indicates that for time-lag fuse-links arc can more easily be established than

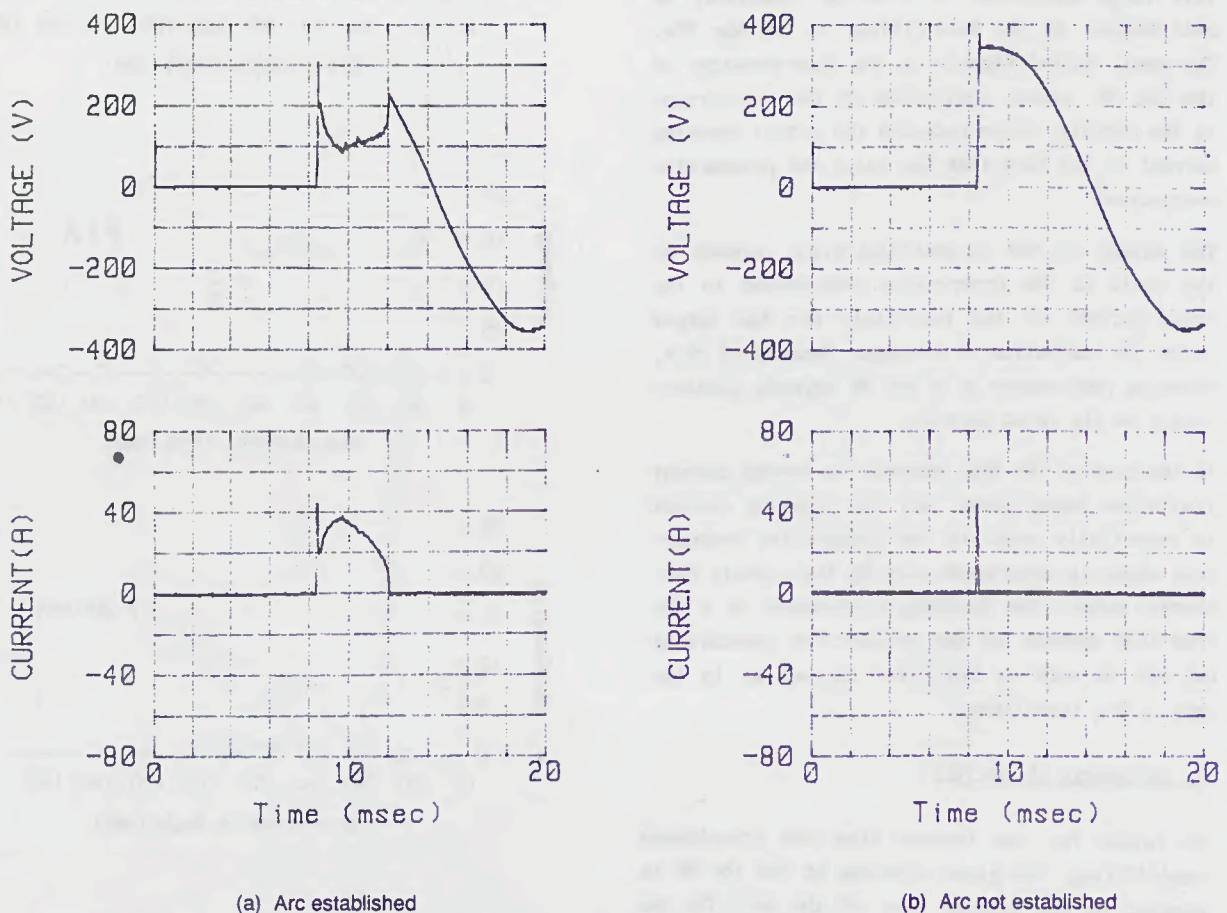


Fig. 2 Arc duration of 500 mA quick-acting fuse-links (Manufacture A)

for quick-acting ones but that the general tendency of the arc-energy which increases with decreasing arc-initiation angle is in common to the quick-acting fuse-links.

Fig. 4 strongly supports our view that arc-energy primarily decides failures in breaking tests of lbc MFs. Here, the diagram shows that failures occurred only for test current 163A and only for the earlier arc-initiation. In these cases the glass tubes and, often, the end-caps could not withstand the intense heat of the arc. The test pieces were all by manufacturer A.

Fig. 5 indicates test result of 3.15A quick-acting fuse-links, made by manufacturer B, for test current 35A at various test voltages. Also in this case, arc-energy was decisive for the failures of the test.

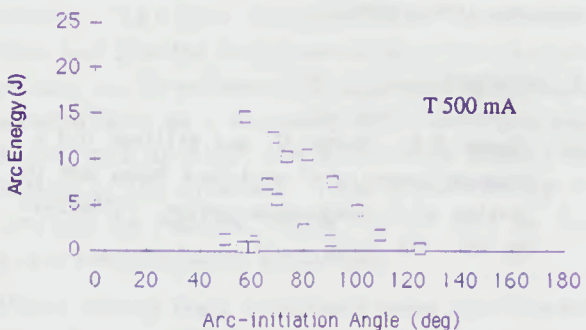
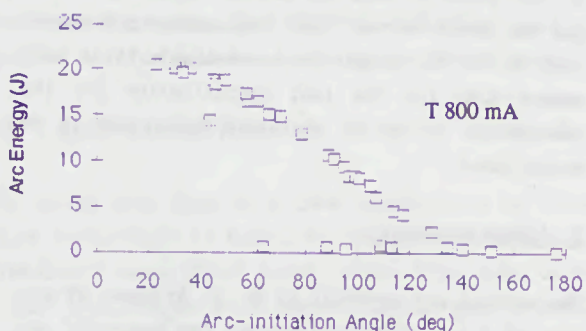
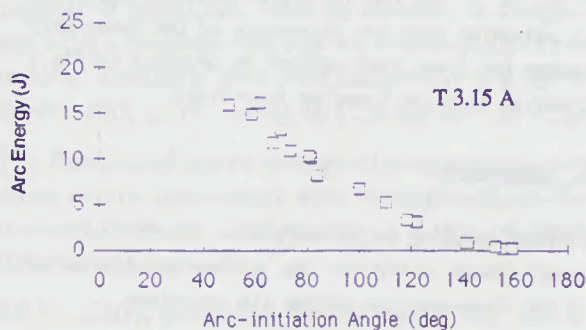


Fig. 3 Test results of 5 x 20 mm fuse-links to IEC 127-2, at 250 V - 35 A (Time-lag, manufacture B)

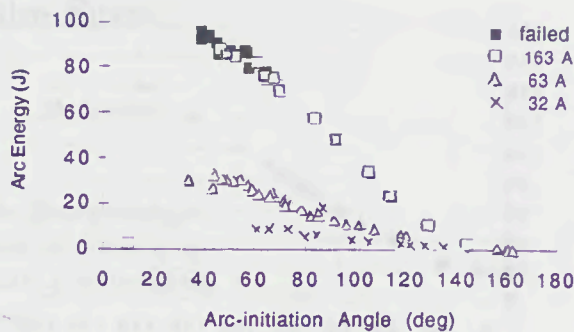


Fig. 4 Arc-energy of 5 x 20 mm quick-acting 6.3 A fuse-links for three test currents (Manufacture A)

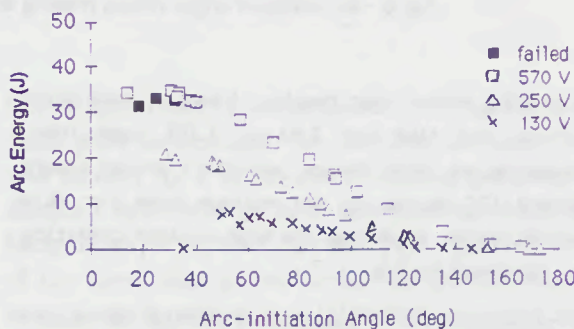


Fig. 5 Arc-energy of 5 x 20 mm quick-acting 3.15 A fuse-links at three test voltages (Manufacture B)

#### 4. Arc-initiation angle versus making angle

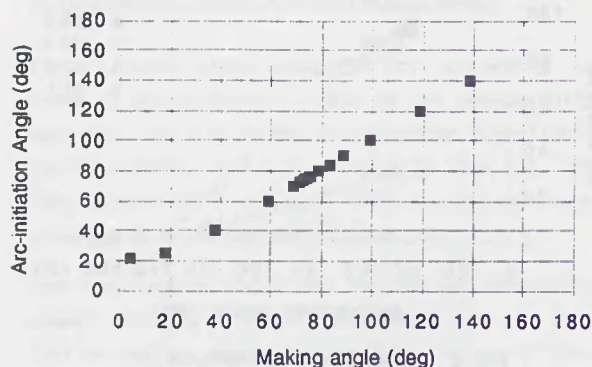
Fig. 6(a) indicates that in the case of small-current lbc MFs, owing to the relatively high test current, making angle on the voltage wave is nearly equal to the arc-initiation angle which distributes widely from 20 to 140 degree.

Fig. 6(b) on the other hand shows the case of fuse links of larger current rating, where arc hardly started before 30 degree. This could be attributed to the slow heating and quick cooling of the fuse-element during its passage of voltage zero because of the relatively small test current.

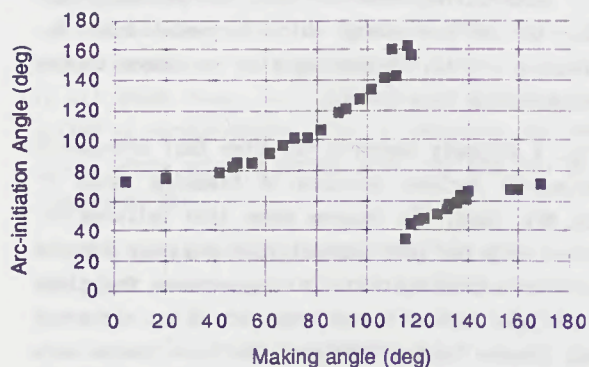
In the case of time-lag lbc fuse-links this tendency is noticeable even for fuse-links of smaller ratings.

#### 5. Test requirements for lbc MFs

At present IEC 127-1, which deals with general requirements for miniature fuse-links, specifies for all breaking tests of all miniature fuse-links, uniquely, making angle of 30 degree on the voltage wave.



(a) 500 mA



(b) 6.3 A

Fig. 6 Arc-initiation angle versus making angle of quick-acting fuse-links (Manufacture A)

According to our test results, however, some quick acting (not time-lag) 2.5A or 3.15A fuse-links, depending on their design, may start arcing always around 150 degree on the voltage wave for this making angle, producing the most lenient condition as suggested by Fig. 1.

Furthermore, if a homogeneous series of quick-acting fuse-links had such a fuse-link as the head and a small fuse-link, say 200mA, as the tail, the test result will be evident before the tests. Thus, the requirement concerning the making angle must needs be re-examined.

IEC 127-1 also requires miniature fuse-links to be tested for currents of approximately 5, 10, 50 and 250 times the rated current not exceeding the rated breaking capacity. The preceding Fig. 4, however, hints that breaking tests for currents lower than the breaking capacity might be useless.

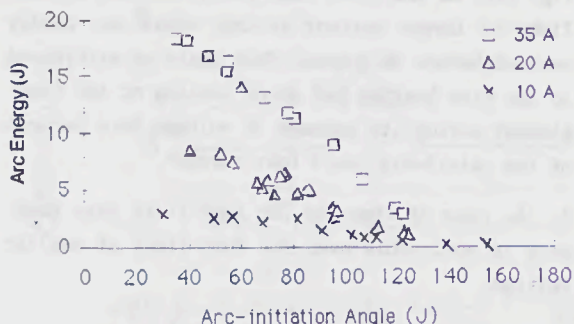


Fig. 7 Arc-energy of 5 x 20 mm time-lag 2A fuse-links for test currents 5I<sub>n</sub>, 10I<sub>n</sub> and the breaking capacity (Manufacture A)

Fig. 7 represents arc-energy of time-lag fuse-links, made by manufacturer A, for test currents 5 I<sub>n</sub>, 10 I<sub>n</sub> and for the rated breaking capacity. It indicates that the phenomenon of the lower arc-energy for lower test current as depicted in Fig. 4 prevails also for time-lag fuse-links.

#### 6. Conclusion

Current-breaking performance of a lbc MF is determined almost solely by the arc-energy dissipated in the fuse-envelope during its operation.

In this point of view the making angle requirement and the lower current test requirement now specified in IEC 127-1 must be re-examined. It is necessary also for the test specification for the homogeneous series of miniature fuse-links to be established.

#### 7. Acknowledgement

The authors are grateful to Mr. H. Arikawa, President of S.O.C. Corporation, who has supported and encouraged our research.

#### 8. Reference

- [1] Turner H.W., Turner C. and Williams D.J.A., Breaking capacity of miniature fuses and the testing of a homogeneous series, ICEFA/1987, pp 169 - 174

# Fusing and Short Circuit Interruption Behaviour of Metal Film Fuses

M. Lindmayer    M. Luther

Institut für Elektrische Energieanlagen  
Technische Universität Braunschweig  
P.O. Box 3329, W-3300 Braunschweig  
Germany

## Summary

This paper presents some experimental results of current limiting and short circuit interruption behaviour of metal film fuses on alumina in comparison with a conventional fuse for semiconductor protection. Breaking tests were carried out in a 250 V-circuit with  $di/dt$ -values of 12 A/ $\mu$ s and 36 A/ $\mu$ s.

The fuse model shows very good interruption properties and in comparison with the conventional fuse the rated current is higher by a factor of nearly three at the same  $i^2t$ .

Additionally, numerical simulations of the melting characteristics are made. They show that the heat resistance between the alumina substrate and its cooled reverse side has to be taken into account.

## 1 Introduction

A metal film fuse is a new application of thick film technology to fuses. In comparison with conventional sand filled fuses, metal film fuses show some advantages with respect to the gap between the rated current and the short circuit let-through current. The heat dissipated from the constrictions and thus the rated current for a certain cross-section can be substantially increased by applying a metal layer on a thermally well-conducting substrate, such as  $Al_2O_3$  and additionally cooling the bottom of the substrate. Thus a quick-acting device can be realized, which can be used for fast power semiconductor protection.

Under steady state conditions some experimental investigations with fast-acting miniature fuses were made by [1], where the fuselinks were manufactured by evaporating silver onto clear quartz disks. In [2]

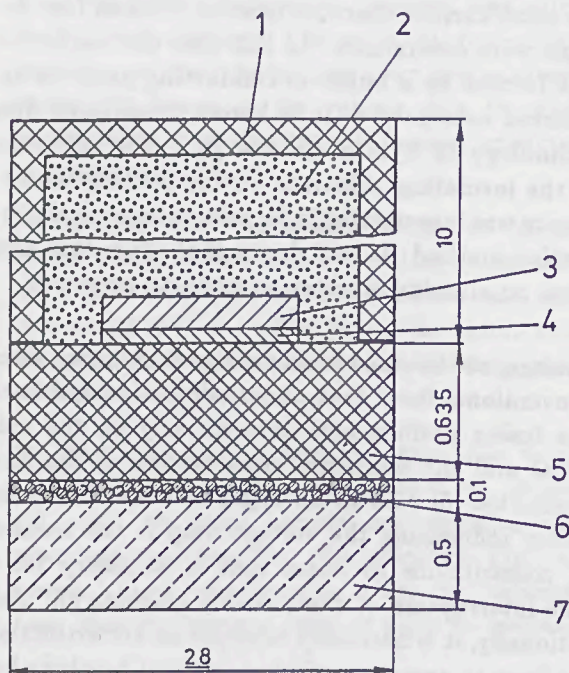
the time/current characteristics of different fuse designs were determined. In this case the conductor was formed by a burnt-in conducting paste on an alumina substrate as it is known from thick film technology of hybrid circuits [3]. The influence of the insulating substrate on the melting performance was investigated in [4] using a numerical simulation method. It was shown that silver thin film fuses on alumina are very sensitive to overloads.

Looking at the short circuit range it is known from conventional fuses that under adiabatic conditions the fusing performance depends only on the material and the minimum cross-section of the fuse conductor [5]. As in all types of fuses, the main factor influencing the voltage drop is the number of constrictions in series that is necessary for a safe interruption of short circuit currents [6]. Additionally, it is necessary to apply an arc extinction medium to assure satisfactory current breaking behaviour. Quartz sand has proved to show optimum behaviour in many respects. It is understood that the large surface area of the sand, together with the microscopic channels between the grains that allow the plasma to flow outward from the hottest zones, are responsible for this performance [5]. The difference with a fuse conductor on a ceramic substrate compared to conventional fuses is that the fuse conductor is only surrounded at one side by the sand.

The following studies were made to establish whether the experiences with conventional fuses can be transferred to metal film fuses in the short circuit range, because there is little information yet about their performance under these conditions.

## 2 Principal Structure of Metal Film Fuses

The principal structure of the investigated fuse models is illustrated in fig. 1. First the conductor is formed by a screen-printed and fired silver paste (4) on an  $\text{Al}_2\text{O}_3$  substrate (5). The thickness of the substrate is 0.635 mm throughout, and its area is  $1 \times 2$  inches. The typical thickness of the burnt-in layer is  $8 \mu\text{m}$ , its specific electrical conductivity is  $\kappa_p = 3.0 \cdot 10^4 \text{ 1}/(\Omega\text{mm})$ . For carrying higher currents, the thickness of the layer is increased by electroplating up to  $70 \mu\text{m}$ . The specific electrical conductivity of the electroplated silver layer (3) is typically  $\kappa_{Ag} = 5.4 \dots 5.8 \cdot 10^4 \text{ 1}/(\Omega\text{mm})$ .



- 1 plastic case
- 2 sand filler
- 3 silver layer ( $20 \dots 60 \mu\text{m}$ )
- 4 silver paste ( $8 \mu\text{m}$ )
- 5  $\text{Al}_2\text{O}_3$  substrate
- 6 heat-conducting adhesive
- 7 copper plate for cooling

Fig. 1: Principal structure of a metal film fuse (all dimensions in mm)

In order to provide a heat sink and to improve the mechanical strength, the substrate is connected to a copper plate (7) by a heat-conducting adhesive (6). The sand filler (2), which is necessary for optimum

arc extinction, is contained in a plastic case (1) mounted on the substrate/conductor combination.

To study the influence of the number of constrictions, the experiments were carried out with two different fuse designs, shown in fig. 2. They consist of 5 or 7 notches in series and two parallel current paths. The width and length of each constriction is 0.5 mm. The geometries were chosen in an iterative process, taking into account the results of nominal current, voltage drop and a large number of interruption tests.

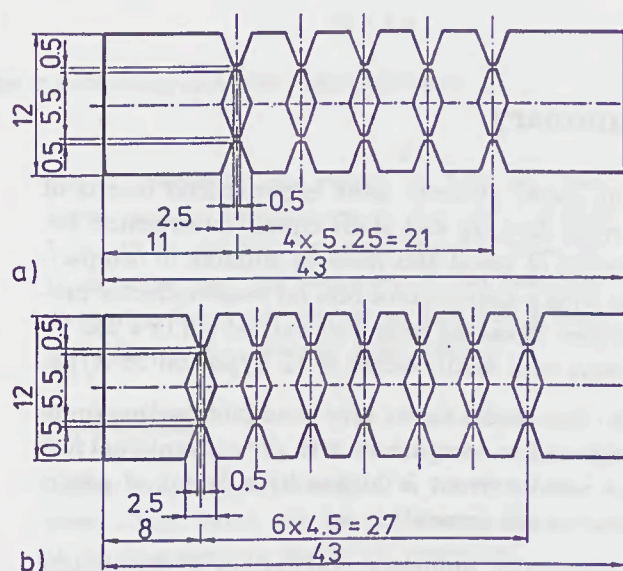


Fig. 2: Investigated fuse designs (all dimensions in mm)

- a) 5 constrictions in series (type 5)
- b) 7 constrictions in series (type 7)

## 3 Test Circuit and Experimental Arrangement

For first experiments under permanent current load in a low voltage DC circuit, the sand was omitted to allow temperature measurements in the metal film constrictions with an infrared thermometer [7]. Under these conditions the role of the quartz sand is negligible because of the main heat dissipation through the substrate.

By water-cooling the bottom of the fuses of fig. 1, the DC current was determined that the fuses are able to withstand for a long time ( $t \rightarrow \infty$ ). It was found that  $200 \text{ }^\circ\text{C}$  are not exceeded in the constrictions then. Though there is no precise coincidence with the definition in fuse standards, this current is referred to as *rated current* of the fuses.

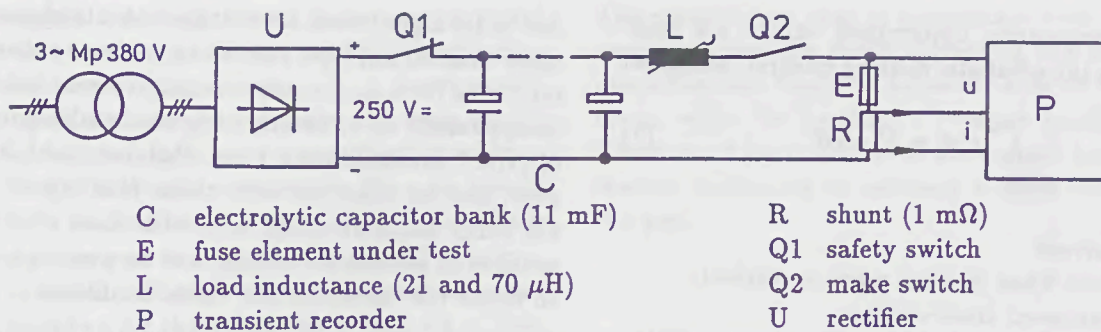


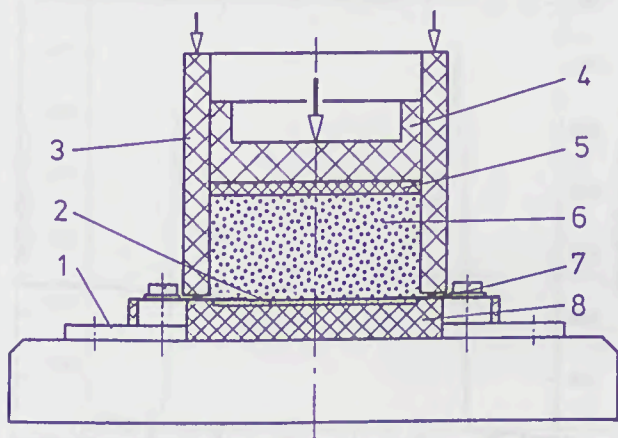
Fig. 3: Test circuit for breaking tests

The short circuit interruption experiments were carried out in the synthetic test circuit of fig. 3. The energy is supplied by a capacitor bank C charged to 250 V. Together with the load inductance L, it constitutes a resonant circuit of 330 Hz and 580 Hz respectively, for the chosen load conditions. The  $di/dt$ -values after closure of Q1 were set by L to 12 and 36 A/ $\mu$ s respectively, equivalent to peak short circuit currents of 38 and 115 kA under 50 Hz conditions. Provided the total interruption time is short in comparison with the resonant frequency, after interruption nearly the full capacitor charge voltage appears and remains across the fuse terminals. Under these conditions the tests are an approximation of a 250 V DC circuit and of the first critical stress in an AC circuit with 250 V momentary line voltage after clearing, respectively. In any case the circuit allows to study the fusing and interruption behaviour and to compare the influence of different fuse parameters. The current and voltage of the fuse are measured by a 20 MHz transient recorder (Nicolet Explorer 2019).

For the interruption tests the fuse model was modified to a demountable test chamber, illustrated in fig. 4. The fuse conductor (2) is contacted with soldered copper strips. The quartz sand (6) is filled into the case (3) and fixed by a top plate (4) under a constant force of 140 N. The inner volume of the chamber is 18 cm<sup>3</sup> and leads to a sand thickness above the conductor of about 12 mm.

#### 4 Experimental Results

The object of the breaking tests was to get some knowledge about the influence of the conductor thickness and the number of constrictions on the fusing performance as well as the interruption capability. The fusing integral, depending on the total thickness of the conductor for the two fuse types at 12 and 36 A/ $\mu$ s, are shown in fig. 5 where every data point represents one interruption test.



- |                                 |                 |
|---------------------------------|-----------------|
| 1 contact terminal              | 5 sealing strip |
| 2 substrate with fuse conductor | 6 sand filler   |
| 3 plastic case                  | 7 seal          |
| 4 bakelized paper top           | 8 bottom plate  |

Fig. 4: Chamber for breaking tests

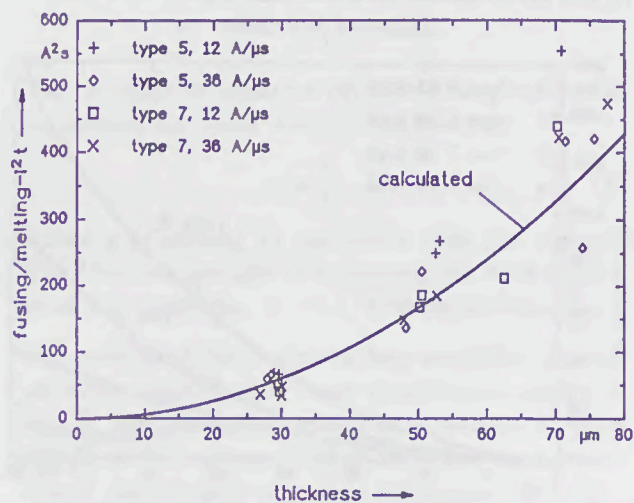


Fig. 5: Fusing and calculated melting integral for different thickness of the fuse conductors

The experimentally determined values are compared with the adiabatic melting integral calculated from [5]

$$\int_0^{t_m} i^2 dt = q^2 \cdot \Delta K \quad (1)$$

where

- $i$  : current
- $t_m$  : time when melting point is reached
- $q$  : minimum cross-section
- $\Delta K$  : material constant ("melting impulse" [5])  
( $6.7 \cdot 10^4 \text{ A}^2\text{s/mm}^4$  for Ag)

As a simplification, the conducting sandwich consisting of  $8 \mu\text{m}$  conducting paste plus electroplated silver is treated as a uniform metal with the  $\Delta K$  value of solid silver.

It can be seen from fig. 5 that especially for larger thicknesses the calculated melting integral is less than the fusing integral. Taking into consideration that the paste has a resistivity of about double the value of Ag and the electroplated silver of about 10 to 15 % higher than solid silver would yield fusing integrals of roughly 25 to 15 % lower, depending on the total thickness of the sandwich. According to [5] the  $\int i^2 dt$  necessary to establish the arc is nearly identical with the value to heat the notches up to the melting point. The results from fig. 5 show that some additional energy, though definitely smaller than the value for complete melting and boiling, is necessary.

In fig. 6 the breaking integrals for the same experiments are summarized. There is no dependence on  $di/dt$  in the investigated range. Both types with 5 and 7 constrictions interrupt the current properly in the investigated range, where type 7 acts faster

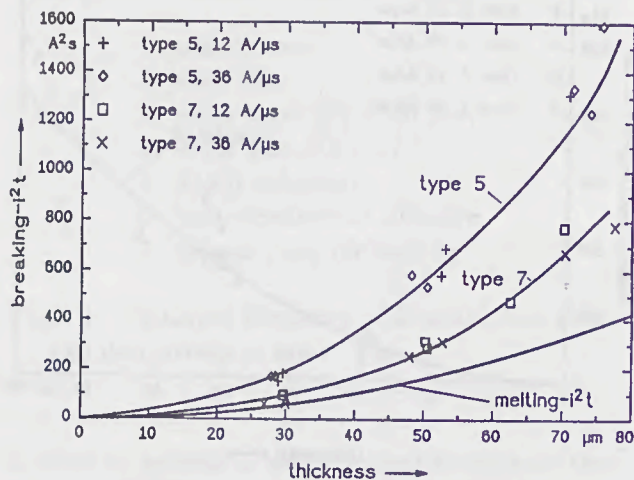


Fig. 6: Breaking integral for different thickness of the fuse conductors

due to its higher total arc voltage. At a thickness of more than  $50 \mu\text{m}$  type 5 shows an increase of breaking times (= time until the residual current tail has disappeared) up to 28 ms, while the breaking times of type 7 are still below 1 ms. Failures could, however, not be observed with these fuse types. On the other hand breaking tests with fuses of only 4 notches in series have shown that they are not able to break the current under these conditions.

A typical oszillogram of a breaking test of a metal film fuse (type 7) is shown in fig. 7. The determined rated current for this fuse pattern is 100 A when the bottom is cooled. For a current rise of  $36 \text{ A}/\mu\text{s}$  the let-through current is 2.7 kA and the breaking time is  $320 \mu\text{s}$ . The fusing integral of this metal film pattern is  $185 \text{ A}^2\text{s}$ , the breaking integral is  $313 \text{ A}^2\text{s}$ , respectively.

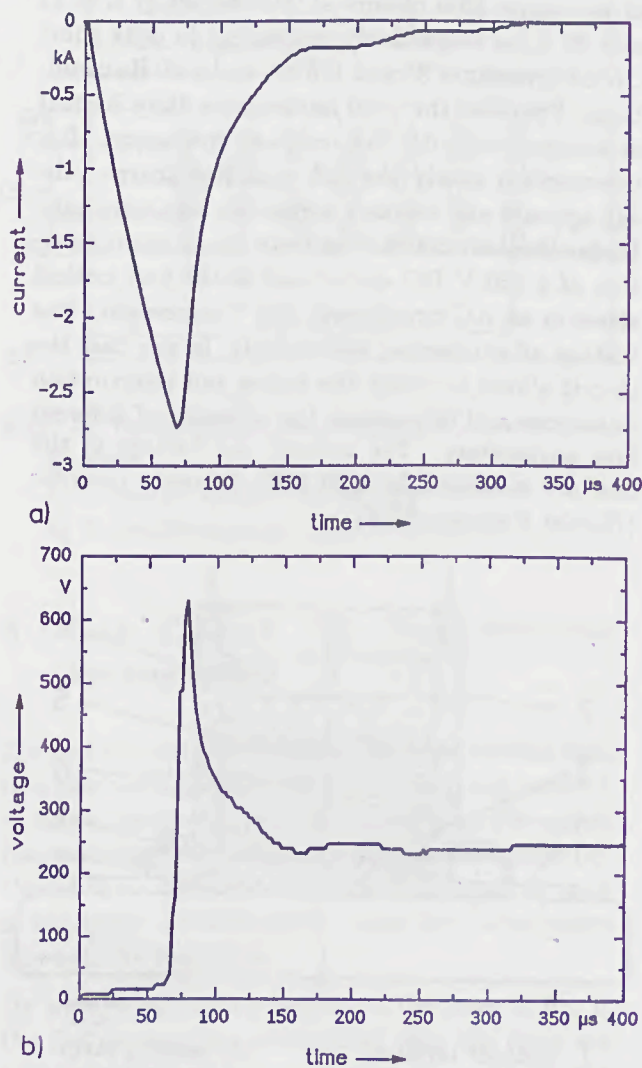


Fig. 7: Breaking test of a metal film fuse (type 7,  $d = 45 \mu\text{m}$ ,  $di/dt = 36 \text{ A}/\mu\text{s}$ )  
 a) current distribution  
 b) voltage distribution

To compare the short circuit behaviour of metal film fuses, breaking tests were carried out with conventional semiconductor fuses. Fig. 8 shows results in the same time range and under the same conditions as in fig. 7 for a conventional semiconductor fuse (35 A/500 V) of approximately the same breaking  $\int i^2 dt$ . It consists of a silver strip 70  $\mu\text{m}$  thick with a pattern of two parallel paths of 7 constrictions in series. The let-through current is somewhat less than for the metal film fuse (2.3 kA), but current zero is only reached after 3.5 ms. The fusing and breaking integrals are 102  $\text{A}^2\text{s}$  and 274  $\text{A}^2\text{s}$ . Comparing the arc voltage of the different fuses, it can be seen that the metal film fuse has a higher peak voltage, resulting in a faster current decay.

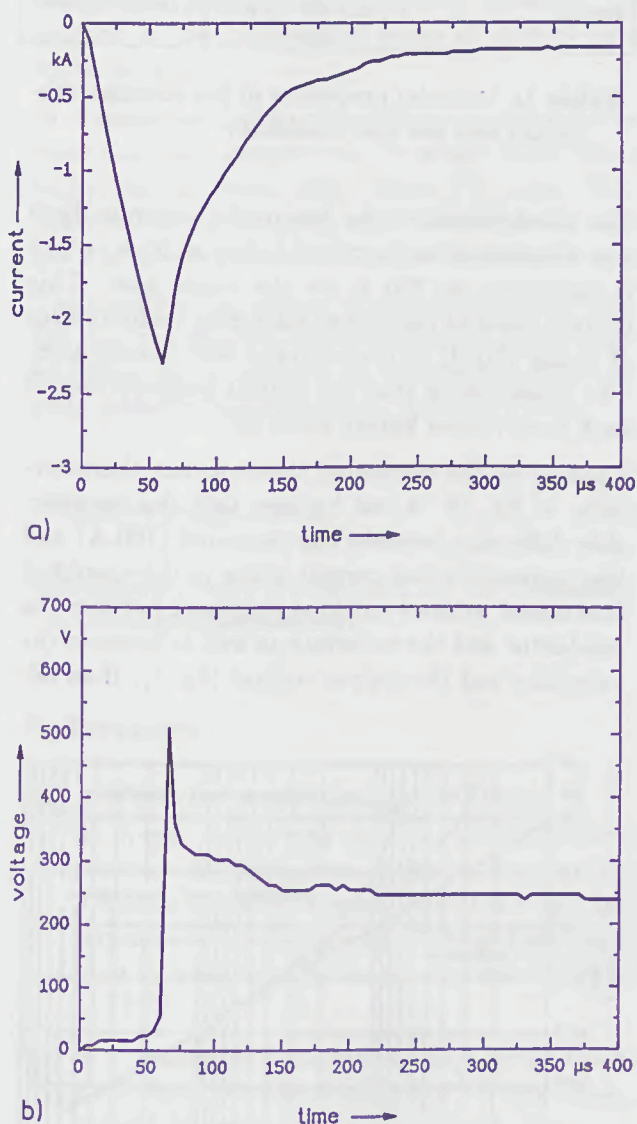


Fig. 8: Breaking test of a conventional semiconductor fuse ( $I_r = 35 \text{ A}$ ,  $di/dt = 36 \text{ A}/\mu\text{s}$ )  
 a) current distribution  
 b) voltage distribution

The results show that in comparison with the conventional fuse the rated current of the described metal film fuse sample is higher by a factor of nearly three, while the breaking  $i^2t$ -values hardly differ. The time of the cessation of the current tail is even shorter, indicating in tendency a faster recovery of the gap.

## 5 Calculated melting characteristic

The melting characteristic of the metal film fuses was studied using the general purpose FEM program ANSYS [8]. The feature of this program is to solve the steady state and transient thermal-electrical coupled field problem with temperature dependent material properties.

The governing differential equation for the heat flow in a conducting solid is given by

$$\text{div}(\lambda \cdot \text{grad}T) - \rho \cdot c \frac{\partial T}{\partial t} = -\eta \quad (2)$$

while the Laplace equation of the electrical current flow is described by

$$\text{div}\vec{J} = \text{div}(\kappa \cdot \text{grad}\varphi) = 0 \quad (3)$$

where

- $\lambda$ : thermal conductivity
- $T$ : temperature
- $t$ : time
- $\rho$ : density
- $c$ : specific heat
- $\eta$ : power density
- $\kappa$ : electrical conductivity
- $\vec{J}$ : current density vector
- $\varphi$ : electrical potential

The coupling of equation (2) and (3) is given by the expression for Joule heating described as

$$\eta = \frac{1}{\kappa} \cdot J^2 \quad (4)$$

where  $\eta$  is defined as generated heat per volume. The iterative solution procedure of the ANSYS program for equations (2) and (3) is treated in [9].

The generated finite element fuse model for the calculations under steady state conditions is shown in fig. 9. Because of symmetry it represents only an eighth section of type 7 (fig. 2b). The model consists of the ceramic substrate (thickness 0.635 mm) and the applied fuse conductor with a thickness of 50  $\mu\text{m}$ . The current load (DC only) is applied at the nodes of the constriction on the left side, while the

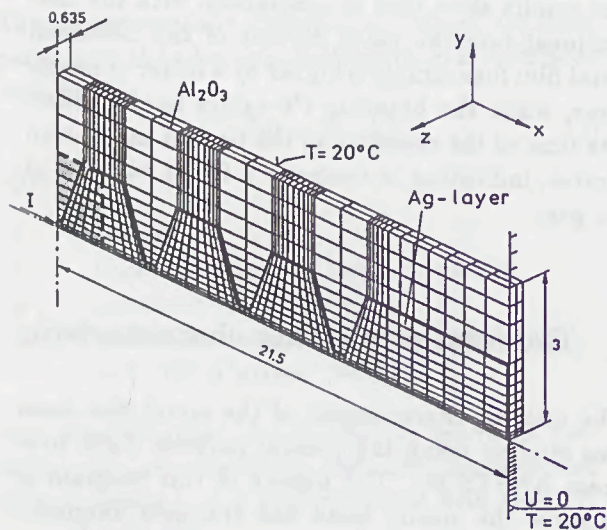


Fig. 9: Steady state FEM fuse model (all dimensions in mm)

electrical potential on the right side of the conductor is fixed to zero. The cooled reverse side of the substrate, as well as the right side of the fuse (fuse terminal), is kept at a temperature of 20 °C. The heat dissipation by convection and radiation can be neglected because thermal conductivity plays the major role in this case. It was assumed first that there is no additional heat resistivity between the conductor and the substrate and between the substrate and the copper plate (fig. 1) of the real fuse.

The melting performance in the overcurrent and short circuit range was computed by increasing the applied current and calculating the time to reach the silver melting point (960 °C). As the calculations proved that the heat conduction between adjacent constricted sections is negligible, the FEM model of fig. 9 was modified into a one constriction fuse model with a finely subdivided ceramic substrate in z-direction. The geometry is indicated by a dashed line in fig. 9.

The temperature dependent material properties (electrical resistivity  $\rho$ , thermal conductivity  $\lambda$ , specific heat  $c$ ) of the  $\text{Al}_2\text{O}_3$  substrate and the conductor are linearized by

$$X(T) = X_0[1 + \alpha_{\rho, \lambda, c}(T - T_0)] \quad (5)$$

where

- $X$ :  $\rho, \lambda, c$
- $\alpha_X$ : temperature coefficients of  $\rho, \lambda, c$
- $T$ : temperature

and the index 0 is used for the properties at 20 °C.

The properties and coefficients for the materials taken from the literature [10, 11, 12, 13] are shown in table 1. The electrical resistivity of the fuse conductor results from the parallel layers of the paste and the plated silver shown in fig. 1. It is higher than the pure silver value ( $\rho_{\text{Ag}} \approx 1.5 \cdot 10^{-5} \Omega\text{mm}$ ).

property	conductor	$\text{Al}_2\text{O}_3$ substrate
electrical resistivity	$\rho_0$	$1.995 \cdot 10^{-5} \Omega\text{mm}$
	$\alpha_\rho$	$4.08 \cdot 10^{-3} 1/\text{K}$
thermal conductivity	$\lambda_0$	$24 \cdot 10^{-3} \text{ W/mmK}$
	$\alpha_\lambda$	$-1.4 \cdot 10^{-4} 1/\text{K}$
specific heat	$c_0$	$1.01 \text{ J/gK}$
	$\alpha_c$	$4.29 \cdot 10^{-4} 1/\text{K}$
density	$\rho$	$10.5 \cdot 10^{-3} \text{ g/mm}^3$

Table 1: Material properties of the alumina substrate and the fuse conductor

The rated current of the fuse model shown in fig. 9 was determined as described before as 55 A, which is equivalent to 220 A for the whole fuse. This current leads to calculated maximum temperatures of about 180 °C in the center of each constriction. The results show that the hottest temperatures of each constriction hardly differ [9].

Looking at the calculated time/current characteristics of fig. 10, it can be seen that the considerable difference between the measured (100 A) and the computed rated current is due to the simplified fuse model without any heat resistance between the conductor and the substrate as well as between the substrate and the copper coolant (fig. 1). If an ad-

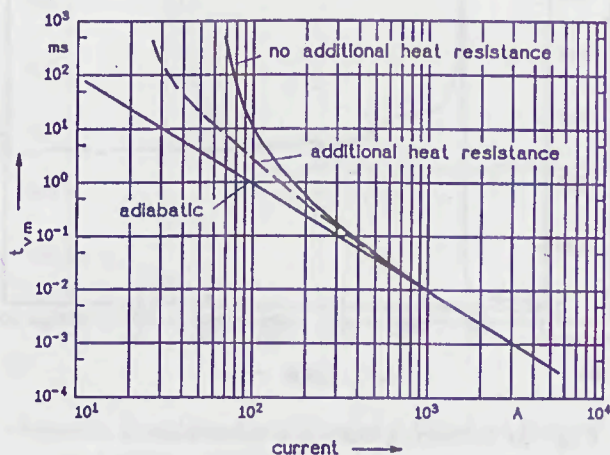


Fig. 10: Calculated time/current characteristics for one eighth section

ditional heat resistance is taken into consideration, the curve shifts to lower nominal current values. First estimations were carried out with the heat resistance of a 0.1 mm thick layer of heat-conducting adhesive (dashed line). The results are in much better agreement. It can be concluded that this resistance plays the major role in this case, and that its reduction will further improve heat dissipation from the notches.

## 6 Conclusion

The investigated metal film fuses have a quick-acting fusing performance. They additionally showed an excellent short circuit breaking behaviour in the investigated range of current rises up to 36 A/ $\mu$ s.

In comparison with conventional semiconductor fuses the rated current can be nearly three times higher for the same short circuit  $i^2t$ -value. This effect is due to the good heat dissipation through the Al<sub>2</sub>O<sub>3</sub> substrate cooled at the reverse side.

The results of the numerical calculations show that the heat resistance of the intermediate layers must be taken into consideration to simulate the complete melting characteristic of metal film fuses.

## Acknowledgement

This research work is supported by the Deutsche Forschungsgemeinschaft.

## References

- [1] A. F. Howe, D. de Cogan, P. W. Webb, N. P. M. Nurse: *Measuring the Pre-Arcing Temperature of High-Breaking-Capacity Fuselinks by Thermal Imaging*, Proceedings of the 2nd International Conference on Electric Fuses and their Applications, Trondheim - Norway 1984, p. 12-23
- [2] A. J. Marriage, B. McIntosh: *High Speed Thick Film Fuses*, Proceedings of the 5th European Hybrid Microelectronics Conference, Stresa - Italy 1985, p. 282-287
- [3] H. Reichel (Publ.): *Hybridintegration, Technologie und Entwurf von Dickschichtschaltungen*, Hüthig-Verlag, Heidelberg 1986
- [4] D. de Cogan, M. Henini: *TLM Modelling of Thin Film Fuses on Silica and Alumina*, Proceedings of 3rd Conference on Electrical Fuses and their Applications, Eindhoven, the Netherlands 1987, p. 12-17
- [5] H. Johann: *Elektrische Schmelzsicherungen für Niederspannung*, Springer-Verlag, Berlin, Heidelberg, New York, 1984
- [6] A. Wright, P. G. Newbery: *Electric Fuses*, IEE Power Engineering Series 2, Peter Peregrinus Ltd., London - New York 1982
- [7] M. Hofmann: *Experimentelle und rechnerische Untersuchungen von Ansprechennlinien und Alterungsvorgängen bei Sicherungsschmelzleitern*, Thesis TU Braunschweig 1984
- [8] G. J. DeSalvo, R. W. Gorman: *ANSYS Users Manual Rev. 4.4*, Swanson Analysis Systems Inc., Houston PA, USA 1989
- [9] M. Lindmayer, M. Luther: *Static and Dynamic FEM Calculation of Current and Temperature Distribution in Metal Film Fuses*, Proceedings of the 5th International ANSYS Conference, Pittsburgh PA - USA 1991
- [10] F. Kohlrausch: *Praktische Physik*, Band 3: Tafeln, B. G. Teubner, Stuttgart 1968
- [11] A. Tslaf: *Combined Properties of Conductors*, Elsevier Scientific Publ. Company, Amsterdam, Oxford, New York, 1981
- [12] R. C. Buchanan: *Ceramic Materials for Electronics*, Marcel Dekker Inc., New York, Basel, 1986
- [13] Y. S. Touloukian: *Thermophysical Properties of Matter, Vol. 5: Specific Heat*, Plenum Press, New York 1975



**Session 5A**

**MOTOR CONTROL FUSES**

Beason SA

MOTOR CONTROL FUSES

# PROTECTION OF MOTOR CONTROLLERS USING NORTH AMERICAN TIME DELAY FUSES

A. J. Flood

Gould Shawmut  
Toronto, Canada

## Summary

European or IEC motor controllers have experienced difficulty in gaining North American market acceptance even though complying with UL and CSA Standards. It is the author's belief that this is due in large part to philosophical differences between North American and European low voltage fuse standards. This paper therefore reviews North American low voltage, current-limiting fuse standards and explains their influence on equipment standards with particular reference to motor controlgear and the application of fuses for short circuit protection of motor circuits. Special reference is given to the North American Time Delay fuse.

## 1. Introduction

North American low voltage fuse, equipment and installation standards are co-ordinated to the extent that when short-circuit protection is provided by current-limiting fuses, it is common practice for the end-user, not the equipment manufacturer, to decide on the class and brand of fuse to be installed. This is contrary to European standards and practice where it is becoming more usual for the equipment manufacturer to have to assume responsibility for the installed fuses.

Introduction of the much smaller European designed IEC contactor into the North American market met with some resistance primarily because some controlgear manufacturers did not fully understand the concepts underlying the North American system of fuse protection and many North Americans did not realize that the IEC type of contactor needs a more current-limiting class of fuse than is commonly used for the protection of the larger dimensioned North American or NEMA type of contactor.

## 2. North American 600 Volt Fuses

For the purposes of this paper, we can say that North American general purpose current-limiting fuses are available in three basic classes - Class R, Class J and Class L.

The Class R fuse, ratings 0.1-600 amps, can be summarized as a large dimension fuse with current-limiting performance adequate for the traditional NEMA type motor controllers. The Class J fuse, ratings 1-600 amps, has overall dimensions similar to IEC 269 fuses and has much better current-limiting performance than the Class R fuse. The Class L fuse is the extension to the Class J range in ratings from 601 amps through 6000 amps.

A significant feature of the North American fuse system is that short-circuit performance limits are specified. That is to say, UL and CSA current-limiting fuse standards specify for each class of fuse the limits of cut-off current, or peak current as it is more commonly referred to in North America, and total operating  $I^2t$  that the fuse can let-through under short-circuit conditions, up to and including its maximum interrupting rating. Note that the normal interrupting rating for current-limiting fuses in North America is 200kA. The class of fuse also determines the dimensions to ensure that fuses of different classes are not readily interchangeable.

Table 1 compares peak current and total  $I^2t$  limits for Class J, R and L fuses at 200kA RMS Sym., 600V, single phase.

Table 1. Some Standard Limits of  $I_p$  and  $I^2t$  for Class J, R and L fuses

Fuse Class & rating (A)	Maximum Limits	
	$I_p$ (kA)	$I^2t$ (A <sup>2</sup> s)
J-60	16	30,000
R-60	26	200,000
J-200	30	300,000
R-200	50	2,000,000
J-400	45	1,100,000
R-400	75	6,000,000
L-800	80	10,000,000
L-1600	150	30,000,000

The significance of the short-circuit peak current and  $I^2t$  limits lies not so much in the actual values specified, but in the fact that equipment and control gear standards can recognize permanent and standardized maximum short-circuit let-through limits which can be used to establish equipment short-circuit ratings when protected by fuses of a specified class. Brand testing of individual manufacturers' fuses is not required.

### 3. The Time Delay Fuse

First introduced in 1939, the North American Time Delay fuse was primarily designed to provide both overload and short-circuit protection in motor circuits. The Time Delay characteristic requires the fuse to carry  $5.0 I_n$  for a minimum of 10 seconds. This delay permits the fuse to be sized close to motor full load current and yet still provide a good motor start characteristic.

A measure of the motor start capability of the Time Delay fuse is that it would require a Non-Time Delay fuse of twice the current rating of the Time Delay fuse to obtain a similar characteristic at 10 seconds.

The Time Delay fuse is normally sized for short-circuit protection at between 125% and 175% of motor full load current. It should be noted that this method of sizing the fuse only requires reference to the motor full load current. With the North American system, it is not normally considered necessary to check Time Delay fuse time-current characteristics for motor start capability or for co-ordination with the overload relay.

Both Class R and Class J fuses can be obtained with either a Non-Time Delay or a Time Delay characteristic. Note that both characteristics have to meet the same cut-off current and  $I^2t$  limits specified for the class of fuse together with the conventional fusing current,  $I_f$ , which for North American general purpose fuses is  $1.35 I_n$ . Figure 1 shows the basic difference between the time-current characteristic of a Non-Time Delay and a Time Delay Class J fuse.

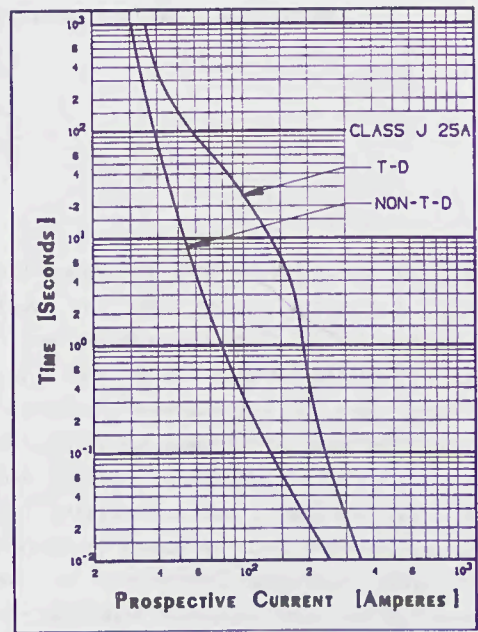


Fig. 1 Class J 25A. Time-current characteristics

### 4. North American Fuses and Equipment Standards

Equipment manufacturers can design and test to standardized fuse short-circuit characteristics. North American fusible equipment standards therefore specify that short-circuit tests must be conducted with test limiters or fuses that have peak current and  $I^2t$  let-through characteristics not less than those specified in the fuse standards for the class and rating of a fuse to be used in the equipment. From the standpoint of short-circuit protection, this system allows for safe interchangeability of fuses of the same class but different manufacture, regardless of any design changes that fuse manufacturers can make from time to time. This in turn enables the end-user to exercise freedom of choice between fuse manufacturers. In North America, the equipment manufacturer is normally responsible only for the fuse class, not the fuse brand.

### 5. Motor Circuits and North American Installation Standards

Not only does the North American standards system recognize fuse peak current and  $I^2t$  limits, but the wiring or installation standards (NEC in the U.S.A. and CEC in Canada) also provide guidance to the end-user by specifying maximum fuse ratings for the short-circuit protection of motor circuits.

These ratings are normally 300% of motor full load current for Non-Time Delay fuses and 175% of motor full load current for Time Delay fuses. If starting difficulties are encountered, they can be increased to a maximum of 400% and 225% respectively.

The installation standards therefore augment the system by identifying standardized fuse ratings to which motor controlgear can be short-circuit tested i.e. 400% motor full load current for Non-Time Delay and 225% motor full load current for Time Delay fuses. Lower test ratings can be used but the equipment must be specially marked to indicate the lower limit.

Again, note the end-user orientation in that the maximum rating of the SCPD is normally determined by the motor full-load current and not by the controller, unless specially marked.

### 6. Short-Circuit Protection of IEC Style Contactors

It is well known that the IEC contactor requires the SCPD to have relatively low cut-off current and  $I^2t$  let-through levels if "no damage" or Type 2 co-ordinated protection is required. In the North American system, the Class J fuse is the most current-limiting general purpose fuse and the Time Delay version is normally installed in motor circuits because it allows a lower current rating to be used and significantly reduces the cut-off current and  $I^2t$  let-through values.

Table 2 compares some typical 3 phase values of peak current and  $I^2t$  let-through at 200kA by Class J and Class R Time Delay fuses when selected for short-circuit protection of a 600V, 3 phase motor circuit having a full load current of 20 amps. To provide a reference point, typical values for a European type gG fuse are also shown.

Table 2. Typical let-through values of  $I_p$  and  $I^2t$ .

Fuse and % of motor full load current	Fuse $I_n$ (A)	$I_p$ (kA)	$I^2t$ (A <sup>2</sup> s.)
Time Delay:			
Class R at 125%	25	14.0	20,000
Class J at 175%	35	6.5	4,500
Class J at 150%	30	6.1	2,200
Class J at 125%	25	5.5	1,600
IEC269:			
Type gG at 200%	40	9.0	10,000

It can be seen from Table 2 that the higher damage levels would be obtained with Class R fuses and that the Class J fuse presents the end-user with the best prospect of obtaining "no damage" protection.

### 7. Motor Controlgear Co-ordination Tests

North American and IEC controlgear standards recognize two levels of short-circuit test currents - a lower level based on the contactor rating and a higher level to establish a higher short-circuit rating. These are known as test currents "r" and "q" respectively in IEC 947-4-1.

This standard also specifies two levels of short-circuit co-ordination for permitted damage levels - Type 1 and Type 2. While North American controlgear standards do not specify short-circuit co-ordination in terms of Type 1 and Type 2, they do not permit the overload relays to be damaged during the low level test when protected by fuses. Damage is however permitted when the SCPD is a circuit breaker.

IEC 947-4-1 also recognizes a third level of test current for verification of discrimination between the overload relay and the SCPD(s). This third level was specified in the old controlgear standard, IEC 292-1, as test currents "p", which were  $0.75 I_c$  and  $1.25 I_c$ , where  $I_c$  represented the cross-over point of the SCPD and overload time-current characteristics.

These test currents "p", contributed to the acceptance problems in North America, partly because discrimination between overload relays and fuses had never been regarded as a problem and partly because IEC292-1 specified that "The SCPD shall not operate in place of the starter for currents up to the maximum overload level in normal service (including stalled current of the motor)." This concept is contrary to that of the North American system which permits the end-user to size a Time Delay fuse close to motor full load running current.

IEC 947-4-1 has modified this part of the standard in that it classifies discrimination between the overload relay and the SCPD as a requirement which may be verified by a special test. Furthermore, it does not specifically require that the cross-over point of the overload relay and SCPD time-current characteristics shall prevent the SCPD from operating at currents up to the maximum overload level.

It should be noted here that limiting the fuse cut-off current and  $I^2t$  characteristics also limits the potential for variation in time-current characteristics among fuses of different manufacture.

A study undertaken by the North American NEMA and EEMAC fuse committees in 1985 for unification discussions with IEC/SC32B/WG8, showed that for operating times of 0.1 seconds or longer, the variation among North American fuse manufacturers' published time-current characteristics for Class J fuses was, for the most part, within  $\pm 10\%$  of the mean value. This relatively small variation among fuse time-current characteristics is obviously important to the concept of safe fuse interchangeability, particularly where equipment withstand limits are critical.

#### 8. Conclusion

North American standardized fuse short-circuit characteristics have resulted in a high degree of uniformity among operating characteristics for fuses of the same Class and rating but different manufacture. They have permitted the development of a standards system based on the concept of safe interchangeability among fuses of the same class but different manufacture.

The Time Delay fuse has provided a simple method of rating fuses for use in motor circuits and the Class J Time Delay is recognized by many motor controlgear manufacturers as providing "no damage" protection for IEC type motor controllers in the North American market.

Under the European system, a controlgear manufacturer would have to test all available fuse brands, and hope their designs did not change, to achieve the level of fuse interchangeability expected in the North American market. It is the author's opinion, therefore, that fuse brand testing for proof of performance with equipment, particularly motor controlgear, is likely to remain the less preferred system in North America.

#### References

1. IEC Standards:
  - IEC 269 - Low voltage fuses.
  - IEC 947 - Low voltage switchgear and controlgear
  - IEC 292-1 - Low voltage motor starters
2. UL Standards:
  - UL 198C - High interrupting capacity fuses, current-limiting types.
  - UL 198E - Class R fuses.
  - UL 508 - Industrial control equipment.
3. CSA Standards:
  - C22.2 No. 14-M1987 - Industrial control equipment.
  - C22.2 No. 106-M90 - HRC fuses.
4. Installation Standards:
  - National Electrical Code 1990.
  - Canadian Electrical Code 1990.

#### Notes:

1. U.S. and Canadian standards are not identical. However, many of the differences tend to be minor in nature and should be eliminated in the standards harmonization process now taking place in North America.
2. A proposal by IEC/SC32B/WG8 to include Class J and Class L fuses in the IEC 269 standard is currently being processed

## CONTACTORS PROTECTED BY FUSES: RISK OF CONTACT WELDING

D. ARATO\*, G. CANTARELLA\*\*

\* Istituto Elettrotecnico Nazionale "Galileo Ferraris"  
Corso Massimo d'Azeglio, 42 - 10125 TORINO - Italy.

\*\* Politecnico di Torino - Dipartimento di Ingegneria  
Elettrica Industriale  
Corso Duca degli Abruzzi, 24 - 10129 TORINO - Italy

### Summary

The risk of contact welding of contactors protected by fuses, when a short circuit occurs, is strictly dependent on the electrodynamic force acting on the contacts of the contactor, the rating of the protective fuses and the value of the prospective short circuit current.

The phenomenon has been dealt with by many authors; some papers on the subject are herewith quoted.

In this paper the results are reported of numerous short-circuit tests performed on contactors protected by fuses, which confirm the considerations made by the above authors.

A brief description of the test carried out on 70 types of contactors, made by 16 different manufacturers with overcurrent up to 50 kA (r.m.s.) at 418 V (1.1 x 380), 50 Hz, is presented.

The results of the tests are illustrated by comprehensive diagrams. In particular the diagrams show:

- the instantaneous value of the current for which the separation of the contacts by electrodynamic effect occurs on each type of contactor;
- the maximum rating of the protective fuses that prevented the tested contactors from contact welding, as a function of the rated operational current of the contactor, for utilization category AC 3;
- the minimum rating of the protective fuses which produced contact welding as a function of the above rated operational current of the contactor.

At last, a comparison is made between the shown test results on contactors protected by fuses and the prescriptions of the new IEC Standards 947-4 (IEC Standards 947-4: Low-voltage switchgear and controlgear. Contactors and motor starters).

### 1. General

In most application, contactors and motor starters are protected by fuses against short circuit currents.

Fuses are suitable for preventing excessive damage to the contactor or its parts. In particular they are capable of limiting the thermal and electrodynamic stresses which can cause the contact welding of the contactor. In the present paper for contact welding is intended a stable union of the contacts, which cannot be easily broken by repeated operations of the contactor control circuit. In other words a welding is meant, which requires the use of a tool for the contact separation, although it also is not always effective.

### 2. Test carried out and relevant methods

The tests were made on 80 types of contactors of 16 different manufacturers and current ratings in accordance with the following table no. 1.

The tests were carried out with alternating current at 418 V (1.1 times the rated voltage), 50 Hz, on a single phase circuit, with overcurrents up to 50,000 A (r.m.s. value of the symmetrical component of the prospective current). The power factor was 0.5 up to 10,000 A, 0.3 from 10,000 to 20,000 A and 0.25 from 20,000 A up to 50,000 A.

The circuit comprised one pole of the contactor in series with a protective fuse, as shown in figure 1. The contactor was in the closed position before the initiation of the overcurrent. The supply source of the electromagnet of the contactor was independent of that of the test circuit.

The tests were repeated under the same conditions on all the poles of the contactor.

Table 1

Manufacturers of contactors	Rated operational current of the contactors tested, for utilization category AC3 ( amperes )																									
a				12			25		40		63		100		160		250		400		630					
b		8		12			25			50		80		125		200	250									
c					16	20			32	40		63		100		160		250		400						
d					16	20				40			80		125		200									
e		8					20			40			80			160			315					630		
f									32		50		80			160		250		400						
g			10			20	25	32	40	50		80	100		160		250						630	800	1000	
h							25			50				125												
i				12									80						315							
l	6		10		16		25		40	50		80	100													
m																160		250		400						630
n					16		25	32	40		63	80	100	125	160		250				500	630				1000
o		8		12	16	20			32		50	63	80													
p											50	63	80		125	160		250								
q									40		63			125		200			315							800

Before any test were carried out, 100 opening and closing cycles were made on each contactor at the rated current and voltage, rated frequency and power factor approaching unity, in order to standardize the initial conditions of the contacts. It has been intended, in such a way, to minimize any accidental differences existing on new contacts which could reduce the reliability of the results. The instantaneous value of the minimum current for which separation of the contacts by electrodynamic effect occurs was first determined on each individual pole of each contactor.

The importance of the knowledge of such a current

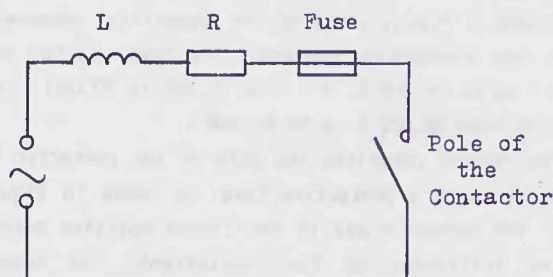


Fig. 1 - Test circuit comprising one pole of the contactor under test and the protective fuse.

value has been discussed in previous papers (1). (2): here is sufficient to remind that the contact welding of the contactor is more probable for short circuit current values near to that for which separation of the contacts by electrodynamic effect occurs, than for greater prospective currents.

The determination was made by means of a suitable equipment causing a sinusoidal half wave of current of given amplitude, at 50 Hz, to flow through the contacts of the pole of the contactor.

The current amplitude was gradually increased, test by test, in successive tests and the voltage drop across the contacts was observed: contact separation is indicated by a sudden increase in the voltage drop, as can be seen in figure 2.

The found values differ, by a few percent, from pole to pole of the same contactor. In the diagram of figure 3, the minimum recorded for each contactor is reported as a function of its rated operational current for utilization category AC 3.

The reported data of the same diagram were smoothed by the least squares method and represented by a dashed straight line statistically equivalent.

The behaviour of each contactor protected by fuses under short circuit conditions was then examined.

The values of prospective test currents were selected for each contactor in the range comprised between a minimum current value slightly lower than

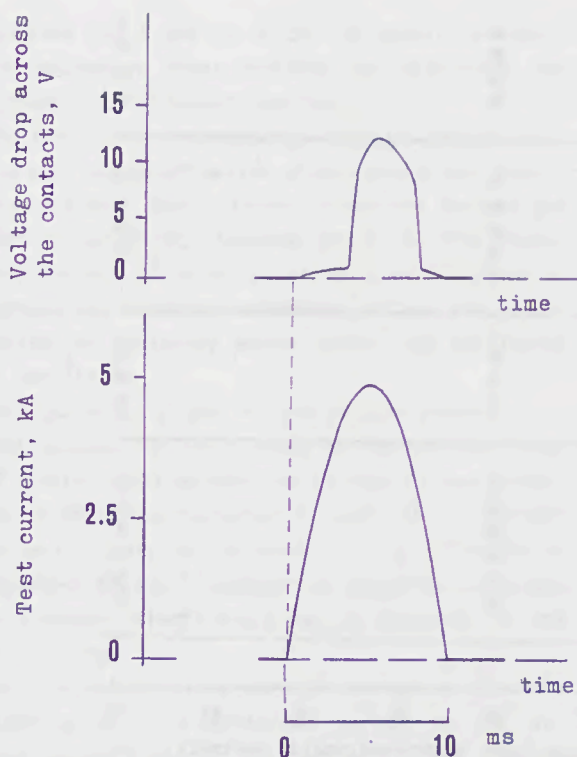


Fig. 2 - Test current and voltage drop across the contacts of a contactor which separate and then return to touch.

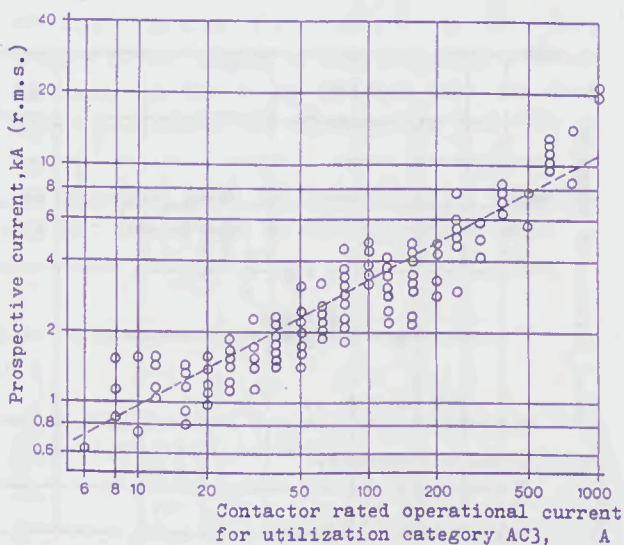


Fig. 3 - Current causing contact separation by electrodynamic effect as a function of the rated operational current of the contactors tested.

that which starts separating the contacts of the contactor by electrodynamic effect and a maximum current value stated in 50,000 A (r.m.s. value of the symmetrical component of the prospective current).

The fuse-links put in series with the contactors were of current limiting type, general purpose application, in accordance with IEC Standards. Their rated current was selected according to the instructions of the contactor manufacturer for a first series of tests, which were carried out in the above range of prospective currents. The fuse rating was then increased or decreased dependently on the results of the first series of tests, for making further series of tests under unaltered remaining conditions.

As a common, general result it can be stated that:

- for prospective currents not causing contact separation by electrodynamic effect no contact damage occurred;
- in the range of prospective currents within which contact welding was expected (1). (2), this occurred;
- for larger prospective currents only erosion of contacts occurred.

Figure 4 shows, for example, the behaviour of the above listed contactors, rated 400 A made by four different manufacturers. As the current rating of the protective fuse increases the range of prospective currents within which contact welding occurred becomes wider.

In the diagram the values can be seen of:

- the maximum rating of the fuse which prevented contactors from contact welding under short circuit currents;
- the minimum rating of fuse which produced contact welding of the contactors.

Figure 5 shows, as a compendium, the maximum rating of fuses which prevented the tested contactors from contact welding as a function of their rated operational current for utilization category AC 3. Note that for many contactors, especially the larger ones, the rating of the protective fuse may become lower than that of the contactor. This fact leads to a certain derating of the operational current of these contactors when a significant reduction of the risk of contact welding is desired.

Figure 6 shows, comprehensively, the minimum rating of fuses which produced contact welding of the tested contactors as a function of their rated operational current for utilization category AC3.

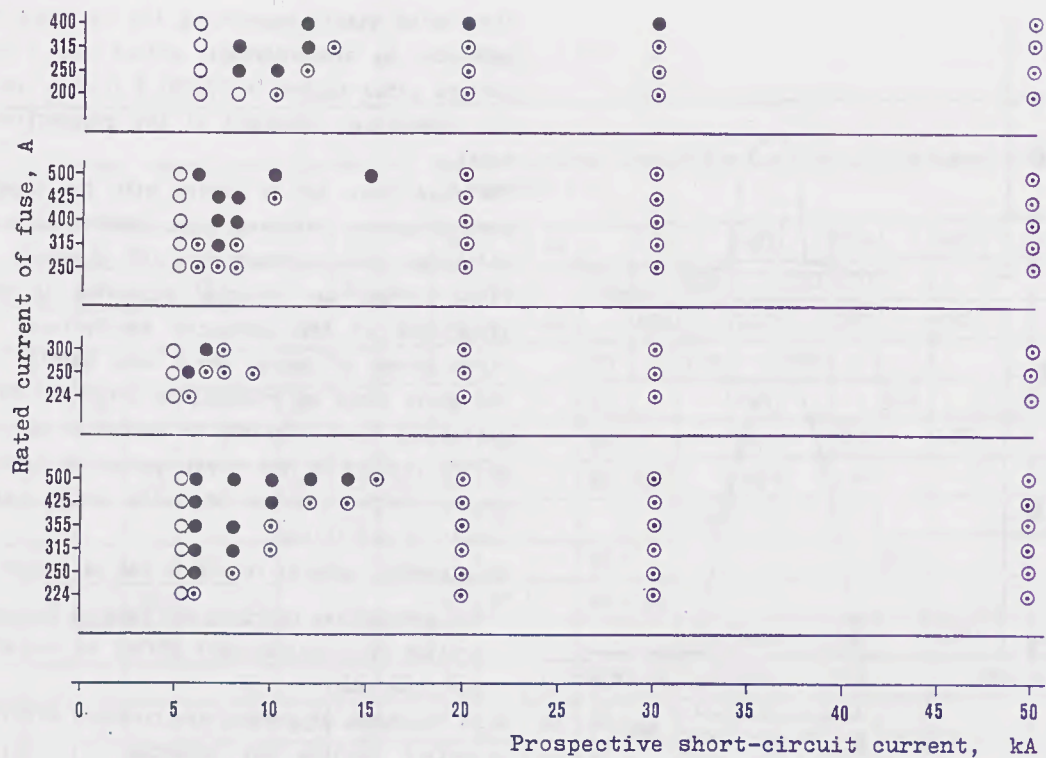


Fig. 4 - Results of tests carried out on 4 types of contactors rated 400 A and protected by fuses of various current rating:

- no damage to contacts
- welding of contacts
- ◐ erosion of contacts

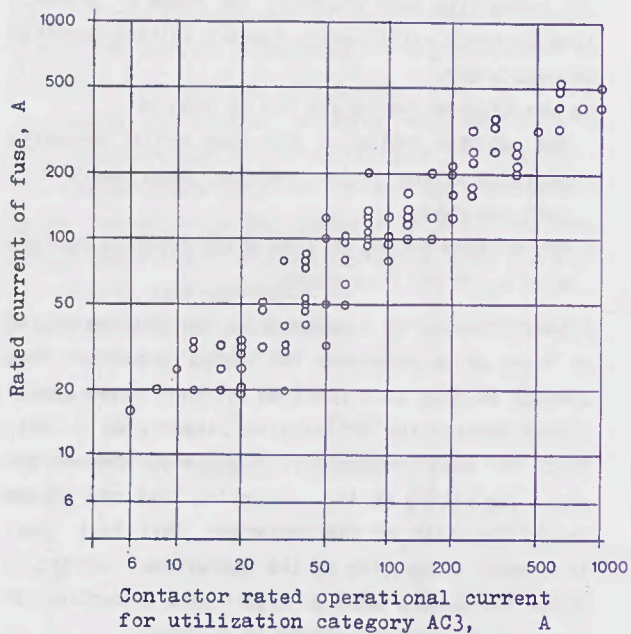


Fig. 5 - Maximum rating of fuses which prevented the tested contactors from contact welding as a function of the rated operational current for utilization category AC3 of the contactors tested.

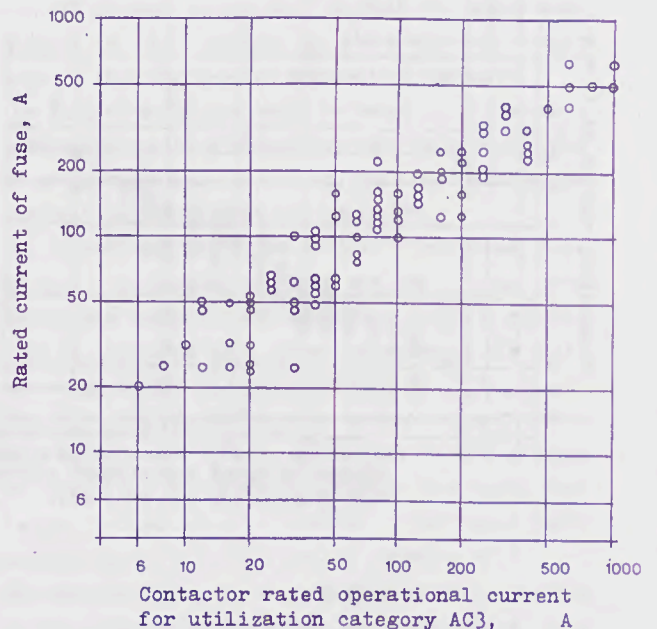


Fig. 6 - Minimum rating of fuses which produced contact welding of the tested contactors as a function of the rated operational current for utilization category AC3 of the contactors tested.

Diagrams no. 5 and no. 6 can be useful to choose the protective fuses suitable for preventing the contactors from contact welding.

The new (1990) international standardization dealing with the coordination of contactors and motor-starters with short circuit protective devices has been issued as IEC Standards 947-4. In this Standards methods of testing can be found intended to improve the contactor conditions of use and application for achieving better safety and continuity of service.

Test currents "q" and "r" aim at this purpose.

Test current "q" corresponds to the maximum value of short-circuit prospective current of the installation where the contactor is used. It is intended to verify that, during short circuit, there be no permanent arcing, flashover or ejection of flames or external effects which may be dangerous to the surroundings.

Test current "r" is a current related at discrete steps to the rated operational current for utilization category AC3 of the contactor. Test current "r" values are specified in the following table 2 and shown in diagram n.7.

Since the origins of the Standardization of contactors, test current "r" was intended as a short circuit current causing a high level of stress to the contactor protected by a given short-circuit protective device. With reference to the above considerations related to the protection afforded by fuses, it has to be reminded that the most severe stresses for the contactor are likely to be experienced for a range of these currents near to the current at which the contacts of the contactor are just thrown apart by electrodynamic effect.

Table 2

Rated operational current $I_e$ (AC-3) (A)	Prospective current "r" (kA)
$0 < I_e \leq 16$	1
$16 < I_e \leq 63$	3
$63 < I_e \leq 125$	5
$125 < I_e \leq 315$	10
$315 < I_e \leq 630$	18
$630 < I_e \leq 1\ 000$	30
$1\ 000 < I_e \leq 1\ 600$	42
$1\ 600 < I_e$	Subject to agreement between manufacturer and user

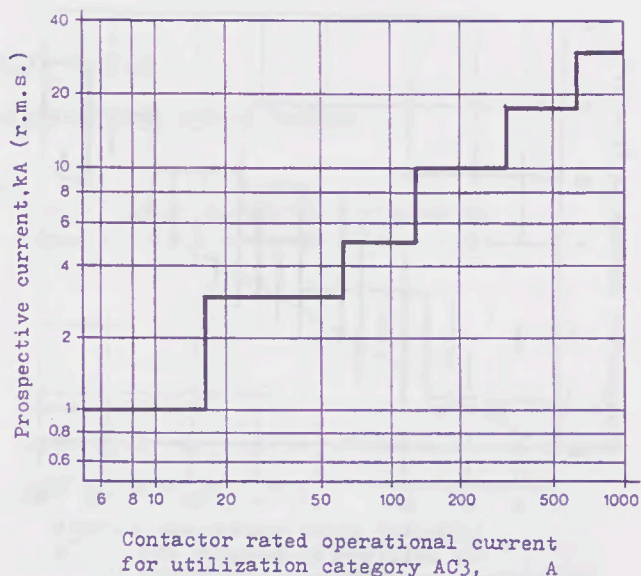


Fig. 7 - Test current "r" at discrete steps as specified in ICE Standards 947-4 as a function of the rated operational current for utilization category AC3 of the contactors tested.

That is particularly true for the risk of contact welding, as can be seen in the above diagram of figure 4.

The opportunity originates from the above considerations of examining whether test current "r", as specified in IEC Standards 947-4, be significant also for the risk of contact welding.

That has been done in figure 8, by comparing the prospective current values for which contact welding were experimentally verified with test current "r" values as specified in the quoted international Standards.

Precisely, in diagram of figure 8, as a function of the rated AC3 operational current of the tested contactors, the following quantities have been plotted for easy comparisons:

- the ranges of the prospective currents of the tests in which contact welding was systematically experienced (the short circuit protective device being the fuse specified in the above diagram of figure 6);
- the test current values "r" at discrete steps as specified in IEC Standards 947-4 (already reported in figure 7);
- the dashed straight line of the above figure 3 statistically equivalent to the current values for which contact separation of the tested contactors occurs.

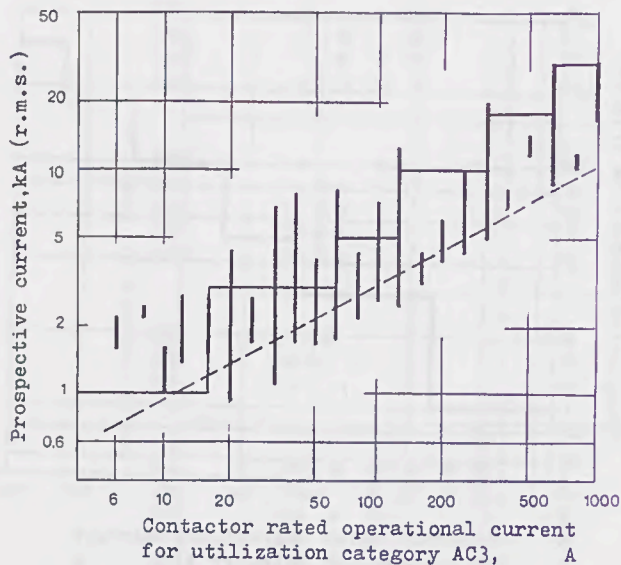


Fig. 8 - Comparison of the prospective current values for which contact welding was experimentally verified with the test current "r" values as specified in the quoted international Standards.

It can be observed that "r" prospective test current values practically comply with the above reminded condition of being near (slightly higher) to those values for which the contacts of the contactors are just thrown apart by electrodynamic effect. In addition, they fall in the prospective test current ranges where contact welding was experimentally verified.

Therefore, it can be deduced that the tests made by current values "r" give also significant results as regards the risk of contact welding of contactors in short circuit conditions.

#### REFERENCES

- [1] Toniolo S.B., Cantarella G.: Protezione di contattori mediante fusibili. *L'Elettrotecnica* - No. 3 bis, vol. LV, 1968.
- [2] Cantarella G., Farina, G., Tartaglia M.: Behaviour of contactors protected by fuses during short-circuit currents. *Proceedings IEE*, vol. 124, No. 12, 1977.
- [3] Wright A., Newbery P.G.: *Electric fuses*. IEE Power Engineering Series 2. Peter Peregrinus LTD., 1982.
- [4] Bellato G., Buccianti R.: Contattori di bassa tensione; indagine sul mercato italiano. - *Elettificazione*, febbraio 1987. pag. 70 - 121.
- [5] Arato D., Cantarella G.: Risultati di prove di corto circuito su contattori e rischio di saldatura dei contatti. *Rendiconti della LXXXVIII riunione annuale dell'AEI - Catania 1987*. Memoria 1.a.3..
- [6] IEC Publication 269-1 Second Edition 1986 Low Voltage Fuses. Part. 1: General Requirements.
- [7] Wilkins R.: Generalised short-circuit characteristics for h.r.c. fuses. *Proc. IEE*, vol. 122 No. 11, November 1975.
- [8] Turner H.W., Turner C.: Phenomena relating to temperature rise and welding in high current electric contacts. *4th International Research Symposium on Electric Contact Phenomena*. 1968.
- [9] Turner H.W., Turner C., Williams D.J.A.: Critical parameters influencing the co-ordination of fuses and switching devices. *Proceedings of the ICEFA 1987*.

## STARTERS PROTECTED BY FUSES

### THERMAL STRESS ON OVERLOAD RELAYS DURING SHORT CIRCUIT CURRENTS

D. ARATO

ISTITUTO ELETTROTECNICO NAZIONALE "GALILEO FERRARIS"  
CORSO MASSIMO D'AZEGLIO 42 - 10125 TORINO - ITALY

AND

C. DUGHERA

ING. L. AUDOLI COSTRUZIONI ELETTRICHE SRL  
CORSO VERCELLI 273 - 10155 TORINO - ITALY

SUMMARY : As well known, the stress and damage that short circuit currents can cause to contactors and their thermal overload relays are directly connected to the rating of the protective fuses.

In this study, a particular attention is paid to the phenomena which concern the thermal overload relays when the rating of the protective fuses is much higher than that of the relay, until 4 times.

#### 1. - PRELIMINARY

On determining the co-ordination between starters and protective devices against short circuit, the Italian rules (CEI 17.7) and the International ones (IEC 947.4) supply the parameters which enable to verify, either experimentally or theoretically, the correctness of the combination. They are the tripping characteristics of the thermal overload relay in the range of the overload currents that the contactor is capable of breaking and that of the short circuit protective device when higher currents occur.

The protection of the starters against short circuit currents is entrusted to fuses or circuit-breakers; however, fuses represent the protective device which is used still today in the majority of the cases.

For example, in figure 1 the average time/current characteristic of a thermal overload relay of a starter having a current setting range 38-60A, set at 50A, and that of a 80A fuse type gG are compared.

The intersection point  $I_{c1}$  of the two characteristics marks the boundary of the respective breaking ranges of the two devices, and has to correspond (according to the prescriptions of the

above mentioned rules) to the maximum breaking capacity of the contactor of the starter : in this case to the value of 650A.

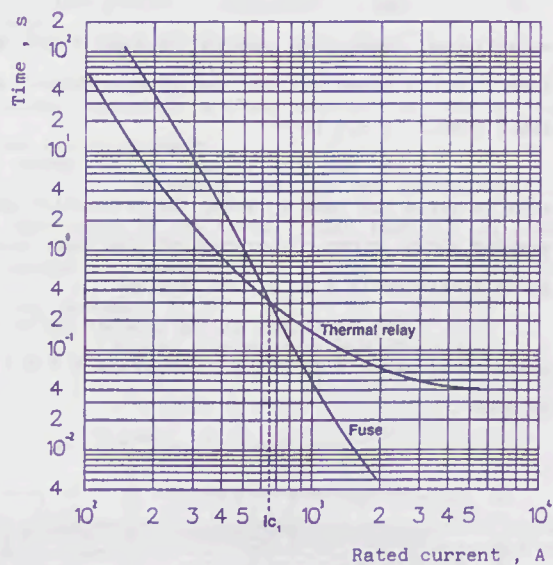


Figure 1 - Average time/current characteristic of a thermal overload relay having a current setting range 38-60A, set at 50A, and that of a 80A fuse type gG.

The subject of this study are the applications in which the rating of the fuses is much higher than that of the thermal overload relay, which is, therefore, submitted to particularly heavy stresses when fault overcurrents occur.

The study has a fair interest because these applications are specifically provided for in the co-ordination requirements of some International standards, such as those of CSA C22.2-14 and UI. 508. One of the conditions prescribed by the above standards is the non-damage of the relay in order to consider the co-ordination as valid.

To this scope, according to the European practice, fuses type aM are chosen with a rated current equal to that of the motor full load current, while fuses type gG are sized from 1,5 to 2,5 times the motor current.

CSA and UL standards establish, on the contrary, the use of delayed fuses sized 2,25 times the motor current, and non-delayed fuses sized 4 times, for the verification of the co-ordination.

This last value can decrease to 2,25 times, but this degrading has to be shown in the nameplate of the starter including the data of the thermal overload relay.

The Canadian Electrical Code establishes, then, the use of delayed fuses sized from 2 to 2,5 times and the use of non-delayed fuses sized from 3 to 3,5 times.

In the following, it is taken into consideration the case in which the protective device against short circuit currents of the same starter above mentioned is a 200A fuse type gG.

The contactor of the starter has a rated operational current of 63A in categories AC3 and AC4, at 500V .

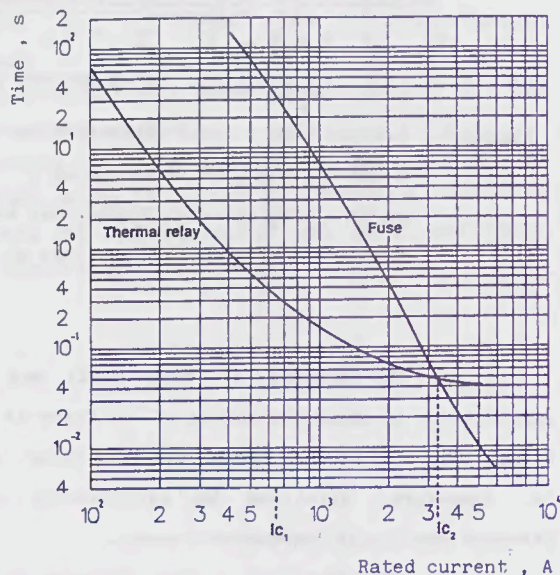


Figure 2 - Average time/current characteristic of a thermal overload relay having a current setting range 38-60A, set at 50A, and that of a 200A fuse type gG.

From the comparison of the time/current characteristics of the thermal overload relay and that of the fuse, represented in figure 2, it clearly results that the contactor is required to operate before the fuse when fault currents higher than 650A, i.e. higher than its breaking capacity, occur.

We shall distinguish two conditions of behaviour of the contactor when fault currents included between the value corresponding to its breaking capacity (650A, point  $I_{c1}$  of figure 2) and the intersection point  $I_{c2}$  (3300A, figure 2) flow through it .

The conditions which can prolong the duration of the fault current are the following :

(a) **Welding of the contactor contacts** : phenomenon which can happen as soon as it manifests a fault current enough to cause the repulsion of the contacts owing to the electrodynamic effect.

This value of current differs from contactor to contactor and rises with the contactor's size.

With reference to the above contactor of the starter, this possibility can occur beginning from a current of 2500A (instantaneous value), corresponding to a current of 1500A (r.m.s value) with power factor 0.5.

This result is drawn from a previous experimental study <sup>(6)</sup>, carried out on 120 contactors of different type and rated current, which enables to establish statistically the value of the repulsion current as a function of the contactor's size, as it can be observed in figure 3, drawn from this study.

(b) **Persistent arc between the contactor contacts** : phenomenon which can happen during breaking operations, if welding does not occur prior, controlled by the thermal overload relay with fault currents higher than the breaking capacity of the contactor itself.

This risk is as much higher as the fault current is near enough to the value  $I_{c2}$  of figure 2.

In both the above-mentioned cases, the thermal overload relay is no longer capable of protecting itself.

The fault current will continue to flow in the circuit until the operation of the fuses.

The thermal stress, due to the persisting current, may cause remarkable damages to the thermal overload relay and even cause the melting of it in case the  $I^2t$  let through is higher than the one tolerable by the temperature sensitive element of the relay itself.

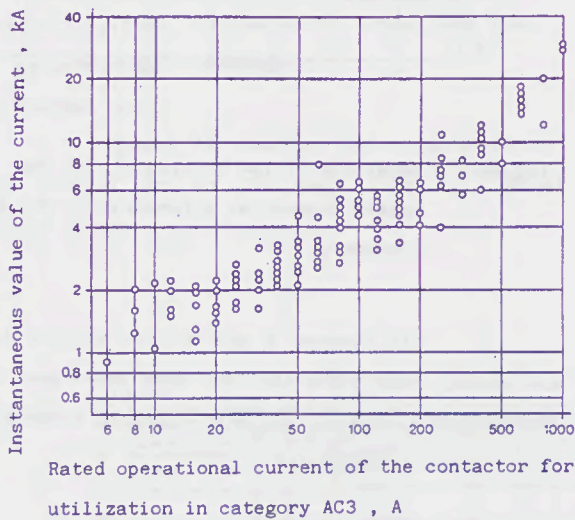


Figure 3 - Current causing contact separation by electrodynamic effect as a function of the rated operational current of the tested contactors .

The melting  $I^2t$  of the temperature sensitive element is a parameter that is clearly definable at level of project, but its definition in an experimental way allows to acquire in addition to the confirmation of the design calculations, further data like as: reliability of the construction, presence of weak parts, imperfection of the weldings or the connections to the incoming and outgoing terminals.

In any case, it is a question of a non-negligible factor of knowledge in the set up of the prototypes and in the settlement of the co-ordination between starter and device for the protection against short circuit.

According to this point of view, an investigation was carried out on the whole line of thermal overload relays, manufactured with the conventional technics of the bimetal element and the heater element, in order to verify the melting  $I^2t$

for each element and to define by consequence the fuses which enable to exclude the probability of such melting, whatever the value of the fault current may be.

## 2. - TESTS CARRIED OUT

The above-mentioned relays were deprived of the tripping device before carrying out the tests.

The incoming and outgoing terminals of each thermal relay, mounted in its plastic housing, were supplied by a single-phase alternating current at 50Hz.

The testing current was made by an auxiliary equipment and switched off by the melting of the heater element.

The supply voltage was maintained, in the major part of the tests, lower than 60V in order to reduce conveniently the arcing time during the melting process.

Figure 4 shows the test circuit.

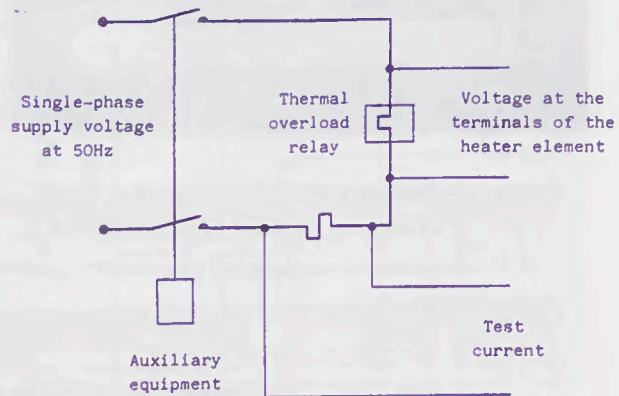


Figure 4 - Test circuit

For each type of heater element, several tests were carried out with values of current increased step by step.

Figure 5 shows a bimetal element complete with its heater element of wounded wire, before the test.

In figure 6, that shows the same element after the tests, the melting of the heater element can be seen.

In each test, the test current, the voltage at the relay terminals, the values of the prearcing time and of the energy which caused the melting of the heater elements were recorded by means of a data acquisition system and a transient recorder.

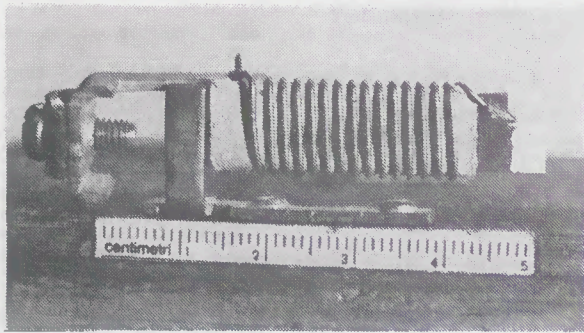


Figure 5 - Bimetal element complete with heater element of wounded wire, before the test .

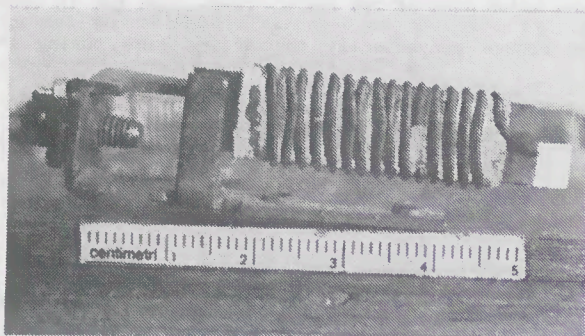


Figure 6 - Bimetal element complete with heater element of wounded wire, after the test. The melting of the heater element is evident .

From the examination of the test results, it was noticed that, at the rising of the test currents, the melting  $I^2t$  decreases progressively of intensity, so much that it reaches a value that remains practically steady, as it can be seen, by way of example, in the graphic representation of figure 7, related to a thermal overload relay with current setting range 29-47A.

The same behaviour was found out in all the tested samples.

About 20 measurements of the melting  $I^2t$  at the changing of the test current were made on each of 22 tested samples.

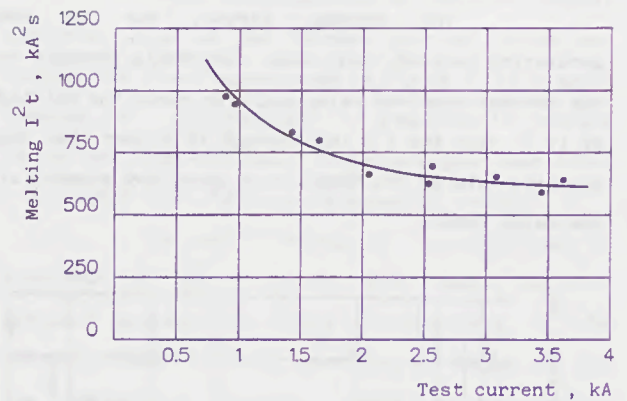


Figure 7 - Behaviour of the melting  $I^2t$  of the heater element as a function of the test current .

In figures 8 and 9, two typical tests are shown, that refer to the same above-mentioned thermal relay, carried out with currents of 950A and 3600A (r.m.s.) respectively.

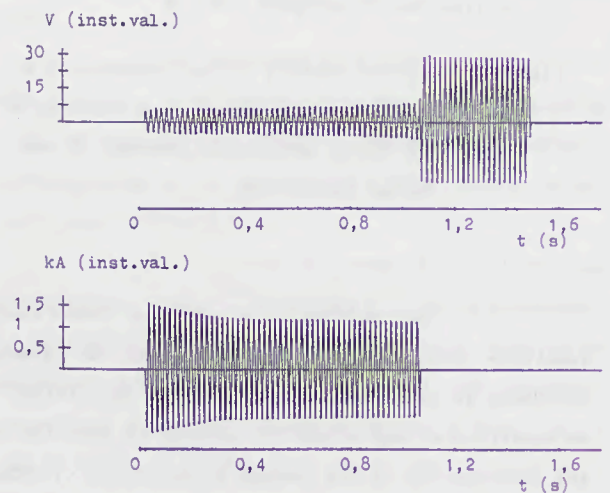


Figure 8 - Test carried out with current 950A

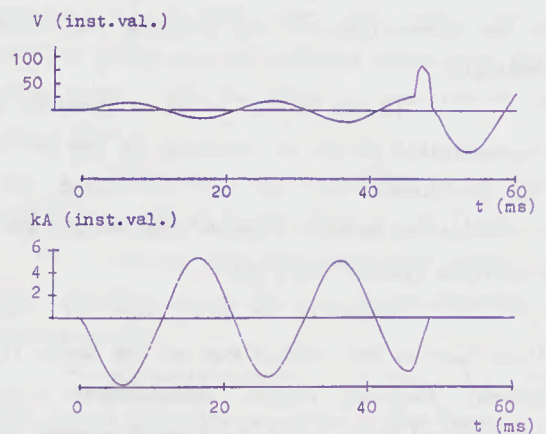


Figure 9 - Test carried out with current 3600A

The equivalent value of the test current was obtained from the relation :

$$I_{eq.} = \sqrt{\frac{I^2 t}{t}} \quad \text{where}$$

$I^2 t$  = thermal stress which caused the melting, experimentally determined  
 $t$  = melting time, limited to the pre-arcing time, experimentally determined

Figure 10 sums up the results of the tests carried out on the whole line of thermal overload relays.

Each thermal relay is represented by a thick line, parallel to the axis of abscissas, the extremes of which define the current setting range of the relay, while the value of the melting  $I^2 t$  is plotted in ordinate.

In the same graph, the values of the melting  $I^2 t$  of the fuses were plotted (pre-arcing  $I^2 t$  + arcing  $I^2 t$  at 500V), either of aM type or gG type, as a function of their rated current.

The above-mentioned values of the fuses were taken from catalogues of some European Manufacturers.

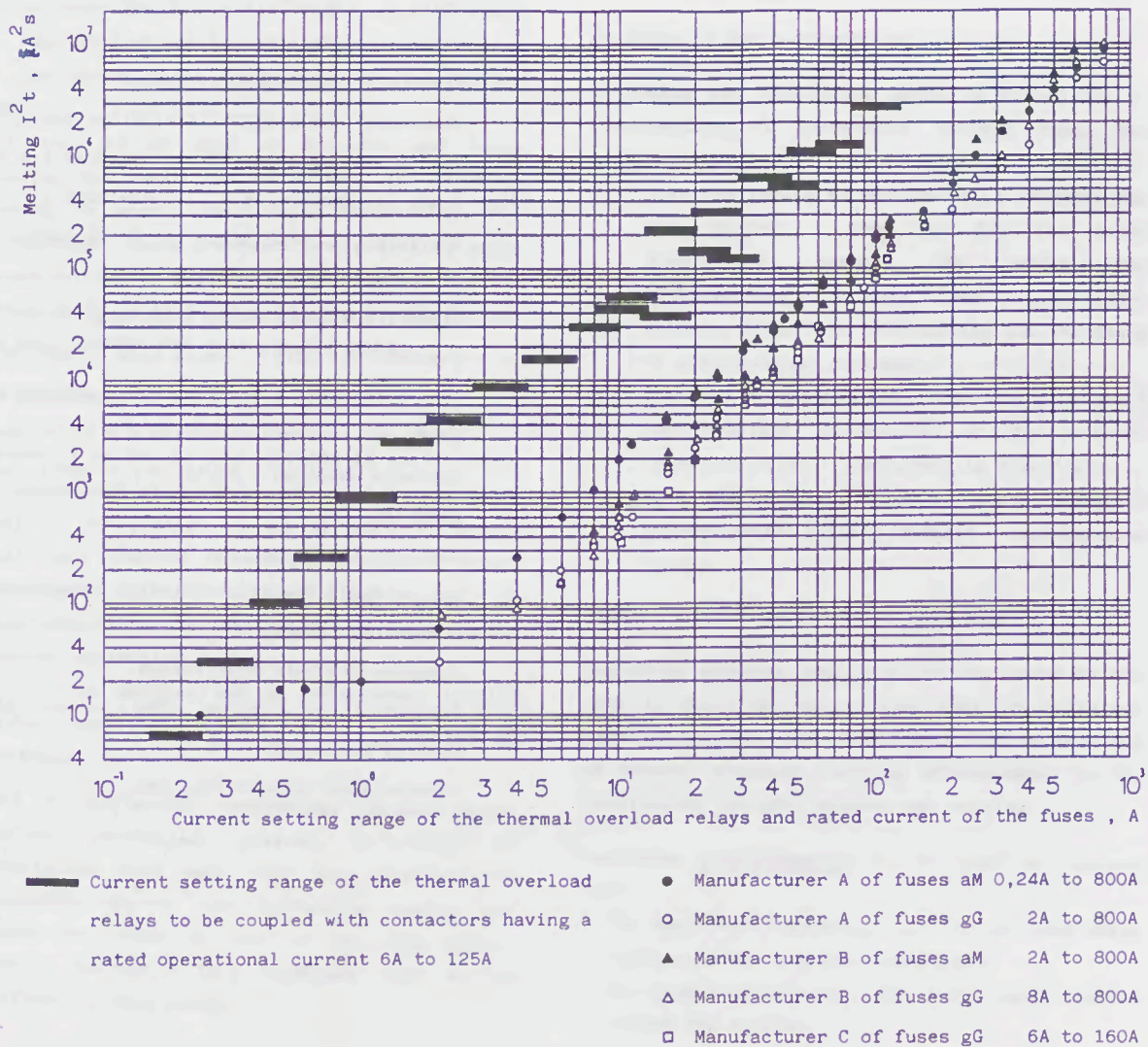


Figure 10 - Comparison of the  $I^2 t$  causing melting of the heater element with the melting  $I^2 t$  of the fuses

### 3. - CONCLUSION

With reference to the above mentioned considerations, it is possible to evaluate graphically the rating of the fuse which guarantees the non-damage of the thermal overload relay when conditions of particular stress occur in presence of the above-described fault currents.

The  $I^2t$  let flow by the protective fuse has to be always lower than the melting  $I^2t$  of the thermal overload relay.

The Authors wish to thank Prof. G. Cantarella and Dott. G. Farina for their valuable advices.

### 4. - REFERENCES

- (1) - Toniolo S.B., Cantarella G. : Protezione di contattori mediante fusibili.  
L'Elettrotecnica - N° 3bis , Vol. LV , 1968
- (2) - Cantarella G., Farina G., Tartaglia M. :  
Behaviour of contactors protected by fuses during short-circuit currents.  
Proceedings IEE , Vol. 124 , N° 12 , 1977
- (3) - Wright A., Newbery P.G. : Electric fuses.  
IEE Power Engineering Series 2 .  
Peter Peregrinus LTD , 1982
- (4) - Bellato G., Buccianti R. : Contattori di bassa tensione ; indagine sul mercato italiano.  
Elettrificazione, Febbraio 1987, pag.70-121
- (5) - Arato D., Cantarella G. : Risultati di prove di corto circuito su contattori e rischio di saldatura dei contatti.  
Rendiconti della LXXXVIII Riunione annuale dell'AEI , Catania 1987 - Memoria 1.a.3
- (6) - Arato D., Cantarella G. : Contattori e avviatori in corto circuito. Prove secondo le norme.  
Elettrificazione, Marzo 1990, pag. 49-52.
- (7) - Standard CEI 32.1 , Aprile 1988 - Fascicolo 1081 : Fusibili a tensione non superiore a 1000V per corrente alternata e a 1500V per corrente continua . Parte 1° : Prescrizioni generali.  
Comitato Elettrotecnico Italiano .
- (8) - Standard C22.2 - N°14 - M1987 : Industrial Control Equipment.  
Canadian Standard Association.
- (9) - Standard UL508 - Septem. 1989 : Industrial Control Equipment.  
Underwriters Laboratories Inc.

## COORDINATION OF FUSES-STARTERS : NEW STANDARDS, NEW NEEDS

M. Bret

Télemécanique

Rueil Malmaison France

### Summary

In the new contactors and motor-starters standard there are new coordination needs and requirements. The behaviour of the devices submitted to these requirements is analyzed in detail. Then, the consequences on the fuses and on their characteristics are considered in order the possible improvements regarding coordination.

### 1 Introduction to Coordination

#### 1.1 General

Issued since May 1990, 947-4-1, IEC standard requires that the manufacturer of a starter shall give the type of coordination of the product and the associated Short Circuit Protective Device (SCPD).

Tests have to be done on starters and fuses following the conditions of 947-4-1 IEC standard in order to permit coordinated association. For this purpose, fuses standards are preparing guide of coordination to explain how to proceed. The aim of this study is to develop how the standards deal with coordination and what are the needs.

#### 1.2 Definition

An assembly of two or more devices in series (e.g. SCPD associated with a contactor and an overload-relay) is coordinated if it is able to permit normal duty and to eliminate unexpected over-current under the following conditions :

- Discrimination (selectivity) between over-current protective devices ensured
- Effects on devices and on environment limited within acceptable limits (e.g.: no danger to persons)
- Back up protection (cascading) between over-current protective devices in case of association with more than one short-circuit protective device (one protective device may assist one other in case of too high short-circuit current). This condition will no be analyzed in this study.

#### 1.3 Applicable standards

Speaking about coordination between fuses and motor starters, the following international standards are to be taken into account :

IEC 947-4-1 dealing with contactors and motor starters

32B(Sec)112 : Application guide for coordination between fuses and motor-starters. It will be part of IEC 269 (dealing with fuses).

IEC 947-4-1 replaces IEC 158 and IEC 292-1 and, although these two standards are well known it is preferred not to speak of them in this study

#### 2. Rules of the coordination

Following the definition given in Sub-clause 1, coordination of protection between fuses and motor-starter implies verification of :

- a) that the rating of the fuses is adequate for the starter : that is for its rated operational current  $I_e$  under the corresponding voltage and utilization category (e.g. AC3 for starting and switching of motors during running).
- b) that the discrimination between the fuses and the overload protection of the starter (overload relay + contactor) is fulfilled
- c) that the protection is ensured: that is short-circuit cleared without unacceptable damage.

These 3 points are developed here below :

Regarding adequate rating a) of the fuses to the load it shall be checked that they can withstand expected currents for normal duty such as starting of motors, plugging, inching corresponding to the utilization category without any melting.

Regarding discrimination b), it shall be checked that :

- for small over-currents, only the overload relay shall operate (the fuses shall not)
- for high over-currents, the fuses shall operate before the starter

Bad discrimination will happen in case of poor accuracy and/or too wide a tolerance of the tripping curve of the overload relay or of the melting curve of the fuses. So, if attention has not been given to discrimination, unexpected melting of the fuses may occur (sometimes inducing the customer to increase the fuse rating) and/or the withstand capabilities of the starter may be exceeded. In both cases the consequences can be damage to the assembly, or worse, to the whole installation.

Regarding protection c), the standards allow two types of coordination, "1" or "2". For both of them, it is required that, under short-circuit conditions, there shall be no danger to persons or installation. In addition, it is said that.

- For type "1", the starter may not be suitable for further use.
- For type "2", the starter shall be suitable for further use, the risk of contact welding (of the contactor) is recognized, in which case the manufacturer shall indicate the measures to be taken as regards to the maintenance of the equipment.

The purpose of this study is to consider mainly coordination type "2" and the corresponding requirements

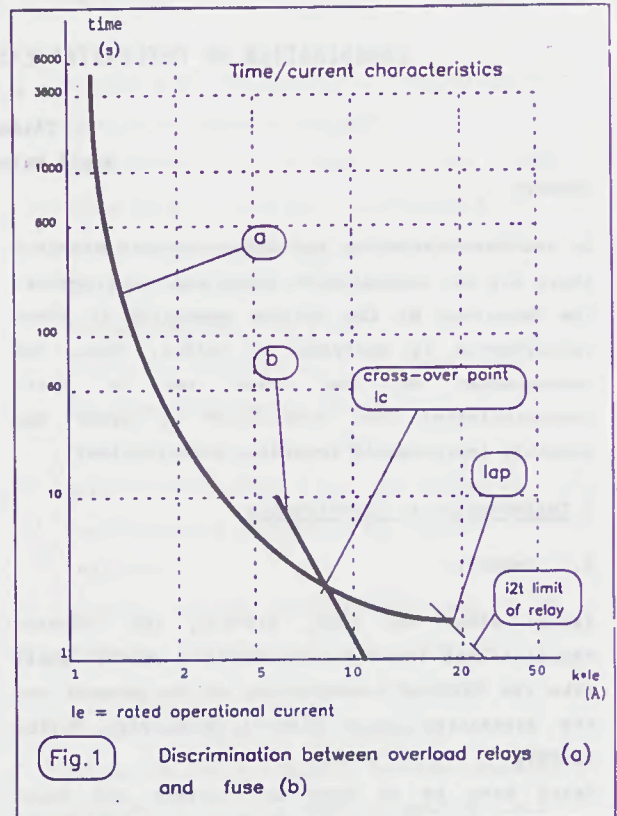
### 3. Requirements and procedures of Standard

#### 3.1 IEC 947-4-1

The best way to consider the standard requirements is to analyse the specific needs of the tests. It can be noticed first that these are three phase tests contrary to single phase tests fuses : sometimes, this may induce some difficulties in finding the optimum fuse rating for the association.

##### 3.1.1 Discrimination test current

The diagram fig. 1 illustrates the tests :



Two tests shall be done, one with a current  $I_{c1} = 0,75 I_c$  and one with  $I_{c2} = 1,25 I_c$ ,  $I_c$  being the current corresponding to the cross-over point of the overload relay and the fuse characteristics respectively. The power factors shall be those corresponding to the utilization category of the starter (e.g. 0,45 for AC3) under the nominal voltage

It shall be verified that :

- After the test  $I_{c1}$  the fuse has not operated and the overload relay has operated to open the starter.
- After the test  $I_{c2}$ , the fuse has operated before the starter.

##### 3.1.2 Short-circuit test current

There are two test currents :

- current "r" which is a conventional prospective test current related to the rated operational current  $I_e$  (AC-3), e.g. 3kA for  $16 < I_e \leq 63A$ . The power factor has generally a higher value than those used to test the fuses (e.g.  $\cos \phi = 0,9$  for "r" current = 3kA)
- current  $I_q$ , which is the rated conditional short-circuit current, stated by the manufacturer of the starter, withstandable satisfactorily by the association (e.g. 50kA).

Note :  $I_q \geq$  current "r"

For each of these short-circuit tests, the current is applied twice, the fuses being changed and, if necessary, the overload relay reset and any welded contacts separated between the two operations (Coordination type "2")

The starter may be replaced between tests at current "r" and tests at  $I_q$ .

It shall be verified, after these tests, that the fault current has been successfully interrupted without any breakdown to earth (or the safety perimeter), without any damage to the conductors and without cracking or breaking of insulating parts.

It shall also be verified that no damage has occurred to the overload relay (by checking its characteristics) and to the contactor (e.g. by checking the making - breaking capabilities after having separated welded contacts if necessary); the adequacy of the insulation shall also be verified by a dielectric test.

### 3.2 32B(Sec)112

This draft is mainly based on IEC 947-4-1. It innovates in the way that it gives tools to likely predict the behaviour of association type "2" between fuse and starter, that by comparison of characteristics of these devices.

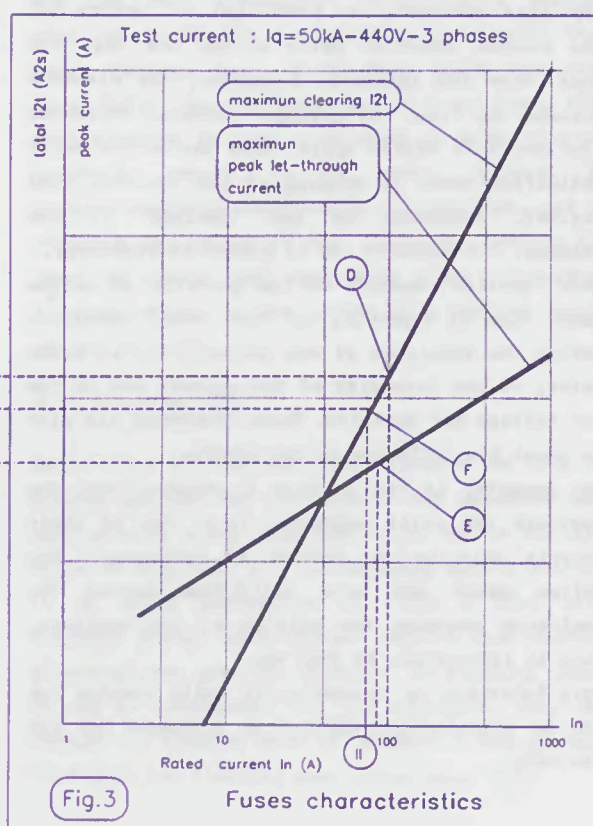
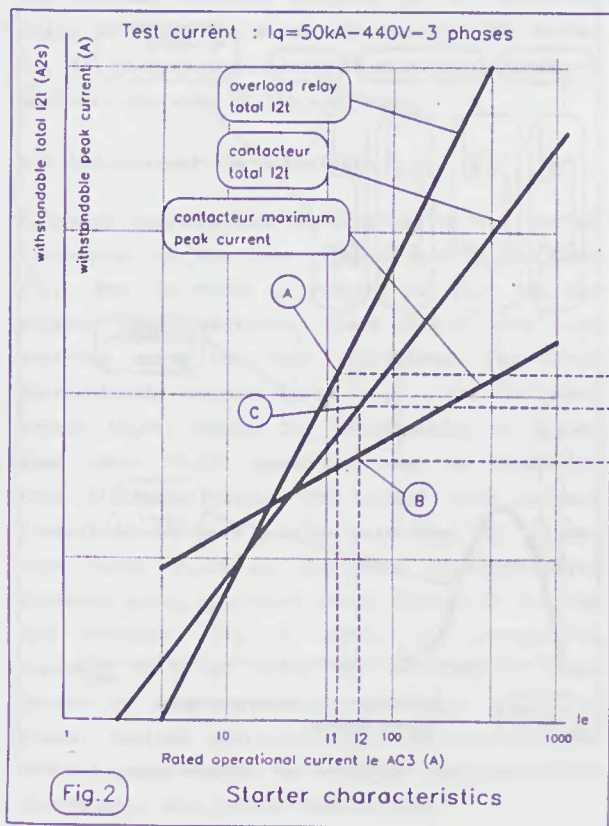
The characteristics taken into account are :

- Peak-current of the fuse and of the contactor
- $I^2t$  of fuse, overload-relay and contactor
- Clearing-time of the fuses

Fig. 2 and 3 (respectively starter and fuses characteristics) illustrate how to choose a suitable fuse rating to protect the starter assembly.

The horizontal axes give the rated operational current  $I_e$  AC3 of the starters and the rated current  $I_n$  of the fuses. The vertical axes give peak-current and  $I^2t$  corresponding values.

Knowing the value of the current setting of the overload-relay  $I_l$  ( $I_l$  = nominal current of the load), it is possible to determine its  $I^2t$  limits (A). Due to having a fixed AC3 rating for the contactors, the rating  $I_2$  of the contactor to be used is often higher than that of the overload relay ( $I_2 \geq I_l$ ). The corresponding peak current limit (B) and the  $I^2t$  limit (C) are shown on fig.2. Then, by comparison of these (D), (E) and (F) of the fuses, find the appropriate fuse rating (only the smallest rating, (II), is valid). These  $I^2t$  and peak characteristics are commonly used for fuses but not usually used for contactors and overload relays: the next clause will give an explanation of this new approach.



#### 4. Behaviour and needs of contactors and overload relays

##### 4.1 Overload relays

The withstand limit of overload-relays is given by withstandable  $I^2t$ . Although this limit may depend on the short-circuit current, a value of  $100 I_e^2$  can be withstood by main overload-relays for the highest short-circuit currents (values of more than  $400 I_e^2$  are often withstandable). This limit is to be taken in account for currents higher than  $I_{ap}$  (e.g. see  $I_{ap} = 17 I_e$  on fig.1).

##### 4.2 Contactors

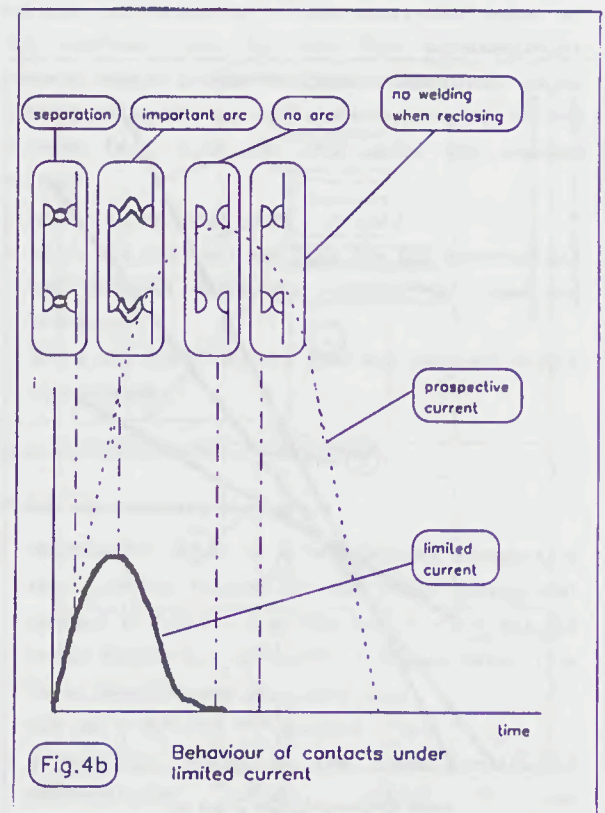
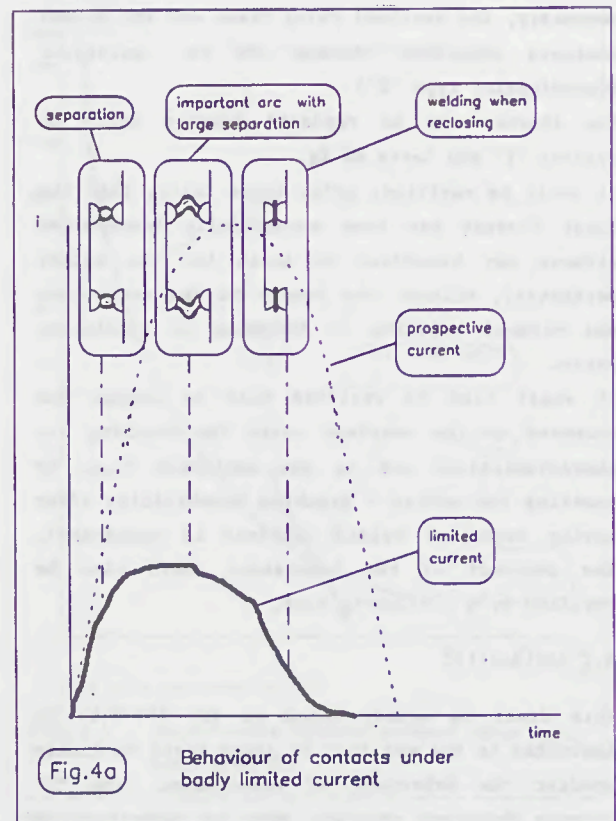
Regarding discrimination problems, it shall be verified that the breaking capacity of the contactor is higher than the crossover current  $I_c$  (see fig.1)

Regarding short-circuit currents area, the behaviour of the contactor is more complex, and can be illustrated by fig. 4.

The electrodynamic forces increase approximately in proportion to the square of the intensity of the current. When the force applied on the moving part of the contact is large enough, this separates from the fixed part : this is the repulsion phenomena. An electrical arc occurs and the contact material melts around the feet arc area. When the intensity decreases, the distance between the fixed and movable contacts decreases also until it closes again. When the molten metal solidifies there is welding of the contacts (see Fig.4a). Depending on the "quality" of the welding, the contacts can or cannot be separated. This "quality" depends on the quantity of molten metal that is depending on the energy developed during the repulsion of the contact, or, in other terms, on the intensity of the current and on the arc voltage and duration. Other phenomena can also be great big influence on the welding.

For example, if the current is cleared when the contacts are still separated (e.g. due to their inertia delaying the instant of reclosing), the molten metal may have solidified before the reclosing avoiding the welding of the contacts. That is illustrated by fig. 4b.

This behaviour is theoretically quite complex but can be practically resolved in a simple way for the user.



Having done several short-circuit tests, the manufacturer knows the withstandable current's characteristic curve of the starter. These waves such as those of Fig. 4b can be described by their peak, their  $I^2t$  and their approximate duration. Then, by analyses on several ratings of starter, it becomes possible to draw characteristic limits as shown on fig. 2.

It must be noticed here that limits given for one short-circuit prospective current under one voltage (e.g. 50 kA, 400 V) cannot be extrapolated to other short-circuit conditions (e.g. 3 kA, 500 V) because the shape of the current characteristic is generally different.

## 5. Consequences and requirements for the associated fuses

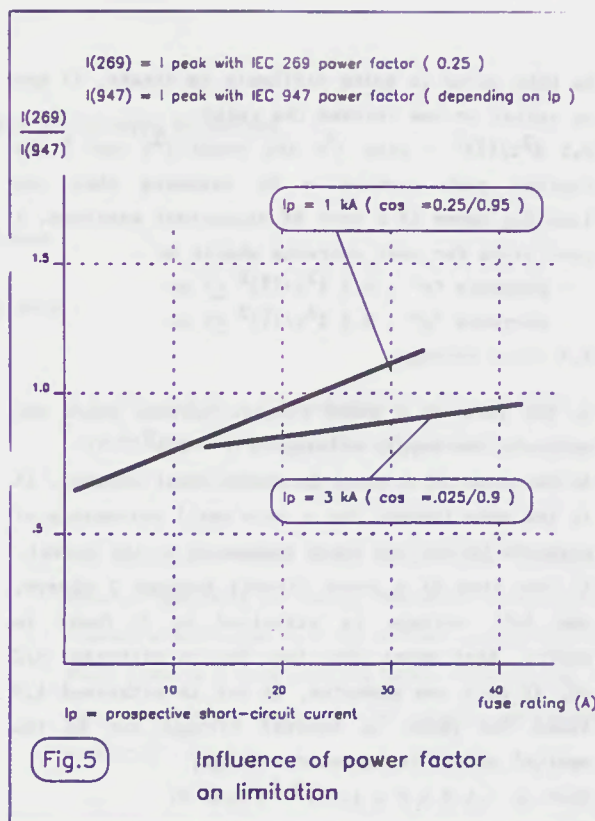
### 5.1 Time - current characteristic

The fuse characteristic must be selected such that the cross over point  $I_c$  (see fig. 1) is greater than the actual starting current ; IEC 947-4-1 requiring the overload relay to trip between 2 or 4 seconds and 10 seconds at 7,2 times  $I_e$  (Trip class 10A or 10 relays), it is hoped that the fuses can withstand these values without melting to be easily coordinated regarding this need.

The minimum breaking capacity of the contactor being 10 times its rated AC4 current (IEC 947-4-1), it is very convenient to have  $I_c < 10 I_e$  to minimize the size of the contactor.

### 5.2 Peak-current characteristic

A better coordination is expected with a better limitation of the fuse (lower peak-current and  $I^2t$ ). But, in order to compare the fuse and the starter characteristics, these should have been obtained using the same conditions. For lower short-circuit current tests (e.g. 1 kA) the power factor (0.95) needed for coordination is higher than those (0.25) generally used for obtaining fuse limiting curves. The actual peak current limitation may have a value more than 20% higher than those shown on the fuse characteristics declared using the lower power factors in the IEC 269 standard. Fig. 5 shows, for prospective currents of 1 and 3 kA, the influence of power factor on peak current for different rating of fuses. Revised characteristics according to IEC 947-4-1 needs should be a useful improvement for determining coordinated associations.



### 5.3 $I^2t$ characteristics

For the same prospective short-circuit current with the total  $I^2t$  are generally lower with high power factors (e.g. 0.95) than which low ones (e.g. 0.25). So, the knowledge of total fuses  $I^2t$  corresponding to test conditions of motor-starter standards should be of great interest to predetermine more accurately coordination, and to optimize the choice of the different devices (It shall be remind that decreasing total let-through  $I^2t$  may conduct to the choice of a smaller rating of the starter).

### 5.4 Clearing time

Long values of clearing time increases the risk of welding because the contacts of the contactor may reclose when there is melted metal due to the arc (case of fig. 4a). For coordination with a starter it is often preferable to use a fuse with slightly higher peak current and  $I^2t$  but shorter clearing time than the opposite. By clearing time, it can be considered, for the contactor, that the current is cleared when it becomes a few percent less than its limiting peak value (e.g. 5%).

As this value is quite difficult to obtain, it can be easier to use instead the ratio  $0.5 I^2 t / (\hat{i})^2$  - with  $I^2 t$  the total  $I^2 t$  and  $\hat{i}$  the limited peak current - by assuming that the limiting curve is a part of sinusoidal waveform. A good ratio for test currents should be :

- currents "r" :  $0.5 I^2 t / (\hat{i})^2 < 6 \text{ ms}$
- currents "q" :  $0.5 I^2 t / (\hat{i})^2 < 5 \text{ ms}$

#### 5.5 Test voltage

In the case of a short circuit between phase and neutral, the supply voltage is  $V = U/3^{0,5}$

In the case of a phase to earth short circuit, it is the same (except for a very small percentage of networks having one phase connected to the earth).

In the case of a short circuit between 2 phases, the full voltage is withstood by 2 fuses in series, that means each fuse has to withstand  $U/2$  or, if only one operates, it has to withstand 1,5 times the phase to neutral voltage due to the neutral point displacement voltage, that is  $1,5 V = U \times 1,5/3^{0,5} = 0,87 U$ .

The same condition appears in case of a 3 phase short-circuit.

That means that it could be of interest to take the limiting characteristic corresponding to 0,87 of the nominal voltage of the fuses to optimize the coordination.

#### VI. Conclusion

The new contactors and motors-starters standard (IEC 947-4-1) gives coordination requirements and that involves some consequences for uses. In particular, attention should be taken regarding :

- time current characteristics (discrimination problem)
- limiting characteristics (short-circuit consequences on the starter)
- conditions of test (power-factor, voltage ...)

In order to facilitate the interpretation of this Standard, an application guide of coordination is under preparation. It will be of good help, mainly if users know the mechanisms of coordination. It will be a very useful tool to :

- estimate the rating of fuses and starters to establish tables of coordinated devices
- compare different kind of fuses (e.g. fuses used for direct tests with others)
- choose device in order to do verification coordination tests

Due to the needs and requirements regarding coordination, a new philosophy of coordination will appear and more adapted fuses characteristics will appear in the futur.

## "aM" FUSE AND ITS COORDINATION WITH STARTERS

R. Deshayes  
Ferraz  
Lyon, France

### ABSTRACT

The coordination between fuses and contactors/motor starters requires a full knowledge of the behaviour of all components so that the contactor and its relay are not damaged during fault conditions.

The new IEC 947-4-1 Publication deals with contactors/motor-starters and the IEC 269-1 and 2 deal with "aM" fuses used in combination with them. In fact, these two documents are not correctly harmonized.

This paper emphasizes the lack of assets of the International Standardization in the field of "aM" fuses. On one hand the information given by IEC 269-1 and 2 Publications do not allow a good assessment of the coordination between starters and fuses. On the other hand the electrical characteristics of these fuses are not up to date.

This leads the author to advise new tests to verify "aM" fuse characteristics, mainly  $I^2t$  and peak let through current, and to suggest new values for them. Moreover it is shown that these actual characteristics are good enough to get the best coordination with starters.

### INTRODUCTION

When a motor starts, a peak current appears, which can reach 25 times the load continuous r.m.s current during the first sinusoidal half-wave.

It is followed by a starting time of around 6 times the normal current of motor. When the speed has reached a steady state, the current recovers its normal value.

The protective device must stand these overloads without operating or ageing. Moreover, when these overloads last longer than the normal starting time or when there is a fault creating higher overcurrents, it must ensure the protection of cables, motor and starter.

To meet these requirements, one combines with the contactor a relay or a release that operates in case of an overload or phase loss, and a short-circuit protective device (SCPD) which operates above the breaking capacity of contactor.

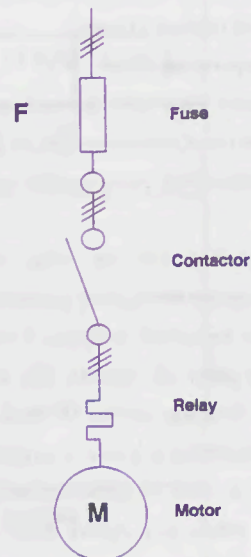


Figure 1 : Motor circuit diagram

When the short-circuit protective device is a fuse, diagram fig. 1 is achieved.

## FUSE-STARTER COORDINATION

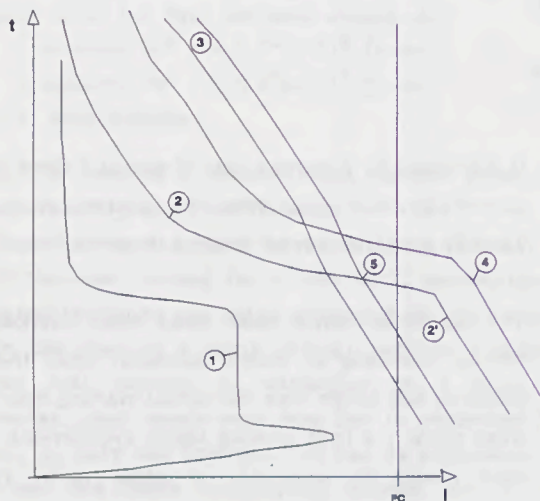


Figure 2 : Coordination of protections

Fig. 2 illustrates the combination between fuse-contactor-relay where the various curves represent :

- (1) starting current of motor
- (2) relay operating curve
- (2') maximum admissible thermal stress of relay
- (3) time/current characteristics of fuse
- (4) protective limit of bus-conductors

In this combination the relay protects the circuit against overcurrents lower than the breaking capacity ( $P_c$ ) of the contactor. Actually, it operates for currents below the point (5) absciss. For example, it must let the motor starting current (1) pass through, but has to limit the duration in order to protect the cables, motor and fuses in case of rotor blocking. It is the same in case of a phase loss. Above point (5) fuse (3) breaks the circuit by limiting the peak current and  $I^2t$  of current wave to avoid the damage of contactor contacts by excessive energy (repulsion with arc) and of relay and cable by thermal effect ( $I^2t$ ).

## COORDINATION TESTS

IEC 947-4-1 Publication on low voltage motor starters has foreseen some tests to check the coordination of the protections of starter-fuse assembly.

Two types or levels of coordination are considered :

- Type "1" admits that the starter, after a short-circuit, may not be capable of operating without repair or replacement of parts. However, it must not cause any danger to people or installations.

- Type "2" requires that in short-circuit condition the equipment does not cause any danger to people or installations and be capable of ensuring its function afterwards.

The risk of contact soldering is admitted. In this case the manufacturer must stipulate the measures to be taken as far as the equipment maintenance is concerned.

Two tests are foreseen to check this coordination :

- One test at the conventional current " $r$ " precised in the table 3 hereafter, corresponding to a condition often severe for the contactor.

Fig. 3 : Prospective current " $r$ "

Rated operational current (A)	Prospective current " $r$ " (kA)	Power Factor
$0 < I_e \leq 16$	1	0,95
$16 < I_e \leq 63$	3	0,9
$63 < I_e \leq 125$	5	0,7
$125 < I_e \leq 315$	10	0,5
$315 < I_e \leq 630$	18	0,3
$630 < I_e \leq 1000$	30	0,25
$1000 < I_e \leq 1600$	42	0,25
$1600 < I_e$	Agreement of manufacturer/user	

- One test at the prospective short-circuit current " $I_q$ " if it is higher than " $r$ ". " $I_q$ " is the combination conditional short-circuit current, i.e. the value of the prospective current that the starter combined with its SCPD can withstand satisfactorily.

During these two tests at currents "r" and "I<sub>q</sub>" the fuse operates before the relay. We are far above point (5) of Fig. 2 in an overcurrent zone where the fuse acts as a limiting device. The behaviour of the contactor and the relay depends on its limiting speed and the values of the cut-off current and the operating I<sup>2</sup>t of fuse are of first importance in the result.

If the starter manufacturer wishes to foresee the chance of the starter-fuse combination good operation he needs to know the fuse performances (operating I<sup>2</sup>t and cut-off current) in the same operating conditions as above.

#### OPERATING CHARACTERISTICS OF "aM" FUSE

Publications 269-1 and 2 define the test conditions and characteristics to be respected or to be issued for "aM" type fuses generally combined with starters.

However, these performances cannot be used to study the behaviour of contactor because they are too far from these of starters.

As a matter of fact, the current "I<sub>1</sub>" of Table XII A of Publication 269-1 (Fig. 4) must be compared with the current "I<sub>q</sub>" defined above. However, the combination test which is carried out in three-phase conditions leads to very favourable results (I<sup>2</sup>t, peak current) in comparison with these of single-phase fuse test. Besides, the current "I<sub>2</sub>" of the same table is close to current "r" but the power factor differs a lot, which cannot be justified in a technical point of view because both devices are combined on the same circuit to be protected.

At last, for the same reasons as above, one can also have a favourable behaviour of fuse in three-phase conditions.

Fig. 4

TABLE XII A of IEC 269-1 Publication

Values for breaking-capacity tests on a.c. fuses

		Test according to Sub-clause 8.5.5.1.				
		No. 1	No. 2	No. 3	No. 4	No. 5
Power frequency recovery voltage		+5 110 -0 % of the rated voltage				
Prospective test current	For "g" fuse-links	I <sub>1</sub>	I <sub>2</sub>	I <sub>3</sub> = 3.2 I <sub>f</sub>	I <sub>4</sub> = 2.0 I <sub>f</sub>	I <sub>5</sub> = 1.25 I <sub>f</sub>
	For "a" fuse-links			I <sub>3</sub> = 2.5 k <sub>2</sub> I <sub>n</sub>	I <sub>4</sub> = 1.6 k <sub>2</sub> I <sub>n</sub>	I <sub>5</sub> = k <sub>2</sub> I <sub>n</sub>
Tolerance on current		+10 -0 %	Not applicable	± 20 %	+20 -0 %	
Power factor		0.2-0.3 for prospective current up to and including 20 kA 0.1-0.2 for prospective current above 20 kA	Same range as used for test No. 1	0.3-0.5		
Making angle after voltage zero		Not applicable	0 +20° -0	Not specified		
Initiation of arcing after voltage zero		For one test : 40° - 65° For two more tests : 65° - 90°	Not applicable	Not applicable		

## NEW PROPOSALS FOR IEC 269-2 PUBLICATION

It seems then necessary to plan some tests for fuses, enabling a comparison of the operating  $I^2t$  characteristics and cut-off current of fuses with the values wished for the contactors. For this, the tests already prescribed should be completed or modified as follows :

- a test should be prescribed at a current corresponding to the rated breaking capacity of fuse but at a voltage equal to the voltage between phases  $3 : 2 = 0,866 \times U$  between phases.

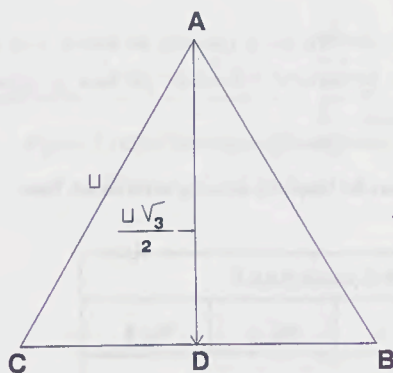


Figure 5 : Applied voltage during a three phase fault

D = middle point of BC

This value is generally admitted as the maximum voltage that a single fuse has to break during a high current three-phase fault (Fig. 5).

As most of these fuses are used under a three-phase voltage close to 400 V, the test voltage would be :  $440 \times 0,866 = 380 \text{ V}$ . For a fuse with a rated voltage of 690V, the test voltage would be :  $760 \times 0,866 = 660 \text{ V}$ .

The operating  $I^2t$  achieved during these tests will be useful for the study of coordination with contactor.

- in the same way, the fuse must be tested at the current "r" with the power factor of table Fig. 3 and under a voltage of 0.866 time the voltage applied between phases.

The values achieved of total operating  $I^2t$  and cut-off current shall be used for the study of coordination with contactor.

## RESULTS ACHIEVED WITH "aM" FUSES TESTED IN THE ABOVE CONDITIONS

### Test of current "r"

We have tested "aM" fuses 500 V designed in accordance with the present IEC 269-2 Publication under a voltage of 380 V corresponding to the maximum value of the voltage applied to a fuse in case of a three-phase fault, in a 400 V network.

A rating has been tested in each rating range precised in the first column of table Fig. 3, at the specified current "r" and power factor.  $I^2t$  values and cut-off current have then been extrapolated to achieve the values corresponding to the other ratings of the range as follows :

$$I^2t \text{ for } I_{N1} \text{ rating} = I^2t \text{ for } I_{N2} \text{ rating} \left( \frac{I_{N1}}{I_{N2}} \right)^2$$

$$I_m \text{ for } I_{N1} \text{ rating} = I_m \text{ for } I_{N2} \text{ rating} \left( \frac{I_{N1}}{I_{N2}} \right)^{\frac{2}{3}}$$

thus considering that each range is homogenous.

The results have then been plotted on the graph Fig. 6 (see annex) in comparison with the withstand capabilities of contactors and overload-relays extracted from the document ref. n° 3.

One can thus check that the "aM" type fuses protect perfectly the contactors of the same rating to which they are combined because the cut-off currents and operating  $I^2t$  of fuses are always lower than the withstand capabilities of contactors. The most critical device seems to be the 63 A rating for which the fuse performances reach exactly the withstand capabilities of contactors.

### Test of current "Iq"

Likewise we have tested these "aM" fuses 500 V at the prospective current "Iq" we have selected at 50 kA, which corresponds to the maximum current achieved in most applications. Under a voltage of 380 V and at a power factor of 0.2, the results achieved are as follows:

$$I^2t = 10 \times I_N^2$$

$$I_m = 600 (I_N)^{2/3}$$

Where :

$I_N$  = Fuse rated current

$I^2t$  = Operating  $I^2t$  under the specified conditions

$I_m$  = Cut-off current

These values are plotted on graph Fig. 7 (see annex) together with the withstand capabilities of contactors and overload-relays (document ref. N°3). This graph shows that the protection of contactors is well ensured on all the rating range.

### "aM" FUSE MELTING CURVE

One must also examine the selection of the gates of the "aM" fuse time-current characteristics.

If one observes Fig. 2, one notices that the fuses has to withstand the motor starting, i.e a first half sinusoidal wave with a peak value that can reach 25 times the rated current, or the r.m.s value 18 times the rated current, for around 15 ms (symmetrical wave), followed by the starting current, 6 times approximately the rated current for 10 seconds.

The fuse must also operate before the relay above the breaking capacity of contactor. To respect this condition, the gate  $12.5 I_N$  within 0.5 second maximum is suitable.

Besides, in case of relay failure, the upper gate  $6.3 I_N$  has to be maintained for 60 seconds maximum.

We thus get the gates of figure 8 which we consider satisfying for most applications.

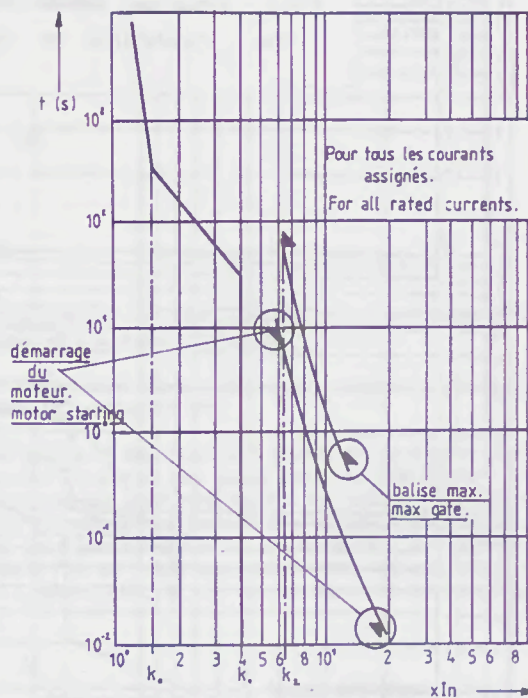


Fig.8 - Zone temps-courant "aM"  
Time-current zone "aM"

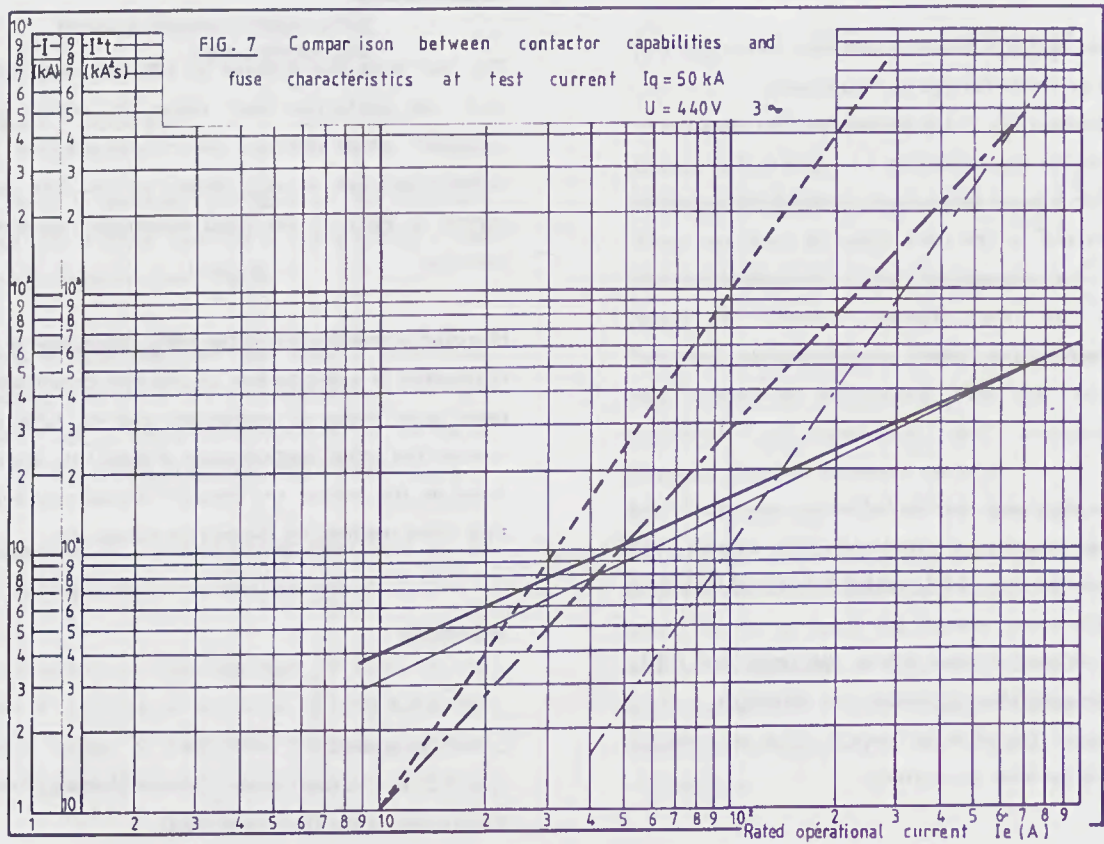
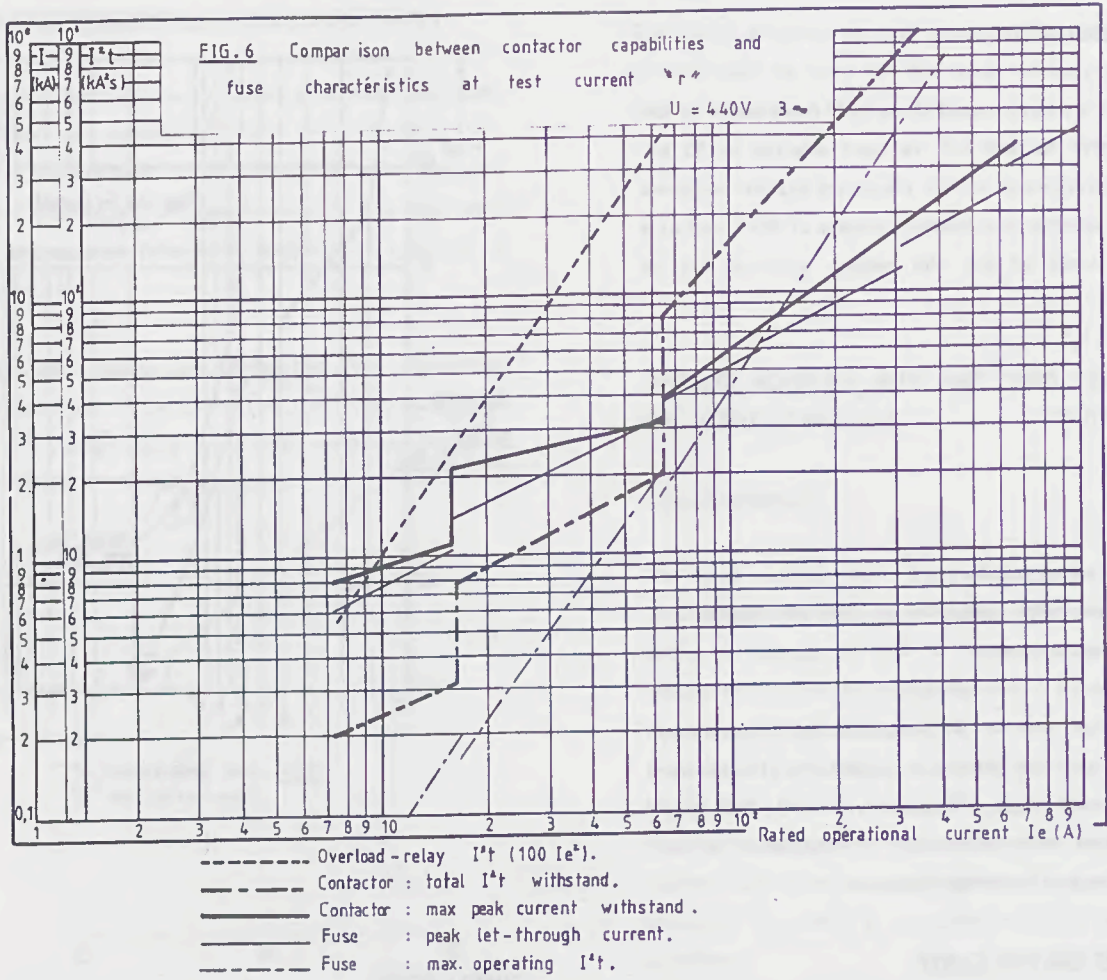
### CONCLUSIONS

The "aM" type fuse ensures an efficient coordination with the contactors and relays to which it is combined, which confirms the current practice. The combination rule is very simple as the fuse rated current is equal to the rated operational current of contactor.

However, a modification of the 269-2 Publication of IEC is required in order to line up the test conditions of fuses with those of contactors and to take into account the actual performances of fuses that are now found on the market and that are appreciably better than these required by the current standards.

### References

- 1/ IEC 947-4-1
- 2/ IEC 269-1 and 2
- 3/ IEC 32 B - Ad Hoc Group - Toronto Meeting - French Experts document (May June 1988).



DUAL-ELEMENT TIME-DELAY CLASS J FUSES FOR  
PROTECTION OF MOTOR CIRCUITS UTILIZING  
IEC CONTROLLERS

by

Steve Schaffer, Member IEEE

Cooper Industries  
Bussmann Division  
P.O. Box 14460  
St. Louis, MO 63178

**I. Introduction**

The motor controller plays an extremely important role in the operation and protection of motors and motor circuits. The importance of motors and motor circuits in the everyday operation of commercial and industrial facilities demands the need for proper protection.

Several factors can determine the optimum performance of a manufacturing facility. Included in these factors, but not limited to them, are the ability to meet production schedules, and the ability to reduce operating costs. This paper will analyze one method of protecting IEC (International Electrotechnical Commission) controllers to enhance these two important factors necessary for optimum performance.

Proper protection requirements dictate that controllers, motor circuits, and the motor should be protected from short circuit damage, overload damage, and single phase damage. No design scheme, no matter how expensive or well planned, can prevent short circuits, overloads, or single phasing. However, the designer does have the ability to protect against the damage caused by these overcurrent conditions. This paper will offer the following recommendations to achieve optimum protection.

1) The IEC philosophy of Type 2 coordination requires "no damage", short circuit protection of the IEC controller. The controller must be capable of being placed back into service following short circuit tests per the IEC publication 947-4 [1]. U.L. (Underwriter's Laboratories) Time Delay Class J fuses can provide Type 2 protection. (The other level of protection is Type 1, which will normally allow damage that requires replacement of the controller).

2) The North American philosophy of "back-up" motor overload protection offers the components a second level of protection from overload and single phase damage. The significance of this back-up philosophy becomes apparent should the controller fail to open the circuit. Welded contacts, or miscalibrated relays are two reasons this can happen. Dual-Element, Time-Delay fuses sized slightly larger than the overload relay, will provide this extra level of protection for most commercial and industrial motors.

**II Branch Circuit Protection Alternatives**

Several protection alternatives are available to the original equipment manufacturer, or system designer. Table I lists the most popular alternatives, and their sizing (rating) philosophies based on motor full load current (FLA).

Table I

Device Type	Rating % of (motor FLA)	Level of Protection	
		IEC Type	Description
Motor Circuit Protector	700%	"1"	Short Circuit only
Fast Acting, Silver Sand* Fuses	300%	"2"	Short Circuit only
Dual-Element, Time-Delay Class J**	125%	"2"	Short Circuit Back up single phase Back up overload

\*This refers to the fuse's construction of pure silver links (99.9% pure) and a sand filler material.

\*\* Class J Fuses are currently under consideration for inclusion under IEC publication 269.

The balance of this paper will compare the performance of motor circuit protectors, fast acting fuses, and Dual-Element, Time-Delay fuses, per the guidelines in Table I. This analysis will be based upon how well each of these devices protects the motor controller, the motor circuit components, and the motor. We will refer to Figure 1 to aid in our comparisons. This reflects components used in a typical 10HP, 3Ø, 460 volt, 14 Amp, 1.15 S.F. motor circuit.



Figure 1.

This figure illustrates several characteristics that should be identified:

- Controller - Overload Relay (2)
- Contactor Breaking Current (6)
- Crossover Range ( $I_c$ )
- Thermal Withstand Limit (5)
- Contactor Withstand (7)

Motor Circuit - #12 Wire Damage (4)

Motor - Motor Start (1)  
Motor Damage (3)

Now let's compare the performance of various protective devices.

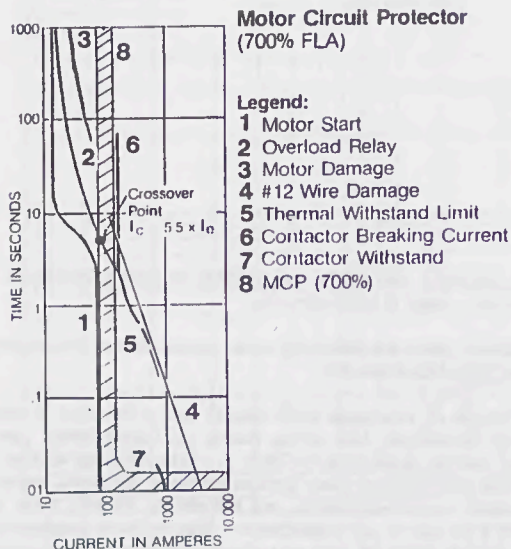


Figure 2.

1. Motor Circuit Protector - Figure 2

A motor circuit protector is a magnetic only (short circuit only) device that will operate under short circuit conditions in excess of its instantaneous trip setting. To allow a motor to start, and prevent nuisance tripping, typical trip settings are 700% - 1300% [2] This device typically takes 1/2 cycle of short circuit current to operate. Unless otherwise noted, these are not considered to be current limiting devices. This brings up two significant points relative to protection - (Note Figure 2)

- a. This device typically affords Type "1" protection under short circuit conditions due to the 1/2 cycle or greater opening time (Note the intersection of the contactor withstand curve with the MCP curve at the .01 second level) This type of protection will require complete replacement of the controller, and
- b. MCP's provide no back-up overload protection for the motor circuit. If the relays are unable to operate in an overload or single phase condition, the motor and other components can be subjected to excessive heating.

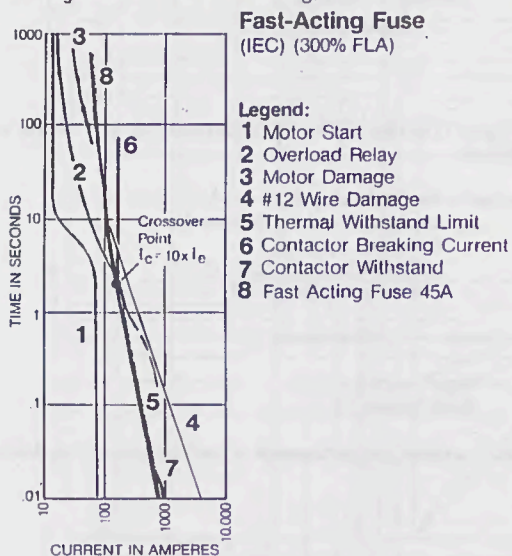


Figure 3.

2. Fast Acting, Silver Sand Fuses. Figure 3

A fast acting fuse is one whose characteristics do not exhibit intentional, built-in time delay during harmless inductive surges (motor starting currents, transformer magnetizing current etc). Because of this lack of time delay, fast acting fuses are typically sized at 300% [2] of motor FLA, to prevent nuisance tripping on motor start-up. However, unlike the MCP, they can exhibit superior short circuit performance due to the silver strips and sand filler material. This is referred to as current limitation. When operating in their current limiting range, these fuses can reduce the damaging energies associated with short circuits. If the characteristics are fast enough, they can protect the motor circuit components, and the motor controller. In many cases, these fuses may provide Type 2 protection for the controller. Two significant points relative to protection can be made here - (Note Figure 3)

- a. Let-thru energy for fast acting fuses, although within type 2 limits, will generally be higher than properly sized, lower rated time delay fuses of the same class.
- b. Fast acting fuses sized at these values offer no back-up overload protection for the motor circuit. If the relays are unable to operate during an overload or single phase condition, the controller and other components may be subjected to excessive heating, and damage.

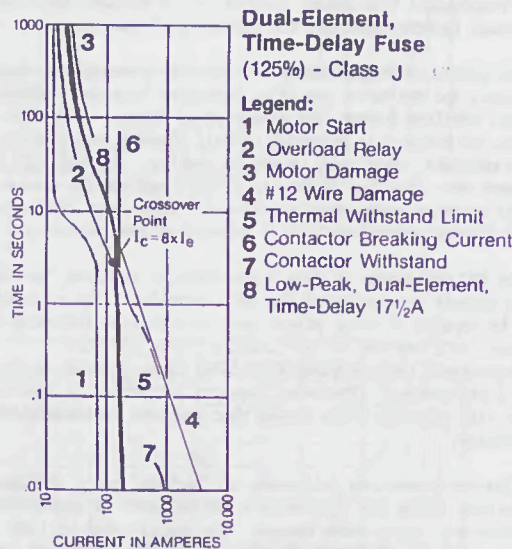


Figure 4.

3. Dual-Element Time Delay Class J Fuses (Figure 4)

A Dual-Element Time-Delay fuse is one whose characteristics have an intentional, built-in delay to withstand harmless inrush currents. This Dual-Element design has two separate elements inside one fuse tube. A spring activated trigger assembly with a heat absorber operates during overloads and single phasing, when sized properly to protect against these conditions. A second element, comprised of a short circuit strip (typically silver) surrounded by sand, operates under a short circuit condition to protect from damaging high fault currents. Short circuits typically occur during the initial start-up of a piece of equipment, or when a maintenance man is working on the equipment.

Sizing Dual-Element Time-Delay Class J fuses at 125% [2] of motor FLA, or the next size larger if 125% does not correspond to a fuse size, affords several distinct protection advantages to the controller, motor circuit, and motor (Note Figure 4)

- a. They provide Type 2 protection under short circuit conditions, due to their excellent short circuit let-thru values. This type of protection does, by definition, require that the controller be reusable following fuse replacement. Note that relay calibration shall not be affected.
- b. They provide practical, inexpensive back-up overload protection for the motor circuit. If the relays are unable to operate in an overload or single phase condition, properly sized fuses will open before the motor damage curve is reached. This sizing philosophy is based on the fuses and relays being sized upon the actual running current of the motor, if the motor is not fully loaded, or the motor nameplate current.

A further study of Figure 4 shows that several other benefits are established when utilizing 125% sizing:

- c. The Dual-Element Time-Delay design allows the motor to start up, even though 125% sizing is used.
- d. The motor circuit conductors are protected from short circuit and overload damage.
- e. Contactor withstand and contactor heating curves are within the protection capabilities of the fuse (which relates directly to Type 2 protection).
- f. The crossover point ( $I_c$ ) is between the optimum coordination limits of 7-10 times contactor ratings. For overloads up to this value, the relay should operate first. If the relays do not operate, for whatever reason, the backup Dual-Element Time-Delay Class J fuse will open before the motor damage curve is reached. For short circuits above this value, the fuse short circuit element will operate, protecting the motor controller and components from damage.

### III. Additional Benefits of Back-up Overload Protection

This paper has dealt with the Class J protection advantages of the motor circuit and its components. There are other economic considerations that make this back-up overload philosophy attractive. These include:

- Reduced downtime
- Reduced installation costs

#### 1. Reduced Downtime

Burned out motors are often the result of improper protection. Overloads and single phasing are major causes of these failures. If overload relays become miscalibrated, the motor loses a major degree of overload protection. If the contacts in the motor controller weld, the relays will offer no protection for the motor. Back-up overload protection with Class J fuses will operate independently of these controller problems, and protect the motor from overload and single phasing damage - protection that is impossible with 300% sizing of fast acting fuses, and 700% sizing of MCP's.

There is less downtime, and lower replacement costs, in changing Dual-Element Time-Delay Class J fuses, as opposed to changing a burned out motor. The type of facility and the processes involved will determine what the downtime can cost.

#### 2. Reduced Installation Costs

Sizing Class J Dual-Element Time-Delay fuses for back-up protection will result in lower fuse ratings than those sized at 300% of motor FLA. This may result in lower fuse costs, lower fuseblocks or disconnect costs, and less space.

To explain let's look at an example:

10HP, 460 Volt, 3 Phase Motor  
14 Ampere FLA

Alternative A - Fast Acting Fuses sized at 300%

	Cost * extended
3 - 40A Fuses	\$42.09
1 - 3 Pole 60A Block	15.82
Total Cost	\$57.91

Alternative B - Dual-Element Time-Delay Fuses sized at 125%

	Cost * extended
3 - 17-1/2 A Fuses	\$22.11
1 - 3 Pole 30A Fuseblock	15.41
Total Cost	\$37.52

\* Suggested resale of one manufacturer's product.

The use of Dual-Element Time-Delay fuses has reduced the initial installation cost of these devices by 35%.

### IV. Summary

IEC controllers, motor circuit components, and motors can be damaged due to overcurrents. The specification of Class J Dual-Element Time-Delay fuses offer several advantages, if sized for back-up overload protection.

- 1) Type 2 protection, under short circuit conditions, for the controller.
- 2) Back up protection under overload conditions. If the relays are miscalibrated or the contacts weld, the fuses can open to protect the motor, motor circuit, and controllers.
- 3) Back-up protection under single phasing conditions. If the relays are miscalibrated for the contacts weld, the fuses will open to protect the motor, motor circuit, and controller.
- 4) Reduced downtime after an overload or fault condition. Resetting of overload relays, or replacement of back-up fuses, is more cost effective than replacing motor circuit components, or a burned out motor. This "second line of defense" will decrease the need to replace burned out motors that have seen an overload or single phase condition.
- 5) Reduced installation cost due to lower fuse ratings and lower fuseblock ratings.

No other overcurrent protective device offers all of these advantages in protecting motor circuits which utilize IEC controllers.

### REFERENCES

- [1] IEC Publication 947-4: Low Voltage Switchgear and controlgear, Part 4: Contactors and Motor Starters.
- [2] National Fire Protection Association' NFPA 70-1990 "National Electrical Code"

## THE DISTRIBUTION OF CONSTRICTIONS IN CORRUGATED FUSE-ELEMENTS

J. Ossowicki and K. Ćwidak

Electrotechnical Institute, Gdańsk, Poland

### SUMMARY

The paper presents preliminary experiments results of an effect of constrictions positioning in the h.v. corrugated strip tape fuse-elements on the overload current breaking process

### 1. INTRODUCTION

The fuse-elements in h.v. fuse-links, with ratings above 100A, consist of several parallel silver (Ag) or, rather rarely, copper (Cu) strips. For the reason of interrupting phenomena these fuse-elements are usually longer than the fuse-body. A rate of both lengths reaches up to 5 and generally depends on the voltage ratings as well as on the fuse design. The lengthening of a fuse-element can be obtained by a winding of the fuse-strips on a ceramic support or by corrugating them. In the case of corrugated fuse-elements a lengthen rate is no more 1.8.

The main draw-back of the first (winding) design is the space inside of a fuse-body is not effectively used (with regard to arc quenching phenomena). On the other hand in the design of parallel corrugated strips it is of rather limited rigidity. A thermo-mechanical endurance when ageing during the multiple overloads was one of the problems intensively investigated up to now. One of the latest publication [1], by Namitokov, Ilyina, and Shklovsky, gives in this matter, a very important theoretical approach, which shows that with respect to ageing the best positioning of constrictions shall be on flat parts located between bent sections. But a thermo-mechanical endurance of the elements, mentioned above, is one aspect of the proper distribution of the constrictions only. Not the less there is also important the question how this distribution impacts on the breaking capacity. That is why authors decided to search this problem

experimentally because there are no test data sufficient enough to analytical approach.

For the being time our tests were limited to the interruption of overloads corresponding to the pre-arcing time of about 0.1 to 120 seconds.

The paper gives results of model test of h.v. motor-protection fuses, with rating 7.2 kV a.c., containing 6 parallel copper corrugated strips, which are fixed, each to the separate insulation support.

### 2. TEST CONDITIONS

The test were carried out on a model h.v. fuse-link 292 mm long, outer diameter 82 mm. As the fuse-elements were used corrugated copper strips with constrictions as shown in Fig. 1. The rigidity problem of corrugated model strips was partially solved by fixing, in several points, of each strip to the separate support. Quarc sand of granulation of 0.2 to 0.5 mm was applied as an arc quenching medium. Its basic chemical composition was: 99.24%  $\text{SiO}_2$ , 0.22%  $\text{Al}_2\text{O}_3 + \text{TiO}_2$ , 0.05%  $\text{Fe}_2\text{O}_3$  and 0.1%  $\text{CaO}$ . When filling with sand, the fuse-links were subjected to shaking to provide minimum porosity [2]. Two types of the copper corrugated strip-elements were investigated. The distinction between each type depends on a location of the constrictions on the folds of a fuse-element [Fig 2] An active length of the fuse-elements was of 450 mm and a thickness of  $0.18_{-0.006}$  mm. The elements were composed of six strips, each  $6_{-0.05}$  mm wide. Every strip contained 43 constriction rows, the constriction rate was 1:6.7. The distance between every next constriction axis was of 10 mm. The formed fuse-elements were placed inside the fuse-body uniformly so, that the minimum distance between the near edges of adjacent strips as well as the minimum distance from the inside part of insulation body were at least 6mm. This

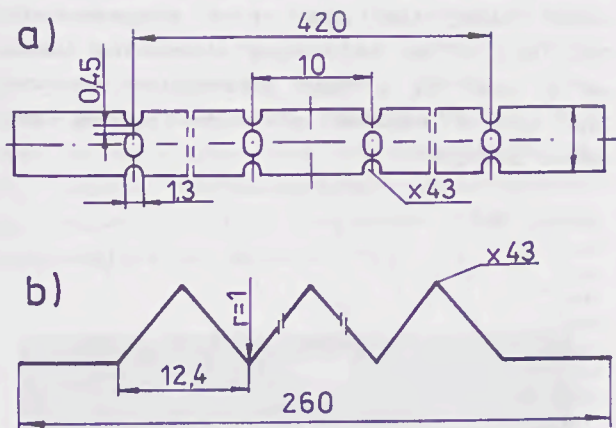


Fig. 1 Tested fuse-elements. a) shape, b) corrugation

arranging of strip-elements inside the fuse-body [4] allows to reach relatively low overload breaking capacity, at which the pre-arcing time is around 200s as well as to reach relatively high breaking capacity, at least of 50kA.

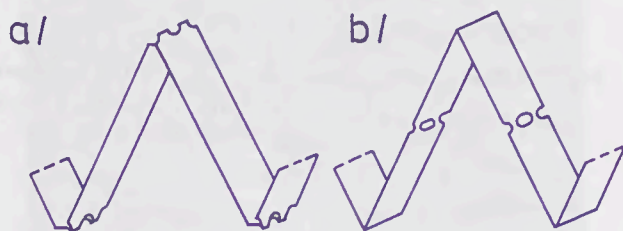


Fig. 2 Constrictions distribution

In consideration of costs, preliminary experiments were carried out on model fuse-links 70mm long inside of which single copper strip fuse-elements 100mm long of cross-section  $6 \times 0.2 \text{ mm}^2$  were inserted. The fuse-element constrictions were distributed on the eight V-shape folds giving the constriction ratio of 1:7. Two utmost distributions were investigated on an every top and in the middle of the V-shape. Test currents were done 2 and 10kA; voltage 1250V; 50Hz; p.f.=0.2.

The overload interruption tests were carried out in synthetic circuit [5]. The test current, of  $3.8I_n$  to  $8I_n$ , was selected to obtain the pre-arcing time of 3 to 120s. For this purpose the fuse under test was pre-heated with a test current at 50V a.c. This current was maintained up to the moment

when its value sharply decreased. It meant that melting process of the fuse-element has started. Next, this current was switched of automatically and a power supply at full value of the test voltage was switched on. The change-over time was of 0.2s. Interruption tests of the current of  $16I_n$  (2560A) were carried out in the circuit shown in Fig.3. Resistors and air-cored reactors were applied for the pre-setting the current and power factor values. The tests were performed at  $7.2^{+0.15} \text{ kV}$  a.c. The test p.f. was  $0.5^{+0.03}$  and  $0.13^{+0.02}$  at the current of  $8I_n$  and  $16I_n$  respectively. In these both tests the making angle was 0 to 10 electrical degrees. The test current and voltage were measured with an error evaluated at  $\pm 5\%$ . The measured values were recorded by means of two channels transient recorder.

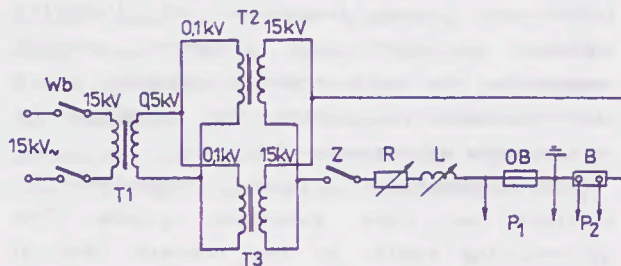


Fig. 3 Test circuitry for test current  $16I_n$ . Wb - master breaker,  $T_1, T_2, T_3$  - transformers  $3 \times 3 \text{ MVA}$ , Z - making switch, R - resistor, L - reactor, OB - fuse model under test, B - shunt,  $P_1$  - recovery voltage measurements,  $P_2$  - current measurements

### 3.EFFECT OF THE CONSTRICTION ARRANGING ON THE BREAKING CAPACITY OF A CORRUGATED FUSE-ELEMENT

The breaking capacity of a non-corrugated strip-element depends on geometrical dimensions of this element but first of all on the constriction number and the distance between themselves [3,4]. There is also additional factor which brings an influence on the breaking capacity of a corrugated fuse-element i.e. the way of constrictions arranging on a fold. If a constrictions number is equal to a fold number, that two extreme cases can be distinguished, respecting to the distance between two next

constrictions i.e.: constrictions on fold tops (Fig.2a) and constrictions in the flat sections middle of the fuse-element (Fig.2b) In the course of an arcing, initiated by an arc ignition in every constrictions, being lengthened arc columns interact. This interaction is the greater if these arcs are closer [4]. It is a result that the heat transfer from the arc column is worsening, hence decreasing of the arc voltage gradient. When these arcs ignite in the fold tops an electrodynamic current effect, in short-circuit breaking conditions, causes additionally the pushing-out the arc column outside the element fold. It causes that the voltage gradient in the arc column increases and in this way the arc column cooling process improve itself.

The voltage, current, arc-energy, breaking Joule's integral records at the voltage 1250V and visual inspection of fulgurite enabled to draw the following general conclusion: the best breaking capacity prove the fuse-elements having the constrictions on the tops of corrugations.

This conclusion was experimentally verified on 7.2kV fuse-link models. The interrupting tests, at the current (3.8, 4, 5, 8 and 16) $\times I_n$ , were carried out on 3 fuse samples with both types fuse-elements. It was found, that the fuse-links of which elements are with constrictions in the middle of flat section (Fig.2b) only in abt. 20% interrupted satisfactorily a test current. So high percentage of interrupting failures related to the whole overload test current range, (3.8-16) $\times I_n$ . In the basis of the visual inspection of fulgurites as well as the analysis of interrupting records it can be pointed out two main reasons of interruption failures. The first one is, just mentioned, thermal interaction of the next arcs when they ignite in the middle of the flat section of a corrugated strip. A relatively short distance between next arc centres (approx. 5.5mm) makes difficult a cooling down of these arcs. On this way relatively low arc voltage gradient is obtained. It leads to an increasing of an arcing time and consequently a fulgurite cross-section increases reasonably. This increasing causes the arcs coming close together up to the moment of converting them

in a single arc. This single arc develops itself along the axis of a strip-element. This kind of an arc length shortening leads, as a rule, to a fuse interruption failure. The typical records of such failures are shown in Fig.4.

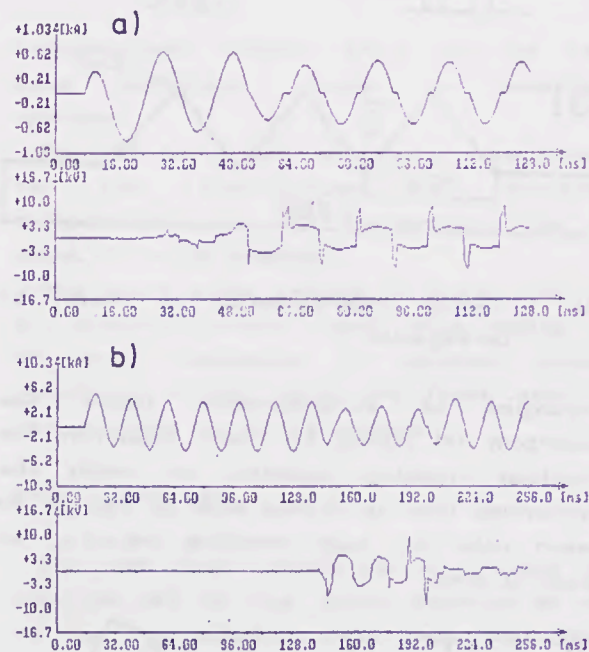


Fig.4 Exemplary records of interruption failure. a)  $U_p = 7050V$ ,  $I_p = 614A$ , b)  $U_p = 7050V$ ,  $I_p = 2560A$

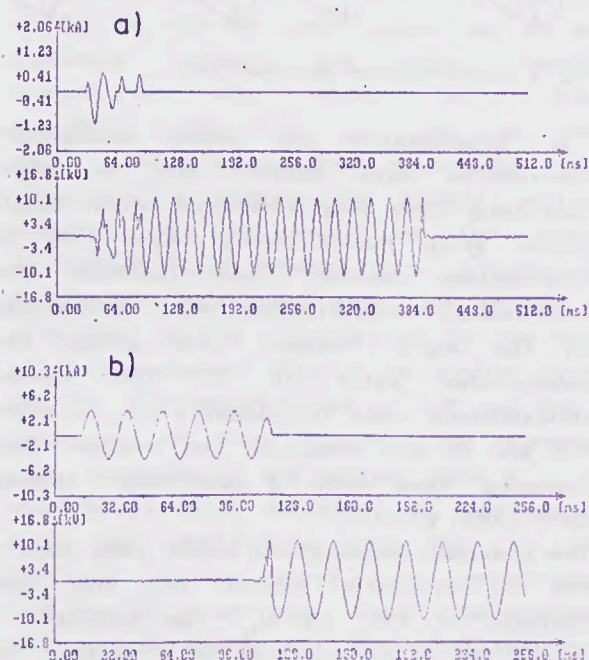


Fig. 5 Exemplary records of interruption. a)  $U_p = 7380V$ ,  $I_p = 630A$ , b)  $U_p = 7450V$ ,  $I_p = 2560A$

On the other hand all the fuse samples of which elements were with the constrictions on a fold top interrupted satisfactorily. The highest arcing time values, when interrupting the test current up to  $5I_n$ , were no more than 50ms and respectively at  $16I_n$  within 10-20ms. Exemplary interruptions are shown in Fig.5. Fulgurites from this interruptions are shown in Fig.6.

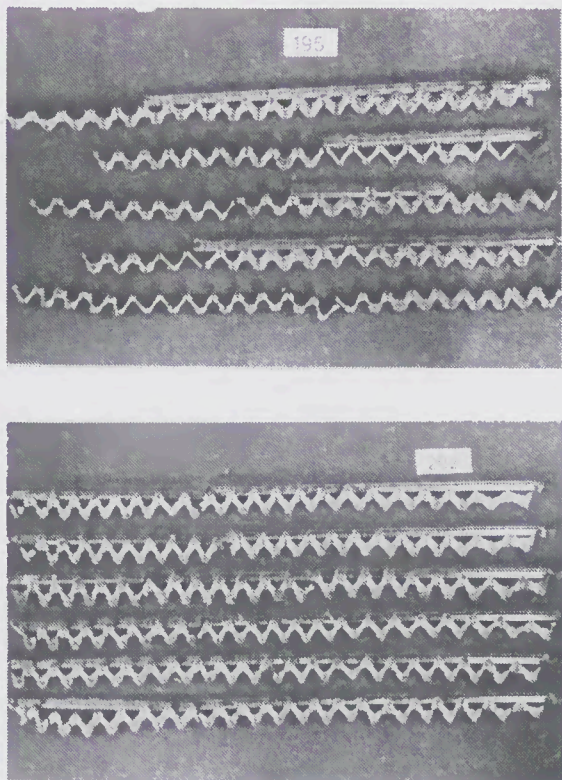


Fig. 6 Exemplary fulgurites of interruption  
 195 -  $U_p=7380V$ ,  $I_p=630A$ ; 202 -  
 $U_p=7450V$ ,  $I_p=2560A$

#### 4. EFFECT OF FUSE-ELEMENTS CONFIGURATION ON THE MULTIPLE OVERLOADS ENDURANCE

As it was concluded in the paper [1] that due to the desired endurance on cyclic overloads it is advisable to have in the strip elements much folds being as close as possible to the constrictions. With regard to an interruption, however, most advantageous is if the constriction is in a top of the fold of a corrugated fuse-element. In the case when whole element is corrugated, there appears favorable tension distribution on particular constrictions, as a result of an expanding

and contracting of the element subjected to the cyclic overloads variations. Amount of these variations can be evaluated by simple calculations, assuming that the temperature rise of an element by  $\Delta T$  causes the every flat section length rise by  $\Delta l$ , of this element. Decreasing of an angle between the flat parts of a fuse element is assumed by  $\Delta\phi$  (Fig.6). The variation of the angle  $\phi$  can be evaluated from the formula (1)

$$\sin\left[\frac{\phi}{2} - \frac{\Delta\phi}{2}\right] = \frac{a}{l(1 + \alpha\Delta T)} \quad (1)$$

Assuming  $\Delta T=300K$ ,  $\alpha=17\exp(-6) 1/K$  for the copper,  $a=6.2mm$ ,  $l=10mm$ , the variation of angle  $\Delta\phi=0.33^\circ$  is obtained as the result when every flat section of the element lengthened itself by  $\Delta l=0.051mm$ . This lengthening by  $\Delta l$  is several times shorter than a diameter of the smallest quarc sand granule used as an arc quenching medium. It seems that, at a normal packing density, these variations of  $\Delta l$  and  $\Delta\phi$  do not cause yet creation in the element constrictions distinctly destructive tensions, which can change a fuse time-current characteristic.

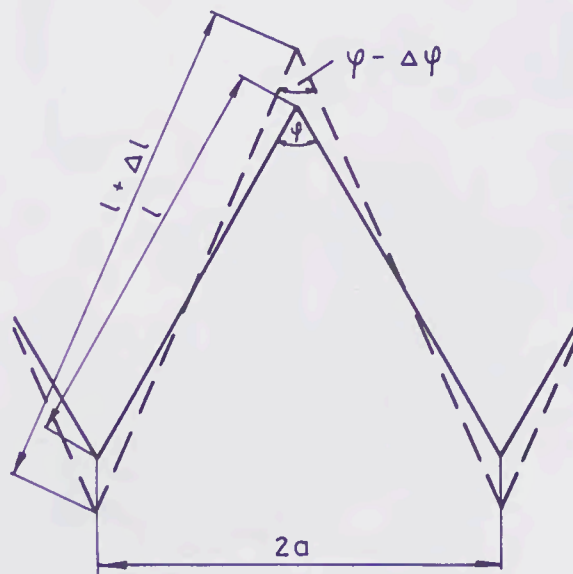


Fig. 7 Fuse-element geometry changes due to heating

Certain verification of the consideration above are endurance on pulse load test results performed on 7.2kV fuse-link models with fuse-elements of constriction on a

fold top (Fig.2a). The pulse load endurance coefficient  $K$ , estimated for these models fuse-links (acc. IEC 644 [5]), is equal 0.72. Comparatively high value of the coefficient  $K$  (in spite the copper fuse-links were used) proves that the pulse load endurance of the copper corrugated fuse-elements with constrictions on the tops is absolutely satisfactorily.

#### 5. CONCLUSIONS

Model overload interruption tests on h.v. fuse-links with corrugated strip fuse-elements prove that the most advantageous is a distribution of constriction on fold tops. By the corrugating of strip elements the tension in a fuse-element was reduced.

Constriction placed in fold tops do not make worse the fuse-links endurance on multiple overloads.

#### REFERENCES

- [1] Namitokov K.K., Ilyina N.A., Shklovsky I.G. Pulse withstandability of semiconductor protection fuses, 1989, Switching Arc Phenomena, Łódź, Poland
- [2] Ossowicki J., Analysis of the process of filling up of fuselinks with quarc sand, Prace IEI, 1970, 64, 31-46 (in Polish)
- [3] Ossowicki J., Pisanko A., Influence of the distance of the constriction in the strip fuse-element on breaking short circuit, 1989, Switching Arc Phenomena, Łódź, Poland, 230-236
- [4] Ossowicki J., The effect of fuse-element shape on breaking phenomena in a.c. circuit, 1987, ICEFA, Eindhoven, Netherlands, 57-62
- [5] IEC Publication 644 (1979), Specification for high-voltage fuse-links for motor circuit applications

**Session 5B**

**FUNDAMENTAL PROCESSES I**



used CSM!  
I<sup>2</sup>t junc<sub>2</sub>

NON ADIABATIC PROCESS IN FUSE ELEMENTS  
WITH HEAVY CURRENT FAULTS

O. Bottauscio, G. Crotti, G. Farina

Istituto Elettrotecnico Nazionale 'Galileo Ferraris'  
Torino, Italy

Summary

The pre-arcing phenomenon in a low voltage fuse operation in the case of high values of short-circuit current is analyzed in order to evaluate relevant quantities as pre-arcing time, cut-off current and pre-arcing I<sup>2</sup>t. The phenomenon is faced both by a numerical simulation of the melting element and by an experimental investigation on different types of fuses. The investigation shows that the values of the pre-arcing I<sup>2</sup>t are higher than those which correspond to the adiabatic conditions even in the case of very high values of the prospective short-circuit current; moreover, the pre-arcing I<sup>2</sup>t, for a definite value of the short-circuit current, depends on the making angle. The tests carried out on three types of fuses show a good agreement with the results of the simulation.

1. Introduction

The knowledge of the fuse operating characteristics in overload and short-circuit conditions is essential when problems of protection of apparatus and coordination of interrupting devices are faced.

The International Standards, concerning low voltage fuses, indicate the operating characteristics to be provided: the time-current characteristics have to be presented for pre-arcing times exceeding 0.1s; in the case of shorter times, the I<sup>2</sup>t characteristics have to be specified. With reference to this last requirement, it has been observed that the heating process is

non-adiabatic even in the case of heavy currents which cause the melting of the fuse in short times. In order to evaluate the relevant quantities, the pre-arcing phenomenon of a low voltage fuse for high values of short-circuit currents has been analyzed both by a numerical approach and an experimental investigation on different types of fuses. The investigation shows that the pre-arcing I<sup>2</sup>t depends on the current value also in the case of short pre-arcing times and, for a defined current value, on the making angle.

2. Numerical simulation of the heating process

The phenomenon of non adiabatic heating of the fuse element has been faced by a numerical simulation. Fig.1 shows a scheme of the fuse element under consideration.

The fuse heating is described by the following equation:

$$\rho_0(1+\alpha\theta)j^2 = -\lambda \frac{\delta^2\theta}{\delta x^2} + c \frac{\delta\theta}{\delta t} \quad (1)$$

where the first term corresponds to the heat supplied to the fuse element, the second represents the heat lost by conduction and the last the heat stored in the element. The transversal conduction of the heat is not taken into account because the thermal conductivity of the sand is negligible with respect to the copper one. In equation (1)  $\rho_0$  is the resistivity at 0°C of the material of the fuse element, a

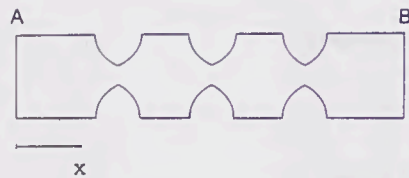


Fig.1 - Schematic representation of the fuse element

is the temperature coefficient of resistivity,  $\lambda$  is the thermal conductivity,  $c$  is the heat capacity and  $j$  is the current density, whose expression is:

$$j(t) = I/S [\sin(\omega t + \psi - \varphi) - \sin(\psi - \varphi) e^{-t/\tau}] \quad (2)$$

where  $\psi$  is the making angle,  $\varphi$  the phase angle of the current,  $\tau$  the time constant,  $I$  the amplitude of the symmetrical component of the prospective current and  $S=S(x)$  the cross section of the fuse element.

In order to solve equation (1), the finite difference method has been used. The computation of the temperature needs the knowledge of the current density in each point of the fuse element. The density, as a consequence of the presence of restricted sections, varies along the length of the element; in order to evaluate it in each subvolume, the current field in the whole fuse element must be computed. To this end, the formal analogy between the electric and the current fields can be advantageously used: in fact, the distribution of the electric field vector is the same for the two fields under consideration, because the electric potential satisfies the Laplace equation in each point of the medium and the same boundary conditions.

On the basis of these considerations the charge simulation method, which is commonly employed to solve the Laplace equation in electrostatic problems, has been used. The method consists in substituting the conducting element with a distribution of discrete charges. Between the surfaces A and B (see Fig.1) a voltage  $V$  is applied. In the equivalence with the electrostatic field, these surfaces can be considered as two electrodes of known potential; then the electrodes A and B and the boundary  $\Omega$  between the conducting

element and the sand are replaced by a discrete charge distribution. The value of these charges is not known, but can be calculated taking into account the boundary conditions:

$$\begin{aligned} V_A &= V \\ V_B &= 0 \\ \left. \begin{aligned} J_n \\ \Omega \end{aligned} \right| &= 0 \end{aligned} \quad (3)$$

The application of these conditions to the boundary points leads to a system of  $n$  linear equations for the  $n$  charges.

This method, that is rather easy to apply and can be used to study field distributions in a complex geometry domain, gives satisfactory results for the aim of this work.

The above method has been applied to study the heating up of different kinds of fuses. The current density distribution has been calculated by the charge equivalent method and the temperature distribution has been obtained by solving numerically equation (1). The knowledge of the temperature distribution along the melting element permits the evaluation of the quantities which characterize the pre-arcing process.

Fig.2 shows the computed temperature distribution in the surrounding area of a restricted section, when the temperature reaches the melting value, for a short-circuit current of 5 kA,  $\cos \varphi = 0.2$  and for two different making angles. The analysis of the two temperature distributions puts in evidence the fact that the process is non adiabatic even at these current values. The phenomenon is more evident for the making angle at which the first loop of current is not sufficient to determine the melting of the element. In this case, at the zero crossing of the current, the energy input reduces and heat is conducted away.

The computed temperature behaviour versus time in the center of the restricted section which first reaches the melting temperature is reported in Fig.3 for two different making angles.

The knowledge of the temperature behaviour in each point of the fuse element

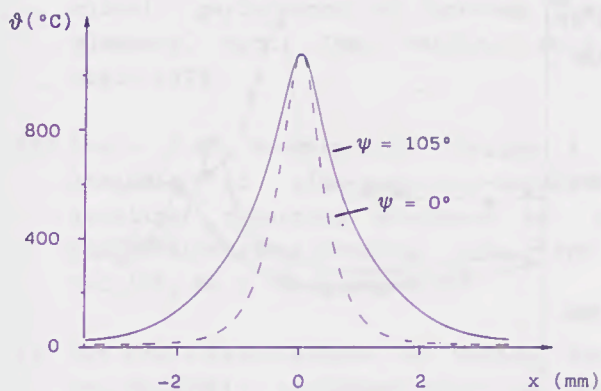


Fig. 2 - Computed temperature distribution in the surrounding area of a restricted section, when the melting temperature is reached, for a short-circuit of 5 kA, power factor equal to 0.2 and for two different making angles.

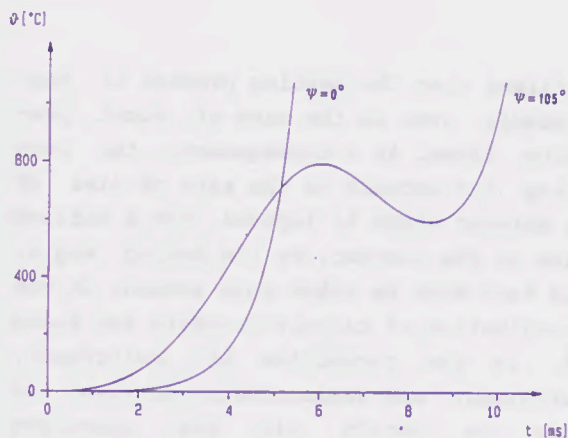


Fig. 3 - Computed temperature distribution versus time in the centre of the restricted section which first reaches the melting temperature for a short-circuit current of 5 kA, power factor equal to 0.2; the curves are referred to two different making angles.

permits the evaluation of the let-through energy ( $I^2t$ ) necessary to lead the element up to the melting temperature. Then, the computed behaviours of the melting  $I^2t$  versus the making angle have been obtained for different current values. These behaviours are shown in Fig. 4 for current values of 5, 10, 25 and 50 kA, power factor equal to 0.2.

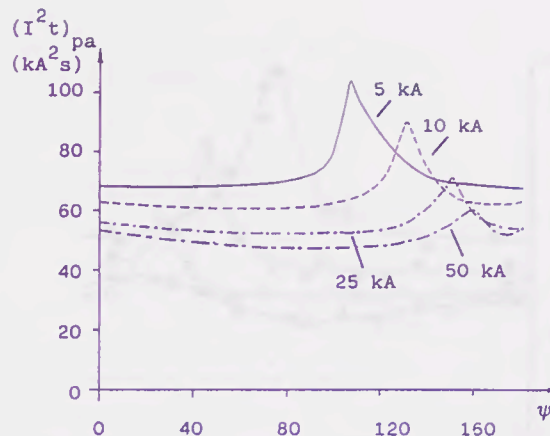


Fig. 4 - Computed behaviour of the melting  $I^2t$  versus the making angle, for different short-circuit currents, in the case of a 160 A fuse.

### 3. Experimental investigation

In order to verify the validity of the computed results, an experimental investigation has been carried out.

Three different kinds of fuses rated 160, 200 and 250 A, 500 V, 50 Hz, have been tested in an a.c. circuit supplied at 418 V with power factor equal to 0.2 with prospective currents of 5, 10, 25 and 50 kA.

For each value of current the pre-arcing time and  $I^2t$  have been recorded for different making angles. The results are illustrated in three diagrams (Fig. 5, 6, 7) corresponding to the three types of fuses.

The experimental behaviours of  $I^2t$  versus the making angle are similar to the computed ones and the making angle corresponding to the maximum  $I^2t$ , is correctly simulated by the calculation. The comparison between the measured and the computed results shows that the calculated  $I^2t$  values are less than the experimental ones. The difference can be explained taking into account the fact that the computation has been stopped at the instant at which the melting process starts; to reach the value of pre-arcing  $I^2t$  the further heating of the fuse until the arc is formed should be considered.

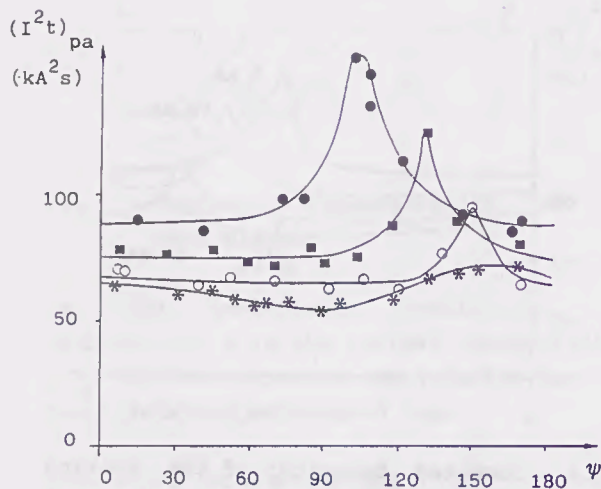


Fig. 5 - Experimental behaviour of the pre-arcing  $I^2t$  versus the making angle for a 160 A fuse:

- ) short-circuit current = 5 kA
- ) short-circuit current = 10 kA
- ) short-circuit current = 25 kA
- \* ) short-circuit current = 50 kA

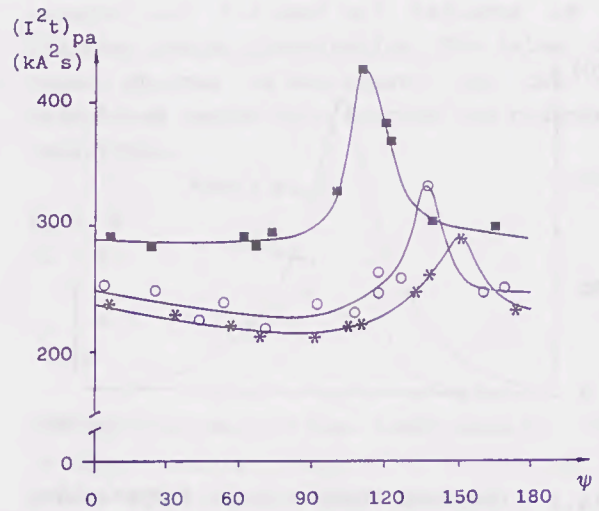


Fig. 7 - Experimental behaviour of the pre-arcing  $I^2t$  versus the making angle for a 250 A fuse:

- ) short-circuit current = 10 kA
- ) short-circuit current = 25 kA
- \* ) short-circuit current = 50 kA

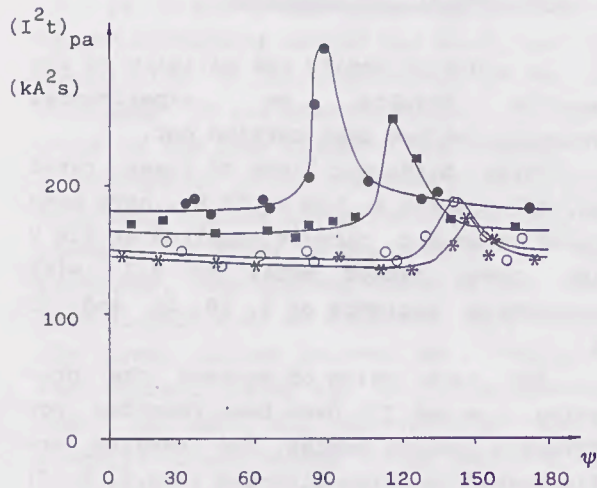


Fig. 6 - Experimental behaviour of the pre-arcing  $I^2t$  versus the making angle for a 200 A fuse:

- ) short-circuit current = 5 kA
- ) short-circuit current = 10 kA
- ) short-circuit current = 25 kA
- \* ) short-circuit current = 50 kA

#### 4. Conclusion

Both from the numerical analysis of the heating phenomenon and the experimental investigation, carried out with test current up to 50 kA on fuses with notched-strip elements, it has been

confirmed that the heating process is non-adiabatic even in the case of short pre-arcing times. As a consequence, the pre-arcing  $I^2t$  depends on the rate of rise of the current which is imposed, for a defined value of the current, by the making angle. This fact must be taken into account in the co-ordination of circuit-breakers and fuses and in the protection of switchgear, controlgear and semiconductor devices, in order to verify all the operative conditions which can occur in actual installations.

#### Acknowledgments

The authors wish to thank Prof. G. Cantarella for his helpful suggestions.

#### References

- [1] Wright A., Newbery P.G., Electric Fuses, 1984, P. Peregrinus LTD, London, UK.
- [2] Jacks E., High Rupturing Capacity Fuses, 1975, E. & F.N. Spon LTD, London, UK.

[3] Wilkins R., McEwan P.M., A.C. short-circuit performance of notched fuse elements, Proc. IEE, Vol.122, No.3, March 1975.

[4] Leach J.G., Newbery P.G., Wright A., Analysis of high-rupturing-capacity fuselink prearcing phenomena by a finite-difference method, Proc. IEE, Vol.120, No.9, September 1973.

[5] Rex H-G., Calculations of models for non-adiabatic processes, Proc. of the 3rd ICEFA, Eindhoven, 11-13 May, 1987.

[6] Weber E., Electromagnetic Theory, 1965, Dover, New York, USA.

MATHematical MODELLING OF THE HEAT TRANSFER PHENOMENA  
IN VARIABLE SECTION FUSIBLE ELEMENTS

Mimi Sasu and Gh. Oarga  
Research Institute for Electrical Engineering  
Bucharest, ROMANIA

Summary

The paper presents a general heating equation, in overload regime, of the fusible elements designed for current-limiting electric fuses, fusible elements made up of silver tapes with rectangular constrictions. An original method for mathematically solving this partial differential equation of a parabolic type and, finally, a comparison between the computation results and the experimental ones obtained when testing some fuse-links for power transformer protection, are presented.

List of symbols

- $\gamma$  - specific mass,  $\text{kg/m}^3$
- $c$  - specific heat,  $\text{Ws}/(\text{kg} \cdot ^\circ\text{C})$
- $\lambda$  - thermal conductivity coefficient,  $\text{W}/(\text{m} \cdot ^\circ\text{C})$
- $K$  - side surface heat transfer coefficient,  $\text{W}/(\text{m}^2 \cdot ^\circ\text{C})$
- $\rho$  - fusible element resistivity,  $\Omega\text{m}$
- $J$  - electric current resistivity,  $\text{A}/\text{m}^2$
- $l_x$  - conductor peripheric length (perimeter),  $\text{m}$
- $A_x$  - conductor cross-section area,  $\text{m}^2$
- $\theta_a$  - ambient temperature,  $^\circ\text{C}$
- $\theta$  - fusible element temperature,  $^\circ\text{C}$
- $\rho_0$  - fusible element resistivity at  $0^\circ\text{C}$ ,  $\Omega\text{m}$
- $\alpha_0$  - resistivity variation coefficient, function of temperature, at  $0^\circ\text{C}$ ,  $1/^\circ\text{C}$
- $g$  - fusible tape thickness,  $\text{m}$
- $a$  - fusible tape minimum half-width,  $\text{m}$
- $b$  - fusible tape maximum half-width,  $\text{m}$
- $d$  - perforation half-length,  $\text{m}$
- $i$  - current instantaneous value, passing through the fusible element,  $\text{A}$
- $I$  - current effective value,  $\text{A}$
- $I_0$  - current effective value on a fusible element in overload regime,  $\text{A}$
- $\theta_0$  - fusible element initial temperature,  $^\circ\text{C}$

- $\theta_f$  - fusible element fusion temperature,  $^\circ\text{C}$
- $t_f$  - time necessary for the fusible element temperature to reach its fusion temperature,  $\theta_f$ , in the  $x = 0$  point,  $\text{s}$
- $\theta_{\text{max}}$  - maximum temperature the fusible element can reach,  $^\circ\text{C}$
- $T$  - time constant,  $\text{s}$
- $n$  - number of the interval divisions  $[0, d]$
- $\Delta x$  - discretization step
- $N$  - system equation number obtained through discretization.

1. Introduction

High-voltage current-limiting fuse-links are widely used for short-circuit and overload protection of the electrical circuits that contain motors, power capacitors or high-power distribution transformers. The complex nature of the heat flux inside the current-limiting electric fuses makes impossible the direct analysis of the phenomena, using classical techniques. The specialized literature briefly presents various computation methods, which mainly make use of finite difference techniques, for establishing the behaviour of the current-limiting fuses under overload and short-circuit conditions [1], [2], [3]. Though the finite difference methods seem to be the most adequate, they require, however, high computer elapse times and large memories, too. Consequently, the paper [4] suggests a decoupled method which, as it is stated, offers accurate enough prediction for the time-current characteristics, without excessive computation times and memories. As it is customary, the current-limiting fuse-links include more fusible elements made up of multiple constrictions (reduced section) tapes. These constrictions can have various shapes: circular, rectangular,

trapezoidal.

The papers [5], [6], [7] present original methods for solving the general heating equation, in non-adiabatic regime, of the variable section fusible elements (tape-shaped of silver, with circular constrictions).

In the present paper, the general heating equation of the fusible elements is written for fusible elements made up of silver tapes with rectangular constrictions and an original method for solving this equation is also presented. The computation results are compared with the experimental ones obtained when testing some high-voltage current-limiting electric fuses, designed for power transformer (short-circuit and overload) protection.

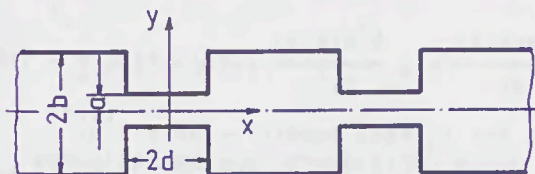


Fig. 1 Fusible element

## 2. Establishing the differential equation of a fusible element heating with rectangular constrictions

We consider a fusible element made up of a rectangular perforation tape, schematically presented in Figure 1.

If one takes into account both the heat conduction in the fusible element and the heat transfer by convection and if one assumes that the fusible element temperature varies with its length only (the element width is much smaller, while the thickness is negligible), then, one can obtain the following general equation for a variable section fusible element heating (in non-adiabatic regime):

$$\begin{aligned} \tau c \frac{\partial \theta(x, t)}{\partial t} = & \lambda \frac{\partial^2 \theta(x, t)}{\partial x^2} + q(\theta) \cdot J^2(x, t) - \\ & - \frac{1}{A_x} K \cdot (\theta(x, t) - \theta_a) \end{aligned} \quad (1)$$

where:

$$q(\theta) = q_0 (1 + \alpha_0 \theta)$$

In the case of the fusible element in Fig. 1 the current density  $J(x, t)$  and the  $1_x/A_x$  ratio have the following expressions:

- for  $0 \leq x < d$ :

$$J(x, t) = \frac{i(t)}{A_x} = \frac{i(t)}{2ag} \approx \frac{I_0}{2ag}$$

where:

$$A_x = 2ag; \quad 1_x = 2(2a + g)$$

$$\frac{1_x}{A_x} = \frac{2(2a + g)}{2ag} \approx \frac{2}{g} \quad (g \ll a)$$

- for  $x \geq d$ :

$$J(x, t) = \frac{i(t)}{A_x} = \frac{i(t)}{2bg} \approx \frac{I_0}{2bg}$$

where:

$$A_x = 2bg; \quad 1_x = 2(2b + g)$$

$$\frac{1_x}{A_x} = \frac{2(2b + g)}{2bg} \approx \frac{2}{g} \quad (g \ll b)$$

As one can notice, in the relations that determine the current density  $J(x, t)$ , the instantaneous value of the current  $i(t) = \sqrt{2} I_0 \sin \omega t$  was replaced by the overload current effective value,  $I_0$ , because the times are high enough for the thermal effect of the alternative current  $i(t)$  to be the same as that of the steady current  $I_0$ . Taking into account the above-given relations, the general equation (1) of a variable section fusible element heating, in the particular case of a fusible element made up of a rectangular constriction tape, will have the following two expressions:

- for  $0 \leq x < d$ :

$$\begin{aligned} \tau c \frac{\partial \theta(x, t)}{\partial t} = & \lambda \frac{\partial^2 \theta(x, t)}{\partial x^2} + q_0 (1 + \alpha_0 \theta(x, t)) \cdot \\ & \cdot \frac{I_0^2}{4a^2 g^2} - \frac{2K}{g} (\theta(x, t) - \theta_a) \end{aligned} \quad (2)$$

- for  $x \geq d$ :

$$\begin{aligned} \tau c \frac{\partial \theta(x, t)}{\partial t} = & \lambda \frac{\partial^2 \theta(x, t)}{\partial x^2} + q_0 (1 + \alpha_0 \theta(x, t)) \cdot \\ & \cdot \frac{I_0^2}{4b^2 g^2} - \frac{2K}{g} (\theta(x, t) - \theta_a) \end{aligned} \quad (3)$$

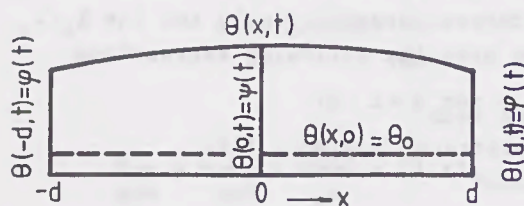


Fig. 2 Limiting conditions

### 3. Initial and limiting conditions

The problem finally raised is related to the determination of the time  $t_f$  necessary for the fusible element temperature  $\theta(x,t)$  to reach its fusion temperature  $\theta_f$  in the  $x = 0$  point, where the fusible element section is minimum, for various overload current values,  $I_0$ . To this purpose, one must solve the differential equation (2) - partial differential equation of a parabolic type - by means of certain initial and limiting conditions. They have the following form:

$$\theta(x,0) = \chi(x) \quad (4)$$

$$\theta(0,t) = \psi(t) \quad (5)$$

$$\theta(d,t) = \varphi(t) \quad (6)$$

and are schematically shown in Figure 2. These conditions were established in paper [8] and have the following expressions:

$$\chi(x) = \theta_0 \quad (7)$$

$$\left. \frac{\partial \theta(x,t)}{\partial x} \right|_{x=0} = 0 \quad (8)$$

$$\varphi(t) = \theta_f - (\theta_f - \theta_0) \exp(-t/T) \quad (9)$$

where  $\theta_f = \theta_{\max}$ .

On the basis of the relations established for the boundary condition determination  $\varphi(t)$  - established on the basis of the differential equation (3) - one has obtained the analytical expression of the heat transfer coefficient  $K$  by the lateral side, as well as of the time constant  $T$ :

$$K = \frac{\alpha_0 c_0 g}{2} \cdot \frac{I_0^2}{4b^2 g^2} \cdot \frac{\theta_f - 1/\alpha_0}{\theta_f - \theta_a} \quad (10)$$

$$\frac{1}{T} = \frac{2}{\gamma c g} K - \frac{\alpha_0 c_0}{fc} \cdot \frac{I_0^2}{4b^2 g^2} \quad (11)$$

One can notice that both the global coeffi-

cient  $K$  and the time constant  $T$  depend on the testing currents, as well as the fusible element sizes.

### 4. Algorithm for solving the fusible element heating equation

in the differential equation (2) the following notations are used:

$$A = \frac{\lambda}{\gamma c} \quad (12)$$

$$B = \frac{1}{\gamma c} \left( \frac{\alpha_0 c_0 I_0^2}{4a^2 g^2} - \frac{2}{g} K \right) \quad (13)$$

$$C = \frac{1}{\gamma c} \left( \frac{q_0 I_0^2}{4a^2 g^2} - \frac{2\theta_a}{g} K \right) \quad (14)$$

then, the fusible element heating equation can be written as:

$$\frac{\partial \theta(x,t)}{\partial t} = A \frac{\partial^2 \theta(x,t)}{\partial x^2} + B\theta(x,t) + C \quad (15)$$

with the initial condition at  $t = 0$ :

$$\theta(x,0) = \theta_0 \quad (16)$$

and the limiting conditions:

$$\left. \frac{\partial \theta(x,t)}{\partial x} \right|_{x=0} = 0 \quad (8)$$

$$\theta(d,t) = \theta(-d,t) = \varphi(t) \quad (17)$$

When writing the limiting condition (17), the symmetry of the fusible element has been taken into account (see Fig. 2).

In order to solve the differential equation (15), a second order partial differential equation of a parabolic type, the DSCT numerical method (Discrete Space, Continuous Time) was used.

By discretizing the space  $x$ , the second order partial differential equation (15) is transformed into a first order ordinary differential equations system, a function of time  $t$ , which can be written in a concentrated form as:

$$\frac{d\theta_i(t)}{dt} = A \frac{\theta_{i+1}(t) - 2\theta_i(t) + \theta_{i-1}(t)}{\Delta x^2} + B\theta_i(t) + C \quad (18)$$

where  $i = 1, \dots, n$ ;  $\Delta x = d/n$  because, as it is shown in Figure 3, the space  $x$  discretization in the interval  $[0, d]$  was made by a constant step.

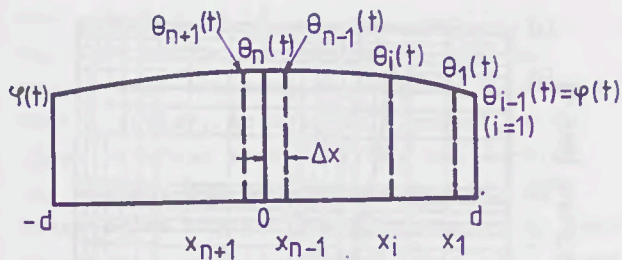


Fig. 3 Discretization of space  $x$  in the interval  $[0, d]$ .

The initial condition (16) is transformed in a set of initial conditions:

$$\theta_1(0) = \theta_0 \quad (19)$$

$$(i=1, \dots, n)$$

and the limiting conditions can be written as (see Fig. 3):

$$\theta_{n+1}(t) = \theta_{n-1}(t) \quad (20)$$

$$\theta_{i-1}(t) = \varphi(t) \quad (21)$$

$$(i=1)$$

#### 5. Establishing the mathematical model for the computer

In order to establish the mathematical model for the computer, the boundary function  $\varphi(t)$  defined by the relation (9) was replaced by its derivative:

$$\frac{d\varphi(t)}{dt} = \frac{1}{T} (\theta_f - \varphi(t)) \quad (22)$$

with the initial condition at  $t = 0$ :

$$\varphi(0) = \theta_0 \quad (23)$$

On the basis of equations (18) and (22), in view of the relations (20), (21) and assigning a certain value to the parameter  $n$ , one can obtain a system of  $N$  differential equations.

If the following notations are used:

$$y_1 = \varphi; y_2 = \theta_1; y_3 = \theta_2; \dots; y_N = \theta_n \quad (24)$$

where  $n = N-1$ , the mathematical model for digital computer will have the following general form:

$$\frac{dy_1}{dt} = \frac{1}{T} (\theta_f - y_1)$$

$$\frac{dy_{j+1}}{dt} = A_0(y_{j+2} - 2y_{j+1} + y_j) + By_{j+1} + C \quad (25)$$

$$\frac{dy_N}{dt} = 2A_0(y_{N-1} - y_N) + By_N + C$$

where:  $j=1, \dots, N-2$

$$A_0 = \frac{(N-1)^2}{d^2} a \quad (26)$$

while the initial conditions are:

$$y_1(0) = \theta_0 \quad (27)$$

$$(i=1, \dots, N)$$

In order to solve the differential equation system (25) with the initial conditions (27), a computation program was carried out on a digital computer, using the integration method RUNGE-KUTTA-GILL.

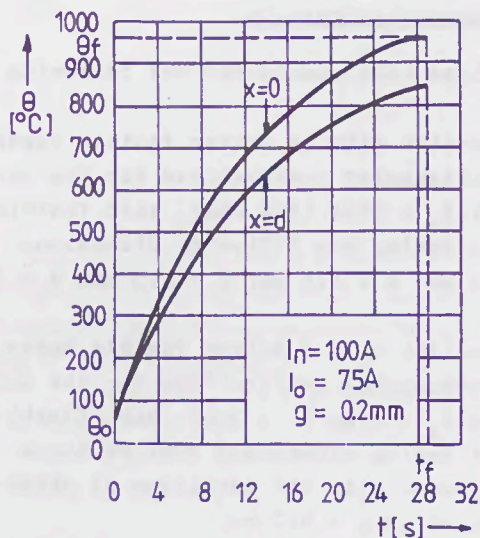
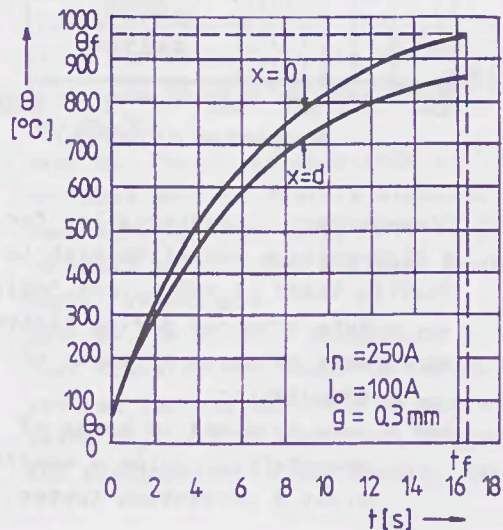


Fig. 4 Computation results.

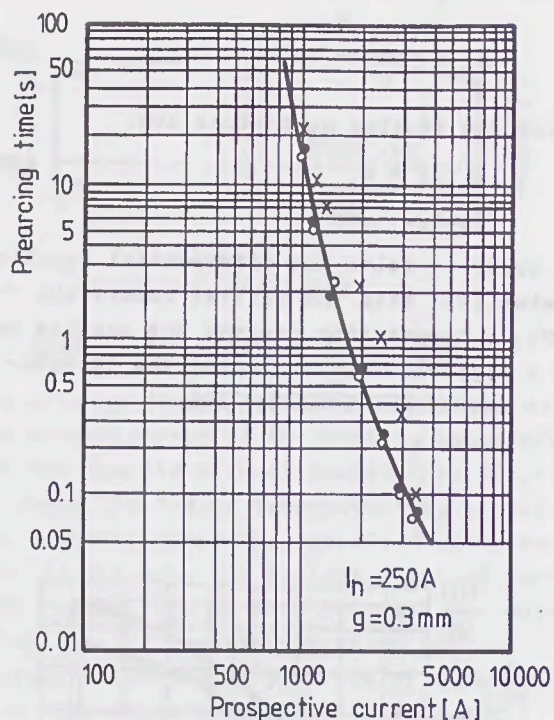


Fig. 5 Time-current characteristics for a high-voltage fuse-link with 10 fusible tapes ( $I_n=250A$ ;  $g=0.3mm$ ):  
 ... - data obtained during testings  
 xxx - data obtained by means of computation  
 ooo - data obtained by means of computation, using a coefficient K correction factor.

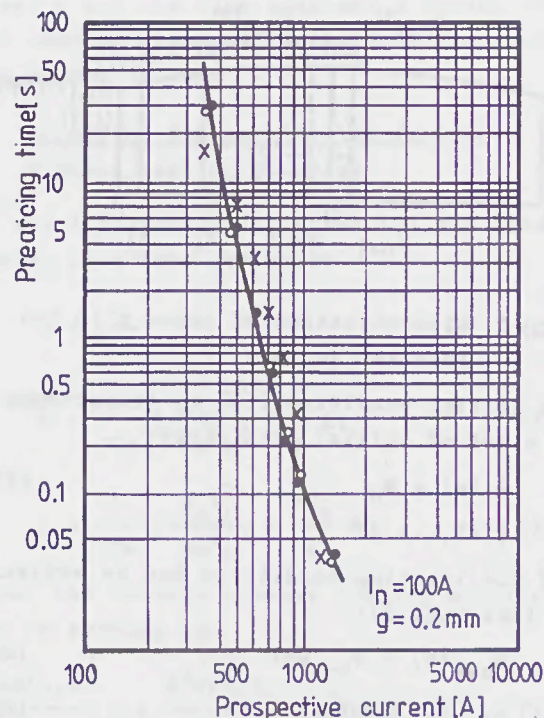


Fig. 6 Time-current characteristics for a high-voltage fuse-link with 5 fusible tapes ( $I_n=100A$ ;  $g=0.2mm$ ):  
 ... - data obtained during testings  
 xxx - data obtained by means of computation  
 ooo - data obtained by means of computation, using a coefficient K correction factor.

#### 6. Computation results

There have been considered the following cases:

a) Fuse-link with 10 silver fusible tapes with rectangular perforations for the rated current  $I_n = 250A$  ( $I = 25A$ ), each fusible element having the following dimensions:  $g = 0.3 mm$ ;  $a = 0.5 mm$ ;  $b = 1.5 mm$ ;  $d = 3 mm$ .

b) Fuse-link with 5 silver fusible tapes, with rectangular perforations for the rated current  $I_n = 100A$  ( $I = 20A$ ), each fusible element having dimensions similar those given above, with the exception of thickness which is  $g = 0.2 mm$ .

In each of the two cases, there were taken into account certain prospective currents, from the time-current characteristics, obtained during the fuse-link overload testing and there were computed the correspond-

ing current by a single fusible element. For each of these overload current values,  $I_0$ , there were established - by means of the digital computer - the temperature time variation characteristics  $\theta = \theta(t)$  in various points of the interval  $[0, d]$ , up to the moment  $t_f$  when the fusible element temperature in the  $x=0$  point reaches the silver fusion temperature,  $\theta_f = 960^\circ C$ . As an example, Figure 4 shows the time variation forms of temperature  $\theta = \theta(t)$  for  $x = 0$  and  $x = d$ , obtained in two computation variants. As one can notice, when analyzing the presented curves, in the constriction (reduced section) area of the fusible tapes, the temperature variations at the moment  $t = t_f$  are of the order of tens of degrees ( $\Delta\theta = 83^\circ C$  and  $\Delta\theta = 108^\circ C$ , respectively).

Figures 5 and 6 present the time-current

characteristics of the two fuse-links analyzed above. In both cases, one can notice that the results obtained by computation differ, to a certain extent, from those obtained when testings are carried out namely, for the same values of the prospective current one can obtain, by computation, generally higher pre-arcing times. However, it was found out that, if in the place of the heat transfer coefficient  $K$ , defined by the relation (10), a corrected coefficient  $K' = k_0 K$  is used in the computations, where the correction factor  $k_0$  is defined by means of the empirical relation:

$$k_0 = 1.1 + \frac{I_0 - 100}{25} \cdot 0.2 \quad (28)$$

then, the obtained computation results are in full agreement with the experimental ones.

#### 7. Conclusions

The heat transfer phenomena in current-limiting electric fuses are mathematically modelled by partial differential equations of a parabolic type. Due to the fact that there occur high prearcing times (of the order of seconds and tens of seconds) when heating, in an overload regime, the fuse-links designed for power transformer protection, the thermal phenomena cannot be considered as adiabatic.

The computation method presented in this paper makes it possible to establish the temperature curves  $\theta = \theta(t)$  for  $x =$  parameter and, implicitly, to establish the time  $t_f$  when temperature  $\theta(t)$  reaches the fusible element fusion temperature  $\theta_f$  in the  $x = 0$  point, where the fusible element section is minimum. The paper presents computation results obtained in various study variants which are compared with the experimental ones obtained during the testings (time-current characteristics).

#### References

- [1] Leach J.G., Newbery P.G., Wright A., Analysis of high-rupturing-capacity fuselink prearcing phenomena by a finite difference method, 1973, Proc. IEE, 120, 987-993.
- [2] Wilkins R., Mc Ewan P.M. A.C. short-

circuit performance of notched fuse elements, 1975, Proc. IEE, 122, 289-292.

- [3] Mc Ewan P.M., Waren L., Survey of numerical methods for solving time-varying fuse equations, 1976, Int. Conf. Electric Fuses and their Applications, Liverpool, England, 21-32.
- [4] Mc Ewan P.M., Wilkins R., A decoupled method for predicting time-current of H.R.C. fuses, 1976, Int. Conf. Electric Fuses and their Applications, Liverpool, England, 33-41.
- [5] Sasu M., A method for solving the variable section fusible elements heating equation, 1981, ETZ Archiv, Berlin, Bd. 3, H. 2, 53-57.
- [6] Sasu M., Metodă de rezolvare a ecuației încălzirii elementelor fuzibile cu secțiune variabilă în regim neadiabatic, 1990, EEA Electrotehnica, București, 38, 71-77.
- [7] Sasu M., Computing algorithm of the variable section fusible elements heating equation, 1990, Int. 90 Conf. "SIGNALS & SYSTEMS", Cetinje, Montenegro, Yugoslavia.
- [8] Sasu M., Oarga Gh., Simulation of the heat transfer phenomena in variable section fusible elements in non-adiabatic regime (the paper was proposed for publication in ETZ Archiv, Berlin).

L.A.V. Cheim  
 CEPEL  
 Rio de Janeiro, Brazil

A.F. Howe  
 University of Nottingham  
 Nottingham, U.K.

Abstract

This paper describes a simple, explicit and unconditionally stable routine, based on Transmission-Line Modelling, for the solution of heat diffusion, to calculate electric fuses operating times. Using the technique it was possible to compute fuse pre-arcing times, at low current, and establish good correlation with practical results.

List of principal symbols

- T = temperature [K]
- H = magnetic field [A/m]
- V = electric potential [V]
- V<sub>i</sub> = incident potential (wave)
- V<sub>r</sub> = reflected potential (wave)
- i = electric current (A)
- R<sub>d</sub> = electrical resistance per unit length [Ω/m]
- R<sub>e</sub> = electrical resistance [Ω]
- R<sub>x</sub>, R<sub>y</sub>, R<sub>z</sub> = thermal resistance in the direction [K/W]
- R<sub>0</sub> = electrical resistance at 293.2 K
- C<sub>d</sub> = capacitance per unit length [F/m]
- L<sub>d</sub> = inductance per unit length [H/m]
- Z = transmission-line impedance [Ω]
- Δl = mesh size in 1-D [m]
- σ = electrical conductivity [1/Ωm]
- ε = electrical permittivity [F/m]
- μ = magnetic permeability [H/m]
- ρ = density [Kg/m<sup>3</sup>]
- c<sub>p</sub> = specific heat [J/KgK]
- k = thermal conductivity [W/mK]

1. Introduction

Transmission Line Modelling (TLM) has been used in a wide variety of applications, including heat transfer, and has proved to be very efficient and often faster than other methods (e.g. Finite Differences).

It is an unconditionally stable technique which means that there is no convergence process for each numerical iteration. Variable meshing and non-uniformity of physical parameters can be easily considered with little extra computation.

It is, therefore, an ideal tool for determining the full range of fuse operating times which may vary from fractions of milliseconds to several hours.

2. Fundamentals of TLM

Although the TLM method was originally designed to analyse electromagnetic problems [1,2] its versatility was soon recognised and the technique was expanded to deal with other problems, including heat transfer [3,4].

Before it is possible to explain how TLM can be applied to analyse the heat diffusion process in electric fuses it is worth considering the fundamentals of the technique, which are summarised in the following sections.

2.1 Diffusion equation

The differential equation which models the potential for the network shown in Fig. 1a is

$$\frac{\partial^2 V}{\partial x^2} = R_d C_d \frac{\partial V}{\partial t} + L_d C_d \frac{\partial^2 V}{\partial t^2} \quad (1)$$

and for the 3-D network shown in Fig. 1b is

$$\nabla^2 V = 3R_d C_d \frac{\partial V}{\partial t} + 3L_d C_d \frac{\partial^2 V}{\partial t^2} \quad (2)$$

Maxwell's curl equation for the lossy-wave in a 3-D space is

$$\nabla^2 H = \mu \sigma \frac{\partial H}{\partial t} + \mu \epsilon \frac{\partial^2 H}{\partial t^2} \quad (3)$$

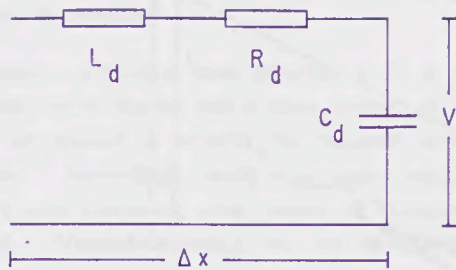
In the case of diffusion  $\mu \sigma \gg \mu \epsilon$  so Eq. (3) becomes

$$\nabla^2 H = \mu \sigma \frac{\partial H}{\partial t} \quad (4)$$

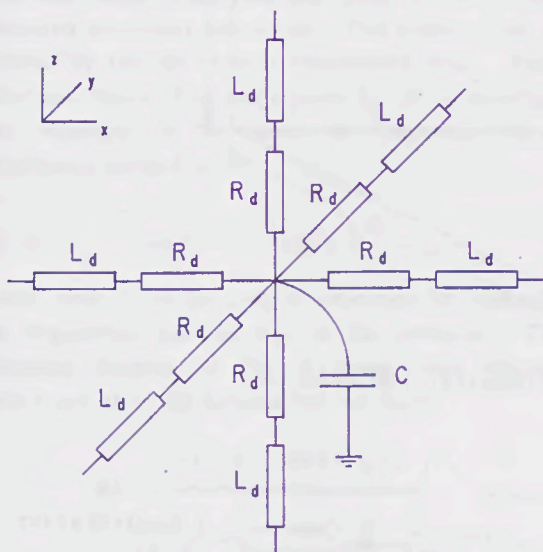
The analogy for the electrical network is that  $R_d C_d \gg L_d C_d$  which means that the second term in Eq. (2) may be neglected i.e.

$$\nabla^2 V = 3R_d C_d \frac{\partial V}{\partial t} \quad (5)$$

Because of the similarity of the last two equations it can be inferred that the potential V in the electrical network shown in Fig. 1 has a wave-like behaviour and hence it can be represented by a travelling wave in a lossy transmission line.



(a) One dimension LRC network



(b) Three dimension LRC network

Fig. 1

## 2.2 Thermal analogue

The Heat Conduction Equation in Cartesian co-ordinates for a 3-D problem is

$$\nabla^2 T = \frac{c_p \rho}{k} \frac{\partial T}{\partial t} \quad (6)$$

There is an obvious analogy between Eqs. (5) and (6) provided that

$$3R_d C_d = \frac{c_p \rho}{k} \quad (7)$$

or

$$\left. \begin{aligned} R_d &= 1/k \\ 3C_d &= c_p \rho \end{aligned} \right] \quad (8)$$

The similarity between Eqs. (5) and (6) leads to the conclusion that the solution of the wave equation (5) yields the temperature distribution in a 3-D space provided that the specific heat is represented by the capacitances, and the thermal conductivity by the resistances of the network (i.e. node voltages in the TLM model represent point temperatures).

## 2.3 Transmission-line modelling (TLM)

The medium to be modelled is divided into a number of interconnected elemental transmission-lines - space discretization. Time is also discretized into steps of  $\Delta t$ , the wave transit time for the transmission-line. The impedance  $Z$  of the transmission-line can be calculated as

$$Z = \Delta l / C \quad (9)$$

where

$$C = c_p \rho \Delta x \Delta y \Delta z / 3 \quad (10)$$

for the 3-D model shown in Fig. 2,

$$Z = 3 \Delta l / c_p \rho \Delta x \Delta y \Delta z \quad (11)$$

In-principle  $\Delta t$  is an arbitrary value, but one should keep in mind that as the whole transmission-line is represented solely by its capacitive component, there is an inductive error  $L_e$ . This error is defined by

$$L_e = \Delta l^2 / C \quad (12)$$

which gets smaller as  $\Delta t$  decreases.

The medium wave velocity is

$$v_m = 1 / \sqrt{LC} \quad (13)$$

and the TLM wave velocity is

$$V_{TLM} = \Delta l / \Delta t \quad (14)$$

which shows that the chosen values for  $\Delta l$  and  $\Delta t$  have to be compromises.

The basic wave equation for the potential at any termination of the transmission-line is

$$V = V^i + V^r \quad (15)$$

So for the Thevenin equivalent of the network shown in Fig. 2

$$V = \frac{1}{3} \sum_{k=1}^6 V_k^i \quad (16)$$

Incident voltage waves will flow along all six branches of the network towards the node, where they will be reflected back, producing corresponding reflected voltages equal to

$$V^r = \frac{R - Z}{R + Z} V^i \quad (17)$$

Expressing Eqs (15), (16) and (17) for the six branches, one has

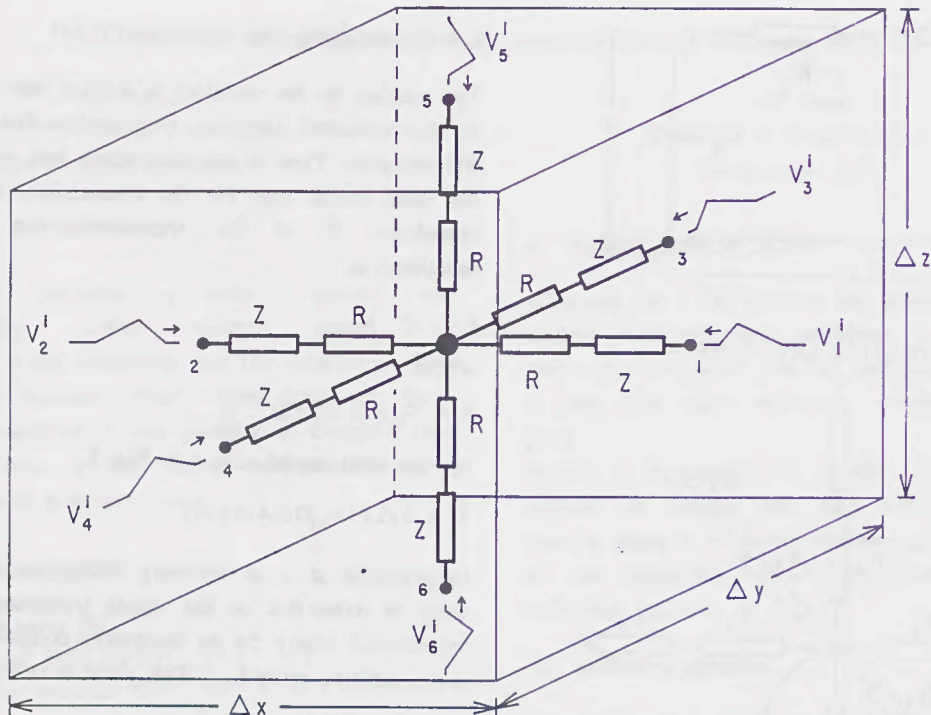


Fig. 2 Three dimension elemental TLM node

$$\begin{bmatrix} V_1^r \\ V_2^r \\ V_3^r \\ V_4^r \\ V_5^r \\ V_6^r \end{bmatrix} = S \begin{bmatrix} V_1^i \\ V_2^i \\ V_3^i \\ V_4^i \\ V_5^i \\ V_6^i \end{bmatrix} \quad (18)$$

where

$$S = \frac{1}{3} \begin{bmatrix} -2 & | & | & | & | & | \\ | & -2 & | & | & | & | \\ | & | & -2 & | & | & | \\ | & | & | & -2 & | & | \\ | & | & | & | & -2 & | \\ | & | & | & | & | & -2 \end{bmatrix} \quad (19)$$

For the first time step all the incident waves are known (initial condition) and from Eq (16) all the potentials at the centre of the node can be calculated. Using the scattering equation (18) all the reflected waves can be determined. This completes the calculation for the actual time step.

For the next iteration each node has to be connected to its neighbour and its 'new' incident wave is set equal to the reflected wave from its neighbour, calculated at the previous iteration (as illustrated in Fig. 3).

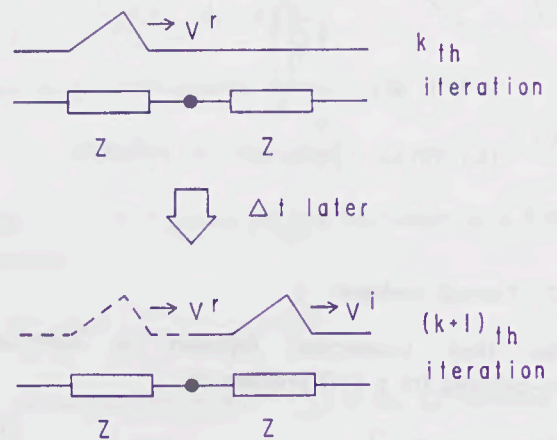


Fig. 3 Connection of two adjacent nodes

Put mathematically,

$$\begin{bmatrix} V^i \\ V^i \\ V^i \\ V^i \\ V^i \\ V^i \end{bmatrix}_{x+1,y} = \begin{bmatrix} V^r \\ V^r \\ V^r \\ V^r \\ V^r \\ V^r \end{bmatrix}_{x,y} \quad (20)$$

(k+1)th iteration      kth iteration

As the new  $V^i$  are known all values of  $V$  can be computed. The process continues step by step until an artificial time limit is achieved. Boundaries can be dealt with by choosing appropriate line terminations.

### 2.4 Variable meshing

Most realistic problems have complex 2-D or 3-D geometries which implies that a large number of small meshes are needed to achieve the required accuracy of results. Accordingly small time steps would be necessary and computing time would be substantially increased. Variable meshing can be introduced in order to minimize this effect. However, meshes of variable sizes have different wave impedances and different transit times (see Eq. (11)). These create undesired internodal reflections. This problem can be avoided by the use of stub transmission lines. These stubs are 'extra' lines terminated by an open-circuit and connected to the centre of the node with a capacitance defined by

$$C_{STUB} = C_{node A} - C_{node B} \quad (21)$$

where 'node A' is the node of reference for balancing the impedances for the rest of the network. The schematic diagram of Fig. 4 shows what happens before and after the inclusion of the stubs.

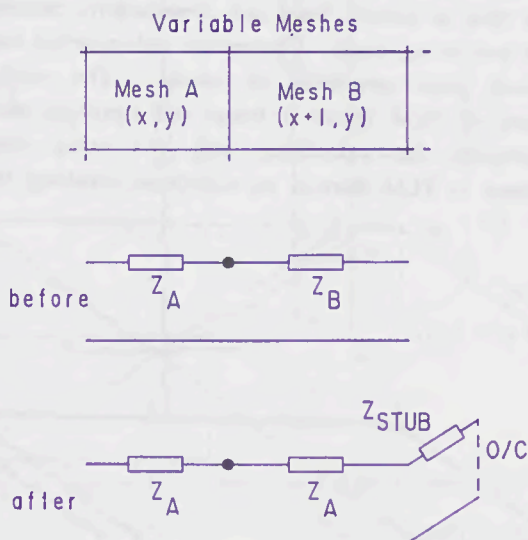


Fig. 4 Effect of adding STUBS to the node

Provided that Eq. (16) is re-defined as

$$V = \frac{\frac{2}{R_x + Z} (V_1^i + V_2^i) + \frac{2}{R_y + Z} (V_3^i + V_4^i) + \frac{2}{R_z + Z} (V_5^i + V_6^i) + \frac{2V_{STUB}}{Z_{STUB}}}{\frac{2}{R_x + Z} + \frac{2}{R_y + Z} + \frac{2}{R_z + Z} + \frac{1}{Z_{STUB}}} \quad (22)$$

then all the above remains valid.

### 2.5 Variable parameters

The method of using stubs will also allow for variations in the physical 'constants' of the material which alter the impedance of the transmission-line. So, in the case of the thermal model where  $c_p$  and  $k$  vary, it will be necessary to adjust the line impedances.

### 2.6 Electrical analogue

Prior to the TLM calculation it was necessary to know the elemental current for each node. It was assumed that each node had the electrical resistance  $R_e$  defined by

$$R = R_0 (1 + \alpha \Delta T) \quad (23)$$

and that the individual resistances were connected as shown in Fig. 5. The elemental currents, and resistances, were updated as temperature increased every time step.

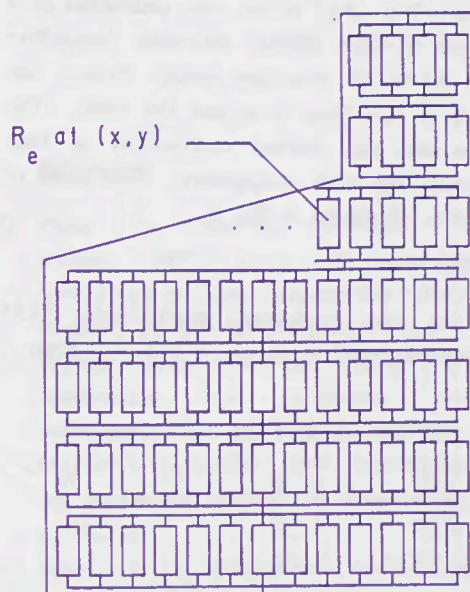


Fig. 5 Parallel-series connection of the electrical resistances of the nodes

### 2.7 Power source

At each time step the amount of energy  $\Delta E$  dissipated in the node shown in Fig. 2, due to the elemental current  $i$ , is given by

$$\Delta E = R_e i^2 \Delta t \quad (24)$$

This energy will cause a rise in temperature of the node.

The internal energy of the node associated with a variation in temperature  $\Delta T$  is defined by

$$\Delta U = c_p \rho \Delta x \Delta y \Delta z \Delta T \quad (25)$$

Assuming that all the energy dissipated in the node is used to increase its internal energy, then  $\Delta E = \Delta U$  and hence the temperature rise is equal to

$$\Delta T = \frac{R_e i^2 \Delta t}{c_p \rho \Delta x \Delta y \Delta z} \quad (26)$$

### 3. Modelling of an industrial fuse

To show how TLM can be employed to model practical fuses, the design illustrated in Fig. 6 was chosen. The silver (Ag) ribbon was embedded in a compact block of silica ( $\text{SiO}_2$ ), with heat conduction assumed to be in all directions except through the narrow edges of the silver strip into the silica. The specific heat and the thermal conductivity of both silica and silver vary with temperature. The limits of these variations are shown in Fig. 6.

#### 3.1 Heat dissipation

To allow for heat conduction longitudinally TLM meshes were connected as shown in Fig. 7. Ports 5

	273 K	1254 K
$c_p$ Ag	0.23	0.28
$k$ Ag	4.27	3.55
$c_p$ $\text{SiO}_2$	0.18	0.28
$k$ $\text{SiO}_2$	1.4E-3	4.3E-3

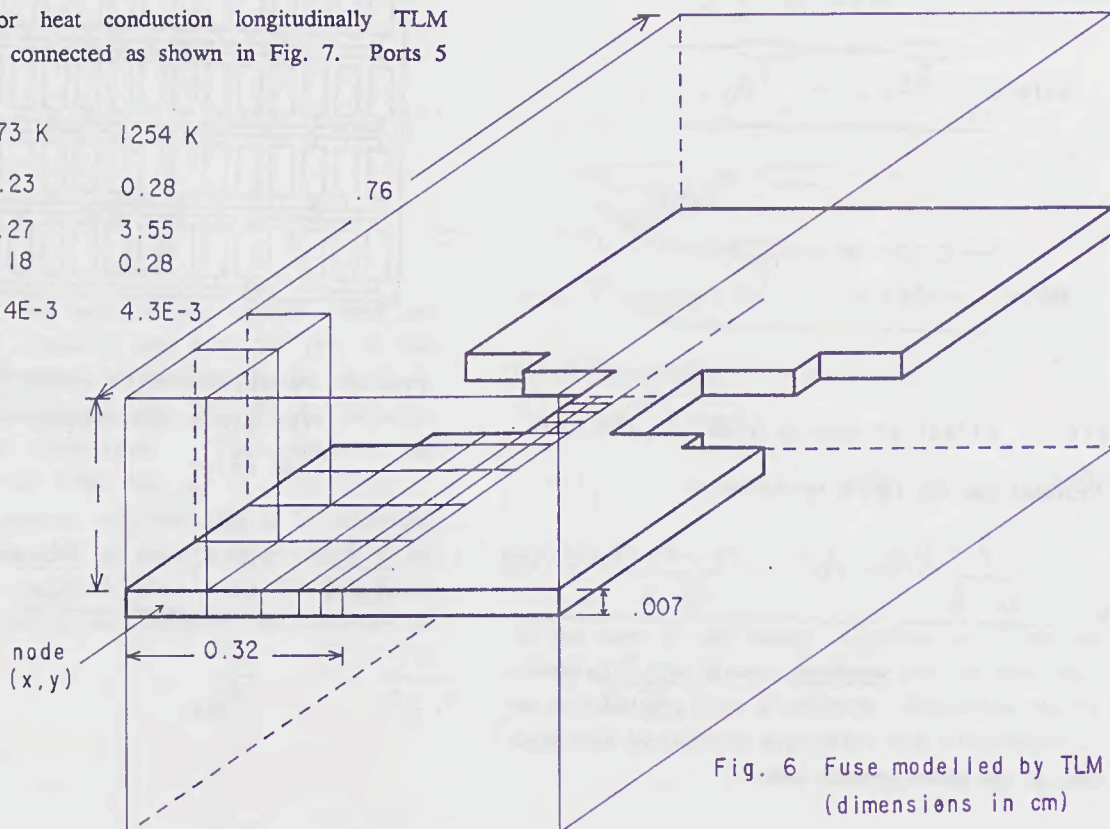


Fig. 6 Fuse modelled by TLM (dimensions in cm)

and 6 for each metallic node were terminated by the thermal resistance of the silica block immediately above or below.

When 100 A flowed through the fuse illustrated in Fig. 6 the temperature distribution in the metallic strip was found to be as shown in Fig. 8.

#### 3.2 Fuse pre-arcing time $\times$ current characteristic

To demonstrate the reliability of TLM to determine the fuse pre-arcing time  $\times$  current characteristic a number of simulations were done for the fuse illustrated in Fig. 6. The results over the time range  $10^{-2}$  to  $10^1$  seconds are presented in Fig. 9. The corresponding computing times varied from a few seconds to 3½ hours. Had it been permitted to run the program for longer periods the simulated characteristic could have been extended, since TLM does not require a convergence process and is explicitly stable.

### 4. Conclusion

It has been demonstrated that using TLM and an orthogonal, irregular mesh, it is possible to model heat flow in electric fuses and consequently, calculate fuse pre-arcing times. Comparison with practical tests showed good correlation of results. The explicit nature of TLM makes it faster and therefore more convenient for calculating long pre-arcing times because in TLM there is no calculation involving two

adjacent nodes for the same time step (unlike Finite Differences where a set of simultaneous linear equations has to be solved each iteration). Although in this work the granular silica was represented by a simple resistor connected to the external ports of the node, this representation could be refined but it would increase computing time. TLM provides a useful tool for the determination of long-time fuse operating characteristics.

### 5. Acknowledgements

Mr. Cheim wishes to thank the Brazilian Government (CEPEL/CNPQ) for its financial support to allow him to study at the University of Nottingham, where he carried out this research in collaboration with Dr. Howe. Both authors are grateful to the University for providing the appropriate facilities.

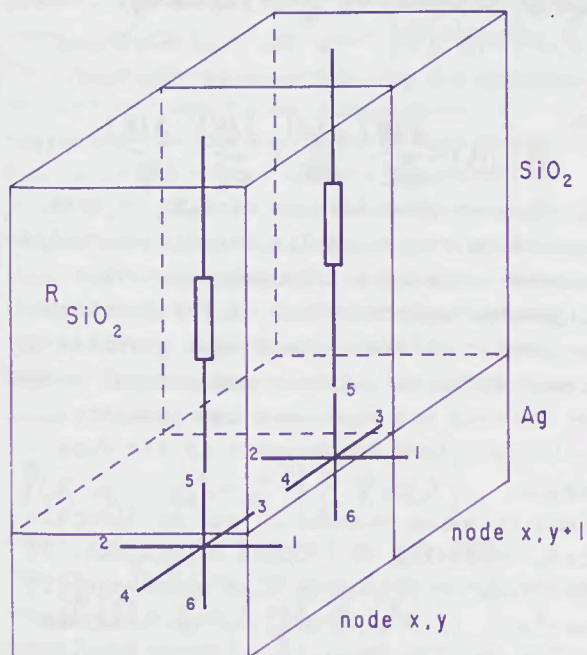


Fig. 7 Metallic nodes and their boundaries

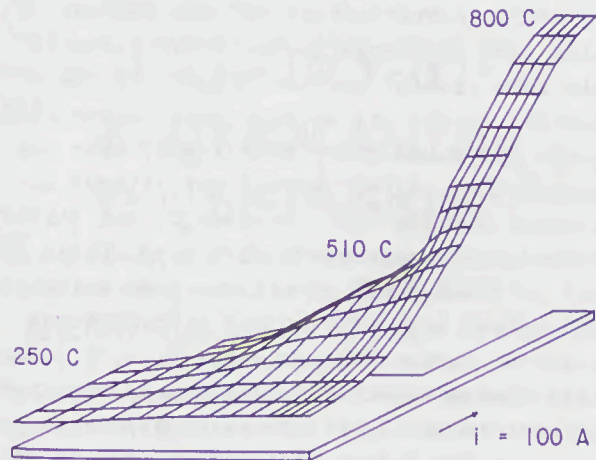


Fig. 8 Temperature profile (3-D) obtained by TLM for the fuse illustrated in Fig. 6

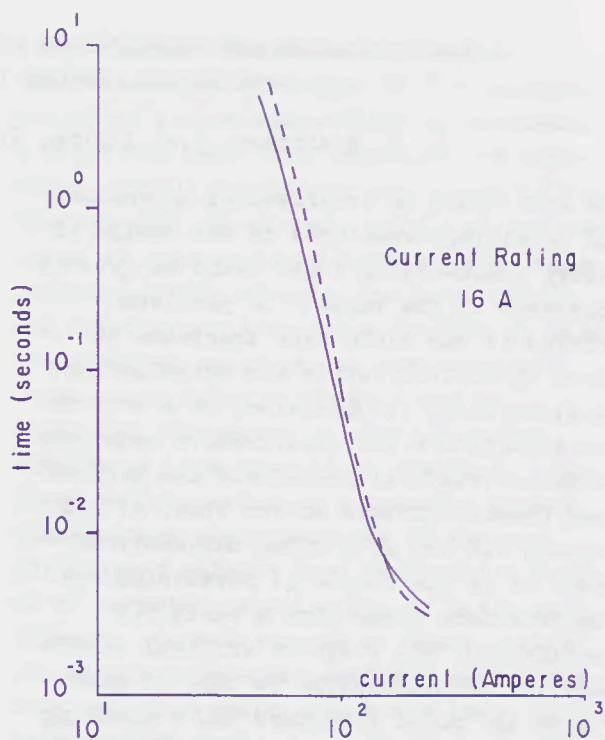


Fig. 9 Time x current characteristics

-- practical results  
 — TLM simulation

### 6. References

- [1] Johns P.B., Numerical modelling by the TLM method, 1977, Proc. of the International Symposium on Large Engineering Systems (Ed. A. Wexler), pp 139-151 (Pergamon Press, Oxford).
- [2] Brewitt-Taylor C.R. and Johns P.B., On the construction and numerical solution of transmission-line and lumped network models of Maxwell's equations, 1980, International Journal for Numerical Methods in Engineering, Vol. 15, pp 13-30.
- [3] Johns P.B., A Simple and unconditionally stable numerical routine for the solution of the diffusion equation, 1977, International Journal for Numerical Methods in Engineering, Vol. 11, pp 1307-1328.
- [4] Pulko S., Mallik A. and Johns P.B., Application of transmission-line modelling (TLM) to thermal diffusion in bodies of complex geometry, 1986, International Journal for Numerical Methods in Engineering, Vol. 11, pp 2303-2312.
- [5] Cook N., TLM Modelling of semiconductor fuses (A feasibility study), 1986, MSc thesis, Nottingham University.
- [6] De Cogan D. and Henini M., TLM Modelling of thin film fuses on silica and alumina, 1987, Third International Conference on Electric Fuses and their Applications (ICEFA), Eindhoven, Netherlands, pp 12-17.

IDENTIFICATION AND OPTIMIZATION AS MAIN APPLICATION AREAS FOR  
MATHEMATICAL METHODS IN FUSE DESIGN

K. K. Namitkov, N.A. Ilyina, G.G. Zhemerov and I.G. Shklovsky

The efficiency of experimental approaches and modelling techniques in the design of modern quick-acting fuses could be greatly increased if the variety of problems arising in the field were tractable in terms of identification and optimization. Identification is understood as a search for qualitative and quantitative relations between structural parameters and performance characteristics of the fuse, either through the use of a known mathematical model or in the course of developing one. The relations found form a basis for predictions. The stage of critical importance for identification is that of elaborating the model structure and evaluating model parameters. The necessity for such a stage in the fuse design is conditioned by the fact that fuses, unlike electromagnetic devices for instance, do not show strict analytical relationships between structural parameters and performance characteristics. In the case of fuses, the relations whose determination can be regarded as classical identification problems include those between

- a) the temperature field in the fuse and structural parameters;
- b) the time-current relation and structural parameters;
- c) cycling capacity and structural parameters and/or type of repeated loading and
- d) functional characteristics (like arcing current,  $\int i_a^2 dt$  and  $\int i_a U_a dt$  functionals, etc.) and structural parameters or those of the short circuit.

Depending on which parameters are known, these problems can be formulated either as direct or inverse. As a direct problem, problem a) can be analyzed, with allowance for nonlinearity and complex geometry of the boundary surfaces, in the variational formulation, using the finite-element technique<sup>1</sup>.

In case the choice of the functional for the finite-element model is difficult, or the proper functional cannot be obtained at all, then a useful finite-element

formulation is provided by Galerkin's scheme. Galerkin suggested a method for solving boundary-value problems through an approximate solution of a partial differential equation<sup>2</sup>. If applied to the field equation characteristic of fuse design problems, i.e.

$$L(\varphi) = \frac{\partial^2 \varphi}{\partial x^2} + \frac{\partial^2 \varphi}{\partial y^2} + Q = 0, \quad (1)$$

then Galerkin's finite-element formulation leads to

$$\iint_{\Omega} [B]^T [B] dy dx \{ \Phi \} - \iint_{\Omega} [N]^T Q dx dy, \quad (2)$$

where  $\varphi = [N] \{ \Phi \}$  is the finite-element approximation for the unknown function, and

$$[B]^T [B] = \frac{\partial [N]^T}{\partial x} \frac{\partial [N]}{\partial x} + \frac{\partial [N]^T}{\partial y} \frac{\partial [N]}{\partial y}. \quad (3)$$

The further procedure is similar to that applied to variationally formulated finite-element equations. If combined with a polynomial approximation of the functions involved, Galerkin's technique provides a highly efficient, simple and general method for solving the equations and boundary-value problems encountered in the fuse design.

Identification problem b) can be diversified, depending on various conditions. In the range of extremely high short-circuit currents,  $(300 \text{ to } 500) I_n$ , the analysis can be based on Meyer's equation disregarding the geometry of constrictions, waveform of the current and the thermal flux from the necks to the wider parts of the fuse element and the filler. If the current values are so high that constricted parts get fused over 14 or 15 ms, then the calculation may be carried out without allowance for the heat transfer to the filler. Indeed, our experiments with both filled and unfilled fuses showed the same value of the fusion integral for all specimens. In case the fusion time exceeds 15 ms, a complete finite-element calculation is required. In certain cases, it proves necessary to consider the rather interesting problem of select such values of the structure para-

Some US file as  
same v bad mes

meter with which its time-current characteristic would pass through at least four given points. The solution procedure is close to that of optimization.

No rigorous models are known for problems c) and d), generally the model structure needs to be developed from basic physical principles (especially for new, non-standard conditions). In many particular cases, however, some a priori knowledge can be used efficiently to simplify the model structure. Then evaluation of the model parameters, which stage is necessary because of the many random factors influencing the results of numerical or instrumental experiments, is reduced to approximation. The latter problem can be efficiently analyzed for the case of fuses within the approach suggested by the present authors and employing the Kolmogorov-Mordashov transformation. As was known by A.N. Kolmogorov, an unknown function  $f(x_1, x_2, \dots, x_n)$  of many variables can be represented, for the purpose of approximation, as a superposition of single-variable functions. V.L. Mordashov further suggested using some transformation rather than a simple superposition of single-variable functions, i.e.

$$f(x_1, x_2, \dots, x_n) = \mathcal{L}^{-1} \left\{ \sum_{i=1}^n \psi_i(x_i) \right\}, \quad (4)$$

where the values assumed by the wanted function  $f(\bar{x})$  at certain points are known and  $\mathcal{L}(f) = \sum_{i=1}^n \mathcal{L}_i f_i = \sum_{i=1}^n \psi_i(x_i)$  is a transformation of  $f(x)$ . The unknown parameters of the transformation are  $\mathcal{L}_i$  and  $\psi_i$ , where the vector  $\vec{\mathcal{L}} (\mathcal{L}_1, \mathcal{L}_2, \dots, \mathcal{L}_n)$  is to be found as the eigenvector minimizing the matrix form  $[\Phi - \Psi - \mathcal{L}N] = 0$ , with

$$\begin{aligned} \Phi &= \left\| \int_{\mathcal{D}} \psi_i(\mathcal{G}_n) \psi_j(\mathcal{G}_n) d\chi(\mathcal{G}_n) \right\|_{i,j}^k \\ \Psi &= \left\| \int_{\mathcal{D}} \psi_i(\mathcal{G}_n) \psi_j(\mathcal{G}_n) d\chi(\mathcal{G}_n) \right\|_{i,j}^k \end{aligned} \quad (5)$$

$\mathcal{G}_n = \{x_1, x_2, \dots, x_n\}$  is the set of independent variables in  $\mathcal{D}$  ( $\mathcal{G}_n \in \mathcal{D}$ );  $d\chi(\mathcal{G}_n) = \prod_{i=1}^n d\chi(x_i)$ ;  $d\chi(x_i) = 1/\rho$ , where  $\rho$  is the number of variation levels for the argument;  $N$  is the matrix parameter;  $N$  a positively defined symmetric matrix of order  $K$  to allow for the importance (weight) of the function arguments, and  $\psi_i$  a set of arbitrarily se-

lected linear-independent functions.

The fundamental advantage of the approach described is the possibility of obtaining a realistic model and improving the accuracy, without increasing the volume of the instrumental experiment, solely at the expense of sophisticated mathematical transformations. The current practical models for solving identification problem c) take the simplest structure at the empirical level (more details can be found in<sup>3</sup>). Among the approaches to identification problem d), one appeals to abstract, idealized models employing a specific preset time-voltage characteristic of the arc. The present authors have performed a series of computer calculations of basic performance characteristics of fuses, using the simplest voltage waveforms across the fuse arc. Generally, the arc voltage can be represented as

$$U_g(t) = 2(U_{g0} - U_{gi})T/T_K + U_{gi}, \quad (6)$$

where  $U_{gi}$  is equal to  $U_{gmin}$  for the waveform  $U_{Li}$ ,  $U_{g0}$  for the mean value and  $U_{gmax}$  for  $U_{pi}$ . The four waveforms used here are  $U_{Li}$  which is voltage reaching the level  $U_{gmin}$  instantaneously and then increasing linearly to  $U_{gmax}$ ;  $U_{pi}$  which becomes  $U_{gmax}$  instantaneously and then decreases in a linear manner towards the level  $U_{gmin}$  (or  $U_c$ ) of the power line voltage;  $U_{g0}$  is the voltage reaching its value instantaneously and staying at that level during the entire arc extinguishing stage; the same value is the mean of  $U_{Li}$  and  $U_{pi}$ ; and finally  $U_{gmax}$  is a constant voltage equal to the maximum admissible level. For the sake of simplicity, we considered the case of an interrupted d.c., assuming that arcing started at the moment  $t_0$  when the current reached the fusion value  $I_0$ . The calculations were performed for  $U_{g0} = 600$  to  $1000$  V;  $I_0 = 10$  to  $20$  kA;  $U_c = 500$  V;  $L = (5 \times 10^{-5}$  to  $6 \times 10^{-4})$  H, and  $R = 5 \times 10^{-3}$  to  $2 \times 10^{-2}$  Ohm. Now we describe some of the regularities established. The arcing time is determined by the mean voltage across the arc, being independent of the voltage waveform. At  $U_g = U_{gmax} = \text{const}$  it is 1.5 times shorter than with other voltage types. Whereas the arc Joule integral and the arc energy both depend

on the voltage waveform across the arc, changing by a factor of 2 or 3 for different waveforms, even with the same mean voltage. The dependence upon this latter is quite essential. E.g. a change of  $U_{go}$  from  $2U_c$  to  $1,2U_c$  results in a nearly five-fold increase in the arc integral. Besides, 90% of the arc energy at  $U_{go}=5U_c$  consist of the energy accumulated in the inductor, while with  $U_{go}=1,2U_c$  this part of energy makes up only 20 to 25% of the total energy.

Optimization is understood as a search for the vector of adjustable fuse parameters minimizing some goal (quality) function with specific functional and/or parametric constraints. All the above mentioned identification problems can be formulated as optimization problems as well. Of the many optimization approaches known for fuses we describe some that have been recognized as the most efficient. One-dimensional optimization with Fibonacci numbers. This is a sequential method of searching, e.g. for a current providing a maximum arc energy, in which the preceding experimental results influence the choice of the domain for the next experiment. In mathematical terms, the problem can be formulated as minimization of the error  $\epsilon$  with which the point  $x^*$  is determined, minimizing the wanted function  $f(x)$  over the interval  $[a_k, b_k]$  after  $n$  steps of the process. According to the method, we select points  $x_k$  and  $x'_k$  within  $[a_k, b_k]$ , determined by the equations

$$x_k = \frac{F_{N-1-k} (b_k - a_k) + a_k}{F_{N+1-k}} \quad (7)$$

$$\text{and } x'_k = \frac{F_{N-1} (b_k - a_k) + a_k}{F_{N+1-k}} \quad (8)$$

where  $F_k = F_{k-1} + F_{k-2}$  are Fibonacci numbers, with  $F_0 = F_1 = 1$ . Thus, at the first step we consider the interval  $[a_k, b_k]$  which is the entire domain of the function. Further steps result in a gradual contraction of the interval, following shifts of one of the boundaries (either the right- or the left-hand one) at the preceding step. If the function assumes at  $x_k$  a smaller value than at  $x'_k$   $f(x_k) < f(x'_k)$ , then the next uncertainty interval can be selected as  $[a_{k+1}, b_{k+1}] = [a_k, x_k]$

Contrary to this, with  $f(x_k) > f(x'_k)$  the interval to be analysed is  $[a_{k+1}, b_{k+1}] = [x_k, b_k]$ . If the two values happen to be equal,  $f(x_k) = f(x'_k)$ , then the next interval can be either  $[a_k, x_k]$  or  $[x'_k, b_k]$ , since both intervals are of the same length  $[b_k - x'_k] = [x_k - a_k]$ . The last points of the process are given by

$$x_{N-1} = (1/2 + \epsilon)(b_{N-1} - a_{N-1}) + a_{N-1} \quad (9)$$

$$x_{N-1} = 1/2 (b_{N-1} - a_{N-1}) + a_{N-1}$$

If we specify the maximum allowable error  $\epsilon$ , then equations (9) yield unambiguously the minimum number of steps  $N$ , and vice versa, for a given number of experiments the limiting error in determining the point of extremum is

$$F_{n+1} \leq L/\epsilon \leq F_{n+2}$$

Here  $\epsilon$  is the error,  $L$  the interval length,  $F_{n+1} \leq L/\epsilon \leq F_{n+2}$  and  $F_{n+1}, F_{n+2}$  are Fibonacci numbers, and  $n$  the number of experiments. By way of example, here are twelve initial members of the Fibonacci series, 1; 1; 2; 3; 5; 8; 13; 21; 34; 55; 89; 144. Hence, to attain a 5 per cent limit to the error ( $\epsilon = 5\%$ ), we would need 6 experimental steps. Indeed,  $F_{6+1} < 20 < F_{6+2}$  or  $13 < 20 < 21$ . With 10 experiments, the error would drop below 0.69%.

Multidimensional optimization of the fuse design can be done most efficiently with the aid of gradient methods. The great advantage of such techniques is that the derivatives of the optimality criterion need not be represented analytically. It is sufficient to calculate partial derivatives of the function at several individual points which can be done in terms of finite increments (both numerically and in an instrumental experiment). The coordinates of point  $\bar{x}^{i+1}$  are calculated at each consecutive step of the procedure as

$$\bar{x}^{i+1} = \bar{x}^i + K(\bar{x}^i) \nabla f(\bar{x}^i), \quad i=1, 2, \dots, n \quad (10)$$

where  $\nabla f(\bar{x}^i) = (\partial f / \partial x_1, \dots, \partial f / \partial x_n)$  is the gradient of  $f(x_1, \dots, x_n)$ . It is a vector whose components are partial derivatives of  $\bar{x}_i$ , specifying the direction of motion from point  $\bar{x}^i$  to  $\bar{x}^{i+1}$ . The proportionality matrix  $K(\bar{x}^i)$  determines the iteration step length. A highly reliable method is Box-Wilson's steepest descent technique

within which the step length is chosen from the condition that the optimality criterion be maximum (minimum) along the gradient vector. In other words, the magnitude of  $K^i$  is found from

$$\max f[\bar{x}^i + K^i \nabla f(\bar{x}^i)] = f[\bar{x}^i + K^i \nabla f(\bar{x}^i)] = f(\bar{x}^{i+1}), \quad K^i > 0 \quad (11)$$

Gradient-based procedures of this kind employ linear approximations to  $f(\bar{x})$ , which allows evaluating first derivatives of the function, along with the function itself. This information is of great importance in the search of optimum. On the other hand, cycling of the process cannot be excluded. To improve the reliability, we can resort to Newton's method in which consecutive points are calculated from the recurrence relation

$$\bar{x}^{i+1} = \bar{x}^i - H^{-1}(\bar{x}^i) \nabla f(\bar{x}^i), \quad (12)$$

with  $H(\bar{x}^i)$  denoting the second derivative matrix (i.e. the Hessian). The method proves particularly efficient near the optimum where the gradient is liable to changes in sign that result in sharp variations of the vector direction and deteriorate the procedure convergence.

Pontryagin's maximal principle. The maximal principle allows obtaining a solution even when other methods fail, e.g. in the presence of constraints and with implicitly specified function to be optimized. It suggests introduction of a set of variables  $P_1(t), P_2(t), \dots, P_n(t)$  for the dual problem, and a scalar Hamiltonian according to

$$H(x, y, P, t) = F(x, y, t) + \sum_{i=1}^n P_i(t) f_i(x, y, t) \quad (13)$$

Let the system under analysis be described by the equation

$$\frac{dx}{dt} = f[x(t), y(t), t] \quad (14)$$

with boundary conditions  $x(t_0) = x_0$  and  $x(t) = Dn$  and let it be necessary to find the control function  $y(t)$  to minimize the functional  $J = \int_{t_0}^t F(x, y, t) dt$ . If the optimum control function  $y(t)$  exists and belongs to the set  $y(t) \in Y$ , and  $\hat{x}(t)$  is the optimum trajectory, then the dual state vector  $P(t)$  should and satisfy

$$\frac{\partial \hat{x}_i(t)}{\partial t} = \frac{\partial H}{\partial P_i(t)} \quad \text{and} \quad \frac{\partial P_i(t)}{\partial t} = -\frac{\partial H}{\partial \hat{x}_i(t)} \quad (15)$$

The maximal principle was used by the present writers to optimize the voltage waveform across the fuse arc.

The sensitivity analysis in fuse design suggests understanding the relations between design variables (such as structural parameters, external conditions and manufacture tolerances) and response of the structure, i.e. variations of its performance parameters. Suppose the equation to describe the structure behaviour is

$$K(b)z(b) = F(b), \quad \text{where } K(b) \text{ is the global rigidity matrix, } z(b) \text{ the solution, and } F(b) \text{ the load.}$$

In most cases the design problem is aimed at minimizing some cost function (or maximize the goal function)  $\Psi[b, z(b)]$  in the presence of constraints on the design variables  $b = [b_1, \dots, b_k]$  and functional characteristics. Then the sensitivity analysis is oriented at finding

$$\frac{d\Psi}{db} = \frac{\partial \Psi}{\partial b} + \frac{\partial \Psi}{\partial z} K^{-1}(b) \frac{\partial}{\partial b} [F(b) - K(b)z] \quad (16)$$

This equation represents the direct differentiation method. A different approach is that of dual variables where the researcher seeks to evaluate

$$\frac{d\Psi}{db} = \frac{\partial \Psi}{\partial b} + \lambda^T \left[ \frac{\partial F(b)}{\partial b} - \frac{\partial}{\partial b} (K(b)z) \right] \quad (17)$$

with  $\lambda^T = K^{-1}(b) \frac{\partial \Psi}{\partial z}$  being the dual variable which is determined from the symmetry of

$K$ . Details of the calculations associated with the two approaches are described in 4. The sensitivity analysis can be complementary to the identification and optimization procedures, either employing their results or accompanying them as a parallel process. Note that direct differentiation is efficient at the preliminary stage of analyzing model problems when the number of variables involved is low. In the majority of practical cases, the dual variable method is preferable.

Gradient methods and the approaches used in sensitivity analysis are largely applicable to optimized parameter scaling for fuse structure modification. A complete recalculation of performance characteristics for new structure parameters can result, with the use of standard high-order models, in forbiddingly high costs and computer time expenditures. The volume of computations can be greatly reduced through the use of

results relating to a reference structure. E.g., let the basic physics in the reference structure be governed by the matrix equation  $[K_0]\{\Psi_0\}=F_0$ , where  $K_0$  is the conductivity matrix (alternatively, the rigidity matrix) specified by the structure parameters, and  $\Psi_0$  the potential (temperature, or mechanical stress) matrix representing response of the structure to the applied load  $F_0$  (electrical, thermal or mechanical). By modifying the structure, the designer changes the matrix  $K_1$ , which leads to the necessity of finding the new response  $\Psi_1$  through the solution of the equation  $[K_1]\{\Psi_1\}=F_1$ . It is possible, however, to make use of the knowledge obtained from the reference equation, and scale the response by generating the series of vectors  $\tilde{\Psi}^{(0)}, \tilde{\Psi}^{(1)}, \tilde{\Psi}^{(2)}$ , etc.

as

$$\tilde{\Psi}^{(i+1)} = \tilde{\Psi}^{(i)} - [K_0]^{-1} \Delta K \tilde{\Psi}^{(i)} \quad (18)$$

with  $\Delta K = K_1 - K_0$  and  $\tilde{\Psi}^{(0)} = \Psi_0$

With moderate (up to 10%) changes in the structure parameters, the sequence  $\tilde{\Psi}^{(0)}, \tilde{\Psi}^{(1)}, \tilde{\Psi}^{(2)}$ , etc. converges to the solution  $\Psi_1$ . Since the best convergence is provided by rational approximating functions, these can be used to obtain a solution with as high parameter variations as 35 to 47%. The required response is sought in the form of the rational function

$$\Psi(x) = [K_0(x) + x_0 K(x)] F.$$

Conclusion. The approaches discussed allow the problem of fuse design and analysis i) to be formulated in rigorous mathematical terms for specific practical cases; ii) to be analyzed on a systematic basis, as a consistent set of logically interdependent algorithms; iii) to be treated by efficient and appropriate methods.

#### REFERENCES

- [1] K.K. Namitokov, N.A. Ilyina, and I.G. Shklovsky. A finite element analysis of the thermal behaviour of notched fuse elements in semiconductor protection fuses. In: Switching Arc Phenomena, Sixth Int'l Conf., 12-15 Sept. 1989, Lodz, Poland. Conference

Materials, 212-217.

- [2] C.A.J. Fletcher. Computational Galerkin Methods. Springer-Verlag, 1984.
- [3] K.K. Namitokov, N.A. Ilyina, and I.G. Shklovsky. Pulse withstandability of semiconductor protection fuses. In: Switching Arc Phenomena, Sixth Int'l Conf., 12-15 Sept. 1989, Lodz, Poland. Conference Materials, 205-211.
- [4] E.J. Hang, K.K. Choi, and V. Komkov. Design sensitivity analysis of structural systems. Academic Press, N.Y., 1986.

THE COMPUTER ANALYSIS OF BREAKING CURRENT PROCESS  
IN SAND FILLER FUSES

Xie Yunxiang  
University of Xi'an Jiaotong  
Dept. of Electrical Engineering  
Xi'an, P.R. China

ABSTRACT

This paper describes breaking current process in sand filler fuses under the short circuit conditions, and analyses the basic characteristic of anode, cathode and arc column during arcing process. A mathematical model that describes the arc phenomena is set up. The results using this model to calculate the arcing process agree with the experiment results well.

1 Introduction

The arc model in sand filler fuses is one of the main subject in fuse research area, a great progress has been made, especially the variations of arc cross-sectional area during the arcing process have been taken account into the model, the calculation results of model become more accurate. However, there are some problems in all of the existing models, all kinds of models are expressed in different mode, angles and respects considered in the models are disparate, so it must be proved that which kind of the model should be used exactly in a specific situation and which one be universal. Meanwhile, a great deal of work need to be done to get some experiment formulae or constants in the models. In order to gain a universal arc model, this paper analyses the breaking current process in sand filler fuses, sets up a mathematical model based on the physics characteristic. The experiment formulae or constants are used in the model as rarely as possible.

2 The mathematical model of arc

When the arc emerge, the voltage across the fuse increases rapidly, so arcing phenomena can be described by the variation of arc current and arc voltage with time.

Generally, the arc can be split into three regions: anode, cathode and arc column, these are considered separately in the following subsections.

2.1 The cathode fall region

A great part of electrons resulting in arc discharge generates in cathode fall region or emits from cathode. This region is about  $10^{-3}$  millimetre long, but there is a regular voltage across it, for low boiling-point cathode, the cathode drop is supposed to be 10V in this paper.<sup>1</sup>

2.2 The anode fall region

This region is also about  $10^{-3}$  millimetre long as with the cathode fall region. However, the process taking place in this region is quite different from that in the cathode fall region. Above 99 percent of electrons and ions generates in the cathode fall region, while below one present of ions is engendered in the anode fall region.<sup>2</sup> The main function of the anode fall region is to change directional motion energy of ions in this region into thermal energy in arc column.

The anode drop could be any value between zero and the ionization potential of anode element material. It is assumed that the anode drop equal to the ionization potential, because field ionization is the probable mechanism for ion production in case of fuse arcs.

2.3 Analysis of arc column plasma

As mentioned earlier, the cathode fall region and anode fall region in an arc are about  $10^{-3}$  mm long, therefore the arc column may be taken to occupy the whole gap length between the electrodes. To derive the mathematical model of arc simply, it is presumed that arc column be cylinder and all of the parameters in arc column be homogeneous. In case of this presumption, it will be considered that the length, cross-sectional area, and conductivity of the arc column vary with time during arcing process so as to determine the resistance of arc column, then the arcing phenomena could be described by mathematical easily.

2.3.1 Electron density of arc column plasma

Arc plasma consists of ions, electrons and neutral particles, when the electrical field is exerted, the discharge particle in plasma will move directionally, therefor current flow in plasma. The current density could be expressed:

$$J = n_i q u_i - n_e q u_e \quad (1)$$

where  $u_i$ ,  $n$  are diffuse velocity and density respectively.

According to condition of quasi-neutral in plasma,  $n_e = n_i$ , then

$$J = n_e q (u_i - u_e) \quad (2)$$

because the discharge particle is accelerated by electrical field, therefore

$$u_i = b_i E \quad (3)$$

$$u_e = b_e E \quad (4)$$

Here,  $b_i$  and  $b_e$  are removal rate of ions and electrons respectively, since electron mass is much lighter than ion mass,  $b_e$  is much bigger than  $b_i$ , so

$$J = n_e q b_e (-E) \quad (5)$$

according to Ohm's law,  $J = \sigma E$ , then

$$n_e = \frac{\sigma}{q b_e} \quad (6)$$

On the basis of gas dynamics theory, electron removal rate can be determined as following:<sup>3</sup>

$$b_e = \frac{q \lambda_e}{m_e V_T} \quad (7)$$

where  $\lambda_e$  is free path of electrons, and  $V_T$  is thermal motion velocity of electrons, it is given by the formula

$$V_T = \sqrt{\frac{8KT}{\pi m_e}} \quad (8)$$

Whereas free path of electrons could be expressed<sup>4</sup>

$$\lambda_e = \frac{KT}{\pi R^2 P} \quad (9)$$

where  $R$  is radius of gas molecule,  $P$  is pressure of arc plasma,  $T$  is temperature,  $K$  is Boltzmann's constant.

therefore electron density is given by the expression

$$n_e = \frac{\sqrt{8\pi m_e R^2 P \sigma}}{q^2 \sqrt{KT}} \quad (10)$$

### 2.3.2 conductivity of arc column plasma

In arc column plasma, electron mass is much lighter than ion mass, therefore velocity of electron which is acquired by effect of electrical field is much higher than that of ion, It is considered that current be mainly delivered by electrons, if ionizability in fuse arc plasma is more than 0.01 percent, conductivity of arc column plasma could be expressed by Spitzer's formula.<sup>5</sup>

$$\sigma = \frac{1.55 \times 10^{-2} T^{3.2}}{\ln(1.242 \times 10^7 T^{3.2} / n_e^{0.5})} \quad (11)$$

### 2.3.3 Length of arc column

Element material corrodes continuously due to the effect of anode and cathode during the arcing process, so the length between electrodes enlarge unceasingly, the rate of its enlargement equals to total burnback rate of anode and cathode.

Burnback rate of electrode material is relate to energy balance in anode and cathode fall region. A.Wright considered this energy balance and obtained that the total energy supplied to anode fall region in each unit time was given by the expression<sup>6</sup>

$$\text{power} = (V_{af} + V_{wf} + V_T) i$$

where  $V_{af}$  is anode fall voltage,  $V_{wf}$  is voltage associated with the work function of the element material,  $V_T$  is voltage associated with the thermal energy of the electrons which enter the anode,  $i$  is arc current.

Meanwhile, he found that corroding degree in two electrode fall region is identical from a large number of X-ray photographs of breaking current tests. Therefore, it could be assumed that energy supplied to cathode be the same as that supplied to anode, the burnback rate of anode equals to that of cathode as a consequence.

A very small part of energy supplied to anode is consumed by radiation and heat conduction. The energy is mainly used up by electrode to rise temperature of electrode and evaporated. A.Wright found that about 20 percent of the total energy is used to complete the process of latent heat of fusion. So the enlargement rate of length of arc plasma could be written as

$$\frac{dl}{dt} = \frac{0.4(V_{af} + V_{wf} + V_T) i}{A_e \rho_e L_f} \quad (12)$$

Here,  $A_e$  is cross-sectional area of electrode,  $\rho_e$  is mass density of electrode material,  $L_f$  is latent heat of element material.

### 2.3.4 Cross-sectional area of arc column

When an arc column is established in a fuse, it receives power from the electrical system, this energy  $E$  could be expressed as

$$E = u i d t \quad (13)$$

where  $u$  is voltage drop along the arc column.

During the earlier part of the arcing period, some of the input power is retained within the arc column and makes dimension and temperature of the

arc column increase. However, in the later part of the arcing period, the changes in energy present in a column during the short period may be very small compared with the total energy input, so it could be considered that power given to column be dissipated by the surrounding filler which will consequently melt progressively, the mass  $m$  of sand filler which will melt in the time interval  $dt$  may be

$$m = \frac{\rho_s u i dt}{\rho_s (C_s \Delta T_s + L_s)} \quad (14)$$

Here  $\rho_s$  is the packed density of sand,  $C_s$  and  $L_s$  are specific heat and fusion latent heat of sand respectively.

Because fuselinks are vibrated after sand is put into them, it is assumed that the volume filling rate of sand should be  $\gamma$ . After sand melts, its volume will increase, the expansion rate of sand on liquefaction is supposed to be  $\beta$ , therefore the volume of liquid sand is  $(1+\beta)\gamma$  times of the originally occupied by sand-air mixture. In addition, a column expands into the space previously occupied by the melted electrode. Then, the total variation in volume can be expressed

$$\frac{dV}{dt} = \frac{[1-(1+\beta)\gamma] u i}{\rho_s (C_s \Delta T_s + L_s)} + A_e \frac{dl}{dt} \quad (15)$$

According to the presumption in the earlier, arc column is cylinder, so the cross-sectional area could be given in the following

$$A_s = V / l \quad (16)$$

### 2.3.5 Energy balance of arc column plasma

When arc column is established, material evaporated from the electrodes often enters it in the form of jets, a number of atoms of this material are accelerated into a column and a fraction  $x$  of them become ionised in any short time interval, meanwhile, almost the same number of atoms and ions would be scattered out of the column. To set up model simply, the following equations are assumed to apply any time interval.

$$N_{a,i} = N_a \quad (17)$$

$$\text{and } N_e = x N_a \quad (18)$$

where  $N_{a,i}$  is the number of atoms and ions which are scattered from arc column,  $N_e$  is the number of electrons which are scattered from arc column, and  $N_a$  is the number of atoms which evaporate from the electrodes.

The total mass melted from the electrodes during the time interval  $dt$  is given by A.Wright

$$\text{total mass} = 0.4(V_{a,r} + V_{w,r} + V_r) i dt / L_f$$

He also found that about 40 percent of this mass will evaporate, if the number  $N_g$  of atoms per each

mass of electrode material is known, the total number of atoms which enter into arc column in time interval  $dt$  could be written as

$$N_a = 0.08 N_g (V_{a,r} + V_{w,r} + V_r) i dt / L_f \quad (19)$$

The energy in arc column is dissipated by the main ways of kinetic energy, compound and radiation.

Kinetic energy could be given in the following

$$\text{kinetic energy} = 1.5 (N_{a,i} + N_e) K T$$

and compound energy is

$$\text{compound energy} = N_e E_i$$

where  $E_i$  is ionization energy of each atom.

For heat radiation, it could be considered as blackbody radiation because the temperature and pressure of arc column is very high. The surface area  $S$  of arc column may be calculated

$$S = (\pi d l) = (4 A_s / \pi)^{0.5} l = 2 l (\pi A_s)^{0.5}$$

therefore heat radiation energy can be expressed as

$$\text{heat radiation energy} = 2 l (\pi A_s)^{0.5} K_s T^4 dt$$

where  $K_s$  is the Stefan-Boltzmann constant.

According to the law of conservation of energy, the following equation is gained

$$(m_s c_s \partial T / \partial t) dt = u i dt - N_a [1.5 K T (1+x) + x E_i] - 2 l K_s T^4 (\pi A_s)^{0.5} dt \quad (20)$$

Here  $m_s$  and  $c_s$  are mass and specific heat of arc plasma.

At any time the temperatures of ions and electrons in a column will be the same because the mean free path is very short and they must experience many collisions before leaving the column, in this circumstance the following equation is applicable

$$\frac{x^2}{1-x^2} = \frac{(2 \pi m_e)^{3/2}}{h^3} (K T)^{3/2} \exp\left(-\frac{E_j}{K T}\right) \quad (21)$$

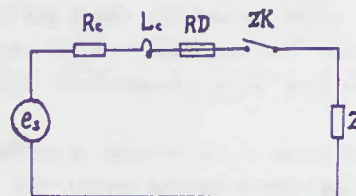
where  $P$  is pressure of arc plasma,  $m_e$  is mass of electron, and  $h$  is Planck constant.

and the pressure of arc column plasma can be expressed as

$$P = \frac{1+x}{x} n_e K T \quad (22)$$

### 2.3.6 Integrated mathematical model of fuse arc

The model of fuse arc are usually described by the equivalent circuit shown in Fig. 1.



$Z=0$  if short circuit occur  
Fig. 1 equivalent circuit

It is often possible to regard a source as having resistance and inductance in series, in this circumstances, the nonlinear equation during the arcing period could be shown as follow

$$e_s = i(R_a n + R_c) + d(L_c i) / dt + n(V_{af} + V_{cf}) \quad (23)$$

Here  $e_s$ ,  $R_c$ ,  $L_c$  are electro-motive force of source, equivalent resistance and inductance of power system,  $R_a$  is resistance of each arc column,  $V_{cf}$  is voltage drop of cathode fall region and  $n$  is the number of arcs or notches in element.

According to Ohm's law, it could be gained

$$R_a = u / i \quad (24)$$

the resistance of the arc column can also be expressed as

$$R_a = \frac{l}{\sigma A_a} \quad (25)$$

Equations (10), (11), (12), (15), (16), (19), (20), (21), (22), (23), (24), (25) are independent and include twelve unknowns  $n_e$ ,  $P$ ,  $\sigma$ ,  $T$ ,  $l$ ,  $A_a$ ,  $V$ ,  $N_a$ ,  $u$ ,  $i$ ,  $R_a$  and  $x$ , if initial conditions are given, these unknowns can be solved.

### 3 Calculation of mathematical model of fuse arc

The twelve equations which describe the arc characteristic could be simplified by using difference method, therefore twelve parameters at time  $t+dt$  would be calculated easily if these parameters at time  $t$  are known.

If the arc length  $l$  is more than or equal to the length between two notches of fuse during the calculation, the arcs will join together and become a single long arc, therefore equation (23) should be changed into

$$e_s = i(R_a' + R_c) + d(L_c i) / dt + (V_{af} + V_{cf}) \quad (26)$$

where  $R_a'$  is the resistance of a single long arc

If this single long arc burnback continuously until the length of it is up to the element length, the calculation should cease, in this circumstance, it is regarded that the breaking current be failure.

#### 3.1 Determination of the initial value

Because the temperature is very low at the beginning of the arcing period, the value of the parameters  $l$ ,  $V$ ,  $A_a$ ,  $x$  are very small and they are taken to be zero, the temperature  $T$  are considered to be the boiling point temperature of element material.

The initial value of arc voltage is difficult to determine. During the prearcing period, the voltage across the notches of fuse is very small, and it changes suddenly at the beginning of the arcing

period. The value of this sudden change depends on the dimension of the notches. Long notches have slightly higher initial voltage than short notches. In this paper, the initial voltage is assumed to be 33 V.

The initial value of arc current can be determined by calculating prearcing period.<sup>7</sup>

#### 3.2 Calculation of arcing period

According to the earlier analysis, the solving the twelve equations by the ways of step by step. The arc voltage  $U_f$  across the ends of the fuses can be calculated

$$U_f = n(V_{af} + V_{cf} + iR_a) \quad (27)$$

If the arcs join together and become a single long arc, the arc voltage will be expressed as

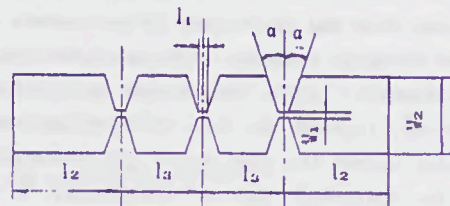
$$U_f = V_{af} + V_{cf} + iR_a' \quad (28)$$

The above arc model are set up on the basis of this presumption which there is only one element in the fuses, if several elements exist in the fuses, the items which are related to current will be changed correspondingly.

### 4 Results

To verify the accuracy of arc model, the fuses in which only one element exist is used to do many practical tests and theory calculations, the results obtained are compared with each other, and they agree well.

The constructions and dimension of the fuse element are shown in Fig. 2.



$$l_1 = 1 \quad l_2 = 21 \quad l_3 = 15 \quad w_1 = 0.7 \quad w_2 = 15 \quad \alpha = 22.5$$

Fig. 2 element structure of a fuse

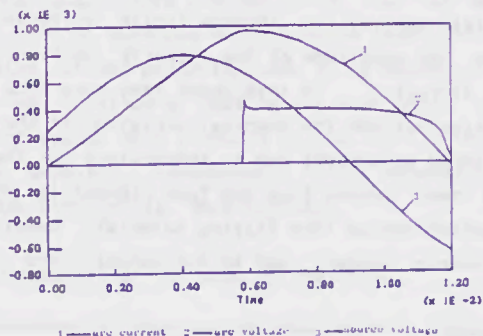
one of the results of tests and calculations are listed in table 1 and Fig. 3.

Table 1 breaking current results under the conditions of  $U=560V$ ,  $I=510A$ ,  $\cos\phi=0.28$

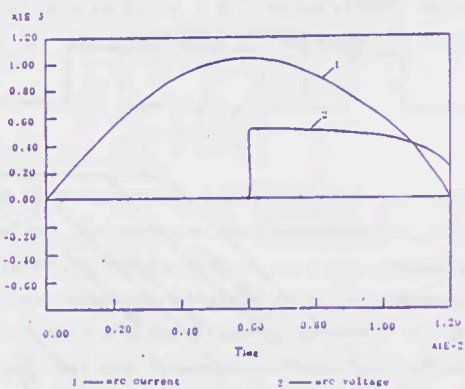
	calculation results	test results
current peak	972.0 (A)	1072 (A)
over voltage	468.6 (V)	531 (V)
arcing time	6.134 (ms)	6 (ms)

### 5 Conclusions

The mathematical model of fuse arc which is derived in this paper could describe breaking current process of fuses. By using this model to study the influences of many kinds of parameters on breaking current process, the work of fuse research become easy, it will advance quickly and economically as well because it is not necessary to do a lot of tests in the study.



( a ) calculation results



( b ) test results

Fig. 3 oscillogram of breaking current

#### References

1. Dolan. W. W, Dyke. W. P: Temperature-and field emission of electrons from metals. Phys.Review. 95, pp.327-332, 1954.
2. A. Erk, M. Schmelzle: Grundlagen der Schaltgeratetechnik. New York, 1974.
3. Wang Qiping: Arc theory in the electrical apparatus. 1982.
4. Cheng Zongzhu, Gao Shuxian: Gas discharge. 1988
5. Spitzer. L, Harm. R: Transport phenomena in a completely ionised gas. Phy. Rev. 89, 1953.
6. A. Wright, K. J. Beaumont: Analysis of high breaking capacity fuselink arcing phenomena. Proc. IEE, Vol.123, March, 1976.
7. Leach, J. G, Newbery.P.G,Wright.A: Analysis of high-rupturing-capacity fuselink prearcing phenomena by a finite difference method. Proc. IEE, 1973, 120, (9). pp987-993.

ANALYSIS OF PREARCING TIME-CURRENT CHARACTERISTIC OF FUSELINKS.

C. Garrido

and

J. Cidras

Dept. of Electrical Engineering, University of Vigo, P.O.Box 62, 36280-VIGO (Spain).

1. SUMMARY.

This paper presents a model for the calculation of the prearcing time in fuse-links, based on the solution of the equations of electrical potential, current density and heat diffusion, by means of the approximation of the partial derivatives through central finite differences. The variations in the values of the different parameters induced by temperature are taken in consideration. Due to the non-linearity of the equations the solution is obtained through an iterative or Gaus-Seidel relaxation process.

2. INTRODUCTION

Gauged conductors (fuse-links) are used in the industry as a means of protecting equipment and installations against the sudden occurrence of current overloads or short-circuits. In order to adequately employ fuse-links as protecting elements one has to know their characteristic intensity/time curve. Normally experimental laboratory test methods are used to obtain such characteristic curves, which bring about a substantial loss of both time and rejected materials. Consequently, a theoretical model which could allow the accurate prediction of the performance of a fuse-link under different conditions of loading and under short-circuit would undoubtedly have a great potential appeal for designers and testers at fuse-link factories.

Due to the fact that the fuse element usually has complicated geometrical forms (see Fig. 1) and that as a rule such parameters as the electric resistivity, thermal conductivity and specific heat vary with temperature, the analytical techniques approach to the study is not possible but it is necessary to appeal to the numerical calculus to be able to build a valid theoretical model of the performance of the fuse.

Several authors have proposed different models for determining the prearcing-time. Leach et al.<sup>1</sup> developed a model which estimates the distribution of the current density by means of the approximation through finite differences of the electric continuity equation. The current density so estimated is used to find out by application of the law of Ohm, the heat generated inside the fuse, which is also expressed by the energetic equation  $Q=Cp.m.dT$ , where  $Q$  is the

heat generated,  $Cp$  is the specific heat,  $m$  is the mass and  $dT$  is the thermal increment produced by the heat generated. Wilkins and others<sup>2</sup> brought forward a model which uses the approximation of the partial derivatives through finite differences to solve the equations of the electric continuity and heat diffusion. In this model they take into consideration neither the eventual variation of the aforementioned parameters due to temperature nor the eventual heat losses from the fuse element to the surrounding medium (the filling material, usually sand or quartz powder) and to the ceramic core of the fuse.

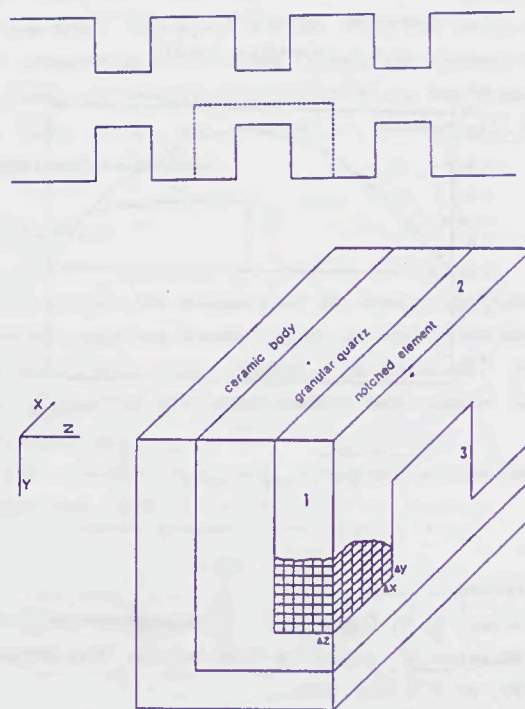


Fig.1: Typical fuselink element, symmetrical part of an element used in our model and finite-difference mesh.

Considering that the electric resistivity of the fuse, the thermal conductivity and the specific heat of the fuse, of the filling material and of the ceramic core vary with temperature, this paper presents a model which uses the method of the finite differences to solve the equations of the electric potential, current density and heat diffusion to estimate the prearcing time in fuses, taking into consideration the variability of the said parameters with variations of temperature.

### 3. MODEL DESCRIPTION.

Considering that the fuse used for the experimental test of the theoretical model presents the shape shown in Fig. 1, by symmetry the part of the fuse shown on the said figure has been used. Although fuses usually present a cylindrical shape, in order to have a simpler modeling we have approximated the cylindrical surfaces which separate the quartz from the ceramic core and the latter from the environment by flat surfaces which contain them. For the evaluation of the prearcing time it is necessary to solve the equation of heat in the fuse using as a source of energy that produced by the Joule effect of current density. Consequently it is necessary to calculate first of all this density.

#### 3.1 Distribution of currents in the fuse.

Considering that a fuse with uniform thickness is used, the current density  $J$  presents components  $J_x$  and  $J_y$  in directions  $x$  &  $y$  respectively, which are related to the components of the electric field  $E$  by:

$$\begin{aligned} J_x &= E_x/\rho \\ J_y &= E_y/\rho \end{aligned} \quad (1)$$

where  $\rho$  is the electric resistivity of the material of fuse and  $E_x$  &  $E_y$  are the components of the electric field in the direction  $x$  &  $y$  respectively. Bearing in mind the relation existing between the electric field and the electric potential  $V$ :  $E = -\text{grad}.V$  and that the divergence of the current density is null (there are neither load sources nor sinks) substituting in (1) gives:

$$\begin{aligned} \text{div}.J &= -\text{div}.\left(\frac{\text{grad}.V}{\rho}\right) = 0 \\ J_x &= -\frac{1}{\rho} \frac{\partial V}{\partial x} \\ J_y &= -\frac{1}{\rho} \frac{\partial V}{\partial y} \end{aligned} \quad (2)$$

The resistivity varies from point to point in the fuse as temperature changes [ $\rho = \rho(T(x,y,z,t))$ ], and bringing this over to equation (2) and operating results:

$$\begin{aligned} \frac{1}{\rho} \nabla^2 V + \nabla\left(\frac{1}{\rho}\right) \cdot \nabla V &= 0 \\ \frac{\partial(1/\rho)}{\partial T} \left[ \frac{\partial T}{\partial x} \frac{\partial V}{\partial x} + \frac{\partial T}{\partial y} \frac{\partial V}{\partial y} \right] + \frac{1}{\rho} \left[ \frac{\partial^2 V}{\partial x^2} + \frac{\partial^2 V}{\partial y^2} \right] &= 0 \end{aligned} \quad (3)$$

To solve equation (3) the following boundary conditions have been assumed:

- 1) on the frontal surfaces which connect the fuse

element with the remaining elements (marked "1" on Figure 1) the distribution of current density is not affected by the presence of the restriction (lengthwise dimensions are usually big enough to hold this as a fact) whereby the current density is constant on each elementary surface, each component presenting the values given by:

$$\begin{aligned} J_x &= -\frac{1}{\rho} \frac{\partial V}{\partial x} = \pm \frac{I}{2 \cdot N \cdot \Delta S} \\ J_y &= \frac{\partial V}{\partial y} = 0 \end{aligned} \quad (4)$$

where  $N$  is the number of elementary areas into which the surface is divided,  $\Delta S$  is its area and  $I$  is the intensity that flows through the fuse. The + sign in the  $J_x$  equation corresponds to the current in-flow surface and the - sign to the current out-flow surface. The division by 2 on the  $J_x$  expression is due to the fact that only one half of the current in and out-flow surfaces is considered.

2) On those boundary surfaces which are parallel to the  $x$  axis (marked "2" on Figure 1) the  $y$  component of the current density is null:

$$J_y = 0 \Rightarrow \frac{\partial V}{\partial y} = 0 \quad (5)$$

3) Finally, on those boundary surfaces which are parallel to the  $y$  axis (marked "3" on Figure 1) the  $x$  component of the current density is null:

$$J_x = 0 \Rightarrow \frac{\partial V}{\partial x} = 0 \quad (6)$$

Through a discretization on the fuse as shown on Fig.1, the approximation of the partial derivatives through central finite differences<sup>2</sup> the electrical potential on a point of discrete coordinates  $(i,j)$  can be obtained and from here the components of the current density are calculated by means of equation 2

#### 3.2 Temperature distribution in the fuse.

To accurately ascertain the distribution of temperatures in the fuse it is necessary to solve the heat diffusion equation, as follows:

$$\begin{aligned} d \cdot C_p \frac{\partial T}{\partial t} &= \nabla(K \nabla T) + Q_v = \\ K \left[ \frac{\partial^2 T}{\partial x^2} + \frac{\partial^2 T}{\partial x^2} + \frac{\partial^2 T}{\partial x^2} \right] + \frac{\partial K}{\partial T} \left[ \left[ \frac{\partial T}{\partial x} \right]^2 + \left[ \frac{\partial T}{\partial x} \right]^2 + \left[ \frac{\partial T}{\partial x} \right]^2 \right] + Q & \end{aligned} \quad (7)$$

where  $d$  is the density of the material,  $C_p$  and  $K$  are its specific heat and thermal conductivity and  $Q_v$  represents the energy generated per unit of volume

and per unit of time in the material. Both  $C_p$  and  $K$  may vary from point to point as temperature changes. To solve equation (7) the following boundary conditions have been assumed as true:

1) By symmetry there is no loss of heat (equal heat flows in both directions) on the surfaces which separate the part under examination from the rest of the fuse, for which reason:

$$\frac{\partial T}{\partial l} = 0 \quad (8)$$

where  $l$  is normal to the separating surfaces. The eventual losses through the external surface of the ceramic core of the fuse are not considered, whereby equation (8) is used for this surface.

This hypothesis is acceptable enough considering that the fuse element is surrounded by quartz grains, which present a very low thermal conductivity thus limiting the heat which passes over to the ceramic core.

2) In the separating surfaces between different materials (copper, quartz and ceramic) the equality of heat-flows in both directions is satisfied:

$$K_1 \frac{\partial T}{\partial l} = K_2 \frac{\partial T}{\partial l} \quad (9)$$

where  $K_1$  and  $K_2$  are the thermal conductivities of the medium 1 and 2 respectively and  $l$  is the normal to the separating surface.

The internal heat generation is due in this case to the Joule effect of the electrical flow and is represented by:

$$Q_v = \rho (J_x(i,j)^2 + J_y(i,j)^2) \quad (10)$$

Bearing in mind the variation in thermal conductivity induced by temperature changes, the new temperature  $T(i,j,k)$  on points of discrete coordinates  $(i,j,k)$  after a discrete interval of time  $\Delta t$ , can be ascertained through the discretization of (7) around central points.

The distribution of the potential with the temperature existing at the beginning of each discrete interval of time or iteration is ascertained through the discretization of equation (3). From the discretization of (2) the current densities can be ascertained and they are used in equation (10) to calculate  $Q_v$ , which applied in (7) permits the obtainment of the new temperature on each point at the end of the interval. The new temperatures substitute those had at the beginning and the process is repeated in subsequent iterations. The process ends

when the fusion temperature of the copper fuse element is reached, thus determining the prearcing time.

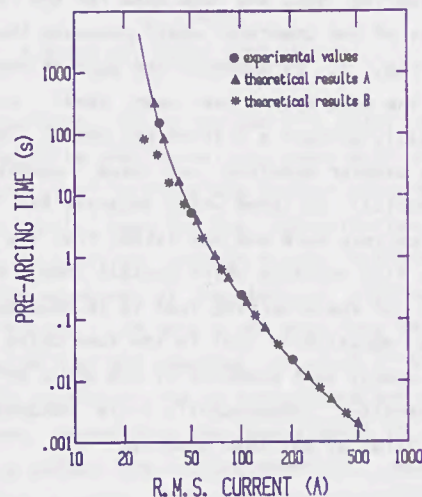


Fig.2: Prearcing time-current curve for a 15 A protection fuselink, 50 Hz symmetrical sinusoidal current.

Table 1: Parameter values of copper used in the model.  $K$ =thermal conductivity;  $\rho$ =resistivity;  $C_p$ =specific heat;  $d$ =density.

$\rho(\Omega m) = 1.785 \times 10^{-8} [1 - 4.1 \times 10^{-5}(T-20) + 0.43 \times 10^{-6}(T-20)^2]$	[4]
$K (W/m^2K) = 418.38 - 6.16 \times 10^{-5} T$	[5]
$K (W/m^2K) = 400$	[5]
$C_p (J/Kg^{\circ}K) = 358 + 0.962 T$	[6]
$d (Kg/m^3) = 8960$	[7]

#### 4. RESULTS.

Figure 2 shows the experimental values and the theoretical results obtained for a fuse with 15 A nominal intensity. Values of parameters are shown on Table I. The theoretical results have been calculated via two different models: through model developed under paragraph 3 Case A results have been reached, whereas on Case B the thermal losses transferred to the quartz powder and the ceramic core have not been taken into account. As shown, both models render identical results for intermediate and high intensities (typical short-circuit values), which coincide with those obtained in laboratory experiments, whereas for intensities close to the nominal intensity of the fuse (typical overload values) the results obtained with the complete model are similar to the experimental values, while those obtained in case B present differences which grow as the intensity values decrease. This results show that the thermal losses by transfer to the surrounding materials of the fuse element are irrelevant for short-

circuit intensities due to the short prearcing times, while they grow bigger as the overload intensity approaches the fuse nominal value due to the longer prearcing times. It is consequently evident that such losses have to be taken into consideration if an accurate model of the performance of a fuse is to be built.

It is interesting to note what effects have some parameters on the performance of the model. Figure 3 shows the temperature reached in the middle of the restriction zone as a function of the current flow-time considering one value for the thermal conductivity of copper as constant and the other as variable. The intensity is 50 A while the remaining parameters vary with temperature. As shown, for short times (low temperatures) similar results are obtained with both conductivity values, and the gap grows with time (and so does the temperature as a result thereof) to the extent that the estimation of the prearcing time with one or the other value of conductivity differ in more than 20%, the minimum value being in no case under 8%. This indicates that if the model is to be adequate the variability of the thermal conductivity of copper as the temperature changes has to be taken into account. Of much less importance is the existence or not of variability in the thermal conductivity of the quartz or the ceramic core because the temperatures on these materials are much lower than those on copper, which implies that the variations in conductivity are so small that they have very little effect on the estimation of the prearcing time.

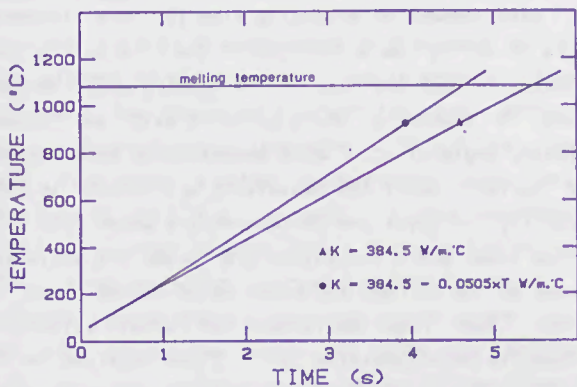


Fig.3: Temperature at the center of the restriction zone as a function of the time for two different values of the copper thermal conductivity.

Figure 4 shows the effect of the circuit closing angle on the thermal development in the middle of the restriction. The intensity is 300 A, using circuit closing angles of 0, 40 and 82° for a sinus function.

A symmetric short-circuit has been assumed, which means that the circuit created presents no reactance.

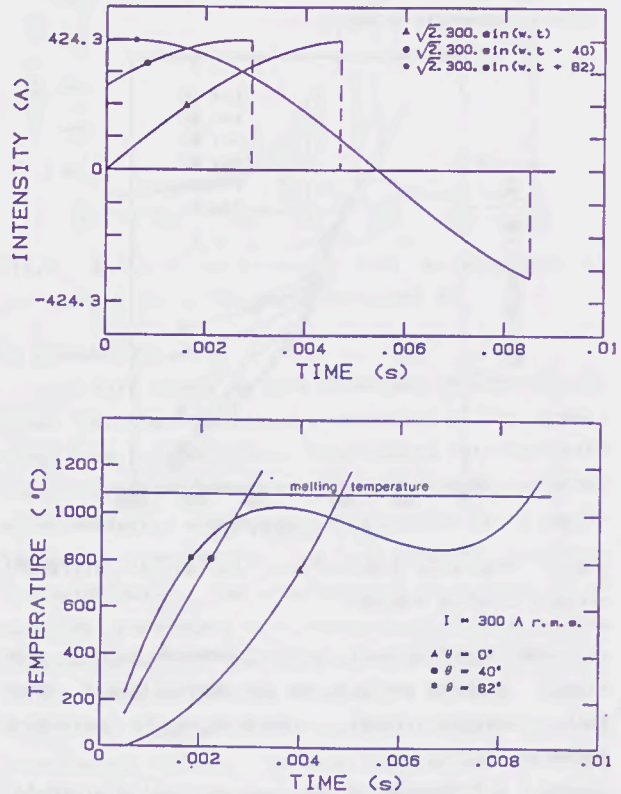


Fig.4: Current intensity and temperature at the center of the restriction zone as a function of the time for three different values of the circuit closing angle.

As shown, depending on the moment the short-circuit is produced (circuit closing angle) the prearcing time obtained varies substantially with differences which are larger than 200% for values obtained with circuit closing angles of 40 and 82°. While for circuit closing angles of 0 and 40° the fusion takes place in the first half-period of the intensity wave, for the circuit closing angle of 82° the fusion cannot take place during the first half-period owing to the high initial stage value, wherefore the temperature -after decreasing slightly- reaches the fusion value (1083 °C) during the 2nd half-period of the intensity wave. This decrease in the temperature is due to the fact that when the intensity wave reaches the null and close to null values, the thermal losses are bigger than the amount of energy brought by the Joule effect. This is shown in detail in Figure 5, which displays the prearcing times as a function of the r.m.s. current for different values of circuit closing angle. As shown, the prearcing time starts to be affected by the circuit closing angle at intensities close to 150 A and the differen-

ces grow with the short-circuit intensity. This shows that the uncertainty in the time it takes a fuse to open increases considerably as the short-circuit intensity grows.

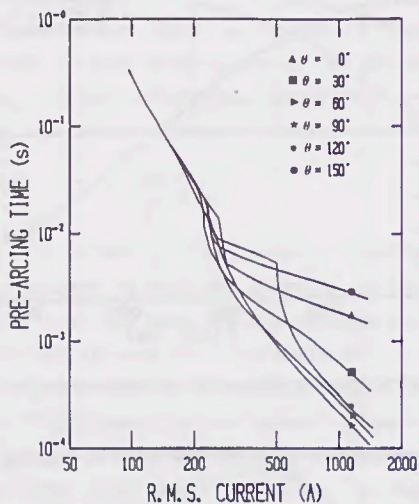


Fig. 5: Prearcing time-current curves for different circuit closing angles.

The short-circuit current depends both on the circuit closing angle  $\theta$  and the short-circuit power factor angle  $\beta$  circuit, according to the following formula:

$$i(t) = 2.I_c[\sin(\omega t + \theta - \beta) - \exp(-\omega t / \tan \beta)] \sin(\theta - \beta) + 2.I \cdot \exp(-\omega t / \tan \beta) \cdot \sin \theta$$

where  $I_c$  is the short-circuit permanent current and  $I$  is the current which flows through the fuse before the short-circuit. One of the advantages of the fuse as against other protecting elements is the capability of the fuse to limit the maximum value of the transient short-circuit current to a value below its maximum peak value. Figure 6 illustrates this limiting effect (cut-off characteristics) for angles of the short-circuit power-factor of 0, 20 & 78°, which represent the maximum transient peak value as a function of the short-circuit permanent current.

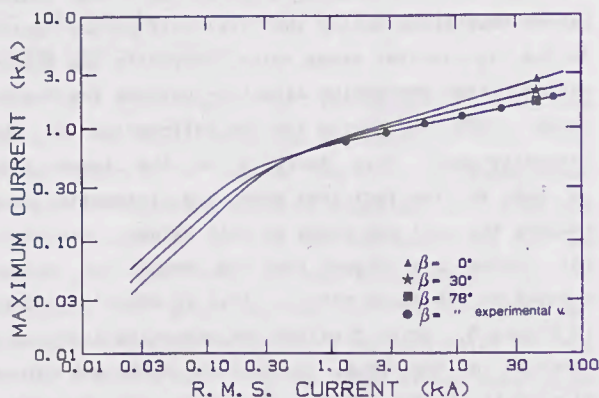


Fig. 6: Fuselink cut-off characteristic for three different short-circuit power-factor angles.

For short-circuit permanent currents under 175, 290 and 350 A, corresponding to angles of 78, 30 and 0° respectively, the fuse exercises no limiting action on the maximum peak transient current due to the fact that the fusion takes place after having reached such a value. Once the limiting effect has started, the maximum value of the thus limited current grows slowly with the increase of the short-circuit permanent current. The limiting effect grows as the impedance short-circuit angle increases. As illustrated the experimental values obtained for an angle of 78° coincide fully with those calculated theoretically.

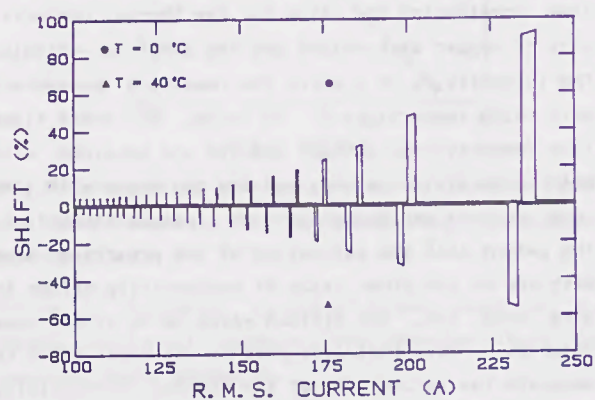


Fig. 7: Shift of the prearcing time (with regard to the prearcing time for the room temperature of 20°) as a function of the current for two different room temperatures.

The effect of the room temperature on the modification of the prearcing time is illustrated in Figure 7, where the deviation is shown in percentages of prearcing time for room temperatures of 0 and 40 °C with respect to prearcing time for room temperature of 20 °C, as a function of the r.m.s. current flowing through the fuse. The results shown correspond to symmetric short-circuits with an circuit closing angle of 0°. With exception of some values of current where the deviations are large, in the majority of cases the deviations are about 1%. In those cases where deviations are large, the deviation grows as the current increases up to values close to 100%. Such huge deviations for certain values of intensity (both positive for 0 °C and negative for 40 °C) are due to the fact that while the fuse reaches fusion for a given number of half-periods of the current wave at 20 °C, at 40 °C room temperature it takes a half-period less, whereas it takes one half-period more for room-temperature of 0 °C. As a consequence thereof the deviation increases as the intensity grows since the relative deviation is larger when the number of half-periods taken to reach fusion decreases. On reaching values of intensities

which make the fuse open in times close to or under one fourth of period, these deviations go down about to 1% because then the difference in room temperature is not enough to cause the aperture in the following half-period. This happens with the deviation by 0°C for obviously at the room temperature of 40° it takes only one half-period. For an intensity of 233 A this is illustrated in Figure 8, where the temperature in the middle of the restriction is represented as a function of time for room temperatures of 20 & 40 °C. As shown, while fusion is reached in the first half-period of the intensity wave ( $t=0.00775$  s) for the room temperature of 40 °C, for the room temperature of 20 °C fusion takes place in the second half-period of the wave ( $t=0.0145$  s). Owing to the difference of 20 ° in room temperature the fusion temperature cannot be reached in the first half-period, although the temperature reached ( $T=1067$  °C) is very close to it.

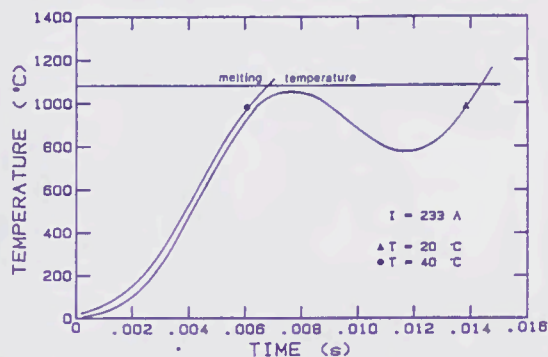


Fig.8: Temperature at the center of the restriction as a function of the time for two different room temperatures.

The effect of variations in thickness of the fuse-element on the prearcing time is shown in Figure 9, where the deviation in prearcing time obtained with a fuse-thickness increased by 5% and the prearcing time with a normal thickness is shown as a function of the r.m.s. current. A room temperature of 20 °C has been assumed. While for intensities over 245 A the deviation in prearcing time is about 7% (because beyond these intensities fusion takes place on both thicknesses within the first wave half-period) at lower intensities the deviation decreases in a discontinuous way after having reached a maximum at 245 A. Such discontinuous decrease is due to the fact that at certain values of intensity fusion is reached within the same half-period on both thicknesses, at other values of intensity fusion takes place one half-period later in the case of the thicker fuse and at other intensities fusion takes place one full period later on the thicker fuse.

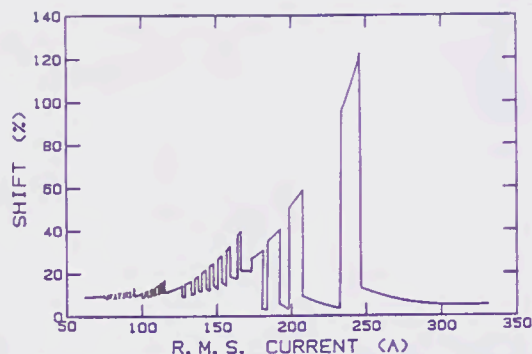


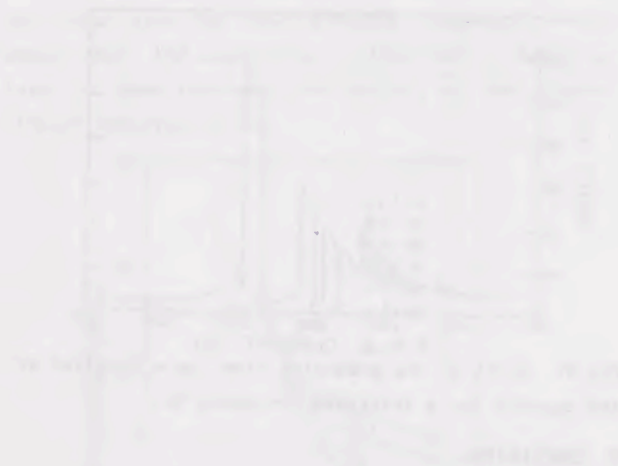
Fig.9: Shift of the prearcing time as a function of the current for a thickness increased 5%.

## 5. CONCLUSIONS

In this paper, we have presented a mathematical model for the theoretical calculation of the prearcing time in fuse-links. The results obtained with the theoretical model coincide with those obtained experimentally, whereby the model proves to be applicable for the design, test and study of fuse-link characteristics. The consideration of variability of equation parameters with temperature as well as the consideration of thermal losses to the materials which surround the fuse element are of major importance for a perfect coincidence of theoretical and experimental values. The model also allows the study of the influence which the variation of the geometry of the fuse element has in the prearcing time as well as the selection of the material most convenient for the fuse specifications required.

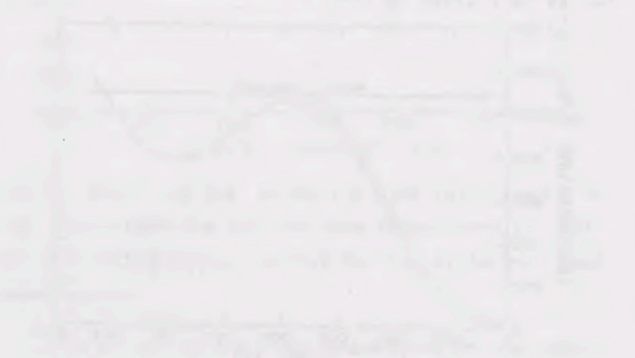
## 6. REFERENCES

- [1] J.G. Leach, P.G. Newbery y A. Wright, "Analysis of high-rupturing-capacity fuselink prearcing phenomena by a finite-difference method", *Proceeding IEE*, 1973, **120** (9), pp. 987-993.
- [2] R. wilkins and P.M. McEwan, "A.C. short-circuit performance of notched fuse elements", *Proceeding IEE*, 1975, **122** (3), pp.289-292.
- [3] D. Euvrard, "Résolution numérique des équations aux dérivées partielles" Ed. Masson, Paris (1988).
- [4] R.G. Lukac, D.A. Silver, R.A. Hartlein and W.Z. Black, "Optimization of metallic shields for extruded dielectric cables under fault conditions", *IEEE Transactions on Power Apparatus and Systems*, 1984, **PAS-103**, pp.3410-3418.
- [5] R.C. Weast, "Handbook of Chemistry and Physics", Ed. CRC Press, Cleveland, Ohio (1974).
- [6] D.E. Gray, "American Institute of Physics Handbook", Ed. McGraw-Hill, New York (1972).
- [7] R.E. Bolz and G.L. Tuve, "Handbook of tables for Applied Engineering Science", Ed. CRC Press, USA (1972).



The graph illustrates the intensity of a signal over time, showing several distinct peaks. The tallest peak is located at approximately the midpoint of the time axis. The peaks are separated by intervals, suggesting a periodic or sequential process. The baseline intensity remains relatively low between the peaks, indicating that the signal returns to a near-zero state between each event. The overall shape of the graph suggests a series of discrete events or measurements recorded over a continuous period.

The data presented in the graph above shows a clear pattern of peaks. The first peak is relatively small, followed by a larger one, and then the tallest peak. This suggests a progression or a change in the underlying process being measured. The intervals between peaks are roughly consistent, which could indicate a regular frequency of events. The final peak is smaller than the previous ones, possibly indicating the end of the recorded period or a change in the signal's characteristics.



This graph shows a single, broad peak, which is significantly wider than the peaks in the first graph. The peak is irregular in shape, with a jagged top, indicating that it may be composed of multiple overlapping components or represents a more complex signal. The rise and fall of the peak are more gradual, and the overall duration of the signal is longer. This could represent a different type of event or a different state of the system being measured, where the signal is spread out over a longer period of time.

**Session 6A**  
**FUSE TESTING**

THE HISTORY OF THE  
CITY OF BOSTON



# Underwriters Laboratories Inc. Standards for Safety for Fuses

Dale A. Hallerberg, P. E.  
Underwriters Laboratories Inc.  
Northbrook, IL U.S.A.

## Summary:

This paper will explain the role of Underwriters Laboratories Inc. (UL) in fuse safety testing and certification. Emphasis is placed on the relationship of UL's standards to the National Electrical Code (NEC<sup>1</sup>), and the general requirements which are common to most UL Listed power fuses.

## Introduction:

For over 95 years, Underwriters Laboratories has tested and certified fuses to standards developed in cooperation with the United States fuse industry and other interested parties. Throughout this time, UL Standards have reflected the safety and performance concerns of the NEC which demand protection of distribution systems, wiring, and utilization equipment from dangerous over-currents. A broad spectrum of tests is used by UL to verify the fuse's performance. These tests include: temperature rise, verification of fuse current rating, full-voltage overload, maximum let-through energy, verification of current-limiting threshold, maximum interrupting capacity, and limitation of let-through current and energy.

For brevity, this paper focuses on power fuses, and no attempt is made to specify every exception or unique case. The exact details of testing, ratings, and requirements are best stated in the standards themselves.

## 1. UL Background

### 1.1 UL History

Underwriters Laboratories is the world's largest independent product safety testing and certification organization. UL was founded in 1894, in response to the alarm-

ing number of fires caused by the new electric light bulb at the Chicago Columbian Exposition. Now, 97 years later, UL continues testing a wide variety of products for safety, as well as performing research testing, developing safety standards, working with local inspection authorities, and educating the public about safety.

### 1.2 UL's Standards and the NEC

In order to assure that all manufacturers of a similar product are treated equitably, consistent standards must be applied. UL develops such product standards through cooperation with manufacturers and other interested parties, taking into consideration the users of the product and any installation codes that apply, such as the NEC.

It is important to note the strong correlation between the NEC and UL's fuse standards. The NEC is an installation code which contains provisions necessary for practical safeguarding of persons and property from hazards arising from the use of electricity. It contains a number of specific requirements for fuses, as well as several general items which also apply. UL's standards are based on the same overall premise of safety, and are carefully written to support and complement the requirements of the NEC with specific requirements for fuses. The result of this relationship is a symbiosis which benefits both fuse users and manufacturers by enhancing the level of electrical safety.

### 1.3 UL Certifications

UL has three types of safety certification: UL Listing, UL Classification, and UL Component Recognition. The type which applies to power fuses is UL Listing.

Products which are Listed by UL have been found to be

in compliance with UL's requirements for the category of equipment involved; they bear the Listing Mark of Underwriters Laboratories. Fuses used to protect distribution systems must be Listed, and all Listed products must meet identical requirements for the specific rating and size involved. They are also required to be suitable for installation in accordance with the NEC<sup>2</sup>. They are considered to be physically and electrically interchangeable with other Listed fuses of the same Class and rating.

#### 1.4 UL Fuse Standards

UL currently has several published standards for power fuses summarized in Table 1.

UL also has published standards for the following fuses: Supplemental Fuses, UL 198G; DC Fuses for Industrial Use, UL 198L; and Mine-Duty Fuses, UL 198M. Special purpose fuses, new or innovative fuses, or novel ratings for a product can be accommodated by using related requirements from UL's present standards, or by evaluating the safety risks involved and designing a new test program to encompass these risks. A common misconception concerning UL is that products outside the scope of present standards cannot be certified. On the contrary, UL is willing to devise an appropriate investigation for any product.

## 2. Fuses for the Protection of Distribution Circuits

UL tests and certifies a broad range of power fuses which are intended to protect power distribution circuits, switching equipment, and wiring. These circuits are often called "branch circuits" because they begin at the utility entrance to the building and branch out to usage equipment around the facility. Several types or Classes of fuse are used to protect these circuits, including Class G, H, J, K, L, R, T, CC, and Plug fuses. The major characteristics of these fuses are summarized in Table 1. Examples of applications of these fuses would be protection of a switchboard, switch, or individual circuits supplied by a distribution panelboard.

### 2.1 Voltages Common in The United States

Several low voltage (600 V ac and less) distribution systems are used in the U.S., depending on the local utility and the needs of the user; voltages of 120, 208, 240, 277,

480, and 600 V are available. These systems are protected by Class G, H, J, K, L, R, T, CC, and Plug fuses with corresponding voltage ratings. A 600 V fuse can be used on any of these circuits, but lower voltage rated fuses are generally smaller, and thus using the closest sized voltage rating will allow the switching equipment to be downsized as well.

### 2.2 Current Ratings

The UL system of fuse classes divides each fuse class into several distinct sizes based on the current range in that size, as shown in Table 1. Intermediate ratings which are between the case size breaks have the same overall dimensions as the next larger case size. For example, ratings of 31-60 A are all sized the same.

### 2.3 Interchangeability

The UL standards for fuses include detailed requirements for the physical dimensions of the fuse. These requirements result in Listed fuses of the same Class, voltage, and current rating being consistent in size so that a cleared fuse can be easily replaced. However, the differences between designs of the fuse Classes and case sizes is such that no fuse is interchangeable with one of a higher voltage rating, lower current rating, lower interrupting rating, or different Class. This is a requirement of the NEC<sup>3</sup>, and an essential aspect of UL Listed fuses; they can be used with confidence that improper replacement is unlikely. This also means that safety is not diminished by allowing replacement by untrained personnel. For example, a Class H fuse rated 100 A and 250 V has a 10 kA interrupting rating and will only fit in a fuseholder specifically designed for these ratings. A Class R, 100 A, 250 V fuse (with a 200 kA interrupting rating) is the same size and will fit into the same fuseholder. The reverse substitution cannot be made because a Class R fuseholder has a rejection feature which allows only Class R fuses to be installed. Thus the lower interrupting rating Class H fuse cannot be installed in a Class R fuseholder where a short circuit current above its rating might be available.

### 2.4 High Interrupting Capability

The design of utility power systems in the United States is such that many industrial and commercial installations have very high available short circuit currents at the

Table 1

Fuse Class	UL Standard	Voltage Ratings	Current Ratings	Interrupting Rating, A rms	Sub-Classes	Size Breaks are at the following Ampere ratings:
G	UL 198 C	300	0-60	100,000	-	15, 20, 30, and 60
H	UL 198 B	250 or 600	0-600	10,000	Renewable and Nonrenewable	30, 60, 100, 200, 400, and 600
J	UL 198 C	600	0-600	200,000	-	30, 60, 100, 200, 400, and 600
K	UL 198 D	250 or 600	0-600	50,000, or 100,000, or 200,000	K1 and K5	30, 60, 100, 200, 400, and 600
L	UL 198 C	600	601-6000	200,000	-	800, 1600, 2000, 2500, 3000, 4000, 5000, and 6000
R	UL 198 E	250 or 600	0-600	200,000	RK1 and RK5	30, 60, 100, 200, 400, and 600
T	UL 198 H	300 or 600	0-1200	200,000	-	30, 60, 100, 200, 400, 600, 800, and 1200
CC	UL 198 C	600	0-30	200,000	-	30
Plug	UL 198 F	125	0-30	10,000	"Edison Base" and Type S	30 15, 20, and 30

Notes: RK1 and K1 fuses have a high level of current limitation  
RK5 and K5 fuses have a moderate level of current limitation

power entrance to their building. Calculated available currents of over 100,000 A rms are common, and for this reason, the industry and UL have selected 200,000 A as the necessary interrupting capability for Class R, L, J, T, and CC fuses. Equipment which uses fuses (Class G, H, and Plug) that have a lower interrupting rating can have interrupting ratings only up to that of the fuse. Class K fuses, because they are interchangeable with Class H fuses, are considered as having a 10 kA interrupting rating for the purpose of fuseholders and usage equipment.

The UL requirements for interrupting testing and ratings are based on Section 110-9 of the NEC. This Section requires equipment which is intended to break current at fault levels to have an interrupting rating sufficient for the system voltage and maximum available short-circuit current.

The ability to simply withstand high fault currents is not enough for many design engineers; in order to determine whether downstream equipment is being suitably protected, they need information on how much current and energy the fuse will allow to pass under short circuit conditions. This need is met by UL Standards which require fuses to meet certain maximum let-through lim-

its when tested at high fault currents. Two specific let-through limits are applied to each fuse size, the peak let-through current,  $I_p$ , and the let-through  $I^2t$ .  $I_p$  is simply the maximum instantaneous current which the fuse lets through during clearing, and is a general indication of the magnetic forces which will be imposed on the equipment.  $I^2t$  is the integral sum of the square of the current during the fuse clearing; it represents the heat energy let through during clearing. Use of let-through information allows system designers to choose fault protection devices which will coordinate to isolate a particular fault without shutting down other circuits. This coordination is required by the NEC<sup>4</sup>.

### 3. Verification of Fuse Characteristics

In order to verify the suitable performance of fuses, samples are tested on several different circuits intended to cover the complete range of possible field situations. Levels of test current range from 110% of the fuse rating (where the fuse shall not clear), through low overloads, to high short-circuit available currents up to 200,000 A.

The maximum ampere rating in each distinct size of fuse

is tested (See Column 7 of Table 1) and represents the range of ampere ratings in that size (eg. 31-60, 61-100 etc.). Any major construction change within a size is also tested; this is common in the 30 A case-size where testing may be needed on a few design breaks in order to properly represent the entire range of ampere ratings.

### 3.1 Verification of Ampere Rating

Several tests are used to verify the ampere rating assigned to a fuse. These tests are not voltage sensitive and thus are performed at a convenient low voltage. The normal test program includes the following tests:

**3.1.1 110% Current-Carrying Capacity:** Fuses are placed in properly sized fuseholders and 110% of their rating is passed through them until they show thermal stability. This test shows the current-carrying ability of the fuse under open-air conditions, which is considered equivalent to the normal maximum load of 80% in an enclosure mandated by the NEC<sup>5</sup>. Temperatures are monitored during the test and must be within set limits. These limitations control the maximum temperatures so the thermal limits of fuse and fuseholder materials and conductor insulation are not exceeded.

**3.1.2 Verification of Clearing-Time:** The time required for the fuse to clear while carrying 135% and 200% of its current rating must be within the limits specified in the appropriate standard. These tests ensure that low overloads are cleared before circuit conductors and equipment are damaged by overheating.

135% Limits		200% Limits			
	Max.	Max.		Max.	
Fuse Rating	Clearing Time	Fuse Rating	Clearing Time	Fuse Rating	Clearing Time
0-60	1 h	0-30	2 m	101-200	8 m
61-600	2 h	31-60	4 m	201-400	10 m
		61-100	6 m	401-600	12 m

Fuses rated above 600 A (Class L and some Class T) are not tested at the above levels, but are required to clear in less than 4h at 150% of current rating.

Fuses specified as "Time-Delay" (discussed below) are allowed longer times to clear at 200%.

**3.1.3 500% Time-Delay:** Fuses which are designed to not clear during short-term overcurrents, such as motor startup, may be designated "time-delay". To obtain this designation, the fuse must not clear within 10s while carrying 500% of rated current. Thus, loads which have fairly high inrush currents of short duration will not cause nuisance clearing of the fuse.

### 3.2 Overload at Full Voltage

In order to evaluate the fuse's ability to clear an overload under full voltage conditions, the fuse is tested at 200% of its rating at rated voltage, with a power factor of 0.8 or less. This test confirms the fuse's ability to operate under overload conditions encountered in everyday use. This is also a test of the materials and construction of the fuse, since this overload will create high temperatures in the fuse, and the fuse must extinguish a full-voltage arc in its overload section.

### 3.3 Verification of Current Limiting Threshold

The term "current-limiting" is associated with Class G, J, L, R, T, and CC fuses. These fuses have a certain threshold above which they limit the instantaneous peak current,  $I_p$ , to a value less than what is available from the circuit, and they will clear in less than 1/2 cycle. This threshold is confirmed by the Maximum Threshold Ratio Test as follows: The available current of the test circuit must be equal to or less than the product of the current rating of the fuse multiplied by the defined threshold ratio for the Class of fuse. The circuit closing is controlled at approximately 90° on the voltage wave and the fuse must clear in less than 1/2 cycle. As an example, a 60 A, Class T fuse has a threshold ratio of 30, and thus must be tested on a 1800 A or less circuit. The circuit is closed at 90° on the voltage wave and the fuse clears at 190°, for a total of 100° to clear. This conforms to the requirements of the standard because the fuse cleared in less than 1/2 cycle (180°).

### 3.4 Verification of Short-Circuit Interrupting Ability

Each short-circuit test is performed at full rated voltage and with a relatively low power factor (0.5 or less for 10 kA circuits, 0.2 or less for circuits above 10 kA). Circuits above 10 kA use controlled closing of the test circuit so the fuse element begins to arc at a point 60° to 90° after voltage zero, typically the most difficult arcing point.

Class H and Plug fuses are not tested above 10 kA since this is their interrupting rating.

#### 3.4.1 Maximum Energy Test

The objective of the maximum energy test is to confirm that each fuse can interrupt a test circuit where the fuse permits a let-through current of 70-100% of the peak available current in the circuit. This criterion subjects the fuse to test at a point where the maximum energy must be absorbed by the fuse.

#### 3.4.2 Interrupting Ability Test

This test verifies the capability of a fuse to safely clear a circuit with an available short-circuit current equal to its interrupting rating (See Table 1 for Interrupting Ratings). For example, Class J, L, R, T, and CC fuses have an interrupting rating of 200 kA and are tested on a circuit calibrated to deliver a minimum of 200,000 rms symmetrical amperes.

#### 3.4.3 Verification of Conformance to Let-Through Limits

As discussed in paragraph 2.4, UL's standards require high interrupting capacity fuses to meet certain let-through limits for  $I_p$  and  $I^2t$  when tested at high fault levels. This assures users of fused equipment that excessive let-through current or energy will not be allowed by a replacement fuse.

The limits for fuse let-throughs correlate with fused equipment testing which requires the use of special test fuses which exceed these limits. Thus, any UL Listed fuse of the correct type is suitable for the equipment. The equipment will be marked with the proper fuse Class.

#### 4. Follow-Up Testing

In addition to the above testing which verifies the performance of new fuses, the NEC<sup>6</sup> also requires that all product Listings include provisions for periodic inspection of products during production. This requirement arises because new products carefully prepared for certification do not always represent those manufactured for sale to users. As a result, UL has a program for regular inspec-

tions of each manufacturer's ongoing production. UL Field Representatives make frequent, unannounced visits to factories to review production controls and conduct detailed inspections. In addition to these follow-up inspections, fuses require follow-up testing since they are complicated combinations of materials which make a simple visual inspection incomplete and since they are so vital to the safety of the electrical system. UL performs regular follow-up testing on fuses which is very similar to the original testing.

#### 5. Conclusion

The combination of several elements in UL's approach to fuse certification produces a line of fuses which provides closely sized overcurrent protection to an enormous range of fuse applications. Non-interchangeability, broad test requirements, let-through limitation, and follow-up inspection and tests are all imperative to UL's process. The genesis of these requirements is the National Electrical Code, providing the safety foundation upon which UL's fuse standards rest. By specifying construction and test requirements, Underwriters Laboratories' standards for fuses make a vital contribution to the overall level of safety in the use of electricity.

#### Footnotes:

- [1] National Electrical Code, NFPA 70 - 1990. National Fire Protection Association, Quincy, MA. All references to the National Electrical Code are to the 1990 edition.
- [2] Ibid, Section 110-3.a(1).
- [3] Ibid, Section 240-60.b.
- [4] Ibid, Section 240-12.
- [5] Ibid, Section 384-16.c.
- [6] Ibid, Article 100 - Definition of Listed.

#### Further Information:

Further information may be obtained by contacting the author at:

Underwriters Laboratories, Inc.  
333 Pfingsten Road  
Northbrook, IL 60062 U.S.A.

Phone: 708-272-8800

FAX: 708-272-8129

# Developments in Small Dimension Fuse Technology and the Impact on a Third Party Independent Certification Organization

Douglas Porteus  
Underwriters Laboratories Inc.  
Melville, NY, USA

## 1. Summary

A brief introduction to Underwriters Laboratories Inc. as a third party independent certification organization will be followed by a discussion of the historical evolution of the UL Standard for Supplementary Fuses, UL198G. The impact of technological advances on the Standard and UL will be noted, as will the UL involvement in the field of international harmonization of small fuse performance requirements.

## 2. Third Party Certification Organizations

### *2.1 In General*

There is a definite need for organizations that can certify that the performance of a product complies with established norms. Such organizations serve to demonstrate that a particular product actually does comply with a formal set of requirements, without bias or a vested interest in the products ultimate profitability. The economic interests of the manufacturer or of a particular segment of industry thus do not influence the determination of product compliance.

Underwriters Laboratories Inc. fulfills the role of a third party certification organization because, as a not-for profit private corporation that does not have any stock holders, it does not market any products and thus has no direct financial reason to endorse or certify a product. Over the years UL has earned and maintained a reputation of fairness. UL has done so not only in the area of product certification, but also in the promulgation of the Standards to which products are evaluated.

### *2.2 UL as a Test Authority*

One way that UL has earned a reputation for fairness is that UL Standards insure that the results obtained during a product evaluation are capable of being repeated with similar or identical results. This demonstrates the level of equality inherent in the test methods and test requirements, and also allows for additional verification of results should a dispute arise. The need for expensive and complicated tests and test equipment has been kept to a minimum, primarily so that smaller manufacturing organizations will have the same opportunity to design, research, and test a product as will the multi-national conglomerates.

### *2.3 UL as a Developer of Standards*

A test authority can maintain a reputation for fairness only if the Standards used for product evaluations allow the determination of compliance to be made in a manner which is inherently unbiased. When UL undertook the responsibility to develop standards, the need for equanimity in standards became a basic part of the approach to accomplishing this task.

As a result, UL has made major efforts to write standards that do not demonstrate favoritism of any kind, and that are not biased in favor of a particular type of product or a particular manufacturer. In so doing, UL has sought input from as many interested sources as possible. The efforts to maintain impartiality do not cease when a standard has been initially published, but continue for any revisions of the standard as they may become necessary.

An additional consideration that has guided UL in the development of standards is that designers of products should be as free as practicable to incorporate technological advances and other factors into their product designs, in an atmosphere of non-restrictive trade.

### *2.4 UL as a Safety Organization*

While fulfilling the roles of test authority and developer of standards, Underwriters Laboratories is also an organization whose prime concern is public safety. Accordingly, when a UL Standard is being developed or revised, the standard must serve to provide a level of safety that is commensurate with the product, the uses to which the product will be put, and the people who will use the product. The UL concern for safety means that any UL Standard is really a UL Standard for Safety, rather than merely a set of construction and performance requirements designed to test the products marketability.

A consequence of this concern for safety is that technological advances which may benefit a concerned industry may not always be incorporated into a UL Standard. Any proposed revision that dilutes the level of safety provided will not be considered.

However, in order to keep up with technical advances in a particular field as covered by the scope of the Standard, and

which can serve to improve the level of safety provided, UL constantly monitors the industry. And UL frequently provides updated revisions in order to satisfy the continuous feedback and response mechanisms.

Similarly, when a product is being evaluated and tested, if any feature of the product is observed that reduces the level of safety provided to a level which is less than that contemplated by the standard, the product may be deemed ineligible for third party certification by UL, even if it meets all the literal requirements of the standard.

Conversely, there is also a need to acknowledge that technological changes may yield a product that does not meet all the exact requirements of the standard, but that does not compromise the level of safety required. Such a product can be eligible for third party certification if the organization responsible for the certification is able to be flexible in its approach to the certification process. As we shall see, UL is such an organization.

### 3. The UL Safety Standard UL198G

#### *3.1 Background*

The requirements for what used to be called "Miscellaneous Cartridge Fuses" were originally added to the UL Standard for Fuses UL198. This standard was for what are now called Class H cartridge fuses and Plug fuses of the Edison base type and those designated Type S.

UL198 formed the nucleus of what later became the entire series of UL fuse standards, and served as the starting point for further fuse standards development. The levels of safety contemplated by UL198, in the form of required test parameters, influenced the development of all subsequent fuse standards.

In terms of test and performance parameters, the requirements for "Miscellaneous Cartridge Fuses" contained in UL198 were basically the same as those already existing for the regular type of cartridge fuses. An important difference in the construction requirements for the miscellaneous fuses was that the physical dimensions were not specified.

This was a direct response to the fuse industry and the various industries that used fuses. Leaving the dimensions unspecified provided the opportunity for third party certification of fuses that had many legitimate uses but which as a consequence of the application also needed to have unconventional shapes and sizes.

In 1972, UL undertook the development of a separate standard for miscellaneous fuses, and during the early

discussions it was decided to include the additional classifications of "miniature" and "micro" fuses. This decision was based on the needs of the industry, which reflected the technological developments of the time.

#### *3.2 The First Edition - UL198.6*

Because the origins of the miscellaneous fuse requirements lay within UL198, certain performance values which had been applicable to the regular type of cartridge fuses were retained for the miscellaneous and miniature fuses when the First Edition of the Standard for Fuses For Supplementary Overcurrent Protection was published on August 24, 1974, with the designation UL198.6.

Performance requirements that were passed on to the miscellaneous and miniature fuses included the 10000A interrupting ability requirement, as well as the test values of 110%, 135%, and 200% of rated current for temperature, current carrying ability, and clearing time evaluation. Micro fuses were given a different set of test parameters in view of the differences in intended use and physical characteristics.

The test values noted above had been chosen years before as the values appropriate to demonstrate an acceptable level of overcurrent and short circuit protection for conductors, as well as for switching and utilization equipment, during the early stages of development of the electrical industry in the United States of America. By the time the first edition of the supplementary fuse standard was published, the need for fuses with a higher interrupting ability rating was apparent. For this reason miscellaneous fuses were able to be rated up to 100,000 amperes, but could not be rated any less than 10,000 amperes. The 10,000A level was kept for the miniature fuse for several reasons, including consistency with other fuse types, and the general agreement by the fuse industry that this value was within the capability of the extant fuse designs.

The micro fuse was assigned an interrupting rating of 50 A at 125 volts ac, based on its anticipated uses and physical characteristics, as previously mentioned. The micro fuse test levels for current carrying ability and temperature, and clearing time verification tests were chosen to be 100%,

150%, and 200% of rated current for the same reasons.

The first edition of the Standard UL198.6 formalized the definitions of what UL identifies as miscellaneous fuses, miniature fuses, and micro fuses, and also formalized the set of performance parameters for these types of fuses.

### 3.2.1 *UL Supplementary Fuse Dimensions*

In keeping with the flexible approach to dimensions for the miscellaneous fuses that had been found in UL198, the First Edition of UL198.6 gave the requirements for the dimensions<sup>1</sup> of the various fuse types in general terms, so that many shapes and sizes would fall under the scope of the Standard.

Miscellaneous fuses have specific dimensions if they are of the ferrule type, and if so, they shall be either 13/32 inch (10.3mm) or larger in diameter, or 1-1/2 inch (38.1mm) or longer in length. If the fuse is not of the ferrule type the dimensions and shape are not specified.

A miniature fuse has envelope dimensions of a) not larger than 9/32 inch (7.1mm) in diameter and 1-7/16 inch (36.1mm) long, and b) not less than 0.197 inch (5mm) in diameter if 0.787 inch (20mm) or longer, or 1/4 inch (6.3mm) in diameter if 5/8 inch (15.9mm) or longer.

A micro fuse also has envelope dimensions. They are a) if tubular shaped with terminals on each end they must fit within the outline 0.197 inch (5mm) in diameter and 0.394 (10mm) long, b) if cylindrical shaped with fuse terminals from base, they must fit within the outline 0.315 inch (8mm) in diameter and 0.394 inch (10mm) high, and c) if rectangular prism shaped with fuse terminals from base, they must fit within the outline 0.236 inch (6mm) wide, 0.394 inch (10mm) high, and 0.591 inch (15mm) long.

### 3.3 *The Second Edition - UL198G*

The Second Edition of the small dimension fuse Standard was published on October 23, 1981. By this time the old Standard UL198 had been retired, and replaced by a number of fuse standards, each dealing with a specific class or a group of classes of fuses. For administrative reasons, the designation of the second edition was changed to UL198G.

The second edition was basically a reissuing of the first edition, with very little change.

### 3.4 *The Third Edition Of UL198G*

The Third Edition was published on February 3, 1988. While the technical specifications including the dimensions have either not changed or not changed substantially from the original, many minor changes have been incorporated into the 3rd Edition in response to the input from concerned parties.

While it is true that the technical requirements of UL198G remain much the same as originally contained in earlier editions, technological advances in the fuse industry have not been ignored. Many needs of the industry have been met on an internal basis, and thus are not as visible as are revisions to a published UL Standard.

This includes the acquisition of a trained, experienced, and knowledgeable staff who can get the job done. And, because UL can be flexible in the approach to third party certification, and also because UL can offer more than one type of third party certification, (as will be discussed below), the job can often be done without the need for formal revision to the Standard.

One area in which UL has responded to the fuse industry is in the number of samples required for test purposes. Many years of test experience demonstrated that the level of safety provided by the original Standard would not be lessened if the number of samples used for testing was reduced. Accordingly, later versions of the Standard provided for reduced sample amounts. For example, the number of glass cartridge miniature fuses with press on ferrules needed for interrupting ability testing has been reduced from the original 10, to 5.

The third edition of the small dimension fuse standard remains in effect at this time. However, as previously mentioned, as a UL Standard UL198G is always under review and UL welcomes any input from interested parties with regard to revising the standard to accommodate technological advances which contribute to fuse performance without reducing the level of safety provided.

## 4. UL Listing and Component Recognition For Supplementary Fuses

A fuse which meets *all* of the performance requirements of UL198G is eligible for UL Listing. The UL Listing Mark identifies the fuse as one which has been fully evaluated to the Standard.

UL also offers a service to fuse manufacturers and fuse users which differentiates UL from most third party certification organizations. Under the Component Program, a fuse may be evaluated that does not meet one or more of the requirements of UL198G. A Component Recognition is conditional, that is, it delineates the known limitations of the fuse performance, including variations from the Standard, and requires that the particular application of the fuse in an end product be evaluated by UL to determine that the fuse is being used in accordance with the limitations of use.

Under the Component Program, many supplementary protection fuse types have been tested by UL and certified for use in applications where the suitability of the combination (fuse and end product) is to be determined by UL.

The flexibility of the Component Program serves two important functions. The first is that a UL Standard need not exist for a fuse to be third party certified. This means that testing can be performed to verify fuse operation to a wide variety of parameters, including those developed by other organizations.

The second is to allow for the manufacture of fuses which do not meet each and every requirement of the existing UL Standard, with the knowledge and understanding that such fuses serve legitimate needs in legitimate applications.

In such applications, particular or limited performance characteristics may be an asset rather than a liability, and the Component Program of Underwriters Laboratories specifically addresses the need for third party certification in this area.

The inherent flexibility of the Component Program contributes strongly to UL's ability to third party certify fuse performance without the need to constantly revise the fuse standard.

#### 5. UL 198G and Fuse Technology Advances

The small dimension fuse industry has been directly influenced by the electronics industry. Electronic components have undergone a practically continuous reduction in size. Advances in miniaturization of electronic components have impacted on the fuse industry because it is still desirable to protect the miniaturized components and associated circuitry. The fuse intended for direct insertion in printed wiring boards was among the first responses to the evolution in electronic circuitry techniques.

UL accommodated this type of fuse in the First Edition of UL198.6, by including miniature fuses with "pig tail" leads and micro fuses with "terminals from base".

Now many components have been made small enough to be mounted directly on the surface of printed wiring boards, and the fuse industry has developed a number of types of surface mounted fuses (called SMT for surface mount type) as a direct response to the needs of those industries which use fuses.

UL198G, in its present form, does not address the SMT fuse. However, UL has been asked to provide third party

certification of safety/performance by a number of manufacturers of SMT fuses.

The UL philosophy has always been that a product which has a form of construction differing from that described in a particular Standard may be examined and tested according to the *intent* of the Standard, and thus may be deemed eligible for UL Listing or UL Component Recognition, and Follow-Up-Service.

This position, which is formally stated in the Forward to every UL Standard, allows the SMT fuse to be tested by adapting the test methodology to fit the product.

In the past, UL has adapted many test methods, such as using a printed wiring board with samples soldered in place, to test the many different types of fuses being submitted for certification.

Working with fuse manufacturers to come up with suitable test methods and procedures has resulted in the desired third party certification of safety in many instances, even when the product being investigated is outside the literal scope of the Standard.

This is a further example of how technological advances have impacted on UL. While UL198G has not yet been revised to specify new ways to conduct fuse testing, UL has changed the way in which some fuses are tested because the changes in fuse designs have in some case rendered the old test methods inadequate. UL also acknowledges the need to change test methodology so that the test results more accurately reflect the fuse performance that will be observed in real world applications.

UL does not need to wait for the Standard to catch up to the industry before investigating a product.

#### 6. The Universal Modular Fuse (UMF)

##### *6.1 Background*

The International Electrotechnical Commission has been attempting to develop requirements for a small dimension fuse that would have universal application and universal evaluation. If all third party certification organizations treat the fuse identically, then the UMF can be regarded as truly universal. Otherwise, the identifying mark of one organization may be judged in some cases and localities as being superior to the mark of another organization, and in other areas as inferior.

With the desired goal of agreeing to a policy that would ultimately yield a UMF that was internationally equivalent, a

meeting was held at the corporate headquarters of UL in April 1987. At the meeting were officials of UL as well as of the IEC. Also attending were a number of interested fuse manufacturers and users.

Agreement was reached on two important items. One was that UL would support the acceptance of a single international fuse standard with active participation in its development. The other was that the gates of 1.25 ("non-fusing") and 1.7 ("fusing") would be reserved by both UL and the IEC as applicable to the UMF and to no other fuse type.

#### 6.2 UL participation

The writer has been involved with UL/IEC activities since 1984-1985, and is a member of the Working Group that has been charged with the responsibility to develop the UMF requirements. At many WG meetings, the question has been asked "What will UL do when the UMF documents are finalized, and what service will UL provide to manufacturers of UMFs?". The answers to these questions were given by Mr. Donald Mader, Vice President of UL, during the WG meetings at Orlando Florida, USA, in January 1989.

UL will use the UMF documents as a basis for a UL Standard, which will be developed via the UL standards development process. UL will then be in a position to offer Listing and Follow-Up-Service to manufacturers of UMFs.

#### 6.2 Follow-Up Service for UMFs

UL differs from many third party certification organizations by conducting ongoing follow ups after an initial certification has been issued. The historical UL follow up for fuses has been comprised of two parts, working together.

Factory inspection is the mechanism by which the fuses being constructed at the manufacturer's factory are compared to a photographic and written description to see that the present construction is the same as that originally evaluated. This verifies continued compliance with the *construction* requirements of the Standard.

Samples are also selected by the UL Field Representative from production samples, and these sample are subjected to Follow-Up-Testing to verify continued compliance with the *performance* requirements of the Standard.

The IEC Working Groups are attempting to develop a scheme for reducing the number of samples tested during an initial submission to a test authority, based on the "homogeneous series" concept. This type of test approach has historically been used by UL when testing fuses. If an IEC

scheme can be agreed to and adopted, the position of the WGs has been that a mandatory plan of follow-up testing must be implemented simultaneously. Accordingly, a follow-up plan has also been under discussion.

At this time, it appears likely that the technical work on the UMF will be finalized before agreement is reached on the reduced sample testing scheme and a follow-up testing plan. The first draft of the UL UMF Standard may therefore be developed with the understanding that, in the absence of an IEC reduced testing scheme and follow-up testing plan, the historical approach to fuse testing will be utilized and that the historical type of UL Follow-Up-Service for fuses will be applicable to the UMF.

In the event that the Working Groups need a substantial amount of additional time to agree on the reduced testing scheme and the follow-up plan, the First Edition of the UL UMF Standard may be published without the incorporation of these aspects of the IEC endeavors. However, it is hoped that while the UL UMF Standard is still going through the development process, the IEC will finalize the reduced sampling and follow-up concepts. They can then be introduced into the UL documents before publication.

In this way the UL and IEC requirements can be truly harmonized, and the culmination of years of efforts and years of technological advances will be a truly universal fuse.

#### 7. Conclusions.

The UL Standard for Fuses for Supplementary overcurrent Protection UL198G has evolved, and continues to evolve, with due regard for public safety, the needs of the concerned industry, and technological advancements.

The methods used by UL to conduct small dimension fuse evaluations have changed in response to the design changes in the fuses being tested.

The UL Listing and Component Recognition Services for fuses fill the ever growing need for third party certification of fuse performance, and do so with a degree of flexibility that cannot be achieved by other organizations. UL can respond quickly to technological advances that are beyond the immediate scope of the written requirements.

UL has supported, and continues to support the international efforts for harmonization of standards, and will continue to participate in developing the Universal Modular Fuse requirements.

[1] Underwriters Laboratories Inc., Standard For Fuses For Supplementary Overcurrent Protection, UL198.6, 1974, Pages 6,7.

THE EFFECTS OF SUPPLY FREQUENCY ON THE PERFORMANCE  
OF A.C. FUSES

R V Wafer  
GEC Alsthom  
Installation Equipment Ltd  
Liverpool U.K.

and

D Osypiw  
Liverpool Polytechnic

SUMMARY:

Computer programs are used to predict the short circuit performance of a.c. fuses at various supply frequencies. Two ranges of low voltage fuses are examined in this way to compare their performance at 50 Hz and 60 Hz. The 400 Hz performance of L.V. fuses is also considered because they are occasionally used at this frequency. Finally, the performance of high voltage fuses, normally used at 60 Hz, is examined when they are installed in a 25 Hz system. Such practice sometimes occurs in North America.

1. INTRODUCTION

Most of the world's a.c. electricity is generated at 50 Hz or 60 Hz. There are some exceptions for which fuse manufacturers have to cater, e.g., 400 Hz in some low voltage applications and 25 Hz in some high voltage installations.

Fuses are therefore proved at either 50 Hz or 60 Hz, and the validity of the resulting test data is sometimes questioned when fuses proved at one frequency are proposed for use at the other. Thus the North American Standards [1,2] specify maximum values of  $I^2t$  and peak current for low voltage fuses related to 60 Hz, and European manufacturers offer fuses which have been proved at 50 Hz. The approvals authorities concerned accept 50 Hz test evidence, but occasionally question the validity of some of the recorded parameters in regard to their applicability to 60 Hz systems.

The suite of computer programs developed by Wilkins [3] is therefore used to examine the performance of fuses at both 50 Hz and 60 Hz, and the results are compared with actual 50 Hz test data to demonstrate the efficacy of the programs.

Since the programs have been shown to be reliable, they can be used with confidence to predict the performance of fuses under conditions at which it is not practicable to test, e.g., at 400 Hz and 25 Hz. This paper reports investigations into performance at both of these frequencies.

2. L.V. FUSE PERFORMANCE AT 50 HZ & 60 HZ

2.1 Verification of Programs' Efficacy

Data on two ranges of fuses commercially available in North America is used to verify the efficacy of the computer programs. The fuse types are HRC1-J and HRC11-C to

reference [2]. Type HRC1-J fuses are also specified in reference [1], where they are identified as Class J. Both types were proved in the U.K. using 50 Hz sources. Whilst both ranges are rated at 600 V in North America, the HRC11-C range was actually tested at 660 V, + 10%.

Table 1 gives the major parameters recorded on approval tests, and shows how the computer predictions compare with those values. The table also gives the standards' limits for  $I^2t$  and peak current for the fuses concerned. Since work is proceeding to produce common North American fuse standards from the existing UL and CSA standards, these limits are referred to as "USC limits" in the table.

The predicted peak currents are generally slightly less than the recorded values on test, but there is good correlation between actual and predicted clearing  $I^2t$  values. There is also good correlation between other parameters not shown in the table (e.g., clearing time and arc voltage). In general, the fuses produce values of peak current which are substantially less than the specified maximum values with the exception of the 600 A rating in the HRC11-C range. The latter produced 90.9% of the maximum value when it was tested at 50 Hz, and it might therefore be argued that it would have exceeded the limit if it had been tested at a different arcing angle in a 60 Hz circuit. The North American standards specify that the arcing angle may be between  $60^\circ$  and  $90^\circ$  when fuses are subjected to tests at their interrupting rating (200 KA in the case of the subject fuse types). Therefore even at a given test plant setting, peak current can vary significantly over this admissible arcing angle range. The performance of the 600 A rating of the HRC11-C range is therefore examined in detail in Section 2.3 of this paper, to demonstrate that it would comply with the standard under the worst test conditions at 60 Hz.

The performances of the 30 A and 60 A ratings in the two subject ranges were also examined, and their let through values at 50 Hz were well within the 60 Hz limits. These results are omitted in the interest of brevity, it being reasonable to assume that conclusions reached about the performances of the larger current ratings are applicable to these smaller ones.

The clearing  $I^2t$  requirements for HRC1-J fuses are stringent, and so inevitably the actual test values approach the permitted limits, particularly as current rating increases. The predicted performance of this range therefore merits close examination.

TABLE 1 Let through values of fuses when tested at 200kA, compared with computer predictions for same fuses at same circuit parameters

Fuse Rating Amps	Data* Status	HRC1 - J fuses			HRC11 - C fuses		
		Arcing Angle Degrees	Peak Current Let through KA	Clearing $I^2t$ A <sup>2</sup> sec x 10 <sup>3</sup>	Arcing Angle Degrees	Peak Current Let through kA	Clearing $I^2t$ A <sup>2</sup> sec x 10 <sup>3</sup>
100	TD	75	12.8	38.1	62	21.1	189
	CP	75	12.3	40.7	62	17.7	180
	USCL		20	80		32	500
200	TD	77	24.7	245	64	32.2	705
	CP	76	23.6	250	65	31	766
	USCL		30	300		50	2000
400	TD	77	37.7	923	76	58.6	2855
	CP	77	36.9	933	75	54.7	3003
	USCL		45	1100		75	6000
600	TD	65	50.3	2280	69	90.9	11020
	CP	66	47.8	2200	69	87.5	12800
	USCL		70	2500		100	12000

\* TD = Test Data

CP = Computer Prediction

USCL = USC Limit

## 2.2 The HRC1-J range at 50 Hz & 60 Hz

In Table 1, the arcing angles for the tests vary from 62° to 77°. The maximum values of clearing  $I^2t$  and peak current do not necessarily occur within such a range. Computer predictions have therefore been obtained over the complete range of 60° to 90° allowed by the standards. The results are shown in Figs. 1 to 4.

The values fluctuate over the arcing angle range, and the scales of the figures are chosen to exaggerate these fluctuations. Thus in Fig 4, the values of clearing  $I^2t$  for a 600 A fuse at 50 Hz change significantly at an arcing angle of about 77°. Such fluctuations occur when a small change in closing angle produces a disproportionate effect on the rate of rise of fault current (see Fig 5).

Table 2 gives a statistical analysis of the clearing  $I^2t$  data shown in Figs. 1 to 4. The maximum and mean values at 50 Hz are slightly greater than those at 60 Hz, except that the maximum value of the 100 A fuse at 60 Hz is 1.1% greater than the 50 Hz value.

## 2.3 The HRC11-C range at 50 Hz & 60 Hz

Table 1 shows that HRC11-C fuses easily comply with the limits specified for  $I_p$  and  $I^2t$ . The tests were taken at 738 V, and only the 600 A fuse yielded values which approach the specified 600 V limits. Fig 6 gives the results of a number of predictions obtained for the 600 A fuse. Predictions for other current ratings in this range show similar trends to those on the HRC1-J range, and so they are not detailed in this paper.

## 2.4 Observations on the 50 Hz & 60 Hz data

2.4.1 Arc energy values at 50 Hz are invariably greater than those at 60 Hz. The fuses themselves are therefore stressed more when they are tested at the lower frequency.

2.4.2 At a given arcing angle, the 60 Hz clearing  $I^2t$  value can be greater than the 50 Hz value. However this difference does not exceed 5% (e.g., the HRC1-J 600 A fuse at arcing angles of 77° to 83° - Fig 4). An approvals engineer might therefore multiply a 50 Hz test value by 1.05 in order to compare it with the specification limit. If this criterion had been applied to the test values detailed in this paper, the fuses would still have complied with the standard.

2.4.3 The peak current ( $I_p$ ) values at 60 Hz are invariably greater than those at 50 Hz, but the fuses generally have no difficulty in meeting the standard requirements in regard to this parameter. In the worst case, the 60 Hz value is about 11% greater than the 50 Hz one (i.e., the HRC1-J 100A fuse at an arcing angle of 74° - Fig 1).

## 3. L.V. FUSE PERFORMANCE AT 400 HZ

Some electrical systems in aircraft are supplied from 400 Hz sources, and a few commercial/industrial installations also require a 400 Hz supply at 380/415 V. In the latter case, the kVA rating of the installed plant can be quite large (e.g., 225 kVA). It is therefore of interest to consider how l.v. industrial fuses are likely to perform in such an installation.

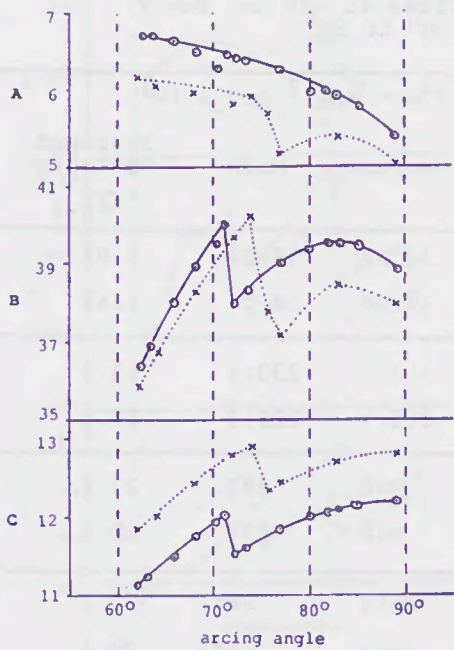


FIG. 1 100A fuse

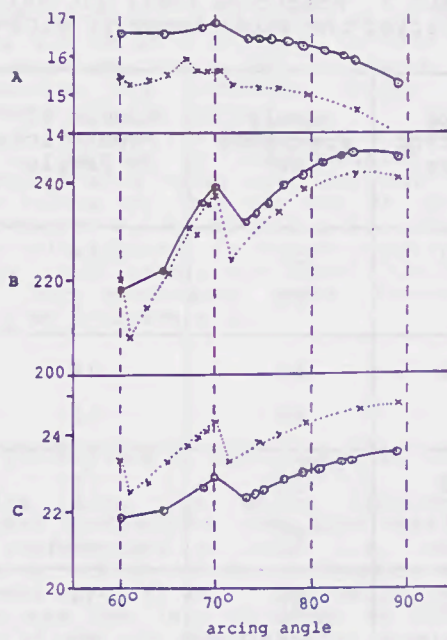


FIG. 2 200A fuse

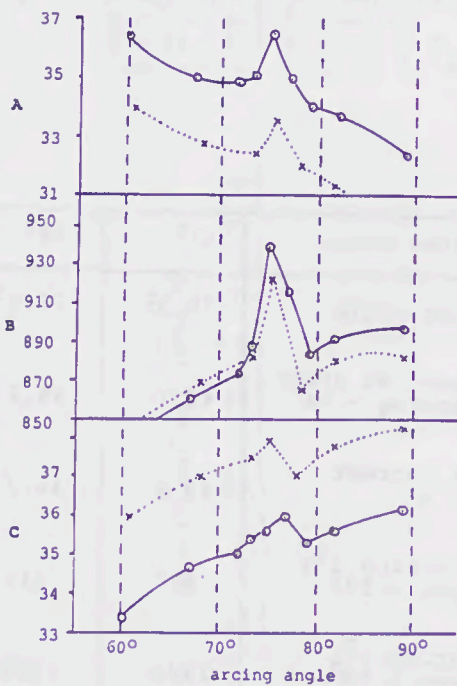


FIG. 3 400A fuse

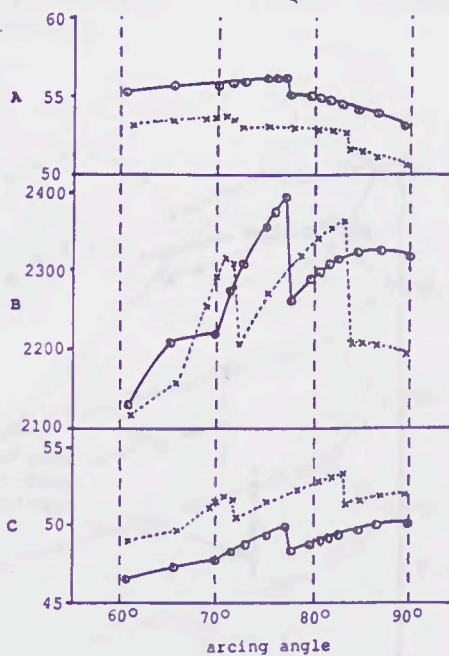


FIG. 4 600A fuse

Key to FIGS. 1 to 4

—○—○—○—○— 50 Hz data

---x---x---x---x--- 60 Hz data

A = Arc energy in kilojoules.

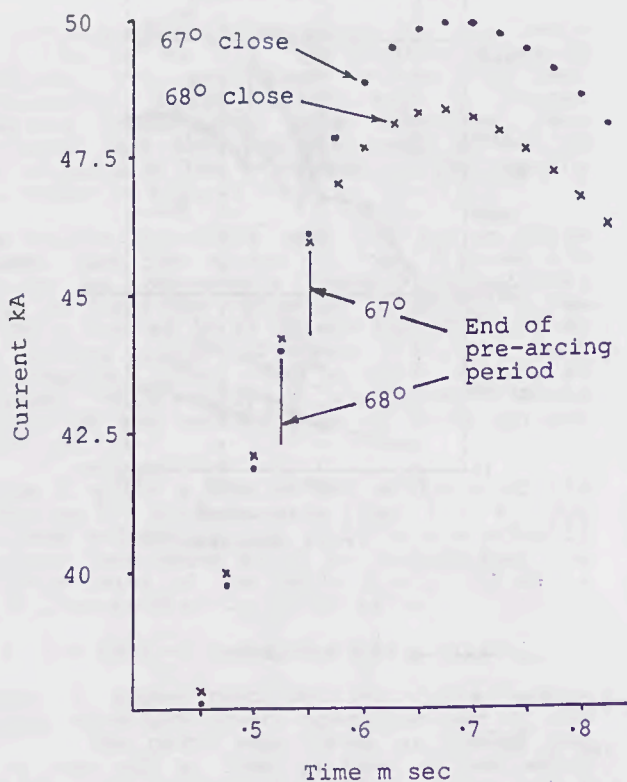
B = Clearing  $I^2t$  in  $A^2 \text{ sec} \times 10^3$

C = Peak current ( $I_p$ ) in kA.

FIGS. 1 to 4 Predictions for performances of HRC1-J fuses at 200 kA, 600 V, 0.11 p.f.

TABLE 2 Predicted total I<sup>2</sup>t values of HRC1-J fuses at 200 kA, 600 V, covering the whole range of arcing angles from 60° to 90°

Fuse Rating Amps	Supply Frequency Hz	Number of Predictions in Sample	Clearing I <sup>2</sup> t - Amp <sup>2</sup> sec x 10 <sup>3</sup>			
			Maximum	Minimum	Mean	Standard Deviation $\sigma_{n-1}$
100	50	14	40.03	36.32	38.68	1.08
	60	9	40.49	35.88	38.04	1.42
200	50	14	245.6	217.2	233.2	13.8
	60	15	241.3	216.5	228.3	10.4
400	50	9	935	842	887	27.6
	60	7	921	848	878	22.6
600	50	17	2396	2019	2281	91.9
	60	17	2358	2023	2244	92.6



Closing angle	67°	68°
Arcing angle	76.9°	77.5°
Current at start of arcing - kA	46.1	44.2
Peak current kA	49.9	48.3
Pre-arcing I <sup>2</sup> t A <sup>2</sup> sec x 10 <sup>3</sup>	387	340
Clearing I <sup>2</sup> t A <sup>2</sup> sec x 10 <sup>3</sup>	2396	2265
Pre-arcing time-m sec	0.55	0.52

FIG.5 Predicted variations of fault current when the circuit is closed at 67° AND 68° to operate HRC1 - J 600 A fuses at 200 kA, 0.11 p.f., 600 V

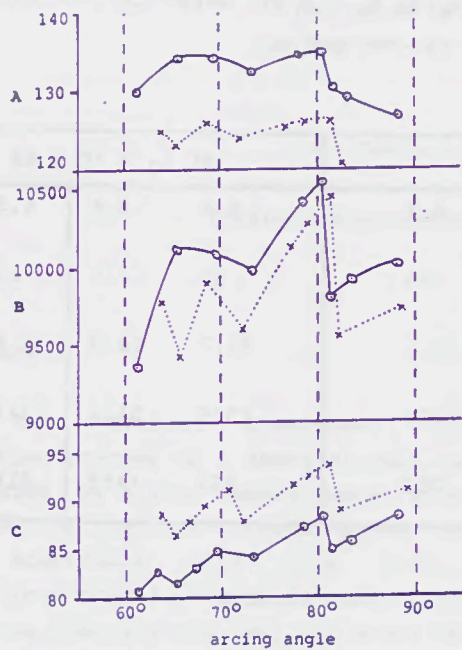


FIG.6 Predictions for performance of HRC11-C 600 A fuse at 200 kA, 600 V, 0.11 p.f. (Key as per Figs. 1 to 4)

### 3.1 Fault levels at 415 V, 400 Hz

A fault of 30 kA, 0.25 p.f., at 50 Hz would become 3.9 kA at 0.032 p.f. if this circuit were supplied from a 400 Hz source instead (neglecting any resulting change in the impedance of the source). If this same circuit then had its power factor modified to 0.9 at 50 Hz by the addition of the resistance of a cable run, the fault current would reduce to 13.5 kA, and at 400 Hz it would become 3.7 kA at 0.25 p.f. From these crude calculations, it can be concluded that 400 Hz fault levels are never likely to be high, but associated power factors will always be relatively low.

### 3.2 Predictions of performance at 400 Hz

Arising from the above considerations, computer predictions have been obtained for the performances of some l.v. industrial fuses at 415 V, 400 Hz, 0.05 p.f., at fault currents up to 40 kA. The results show that fuses are far less stressed at 400 Hz in terms of the arc energies they dissipate and the clearing  $I^2t$  values they produce. However, their peak current values are 60-80% greater than 50 Hz values at the same fault levels (with assumed power factors of 0.1 - 0.2 at 50 Hz). Figure 7 shows these differences.

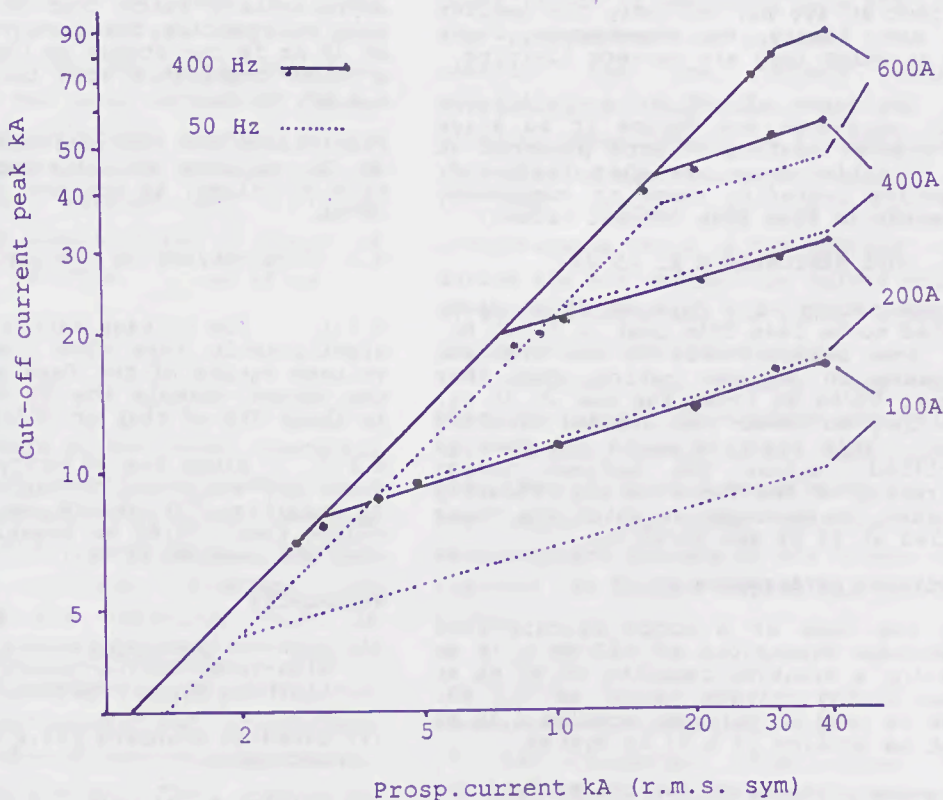


FIG.7 Cut-off current characteristics of l.v. industrial fuses to B.S.88-2 at 50 Hz and 400 Hz, 415 V

TABLE 3 Predictions of let through values for a 250 A, 7.2 kV, motor circuit fuse at the voltages and frequencies shown

	At $I_1 = 46$ kA			At $I_2 = 20.7$ kA		
	6.4	6.4	4.8	6.4	6.4	4.8
Applied voltage (kV)	6.4	6.4	4.8	6.4	6.4	4.8
Frequency (Hz)	50	25	25	50	25	25
Peak current - $I_p$ (kA)	29.4	23.4	22.1	21.7	20.3	15.6
Clearing $I^2t$ ( $A^2$ sec $\times 10^3$ )	2228	5052	1908	2366	5132	2321
Arc energy (kJ)	739	1429	753	832	1453	916

### 3.3 Observations on the application of fuses at 400 Hz

3.3.1 Fault levels are low compared with 50 Hz industrial values, and fuses easily cope with any fault conditions they are likely to encounter.

3.3.2 Fuses produce much larger values of peak current at 400 Hz, but only the smaller ratings are likely to experience fault currents at which they are current limiting.

3.3.3 Designers of 400 Hz installations use 50 Hz equipment and derate it to allow for the greater heating effects produced at 400 Hz. Cable sizes are also increased. This practice therefore tends to compensate for increases in fuse peak current values.

### 4. H.V. FUSE PERFORMANCE AT 25 Hz

The voltage rating of a fuse at 25 Hz might be expected to be less than that at 50/60 Hz. However, some manufacturers do not indicate any decrease in voltage rating when they offer their 50/60 Hz types for use at 25 Hz, although they do lower the claimed breaking capacity. This practice would not seem to be justified, unless the maximum design voltage rating of the fuses is significantly greater than the voltages at which the fuses are applied at 25 Hz and 50/60 Hz.

#### 4.1 Predicted performance at 25 Hz

Consider the case of a motor circuit fuse with cartridge dimensions of 403 mm x 76 mm dia., having a breaking capacity of 45 kA at a maximum design voltage rating of 7.2 kV. This fuse is used at voltages down to 4.16 kV and might be applied in a 25 Hz system.

Table 3 gives predictions for the performance of this fuse at  $I_1$  and  $I_2$  when tested at 6.4 kV, 50 Hz (i.e., approximately 87% of 7.2 kV in accordance with IEC 282-1).

The  $I_2$  duty stresses the fuse slightly more than the  $I_1$  duty, and this accords with actual test data recorded on this type. The table also indicates the performances of this type when it is subjected to 6.4 kV and 4.8 kV, both at 25 Hz.

At 6.4 kV, 25 Hz, the stress on the fuse in terms of arc energy and clearing  $I^2t$  is approximately twice that at 6.4 kV, 50 Hz. Only by reducing the test voltage to 4.8 kV at 25 Hz is the stress on the fuse reduced to a level comparable with that encountered at 6.4 kV, 50 Hz.

Predictions for the performance of this type at 30 kA show no alleviation in the let through values, as compared with those at 46 kA.

#### 4.2 Observations on the application of fuses at 25 Hz

4.2.1 The voltage rating at 25 Hz must be significantly less than the maximum design voltage rating of the fuse at 50/60 Hz. In the chosen example the 25 Hz voltage rating is about 75% of that at 50/60 Hz.

4.2.2 Since the majority of high voltage fuses are subjected to maximum stress at the  $I_2$  condition, it should not be necessary to reduce their 50/60 Hz breaking capacity when they are used at 25 Hz.

### REFERENCES

- (1) Underwriters Laboratories Standard for High-Interrupting-Capacity Fuses, Current Limiting Types - UL198C.
- (2) Canadian Standard C22.2 No.106 - M1985, HRC Fuses.
- (3) Wilkins R: "A suite of interactive programs for fuse design and development" Int.Conf.on Electric Fuses and their applications, NTH, Trondheim, 13-15 June 1984, p.p. 227-235.

INFLUENCE OF SHORT-CIRCUIT POWER FACTOR  
ON THE CUT-OFF CURRENT OF LOW VOLTAGE FUSES

O. Bottauscio, G. Crotti, G. Farina

Istituto Elettrotecnico Nazionale 'Galileo Ferraris'  
Torino, Italy

Summary

The severest conditions in the breaking process of a short-circuit current operated by a fuse usually occur with low values of the short-circuit power factor. In accordance with this fact, the Electrotechnical Standards concerning low voltage fuses, establish, for short-circuit tests, the value of the power factor as a function of the prospective test current; this value corresponds to the lowest occurring in actual installations. However, as regards the cut-off characteristics, the maximum peak values of the current likely to be experienced in the case of power factors close to unity are higher than those indicated by the manufacturers, usually given for lower values of power factor. After an analytical approach to the problem, the paper presents the results of numerous tests, carried out in our laboratories, on several types of fuses of different rated currents.

1. Introduction

The knowledge of the fuse operating characteristics, which is useful to estimate the fuse behaviour under overload and short-circuit conditions, becomes essential in solving problems of coordination of the apparatus (such as circuit-breakers, contactors, motor-starters, disconnectors, etc...) and protection of controlgear and controllers (such as semiconductor devices, capacitors, etc...). In particular, the quantities involved in the interruption process of a short-circuit current, in a circuit protected by a fuse, are the let-through energy  $I^2t$  and the cut-off current  $I_p$ .

These quantities are functions of the mode of operation of the fuse as well as of the circuit parameters, which determine the prospective current and power factor.

As known, damages to the devices to be protected strictly depend on the values of the cut-off current and  $I^2t$  as well as on the rate of rise of the current ( $di/dt$ ). As a consequence, in order to represent the most severe conditions that can be experienced in the installations, the International Electrotechnical Standards, concerning low voltage fuses, establish the conditions for short-circuit breaking tests; in particular, the value of the power factor is expressed as a function of the prospective test current (\*). Since, usually, the most severe conditions correspond to low values of the short-circuit power factor, as a consequence of the greater electromagnetic energy stored in the circuit and of the higher instantaneous value of the applied voltage during the arc period, the values indicated by the Standards are the lowest which occur in the actual installations.

However, as regards the cut-off characteristics, the maximum peak values of the current, likely to be experienced in the case of power factors close to unity, are higher than those indicated by the manufacturers because of the higher rate of rise of the current during the pre-arcing period.

---

(\*) IEC Standards (Publication 269-1) indicate the following power factor ranges: 0.2-0.3 for prospective test currents up to 20 kA; 0.1-0.2 for prospective test currents above 20 kA.

## 2. Simulation of the fuse behaviour

The current in a single-phase circuit protected by a fuse, under short-circuit conditions, can be obtained by the following equation:

$$e = Ri + L \frac{di}{dt} + v_a \quad (1)$$

where  $e=e(t)$  is the supply voltage,  $R$  and  $L$  are the resistance and the inductance of the circuit and  $v_a$  the arc voltage.

In order to represent the arc voltage behaviour the V-I arc characteristic is represented by [5]:

$$v_a = v_0 + ri \quad (2)$$

where, for low voltage fuses,  $v_0$  is 0.6 times the r.m.s. value of the supply voltage  $E$  and  $r$  is equal to  $0.7 E/I_{\pi/2}$ ;  $I_{\pi/2}$  is the so called "one-half-cycle fusing current".

By introducing expression (2) in equation (1), the expression of the current can be evaluated:

$$i(t) = c e^{-(R+r)/Lt} - \frac{v_0}{R+r} + \frac{E}{(R+r)^2 + (\omega L)^2} \sin(\omega t + \psi - \varphi) \quad (3)$$

where  $c$  is the integration constant,  $\varphi$  is the phase angle of the current,  $\psi$  the making angle and  $v_0$  and  $r$  are equal to zero during the pre-arcing period.

The knowledge of the current behaviour permits the evaluation of the cut-off current. The peak of the current is computed as a function of the making angle for a defined prospective power factor; then it is possible to evaluate the maximum cut-off current, with respect to the making angle, versus the power factor. Different circuit conditions of installations protected by fuses of different rated currents have been analyzed. In particular, the behaviour of fuses with rated currents of 16, 25 and 50 A in short-circuit tests with prospective currents from 3 kA to 10 kA has been considered. For each condition,

the cut-off current, obtained in the case of the power factor indicated for the breaking tests by the Standards, has been compared with the one which results when the power factor is close to unity. As an example Fig.1 shows the behaviour of the cut-off current versus the making angle for a prospective short-circuit current of 3 kA, with a 16 A fuse, for a power factor of 0.28 and for a power factor of 0.98. It can be noted that the maximum value of current is reached with the highest value of power factor.

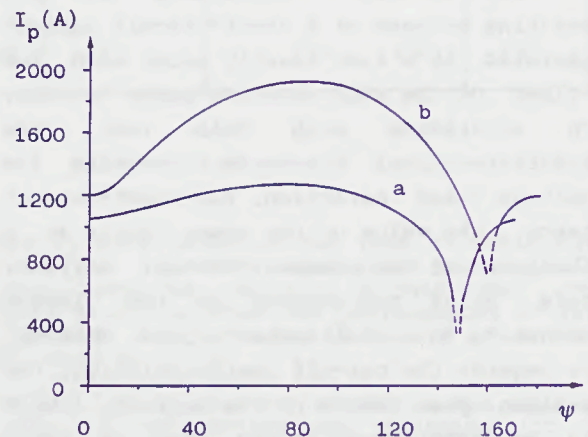


Fig.1 - Computed behaviour of the cut-off current versus the making angle, for a prospective short-circuit current of 3 kA, with a 16 A fuse:  
a) power factor = 0.28  
b) power factor = 0.98

In order to put in evidence the dependence of the maximum cut-off current on the prospective power factor, the computation results have been summarized in Fig.2, 3 and 4, which correspond respectively to prospective short-circuit currents of 3, 5 and 10 kA. It can be seen that the cut-off current values increase when the power factor tends to unity.

As regards the actual installations, the maximum and minimum power factor values that can be experienced must be taken into account. Fig.5 shows these values as a function of the supply transformer rated power for short-circuit currents of 3, 5, 10 and 20 kA. As can be seen, the higher the rated power of the transformer, the higher the possibility of high values of power factor.

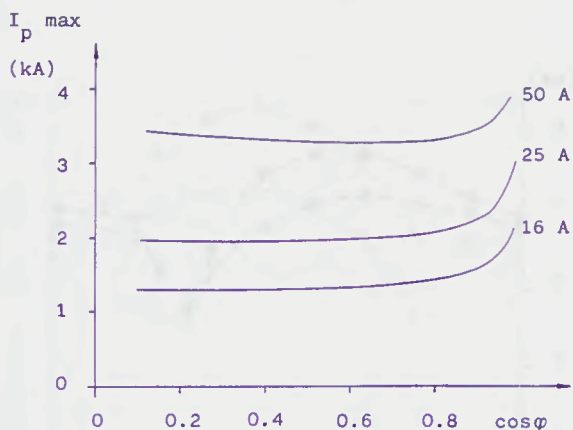


Fig.2 - Maximum cut-off current versus the prospective power factor for a short-circuit current of 3 kA. The rated current of the fuse is indicated as parameter.

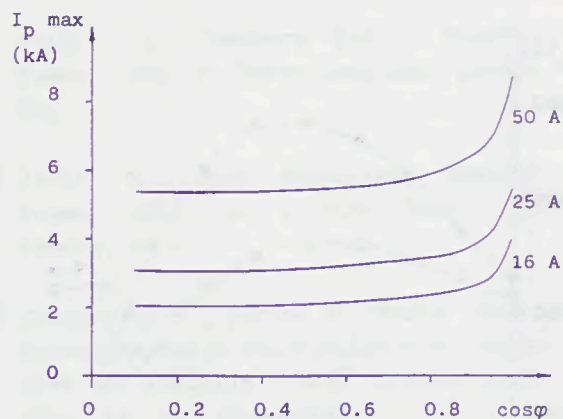


Fig.4 - Maximum cut-off current versus the prospective power factor for a short-circuit current of 10 kA. The rated current of the fuse is indicated as parameter.

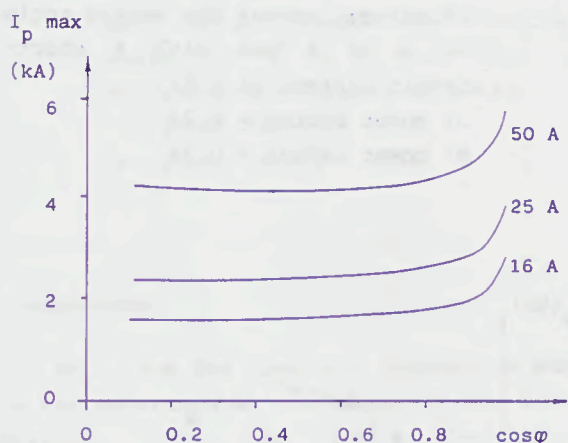


Fig.3 - Maximum cut-off current versus the prospective power factor for a short-circuit current of 5 kA. The rated current of the fuse is indicated as parameter.

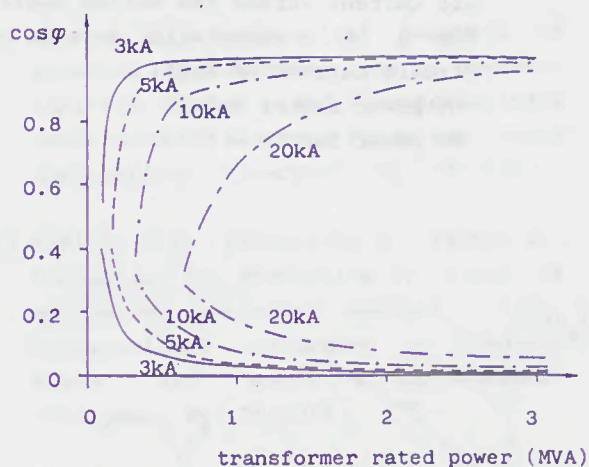


Fig.5 - Maximum and minimum power factor obtainable in actual installations versus the transformer rated power for different short-circuit currents.

### 3. Experimental results

The indications obtained by the simulation have been compared with the results of an experimental investigation carried out on several types of fuses. The single-phase test circuit was supplied at 420 V, 50 Hz and the tests were carried out with prospective currents of 3, 5 and 10 kA. The making instant was determined by

two controlled thyristors connected in antiparallel. Each type of fuse has been tested with the lowest and the highest power factor available in the laboratory test circuit.

The experimental data are summed up in Fig.6-10. The diagrams confirm the previous considerations and are in accordance with the computation results.

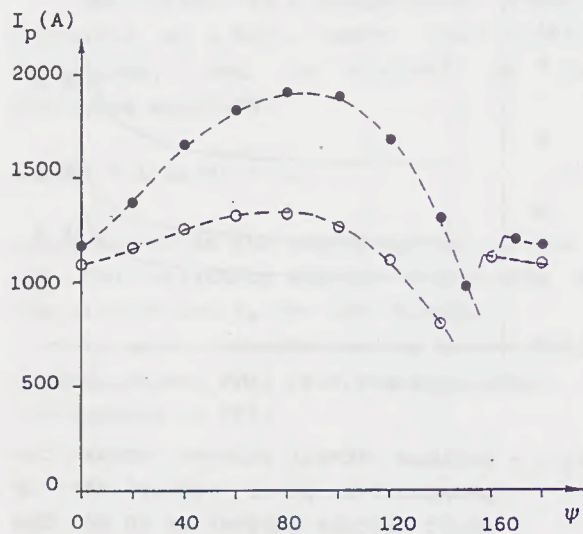


Fig.6 - Experimental behaviour of the cut-off current versus the making angle for a 16 A fuse with a short-circuit current of 3 kA:  
 ○) power factor = 0.28  
 ●) power factor = 0.98

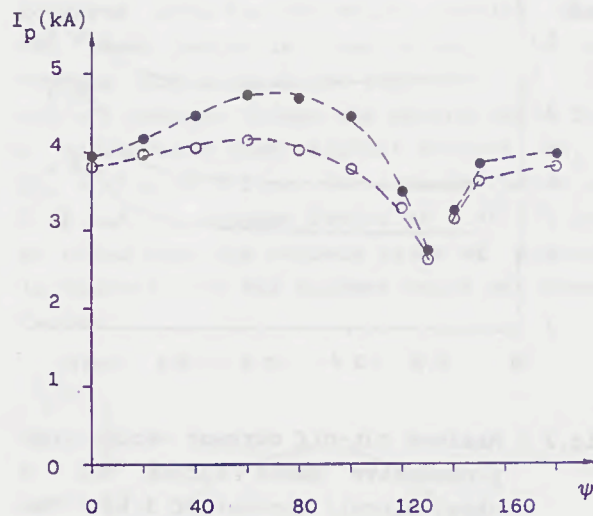


Fig.8 - Experimental behaviour of the cut-off current versus the making angle for a 50 A fuse with a short-circuit current of 5 kA:  
 ○) power factor = 0.29  
 ●) power factor = 0.94

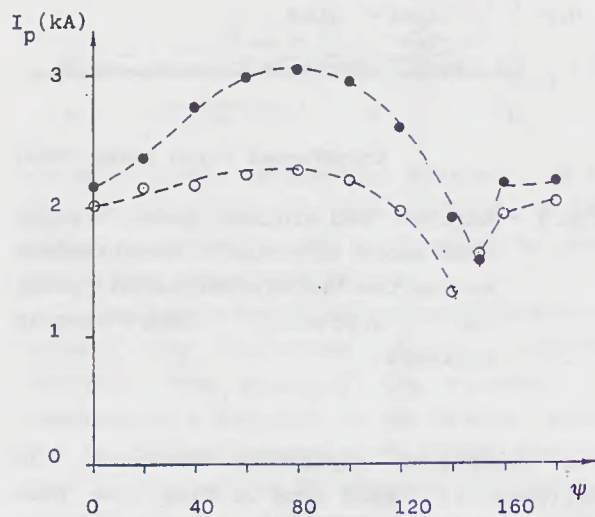


Fig.7 - Experimental behaviour of the cut-off current versus the making angle for a 25 A fuse with a short-circuit current of 5 kA:  
 ○) power factor = 0.29  
 ●) power factor = 0.94

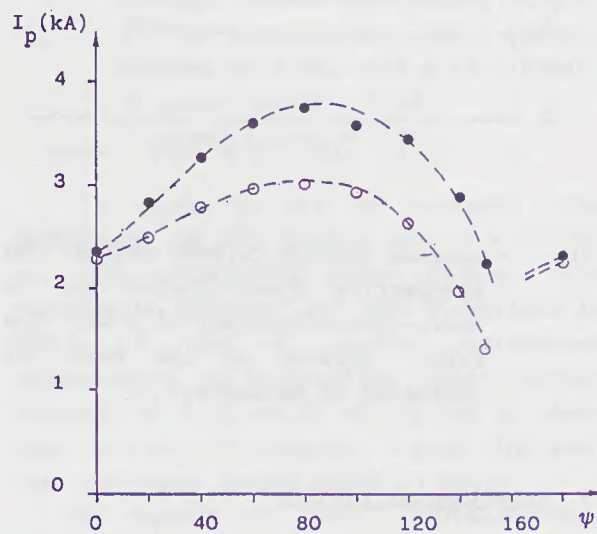


Fig.9 - Experimental behaviour of the cut-off current versus the making angle for a 25 A fuse with a short-circuit current of 10 kA:  
 ○) power factor = 0.35  
 ●) power factor = 0.96

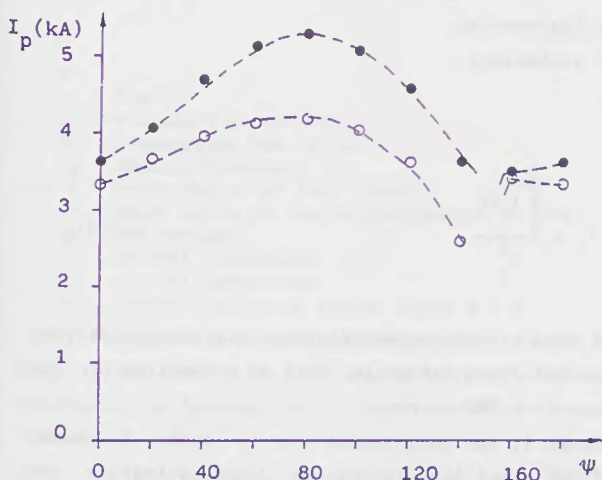


Fig.10 - Experimental behaviour of the cut-off current versus the making angle for a 50 A fuse with a short-circuit current of 10 kA:

- ) power factor = 0.35
- ) power factor = 0.96

#### 4. Conclusions

Both from the numerical simulation and the the experimental procedure, it has been verified that the test conditions representative of the severest conditions, as regards the cut-off current, are those corresponding to power factor values approaching to unity. Therefore, for particular applications, in order to verify completely the fuse behaviour as regards the maximum cut-off current, tests, carried out with the highest values of the power factor that can be experienced in the actual installations, may be necessary.

#### Acknowledgments

The authors wish to thank Prof. G. Cantarella for his helpful suggestions.

#### References

- [1] Wright A., Newbery P.G., Electric Fuses, 1984, P. Peregrinus LTD, London, UK.
- [2] Jacks E., High Rupturing Capacity Fuses, 1975, E. & F.N. Spon LTD, London, UK.
- [3] Cantarella G., Farina G., Sulla determinazione delle caratteristiche operative dei fusibili, 1973, L'Elettrotecnica, LX, 11, 1089-1096.
- [4] Ambrosione F., Bottauscio O., Crotti G., Influence of power factor on short-circuit tests on circuit-breakers for household installations, 1989, Switching Arc Phenomena, Lodz, Poland, 124-127.
- [5] Hirose A., Mathematical analysis of breaking performance of current-limiting fuses, 1976, International Conference on Electric Fuses and their Applications, Liverpool, UK, 182-191.
- [6] Toniolo S.B., Cantarella G., Farina G., Tartaglia M., Protection by fuses of mechanical switching devices, 1976, International Conference on Electric Fuses and their Applications, Liverpool, UK, 212-215.

## CHOICES FOR THE PRESENTATION OF FUSE MELTING CURVES.

J.G.J. Sloot and X. Meng  
 Department of Electrical Engineering  
 Eindhoven University of Technology  
 Netherlands.

### Summary.

Fuse manufacturers generally present time-current characteristics which are guaranteed within 10 % (of the current). This paper shows experimental results with a considerable stronger spread, in the case of asymmetrical currents. The increased spread is in agreement with expectations from former computer simulations using a thermal model for the fuse. The experiments show a reduced influence of the switching angle, when the melting time is plotted as a function of the so called virtual current (the expanding RMS current). Purpose of this study was to present an experimental justification for the use of virtual currents for fuse melting curves. The method can be of help in the case of sharp coordination studies, or for non sinuous currents.

### 1. Introduction.

For operating times above about 100 ms, the pre-arcing-behaviour of fuses can usually be represented by time-current characteristics, where the pre-arcing-time is plotted as a function of the RMS- value of the prospective current. For faster pre-arcing-times, graphs are used where the pre-arcing Joule integral  $I^2t$  is plotted as a function of the RMS- value of the prospective current. This  $I^2t$  stands for the time integral of the square of the instantaneous current passing through a fuselink between the instant when a circuit fault occurs and the instant  $t_m$  of arc initiation :

$$I^2t = \int_0^{t_m} i^2 dt \quad (1)$$

The preference for  $I^2t$  curves is based on the assumption that, at a particular prospective current  $I_p$ , different wave shapes can lead to a range of melting times, but are coupled with the same Joule integral. In fact, this assumption only holds, when the heat loss from the fuse strip is the same for any current shape.

Equivalent to the Joule integral, also a quantity is used, termed virtual time, defined as the  $I^2t$  value divided by the square of the value of the prospective current :

$$t_v = \frac{\int_0^{t_m} i^2 dt}{I_p^2} \quad (2)$$

Fuse manufacturers generally supply graphs of virtual times and Joule integrals, both as a function of the prospective RMS current.

Although it has been warned even in basic textbooks on fuses<sup>1</sup> that the values of Joule integrals (or virtual times) not only depend on the current level, but also on the shape of the prospective current, the latter is often not taken into account in practice.

Especially for fuses with elements on a substrate such simplifications can lead to faulty fuse coordinations. Purpose of this study was :

- to determine experimentally the influence of the current asymmetry on the spread of virtual time (or Joule integral) curves,
- to justify experimentally the alternative presentation of time current characteristics, using 'virtual currents'. This method was introduced formerly, only on the basis of computer simulations<sup>2,3,4</sup>.

### 2. Definition of virtual currents.

As an alternative for the Joule integral  $I^2t$  or the virtual time  $t_v$  we suggest to choose for the virtual current  $I_v(t)$ .

For any momentary current  $i(t)$ , a virtual current  $I_v(t)$  can be defined similarly to the prospective RMS current  $I_p$ , with the difference that the integration is not limited to time periods (for instance 10 ms for a 50 Hz current). In formula :

$$I_v(t) = \sqrt{\frac{\int i^2 dt}{t}} \quad (3)$$

In fact, the virtual current  $I_v(t_1, t_2)$  can be considered as a measure for the average heating power per unit of resistance, for the time difference between moments  $t_1$  and  $t_2$ . Only one time parameter is left, when  $t_1 = 0$  for fault currents.

With a voltage source :

$$u(t) = U_p \sqrt{2} \sin(\omega t + \psi) \quad (4)$$

the general expression for an asymmetric current after  $t = 0$  is given by :

$$i(t) = I_p \sqrt{2} [\sin(\omega t + \psi - \phi) - e^{-Rt/L} \sin(\psi - \phi)] \quad (5)$$

with :

- $t$  : time
- $i(t)$  : momentary ac current
- $I_p$  : prospective RMS current
- $\omega$  : angular frequency
- $\cos \phi$  : power factor of the circuit
- $\psi$  : phase angle of the voltage source at  $t=0$
- $U_p$  : RMS voltage
- $R$  : circuit resistance
- $L$  : circuit inductance
- $\alpha$  : current switching angle, with  $\alpha = \psi - \phi$
- $\tau$  : circuit time constant with  $\tau = L/R$

The virtual current  $I_v(t)$  related with  $i(t)$  can be determined by integration :

$$I_v(t) = I \left[ 1 - \frac{1}{\omega t} \sin \omega t \cos(\omega t + 2\alpha) + \frac{\tau}{t} \sin^2 \alpha (1 - e^{-2t/\tau}) - \frac{4 \sin \alpha \sin \phi}{\omega t} \left\{ \sin \psi e^{-t/\tau} \sin(\omega t + \psi) \right\} \right]^{0.5} \quad (6)$$

The use of virtual currents was already suggested by Hulsink<sup>3</sup> and Takach<sup>4</sup> for transformer protection applications. Also the IEC Technical Committee 32 considered its relevance<sup>5</sup> but preferred the use of virtual times. As a main critic they judged the virtual current method difficult to use. This argument has become weaker during the last twenty years because of the increased possibilities of personal computers. The committee did not recognize the less spread in the characteristic for the case of short time constants of the fuse element. A stronger negative point of virtual times was not considered by the TC : what to do with transformer inrush? The common analogy with  $25 I_n$  at 10 ms is weakly motivated, while the translation to virtual currents is performed easily.

### 3. Experiments.

For the thermal tests, a low voltage circuit was chosen (Figure 1).

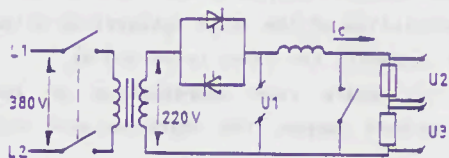


Figure 1. Test circuit for the determination of current-time characteristics.

The RMS value of the current ( $I = 10-100A$ ) and the

power factor ( $\cos \phi = 0.1$ ) of the circuit were realized with air coils.

The switching angles ( $\psi = 0, 30, 90, 150^\circ$ ) were accurately established with thyristors. Commercial high voltage fuses (12 kV, 40A) served as test objects. These fuses consist of 15 parallel strips. For reasons of economy and test set up requirements, the strips were tested individually (deviations between the behaviour of the total fuse and individual strips were only expected in the low current range).

The experimental results are plotted in Figure 2 (virtual time  $t_v$  as a function of prospective RMS current  $I$ ), together the manufacturer curve.

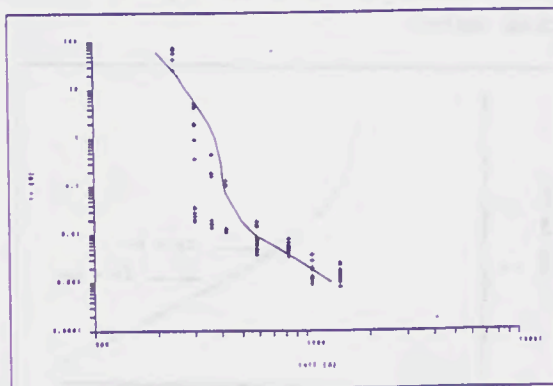


Figure 2. Comparison of the manufacturer's curve with experimental values of the virtual melting time  $t_v$  as a function of the RMS current, for several switching angles.

From Figure 2 it is evident that the virtual time can hardly be presented by just one single curve. The manufacturer curve is in closest agreement with the experimental points for  $\psi = 90^\circ$ . Obviously, the manufacturer's test was performed with symmetrical currents. The observed spread of results is not typical for this particular type of fuse, for instance Cranshaw<sup>6</sup> reported similar results for semiconductor fuses.

A reduction in the spread of the experimental results can be reached, by presenting them in Figure 3 (real melting time  $t_m$  as function of the virtual current  $I_v$ ). This observation is in accordance with former computer simulations<sup>2</sup>. Together with the experimental points, the manufacturer's curve is plotted in Figure 3. This curve ( $t_m, I_v$ ) can consist of the original curve ( $t_v, I_p$ ) without translation, which simply can be realized by changing the axis names<sup>2</sup>. Figure 4 illustrates this similarity.

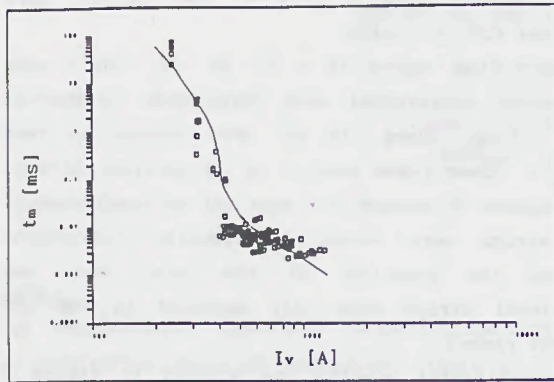


Figure 3. Comparison of the manufacturers curve with experimental values of the real melting time  $t_m$  as a function of the virtual current  $I_v$ , for several switching angles.

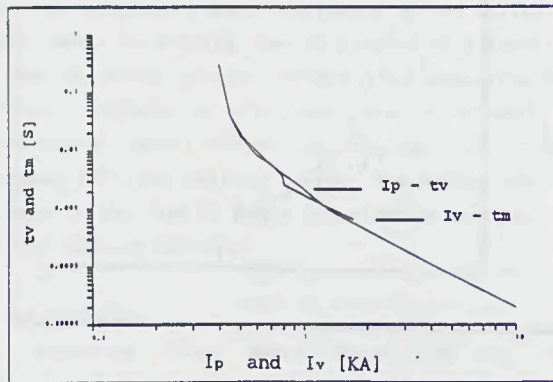


Figure 4. Original manufacturers curve (virtual melting time versus RMS current) and translated version (real melting time versus virtual current). This fortunate possibility is understandable from Figure 5: the virtual current of a symmetrical sinus reaches the prospective value within about 5 ms. This is short enough for nearly adiabatic heating (so  $I_p^2 t = I_v^2 t$ ), while later on  $I_v = I_p$ .

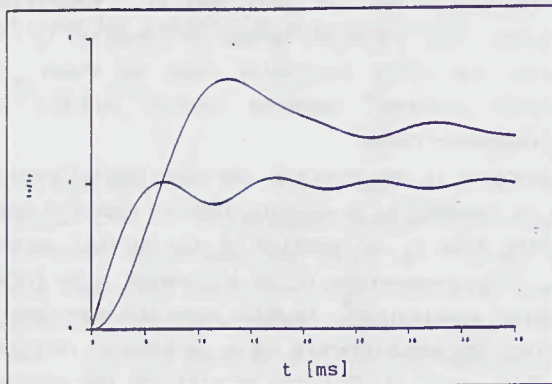


Figure 5. The virtual currents  $I_{v1}(t)$  and  $I_{v2}(t)$ , belonging to an almost symmetrical ( $\psi=90^\circ$ ) and an asymmetrical momentary current ( $\psi=0^\circ$ ) with the same prospective value and  $\cos\phi = 0.1$ .

#### 4. Application example of the virtual current method

The practical use of the virtual current method for fuse coordination is illustrated in Figure 6.

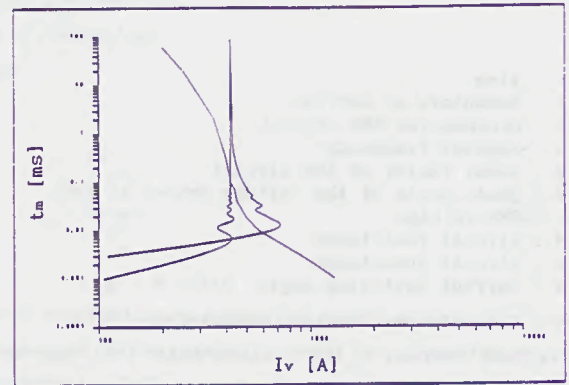


Figure 6 Manufacturers fuse melting curve for 40 A, presented for virtual times and RMS currents, together with the transformed curve for real melting times and virtual currents.

In Figure 6, the conventional manufacturers curve ( $t_v, I_p$ ) is plotted without changes in the  $t, I_v$  graph. To determine fuse functioning for a current with prospective value  $I_p = 420$  A, with symmetrical and asymmetrical current shape, their virtual patterns are plotted in Figure 5. From the intersections, fuse functioning for  $t = 100$  ms and 10 ms is found, for symmetrical and asymmetrical shapes. This is in accordance with the experimental values of Figure 3 (96 ms and 8 ms respectively). It is clear that the conventional method with virtual times would result in the value 100 ms for both wave shapes. Other examples of virtual current applications are described elsewhere for transformer inrush<sup>2,8</sup> or fuse selectivity<sup>7</sup>.

#### 5. Conclusion and recommendations.

As a result of this and former studies it can be stated, that for the every day use of fuses, it is advisable to choose:

- characteristics of the real melting time as a function of RMS currents, for times above 100ms.
- characteristics of the Joule integral as a function of RMS currents, for times below 100 ms.

However for sharp fuse coordination or for non sinuous current shapes, the characteristic with the real melting time as a function of virtual current offers a more reliable instrument for the fuse application specialist. This characteristic can be considered identical to the available conventional virtual time characteristic, if the latter is determined for symmetrical sinus currents. One has to

keep in mind that the virtual current method is also an approximation, it offers however a time and cost saving alternative to computer simulations or real experiments.

#### Acknowledgement.

The authors want to thank Mr. P.Klijn for the construction of the experimental setup and Mr. R.VanBezooen for the assistance during the measurements.

#### References.

- [1] Wright A. and Newbery P.G., 1982, Electric Fuses, Peregrinus, Stevenage, Great Britain.
- [2] Sloot J.G.J. and VandenHeuvel W.M.C., A new method for the presentation of fuse melting curves, 1989, Proc. 6th. Int.Symp. on Switching Arc Phenomena, Lodz, Poland, 250-254.
- [3] Hulsink G.J., Inschakelstromen in net transformatoren, 1961, Smit mededelingen, Vol 16, nr.4, 1-11.
- [4] Takach D.S., Distribution transformer primary fuse coordination, 1982, IEEE Trans. on Power App. and Syst., Vol. PAS-101, 2278-2285.
- [5] IEC Report of TC32, 1970, 1-3.
- [6] Cranshaw A.J., Optimization of H.V.Fuse-link contactor combinations by study of the effects of circuit conditions and fuse-link manufacturing tolerances on time-current curves for times less than 0.1 seconds, 1987, Proc. Third Int.Conf.on Electrical Fuses and their Applications, Eindhoven, Netherlands, 142-146.
- [7] Sloot J.G.J., Klijn P.N. and Bollen M.H.J., Rules for transformer protection with fuses., 1990, Proc. 4th Int.Symp. on Short Circuit Currents in Power Systems, Luik, Belgium, 4.2, 1-5.
- [8] W.M.C. van den Heuvel, V.K.I. Kalasek, J.G.J. Sloot, The thermal load by transformer inrush currents on fuses selected for short circuit protection, 1990, Proc. 4th Int.Symp. on Short Circuit Currents in Power Systems, Luik, Belgium, 4.4, 1-5.

The first part of the paper is devoted to a general discussion of the problem. It is shown that the problem is of great importance in the theory of differential equations. The author then proceeds to a detailed analysis of the problem, showing that it is equivalent to a problem in the theory of integral equations. This is done by introducing a suitable transformation of the variables.

In the next section, the author discusses the properties of the integral equation. It is shown that the kernel of the equation is symmetric and positive definite. This implies that the equation has a unique solution. The author then proceeds to a detailed analysis of the properties of the solution, showing that it is continuous and differentiable. This is done by using the theory of integral equations.

Finally, the author discusses the numerical solution of the problem. It is shown that the problem can be solved by using the method of successive approximations. This is done by introducing a suitable sequence of functions. The author then proceeds to a detailed analysis of the convergence of the sequence, showing that it converges to the solution of the problem. This is done by using the theory of integral equations.

The second part of the paper is devoted to a detailed analysis of the problem. It is shown that the problem is equivalent to a problem in the theory of integral equations. This is done by introducing a suitable transformation of the variables. The author then proceeds to a detailed analysis of the properties of the integral equation, showing that it has a unique solution.

In the next section, the author discusses the properties of the solution. It is shown that the solution is continuous and differentiable. This is done by using the theory of integral equations. The author then proceeds to a detailed analysis of the numerical solution of the problem, showing that it can be solved by using the method of successive approximations.

Finally, the author discusses the convergence of the sequence of functions. It is shown that the sequence converges to the solution of the problem. This is done by using the theory of integral equations. The author then proceeds to a detailed analysis of the properties of the solution, showing that it is continuous and differentiable.

**Session 6B**

**FUNDAMENTAL PROCESSES II**

2000

FUNDAMENTAL PRINCIPLES II

## DEVELOPMENTS IN THE MODELLING OF FUSE BREAKING TESTS

R. Wilkins  
Consultant  
Heswall, UK

and  
D. Suuronen, L. O'Shields  
Gould Shawmut  
Newburyport, USA

### Summary

The paper describes a number of improvements to the modelling of short-circuit tests on current-limiting fuses with multiple parallel notched elements in a granular filling medium. Some of these improvements are concerned with the physical models while others are concerned with the numerical methods required to obtain fast and accurate solutions. Some typical results are given, and the need for improvements to the test-plant model is discussed.

### 1. Introduction

In 1980 Gnanalingam and Wilkins described a method for computing the complete current and voltage transients for a short-circuit test on a current-limiting fuse [1]. The method used a finite-difference method to calculate the transient temperature distribution during the prearcing period, and the arcing period was modelled using a quasi-static model of the arcs in the notch zones, which expanded radially due to fusion of the filler, and axially due to burnback. The method was based upon experimental work on silver fuse elements with uniformly spaced rectangular notches, in a particular type of quartz sand [2].

The arcing models required a number of non-linear ordinary differential equations need to be solved. During each integration time step the arc length increases due to burnback, and this was allowed for by creating a new "lumen segment" to represent the additional part of the arc. The cross-sectional area of the new lumen segment was then added to the list of variables to be integrated, and so the order of the model increased after each time step.

Subsequent work by Daalder and Schreurs [3], Leistad et al [4], and Eger and Rother [5], has confirmed that this type of fuse model gives a realistic representation of the breaking process.

An interactive program based upon this model was described at Trondheim in 1984 [6].

In this paper a number of improvements to the basic model of 1980 are described. These improvements can be grouped into three categories as follows :

- (a) Improvements to the physical models. These are almost all connected with the arcing phase, as the physical basis of the prearcing phase is well understood and documented.
- (b) Improvements to the computational algorithms. These are needed to improve the flexibility, speed and accuracy of the computations to enable the user to model a much wider range of fuse designs.
- (c) Extension of the range of materials which can be specified for the element and filler. Whilst the standard thermophysical properties of most materials are known, some of the properties used in the arcing models need to be estimated from controlled experiments.

Some typical results obtained with the improved models are given, and the accuracy, usage, and possible future developments are discussed.

### 2. Improvements to prearcing computations

It is desirable for the program user to be able to select the fuse element design very easily, using a menu to choose the shapes of the reduced sections and their axial location along the fuse element. When running the program the required finite-difference meshes need to be generated automatically, with the mesh sizes reduced in regions of high current density, to give higher accuracy.

#### 2.1 Solution method

The program described in 1980 used the Crank-Nicholson formulation of the finite-difference methods, with the new element temperature distributions being computed by iteration after each time step. Experience has shown that the fully implicit formulation is preferable for general-purpose use, with direct rather than iterative solution. When sudden changes occur, for example in the solution time-step, stable oscillations are generated if the Crank-Nicholson method is used. These oscillations are well-known [7], and can be sometimes be troublesome. No such oscillations occur with the fully implicit method, which has been found to be more robust for general-purpose use. (Similar considerations apply if finite-element methods are used for the discretisation of the space variables [8]. Again a fully implicit formulation for the time-derivative is preferable).

A linear set of equations for the temperatures at the nodal points on the fuse elements has to be solved at each time step [6], for each notch design, and for the plain element sections between the notch zones. These equations are most efficiently solved using sparse-matrix methods, with triangular factorisation and back-substitution [9]. The mesh-generation algorithms need to generate a node numbering scheme which is near-optimal, which gives a dramatic reduction in solution time. The equations only need to be retriangularised when a change in time step occurs.

#### 2.2 Time step control

A general purpose program must incorporate schemes to automatically set the initial solution time step  $\Delta t$ , and to subsequently alter  $\Delta t$  as necessary. If the accuracy of the solution is too low the time step must be reduced, while if the accuracy is unnecessarily high, it must be increased, to give acceptably fast solutions. Experience has shown that this can be achieved, as far as the element temperatures are concerned, by reducing the time step if the maximum increment in the temperature of any node is about to exceed  $\Delta T_m/50$  and increasing it if the maximum increment falls below  $\Delta T_m/80$ , where  $\Delta T_m$  is the temperature rise required to reach the fusion point from the initial ambient value.

However with notches of different styles on the same element the situation occurs that arcing is in progress at some notch zones while others have not yet melted. So the above scheme for time step control needs to be combined with one suitable for the arcing variables. This combined scheme will be discussed later.

### 3. Improvements to arcing models

Although the basic concept of the arcing process is unchanged, some substantial improvements to the detailed physical models have been made.

#### 3.1 Arc quasi-static characteristic

Gnanalingam's work [2] was principally concerned with the high-current end of the arc characteristic, and in [1] a very rough correction was made to allow for the fact that the slope of the characteristic becomes negative as the current falls. More recent work [10] has extended the theoretical model of the quasi-static characteristic into the low-current zone, which gives improved modelling of the behaviour during the later stages of arcing.

#### 3.2 Characterisation of different fillers

During arcing radial expansion of the arc channel is determined by the input power from the arc and the enthalpy required to heat the filler to the effective fusion temperature [1],[3]. However, this model alone is not sufficient to explain the differences between fillers in their ability to control the arc. For example, the radial expansion of an arc in bonded sand is very much lower than in loose sand, despite the fact that the required enthalpy differs very little for the two materials. This must be attributed to differences in the viscous flow properties of the liquid filler [3]. It appears that the flow into bonded sand is much lower, and this effect can be taken into account by multiplying the lumen expansion rate by a flow coefficient, determined experimentally for each type of sand. Loose sands have flow coefficients around 1.0, while with bonded sand, values as low as 0.2 are found.

#### 3.3 Burnback rate

The rate of burnback used in [1] was obtained from an empirical power-law, derived from experiments on the burnback of silver strips in quartz sand [2]. Subsequently Daalder developed a model for the burnback process which included the effect of the temperature of the strip ahead of the arc root [3]. Although the difference in results is small, Daalder's model has a more sound physical basis and should be used in preference to the power-law formula. It has however been found desirable to make an adjustment for the effect of the filler material. During burnback, element metal is removed principally in liquid form which is forced away from the arcing zone through the gaps between the sand grains. Thus the porosity of the sand to this flow has an influence on the burnback rate.

#### 3.4 Effect of sand volume

It is well known that the arcing  $I^2t$  for a given element design falls significantly if the inner diameter of the fuse tube is reduced [11]. During arcing the sand is compressed due to the pressure exerted by the arc column, resulting in an additional increase in the lumen cross-section. Pastors [12] has demonstrated that the arcing  $I^2t$  can be reduced by application of external pressure from a piston on the sand grains (although the intergranular gas pressure remains atmospheric).

If the arc column pressure is  $p$ , the increase in lumen cross-section will be given by  $pA_s/K$ , where  $A_s$  is the total sand cross-section per unit length, and  $K$  is the compression modulus of the sand. Thus if the sand volume  $A_s$  is reduced, the increase in section will fall, resulting in a higher arc voltage gradient and a lower arcing  $I^2t$ .

This gives a very simple model for correcting for the effect of the inner diameter of the fuse tube, by adding a small time-dependent area to the lumen cross-section during solution.

#### 3.5 Initial arc voltage

When the centre of a notch zone reaches its melting point a short arc is formed, and for rectangular notch the initial arc length can be taken as equal to the notch length [1]. However, with other notch profiles, for example semicircular, there is some doubt as to the value to be assumed for the initial arc length. One possibility is to assume a length of zero and then allow the arc to extend along the notch zone using the usual burnback formula. However the notch disintegration is explosive and an initial arc length greater than zero is more realistic. A good compromise is to set the length to the value at which the element cross-sectional area is 20% larger than the minimum at the centre of the notch, although this value is not critical.

A more important effect with semicircular or tapered notches during the early stages of arcing appears to be a more rapid rate of lumen expansion due to the very low quantity of entrapped liquid metal from the element in the adjacent fulgurite wall. To quote from Daalder "... It seems that metal droplets increase the cohesion between the sand grains and improve, by a kind of glueing effect, the solidity of the wall around the arc." [3]. This does indeed appear to be the case. Using this concept a correction to the lumen expansion rate can be made to allow for the low density of entrapped metal in the notch zones, and this has been found to give better results for semicircular and similar notch designs.

### 4. Automatic control of solution time step

The arcing models give rise to a non-linear set of ordinary differential equations, in which the principal state variables are the circuit current, the lengths of the arcs in the notch zones, and the cross-sectional areas of the arc lumen segments. There are also auxiliary variables such as arc energy and  $I^2t$  which can be conveniently added to the set [1]. During some parts of the arcing period these variables change rapidly, and a small time step is needed to follow them, while at other times, usually during the later stages of arcing, a much larger time step is possible. Runge-Kutta integration with automatic adjustment of the time step to achieve a preset accuracy [13] has been found to be most convenient. In this method the equations are first solved using 3rd-order R-K integration, and then the solution is repeated using a more accurate 4th-order method. The difference between the two results is used to estimate the maximum truncation error and if this is greater than a preset tolerance, the time step is halved and the calculations are redone. If during computation the truncation error falls below one-tenth of the tolerance, the time step is increased by 50% at the succeeding integration step.

Although this scheme works well for controlling the solution for the arcing variables, it is insufficient for checking on the accuracy of the transient heating calculations as described in

section 2.2. One possible way to do this is to reformulate the finite-difference equations as a set of linear o.d.e.'s [7], add these to the list of state variables, and to use R-K integration to solve for all the variables, including temperature rises, simultaneously. This method has been tried but it is not efficient. Open-type integration schemes such as R-K require the time step to be much smaller than the smallest time constant in the set of equations [13]. If the heating calculations are included, the solution time step becomes (unnecessarily) dictated by the thermal time constants of the notch zones, yielding a very small time step and unacceptably long solution times.

It is much better to use the direct implicit method described in section 2 to calculate the element temperature distribution and to use a combined scheme for controlling the time step. A typical method is given below. (Omitting model switching and associated logic).

- (i) Integrate the non-linear set for the new state variables, reducing the time step if necessary to ensure accuracy. This will yield, among other things, the new circuit current.
- (ii) Calculate the new temperature distributions for the notch zones not yet arcing. If the maximum temperature increment exceeds  $\Delta T_m/50$ , reset all state variables and temperatures to "old" values and return to step (i).
- (iii) Increment the time variable.
- (iv) If the truncation error from the R-K exceeds one-tenth of the required tolerance, leave  $\Delta t$  unchanged. Otherwise increase the time step as follows:
  - (a) If all notch zones are arcing increase  $\Delta t$  by 50%
  - (b) Otherwise increase  $\Delta t$  by an amount which by extrapolation is expected to give a maximum temperature increment of  $\Delta T_m/80$  on the next step
- (v) Go to step (i).

This scheme gives fast efficient solutions for all fuse designs encountered to date.

## 5. Other computational techniques

### 5.1 Switching of models and logical control

During the numerical solutions described above to obtain the transient temperatures and arcing variables, there are many stages at which the models need to be changed, enabled or disabled, consequent upon the occurrence of some "event". Typical events include fusion of the notch zones, merging of arcs between adjacent notch zones, arcs reaching the end-caps, commutation of arc current between parallel elements, arc extinction, and so on. In a fuse with several different notch designs, some notch zones may be arcing while some are not, and the merging of adjacent arcs may take place at different points on the elements at different times. It is a very complex job to keep track of the state of all parts of the total system model. It is necessary to have a formally-structured procedure for doing this, firstly to ensure reliability, and secondly to enable upgrades to be added to the models with the minimum of difficulty.

The basic procedure is to have a set of logical variables describing the states and sub-states of the model, and at the end of each integration time

step, logical tests are made to see whether a change of state has occurred during the step. If so, the time at which the change occurred ( $t'$ ) is calculated by linear interpolation, the state(s) are switched, and the values of all numeric solution quantities are reset, by interpolation, to their values at time  $t'$  before resuming solution.

This basic procedure is not enough, however, as sometimes more than one state change can occur during a time step. Thus it is necessary first to record all state changes which occur and then to determine which of these changes occurred earliest, i.e. with the lowest value of  $t'$ . The model is then switched to this point before resuming, which ensures that the changes of state occur in the right order. In some cases this can be an important consideration [10].

Within this scheme, however, special consideration needs to be given to the case of merging of arcs between adjacent notch zones. Whilst in general each notch zone needs to be treated individually, it is very common to have a uniform spacing of notches, in which case merging takes place almost simultaneously along the length of the element. For a high-voltage fuse there may be a hundred or so series notches, and if they are uniformly spaced, the above solution procedure would reset the models a hundred or so times during the time step when merging occurred, in an order which depended upon the rounding error in the solution for the arc lengths. To give a more efficient procedure, the states should be reset after logical testing for all arcs about to merge whose lengths do not differ by more than 1%. This gives a much more rapid progress through the transition with negligible change in accuracy.

### 5.2 Addition of new lumen segments

In the original scheme [1], a new axial lumen segment was added to each arc at every time step. During the later stages of arcing, when the arc current becomes low, these new segments are very short, because the burnback velocity is very low. In these cases a large reduction in computing time can be achieved if, instead of creating a new lumen segment, the extra arc length is simply added to the previous segment. This drastically reduces the number of state variables generated during solution. Experience has shown that if this procedure is adopted when the extra length is less than about 1% of the total arc length, there is negligible difference in the results obtained.

## 6. Software design

### 6.1 User interface

It should be emphasised that the models and computational algorithms described in this paper must be transparent to the software user, who is interested in the final results and not usually in the means used to achieve them. Developing a simple system for the input of fuse designs and the output of results requires considerable effort but the ever-increasing availability of cheap computer power makes large improvements possible in this area.

### 6.2 Structured design

With increased complexity of the models and algorithms, and with a modern user interface, structured design of software is essential. All significant software functions should be contained within modules which are planned to combine together in a way that allows for future alterations and additions. Thus if it is decided that an improved burnback model is to be adopted, it must be possible

to do this very simply, by changing one program module, with little or no alteration to the remaining modules.

### 7. Typical results

Fig.1 shows a comparison between the measured breaking transients and the values computed using the improved models and algorithms described above for a 600A fuse tested nominally at 600V 100kA. The curves show a prearcing period followed by a small voltage increase when one of the notches begins arcing. Somewhat later the remaining notches, which have larger widths, melt and the fuse voltage increases further, followed by a rapid rise in voltage as all arcs burn back. Later, as the current falls and the arcs merge into one (in stages) the fuse voltage falls along with the current until arc extinction occurs.

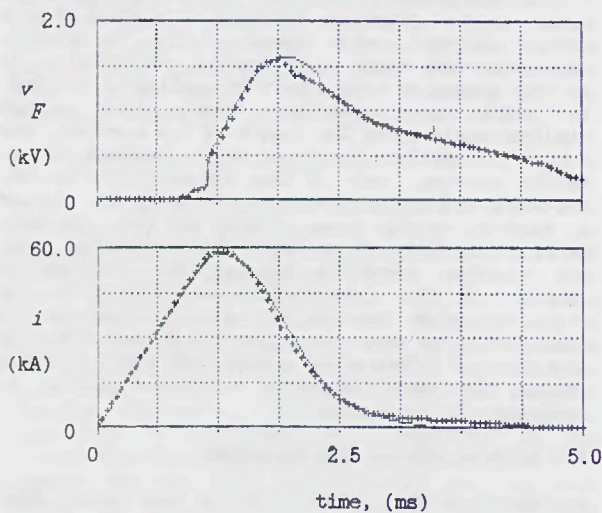


Fig. 1 Short-circuit transients for 600A fuse at 600V, 100kA nominal

————— computed  
 + + + + + test results

Using the improved models and algorithms, with a variety of fuse designs and filling media, peak let-through currents can usually be computed within 5%, while peak arc voltage, arc energy, and  $I^2t$  are usually within 15%.

The results for unbonded sand are better than for bonded sand, and so there is scope for improving the models of the arcing process within bonded sand.

### 8. Test plant model

Apart from the modelling of arcing in bonded sand, there is little scope for improvements to the fuse models described above. If further improvement in accuracy is required, a better model of the test circuit is needed. The results shown in Fig.1 were obtained by representing the source circuit in the usual way, by a fixed R-L series circuit, determined from the nominal test conditions, i.e. voltage, prospective current, and power factor. However recent experience has shown that this model is inadequate if high accuracy is required.

In most laboratories the short-circuit current is obtained from a synchronous generator, the inductance of which is time-varying. The total circuit inductance consists of the generator inductance plus the inductance external to the generator and is therefore not constant. Studies

have shown that this can typically cause an error of 3-4% in the computed value of  $I^2t$ .

However a much more important consideration is that the test circuit resistance is not constant. The estimate of R usually used is based upon a power-factor value derived from a calibration shot. It is obtained from the d.c. decrement one half-cycle after switch-on, i.e. after 10ms for 50 Hz, and this gives a measure of the d.c. resistance of the test circuit. However most fuse breaking tests are over within a few milliseconds, and during this period the transient resistance of the circuit is much higher than the d.c. value, because of the transient skin and proximity effects and transients induced in other conductive parts external to the test circuit. The power for these losses must be met from the test circuit and they are made manifest by a transient increase in the test circuit resistance.

The above errors in the test-circuit model give rise to errors of the same order as those due to the fuse model. Significant further improvement is only possible if progress in the modelling of the test plant, as well as the fuse, can be made.

### 9. Conclusions

The paper has described a number of extensions and improvements to the modelling of fuse breaking tests. For computing transient element temperatures a fully implicit formulation is recommended, with direct solution using sparse-matrix methods. Improvements to the arcing models include extension to the quasi-static arc characteristic, representation of the flow properties of different fillers under arcing, improved burnback models, and a method for representing the effect of the inner diameter of the fuse tube.

Automatic control of the solution time step is needed to obtain fast and accurate results, and a suitable method has been described, which combines the differing requirements of the prearcing and arcing models. A structured scheme for model switching and logical control is needed for reliability and extensibility. The improved models have been tested with a variety of different fuse designs and give results which are close to those obtained by short-circuit tests, but further improvement requires a simultaneous improvement in the modelling of the short-circuit test plant.

### 10. References

- [1] Gnanalingam S. and Wilkins R., Digital simulation of fuse breaking tests. 1980, Proc.IEE, 127, 434-440.
- [2] Gnanalingam S., Ph.D Thesis, Liverpool Polytechnic, 1979.
- [3] Daalder J.E. and Schreurs E.F., Arcing phenomena in high-voltage fuses. 1983, EUT Report 83-E-137, Eindhoven University of Technology.
- [4] Leistad P.O., Kongsjorden H. and Kulsetas J., Simulation of short-circuit testing of high-voltage fuses. 1984, Int. Conf. on Electric Fuses and their Applications, Trondheim, 220-226.
- [5] Eger D. and Rother W., A mathematical model for the arcing period of high-voltage fuses. 1989, IC-ECAA, Xi'an, China.

- [6] Wilkins R. Wade S. and Floyd J.S. A suite of programs for fuse design and development. 1984, Int. Conf. on Electric Fuses and their Applications, Trondheim, 227-235.
- [7] Smith G.D. Numerical solution of partial differential equations : finite difference methods. 1986 (3rd edition), Oxford University Press.
- [8] Davies A.J. The finite element method : A first approach. 1980, Oxford University Press.
- [9] Pissanetzky S. Sparse matrix technology. 1984, Academic Press.
- [10] Wilkins R. Commutation of arcs between parallel fuse elements. 1989, 6th Int. Symp. on Switching Arc Phenomena. Lodz, Poland, 237-241.
- [11] Oliver R. 1973, 2nd Int. Symp. on Switching Arc Phenomena. Lodz, Poland, Transcript of discussions, 180-181.
- [12] Pastors Y. and Ledinsk H.A. Switching arc in sand-liquid-filled fuses. 1977, 3rd Int. Symp. on Switching Arc Phenomena. Lodz, Poland, 320-323.
- [13] Conte S.D. and De Boor C. Elementary numerical analysis. 1981, McGraw-Hill.

Seems a sensible description.  
 Droplet pressed into sand  
 - see my paper

AN INTEGRATED PHYSICAL MODEL OF THE H.B.C. FUSE ARCING PROCESS

K. Jakubiuk, T. Lipski  
 Technical University of  
 Gdańsk, Poland

and A. Pisanko  
 Electrotechnical Institute  
 Gdańsk Branch, Poland

**S u m m a r y.** Paper gives a phenomenological description of the whole arcing process which has take place in a fuse with single notched fuse-element, but particularly the fuse element burn-back and arc-channel physics. All considerations are based upon existing literature and own extensive short-circuit experiments in the range 3-30 kA(RMS) 550 V, 50 Hz. Three stages are considered: arc-ignition, arc-burning, post-arc recovery withstand.

1. Introduction

The paper deals with the arcing phenomena in high breaking capacity fuses (h.b.c.) during short-circuit current interruption. The arcing under consideration takes place in a fuse within multi-notched single strip fuse-element. In such a case known approaches do assume several simplifications about the arcing physics to facilitate the calculations. In this respect usually two arc aspects are considered: the arc-elongation due to fuse-element burn-back and secondly,- the arc-column conditions in time. Both make possible the arc-voltage calculation, hence the analytical prediction of h.b.c. fuse behaviour in a given electric circuit is possible.

Meanwhile the whole arcing process contains 3 following stages: arc-ignition, arc-burning, post-arc recovery strenght. The existing literature concentrates mainly on the second stage. So one aim of the paper is to give an integrated approach which includes mentioned 3 stages. Not less important is another aim, to show an improved look onto the burn-back process and arc-column behaviour during the second stage.

2. Arc-ignition

Two groups of parameters are responsible for arc ignition in the notches: first,- for a given fuse-element material, the fuse-element geometry, but particularly so-called the "constriction ratio"; second,- the short-circuit parameters amongwhich the most important is the prospective current. Under "constriction ratio" one has understand the ratio of the fuse-element shoulder cross-

section to the notch cross-section. If by a given constriction ratio the short-circuit current is of the magnitude, which can lead to the multiple arcing, such case is excluded from considerations.

The arc-ignition voltages  $u_1$  in a notch one can calculate using a number of the Hibner's empirical relations. The newest one for round notches is given in a paper for this ICEFA [1]. Earlier 8 Hibner's publications on this subject one can trace using "Digests" [2]. The general form of all those relations is

$$u_1 = c i_0^a S^{-b} \quad (1)$$

where:  $c$  - some constant;  $i_0$  - cut-off current  $S$  - notch cross-sectional area;  $a, b$  - constants (e.g.  $a=0.5, b=-0.2$ ). Besides, there is a number of consecutive approaches to the arc-ignition physics [3-5]. The newest one is given in a paper for this ICEFA [6].

During the arc-ignition appears the pressure exploding component [7]. A clear record of such a component is shown in Fig.1.

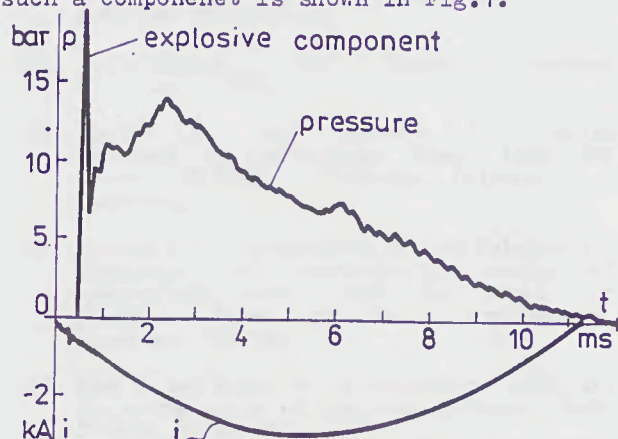


Fig. 1 Record during arc-ignition and burning in ice tube 10 mm dia, 150 mm long

Although the record refers to the ablative arc investigations [9], but the arc was ignited by 0.1 mm Cu wire in 150 mm long ice hole. The Figure was not shown in the paper [6], but belong to the same series of tests as described in that paper (by courtesy of Prof. A.D. Stokes). The physics ruling the wire explosion and the arc ignition in notches is nearly analogous. As a result of notch-explosion X-ray photography after current interruption shows typical explosion region (encircled in Fig.2). The region

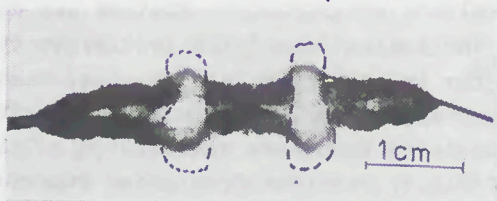


Fig. 2 X-ray picture of a fulgurite, side view, Cu-strip  $6 \times 0.2 \text{ mm}^2$ , 2 constrictions  $1.2 \times 0.2 \text{ mm}^2$ , 12 mm apart, 3.1 kA

shows complete lack of the metal particles. Moreover the cavity after explosion indicates the largest cross-section. As it will be demonstrated farther, the encircled region is one of the major component of the post-arc gap to withstand the recovery voltage.

## 2. Arc-burning

### 2.1 Burn-back process

One of the most advanced approach to the burn-back process is done by [9] which exploits very much the results of a basic work [10]. Repeated after [9] Fig.3 shows phases distributed along the element-end during the burn-back process. At the arcing front  $x=x_l$  the liquid silver is overheated up to abt 1700 K, whereas in the case Cu-strip the liquid reaches  $T_{\text{drop}} = \text{abt melting point}$ , i.e. 1356 K [10].

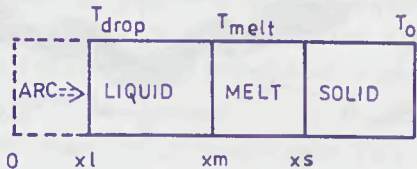


Fig. 3 Phases within fuse-element during burn-back process [9]

To verify the model taken in calculations [9, 10] a number of tests were carried out, described in details in [11] using strip Cu-elements,  $6 \times 0.2 \text{ mm}^2$  with notches  $1.2 \times 0.2 \text{ mm}^2$  (constriction ratio 5). The number of notches 1 to 5 within distances up to 15 mm.

Standard fuse quartz sand of 0.2-0.5 mm sieve dimension was packed into the tested DIN dimension 500 V fuse-links by a standard procedure. The active fuse-element length was 56 mm. Tests were performed within 3.1, 9.99 and 32 kA (RMS), p.f.=0.24 and 550 V, 50 Hz. After every shot the test voltage was maintained 15 sec between fuse-terminals.

From the literature are well known descriptions of the fulgurites after short-circuit interruption (e.g. [10, 12]). But our inspection of more than hundred fulgurites after above tests shows some new details essential for the burn-back process. Several of them only one can deduce from the Figs 2 and 4. One can distinguish yet not described two processes: droplet formation and acceleration and droplet penetration into the sand. The energy needed to get both processes shall be drawn from the heat of overheated element-end (at arcing front  $x_l$  in the Fig.3). That is why suggested in [10] for copper the droplet formation temperature 1356 K shall be higher, otherwise the droplets penetration into the sand is impossible.

In the literature the droplets formation and acceleration processes are described for arc cathode root on contact switches only [13, 14]. In this case the surface in touch with the root is practically unlimited in comparison with the cathode-spot dimensions. Whereas in fuses the element-end area at the arcing front  $x_l$  (Fig.3) is restricted, for example in our experiments up to  $1.2 \text{ mm}^2$ . So in both cases the droplet process can show some differences. But qualitatively it seems is similar one to that demonstrated in the Fig.5.



Fig. 4 Cross-section of fulgurite cut along the arc-channel axis, Cu-strip  $6 \times 0.2 \text{ mm}^2$ , 2 constrictions  $1.2 \times 0.2 \text{ mm}^2$ , 1 mm apart, 3.1 kA, 1 - bright dots on the rim are Cu droplets

From the fulgurite inspection remarkably is that the droplets diffusion into the sand the very element-end shows nearly ideal symmetry, i.e. half of the strip metal is removing in one and second half in opposite direction, both perpendicular to the strip flat surface.

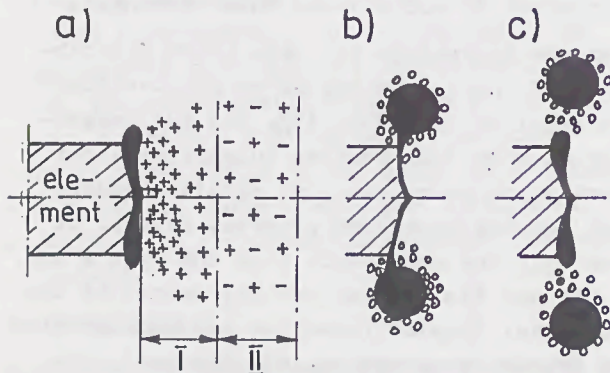


Fig. 5 Consecutive pictures showing droplets ejection from the cathode-element-end a - melting and deformation of liquid b - droplets ejection, c - heating and vaporization of droplets, I - space charge zone, II - ionization zone Note: Zones I and II in Figs b and c are not shown.

The droplet penetration into the sand shall depend first of all upon:

- the kinetic energy of droplets in the instant of the clashing into the sand wall,
- the dynamic viscosity and mass density of droplets,
- the sand wall porosity,
- the dynamic pressure of the arc-column,
- the pressure distribution in direction z (Fig.4).

The hydrodynamics of that penetration can be formulated as follows [15]

$$-\frac{dp}{dz} = \alpha \mu G + \beta v G^2 \quad (2)$$

where: left hand side means the local pressure gradient in z direction,  $\alpha$  - dynamic coefficient of resistance between sand and droplets due to adhesion,  $\beta$  - resistance of sand due to inertia,  $\mu$  - dynamic coefficient of viscosity,  $v$  - specific volume of metal. Unfortunately all the right hand side parameters are not known quantitatively.

During the droplets filtering through sand their temperature is decaying eventually up to the metal solidification, unless immediately after a heat wave from the arc-column will overtake the thermal conditions of alres-

dy dispersed metal.

Two velocities are deciding on the dynamic shape of the droplet layer dispersed into sand in the vicinity of the element-end, viz.: one is the burn-back velocity, which is axial, and second, - the initial velocity of droplet penetration into sand, eventually perpendicular to the axis (Fig.6). The burn-back velocity one can calculate, for example by method demonstrated in [9], whereas the droplet velocity is not yet possible even evaluate analytically. What we can do now is the evaluation of the last velocity from X-ray images of fulgurites, e.g. taken from our experiments, in a combination with the calculated burn-back velocity [9]. The angle  $\alpha$  (Fig.6) received from those experiments is between abt  $25^\circ$  and  $65^\circ$  and relates to the test current and the fuse-element geometry. For mean value  $45^\circ$ , assuming penetration velocity perpendicular to the axis, the penetration velocity shall be equal to the burn-back velocity. By current density range 1 to 4 kA/mm<sup>2</sup> the measured burn-back velocity [10] was between abt 1 and 5 m/s correspondingly. This means the droplet penetration velocity of this same order.

The final point with droplet filtering into sand is on the enthalpy  $H_{con}$  increase per unit volume needed to raise the temperature from the initial fuse-element temperature to

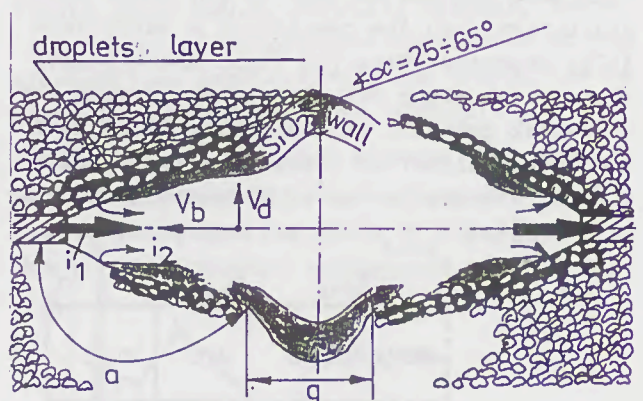


Fig. 6 Image of the arc

$i_1$  - main current path;  $i_2$  - partial current path;  $v_b$  - burn-back velocity;  $v_d$  - droplet velocity;  $\alpha$  - angle between droplets layer and axis;  $g$  - recovery withstand gap between droplets layers which in fact is the gap after explosion; a - points of connection

$T_{drop}$ . To get reasonably good agreement of voltage and current traces for the calculations based upon method given by [10] and recorded in our experiments we needed to assume  $H_{con}$  as a variable depending upon test conditions and the fuse-element geometry. For Cu, for instance, the magnitudes of the  $H_{con}$  shall be as in the Tables 1 and 2, shown in our paper [16]. Those magnitudes are between 0.7 and 1.18 times  $10^9$  J/m<sup>3</sup> if the calculating errors of the current have to be not greater than abt 20 %, the voltage 25 % and the final arc length abt 7 %. Moreover similar enthalpy but for sand  $H_{ag}$  shall vary between 4.9 and 7 J/m<sup>3</sup> times  $10^9$ . So a remark in [10] that  $H_{con}$  shall not necessarily be constant is confirmed by our experiments and calculations.

All said means that also in the Cu case the  $T_{drop}$  shall be higher than the melting temperature and the degree of metal overheating shall be different for various short-circuit conditions and the fuse-element geometry.

Mentioned earlier the dynamic pressure of the arc-column it seems is responsible for farther pressing into the sand of the liquid metal particles.

Another observation from the fulgurites indicate that the droplets pressed into the sand in the vicinity of the element-end are still in a direct touch with the arc column. In this region is not yet arised any shield made from the molten silica sand, which can isolate the arc-column from dispersed metal. It denotes that some portion of the current  $i_2$  in Fig.6 also flows through dispersed metal in parallel to the current  $i_1$  of the main feeding path. But due to droplets dynamic and their very high temperature the magnitude of current  $i_2$  supposed to be negligible in relation to  $i_1$ . As a result also electromagnetical influence on the mobile liquid metal can be omitted.

Next important observation based upon fulgurites inspection shows that the dispersed metal (Fig.4) is in very good galvanic connection with the element-end. Such a connection exists even up to the farthest droplets apart to the element-end. Also a galvanic connection with the element-end demonstrates inner wall of the arc-channel just in the vicinity of the element-end. The connection in

this region is likely due to yet lack of the developed tight silica shield, isolating the arc-column from the dispersed metal. Obviously the observations described refer to the fulgurites after completing of interruption. During the arc-burning those galvanic connections could not exist. But, in any case, very close to the final current zero such connections should already become actual due to droplets merging into one connecting layer. From this follows an important behaviour of the fuse during the post-arc recovery withstand stage.

## 2.2 Arc-column behaviour

It is already well known and is confirmed by Figs.4 and 6 that the arc-column is surrounded by a tight tube made from molten sand which includes chemically bound Cu. Detailed inspections of the inner walls of fulgurites in an arbitrary distance to the element-end does not show any axial draught traces on those walls. It seems, it witnesses of the lack of considerable axial plasma jets originated in its constricted region in the vicinity of electrode-ends. In fact a simple calculation shows, for example, that for conditions corresponding to our experiments, the overpressure in the vicinity of the electrode-ends against arc-column should be abt 0.1 to 0.5 MPa only. That's why the existing approaches which treat the arc as a SiO<sub>2</sub> wall stabilized one, of course, are correct. Arc is assumed in LTE and characterized by temperature, pressure, cross-sectional area and velocity of the plasma in perpendicular direction to the strip flat surface induced by the column expansion and the opposite ablation process.

## 3. Post-arc recovery withstand

Coming back to the fulgurite inspection after our experiments (Figs.4, 6) one can come to the conclusions about the post-arc withstand. The processes responsible for recovery withstand are concentrated along two parallel paths. One is the gap between the metal layers dispersed into the sand and galvanically connected to the element-ends. The second is along the molten silica wall. That's why a first step in analytical prediction of that withstand should be the heat transfer calculation from the elongating arc-column to the sand. This heat, first of all, cause

the growing of molten wall thickness. But penetrating farther the heat can reach earlier dispersed droplets bringing them eventually to the boiling point. In a result the metal can evaporize giving the elongation of mentioned gap.

Above sketchy description of phenomena associated with the post-arc recovery withstand are crucial for the final arc-extinction and for the time being are awaiting on extensive investigations.

#### 4. Final remarks

We tried to give an integrated physical picture of the arcing in h.b.c. fuses equipped within a notched single strip fuse-element overloaded by a short-circuit current. The picture contains some new aspects, among them: droplets formation, their penetration into the sand, the galvanic contact of those droplets with the element-ends. Moreover a very crucial for the final arc-extinction problem was mentioned, namely the post-arc recovery withstand of the hot fulgurite, which waits for investigations.

#### References

- [1] Hibner J., Calculation of the arc ignition voltage of fuse elements with round bridges, 1991, ICEFA-1991, Nottingham, U.K.
- [2] Turner H.W. and Turner C., Digests of information on fuses, protective and switching devices, ERA 2799, Leatherhead, U.K.
- [3] Hibner J., Jakubiuk K. and Lipski T., Evaluation of pressure explosive component of high rupturing capacity fuses, IX Int. Conf. on Gas Discharges and Their Appl., 1988, Venezia, Italy, 583-587.
- [4] Jakubiuk K. and Lipski T., An improved evaluation of exploding pressure component (EPC) of H.B.C. fuses, XII Symp. on Electr. Discharges in Gases, 1989, Pasym, Poland, 284-295.
- [5] Jakubiuk K. and Lipski T., An improved analytical model of the explosive component pressure generation in a H.B.C. fuse VI SAP, 1989, Łódź, Poland, 185-189.
- [6] Jakubiuk K., Electrothermal fuse-element disintegrating mechanism by short-circuit currents, 1991, ICEFA-1991, Nottingham, U.K.
- [7] Lipski T., Generation and propagation of the pressure due to the fuse-element disintegration in h.b.c. fuses, Int. Conf. on Gas Discharges and Their Applications, 1985, Oxford, U.K., 87-90.
- [8] Stokes A.D. and Cao L.J., Ablation arcs I: Arcs in ice, J. Phys. D.: Appl. Phys., U.K. Vol. 22, 1989, 1697-1701.
- [9] Sloot J.G.J., Kalašek V.K.I. and Sikkenga J., A one dimensional mathematical model for the dynamical burn-back velocity of silver strips, 1987, ICEFA 1987, Eindhoven, The Netherlands, 99-111.
- [10] Daalder J.E. and Schreurs E.F., Arcing phenomena in high-voltage fuses, EUT Report 83-E-137, Eindhoven, The Netherlands, Technical University.
- [11] Ossowicki J. and Pisanko A., Influence of the distance of the constriction in the strip fuse element on breking short circuit, VI SAP, 1989, Łódź, Poland, 230-236.
- [12] Lakshiminarashima C.S., Barrault M.R. and Oliver R., IEE Proc., 1978, Vol. 125, 391-399.
- [13] Bolanowski B. and Kołaciński Z., A model of cathode plasma jet, (in Polish), VII Symp. Podstawy Teorii Wyładowań Elektrycznych w Gazach. Politechnika Warszawska, 1983, Warszawa, Poland, 8-18.
- [14] Hantzsche E., Droplet emission from vacuum arc spots. Proc. 7th Int. Symp. Disch. Electr. in Vacuum, 1976, Novosibirsk, USSR, 324.
- [15] Vasiljev L.L. and Majorov V.A., An analytical study of resistance, heat transfer and stability in evaporative cooling of a porous heat-producing element, Ind. J. Heat Mass Transfer, 1977, Vol. 22, 301-307.
- [16] Lipski T. and Pisanko A., Could a short-circuit protection by h.r.c. fuse be selected upon fuse arc-voltage? 4th Int. Symp. on Short-circuit Currents in Power Systems. 1990, Liège, Belgium, 4.1.1.-4.1.5.

THE USE OF OPTICAL SPECTROSCOPY IN THE ANALYSIS  
OF ELECTRIC FUSE ARCING

D.R. Barrow  
Davy Computing Limited  
Sheffield, UK

and

A.F. Howe  
University of Nottingham  
UK

*Low temps  
disagree with  
Chikata  
Franchard July?*

**Abstract**

Optical fibres were inserted into electric fuselinks to observe the light emission from fuse arcs. By recording the emission spectra using a rapid-scanning spectrometer and photo-multiplier tube and measuring the relative intensities of the most prominent wavelengths it was possible to estimate fuse arc temperatures. The results indicated that these temperatures were of the order of 7000K. and remained virtually constant throughout the duration of the arc.

**1. Introduction**

The high temperature of a fuse arc plasma causes it to emit light with characteristic spectral lines [1]. By obtaining the spectrum of the light it is possible to assess the temperature of the arc, providing that the time taken to collect the spectrum is short enough for the temperature to be regarded as constant and long enough for the area observed to be in local thermodynamic equilibrium.

Inserting quartz optical fibres into fuselinks it is possible to observe light emissions from electric fuse arcs. Employing fibres with diameters roughly equal to the mean sand grain diameter it follows that the operation of the fuse, even during arcing, will only be marginally affected.

**2.0 Test Fuses**

Test fuses were constructed as illustrated in figure 1, using glass reinforced plastic bodies with zinc end caps and copper tags.

Elements comprised a length of 7.14mm ( $\pm 0.7\%$ ) wide, 0.1 mm ( $\pm 2.5\%$ ) thick, 99.97% pure silver strip, with a single notch punched at its centre.

Notch dimensions were controlled to better than 2%. The fuse body was drilled perpendicular to the plane of the element using a 1mm drill. A glass capillary tube was inserted to within 3 mm of the element and glued into place using epoxy resin. A 200 micron quartz optical fibre was introduced and allowed to rest on or near to the restriction. It was then glued into place using epoxy resin. The fuses were filled

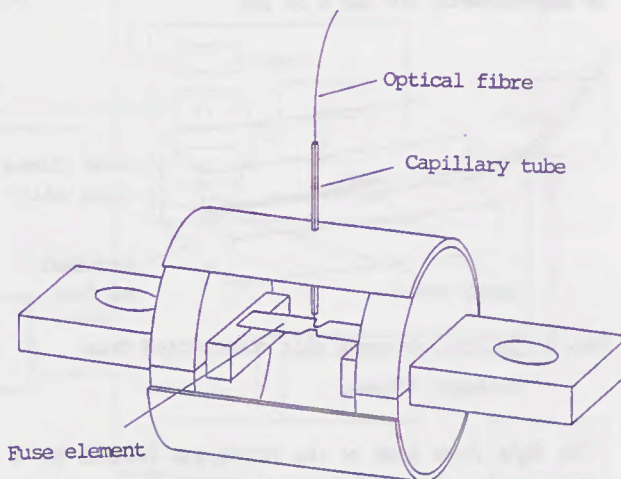


Fig. 1 Test fuse showing placement of optical fibre.

with 97% pure silica grains with a minimum diameter between  $250\mu\text{m}$  and  $640\mu\text{m}$ . The sand was compacted into the fuse body by precisely controlled vibration.

**3. Rapid Scanning Spectrometer**

A rapid scanning spectrometer (RSS) was constructed, as shown in Fig. 2 to enable the spectra of light emitted from test fuselinks during arcing to be analysed.

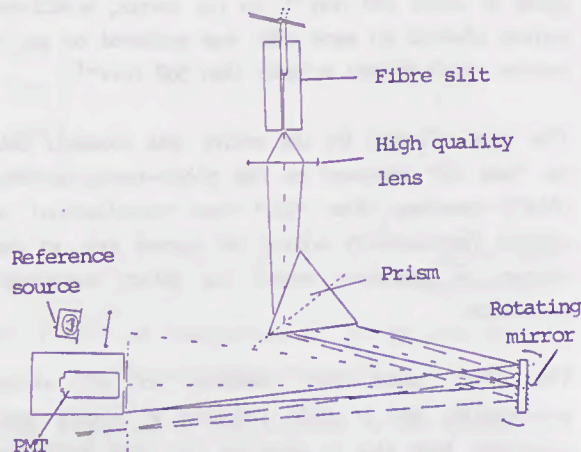


Fig. 2 Rapid Scanning Spectrometer.

The light emanating from each test fuse was transmitted through the optical fibre inserted in its body and a standard connector to a bundle of four  $50\mu\text{m}$  fibres. The free end of the bundle was exposed

from its protective sheath, and the four fibres glued to a machined-flat surface, using clear epoxy resin. The fibres were laid down touching their neighbours, with the final centimetre aligned horizontally. (Fig. 3). The front surface of the block, including the ends of the fibres, was then machined flat and polished. This formed the "entrance slit" to the RSS with dimensions of approximately  $200\ \mu\text{m} \times 50\ \mu\text{m}$ .

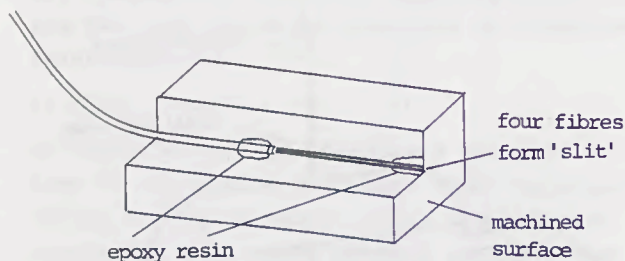


Fig. 3 Optical entrance slit constructed from multiple fibres.

The light from ends of the fibres was focused by a high quality 50mm camera lens. The optical path length was of the order of 1000mm giving a magnification of almost 20, and a final image width of around 1mm.

The light was then dispersed by a  $60^\circ$  prism onto a rotating mirror. To achieve a wavelength resolution of better than 1.5nm a complete spectrum (from  $\sim 450\text{nm}$  to  $\sim 850\text{nm}$ ) had to be collected in  $30\ \mu\text{s}$ . Prism dispersion was about  $5^\circ$ , so the mirror had to rotate through  $5^\circ$  in less than  $30\ \mu\text{s}$ , and complete one revolution in 2.2ms. This corresponds to a rotational speed of about  $460\ \text{revs}^{-1}$ . So the mirror, which was surface silvered on each side, was mounted on an air turbine which rotated at more than  $500\ \text{revs}^{-1}$ .

The light reflected by the mirror was focussed onto the "exit slit" mounted on the photo-multiplier tube (PMT) housing. The "slit" was manufactured to operate symmetrically around the optical axis, so that changes in aperture would not affect wavelength calibration.

The PMT used was sensitive to all visible wavelengths, had a rapid response to ensure good resolution, high gain to cater for low light levels and low dark current to improve final signal to noise ratio.

Barrow [2] provides fuller details on the construction of the RSS, along with the method of calibration. Fig. 4 shows the variation in system response with wavelength.

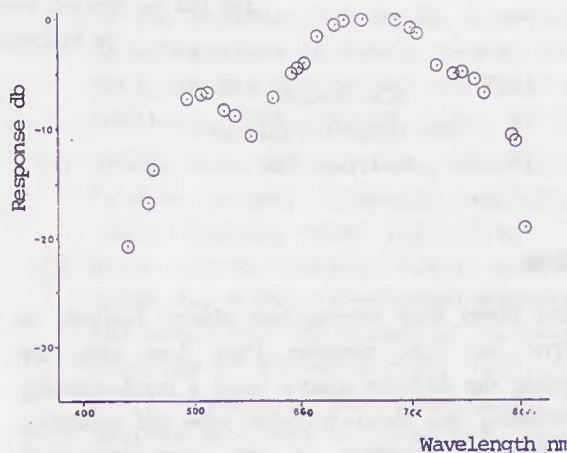


Fig. 4 System response: sensitivity vs. wavelength.

#### 4. Experimentation

The test configuration is shown in Fig. 5. With the applied voltage set at 255V, the prospective fault current was 525A at a power factor of 0.2 lagging. Using point on wave control, accurate to two electrical degrees, the circuit was closed at the applied voltage zero, to ensure substantial arcing. The fuse current and voltage waveforms were recorded and the fuse arc spectrum during a preselected "time window" in the arcing period was captured.

Fig. 6 shows a sample trace of the PMT output. Three multiplets are readily observed. The wavelengths of the component parts are:

- i) 635.5nm: 634.7nm and 637.1nm
- ii) 505.1nm: 504.1nm and 505.6nm
- iii) 597.2nm: 595.8nm and 597.9nm

Because of the variation in system response with wavelength (Fig. 4) the peaks recorded were multiplied by appropriate correction factors to find their relative intensities.

##### 4.1 Possible sources of error

The possible sources of error which could affect these results are that

- (i) the optical fibre will act as a heat pipe, causing a localised reduction in temperature particularly during prolonged pre-arcing.
- (ii) light energy will escape from the arc, potentially reducing the arcing time and arc energy.

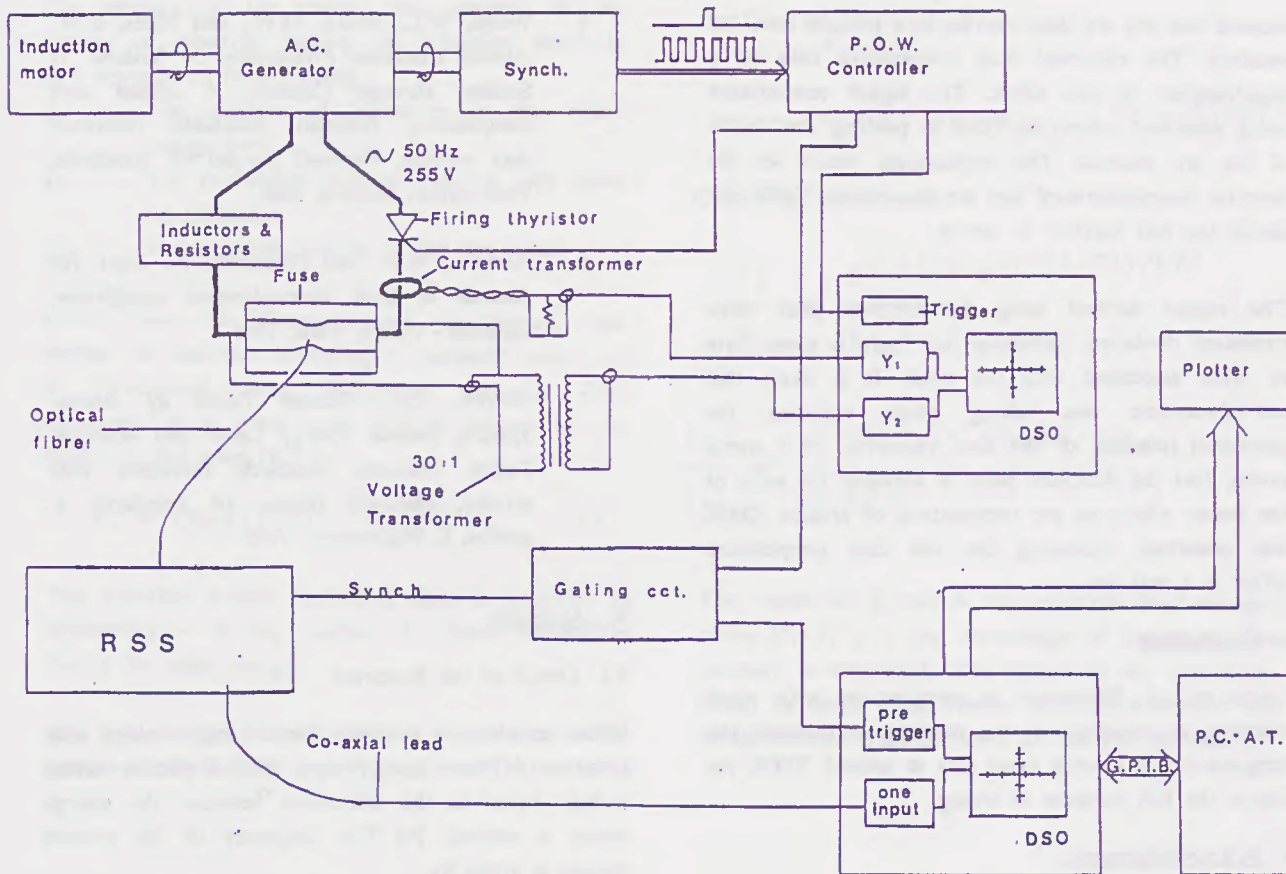


Fig. 5 Test system configuration with Rapid Scanning Spectrometer.

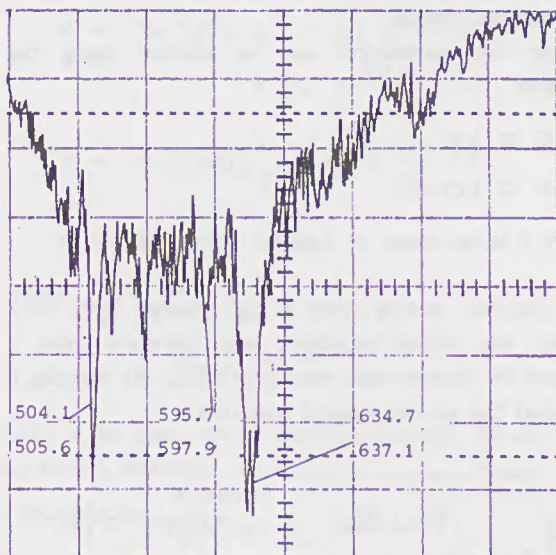


Fig. 6 Emission spectrum of HBC fuse arc.

### 5. Interpretation

To find the arc temperature from the spectral lines it is necessary to compare the intensities of the lines, as explained in the appendix 9. The temperature derived

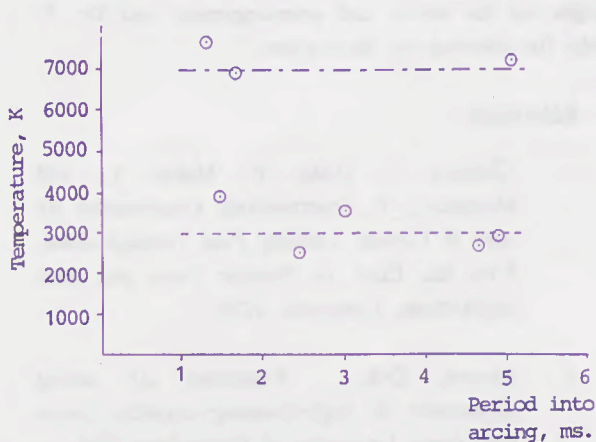


Fig. 7 Plot of temperature vs. period into arcing from emission spectroscopy.

from comparison of the intensities of the 505.1nm and 597.2nm peaks appears to be at one of two discrete levels centred around 7000K and 3000K, see Fig. 7.

In a separate study by the authors, described in another paper to this conference [3] five optical fibres were inserted into fuse links so that the ends of the fibres formed a straight line above the fuse element starting at the restriction. The results of this work

showed that the arc does not lie in a straight line, but wanders. The observed dual temperature may be a manifestation of this effect. The higher temperature being observed when the fibre is probing the centre of the arc channel. This explanation would set the electron temperature of the arc at around 7000K for almost the full duration of arcing.

The results derived using the 635.5nm peak show consistent deviation, indicating that there is some form of error associated with this peak. It is likely that self-absorption was taking place reducing the perceived intensity of the line. However, it is worth noting that the 635.5nm peak is elevated on each of the traces where an arc temperature of around 7000K was observed, indicating that the dual temperature effect is a real one.

## 6. Conclusions

Using optical fibroscopy in conjunction with rapid scanning spectroscopy it was possible to measure the temperature of electric fuses arcs at around 7000K for almost the full duration of arcing.

## 7. Acknowledgements

The authors wish to thank Hawker Fusegear Limited for sponsoring this work, the University of Nottingham for providing the facilities, Professor A. Wright for his advice and encouragement and Dr. F. Hicks for drawing the illustrations.

## 8. References

- Chikata, T., Ueda, Y., Murai, Y., and Miyamoto, T: *Spectroscopic Observations of Arcs in Current Limiting Fuse Through Sand*, Proc. Int. Conf. on Electric Fuses and their applications, Liverpool, 1976.
- Barrow, D.R.: *Evaluation of arcing parameters in high-breaking-capacity fuses*. PhD thesis University of Nottingham 1988.
- Barrow, D.R., and Howe A.F., *A comparison of the computer modelling of electric fuse arcing and their real-life performance*. Proc. 4th Int. Conf. Electric Fuses and their Applications, University of Nottingham, Sept. 1991.
- Griem, H.R.: *Plasma Spectroscopy*, McGraw-Hill, NY, 1964.
- Weise, W.L., Smith, M.W., and Miles, B.M.: *Atomic transition Probabilities - Volume II Sodium through Calcium. A critical data compilation*, National standards reference data service, National Bureau of Standards, Washington, October 1969.
- Drawin, H.W. and Felenbok, P.: *Data for plasmas in local thermodynamic equilibrium*, Gauthier-Villars, Paris, 1965.
- Moore, C.E.: *Selected Tables of Atomic Spectra, Atomic Energy Levels and Multiplet Tables*, National standards reference data service, National Bureau of Standards 3, section 1, Washington, 1965.

## 9. Appendix

### 9.1 Origin of the Spectrum

When an electron traverses from a high energy state ( $E_m$ ) to a lower energy state ( $E_n$ ) a photon having energy equal to the difference between the energy levels is emitted. [4] The frequency of the emitted photon is given by

$$E_m - E_n = \Delta E = h\nu$$

where  $h$  is Planck's constant and  $\nu$  is the frequency of the emitted photon.

Hence the wavelength can be derived using the relation

$$c = \lambda\nu;$$

$$\lambda = hc/\Delta E$$

where  $c$  is the speed of light.

An electron moving from a high energy level to a lower one within an atom will therefore emit a photon of characteristic wavelength (Fig. 8) forming a spectral line on the emitted spectrum.

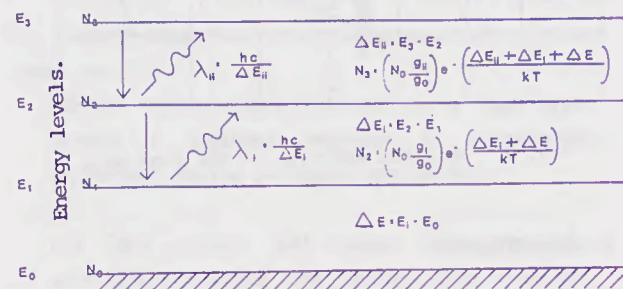


Fig. 8 Illustration of Boltzmann distribution.

The intensity of the emitted line depends on the number of electrons making the transition which in turn depends on three factors.

- i) The number of electrons in the raised energy level.
- ii) The probability that an electron will make the transition.
- iii) The statistical weights of the two states.

Where there is thermodynamic equilibrium, the number of electrons occupying a particular level can be determined using Boltzmann statistics. The population of a given level ( $N_j$ ) is related to the energy of that level ( $E_j$ ) by

$$N_j = (N_0 g_j / g_0) e^{-E_j/kT} \quad (1)$$

The statistical weight ( $g_n$ ) of a state is equal to its degeneracy - ie the number of distinct sub-states having the same energy.

The total number of particles ( $N$ ) is the sum of the number of particles in a particular level ( $N_i$ ) over all levels.

ie

$$N = N_0 + N_1 + N_2 + \dots$$

combining with equation 1 obtains

$$N = (N_0/g_0) (g_0 + g_1 e^{-E_1/kT} + g_2 e^{-E_2/kT} + \dots)$$

$$N = (N_0/g_0) \sum_{j=0}^i g_j e^{-E_j/kT}$$

$$N = (N_0/g_0) U(T)$$

where

$$U(T) = \sum_{j=0}^i g_j e^{-E_j/kT}$$

$U(T)$  is the state sum or partition function. Hence equation 1 becomes:

$$N_j = (N/U(T)) g_j e^{-E_j/kT}$$

For a volume of gas containing  $N_j$  particles in a raised energy state, and with a probability of  $A_{j,j-1}$  for the transition under review, the number of transitions in a second is  $N_j A_{j,j-1}$ . The transition emits a photon with energy  $hc/\lambda$  and hence the energy emitted per second (intensity) is

$$I = N_j \cdot A_{j,j-1} \cdot hc/\lambda$$

$$I = (N_j/U(T)) g_j A_{j,j-1} \frac{hc}{\lambda} e^{-E_j/kT}$$

Comparing the intensity of two lines obtains:

$$\frac{I_1}{I_2} = \frac{g_1 \cdot A_{1,2} \cdot e^{-((E_1-E_2)/kT)}}{g_2 \cdot A_{2,1}}$$

$$\frac{I_1}{I_2} = \frac{g_1 \cdot A_{1,2} \cdot e^{- (hc/kT) ((1/\lambda_1)-(1/\lambda_2))}}{g_2 \cdot A_{2,1}}$$

The values of  $g$  and  $A$  are available from standard tables [5,6,7].  $\lambda$  is the wavelength of the line whose intensity is measured. The values of  $h, c$  and  $k$  are found in many texts. Hence, the temperature  $T$  can be determined from the ratio of two line intensities.

ELECTROTHERMAL FUSE-ELEMENT DISINTEGRATING  
MECHANISM BY SHORT-CIRCUIT CURRENTS

K. Jakubiuk

Technical University of Gdańsk  
Gdańsk, Poland

Summary

The paper gives a new hypothesis of the striated disintegration of the fuse-elements. The hypothesis name is electrothermal mechanism of the striated disintegration. From general assumptions of the synergetics is shown a possibility of generating of the electrothermal instabilities by means of the relation of dispersions. For a simplified model by a numerical analyses are determined the conditions of the arising of those instabilities.

1. Introduction

During short-circuit interruption a uniform fuse-element of h.b.c. fuses disintegrates in form of the striation. Such a multiple arc-ignition shows also the shoulders (thicker parts) of notched fuse-element if those shoulders length, between notches is sufficient and the prospective current is large enough. Criteria of striation appearance for uniform wire elements, in form of a relation: the wire diameter versus the current density, are given by Nasiłowski<sup>8</sup>. Experimental formulae for average modulus  $h_w$  of striation for Cu and Ag wires is

$$h_w = 0.555 + 2.08 \cdot d \quad (1)$$

where:  $d$  - wire diameter,  $h_w$  and  $d$  in mm. But for uniform strip Cu and Ag elements that modulus  $h_s$  in mm, also established experimentally by Hibner<sup>5</sup> is

$$h_s = k_c \cdot S^{0.3} \quad (2)$$

in which:  $k_c = \text{const.} = 3.1 \text{ mm}^{0.4}$ ,  $S$  - strip cross-sectional area in  $\text{mm}^2$ . A defined minimal current density and a minimal energy stored in the circuit at the instant of disintegration shall be fulfilled to get striation.

In the literature there is a number of the hypothesis given on the striation origin in the frames of discussion on the wire explosion. The major are:

- a) magneto-thermo-elastic vibrations, Liebidiew<sup>7</sup>,
- b) magneto-hydrodynamic vibrations, Liebidiew<sup>7</sup>,
- c) wire vibrations, Nasiłowski<sup>8</sup>,
- d) nonuniform wire heating, Liebidiew<sup>7</sup>.

In the case a) and b) the disintegration is due to local deviation of the wire from the straight line or local deviation of the outer wire surface from cylinder. In the case c) the vibration starts immediately after first arc-ignition, whereas in the case d) some geometrical or structural inhomogenities generate the disintegration. According to up to date opinion (e.g. Liebidiew<sup>7</sup>), which shares also author of this paper, the pinch-effect in an exploding wire in h.b.c. fuses can be neglected as a cause of disintegration suggested by hypothesis a) and b). However, the last one still have lot of followers hypothesis b). X-ray pictures showed, Arai<sup>1,2</sup>, that the arc ignites only after the wire disintegration, which is in contradiction to the hypothesis c). Author is of opinion that hypothesis d) is the most adequate to reality, however, it explains the initiation of striation only.

The paper gives an attempt of extension of this hypothesis, which brought practically a new one, called farther the electrothermal mechanism.

Outgoing from the general assumptions of the synergetics, Wasiliew<sup>9</sup>, has been shown a possibility of appearance of the electrothermal instability by means of dispersion relations. For a simplified model by the numerical approach the conditions of that instability arising have been defined.

## 2. Striated disintegration as a dissipative structure

Dissipative structures are one of forms of the selforganization of the active systems, Wasiliew<sup>9</sup>. These structures are leading to distortion of the uniformities of non-equilibrated thermodynamical systems. Such structures show very often the periodical distribution in the space. The active systems are described by the nonlinear equations of diffusion. So our exploding wire, as an active system is described by the equation of the electromagnetic field diffusion

$$\frac{\partial j}{\partial t} = \frac{1}{\mu_0} [-\nabla (\nabla \cdot \frac{j}{\sigma}) + \nabla^2 (\frac{j}{\sigma})] \quad (3)$$

and the transient heat conduction equation

$$\frac{\partial T}{\partial t} = \frac{j^2}{\rho \cdot c_p \cdot \sigma} + \frac{1}{\rho \cdot c_p} \nabla \cdot (\lambda \nabla T) \quad (4)$$

where:  $\rho, c_p$  - mass density and specific heat,

$\sigma, \lambda$  - electrical and thermal conductivities respectively, which are functions of the temperature,

$T$  - temperature,

$j$  - vector of density currents.

In active systems described by (3) and (4) can arise dissipative structures, Wasiliew<sup>9</sup>, - i.e. striation.

## 3. Conditions of arising of the electrothermal instabilities

During fast heating up by Joule's heat some geometrical and structural nonuniformities of a conductor cause small local overheating. Because the time-constant of diffusion in equation (3) for Cu and Ag is 2 order smaller than the time-constant of equation (4), Jakubiuk<sup>6</sup>, so according to equation (3) will be overheated nearly adiabatic a number of cross-section perpendicular to the current direction. But over a it can not be overheated. This observation striation for the wire diameter above certain magnitude, Nasiłowski<sup>8</sup>. So one can assume that the temperature distribution along a wire, being already in melted state, is stochastic one.

In electrothermal analysis we get the temperature distribution in the form

$$T(z, t) = T_0(t) + \sum_{k=1}^{\infty} T_k(t) e^{ikz} \quad (5)$$

where:  $k = \frac{2\pi}{\lambda_k}$  - wave number,  $i = \sqrt{-1}$ ,  
 $\lambda_k$  - wave length,

$T_0(t)$  - constant temperature component along wire axis,

$T_k(t)$  - amplitude of  $k$ -waves of temperature.

Assuming  $\rho \cdot c_p = \text{const.}$ ,  $\lambda = \text{const.}$  and

$$\sigma = \frac{\sigma_{\infty}}{1 + \alpha \cdot \Delta T} \quad (6)$$

in which:  $\sigma_{\infty}$  - electrical conductivity in the temperature  $T_{\infty}$ ,  $\Delta T = T - T_{\infty}$ ,  
 $T_0$  - one can get the relation

$$\frac{dT}{dt} = \frac{j^2}{\rho \cdot c_p \cdot \sigma_{\infty}} (1 + \alpha \cdot \Delta T) \quad (7)$$

But the amplitude  $T_k$  of  $k$ -temperature wave fulfils the equation

$$\frac{1}{T_k} \frac{dT_k}{dt} = \frac{1}{\rho \cdot c_p} \left( \frac{j^2}{\sigma_{\infty}} - \lambda \cdot k^2 \right) \quad (8)$$

From (8) is seen that short wave temperature distortions will be damped whereas long wave ones will grow. The boundary wave expresses the relationship

$$\lambda_{kb} = \frac{2\pi}{j} \left( \frac{\sigma_{\infty} \cdot \lambda}{\alpha} \right)^{0.5} \quad (9)$$

Because in a wire arise mainly short-wave distortions it shall be expected appearance of the waves  $\lambda_k \geq \lambda_{kb}$ . For example for Cu wire and  $j = 5 \text{ kA} \cdot \text{mm}^{-2}$  -  $\lambda_{kb} = 2.95 \text{ mm}$ . From this the modulus is  $h_g = 0.5 \cdot \lambda_{kb} = 1.47 \text{ mm}$ , i.e. after (1) it gives the wire diameter 0.44 mm. The results, despite simplified analysis, are close to the experimental results.

#### 4. Investigations of the development of electrothermal instabilities

Electrothermal instabilities can arise if the fuse-element is in liquid dynamic overheated state above the boiling point. In such conditions the conductivity depends on the temperature and the mass density by means of exponent  $\gamma$  ( $\gamma > 1$ ) in the relation

$$\sigma = \sigma_{o1} \cdot \left( \frac{T_{o1}}{T} \right)^\gamma \quad (10)$$

In calculations the temperature was taken as

$$T(z,t) = T_o(t) + T_1(z,t) \quad (11)$$

where the component  $T_o$  fulfils the equation

$$\frac{dT_o}{dt} = \frac{j^2}{\rho \cdot c_p \cdot \sigma_{o1}} \cdot \left( \frac{T_o}{T_{o1}} \right)^\gamma \quad (12)$$

whereas  $T_1$  the equation

$$\frac{\partial T_1}{\partial t} = \frac{j^2}{\rho \cdot c_p \cdot \sigma_{o1}} \left[ \left( \frac{T_o + T_1}{T_{o1}} \right)^\gamma - \left( \frac{T_o}{T_{o1}} \right)^\gamma \right] - \frac{\lambda_{o1}}{\rho \cdot c_p} \frac{\partial^2 T_1}{\partial z^2} \quad (13)$$

where:  $\sigma_{o1}, \lambda_{o1}$  - values in temperature  $T_{o1}$ .  
Introducing non-dimensioned variables

$$\vartheta = \frac{T}{T_{o1}}, \quad \vartheta_o = \frac{T_o}{T_{o1}}, \quad \vartheta_1 = \frac{T_1}{T_{o1}}, \quad (14)$$

$$\eta = \frac{z}{l_o}, \quad \tau = \frac{t}{\frac{\rho \cdot c_p \cdot \lambda_{o1}^{-1} \cdot l_o^2}{j^2}}$$

in which:  $l_o$  - characteristic linear parameter,

and taking the non-dimensioned constant

$$D = \frac{j^2 \cdot l_o^2}{\sigma_{o1} \cdot \lambda_{o1} \cdot T_{o1}} \quad (15)$$

the equations (12) and (13) are reducing to the form

$$\frac{d\vartheta_o}{d\tau} = D \cdot \vartheta_o^\gamma \quad (16)$$

and

$$\frac{\partial \vartheta_1}{\partial \tau} = D \cdot [(\vartheta_o + \vartheta_1)^\gamma - \vartheta_o^\gamma] + \frac{\partial^2 \vartheta_1}{\partial \eta^2} \quad (17)$$

Equation (16) is to be integrated analytically. By  $\gamma > 1$  and initial condition  $\vartheta_o(\tau=0) = 1$  the solution is done by

$$\vartheta_o = [1 - (\gamma - 1) \cdot D \cdot \tau]^{1/(\gamma-1)} \quad (18)$$

From (18) outcomes, that in a finite time span the temperature will reach the infinity, what is possible in a non-linear relation only.

The solution of equation (17) was done numerically for the initial conditions given in the Fig.1 and boundary conditions

$$\left. \frac{\partial \vartheta_1}{\partial \eta} \right|_{\eta=0} = \left. \frac{\partial \vartheta_1}{\partial \eta} \right|_{\eta=1} = 0 \quad (19)$$

which denote thermal isolation of the wire section.

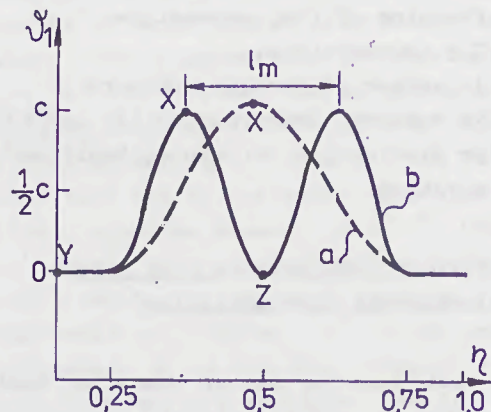
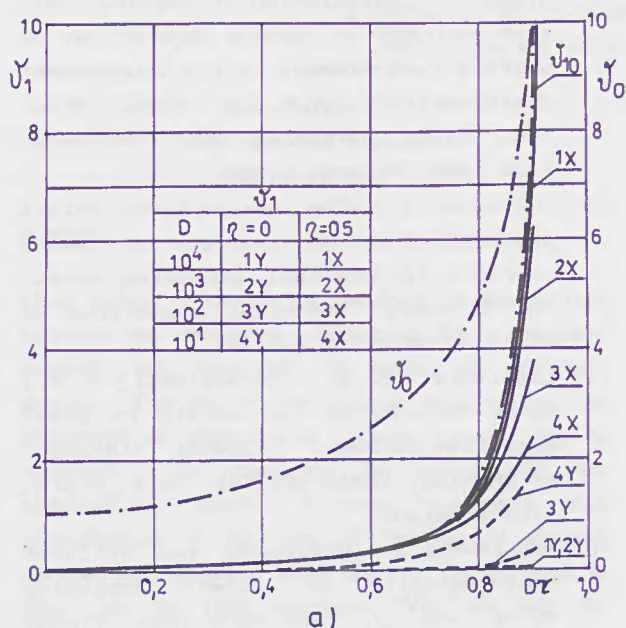
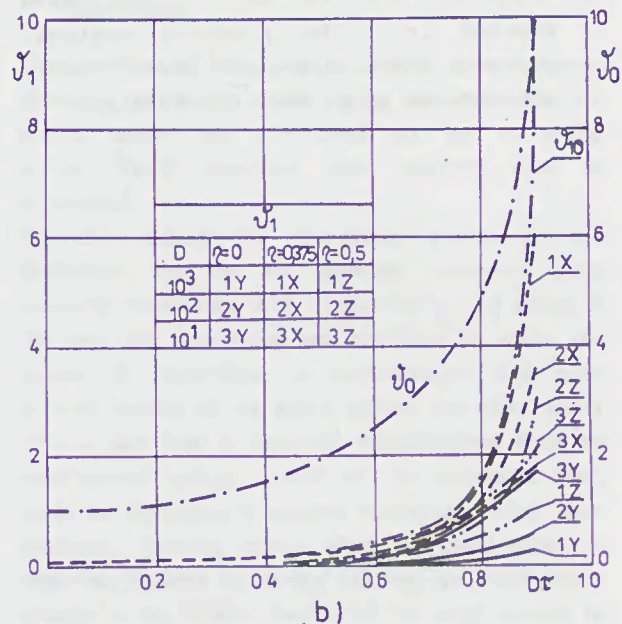


Fig. 1 Initial conditions for equation (17)  
X, Y, Z - points for which the temperature profiles are given in Fig.2.  
 $l_m$  - distance between overheated regions.

The calculations are made for different magnitudes  $\gamma$ ,  $D$  and initial amplitudes of the distortion  $c$  (Fig.1). Exemplary results of the calculations are given in Fig.2. To enable comparison the profiles are given as the function of  $D \cdot \tau$ . The diagrams show the temperature profiles of  $\vartheta_o$  and  $\vartheta_1$  in different wire points (Fig.1). Moreover for a



a)



b)

Fig.2 Temperature  $\vartheta_0, \vartheta_1, \vartheta_{10}$  profiles in the points indicated in Fig.1 as function of time  $D\tau$  for  $\gamma = 2$  and  $c = 0.05$

- a) initial condition a (Fig.1)
- b) initial condition b (Fig.1)

comparison the difference of the temperatures  $\vartheta_{10}$  between points X and Y is shown, but the thermal conductivity was neglected. It gives the maximal possible difference temperature in the wire.

From Fig. 2a and some results, not enclosed to this paper, a conclusion is, that for every magnitudes of the exponent  $\gamma > 1$  exist

a defined boundary value of the constant  $D = D_b$  above which the thermal conductivity is not able to equilibrate of the non-uniform temperature distribution.

As a criteria of  $D_b$  selection by a convention was taken non-changeable temperature difference  $\vartheta = \vartheta_0 + \vartheta_1$  in the points X and Y at the initial instant and in the instant when  $\vartheta_0 = 10$ .

The following results are obtained:

for  $\gamma = 1.2 - D_b = 50$ ; for  $\gamma = 1.5 - D_b = 20$ ; for  $\gamma = 2.0 - D_b = 10$ ; for  $\gamma = 3.0 - D_b = 5$ . For Cu and Ag wires one can take approximately  $\gamma = 2.0$ . Obtained results  $D_b$  make possible, for given magnitude  $j$  and material data at the melting point  $T_m$  ( $T_{01} = T_m$ ), to determine after (15) at which dimensions those temperature non-uniformities can be equalized. For example, at  $j = 5 \text{ kA} \cdot \text{mm}^{-2}$ ,  $\gamma = 2.0$  and Cu wire the non-uniformities  $l_0 < 0.88 \text{ mm}$  should give the temperature equalization.

From Fig.2b and results not shown in this paper, can define boundary value of the constant  $D = D_w$  that two regions with distance  $l_m$  apart will join together due to the heat transfer. It would correspond to the short wave damping of length  $l_m$  and shorter. As a criterion to define  $D_w$  for given  $\gamma$  we took connection in one two regions heated up when  $\vartheta = \vartheta_0 + \vartheta_1 = 10$ . In this way we get:

for  $\gamma = 1.5 - D_w = 100$ ; for  $\gamma = 2.0 - D_w = 80$ . The parameter  $D_w$  enables approximative calculation of the disintegrating modulus after the formulae

$$l_m \leq \frac{(D_w \cdot \sigma_{01} \cdot T_{01} \cdot \lambda_{01})^{0.5}}{4 \cdot j} \quad (20)$$

Comparison of the results of experiments and after the formulae (14) are given in the Table 1.

The conclusion from the Table 1 is that for current-density actual in fuses the formulae (20) gives a satisfactory agreement. But for higher current-density, typical for so-called fast explosions the differences are great. Possibly it is due to considerable overheating of the liquid metal for fast explosions and changes of the material parameters.

Table 1 Juxtaposition of experimental and analytical results

Material	Diameter (mm)	$j$ ( $\text{KA} \cdot \text{mm}^{-2}$ )	Modul. exper. (mm)	Modul. calcul. (mm)	Source
Ag	0.3	8.2	0.31	0.39	[2]
Ag	0.5	6.0	0.36	0.54	[2]
Ag	0.5	12.0	0.24	0.27	[1]
Cu	0.625	170.0	0.23	0.018	[4]
Cu	0.625	260.0	0.20	0.020	[3]

*vhigh. expl. wire.*

### 5. Conclusions

The paper pointed out, that the striated disintegration of a fuse-element, or more wide, of an exploding wire can arise due to development of the electrothermal instabilities, which are appearing with the non-linear volumetric heat sources taking into account the heat transfer. An analysis of a simplified model we got a formulae to determine the striation modulus. The calculating results are in agreement with the experiments for fuses, but are in disagreement for the exploding wires. This problem now is under further investigations.

### 6. Acknowledgements

The autor wishes to acknowledge the friendly and constructive advice given by Prof. J. Hryńczuk and Prof. T. Lipski in discussions during the progress of this work.

### 7. References

- [1] Arai S., Deformation and disruption of silver wires, Proc. ICEFA 1976, Liverpool Polytechnic, p.50.
- [2] Arai S., Deformation and disruption of silver wires, Private communications, 1977.
- [3] Bennett F.D. et. al., Expansion of superheated metals, J. Appl. Phys., 1974, vol. 45, p.3429
- [4] Fansler K. S., Shear D. D., Correlated X-ray and optical streak photographs of exploding wires, Exploding Wires, vol.4, New York 1968. Plenum Press. p.185

- [5] Hibner J., Calculation of the arc-ignition voltage on single disruption of uniform fuse-element by its independent disintegration in h.b.c. fuses. Proc. Int. Symp. Switching Arc Phenomena, Łódź 1985, Poland, p.368.
- [6] Jakubiuk K., The analysis of select phenomenons in the first part of impuls currents in the fast exploding wires, Ph. D. Thesis, Technical University of Gdańsk, 1981, (in Polish).
- [7] Lieblediew S. W., Sawwatimskij A. F., Quick heating of the metals by great densities current, Uspechi Fiziczeskich Nauk, 1984, vol.144, no 2, p.215, (in Russian).
- [8] Nasiłowski J., Unduloids and striated disintegration of wires, Exploding Wires, vol. 3, New York 1964, Plenum Press, p.295.
- [9] Wasiliew W.A. et. al., Self-wave process in the kinetics systems, Uspechi Fiziczeskich Nauk, 1971, vol.128, no 4, p. 625, (in Russian).

A COMPARISON OF THE COMPUTER MODELLING OF ELECTRIC  
FUSE ARCING AND THEIR REAL-LIFE PERFORMANCE

D.R. Barrow  
Davy Computing Limited  
Sheffield, UK

and

A.F. Howe  
University of Nottingham  
UK

### Abstract

Using optical fibroscopy the burnback of electric fuse elements was monitored. Alongside this a computer program was developed to model the burnback process. The rate of burnback is dependent on the percentage of eroded fuse element material that is vaporised. By comparing the experimental and computational results it was established that approximately 10 per cent of the eroded element material was vaporised whilst the rest flowed away as liquid into the filler interstices. With this data the accuracy of fuse arc models should be improved.

### 1. Introduction

The operation of fuses may be divided into two parts, namely a pre-arc period during which elements are heated, melted and then break up, and an arcing period which continues until current flow is interrupted.

Behaviour during the pre-arc period is well understood and can be modelled accurately using numerical techniques [1,2]. Behaviour during arcing is still not fully understood and continues to attract the interest of researchers, as manufacturers seek more accurate models of the arcing period. Currently, every time a new fuse is designed manufacturers must do experimental testing. Much of this expensive work could be eliminated if accurate numerical models were available. Existing models which are based either on empirical methods or energy balances are insufficiently accurate to be reliable because of the large number of interactive parameters that are associated with the arcing process [3]. This paper describes work, which was designed to try to relate two of these parameters, burnback rate and the proportion of element material which is vaporised.

Wright and Beaumont [3] examined microscopically the fulgurite which surrounds an operated fuse element and discovered that during arcing some of the element material flowed out in liquid form into the spaces among the filler granules, whilst other element material was vaporised, forced out into the interstices by the pressure of the arc and deposited finely on the filler material. As the amount of energy required to melt a particular volume of material is far less than

that necessary to vaporise the same volume, the percentage of eroded element material that is vaporised will have a significant effect on the fuse burnback rate and hence its operating characteristic. This work, which was designed to ascertain this percentage, had two parts. The first was experimental to measure the burnback rate and the second was computational.

### 2. Burnback experiments

This work has been described previously [4] but for the convenience of the reader the salient points are repeated here.

Fuselinks were constructed with a narrow slot cut longitudinally in the fusebody perpendicular to the plane of element. Five optical fibres were inserted so that the first lay approximately over the restriction and the remainder formed a line with each touching its neighbour as shown in Fig. 1. Each fuse was then filled with sand to normal packing density.

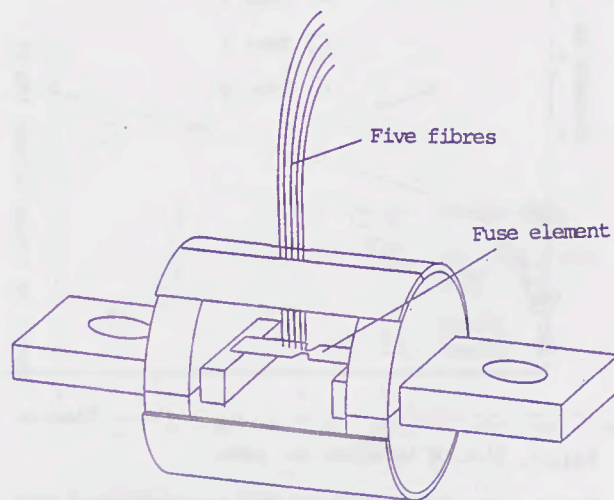


Fig. 1 Fuse design for burnback measurement.

When each fuse was operated, its arc length increased and light from the arc appeared first from the fibre over the centre of the restriction and then from the others successively. Fig. 2 shows the light outputs during one test.

The traces fall when light is emitted from the fibres. The top trace is the one from the fibre over the restriction in the element, the lower traces being in

the order of the fibres. From these results it was possible to plot graphs of burnback versus time. Fig. 3 shows the results from three tests.

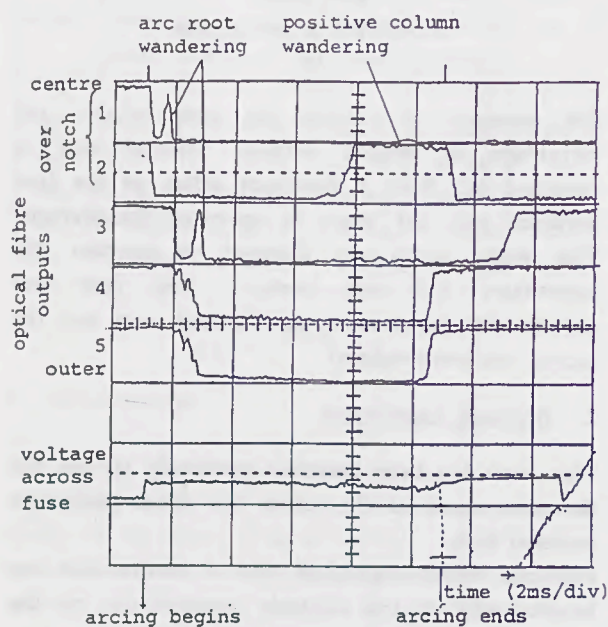


Fig. 2 Multi-trace plot of burnback (Test 1).

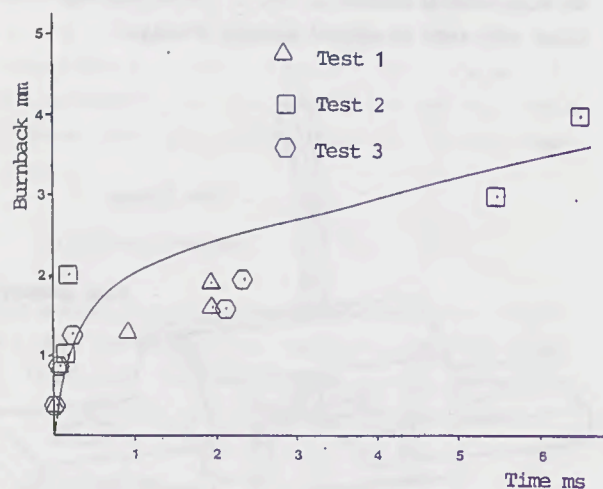


Fig. 3 Plot of burnback vs. time.

Examination of the traces of light output showed that sudden diminutions in light intensity occur for periods of up to 3 ms, indicating that the arc wanders [5]. Signals from the outer fibres cease abruptly about 0.5 ms before the drop in arc voltage, normally associated with the end of arcing. Light continued to be emitted from the inner fibres after the end of arcing probably due to incandescence of the fulgurite.

### 3. Numerical modelling

The numerical model was based entirely on the concept of energy balances. No consideration was

given to the processes taking place within the arc and it was assumed that the arc itself had no intrinsic energy.

When the duration of electric fuse arcing is only a few milliseconds then the arcing process may be considered to be essentially adiabatic, so that negligible heat is transmitted beyond the immediate layer of the filter surrounding the element. Because of this, it was possible to construct a numerical model based upon the electrical energy supplied acting solely upon the surface layer of the filler.

#### 3.1 Fuse model

The fuse was considered as a section with width equal to the width of the element and with infinite height and length as illustrated in Fig. 4. The element was situated at the centre and was represented by a layer with a thickness equal to that of the element and with the physical attributes of the element material. The rest of the model which represents the filler was divided with layers  $\Delta z$  thick.

The model was divided longitudinally into segments  $\Delta x$  long.

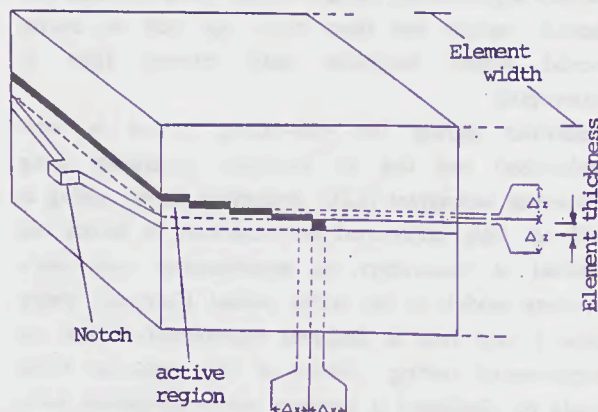


Fig. 4 Fuse element showing modelling sub-volumes.

The heat capacity of the filler and the element material were derived for the temperature ranges 293K to their respective melting points, since in the physical tests the fuses had equilibrated with room temperature and were not pre-heated. The heat capacity of the filler and the element were derived using the expression

$$C_p = a + b \times 10^{-3}T + c \times 10^{-6}T^2 + d \times 10^5/T^2$$

where  $a$ ,  $b$ ,  $c$  and  $d$  are constants and  $T$  is the temperature [6].

The constants have different values for the solid and liquid phases. In order to obtain values for the heat capacity of the materials, values were calculated in 10K intervals up to their melting point. The values so derived were integrated to provide a lumped value

for heat capacity up to the material's change of state. The latent heat of melting and the latent heat of vaporisation were added to the integrated value to provide the total heat to vaporise unit mass of material. In the case of the filler vaporisation does not occur since silica decomposes directly from its liquid phase at 2523K. The decomposition requires an amount of energy equal to the heat of formation of silica from its elements at that temperature, and so this value was used in place of the latent heat of vaporisation.

### 3.2 Energy considerations

The total energy supplied to the fuselink in the time interval  $\Delta t$  was equal to  $i v \Delta t$

where  $i$  = instantaneous current

$v$  = instantaneous voltage across the fuse.

As the system was assumed to be adiabatic all of this energy was used to:

- i) heat up and erode the element, and
- ii) heat up and decompose the filler material adjacent to the surface of the element.

The energy required to erode the element has been quoted by a number of authors [7-9] as being equal to  $i v_{ar} \Delta t$

where  $v_{ar}$  = arc root voltage.

For simplicity some authors have ignored the heat conduction from the arc along the element. However, as some of this energy must be dissipated in raising the temperature of the element, this effect was considered here.

The rest of the supplied energy was available for heating and decomposing the filler material surrounding the element.

### 3.3 Modelling implementation

The model was initialised at the moment the restriction was broken, and then progressed in  $1 \mu s$  time steps.

At each time step,  $\Delta t$ , the total energy supplied to the fuse during that interval was calculated. To do this the instantaneous current,  $i$ , and voltage,  $v$ , measurements made during the burnback experiments were supplied as data.

As the percentage of eroded element material that is vaporised was unknown an arbitrary value was chosen initially. Then using the concept of arc root voltage the energy supplied to the element subvolume adjacent to the break in the element was calculated, assuming that the arc root voltage was 14V. After determining the proportion of this energy, that is necessary to heat the element ends [5], the remainder was added to the total stored energy in the element

subvolume. When the total energy exceeded the amount required to vaporise the chosen percentage of element material in the subvolume, this section was set aside and the excess energy was used to start heating the next subvolume.

The energy supplied during each time step to the surface of each subvolume of filler was then determined and added to the previous value for that subvolume. When sufficient energy had been provided to decompose the subvolume that segment was discarded and the excess energy was used to start heating the next layer.

Iterations continued until the current reached zero.

The procedure was then repeated for other percentages of eroded element material.

### 3.4 Results

The computations gave consistently high rates of element erosion when the heating of the element was ignored (as illustrated in Fig. 5, graph labelled "arc root volts only"). However, reasonable correlation with the experimental results was achieved when the heating of the element ends was included and it was assumed that 10% of the eroded element material was vaporised and 90% was forced away from the arc as liquid. This is the "normalised" graph in Fig. 5.

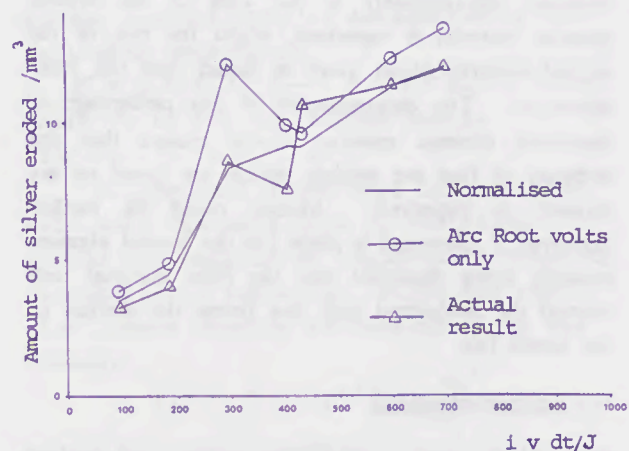


Fig. 5 Amount of silver eroded vs. supplied energy (computed and practical results)

Fig. 6 shows the same comparison in the form of a graph of burnback length versus time. Again there is reasonable correlation. The error at short elapsed times was due to simplified modelling of the element restriction.

A number of authors have noticed variations in the burnback rate when elements are preheated. To examine whether this effect could be demonstrated using the computer program the initial temperature of

the element was raised, and it was found that temperature rises as small as 25K had a marked effect on burnback rate.

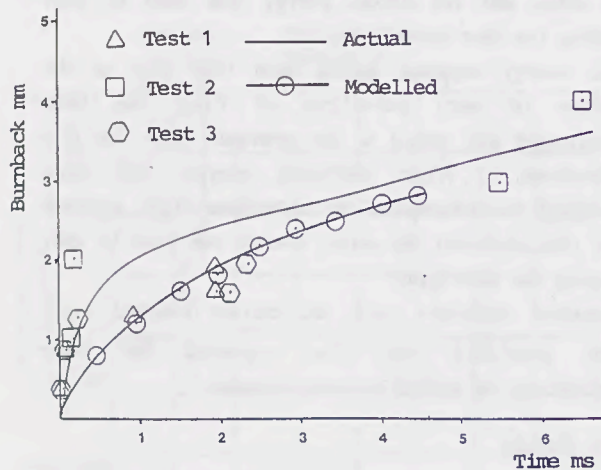


Fig. 6 Burnback vs. time.  
(Computed and practical results)

#### 4. Conclusions

The rate of fuse element burnback has been measured using optical fibres. Using these results and a simple numerical model of the erosion mechanism, it has been established that providing the arcing process is adiabatic approximately 10 per cent of the eroded element material is vaporised, whilst the rest of the eroded material flows away as liquid into the filler interstices. The determination of this percentage of vaporised element material should ensure that the accuracy of fuse arc models, which are based on arc physics, is improved. Models could be further improved if allowance is made for the eroded element material being dispersed into the filler material well beyond the isothermal wall that forms the surface of the lumen [10].

#### 5. Acknowledgements

The authors wish to thank Hawker Fusegear Limited for sponsoring this work, the University of Nottingham for providing the facilities, Professor Wright for his advice and encouragement and Dr. F. Hicks for drawing the illustrations.

#### References

- [1] Leach J.G., Newbery P.G. and Wright A., Analysis of high-rupturing-capacity fuselinks prearcing phenomena by a finite difference method, 1973, Proc. IEE, 120 (9), pp. 987-993.
- [2] Wilkins R., Wade S. and Floyd J.S., A suite of interactive programs for fuse design and development, 1984, Proc. of International Conference on Electric Fuses and their Applications, Trondheim, Norway, pp. 227-235.
- [3] Wright A. and Beaumont K.J., Analysis of high-rupturing-capacity fuselink arcing phenomena, 1976, Proc. IEE Vol. 123, (9), pp. 252-260.
- [4] Barrow D.R., Howe A.F. and Wright A., Methods of determining fuse arc parameters, 3-7 May 1989, International Conference on Electrical Contacts, Arcs, Apparatus and their Applications, Xi'an Jiaotong University, Xi'an, China.
- [5] Barrow D.R., Evaluation of arcing parameters in high breaking capacity fuses, 1988, PhD thesis, University of Nottingham.
- [6] Weast R.C., Handbook of chemistry and physics (CRC Press, Boca Raton, Florida, 1986, 67th edn.)
- [7] Daadler J.E. and Schreurs E.F., Arcing phenomena in high voltage fuses, 1983, EUT report 83-E-137, ISBN 90-6144-137-4, Eindhoven, Netherlands.
- [8] Wilkins R., Semi-empirical modelling of arcing in current limiting fuses, 1976, Proc. Conference on Electric Fuses and their Applications, Liverpool Polytechnic.
- [9] Hoyaux M.F., Arc physics, 1968, Springer-Verlag, New York.
- [10] Beaumont K.J., The analysis of HRC fuselink arcing phenomena, 1976, PhD thesis, University of Nottingham.

Z. Frenkel

Kharkov Institute of Municipal Engineers  
Kharkov, USSR

1. Abstract

Developed in the channel model approximation is a mathematical model of an electric arc in a quartz filled fuse with a foil strip fusible element. The arcing takes place in quartz (SiO<sub>2</sub>) vapours. The model accounts for molecular dissociation of SiO<sub>2</sub> into SiO, Si and O, ionization of Si atoms, dissipation of energy from the arc channel by radiation and thermal conduction. The model allows to calculate the channel plasma temperature, arc channel thickness, axial electric field value and particles density during the whole arc extinction process from known values of current and pressure in the arc channel.

2. System of equations

When emergency currents are cut off by a fuse with strip fusible elements there appears an electric arc, the arcing taking place in a closed chamber within fulgurite. In the first approximation the chamber can be considered as a right-angle prism of width  $\alpha$ , thickness  $2\beta$  and length L.

Within the scope of the channel model Namitokov and Frenkel<sup>1</sup> obtained a system of equations describing such a discharge

$$I = 2\alpha x_0 \sigma(T_0) E \quad (1)$$

$$IE = \frac{2\alpha}{\beta - x_0} \int_{T_w}^{T_0} \chi(T) dT' + 2\alpha x_0 \mathcal{U}(T_0) \quad (2)$$

$$\frac{[IE - 2\alpha x_0 \mathcal{U}(T_0)]^2}{8\alpha^2} = E^2 \int_{T_w}^{T_0} \chi(T) \sigma(T) dT' - \int_{T_w}^{T_0} \chi(T) \mathcal{U}(T) dT' \quad (3)$$

Here I - arc current; E - axial electric field intensity in arc;  $2x_0$  - thickness of arc channel;  $\sigma$  and  $T_0$  - conductivity and temperature of arc plasma, respectively;  $\chi$  - thermal conduction of gas surrounding the channel;  $\mathcal{U}$  - density

of radiation losses;  $T_w$  - chamber wall temperature. The arc channel width is accepted to be equal to the chamber width.

The system of equations (1) - (3) allows to find the main discharge parameters  $T_0$ ,  $x_0$  and known values of the arc current and pressure (P) in the chamber. For further calculations it is necessary to know the dependence of quantities  $\sigma$ ,  $\chi$  and  $\mathcal{U}$  on the plasma temperature and pressure.

To find these relationships we assume that in a quartz filled fuse the arcing takes place in quartz vapours, the ionized gas being silicon (Si) vapours, the chamber pressure reaches the value of few tens of atmospheres, and the plasma temperature reaches 20000 K. Such a discharge can be considered as a high-pressure electric arc and the discharge plasma as strongly ionized. Marshak<sup>2</sup> has shown that in this case plasma conductivity is determined by the following expression

$$\sigma = 3.4 \cdot 10^{-6} \frac{T^{5/2}}{\varphi_i} = 4.05 \cdot 10^{-7} T^{5/2} \quad (4)$$

where  $\varphi_i$  is the ionization energy (for Si  $\varphi_i = 8.15$  eV).

Raiser<sup>3</sup> has shown that in high-pressure arcs the main type of radiation within the considered temperature range is recombination radiation. Hence the radiation losses density is determined by the formula

$$\mathcal{U} = 5.4 \cdot 10^{-35} \frac{N_e^2}{\sqrt{T_0}} \quad (5)$$

where  $N_e$  is the electrons density in plasma.

To find the thermal conduction we use the known expression for thermal conduction of monatomic gas

$$\chi = \chi_0 \sqrt{T_0} \quad (6)$$

where  $\chi_0$  is a constant found from experimental data.

The SiO<sub>2</sub> molecules which evaporize

from the chamber walls dissociate in the chamber space. The dissociation thereat takes place in two stages. At first, the reaction  $\text{SiO}_2 \rightarrow \text{SiO} + \text{O}$  takes place, the dissociation energy ( $\varphi_d$ ) being 4.95 eV. Then the reaction  $\text{SiO} \rightarrow \text{Si} + \text{O}$  takes place with the dissociation energy equal to 7.8 eV. The latter value is close to the silicon ionization energy. Therefore, during calculation it should be taken into account that in the arc channel, besides Si and O atoms, there could be SiO molecules.

According to Dalton's law, the pressure in the chamber with account of the dissociation and ionization reactions, and in the assumption that the reaction  $\text{SiO}_2 \rightarrow \text{SiO} + \text{O}$  has fully taken place, is found from the equation

$$P = K T_0 (N_{\text{O}_2} + N_{\text{SiO}} + N_{\text{Si}} + N_{\text{Si}}^+ + N_{\text{O}_2} + N_e) \quad (7)$$

where  $N_{\text{O}_2}$  - density of oxygen atoms arising in the reaction  $\text{SiO}_2 \rightarrow \text{SiO} + \text{O}$ ;  $N_{\text{SiO}}$  - density of SiO molecules;  $N_{\text{Si}}$  - density of silicon atoms;  $N_{\text{Si}}^+$  - density of Si ions;  $N_{\text{O}_2}$  - density of oxygen atoms arising in the reaction  $\text{SiO} \rightarrow \text{SiO} + \text{O}$ ;  $N_e$  - density of electrons;  $K$  - Boltzmann's constant.

Equation (7) can be simplified. Let us introduce the designations:  $N_{\text{SiO}}^s$  - density of SiO molecules prior to their dissociation;  $N_{\text{Si}}^s$  - density of silicon atoms prior to their ionization.

Then, taking into account that

$$N_{\text{Si}} + N_{\text{Si}}^+ = N_{\text{Si}}^s; \quad N_{\text{Si}}^+ = N_e;$$

$$N_{\text{SiO}} + N_{\text{O}_2} = N_{\text{SiO}}^s = N_{\text{O}_2}$$

we obtain

$$P = K T_0 (2 N_{\text{SiO}}^s + N_{\text{Si}}^s + N_e) \quad (8)$$

We can ignore ionization of oxygen atoms because the oxygen ionization energy is significantly greater than the silicon atoms ionization energy.

The processes of dissociation and ionization in equilibrium isothermic plasma which is present in high-pressure arcs are described on the basis of the

mass action law by the following equations:

$$\frac{N_{\text{Si}}^{s^2}}{N_{\text{SiO}}^s - N_{\text{Si}}^s} = K_1(T_0) \quad (9)$$

$$\frac{N_e^2}{N_{\text{Si}}^s - N_e} = K_2(T_0) \quad (10)$$

where  $K_1(T_0)$  and  $K_2(T_0)$  are the dissociation and ionization constants, respectively.

According to Smirnov<sup>4</sup>, the dissociation constant for diatomic molecules is of the form:

$$K_1(T_0) = \frac{\varphi_{\text{Si}} \varphi_{\text{O}}}{2 \varphi_{\text{SiO}}} \times \frac{(1 - e^{-\frac{h\nu}{K T_0}})}{2 \pi \tau_0^2} \times \sqrt{\frac{\pi \mu K T_0}{h^2}} e^{-\frac{\varphi_d}{K T_0}} \quad (11)$$

where  $\varphi_{\text{Si}}$ ,  $\varphi_{\text{O}}$  and  $\varphi_{\text{SiO}}$  are the statistical weights of the silicon and oxygen atoms and SiO molecule;  $h\nu$  - distance between the molecule oscillation levels;  $\tau_0$  - equilibrium distance between atom nuclei in the molecule;  $h$  - Planck's constant;  $\mu$  - reduced mass of atoms.

For SiO we have:  $\mu = 1.69 \cdot 10^{-26}$  kg;  $h\nu = 1241 \text{ cm}^{-1} = 0.154$  eV;  $\tau_0 = 1.51 \cdot 10^{-10}$  m;  $\varphi_{\text{Si}} = \varphi_{\text{O}} = 9$ ;  $\varphi_{\text{SiO}} = 2$ . Substituting these values into (11), we obtain:

$$K_1(T_0) = 5.16 \cdot 10^{29} (1 - e^{-\frac{1790}{T_0}}) \times \sqrt{T_0} \exp(-\frac{9.048 \cdot 10^4}{T_0}) \quad (12)$$

Taking into account that the statistical weight of the silicon ion is equal to 6, the ionization constant takes the form:

$$K_2(T_0) = 3.23 \cdot 10^{21} T_0^{3/2} \exp(-\frac{9.454 \cdot 10^4}{T_0}) \quad (13)$$

Finding  $N_{\text{SiO}}^s$  from (9), and substituting its expression into (8), we obtain:

$$P = K T_0 \left( \frac{2 N_{\text{Si}}^{s^2}}{K_1(T_0)} + 3 N_{\text{Si}}^s + N_e \right) \quad (14)$$

Combining equations (1) - (3), (10) and (14) with expressions (4) - (6), (12) and (13), we obtain a system of equations

allowing to find  $T_0$ ,  $X_0$ ,  $E$ ,  $N_{Si}^s$  and  $N_e$  from I and P. But before starting to solve this system of equations we shall perform a number of simplifications.

### 3. Solving the system of equations

Preliminary calculations have shown that in the pressure range being considered, at small temperatures  $N_{Si}^s \gg N_e$ , hence the quantity  $N_e$  in the denominator of equation (10) and in the r.h. side of equation (14) can be ignored. Then, as the temperature rises, the quantity  $2N_{Si}^s/K_1(T_0)$  in (14) becomes small as compared to  $N_{Si}^s$ . As before,  $N_e$  thereat remains small. Thus, the whole temperature range can be divided into two regions. In the first region at low temperatures  $N_e$  can be ignored in the denominator of (10) and in the r.h. side of (14). Then from these equations we obtain:

$$N_{Si}^s = -\frac{3}{4} K_1(T_0) + \sqrt{\frac{9}{16} K_1^2(T_0) + \frac{PK_1(T_0)}{2KT_0}} \quad (15)$$

$$N_e^2 = -\frac{3}{4} K_1(T_0) K_2(T_0) + K_2(T_0) \sqrt{\frac{9}{16} K_1^2(T_0) - \frac{PK_1(T_0)}{2KT_0}} \quad (16)$$

Substituting (16) into (2), (3) and (5), and computing the integral in (3) with account of  $T_0 \gg T_w$ , from the system of equations (1) - (3) we obtain:

$$\bar{I} = 2\alpha X_0 \sigma_0 T_0^{5/2} E \quad (17)$$

$$\bar{I}E = \frac{4\alpha X_0 T_0^{3/2}}{3(\delta - X_0)} - 8.1 \cdot 10^{-25} \frac{\alpha X_0}{\sqrt{T_0}} \times K_1(T_0) K_2(T_0) + 1.08 \cdot 10^{-34} \frac{\alpha X_0}{\sqrt{T_0}} \times K_2(T_0) \sqrt{\frac{9}{16} K_1^2(T_0) - \frac{PK_1(T_0)}{2KT_0}} \quad (18)$$

$$\frac{2X_0 T_0^2}{9(\delta - X_0)^2} = 1 \cdot 10^{-2} E^2 T_0^3 + 4.05 \cdot 10^{-35} \times$$

$$\times \frac{K_1(T_0) K_2(T_0) T_0^2}{\psi_i + \psi_d} - \frac{4.05 \cdot 10^{-35} K_2(T_0)}{2K_1(T_0) \left(1 + \frac{\psi_d}{T_0}\right)} \times \left[ K_1(T_0) + \frac{4P}{3KT_0} \right] \sqrt{K_1^2(T_0) + \frac{8K_1(T_0)P}{3KT_0}} - \frac{32P^2}{9K^2 T_0^2} \operatorname{erf} \left[ \sqrt{1 + \frac{3KT_0 K_2(T_0)}{8P}} + \sqrt{\frac{3KT_0 K_2(T_0)}{8P}} \right] \quad (19)$$

In the second temperature region we ignore the term  $2N_{Si}^s/K_1(T_0)$  in the r.h. side of (14). In this case, from (10) and (14) we obtain

$$N_e = \frac{2}{3} K_2(T_0) \left[ \sqrt{1 + \frac{3P}{4K_2(T_0)KT_0}} - 1 \right] \quad (20)$$

$$N_{Si}^s = N_e + \frac{N_e^2}{K_2(T_0)} \quad (21)$$

Using (20) in the same way as (16), and performing the same transformations, from (2) and (3) we obtain:

$$\bar{I}E = \frac{4\alpha X_0 T_0^{3/2}}{3(\delta - X_0)} + 4.8 \cdot 10^{-35} \frac{\alpha X_0}{\sqrt{T_0}} \times$$

$$\times K_2^2(T_0) \left[ \sqrt{1 + \frac{3P}{4K_2(T_0)KT_0}} - 1 \right]^2 \quad (22)$$

$$\frac{2X_0 T_0^2}{9(\delta - X_0)^2} = 1 \cdot 10^{-2} E^2 T_0^3 -$$

$$- 2.4 \cdot 10^{-35} \frac{T_0}{\psi_i} K_2^2(T_0) +$$

$$\begin{aligned}
& + \frac{2.4 \cdot 10^{-35}}{1.5 + \frac{\varphi_i}{T_0}} \left\{ \left[ K_2(T_0) + \frac{3P}{8KT_0} \right] \times \right. \\
& \times \sqrt{K_2(T_0) + \frac{3P}{4KT_0}} - \frac{9P^2}{32K^2T_0^2} \times \\
& \times \ln \left[ \sqrt{\frac{4K_2(T_0)KT_0}{3P}} + \right. \\
& \left. \left. + \sqrt{1 + \frac{4K_2(T_0)KT_0}{3P}} \right] \right\} - \\
& - 1.8 \cdot 10^{-35} \frac{PK_2(T_0)}{K\varphi_i} \left( 1 - \frac{5}{2} \frac{T_0}{\varphi_i} + \right. \\
& \left. + \frac{35}{4} \frac{T_0^2}{\varphi_i^2} \right) \quad (23)
\end{aligned}$$

The third equation of this system is equation (17).

The boundary between two temperature regions is determined conventionally by the inequality

$$\frac{2N_{Si}^s}{3K_1(T_0)} > 0.05 \quad (24)$$

This inequality means that the boundary between the first and second temperature regions passes through the temperature at which the first summand in the r.h. side of (14) is 20 times smaller than the second one. Substituting (15) into (24) we obtain

$$0.5 \sqrt{1 - \frac{8P}{9KT_0 K_1(T_0)}} - 0.55 > 0 \quad (25)$$

In the first temperature region this inequality is satisfied, and in the second one it is not.

The obtained systems of equations are solved on a PC.

If the solution is obtained in the first temperature region, then besides quantities  $T_0$ ,  $X_0$ ,  $E$ , and we can find

$$\begin{aligned}
N_{Si} &= N_{Si}^s - N_e \\
N_{Si0} &= \frac{N_{Si}^{s2}}{K_1(T_0)}
\end{aligned}$$

$$N_0 = N_{Si0} + 2N_{Si}^s \quad (26)$$

If the solution is obtained in the second temperature region, then additionally we can find

$$N_{Si} = N_{Si}^f - N_e; \quad N_0 = 2N_{Si}^f \quad (27)$$

Besides, knowing the arc voltage ( $U_d$ ), we can find the arc length

$$L = \frac{U_d - U_{ac}}{E} \quad (28)$$

Here  $U_{ac}$  is the potential drop in the electrode vicinity. Namitokov and Frenkel<sup>5</sup> have shown that for fusible elements Al, Cu and Ag  $U_{ac} = 40$  V.

The value of  $X_0$  was chosen by comparing the calculated and experimental values of  $L$ . For aluminum  $X_0 = 1 \cdot 10^{-3}$  mkg/s<sup>3</sup>K<sup>3/2</sup>; for copper and silver  $X_0 = 1.6 \cdot 10^{-3}$  mkg/s<sup>3</sup>K<sup>3/2</sup>.

#### 4. Calculation results

The obtained model was used to calculate the plasma parameters of an arc discharge in a fuse according to Namitokov's and Frenkel's<sup>6,7,8</sup> experimental data.

Shown in Fig. 1 are the results of calculating the plasma temperature, axial electric field intensity and burn-out length of a fuse with a copper fusible element 10 mm wide, 0.14 mm thick and one rectangular neck in the centre 1 mm long and 1 mm wide. Tests were carried out in a d.c. circuit with voltage 500 V, anticipated current 1400 A, time constant 2.3 ms. The whole process lasted for 71 ms. Calculations began in 4.4 ms from the moment of arc emergence. As seen from the given calculations, at the initial stage of the arc extinction process the plasma temperature is exceedingly high and reaches  $18 \cdot 10^3$  K. This corresponds to values obtained by spectroscopy measurements. Further the plasma temperature drops, but even at the end of the arc extinction

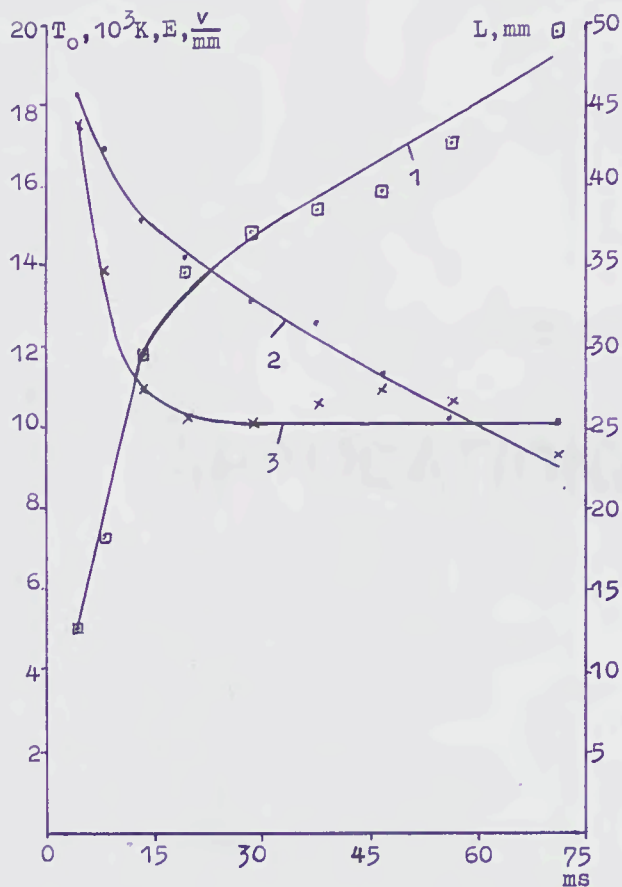


Fig.1 1 - L; 2 -  $T_0$ ; 3 - E

process the plasma remains strongly ionized. The presence of SiO molecules can be ignored during the whole process. The behaviour of the axial electric field intensity value corresponds to that obtained experimentally by Ranjan R. and Barrault M.<sup>9</sup> At the initial stage the fusible element burn-out process is intensive, and then it slows down. The final burn-out length value obtained experimentally is 44 mm, and the calculated value is 49.5 mm.

Shown in Fig. 2 are the results of calculating the particles density in the arc plasma of a fuse with a silver fusible element 2.5 mm wide and 0.14 mm thick with one neck on the centre 1 mm long and 1 mm wide. Experiments were carried out with d.c. voltage 500 V, anticipated current 3000 A, time constant 5.1 ms. Arcing time was 23.6 ms. These experiments were distinguished by very high pressure in the fuse arc channel. Thus, measurements have

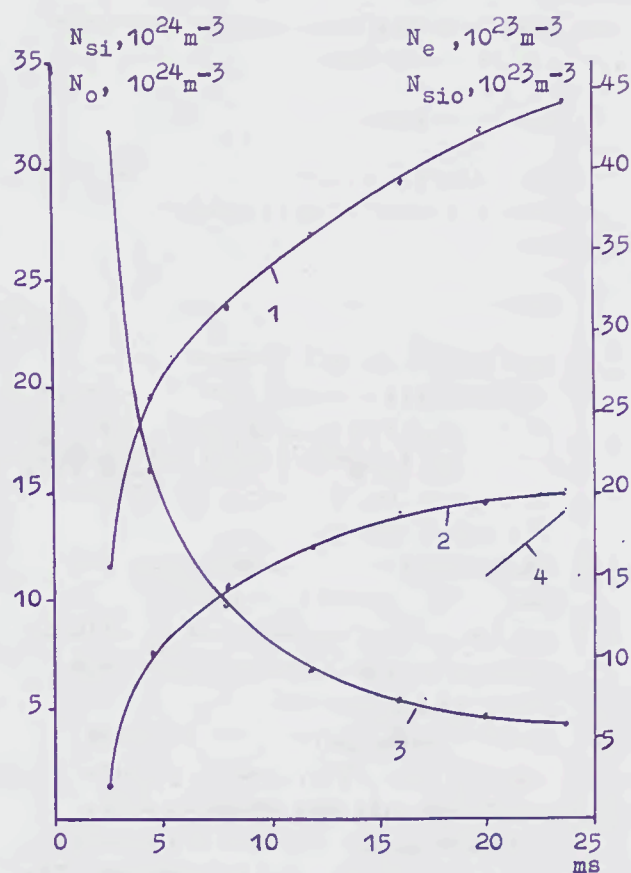


Fig.2 1 -  $N_0$ ; 2 -  $N_{Si}$ ; 3 -  $N_e$ ; 4 -  $N_{SiO}$

shown that at the end of the arc extinction process the pressure in the arc channel reaches  $56.5 \cdot 10^5$  Pa. This accounts for the high particles density in the arc channel. At the final stage of the process it is necessary to take into account SiO molecules, and calculations are carried out in the first temperature region. At the early stages of arc extinction calculations are carried out in the second temperature region. The final burn-out length value obtained experimentally is 46 mm, and the calculated value is 47.4 mm.

### 5. Conclusion

The developed mathematical model of an electric arc in a quartz filled fuse allows to calculate the discharge parameters of gas-discharge plasma during the whole arc extinction process. Checking the behaviour of the obtained relationships

requires experimental determination of these parameters. Calculation of discharge parameters at the end of the arc extinction process shows satisfactory agreement with experimental data.

#### Acknowledgement

The author is grateful to Prof. Namitokov K.K. for general guidance of the work.

#### References

- [1] Namitokov K.K. and Frenckel Z.M., Mathematical model of the final stage of arc extinction in a fuse, 1990, Proc. The IX Czechoslovak Symposium on Physics of Switching Arc, Tatranska Strba, October.
- [2] Ed. Marshak I.S., Pulsed light sources, 1978, Energia, Moscow.
- [3] Raizer Yu.P., Fundamentals of modern physics of gas discharge processes, 1980, Nauka, Moscow.
- [4] Smirnov B.M., Physics of slightly ionized gas, 1978, Nauka, Moscow.
- [5] Namitokov K.K. and Frenckel Z.M., Pressure in an electric arc channel in a fuse, 1989, Elektrotehnika, 12.
- [6] Namitokov K.K. and Frenckel Z.M., Influence of design features of a fuse fusible element on the arc processes therein, 1984, Elektrotehnika, 9.
- [7] Namitokov K.K. and Frenckel Z.M., Specific features of arc processes in fuses depending on the fusible element geometry, 1985, Izv. VUZov, Elektromekhanika, 11.
- [8] Namitokov K.K., Frenckel Z.M. and Kimmelnitzky R.S., Pressure inside the fusible element enclosure of a fuse with a filler, 1988, Elektrotehnika, 4.
- [9] Ranjan R. and Barrault M., Axial electric field measurements of d.c. arcs in current-limiting fuses, 1980, Proc. IEEE, 127, May, 3.

**Session 7**

**APPLICATIONS AND TRENDS**



## PERFORMANCE CRITERIA FOR COMPACT INDUSTRIAL FUSELINKS

by H W Turner, C Turner and D J A Williams

### Summary

The International Electrotechnical Commission are seeking to harmonise a type of low-voltage, high breaking-capacity fuse which is suitable for use world-wide as a normal standard preferred item. A compact industrial fuse system with rated currents up to 125 A has been developed in the United Kingdom which achieves the criteria proposed by the IEC and has proved its effectiveness in practical use in a large number of industrial installations. Limitation of the rated voltage to 415 V has allowed significant reductions in power dissipation and size. This system is a most suitable choice for international harmonisation as the preferred system for the harmonised system voltage of 230/400 volts.

### 1. Introduction

During the last quarter century there have been many attempts to secure an internationally harmonised system of low-voltage fuses. The idea has many theoretical attractions. A manufacturer of equipment could make provision for the fuses within that equipment without having to make special provision for the exchange of fuse-bases to accommodate the various designs which have become established in different countries during this century. There are types which are bolted into position, others with blade contacts, ferrule contacts, and in medium and low current ratings there are types which are placed within the fuse holder and secured in position by a screw-down cap, and another type with a fuselink constructed like a plug with two contact pins between which the enclosed fuse element is connected. The latter is inserted into a fuse-base in the form of a socket. How much simpler it would be if there was only one design for each current and voltage rating. The equipment designer could provide for it in the knowledge that anywhere in the world there would be an exact replacement readily obtainable. The replacement would also be certified to the IEC standard and have identical characteristics to the item being replaced, giving no problems with respect to discrimination etc. So goes the theoretical argument.

In practice the aim of harmonisation is not so easy to achieve as would appear from the theoretical argument. There are many practical difficulties.

Billions of fuses are already installed in apparatus throughout the world and require replacement fuselinks for "Blown" fuses. Enthusiasm in a given country for a harmonised system rapidly dies if the fuselinks do not fit in the available fuse-bases with the same degree of protection. A completely new harmonised system is therefore universally unpopular because it is seen everywhere as just an additional system, which would need to have exceptional economical and technical advantages before its use would even be considered.

It appears therefore that any International harmonisation needs to be based on existing systems. These are continuously being improved by normal technical evolutionary development, and IEC SC32B and its working groups are constantly assessing the new types as they become established in use, with a view to identifying a type or types most suitable as preferred designs in any future harmonisation, reducing proliferation and ensuring good reproducible performance.

In spite of the practical difficulties there has been considerable progress in the last few years toward the achievement of these aims, particularly in achieving common characteristics and performance standards. These achievements are summarised below together with details of the schemes being proposed for the "Neutral" evaluation of the various available types, and an examples of the application of the proposed evaluation criteria which identifies the British compact industrial fuselink as the most suitable for harmonisation within its range.

## 2. Progress to Date

The process of harmonisation has been considerably advanced in recent years, as is evidenced in the latest edition of IEC 269 "Low-voltage fuses", every part of which has been or is being revised in accordance with these aims. IEC 269-1 "General Requirements" and IEC 269-2 "Supplementary requirements for fuses for use by authorised persons (fuses mainly for industrial application)" have both been published and incorporated in national standards.

It was early realised that before any thought of dimensional standardisation could be attempted, it was necessary to proceed towards standardisation of characteristics and performance. A survey carried out on behalf of IEC 32B/WG8 at the commencement of this work revealed that at that time the fuses in use throughout the world differed by as much as 5 to 1 in certain characteristics. It was appreciated that although special characteristics might be needed for certain specialised applications, the bulk of the applications of fuselinks were of a general purpose type where it was desirable to have similar characteristics when replacing a fuselink by one of similar dimensions and rating but of different manufacture. Designers of equipment specifying the use of "100 A general purpose fuse to IEC 269", for example, should also be able to get the same protection whatever the national system.

The achievement of 32B can be recognised in IEC 269-1 and IEC 269-2 where a general purpose fuse is defined within specified gates of time/current and  $I^2t$  which ensure discrimination between fuses of 1.6 to 1 in current rating. Fig 1 is an example of how this has been achieved for fuselinks to the British Standard BS 88, but similar time/current zones are obtained if the values are taken from the German Standard, the French Standard, or any other National Standard complying with IEC 269-1 and IEC 269-2. More detail of the various national types complying with all sub-clauses of IEC 269-1 and IEC 269-2 is given in IEC 269-2-1 "Supplementary requirements for fuses for use by authorised persons (fuses mainly for industrial application) Sections I to III" in which special features and dimensions of the various systems are recorded.

The only variation still existing is in fuses to the American national standards which are still classified according to a historical philosophy of fuse current rating, but at the same time of writing a special working group with a US convener is actively proceeding with supplementary requirements which should enable the American system to be added to IEC 269-2-1.

The other essential performance factors of the fuses are harmonised in IEC 269. In particular the breaking capacity of fuses up to a rated voltage of 660 V, mainly for industrial applications has been set at a minimum level of 50 kA. The criteria for establishing rated current and rated voltage, the temperature rise of contacts and terminals, interpretation of oscillograms, the number of samples to be tested, and the methods of test for power dissipation, protection against electric shock etc, are also all specified so as to ensure equal conditions of high safety and reliability in application to all systems which comply with the standard.

All new refinements to the standard under consideration are now applied universally to all systems included in IEC 269-2-1.

It could justifiably be claimed that the framework for world-wide harmonisation of low-voltage fuses on the basis of performance and characteristics has been attained in IEC 269-1 and IEC 269-2.

## 3. Future Tasks and Philosophy

Because of the evolutionary nature of fuse development and use, established systems need to be considered when selecting a particular fuse system as a preferred system for international harmonisation. However, because of the strength of local preference for each national system it is difficult to make an objective analysis on a world-wide basis. However, 32B/WG13 has been given the task of attempting this analysis, and has proposed that a "Neutral" system of assessment be used to compare the advantages and disadvantages of the different fuses within the national systems, to select the best fuse for harmonisation. The philosophy of the proposed system of comparison is outlined below and appears to be a very fair one. However, it must be said at the outset that early study shows that the result of any comparison is dependent upon the specific application of the fuse and the geographical area in which it is used. This is a major drawback to the philosophy, but it still produced interesting results, as is shown in Section 4 where the philosophy is applied to the British compact industrial fuselink compared with other types with similar performance.

The philosophy developed by IEC 23B/WG13 starts by assembling a list of desirable attributes of a Fuse System. This list is based on a collation of attributes obtained by the circulation of questionnaire to all the National Committees of the IEC asking them to proposed such desirable attributes. The list of attributes proposed is as follows:-

- 1 High breaking-capacity
- 2 Optimum number of ratings based on the R10 series
- 3 Good cycling withstand ability
- 4 Defined total  $I^2t$  values
- 5 Electrical shock protection
- 6 Fuse-link easy to replace
- 7 Low power dissipation
- 8 Compact physical size
- 9 Indicator system
- 10 Low cost
- 11 Non-"repairable" design
- 12 Contact pressure independent of user's skill
- 13 Non-interchangeable by voltage rating
- 14 Non-interchangeable by current rating
- 15 Safe replacement under load conditions
- 16 Provision for safe replacement without danger in a high prospective fault area
- 17 Non-interchangeable with other systems of different specification
- 18 Easy mounting of fuse holder
- 19 DIN rail mounting option
- 20 Modular design
- 21 Access for voltage tester
- 22 Fuse handle an integral part of the fuse
- 23  $I_6$  test duty
- 24 Defined dc rating.

These attributes are all desirable in a fuse system, and the intention is that a panel of experts would examine each competing system and allow a percentage "score" representing the extent to which the system achieves each parameter. However, before these "scores" can be used to provide the yardstick to measure the relative advantages of one system above any other, it is necessary to establish an agreed order of importance of the attributes. It is proposed that this be accomplished by considering each attribute in comparison one at a time with each of the others, and thus establish an order of importance, with the least important at the bottom of the list and the most important at the top. A simple tabular method has been devised for this purpose. The position in the table will then determine the weighting to be applied to each attribute. The scores will then each be multiplied by the appropriate rating and added up. The optimum system will be that with the highest total.

In theory this appears to be a completely "Neutral" system but in practice it is again fraught with difficulty. Even assuming that a panel of completely independent experts could be found, their assessment of relative importance of the attributes would differ, depending on their country of origin. These differences of opinion are not chauvinistic but represent significant differences in the conventional wisdom in different countries. To take one example: the fuse indicator. In some European countries it is usual to fit an indicator to each fuse-link to identify a fuse which has blown. It is generally accepted by the users in those countries that this feature is of significant value, and that its advantages outweigh the disadvantage that indicators are not 100% reliable. In the UK this matter was studied at BSI many years ago, and the reverse conclusion was reached. Early fuselinks to BS 88 were fitted with such indicators, but in later editions of BS 88, they were removed because it was decided that the occasional maloperation of an indicator could have safety implications which far outweighed the convenience of the indication. Furthermore, the removal of the indicators reduces manufacturing cost, and thus gives a better score to item (10). Item (10) is of primary importance to many users.

The last point brings out a further difference in the voting of experts. In attempts already made to make this assessment in one country with a large number of respondents, it was found that if the respondents were divided into two groups, users and manufacturers, there was good consistency in the opinions within each group, but the conclusions of each group were very different.

Finally there is the question of establishing what basis we should establish for the ultimate use of the fuse system. A lot of the views which have been expressed in these discussions have tended to seek a fuse system which would be usable in every possible application up to 690 volt systems. Item (24) suggests that the same system should also be usable on dc, whereas the number of dc installations and the number of 660 volt installations is small compared with ac installations up to 415 volts. A "universal" fuse could be regarded as over-engineered, and the inefficient compared with a fuse designed to be restricted to the lower ac voltage used in the majority of applications. The latter fuse could contain the same electrical performance at the lower voltage within smaller dimensions, saving material cost, and more importantly saving expensive space. The lower voltage rating enables a fuse to be made with a lower power loss, which reduces the heat dissipated within the enclosure, and also saves energy - an environmental bonus when we consider the enormous number of current-carrying fuses in service.

Thus we see that there is a philosophical basis which colours the judgement in assessing the relative merits of different fuse systems, and that it is unlikely that any system would have over-riding superiority above all others. However it is clear that in restricted circumstances one type can be superior, as we can illustrate with the British compact industrial fuse.

#### **4. Application of the Philosophy to the Compact Industrial Fuse**

The basis of the argument is contained in the penultimate paragraph of the last section. This fuse meets all the requirements of IEC 269-2 and IEC 269-1, and thus it achieves all that is at present required of it in parameters (1), (2), (3), (4) and (5), and proposed improvements to these specifications. It is restricted to 415 volts ac use. This enables it to score high marks on all these items. Now the other attributes of the fuse can be compared with other fuses to the same standard. (6) Fuselink easy to replace: With their offset blade construction (see Fig 2) a blown fuse is easily lifted out and replaced. (7) Low power dissipation: due to the restriction to a maximum of 415 volts, these fuselinks have a significantly lower power dissipation than other BS 88 fuses with the same rated current. (8) Compact physical size: this is a special feature of these fuses (see Fig 2). (10) Low cost: these fuses use less materials than other comparable types and also occupy less expensive space. There are thus significant cost savings. There is a further on-going cost saving in the reduced power dissipation. (11) Non-"repairable" design: Yes (12). Contact pressure independent of user's skill: Yes. (13) Non interchangeable by voltage rating: Yes, these fuselinks are of unique designs and of dimensions which provide non-interchangeability. (14) Non-interchangeability by current rating: Non-interchangeability is specified in four current bands with maxima at 20 A, 32 A, 63 A and 125 A. This has proved sufficient in wide experience of use of these fuses, and although the system is capable of additional keying features to give complete non-interchangeability, this was judged unnecessary. (15) safe replacement under load conditions: this is provided by attribute (22). (16) provision for safe replacement without danger in a high prospective fault area: It is arguable that replacement without isolation in such an area cannot be without hazard, although feature (22) reduces such hazard. (17) Non-interchangeable with other systems of different specification: Yes, this is a unique type of fuse. (18) Easy mounting of fuse holder: Yes (19).

DIN rail mounting option: Yes. (20) Modular design: Yes. (22) Fuse handle an integral part of the fuse: Yes. Two aspects are yet to be decided, ie: (21) Access for voltage tester, which could readily be provided, and (23)  $I_g$  test duty which is not required in IEC 269 although experience with these fuses in practice indicates that there should be no difficulty in successfully passing any additional breaking capacity test in the specified range. We see that this system will score high marks on all these attributes, and therefore, whatever the order of importance assigned, it is sure to be outstanding in its assessment.

There were two attributes to which answers could not be provided: (9) Indicator system and (24) defined dc rating. However it was explained that the British national committee had decided that indicators should be separated from the fuselinks and thus (9) was a separate matter, and with respect to (24) these fuselinks are restricted to ac use.

It is seen therefore that a fuse system can have considerable advantages above other systems if restrictions are applied to its use. There is no hazard introduced, provided the fuses are non-interchangeable with other types. Such a case is illustrated above.

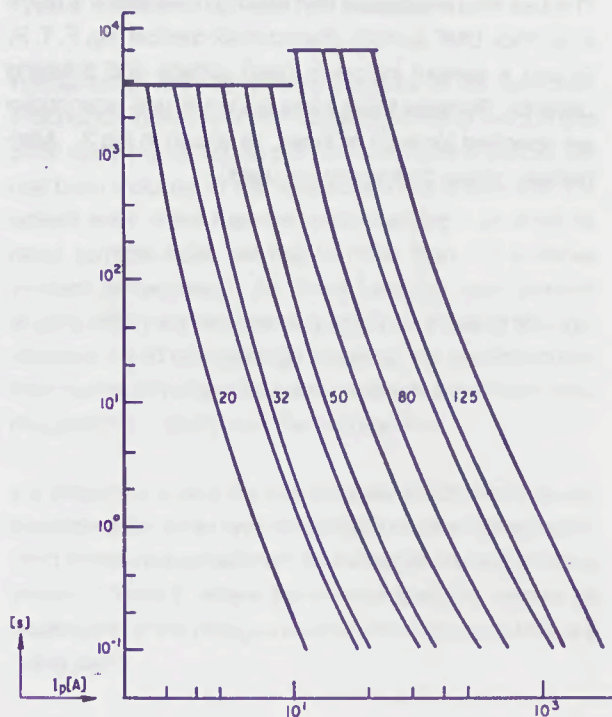
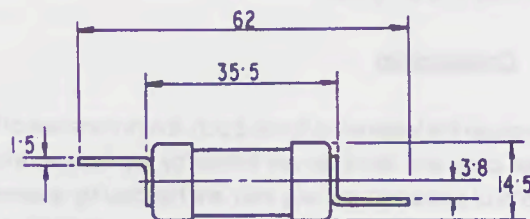
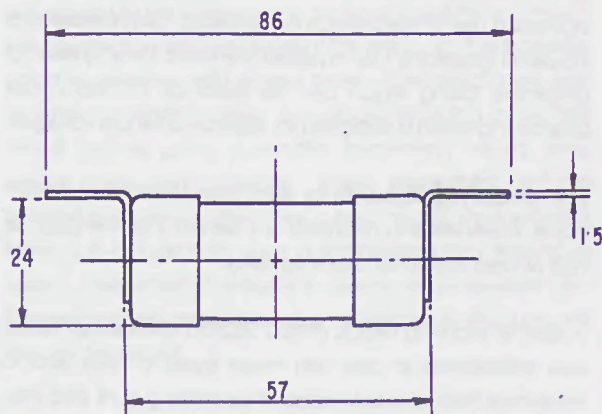


Fig. 1 Time/examples of current characteristics specified in BS88

## 5. Conclusions

- 1 Considerable progress has been made in international harmonisation of requirements for performance and characteristics of fuselinks to IEC 269-1 and IEC 269-2.
- 2 Progress in harmonisation of dimensions is slow, due to a variety of practical considerations.
- 3 A new attempt is being made to assess existing systems on the basis of agreed desirable attributes of the fuse, to select the best preferred types and reduce proliferation.
- 4 Although a "Neutral" method of assessment has been devised, practical and theoretical difficulties exist in establishing an order of importance of the attributes.
- 5 In spite of the difficulties, it is clear that certain fuses will stand out from the others by their many advantages, provided their range of use is limited.
- 6 An example of such a fuse is the British compact industrial fuse.



All dimensions in mm

Fig. 2 Comparison of the dimensions of the British compact industrial fuselink (below) with the conventional design of industrial fuselink (above)

## Requirements for Universal Modular Fuses (UMF's)

C Turner, H W Turner, D J A Williams

### Summary

A new type of miniature fuse-link is described, which is specifically designed for use on printed circuit boards. These fuse-links are particularly suitable for use at low voltages, down to 32 V and currents up to 5 A. The requirements for such fuse-links, both dimensional and electrical, are discussed. Achievements to date and possibilities for future developments are considered.

### 1. Introduction

The increasing tendency towards miniaturisation and the increased use of electronics in domestic, commercial and industrial situations has revealed the need for a system of protective fusing which can be used on printed circuit boards and which is designed for application at low voltages.

The special requirements for such fuses lie in their dimensions, materials and methods of insertion into the pcb, as well as their electrical characteristics.

A special Working Group of IEC SC32C (Miniature Fuses) was established to deal with these types of fuse, and to determine their characteristics, thus making sure that they are universally accepted, so that they can be used in electronic equipment which is likely to be moved freely from one country to another.

The specification for these fuses will be Part 4 of the IEC series on miniature fuses (IEC 127). A unique symbol will be used to identify them.

### 2. Construction

Because the fuses must fit into a pcb, the dimensions of the fuse body and terminals are limited by the normal dimensions of pcb's and the way they are handled by automatic insertion machinery. The two different types of UMF which are being standardised are the through hole radial type, designed for soldering directly into a printed circuit board, and the surface mounting type, which is designed to be attached into the surface of a substrate by solder or other means.

For the through hole type, the terminals (pins) must go through the hole in the pcb (1 mm), which gives a maximum cross-sectional area, but they must also be able to carry the required current without overheating, and this determines the minimum cross-sectional area of the pins. The spacing of the pins corresponds to multiples of the hole spacing in the pcb and depends on the rated voltage of the fuselink, as shown in Fig 1.

The terminals of the surface mounting types are arranged as shown in Fig 2, and their dimensions and spacing are only limited by the creepage and clearance requirements for the rated voltage and by the stacking dimensions of the components on the pcb.

The fuse element is completely enclosed. The enclosure should be made of a material which can withstand the heat required for soldering the terminals into or onto the board and its other maximum dimensions are standardised as shown in Figs 1 and 2.

The fuse links are marked with rated current, maker's name or symbol, UMF symbol, characteristic symbol (eg, F, T, R, S) and a symbol indicating rated voltage and breaking capacity. Because these fuses are small, one-letter codes are specified for each of these, as shown in Fig 3. Alternatively, colour coding may be used.

### **3. Electrical Properties**

The electrical requirements for these fuses are very similar to those of the more familiar miniature cartridge fuses, as they are meant to perform a similar protective function.

The range of current ratings is the same as for miniature cartridge fuses, from 32 mA, to 5 A, and voltage ratings are 32, 63, 125 and 250 V, with low breaking capacity only up to 125 V, and low, intermediate and high breaking capacity at 250 V. These breaking capacities are defined as shown in Table 1.

Four types of time/current characteristic are envisaged for these fuse-links: R: super-quick acting; F: quick-acting; T: time-lag; S: super time-lag.

All fuses should operate within the harmonised system of time/current gates, ie their pre-arcing times at 1.25 times rated current should be at least one hour, and at 1.7 times rated current they should not exceed 5 minutes.

At 10 times rated current the pre-arcing times depend on the type:-

- Type R: not exceeding 0.005 seconds
- Type F: between 0.005 and 0.015 seconds
- Type T: between 0.015 and 0.100 seconds
- Type S: between 0.100 and 1.00 seconds.

Temperature rise for these fuse-links is of particular importance, because of their close proximity to the pcb and other components on the pcb, and therefore a special test has been included in the specification to ensure that the hottest point of the fuse-link when carrying 1.25 times its rated currents does not rise to more than 135 K above ambient temperature. As these fuselinks have element lengths which are considerably less than those of the conventional 5 x 20 mm cartridge fuselinks, it is possible to limit their maximum voltage drop and maximum sustained power dissipation to comply with this requirement.

It is important to limit the overvoltages which occur during fuse operation, so as to avoid damage to other components, and therefore the maximum overvoltages are laid down as shown in Table 2, where the overvoltages are seen to be dependent on the voltage system in which the fuse-links are being used.

### **4. Future Developments**

At present these fuselinks are being manufactured to a limited degree. Some examples of the fuses available are shown in the photograph. It is expected, however, that a considerable expansion of the manufacture and use of these types will follow the general acceptance of the new IEC specification, and in particular that these fuses will be developed in low voltage and low current ratings. It is difficult to manufacture conventional miniature fuse types with such ratings because of their inherently larger volt drop and the fact that sophisticated design methods are necessary to produce elements with reproducible time/current characteristics and the required mechanical properties.

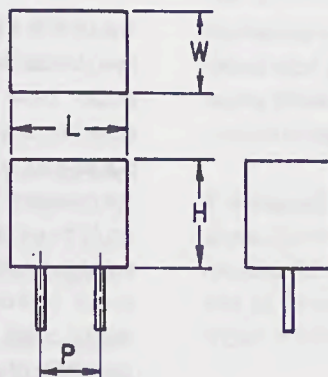
### **5. Conclusions**

The UMF is a type of fuselink, which, if accepted world-wide as a standardised fuse type for use on printed circuit-boards, would have considerable economical and technical advantages over the fuses in use at present. Their use would put an end to the ambiguity in rating philosophy at present still prevalent in different parts of the world, so that fuselinks could be replaced with greater safety. The designs are also suitable for direct insertion or surface mounting on printed circuit boards using automatic machinery, saving time, labour costs, and materials. These economics give the possibility of using more fuses in each circuit, thus isolating faulty sub-circuits with good discrimination and enhanced safety. Identification of faults in design or component performance which cause the return of electronic products will thus be facilitated.

**Fig.1 Fuselinks-UMF  
Through hole radial type**

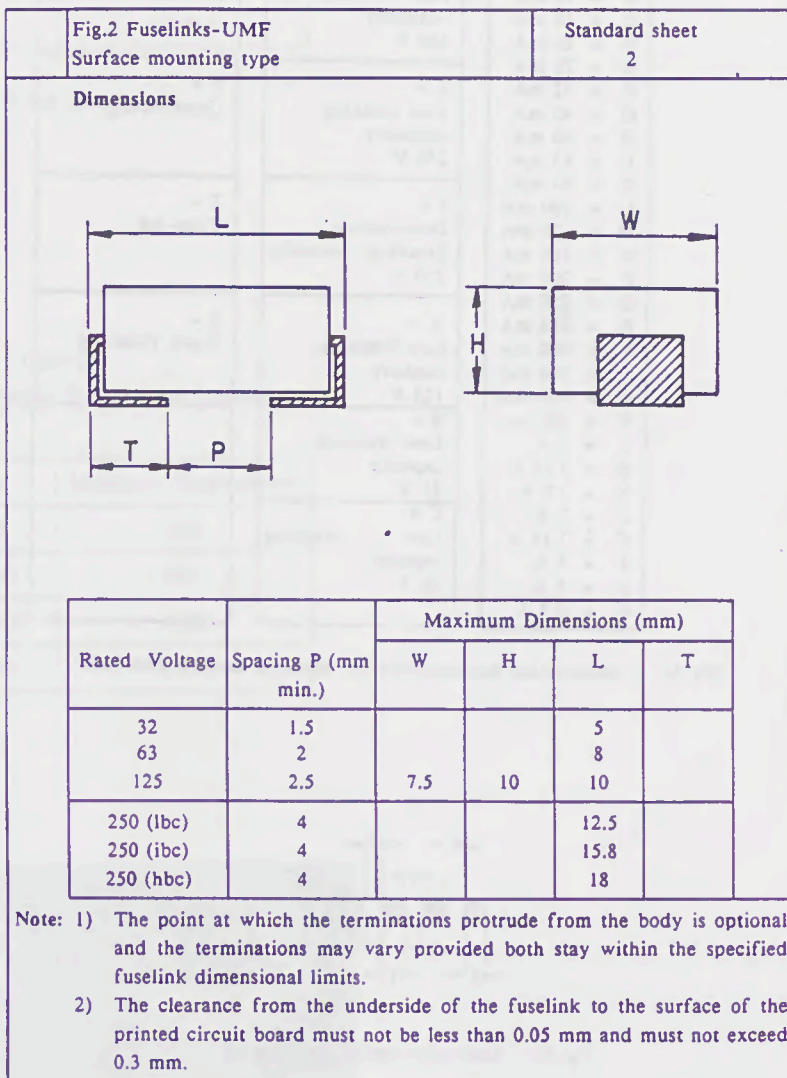
**Standard sheet  
I**

**Dimensions**



Rated Voltage	Pin Spacing (mm) P	Maximum Dimensions (mm)		
		W	H	L
32	2.5			8
63	2.5			8
125	5	7.5	10	10.5
250 (lbc)	7.5			12.5
250 (ibc)	10			15.0
250 (hbc)	12.5			18

**Note:** The termination must go through a in hole and have a minimum cross-sectional area of 0.15 m<sup>2</sup>. The geometry of the cross section is optional.



Example :

UMF of 200 mA rating Low Breaking-capacity Quick-acting Reflow type SMT:-

UMF Symbol		
A = 10 mA	H = High breaking -capacity 250 V	R = Super Quick-acting
B = 12 mA	L = Low breaking -capacity 250 V	F = Quick-acting
C = 16 mA	I = Intermediate breaking capacity 250 V	T = Time-lag
D = 20 mA	A = Low breaking capacity 125 V	S = Super Time-lag
E = 25 mA	B = Low breaking capacity 63 V	
F = 32 mA	C = Low breaking capacity 32 V	
G = 40 mA		
H = 50 mA		
J = 63 mA		
K = 80 mA		
L = 100 mA		
M = 125 mA		
N = 160 mA		
P = 200 mA		
Q = 250 mA		
R = 315 mA		
S = 400 mA		
T = 500 mA		
U = 630 mA		
V = 800 mA		
1 = 1 A		
W = 1.25 A		
X = 1.6 A		
2 = 2 A		
3* = 3.15 A		
4 = 4 A		
5 = 5 A		
6 = 6.3 A		

Fig 3a Abbreviated marking code for universal modular fuse links

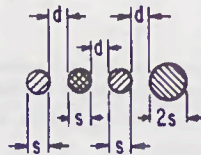


Fig 3b Alternative colour dot marking

Table 1  
Breaking Capacity

Rated Voltage	Breaking Capacity
32 (lbc)	35 A or $10I_n^*$
63 (lbc)	35 A or $10I_n^*$
125 (lbc)	50 A or $10I_n^*$
250 (lbc)	100 A
250 (ibc)	500 A
250 (hbc)	1500 A

\* whichever is the greater

Table 2  
Maximum Overvoltages During Fuse Operation

Rated Voltages	Maximum Overvoltage
$0 < U_n \leq 50$	500
$50 < U_n \leq 100$	800
$100 < U_n \leq 150$	1500
$150 < U_n \leq 300$	2500

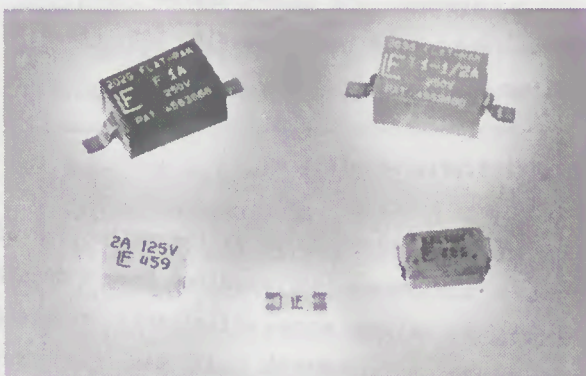


Fig.4 Photograph of UMF's available at present

# APPLICATION OF THE EXPERT SYSTEM FOR THE SELECTION OF CAPACITOR FUSES

S. ARAI

Department of Electrical Engineering

Tokyo Denki University

Tokyo Japan

Summary: An expert system application is tried to design shunt capacitor banks in order to correct power factor and to select line fuses for the capacitor bank protection. The programming language of the expert system is the PROLOG, and it runs on the personal computer. It is shown that the expert system aids and is useful to design shunt capacitor banks and to select line fuses quite well.

## 1. Introduction

The power factor improved by shunt capacitors connected in parallel with electrical distribution lines reduces the size of each components in distribution system, so that electric utilities in our country provide to reduce the rate of customer charge and urge for consumers to install capacitor banks at their electrical receiving system.

The combinations of a load-breaking switch and a current limiting fuse (clf) are often installed in series to control and protect capacitor bank circuit.

Clfs applying to line fuses provide backup protection against ruptures of shunt capacitor tanks.

This paper reports the application of expert system to design shunt capacitor banks and to select applicable line fuses to the shunt capacitor banks installed at consumer's electrical receiving-end.

The commercial expert system tool that belongs to DECsystem-10 PROLOG is used for expert system construction. The programming language of the expert system is the Prolog, and the system is used on the personal computer which

has 640kB memory capacity. It is recognized that the expert system aids to design shunt capacitor banks and to select suitable line fuses quite well within short executive time.

## 2. The Expert System in Prolog

Prolog programming consists of three types of clauses of facts, rules and questions. Facts called data express the objects and their relationships and always unconditionally true. Rules express true relationships between facts depending upon a given condition. Question looks like a expression of fact, except the special symbol of a question mark and a hyphon, gives answers of Prolog that consists of a set of objects satisfying the questions. A question except a question mark and a hyphon is called a goal.

Informations in an expert system can take the form of facts and rules. Facts and rules are contained as the knowledge base in an expert system, the expert system uses these facts and rules as the basis for decision making.

### 2.1 Knowledge Acquisition

The knowledge base which is the collection of domain knowledges is acquired from a domain expert who solves more efficiently problems in a particular field. It may also get expertise from various sources as stating later.

### 2.2 Inference Execution

Each clause of rule consists of a head and a body. They are connected by the symbol ":-". The clause of a rule has the form as follows

```
conclusion:-condition_1,condition_2,
          ...,condition_n.      (1)
```

A set of conditions on the right-hand side of the rule is the body of a clause, can be tested for their truth value. The conclusion on the left-hand side of the rule is the head of a clause is true if its conditions can be proved true. Each term of above clause(1) is called a predicate.

A condition is compared with the conclusions of the stored clauses. When it finds a match, it tries to prove the goal by considering the conditions of the matched conclusion as subgoals. When all subgoals are shown to be true, the goal itself is proved.

These inference proceedings are rigidly controlled by the interpreter, which has the principal mechanisms of backtrack, pattern matching called unification, syllogistic inference and a scheduler.

### 3. Data Base Representation

The main data structures of this expert system can be represented in the form of list structures. The values of elements of a list are mostly obtained by the manufacture's catalogues. The list is an ordered sequence of

```
rating_lf(pt_t_uco_1,[rated_volt('7.2'),
                    rated_current(3),
                    rated_breaking_current(63),
                    reted_min_breaking_crrnt(27),
                    fusing_current_7200s(28),
                    fusing_current_60s(29),
                    fusing_current_100ms(71),
                    fusing_current_2ms(1800),
                    breaking_current_13ms(342)]).
```

Fig.1 An example of data for a line fuse

elements of capacitors and clfs data, so that facts are organized to be able to get necessary informations on relations between data.

As shown in fig.1, in the example of this data structure, rating\_lf is the name of data kind, pt\_t\_uco\_1 is the name of data, the elements in the list are names of ratings and of fusing and breaking charateritics about a clf, the value in each parentheses of elements is the voltage or current value of ratings and of fusing and breaking charateritics.

### 4. Rule Base Representation

Knowledge in this expert system originates from many sources, such as electrical regulations, research papers, case studies, reports, manufacture's manuals, empirical data, books, and domain expert experiences. Knowledges that includes procedures, intuitive method and strategeies for problem solving are necessary for the expert system to build into a computer program.

#### 4.1 Rule Base of Design Capacitor Bank

One of necessary imformations for the design of shunt capacitor bank is total capacity of the capacitor bank in full load at the consumer's receiving-end. And other required informations are original and desired improving power factor. The total capacity of capacitor bank is calculated by using the following well known formula

$$Q = P(\sqrt{(100/Pf_b)^2 - 1} - \sqrt{(100/Pf_a)^2 - 1}) \quad (2)$$

where

Q = total capacity of the capacitor bank (kVA)  
P = consumer's recieving power capacity (kW)  
Pf\_b = original receiving-end power factor at full load (%)

Pf\_a = desired improving receiving-end power factor at full load (%).

P, Pf<sub>b</sub> and Pf<sub>a</sub> are not provided as data base in the expert system, so that the expert system asks for the user to supply these informations. The values of P, Pf<sub>b</sub> and Pf<sub>a</sub> are input to the running expert system from the computer terminal.

When the receiving power is greater than 500kVA, the total capacity of capacitor bank is divided into a few banks in practice, so that the necessary capacity of capacitor bank is timely adjusted to meet the changing demand of reactive power as close as possible. In our country, individual divided capacitor bank is usually used in a series reactor, the capacity of series reactor is 6% of the capacity of the individual capacitor.

The divided capacitor bank and its series reactor are selected from the manufacturer's cataloged capacity to meet just or just over the calculated capacity.

#### 4.2 Rule Base of Selection CLFs

The applicable clf to capacitor circuit is selected from one of clfs passed all selecting rules with aim of short circuit protection of capacitor banks and series reactors.

Selecting rules are as follows,

(1) the rated voltage Vr of clf equals or is larger than the circuit voltage V<sub>l1</sub>, and Vr is equals or smaller than the voltage of 1.2 times V<sub>l1</sub>.

$$V_{l1} \leq V_r \leq 1.2 \times V_{l1} \quad (3)$$

(2) the rated frequency of clf equals the circuit frequency.

(3) the clf is able to carry the current of 1.5 times the circuit full load current, that is, the rated current of clf Inf is greater than the current of 1.5 times the capacitor rated current or capacitor circuit current Inc.

$$1.5 \times Inc \leq Inf \quad (4)$$

(4) the rated breaking current of clf I<sub>l</sub> is greater than the short circuit current I<sub>s</sub>.

$$I_s < I_l \quad (5)$$

(5) the overcurrent of the circuit to be less than the minimum breaking current of clf I<sub>mb</sub> is broken by the series switchgear such as load breaking switch. That is, an intersection point of the operating time-current characteristics of clf and the series switchgear is greater than the minimum breaking current of clf.

$$I_{mb} < I_f \text{ and } I_f = I_s \text{ at } T_f = T_s \quad (6)$$

(6) the minimum pre-arcing current of clf Immf is greater than the current of 2 times the circuit current.

$$2 \times Inc < Immf \quad (7)$$

(7) the current of 10 times the circuit current is greater than the 60s pre-arcing current of clf I<sub>f60</sub>.

$$10 \times Inc > I_{f60} \quad (8)$$

(8<sub>1</sub>) in the case of no series reactor, clf does not melt by flowing the over current of 70 times the circuit current during 2ms and can repeat it 100 times. That is, the over current is smaller than the current of S-factor times the 2ms pre-arcing current.

$$70 \times Inc < S \times I_{f2m} \quad (9)$$

(8<sub>2</sub>) in the case of installation of series reactor, clf does not melt by flowing the current of 5 times the circuit current during 100ms and repeating it 100 times. the over current is smaller than the current of S-factor times the 100ms pre-arcing current.

$$5 \times Inc < S \times I_{f0.1} \quad (10)$$

(9) the maximum Juele-integral of 10% breaking probability of capacitor bank during 13ms is greater than the maximum Juele-integral of 13ms operating current of clf.

$$(I_{f13m})^2 < (I_{c13m})^2 \quad (11)$$

I<sub>f13m</sub> is operating current of clf at 13ms, I<sub>c13m</sub> is current on the characteristics of 10% breaking probability of capacitor at 13ms.

(10) operating time-current characteristics of clf is under 10% breaking probability characteristics of capacitor bank.

$$I_{fi} < I_{ci} \text{ at } T_{fi} = T_{ci} \quad (12)$$

Tfi, Ifi are time and current of the clf at the 'i'th point on the operating time-current characteristics of clf, Tci, Ici are time and current of the capacitor at the 'i'th point on the 10% breaking probability characteristics of capacitor.

Rule (1) is expressed in a program as shown in fig.2. When a capacitor rated voltage Vnc and a clf rated voltage are given, the condition of 'float' calculates  $Vnc_{12} = 1.2 \times Vnc$ , next condition of 'ge' decides  $Vnc \leq Vnf$ , and the last condition decides  $Vnf \leq 1.2 \times Vnc$ . If every condition is true, the conclusion is true.

```

rated_voltage_clf(Vnc,Vcf):-
  float(*,'1.2',Vnc,Vnc_12),ge(Vnf,Vnc),
  ge(Vnc_12,Vnf).

```

Fig.2 A program of rule(1) of the clf selecting rules.

## 5. Support Facilities

In the expert system, general problem-solving knowledge is organized by separation from the knowledge about the problem domain.

### 5.1 Data Base Processing

The data base processing is composed of capacitor data base processing and clf data base processing. After menu selection, the data base processing asks for the user to input pertinent data in conversing with the expert system and stores data in the data base during the expert system executing. Other data base manipulations are executed by the editor and the built-in clauses in Prolog.

### 5.2 Explanation of Results

Explanation facility explains how the system arrived at its conclusions or answers. Users tend to have more faith in the results, more confidence in the system by the explanation of

process getting at its answer.

The successful way leading to the conclusion is explained after the completion of clf selection. The expert system indicates the specified conditions of power factor correcting circuit and the designed capacitor bank. The comparison is displayed between the specified selecting rules of clf and the characteristics of selected clf, then time-current characteristic is displayed between the clf and the capacitor bank on graph or by the values.

### 5.3 Support Facilities of Tool

Main components of this expert system support environment are knowledge base debugging aids, input/output facilities and knowledge base editor. This expert system tool has usual facilities such as normal display, windows, a mouse pointing device and manipulating fundamental mathematical formula. The editor of expert system tool includes lots of predicates of various functions and common programming languages such as writing, reading, displaying, deleting, copying, etc.

## 6. An Example of the Expert System Execution

As shown in fig.3(a), the expert system may start after inputting question of goal 'run.' in the interpreter. Information under  means user input.

The user selects next processing from the contents of menu as shown in fig.3(b). Here user selects item 3 for design a capacitor bank circuit and selection clfs to achieve the power-factor correction for a system.

The running expert system communicates with the user and asks for the user to input the suitable informations about capacitor banks circuit design and switching controllers of capacitor bank.

After the user inputs the required information as shown in fig.4, the expert system shows the

|?-run|

(a) the expert system starts running

- 1 data base processing of clfs
- 2 data base processing of capacitors
- 3 design of capacitor banks circuit and selection of clfs
- 4 finish

(b) processing menu

Fig.3 The expert system starts running and the processing menu

Input according to the following request;  
Circuit voltage(kV) = 6.6  
Consumer's receiving power capacity (kVA)  
= 1500  
Original receiving-end power factor at  
full load(%) = 75  
Desired improving receiving-end power  
factor at full load(%) = 95

Fig.4 An example of system requests for capacitor banks

given data about capacitor bank circuit and calculated results on the display.

Afterwards the expert system arrives at the conclusion of capacitor bank circuit design as shown in table 1.

Next, the system goes to the selection of applicable clf to the above designed capacitor circuit by the user picking the item of selection clf processing from the second menu omitted as next action.

The capacities of capacitor bank and reactor are shown about the object selected from the designed capacitor bank as shown in table 1. The method of selection clf executes the elimination of the clf data base which does not meet each step of the selecting rule as shown in fig.5(a). The passed data names are shown on the display.

During the executing, the user gives appropriate informations such as short circuit current of capacitor bank circuit, breaking capacity of load-switch, S-factor of clfs for the requirement of the expert system. The expert system decides the clfs which passed the all selecting rule to be applicable as shown in fig.5(b). After the selection of clf is completed, the expert system shows data for the selected capacitor bank and clf on the display.

As final process, the expert system goes to

Table 1 Number of divided bank, calculated one capacitor bank capacity, designed capacitor bank capacity and series reactor capacity to design number

design number	number of dividing	calculated capacity(kVA)	recommending capacity(kVA)	reactor capacity(kVA)
1	6	138.0	150	9.0
2	5	166.0	200	12.0
3	4	207.0	250	15.0
4	3	277.0	300	18.0
5	2	415.0	500	30.0
6	1	830.0	1000	60.0

the indication of the comparison between the specified conditions of power factor correcting circuit and the designed one capacitor bank and its circuit. The

```
[data passed 1st rule]
pt_t_uco_1,pt_t_uco_2,pt_t_uco_3,
pt_t_uco_4,pt_t_uco_5,pt_t_uco_6,
pt_t_uco_7,

[data passed 3rd rule]
pt_t_uco_4,pt_t_uco_5,pt_t_uco_6,
pt_t_uco_7,
```

(a) data names of clfs passed 1st, 3rd rule

```
[data passed 9th rule]
pt_t_uco_4,pt_t_uco_5,
```

(b) clfs passed all rules

Fig.5 Selecting execution of clf

confirmation of appropriate clf selection is the comparison between the all specified selecting rules of clf and the characteristics of selected clf, then operating time-current characteristic curve of the clf between 10% breaking probability characteristics of the capacitor bank on graph or by the values.

Lastly, the user picks the next action or the finish processing. We obtained the selected clf to agree entirely with the manufacture's data.

## 7. Conclusion

It was proved that the developed expert system aided electrical designing engineer in his designing job of power-factor correcting circuit.

The developed expert system is quite simple and remains many problems to improve its

performing better, but we can suggest that the developed expert system is available and useful for diagnosis of distribution circuits.

The tool was chosen because it was efficient one available that ran on our personal computer.

## References

- [1] Waterman D.A., A Guide to Expert systems, 1986, Addison-Wesley
- [2] Shibayama H., Sakuragawa T, Hagino T, An Introduction to Prolog-KABA(Japanese), 1986, Iwanami
- [3] Prolog-KABA Reference Manual (Japanese)
- [4] Cloksin W.F., Mellish C.S., Programming in Prolog, 1981, Springer-Verlag
- [5] JEM 1348-1984, Fuses for High Voltage Capacitors(Japanese), 1984, The Japanese Electrical Manufactures Association
- [6] JEC-2330, Power Fuses(Japanese), 1986, Standard of The Japanese Electrotechnical Committee
- [7] Walker A., McCord M., Sowa J.F., Wilson W.G, Knowledge Systems and Prolog, 1987, Addison-Wesley

PROTECTION OF ESI EQUIPMENT WHERE PRIVATE GENERATORS  
ARE CONNECTED TO THE DISTRIBUTION SYSTEM

D J Williams  
ERA Technology Ltd  
Leatherhead, Surrey, UK

H W Turner  
ERA Technology Ltd  
Leatherhead, Surrey, UK

SUMMARY

It is now a legal requirement for private generators producing 1 MW of power or more to be able to sell electricity to Regional Electricity Companies (RECs) for their distribution systems. The RECs need to ensure that safety and security of supply are not impaired as a result. Equipment whose rating was adequate before the connection of private generators may therefore require uprating or additional protection. This paper focuses on the additional protection that current limiting fuses can provide for circuit breakers whilst optimising co-ordination. The possible prospective fault currents after the connection of private generators and the times in which they must be disconnected are considered.

1. Introduction

With recent legislation empowering private generators to sell electricity for distribution on Regional Electricity Company systems, consideration must be given to the continued safety and security of supply. ERA, in collaboration with the Electricity Council (now the Electricity Association), has therefore conducted an investigation into some protection aspects of this increasingly important commercial activity. In order to provide the necessary background to the changing situation, discussions were held with representatives of a major electricity board at various stages of the investigation.

The objective of this work is to determine what sort of protection device is most suitable for limiting fault currents on distribution networks at 'medium' voltage (11 kV) in situations where the addition of private generators might cause faults in excess of the breaking capacity of existing protection equipment and of the fault current withstand of other circuit components. At this stage, ERA's study does not include low voltage (415 V) circuits because the connection of small private generators at this voltage rarely causes fault level problems, except occasionally where interconnection between 415 V systems exists. Interconnection increases the fault level and the connection of private generators may then cause the declared fault level to be exceeded. However, in such cases, the relatively low cost, simple solution of removing interconnections can be used to reduce fault levels.

At medium voltage, the characteristics of the combined circuit resulting from the addition of private generators to the distribution system are such that special types or combinations of fuses will probably be necessary to provide full protection, as described below.

2. Normal and Fault Current Levels

2.1 Before the Connection of Private Generators

From discussions with the Electricity Council it is understood that normal full load currents in the systems under consideration are approximately within an order of magnitude of the fault currents.

The fault level on an 11 kV system normally lies in the range 100 MVA to 175 MVA (5.2 kA to 9.2 kA), but the extremes are 50 MVA to 250 MVA (2.6 kA to 13.1 kA)<sup>7</sup>. Usually, a margin of approximately 30 MVA to 40 MVA (1.6 kA to 2.1 kA) exists for the accommodation of the fault level from private generation and induction motors. Existing switchgear can safely disconnect a fault level of 13.1 kA.

The contribution from the motor load on the system is variable, but is typically well within the 30 MVA to 40 MVA margin. However, in some circumstances there may be a much larger contribution; for instance Williams and Corcoran<sup>1</sup> quote up to 35% when induction motors are electrically close to a faulted busbar. In this extreme case, larger margins would be necessary to prevent existing switchgear experiencing fault levels higher than their rating, even before the connection of private generators. However, the presence of large motors or groups of motors would be known to the REC concerned, and allowance made for them. Guistiniani<sup>5</sup> states that the contribution from induction motors decays to a relatively small value after 5 to 10 cycles, ie 0.1 to 0.2 seconds. If a REC circuit breaker takes 0.4 seconds to operate<sup>7</sup> then the contribution from induction motors would be negligible. However, more rapid disconnection is presumably desirable, and could be achieved by fusing.

## 2.2 After the Connection of Private Generators

The total private generation capacity that could be connected to any one 11 kV system is expected to be in the range 1 MVA to 7.5 MVA<sup>7</sup>, with corresponding current levels of 0.05 kA to 0.4 kA. It is expected that the minimum generator size will be 1 MVA because it is unlikely that it will be economic for smaller generators to be connected at 11 kV. The order of fault level contribution from a generator is typically 5 to 6 times its rating for a short circuit, ie at present, a private generator could add 5 to 45 MVA, or 0.3 to 2.4 kA, to the short circuit current. For larger private generators, the fault level margin of the existing system may be insufficient to accommodate their fault level contribution. If several large private generators were connected in parallel without additional fault level reduction measures, then the rating of 13.1 kA switchgear could be significantly exceeded. The contribution from motor loads must also be considered when deciding on fault level reduction measures.

To enable switchgear to be used when fault levels can rise to values significantly above its rating, some back-up device (eg fuse) for interrupting fault currents in approximately a quarter of a cycle, ie 5 ms, is required. Co-ordination would be achieved by disconnection of currents above the switchgear rating by the back-up device, leaving the switchgear to disconnect currents below its maximum breaking capacity.

Two examples of sites being proposed for private generation were considered using the 11 kV system diagrams for the areas supplied by grid supply points called X and Y for the purposes of this paper. 1.5 MVA may be exported from Site A, which is connected to grid supply point X by approximately 6.7 km of cable, and 4 MVA from Site B, which is connected to grid supply point Y by approximately 3.9 km of cable. In the former case there is the complication of home based patients who are presumably noted on the diagram because they are highly dependent on a continuous electricity supply. They are between grid supply point X and generation site A.

In these cases, the highest prospective current would occur if there was a fault close to the grid supply point. There would then be some limitation of the contribution to the fault from the private generator by the intervening cable. A worse case would therefore exist if a private generator was connected close to the grid supply point.

Information from an electricity board<sup>7</sup> gave a range of normal currents of 0 to 400 A flowing either from or to a private generator at its point of connection to the distribution system. A protective device at this point (B

in Fig.1) must therefore carry 400 A without deterioration. The maximum current of 400 A into the distribution system could only be provided by a 7.5 MVA private generator, and the maximum current through the protective device feeding into a fault on the distribution system would be approximately 2.4 kA<sup>7</sup>, or 6 times the rating of a fuse used for protection at this point. The use of two type K fuses in parallel (discussed in Section 3.4) would give a pre-arcing time of 100 seconds, and would therefore offer no protection from the private generator's output to the electricity board's circuit breakers. This would apply in a similar way for less powerful private generators used in conjunction with correspondingly lower fuse ratings.

If a fuse was placed in series with a private generator (C in Fig.1), but did not carry any current input from the distribution system, it would again have to be rated to carry the maximum power generated. A fault on the distribution system would not cause currents from the generator to the distribution system higher than those described above, and hence disconnection times would be similarly long. This arrangement would also have the disadvantage of disconnecting the private generator from any load it was primarily intended to supply when there was a fault on the main 11 kV system. However, the generator might be tripped whatever the position of the protection because of instabilities on the 11 kV system resulting from the fault and its disconnection. The advantage to the private generator of installing protection at B rather than C is that supply to its load could be resumed without waiting for a fault on the distribution system to be remedied.

This would also apply if there was protection at positions such as A in Fig.1. The prospective fault current would be higher here than at B and C and current sensitive protection devices used to protect the circuit breakers would therefore operate more rapidly. Damage to the circuit breakers from fault currents in the main 11 kV system could be prevented, although current from the private generators could still flow into the local part of the 11 kV system. However, a separate protection system should then rapidly disconnect the private generator from the local system. It would be necessary to ensure that protection at A was co-ordinated correctly with the circuit breakers so that the latter disconnected low fault currents and the former disconnected high fault currents.

### 3. Methods of Protection with Private Generators Connected to the 11 kV system

In the event of a fault, it is necessary to prevent the combination of main and private generation from damaging REC switchgear. Sometimes, a possible method of accomplishing this is to disconnect private generators from the distribution system to prevent them adding to fault currents whenever running arrangements which give rise to high fault levels are adopted. Alternatively, if the fault is cut off before the current reaches a damaging level, rapid disconnection of the private generators might be unnecessary. Various means of protection are possible and are discussed below.

#### 3.1 The Calor-Emag $I_S$ Limiter

The Calor-Emag  $I_S$  limiter<sup>2</sup> is a device intended to provide rapid disconnection of faults. It has a fusible link with an element of considerably lower rating than the normal circuit current in parallel with a tubular conductor, or bursting bridge, which normally carries most of the current. An explosive in the centre of this tube is detonated by an electronic circuit in the event of a fault, diverting all the current through the fusible link. Calor-Emag give a bursting time for the tube of 0.1 ms and a time for limitation of the current by the fusible link of 0.5 ms.

The Calor-Emag  $I_S$  limiter<sup>2</sup> is already in use for disconnecting fault currents at some sites where private generators feed power into area board systems. However, the limiter is not a failsafe device, and is understood to have failed. Problems may arise in the circuits which initiate operation of the limiter or in the detonation of the bursting bridge connection. There is no system to indicate the presence of a malfunction before the limiter is required to operate.

If a fuse with a rating appropriate to the normal current and voltage of the circuit was connected in series with the  $I_S$  limiter, then the combined system would fail to safety if the bridge failed to burst. The breaking capacity of the fuse would be sufficient to disconnect safely the maximum fault current if the  $I_S$  limiter failed to operate correctly for whatever reason. This would add to the cost of protection and it would be simpler and cheaper to use a single fuse system which would disconnect faults sufficiently rapidly (see Section 3.4). However, the back-up function could be performed using present designs of fuse, which are not fast enough to provide complete protection. The switchgear would not be fully protected by such a system, but it would be safer than with an  $I_S$  limiter alone.

Also, the connection of such a series fuse would not have prevented the type of limiter failure reported to the Electricity Council<sup>7</sup> in which the bridge was burst but the fault current was insufficient to be cleared by the parallel fusible link. The link then overheated and a flashover occurred. Calor-Emag do not use a sealed cartridge fuselink in their limiter, but replace the element and quenching material in the same barrel after operation. The performance in this respect could probably be improved by the use of a general purpose fuselink conforming to BS 2692 Part 1. Such a fuselink would have to be replaced in its entirety after operation of the limiter.

The Calor-Emag is the oldest device of its type, and is in use in various locations, but other companies such as the G & W Electric Co and the S & C Electric Co produce similar devices. They may have advantages, but this would have to be ascertained by comparative testing.

#### 3.2 Uprating Switchgear

An alternative solution to the problem of increased fault current levels is uprating the switchgear whose rating may be exceeded. According to GEC<sup>1</sup>, economical switchgear ratings are now available at ratings higher than 250 MVA, eg 475 MVA and 600 MVA. The smaller of these ratings would be sufficient to disconnect the present maximum fault levels, allowing for significant contributions from induction motors (87 MVA) (see Section 2.1) and the anticipated contribution to a fault from a large private generator (45 MVA) (see Section 2.2), whilst still allowing for some future increase in generating capacity.

When a private generator wishes to be connected to the distribution system, the fault levels after connection should be carefully calculated, taking into account the distance of the generator from any switchgear. The Electricity at Work Act does not permit switchgear ratings to be exceeded, so if this is found to be possible, then the uprating of switchgear may be necessary if a private generator is to be connected. The effect of the rate of rise of the increased fault current, which may adversely affect the switchgear even if the current is cut-off before rated values are reached, should also be considered, and switchgear manufacturers consulted.

Even if switchgear with ratings of the order of 475 MVA is now more economical than before, it is unlikely that the RECs would want to go to the expense of uprating switchgear unless it becomes due for replacement. However, this could be a solution if the private generating company met all or some of the cost of necessary uprating of the protection to accommodate the addition of their

supply. Such additional costs may make the connection of some private generators uneconomic, and other protection methods should then be considered.

### 3.3 GEC's Short-Circuit Limiting Coupling

In the same paper<sup>1</sup>, the authors suggest the use of a 'short-circuit limiting coupling' (SLC) developed by GEC. The device consists of a reactor in series with a capacitor, and the combination resonates at power frequency thus adding a low impedance to the circuit. An iron-cored reactor in parallel with the capacitor saturates if the voltage drop across the capacitor increases due to an excessive current. The tuning of the circuit is then changed, producing a high impedance. This device appears to give rapid limitation of fault currents, but has the disadvantages of being bulky and expensive. Also, it may be possible for it to fail to operate, for instance in the case of a fault in the capacitor. However, it is more likely to be reliable than a device incorporating explosives.

### 3.4 Conventional Fusing

The use of fusing is an alternative to the protection options described above. Fuses are failsafe devices when used within their specification, they have very high breaking capacity and are compact and economical. They are most economical if a device from normal production can be used, rather than a specially made one. Electricity boards and the Electricity Council have examined the characteristics of fuselinks produced by various manufacturers, including GEC's standard, type K, high voltage, high breaking capacity fuselinks<sup>3</sup>, which are rated at 12 kV. However, the maximum current rating available in a single fuselink is 350 A and the application under consideration was a private generator with a total load current of 410 A (slightly higher than the usual range<sup>7</sup>).

GEC suggest the use of two identical fuses in parallel to achieve higher current ratings, which are less than the sum of the two ratings used. The characteristics of such a pair of fuses were supplied to ERA by GEC. An appropriate fuse with a rating of 450 A can be produced by connecting two 250 A fuselinks in parallel. Combining two fuselinks in parallel also has the advantage that the combination's time/current characteristic is steeper than that of a single fuselink, giving faster operation at high fault currents.

Similar characteristics were provided by Hawker Fusegear<sup>4</sup>. To save space, the following examples are taken from the GEC data, but other manufacturers' products could be used in a similar manner.

The characteristics for this combination show that prospective fault currents (symmetric rms) above 10.2 kA are cut off, and at this current, the pre-arcing time is 50 ms, or between 2 and 3 cycles. At the maximum fault current without private generators, 13.1 kA, the pre-arcing time would be 25 ms (1 to 2 cycles) and with the addition of a 7.5 MVA private generator, the maximum fault current of 15.5 kA would give a pre-arcing time of 12 ms (0.5 to 1 cycle). Switchgear would therefore be exposed to a current exceeding its rating for part of this time, and for part of the arcing time. Thus although this combination fuse operates much more rapidly than the circuit breakers normally in use, it does not provide sufficient protection. At such fault currents, the pre-arcing  $I^2t$  would be close to its minimum value of  $1200 \times 10^3 \text{ A}^2\text{s}$ .

However, it may be possible to achieve the required protection by taking the process of combination further, ie connecting more fuselinks in parallel. For example, GEC gives characteristics for two 125 A fuselinks in parallel for which the combined rating is 225 A. Thus GEC derate the sum of the ratings combined in parallel by 10%. Combining two such pairs of fuselinks in parallel would therefore presumably give a fuselink with a rating of 405 A. Fuses are derated because of the effects of heating by adjacent fuses and because there will be some uncertainty about the exact distribution of current in parallel fuses, whose resistances may be slightly different. Less derating may therefore be required if the fuselinks are spaced to allow better heat dissipation. Also, when more than two fuses of the same rating are connected in parallel, it is statistically more likely for there to be a more even current distribution.

Four 125 A fuselinks in parallel would provide suitable protection for the case of the maximum normal current of 400 A expected by some electricity boards (Section 2.2), and possibly when there is a slightly higher current of 410 A<sup>7</sup> as in some applications. The time/current characteristics would be steeper than for a pair of fuselinks and it is possible that fault currents exceeding the switchgear rating could be disconnected sufficiently rapidly. However, it would be necessary to determine characteristics for such a combination experimentally to establish its suitability for the application. The use of more than four fuselinks in parallel may be necessary if this method of protection is to be used.

The rating of approximately 405 A may be too small for some applications, but combining four 160 A fuselinks, the next rating above 125 A provided by GEC, should give a rating of approximately 520 A. This would probably be too high to provide sufficient protection, and the manufacture of fuselinks with a rating between 125 A and 160 A may be necessary. Alternatively, it may be possible to use mixed ratings in parallel if the difference between ratings is produced by variations in the number of parallel elements of the same design. The current distribution would have to be checked to ensure that the current through each fuse was proportional to the rating. However, this is a departure from existing practice and careful investigation and testing would be required before this concept could be accepted by fuse manufacturers and users. Such a combination of fuses should then only be used as recommended by the manufacturer, and this could be accomplished by connecting the fuses in a single unit which could only be fitted to a specially modified fuse holder.

At B or C in Fig.1, the fault current flowing to or from the private generator should be much less than the values of 10 to 15 kA for which operating times are given above, giving longer operating times and greater values of pre-arcing  $I^2t$ . The use of such a fuse system at these positions would therefore provide the required protection. The combination fuselink must therefore be connected at positions such as A where current from the grid and the private generator flows. Fuses with ratings of the order of magnitude described above would only be appropriate in branches of the 11 kV system supplying currents of approximately 400 to 500 A. Fuses with higher ratings will be required closer to grid supply points, and can be produced with fast characteristics using the principles described above.

### 3.5 Special Fuse Types

It may be possible to achieve the required protection using a device similar to that being developed by General Electric<sup>6</sup>. It is based on a conventional fuse element, but has chemical charges attached to it. It is hoped that it will be possible to use a microprocessor monitoring system to blow the charges and hence disconnect the current. This device might give operating times of the order of those claimed for the Calor-Emag  $I_S$  limiter (Section 3.1). However, there is no evidence that General Electric have yet produced a successful prototype.

The General Electric Device could presumably be set to operate at any current level required. It would have a great advantage over the Calor-Emag  $I_S$  limiter because the fuse element could operate in the normal way if the charges or their triggering circuits failed. The General

Electric element has an M-effect blob to dissolve the element and operate the fuse at low overcurrents, and a series of constrictions at which multiple arcs would be created by a high overcurrent. These features would presumably be designed in the same way as in a conventional fuse of similar rating, making the device failsafe if similarly filled and enclosed. However, the article<sup>6</sup> does not make clear how the device was to be enclosed such that products of the explosion did not create a hazard.

Also, the reliability of the operation of the explosive is not assessed and there could be other hazards associated with its presence. Its stability in its working environment would have to be proved. Explosive devices have historically been less reliable than required when used in protection applications. For instance, explosive indicators were removed from British low voltage fuses because of unreliability, occasional spurious operation, possible association with the initiating of arcing faults and the known failure record of the Calor-Emag  $I_S$  limiter. In contrast, conventional fuses (Section 3.4) have extremely high reliability and repeatability.

## 4. Conclusions

At present, it appears that combining fuselinks in parallel (Section 3.4) offers the most reliable, safe and economical method of protecting existing switchgear. However, the number of fuselinks required to give sufficiently rapid operation is excessive. If fuse manufacturers can develop a fuselink that operates more rapidly than existing designs, then complete protection against increased fault levels caused by the connection of private generators could be provided. It is also possible that in future, a reliable fusible element combined with an explosive charge (Section 3.5) could give more rapid protection. Such a device would have to be thoroughly tested to ensure reliability and safety.

If funds were available, a straightforward method of preventing problems due to the contribution of fault currents by private generators would be to replace existing circuit breakers with new ones of higher breaker capacity.

### 5. References

- [1] Williams W.P. and Corcoran J.C.W., Progress in design of industrial power networks, 1987, GEC Review, Vol.3, No.3.
- [2] Calor Emag, Technical/Advertising Leaflet No.1357/6E on  $I_s$  limiters.
- [3] GEC Alsthom catalogue for fuselinks to BS 2692.
- [4] Hawker Fusegear catalogue for fuselinks to BS 2692.
- [5] Guistiniani D., Presentation on the operation of private generating plant in parallel with the grid distribution system, Ref.7R/53/7, East Midland Electricity Board.
- [6] Martin D., Smart fuses enter with a small bang, 1960, Electrical Review, p7.
- [7] ERA investigation into the possible use of HV fuses for restriction of generator fault current contribution; information requested at meeting arranged with an Electricity Board by the Electricity Council (27 Sept 1989). (Not available except with the permission of the electricity board concerned.)

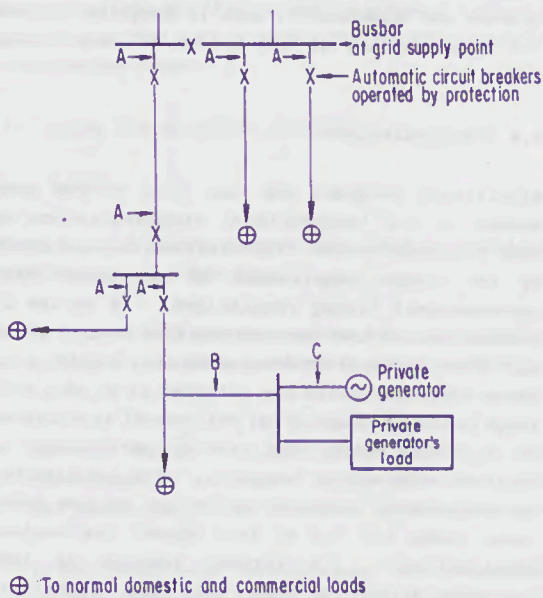


Fig. 1 Schematic distribution network with private generator

P.G. Newbery  
Hawker Fusegear Ltd.  
Leicestershire, UK.

### Summary

This paper outlines the advantages of fuse protection in low voltage distribution systems and covers the recent progress made in standardisation. Significant advances have been made in fuselink technology resulting in higher performance products in standard packages, or more compact fuselinks. The evolution of fuse systems must however include the associated fusegear and two examples are illustrated of recent innovations in fuseholders and fuse distribution boards by one manufacturer in the United Kingdom.

### 1. Introduction

Fuse protection has been used for over 100 years and is still widely used in high and low voltage applications, and for the protection of electronic circuits with miniature fuselinks. Recent developments in all these fields have been illustrated in this conference and the wide variety of papers from over 20 countries confirms that fuse protection is still evolving to meet the present and future needs of overcurrent protection. This paper will focus on fuses for low voltage industrial and commercial applications, and, in particular, for final distribution circuits.

### 2. Advantages of Fuse Protection

#### 2.1 General

The following section highlights some of the main advantages of fuse protection in low voltage systems and takes into account the growth of other protective devices such as mcbs and mccbs.

#### 2.2 Safe Operation and Safe Replacement

These two fundamental aspects of fuse operation are taken for granted and consequently often overlooked. First taking safe operation - when a cartridge fuselink operates, it does so quietly, and the by-products of arcing are safely enclosed within the fuse cartridge. The same cannot be said for mcbs and mccbs which can emit arc products and the position of the associated venting is not standardised which means they can only be replaced with identical products.

Turning to safe replacement - when a fuselink operates the reason for the fault has to be identified and corrected. A brand new fuselink is then inserted and the system is restored to its

original state of security. When circuit breakers operate there is inherently some erosion of the contacts etc. Many of these breakers when tested to their "ultimate breaking capacity" are only capable of a limited number of operations and have to be replaced. The time taken to replace a fuselink is often quoted as a disadvantage. It is, however, insignificant compared with the fault diagnosis time, and that for corrective action.

#### 2.3 High Breaking Capacity

The current and energy limitation provided by modern cartridge fuselinks gives them the ability to clear the highest of fault currents likely to arise in service. For example fuselinks used in North America are tested to 200kA to meet fault levels that can occur, such as in high-rise buildings. This current and energy limitation can occur at much lower fault currents, for example 20A industrial fuselinks can become current limiting at a current as low as 100A. Magnetic and thermal stresses in the faulty circuit are thus dramatically reduced, even at these low fault currents, restricting the damage at the seat of the fault and thus protecting sensitive circuit components.

This high breaking capacity means that detailed fault level calculations with fuse protected systems are unnecessary, and, in addition, allows for strengthening of the system at some future date.

#### 2.4 Standardisation

Significant progress has been made in the past decade on the international standardisation of fuse characteristics. This has been brought about by the common requirement of compliance with international wiring regulations. A series of points or gates have been established through which all manufacturers characteristics should lie. These characteristics are referred to as gG - full range breaking capacity (g) and general application (G). This means that similar performance is achieved with any gG fuselink. The mcb also has non-adjustable characteristics but on the other hand, there are up to four types for various applications. A further feature of fuse characteristics is that they are relatively insensitive to changes in ambient temperature for example when placed inside an enclosure. Ambient temperature can have a significant effect, however, on the tripping current of breakers.

The gG characteristics do not cover North American practice, but standardisation work is currently addressing this aspect.

## 2.5 Discrimination

The gG fuselinks give a discrimination ratio of 1.6:1 (two steps in the R10 series). In circuit breaker protected systems, a ratio of up to 4:1 in current rating is required and a detailed study of characteristics is required.

A fuselink is often used to give back-up protection for circuit breakers and this is an area where further standardised information is required on the withstand capabilities of modern breakers to co-ordinate with fuse characteristics.

## 2.6 Motor Circuit Protection

Recent papers show how the fuselink is the only effective means of giving Type 2 co-ordination of modern motor starters to IEC 947-4-1. There are special motor circuit fuselinks for example gM, aM or dual element which take account of the short time nature of the motor starting surge to give compact fuselinks. It should however be stressed that a large number of applications are covered with the appropriate selection of standard gG fuselinks.

Current work is being undertaken in the IEC low voltage standardisation committee which should enable the setting of universal total  $I^2t$  limits for gG fuselinks. These will be established on the requirements for protecting sensitive modern motor starters. This should in turn simplify fuse selection for the protection of motor circuits and obviate the undesirable practice of selective combination tests.

## 3. Final Distribution Circuits

### 3.1 General

Considerable advances have been made in fuselink performance for example:-

- In Europe 660V performance is now available in packages that were previously rated at 500V or less.
- In the United Kingdom there has been the consolidation of compact blade type fuselinks and associated fully shrouded fuseholders.
- In mainland Europe there has been the development of the compact size 000 or C00 fuselinks for ratings up to 100A.

- In North America there is the use of very compact class T fuselinks for non-motor circuit applications and a trend towards time delay fuselinks in the class J package.

To fully exploit the advantages of high breaking capacity fuselinks, consideration must also be given to the associated fusegear in which they are used and consequently the fuse system. In addition to performance requirements, other important aspects have to be addressed such as simplicity of application, ease of installation, aesthetics, availability, safety and of course cost competitiveness with other protection systems.

An IEC Working Group has been examining the feasibility of a unified system of fuses. The feasibility aspect must be stressed rather than any definitive proposals. In a similar way to the universal plug and socket system, such a task is fraught with dimensional rather than technical constraints, particularly with regard to the large and longstanding replacement need for existing systems. The Working Group concluded that in the short term it was not feasible to have a universal fuse system and the Working Group was redirected to consider a list of attributes for a future system so products can evolve with enhanced features.

This list of attributes includes a number of technical requirements such as defined characteristics and properties of materials. In addition safety and constructional features have been identified and include:-

- \* Electrical shock protection.
- \* Contact pressure independent of users skill.
- \* Good contact design including terminal connections.
- \* Fuselink easy to replace.
- \* Fusehandle an integral part of the fuse.
- \* Non interchangeable with different levels of rated current.
- \* Indicator, if required, to be a separate reliable unit.
- \* Compact physical size.
- \* Rail mounting option.
- \* Modular design.

These attributes have been addressed by one manufacturer in the United Kingdom in the development of innovative fuseholders to take standard bolted fuselinks and of a new generation of fuse distribution boards.

### 3.2 New Fuseholder

Safety requirements are becoming increasingly prevalent in both national and international legislation for installation equipment and the requirement for the protection against electric shock is an important feature for new designs of fuseholders. British fuseholders have traditionally been well shrouded and have an IP-2X degree of protection for all three states of installation i.e.

- when the complete fuse is properly mounted.
- during the replacement of the fuselink
- when the fuse carrier is removed

In the new fuseholder, particular attention has been given to these aspects and includes captive hinged internal terminal shields which overcome the nuisance factor on many existing designs where the shields are not captive and may get lost during installation.

A problem worldwide in electrical power components is the provision of an effective hand operated system to give ease of insertion and particularly withdrawal against the necessary high contact pressures. This is a problem with conventional British fuseholders and foreign fuse-bases where a compromise has to be made on contact pressure. The new fuseholder overcomes this problem with a simple cam and lever action giving a mechanical advantage to remove the fuse carrier with a low application of force whilst maintaining a high contact pressure. This cam action enables safe withdrawal and insertion of the fuse carrier which is independent of the users skill. It also enables the design to have high contact pressures to give enhanced reliability and performance.

The main requirement regarding cable connection for British Standard fuseholders is to fit the stripped cable end directly into the fuseholder terminals, and is generally referred to as "front connected". Normally these fuseholders have tunnel type terminals machined or extruded in brass with a grub screw for fastening. Special measures are required to give effective clamping for all sizes of cable for a reliable connection without damaging the conductors. The new fuseholder has a saddle type connection and the main electrical contact is made directly onto the high conductivity top plate (Fig. 1). This in turn is an integral part of the double sided fuse base contacts.

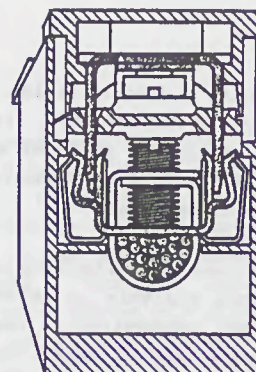


Fig. 1 Saddle Type Terminal

The use of stainless steel saddles and hardened terminal screws coupled with profiling of the cable contact enables high tightening torques to be achieved. This is particularly important in applications where undersized cables are inadvertently used which could result in excessive temperatures in this terminal zone. The design permits the saddle to "breathe" during normal expansion and contraction of cables during normal load variations, maintaining a constant clamping pressure. This obviates the need for re-tightening as is often required in conventional arrangements. In addition to the requirements of IEC 269 the terminals have been tested to the requirements of the new Low Voltage Switchgear and Controlgear Standard IEC 947-Part 1, which require tests for:-

- Mechanical strength
- Damage and accidental loosening of cable
- Pull out force

The terminal designs gave values well in excess of these modern requirements

Fuseholders generally have the cable clamping screws firmly screwed home, and they have to be released (often forcibly) before the cable can be inserted. The new fuseholder has these screws "backed-out" leaving the cable aperture open, thus saving installation time.

The cam action well covers the attribute of "simple and swift facility for safe fuselink replacement" and in addition, hinged captive screws are a feature of the fuse carrier, particularly important for the busy electrician (Fig. 2). Often the fuselink

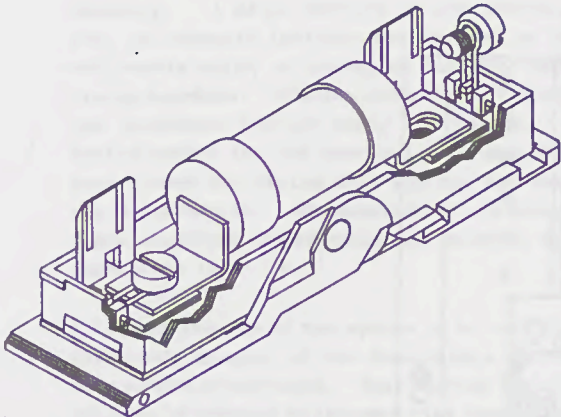


Fig. 2 Hinged Captive Screws

has to be replaced in difficult situations and in traditional products it is easy to loose the screw and they are often difficult to locate.

In the British system, the fuse carrier is an integral part of the fuse; this is an advantage over the "DIN system" with a replaceable handle which may be lost and unsafe improvisation may be attempted.

Non-interchangeability with different levels of rated current at 20, 32 and 63A and beyond, are achieved in British fuseholders through dimensional constraints on the fuselinks. The bulk of the market requirement for final distribution circuits in industrial and commercial application is up to 63A. The new fuseholder is, however, available up to 100A, using modern compact bolted fuselinks. For higher current ratings the modern cost effective approach is to use fuse combination switches, switch fuses or fuse switches.

An optional optical indicator is available as an accessory to be fitted into the fuse carrier meeting another of the desirable attributes. This means the fuselink is not complicated with the provision of an indicator, sometimes of questionable reliability.

Rail mounting is a feature of modern equipment and the new fuseholder offers DIN rail mounting - the modern approach - and bolted panel mounting, the conventional approach, as standard thus obviating the need for stocking the individual types. The DIN rail mounting facility for each of the sizes are designed to have equal height and depth above the DIN rail, thus giving a functional and aesthetic appeal to installations of mixed ratings.

There is a requirement for the electrical connections to be made through back studs for example, on surface panel mounted applications for control circuits on distribution switchgear. The new fuseholder can be readily converted to a single or double back stud version with a conversion kit and the aid of a screwdriver. Traditional products cannot be converted and are factory assembled. Availability of these back stud versions with inherent lower demand is, therefore, greatly enhanced and stockholding can be minimised at appropriate points down the distribution chain.

### 3.3 New Distribution Fuseboard

In the United Kingdom up to the 1970's fuseboards with semi-enclosed or rewirable fuses were popular in final distribution circuits. The large potential market to supersede these old technology devices has largely been taken by mcb boards, mainly due to their ease of installation and competitiveness. Similar progress has been made by mcbs throughout the world in applications where their breaking capacity meet the installation requirements.

The features of modern mcb boards were examined and a fuseboard developed incorporating the desirable features of such a system and giving the added advantages afforded by modern cartridge fuses. A survey showed that the vast majority of requirements are covered by fuse ratings of 63A or less and of these the bulk are below 32A

It was decided to use fuselinks to BS88 part 6 with blade contacts, removing the need for a special tool (screwdriver) to put the fuselinks into the fuse carrier. The desirable features of the fuseholder with the cam action was incorporated with a common modular envelope size for the 32 and 63A ratings. These include non-interchangeable features in the fuse-base and carrier so that the 32A fuse carrier cannot be "over-fused" and the 63A fuse carrier will not fit into the 32A fusebase. This modular design overcomes one of the problems of British fuseboards in that if only one outgoing circuit requires a 63A size fuselink then a multiway board with 63A fuses has to be used in all circuits.

The new fuseboard takes a similar form to the mcb board and for ease of installation a pan assembly is used incorporating protected vertical 200A bus-bars (Fig. 3). The appropriate fuseholders for a specific application are assembled onto the pan assembly. The fuseholders are fitted with stab connectors at the bus-bar end which are orientated for the phases (Fig. 4) and simply docked into the rising bus-bars and secured into position by means of a captive screw on the pan

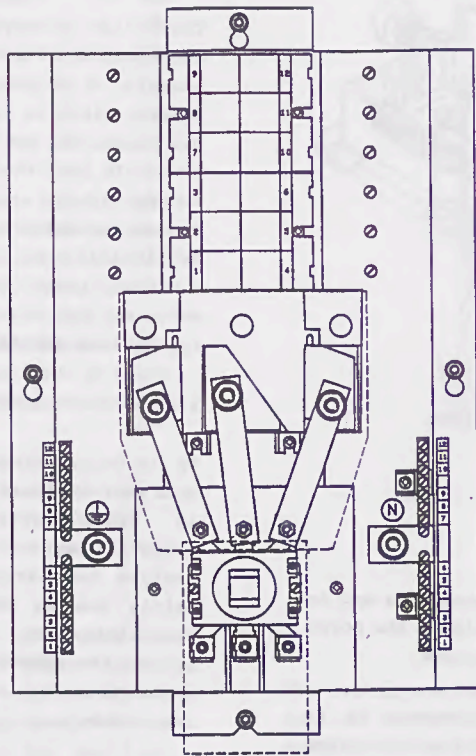


Fig. 3 Pan Assembly with Integral Isolator

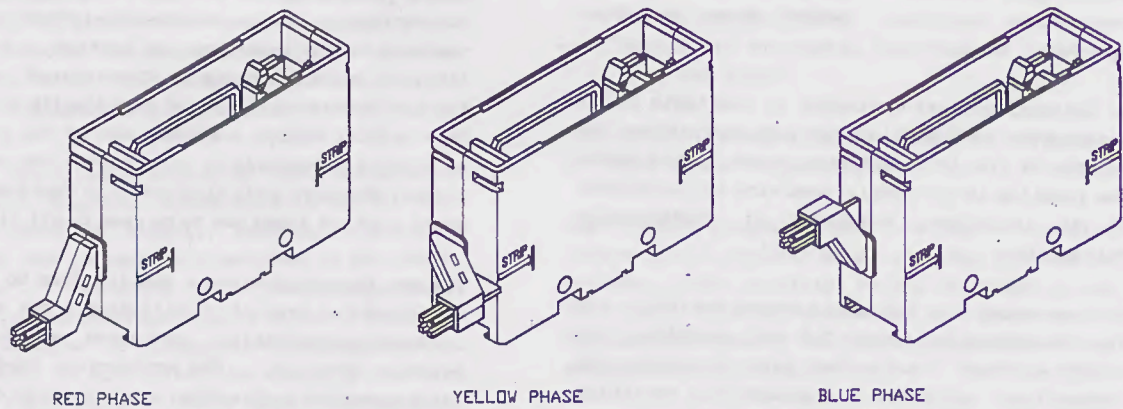


Fig. 4 Stab Connectors

assembly. A major feature of the fuseboard is that an integral isolator can be used as in the mcb boards which is connected directly onto the rising bus-bars. The pan assembly is fitted into the enclosure and is ready for wiring. The configuration for the vertical arrangement gives good access for wiring in a similar and familiar way to mcb boards. The addition of the Escutcheon plate completes the assembly and gives an elegant appearance (Fig. 5).

A further feature of the system is to have two and three pole ganging of the fuseholders by the use of standard accessories. This enables the correct poles to be removed at the same time thus providing improved safety to the isolation of 2 and 3 pole circuits. Prominent circuit identification labels are also provided on the fuse carrier and bus-bar covers.

The new fuseboard forms part of a range of fusegear, bus-bar chambers, fuse combination switches, isolators etc. to give an integrated system with all the technical advantages of fuse protection in a modern and economic way with an emphasis on ease of installation.

#### 4. Conclusions

The longstanding advantages, versatility, simplicity of selection and well proven experience of high breaking capacity fuselinks, coupled with the evolution of new compact products, are strong factors for the longevity of fuse protection in final distribution circuits.

These desirable features of the fuselink cannot be fully exploited without considering its integration into the associated fusegear to give a complete system. Innovations in fusegear, such as fuseholders and distribution boards as illustrated in this paper, are of paramount importance. Advances in ease of installation, availability, aesthetics, safety and cost effectiveness can be achieved to enable fuse protection to play a dominant role in protecting electrical circuits in the future.

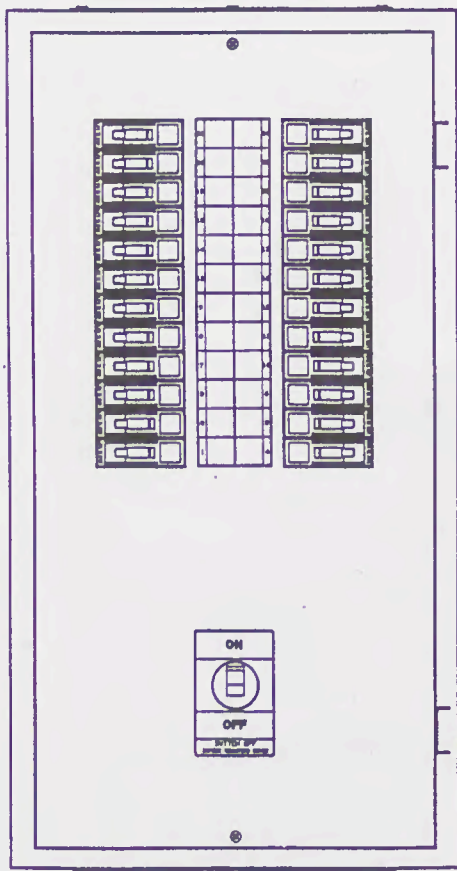


Fig. 5 New Distribution Fuseboard (door removed)

Faint, illegible text at the top left of the page, possibly a header or introductory paragraph.

Faint, illegible text at the top right of the page, possibly a header or introductory paragraph.

Faint, illegible text in the middle left section, likely a descriptive paragraph.

Faint, illegible text in the middle right section, likely a descriptive paragraph.



Faint, illegible text at the bottom right of the page, possibly a concluding paragraph or a note.



Faint text below the large diagram, likely a caption or title for the drawing.



# OVERLOAD TESTS FOR FUSES IN ROLLING-MILLS

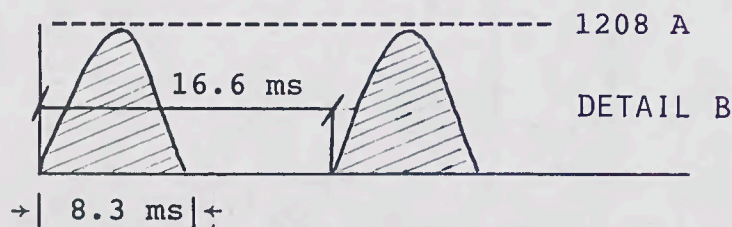
PAPER TO BE PRESENTED AT THE ICEFA 91 - CONFERENCE

## SESSION 1

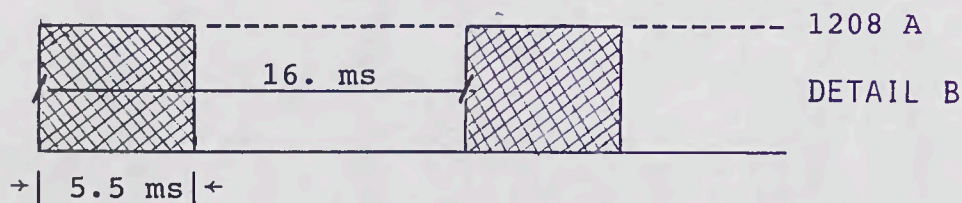
### CORRIGENDUM:

A) FIGURE 1 - REPLACE DETAIL B

FROM:



To:



- B) FIGURE 2 - REPLACE IN THE FIGURE THE SYMBOL  $\frac{1}{4}$  BY  $\frac{1}{4}$
- C) FIGURE 7 - REPLACE "T = 186S" BY "T = 180S"
- D) ITEM 4 - PAGE 5 - LEFT COLUMN:
- D.1) 1<sup>ST</sup> LINE:  
REPLACE "TEXT" BY "TEST"
- D.2) 3<sup>RD</sup> LINE AFTER THE TITLE OF FIGURE 7  
REPLACE "27.6 x 10<sup>6</sup>" BY "26.5 x 10<sup>7</sup>"
- D.3) 7<sup>TH</sup> LINE AFTER THE TITLE OF FIGURE 7  
REPLACE "27 x 10<sup>6</sup>" BY "26.5 x 10<sup>7</sup>"



ISBN 0 9514828 1 5